S. F. Carter (p. 245). See January 1950. . . . Sven Fornander (p. 256). See January 1950. . . . Folke Nilsson (p. 256). See January 1950. . . . M. Cohen (p. 261). See September 1949. . . . V. G. Paranjpe (p. 261): born in Bombay, India and there attended Elphinstone high school. Received B.S.-Metallurgy degree from Benares Hindu University and Sc.D.—Met. from M.I.T., in which he was for a time Research Assistant and currently Research Associate. . . . M. B. Bever (p. 261): born in Germany and obtained degree of Doctor of Science from M.I.T. Is a member of AIME and lives in Cambridge, Mass. Associate Professor of Metallurgy at M.I.T. teaching physical metallurgy and metallurgical thermodynamics. Has been member of Program Committee and Membership Committee, IMD., Membership Committee, Extractive Metallurgy Div., and Physical Chem. of Steelmaking Committee. Mr. Bever has previously presented papers as co-author on the Solubility of Various Elements in Copper, Iron and their Alloys; On the role of Oxygen in the Iron Blast Furnace, the Age-hardening of Aluminum Alloys and the 1946 Annual IMD articles on physical metallurgy. He enjoys music and mountain climbing. . . . C. F. Floe (p. 261); born in Dawson, Y.T., Canada, and graduated from Washington State College receiving B.S. and M.S. degrees and obtained Sc.D. in Metallurgy from M.I.T. Was Instructor and Asst. Professor at Washington State College; Asst. Professor, Univ. of Notre Dame and currently Executive Officer, Dept. of Metallurgy, M.I.T. Is a member of AIME and lives in Belmont, Mass. Mr. Floe has previously presented AIME papers on Gases in Copper and Copper Alloys; Carbon in Copper. . . .W. L. Finlay (p. 277). See October 1949. . . . F. Libsch (p. 287); born in Rockville, Conn., attending high school there and received degrees of B.S., M.S. and Sc.D. in Metallurgy, at Mass. Inst. of Tech. Is a Junior member of AIME and lives in Bethlehem, Pa. His experience has been primarily in the field of Physical Metallurgy, specializing in Heat Treatment; development and research on sintering of iron powder; Research Fe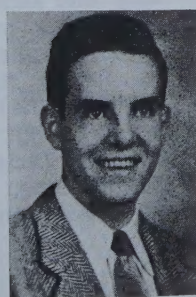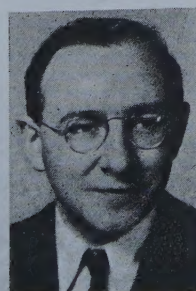llow for Nitralloy Corp. at M.I.T.; Captain, U. S. Army Ordnance Dept. at Springfield Armory, for metallurgical development and research in small arms; currently Asst. Professor, Dept. of Metallurgical Eng., Lehigh Univ., Bethlehem, Pa. and Metallurgical Consultant, Lepel High Frequency Lab., Inc., N. Y. . . . E. Both (p. 287); born in Ahrweiler, Germany, and attended high school there, graduating from University of Bonn, Germany, with degree of Ph.D. His home is in Oakhurst, N. J. Was for some time with the Heraeus Vacuumschmelze A.G., at Hanau, Germany, subsequently becoming Director of the Research and Development Laboratories of that company. At present Mr. Both is on the staff of the Signal Corps Engineering Laboratories, Fort Monmouth, N. J. . . . Donald Warren (p. 287); born in Carbondale, Pa., and attended Lafayette high school, Lexington, Ky. Obtained B.S. and M.S. degrees from University of Kentucky and Lehigh Univ. He is a student member of AIME and lives in Springtown, Pa. Is Engineering Aid at Cleveland Laboratory of N.A.C.A. Mr. Warren's chief interests are philately and photography. . . . T. E. Leontis (p. 297); see December 1949. . . . R. S. Busk (p. 297); born in Brooklyn, N. Y., went to high school in Poughkeepsie, N. Y., and graduated from Colgate University with B.A. degree and obtained D.Eng. from Yale. He is a member of AIME and lives in Midland, Mich., and is on



M. B. Bever



F. Libsch



E. Both



D. Warren



R. S. Busk

# *Journal of* METALS

# IN THIS ISSUE

VOL. 188, NO. 2                     FEBRUARY, 1950

### COVER
The world's greatest iron ore lode. This is the first picture and first disclosure of U. S. Steel's spectacular discovery, Cerro Bolivar (La Parida), in Venezuela, a mountain of iron ore of great purity and of stupendous tonnage. Cerro Bolivar will be shipping 15 million tons yearly by 1955. For full story see p. 222.

S. F. Carter (p. 245). See January 1950. . . . Sven Fornander (p. 256). See January 1950. . . . Folke Nilsson (p. 256). See January 1950. . . . M. Cohen (p. 261). See September 1949. . . . V. G. Paranjpe (p. 261): born in Bombay, India and there attended Elphinstone high school. Received B.S.-Metallurgy degree from Benares Hindu University and Sc.D.—Met. from M.I.T., in which he was for a time Research Assistant and currently Research Associate. . . . M. B. Bever (p. 261): born in Germany and obtained degree of Doctor of Science from M.I.T. Is a member of AIME and lives in Cambridge, Mass. Associate Professor of Metallurgy at M.I.T. teaching physical metallurgy and metallurgical thermodynamics. Has been member of Program Committee and Membership Committee, IMD., Membership Committee, Extractive Metallurgy Div., and Physical Chem. of Steelmaking Committee. Mr. Bever has previously presented papers as coauthor on the Solubility of Various Elements in Copper, Iron and their Alloys; On the role of Oxygen in the Iron Blast Furnace, the Age-hardening of Aluminum Alloys and the 1946 Annual IMD articles on physical metallurgy. He enjoys music and mountain climbing. . . . C. F. Floe (p. 261); born in Dawson, Y.T., Canada, and graduated from Washington State College receiving B.S. and M.S. degrees and obtained Sc.D. in Metallurgy from M.I.T. Was Instructor and Asst. Professor at Washington State College; Asst. Professor, Univ. of Notre Dame and currently Executive Officer, Dept. of Metallurgy, M.I.T. Is a member of AIME and lives in Belmont, Mass. Mr. Floe has previously presented AIME papers on Gases in Copper and Copper Alloys; Carbon in Copper. . . . W. L. Finlay (p. 277). See October 1949. . . . F. Libsch (p. 287); born in Rockville, Conn., attending high school there and received degrees of B.S., M.S. and Sc.D. in Metallurgy, at Mass. Inst. of Tech. Is a Junior member of AIME and lives in Bethlehem, Pa. His experience has been primarily in the field of Physical Metallurgy, specializing in Heat Treatment; development and research on sintering of iron powder; Research Fellow for Nitralloy Corp. at M.I.T.; Captain, U. S. Army Ordnance Dept. at Springfield Armory, for metallurgical development and research in small arms; currently Asst. Professor, Dept. of Metallurgical Eng., Lehigh Univ., Bethlehem, Pa. and Metallurgical Consultant, Lepel High Frequency Lab., Inc., N. Y. . . . E. Both (p. 287); born in Ahrweiler, Germany, and attended high school there, graduating from University of Bonn, Germany, with degree of Ph.D. His home is in Oakhurst, N. J. Was for some time with the Heraeus Vacuumschmelze A.G., at Hanau, Germany, subsequently becoming Director of the Research and Development Laboratories of that company. At present Mr. Both is on the staff of the Signal Corps Engineering Laboratories, Fort Monmouth, N. J. . . . Donald Warren (p. 287); born in Carbondale, Pa., and attended Lafayette high school, Lexington, Ky. Obtained B.S. and M.S. degrees from University of Kentucky and Lehigh Univ. He is a student member of AIME and lives in Springtown, Pa. Is Engineering Aid at Cleveland Laboratory of N.A.C.A. Mr. Warren's chief interests are philately and photography. . . . T. E. Leontis (p. 297); see December 1949. . . . R. S. Busk (p. 297); born in Brooklyn, N. Y., went to high school in Poughkeepsie, N. Y., and graduated from Colgate University with B.A. degree and obtained D.Eng. from Yale. He is a member of AIME and lives in Midland, Mich., and is on

M. B. Bever

F. Libsch

E. Both

D. Warren

R. S. Busk

M. F. Hawkes

G. H. Enzian

R. Wachtell

K. M. Goldman

the staff of the Magnesium Lab. Dow Chemical Co. Mr. Busk has previously presented an AIME paper. His hobby is woodworking and golf is his chief pastime. . . . **M. F. Hawkes** (p. 307); born in Los Angeles, and attended high school in Fresno, Calif. Received B.S. degree from Univ. of Calif., and M.S. and D.Sc. from Carnegie Tech. He is a member of AIME and lives in Pittsburgh. Was with Bethlehem Steel Co., Los Angeles, on the staff of the Metallurgical Dept. of the steel plant, and currently Associate Professor at Carnegie Tech. Mr. Hawkes has previously presented an AIME paper on Austenite Transformation in Cobalt Steels; Austenite Grain Size in Cast Steels. His interests range from deep-sea fishing when in California to loafing in the sun in Florida, as well as softball, bridge and chess. . . . **C. W. Sherman** (p. 334); see November 1949. . . . **G. H. Enzian** (p. 346); born in Forty Fort, Pa., attended high school in Windber, Pa., graduating from Lehigh University with B.S. and Met. E. degrees. He is a member of AIME and now resides in Fox Chapel outside Pittsburgh. Began working in J & L mill as metallurgical inspector. Became metallographer in Research & Development Div., and is currently Assistant Manager, Metallurgical Research. Mr. Enzian has previously presented an AIME paper as co-author on Effect of Deoxidation on the Strain-Sensitivity of Low Carbon Steels. His major activities are hunting, fishing, golf. . . . **R. Wachtell** (p. 354); born in New York City and attended DeWitt Clinton high school graduating from Columbia University with B.S. degree. He makes his home in Mamaroneck, N. Y. Was for a time with Bureau of Standards; Metallurgist for Inspection Control Lab., at Republic Aviation Corp.; Metallurgist, Air Reduction Co., and at present Research Metallurgist with American Electro Metals Corp. Mr. Wachtell's hobby is model-making and photography besides his interests in music as a flautist. . . . **W. O. Philbrook** (p. 361); born in Chicago, attended Hyde Park high school and received degree of B.S.-Chem. from University of Chicago. Is a member of AIME and makes his home in Pittsburgh. Was routine analyst for Wisconsin Steel Wks., Int. Harvester Co.; for a time Research Chemist-Foreman of Metallurgical Div.; and currently Associate Professor Met. Eng. and Member of Staff, Met. Res. Lab. Mr. Philbrook has previously presented AIME papers on Basic Openhearth Steelmaking. His chief interests are fishing, fly-tying, bridge. . . . **Kenneth M. Goldman** (p. 361); born in Pittsburgh, attended Fifth Avenue high school and graduated from Carnegie Inst. of Technology with degree of B.S. in Metallurgical Eng. Is a junior member of AIME and lives in Pittsburgh. Was student engineer at National

Tube Co.; Junior scientist at Los Alamos, New Mexico, while in U. S. Army Corps of Engineers T/Sgt.; Research Asst., Metals Research Lab., Carnegie Tech.; currently full time graduate student in Metallurgy at that Institute. His pastime is devoted to tennis, hiking and reading. . . . **Martha M. Helzel** (p. 361); born in Greensburg, Pa., attended high school in Jeannette, Pa., and graduated from Seton Hill College, Greensburg, with B.S. degree. She makes her home in Massena, N. Y. Was Chemist for Beech Bottom Power Co., Wheeling, W. Va.; and later Research Associate at Carnegie Institute of Technology. Miss Helzel's chief interest is collecting music records and is a pianist and singer in her own right. . . . **C. G. Dunn** (p. 368); born in Wenatchee, Wash., and went to Fergus County high school in Lewistown, Montana, graduating from Montana State Univ. with degree of B.A. and obtaining Ph.D. from University of Illinois. Is a member of AIME and lives in Pittsfield, Mass. Was graduate assistant at Univ. of Illinois, subsequently becoming Physicist at General Electric Co., Pittsfield, dealing with research and development of magnetic materials. Mr. Dunn has previously presented a number of AIME papers. His chief pleasures are bowling and photography. . . . **C. E. Birchenall** (p. 378). See January 1950. . . . **W. F. Craig, Jr.** (p. 389); born in Winterset, Iowa and attended high school there. Received B.S.-Chem. Eng. degree from Iowa State College. His home is in Chicago. Has worked for Carnegie-Illinois Steel Corp., Gary, Ind. as Research Metallurgist and now Supervisor, Ferrous Metals Research, Armour Research Foundation, Chicago. . . . **J. P. Sheehan** (p. 389); born in Ossining, N. Y., attended high school there and received degrees of B.S. and M.S-Met. from University of Kentucky and Notre Dame. He makes his home in Chicago. Has worked on the Ear Research Project of University of Kentucky; was Quality Control Metallurgist for Republic Steel, and currently Research Metallurgist for Armour Research Foundation. His chief recreation is golf. . . . **D. J. Carney** (p. 397); born in Charleroi, Pa. and went to high school there. Attended Penn State, Carnegie Inst. of Tech., and Mass. Inst. of Tech., receiving degrees of B.S. and Sc.D. and makes his home in Chicago. Was with Pittsburgh Steel Co., the Naval Research Lab., Carnegie Inst. of Tech., Mass. Inst. of Tech., Duquesne, Clairton and South Works of Carnegie-Illinois Steel Corp. . . . **N. J. Grant** (p. 397). See November 1949. . . . **D. C. Hilty** (p. 414). See September 1949. . . . **W. Crafts** (p. 414). See December 1949.

* The greatest and richest iron ore body in the world was discovered by U. S. Steel in Venezuela in April 1947 and is disclosed for the first time in this issue (p.222). One solid mountain of ore, Cerro Bolivar, will furnish more tonnage than the famous Hull-Rust pit at Superior has or ever can. Total resources are on the order of 1-1/2 billion tons plus.

Big steel is now moving with great speed on construction to bring out this ore, and 10 million tons are scheduled for shipment into Baltimore and Birmingham by late 1952. This ore will arrive at Pittsburgh at a price lower than present natural ores from Superior. The Venezuelan properties will be completely mechanized.

* U. S. Steel and independent companies are embarking on a taconite beneficiation program of tremendous proportions which must be speeded to completion in the 1950's. (see p. 222).

By 1960 over $1.2 billion dollars will be spent on Venezuela, taconite, and Labrador to solve the U. S. iron ore crisis. In addition, U. S. Steel will spend another $300 million plus for a new steel mill at Trenton, N. J. before 1955.

* New data on the effect of varied melting practice in electric arc-furnace steels on hydrogen content are given by Sam Carter (p. 245).

* Effect of inductive stirring during the reducing period, the effects on refractory linings and economic aspects of its use are shown in detail on p. 256.

* New experimental data on the manganese equilibrium in liquid steels under simple slags are given on p. 341.

* Simultaneous small variations in phosphorus and nitrogen have concomitant effects on the properties of low-carbon steels, according to G. H. Enzian, (p. 346).

* A 50 pct non-cobalt alloy, prepared by powder metallurgy methods, exhibits optimum magnetic properties when heatreated in a magnetic field. Small amounts of nickel appear to be detrimental. (See p. 287).

* Direct extrusion of magnesium-alloy powder is described (p. 297) and used to produce four new alloy types by controlled solid-state diffusion.

* On Dec. 23 the French celebrated the start of a large continuous mill project by the Societe Lorraine de Laminage Continu (SOLLAC), financed with ECA dollars. A vast heavy industrial project such as this to offset resurgence of the German Ruhr has long been a French dream.

Meanwhile, in Germany, the Thyssen works, once the largest iron and steel plant in Europe, has had its steel capacity reduced to 117,000 tons whereas its pig iron capacity has been left at 600,000 tons a year. The Germans ask for retention of at least one blooming mill, now dismantled and crated for delivery to England. The Ruhr's only broad continuous mill has been sent to Russia.

All indications are that the Adenauer government in western Germany will succeed in eliminating the 11.1 million-ton restriction on steel output and will secure jurisdiction over the reorganization of the Ruhr steel trusts, which German experts are at present being required to carry out under Military Government Law 75. If so, an effort will be made to secure American or Swedish capital to rebuild the Ruhr with modern equipment to take the place of the outdated facilities that the victorious Allies so busily hauled away.

# It's Everyone's Business

JAN. 17—In what appears to be a general spirit of post-Christmas emotional malaise, most adult Americans have bidden farewell to the Forties and turned with no perceptible enthusiasm toward the Fifties. The dying decade had started amid a phoney war which verged on the romantic, stirred the pulse with excitement and seemed far away. A phoney peace dominates the new decade. The romance is no longer there. Nor is the excitement. Nor is the distance.

While most of the world preferred to be chronologically correct and hold off for another year before celebrating the demise of the first half of the twentieth century, the United States with true competitive enterprise and a great whirl of words scurried into the second half a year early. This undue haste might perhaps have been dictated unconsciously by a yearning for the pattern of history to be repeated. For many centuries, ever since Roman times, the second half of most centuries tended to be far more tranquil than the first half.

In Washington, Mr. Truman got on both sides of the mid-century line with all the aplomb of a good politician. He told Congress early in January that "the state of the Union continues to be good," as it nears "the midpoint of the twentieth century." Later he spoke of moving forward into the second half of the century. He promised an infinitely better life for everyone, whichever side of the mid-century line, and reaffirmed his prescription toward that end: assistance for small businesses; more houses for the middle-income groups; tougher anti-monopoly laws, retention of rent controls; development of natural resources; better insurance against the hazards of old age, idleness and unemployment; better medical care and education, civil rights legislation; new labor relations law and production payments to support farm incomes. All this was to be coupled with suggestions on how to balance the budget.

The bloody and confusing 1940's had brought to most men's minds a fear of the future such as they had not known for centuries, and Mr. Truman's objective is to temper that fear. Only time will tell whether the terminal point of such a philosophy would or would not belie the old English proverb citing inability to both eat and have a cake.

Brave words to the contrary, the national budget persisted in sliding off into the red. The smell of further inflation was equally persistent. And just to impart a little more zip to the trend, the American Federation of Labor announced its intention of seeking "substantial" and "large" wage increases this year. The AFL forewarns of a business slump after June and a 10¢ an hr wage increase for each worker "will be enough to reverse the prospective downward trend and start a rise." Thus it goes—"the way to halt a drop in demand for labor is to raise the price of labor."

**Elsewhere in the harassed world,** beleagured individualists in New York achieved a local triumph of sorts for one of the freedoms denied by the Soviet and Nazi systems—the right of escape, some escape at least, from the servitude to decibels. Grand Central Station weakened percepti-

bly at Christmas on its 5-min commercials and bore down heavily on "Hark, The Herald Angels Sing," and on New Year's Day capitulated entirely by abandoning the broadcasting of canned music and slugs of advertising slogans. In Europe, M. Bidault's Assembly majority fell away and newspaper accounts of the incredible monstrosities of political trials beyond the iron curtain were supplanted by headlines marking the birth of Princess Yasmin. The latter was surrounded by Byzantine splendor but otherwise
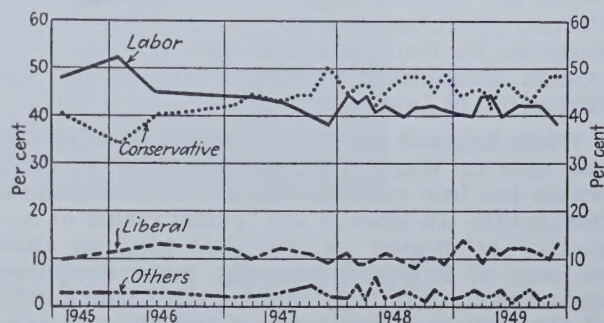


showed no apparent deviation from the accepted norm. In Western Germany, Dr. Adenauer began to speak up more boldly, and the whole fabric of Allied policy towards the defeated enemy further dissolved under the impact of rivalry with the Russians. In the Far East both the Americans and British seem somewhat embarrassed by Chiang Kai-shek's refusal to lie down. Dual thinking regarding the "squalid and useless struggle in the China seas" is such that newspapers give sympathetic accounts to an American ship running supplies to the Communists at Shanghai while calling for help for the recognized Chinese government in Formosa. And with Britain recognizing Communist China they may well have to team up with Russia against the United States to kick the Chinese representative off the UNO Security Council, the Far Eastern Commission and the Allied Council in Tokyo.

Far Eastern policy has never been a bipartisan matter and as General Chiang retreated to his final redoubts in Formosa and Hainan, a number of Republicans pecked away at Administration lassitude. Senator Smith advocated the occupation of Formosa and Messrs. Hoover and Taft asked for use of the Navy. Mr. Acheson has stood firm, however, against military aid. None the less, a study will be made of the Generalissimo's chances. Mr. Truman has a private purse of $75 million for the Far East and some $94 million in frozen ECA funds. Mr. Truman will likely trade some of this money for support of new Marshall plan appropriations, always mindful, of course, of Mr. Acheson's plan to drive a wedge between the Chinese and Moscow, and his wish to avoid any revival of imperialist nightmares throughout the Orient. Mr. Acheson is very convinced that the victories of Communism in China will be short-lived and South Asia will not fall

under the Soviet yoke if the West can win the friendship of the independent Asiatic people and convince them that real efforts are being made for their welfare and progress. It is tact and human understanding in official and unofficial contacts, and also Mr. Truman's Fourth Point, which will tip the balance and stem the communist flood—not the mailed fist.

In Britain an electorate is getting readied for a general election in late February, the first since 1945. Despite the steady victories in local by-elections, the tide has tended to run steadily against the Labor Party. Ever since 1945 Dr. Gallup's British Institute of Public Opinion has periodically asked the question: "If there were a general election tomorrow, how would you vote?" The results are shown here in graph form. While Mr. Truman all too recently proved that election prediction is indeed an unproductive occupation, Dr. Gallup's figures have been accorded enough recognition to wring most of the optimism out of Labor politicians.

**While England debates the merits of Socialism,** the eyes of Western Europe continue to stray across the iron curtain with a certain degree of fascination. In Moscow the "genial father of humanity" celebrated his seventieth birthday amid an orgy of idolatrist vulgarity, mass obeisance and orations of flattery running the entire gamut of the richest superlatives of the Russian language, all interlarded with some genuine respect and sincere personal feeling. Only in Tito's Yugoslavia was the great day ignored—perhaps there all energy is being hoarded for a bang-up competitive celebration on May 25, Tito's birthday!

Stalin's birthday was marked by orations by Politburo members, all written by central headquarters and therefore indicative of the grand strategy of communist thinking. Apparently Stalin fully intends to prove anew the astonishing longevity of Caucasians, and furthermore, has no intention of retiring to an elder statesman role. He is and will be the master-mind behind unrelenting pressure on western countries. The revolution must not be permitted to lag. Flexibility and cunning are to mark all relations with the capitalist countries and attempts will be made to split the western bloc by dangling before the United States offers promising bans on atomic weapons and agreements to divvy up the world into spheres of influence.

Down in Bulgaria the testimony released on the trial of communist Secretary-General Kostov indicates that the Soviet world is far less strong, far less monolithic than its champions claim. Apparently Kostov, a long-time dependable Comintern agent, refused at times to sell exclusively to Russia when better prices could be obtained for certain products in Europe. He also considered accepting Marshall aid and tended to view Tito's Yugoslavia as having "a sober and realistic policy." In satellite Russia such thinking leads straight to the hangman's noose. Kostov's failure to stick by his "confession" in the trial parody in the Military Club ballroom so infuriated and confused the functionaries as to make them speechless for 48 hr, until *Pravda* laid down the line by describing him as a "shrewd, experienced and determined enemy . . . soft and oily voice . . . cunning eyes of a thief." *Pravda* also derided Kostov's "bent back," not mentioning that the

hunchback dates from 1924 when, as a communist organizer, he threw himself from the Sofia police building roof to escape torture. Elsewhere around the Russian periphery other nooses are being readied for other "diversionist" communist necks.

Back in the United States the stock market jumps around while industry as a whole operates steadily at its best level since last spring. Order books for most consumer goods are well filled; the steel industry is working at forced draft to plug up strike-reduced inventories, coal stocks need replenishing, and Detroit is scheduling higher activity for early 1950 than in the com-



parative 1949 period. Construction contracts remain very high. As the Treasury starts paying $2.8 billion of insurance premium refunds to veterans, there is every indication that industrial output during the winter will inch further upward.
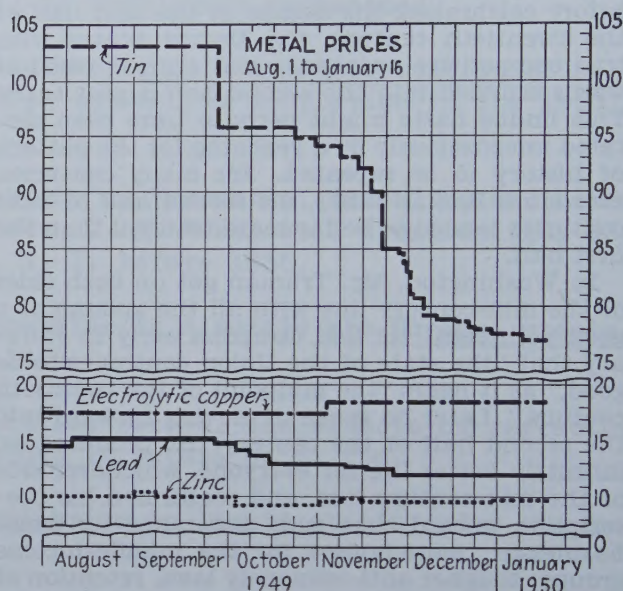
As for base metal prices, the release of inflationary pressures is such that a general rise in nonferrous prices is not out of the question. In most base metals, excepting tin, American demand has recovered along with a firming in price tone. Consumption of copper has been maintained at a high level and deliveries from producers and custom smelters are heavy. The strength of the market is best gaged by hardening in the copper scrap market. Lead scrap and the forward price of zinc have also tended to rise. Tin, however, has persistently strayed to the downward side, with prices virtually dictated by the RFC which sells the output of the Texas smelter. Recently the British Ministry of Supply transferred 3,000 tons of tin to New York for the spot market, only to be met by the RFC announcement that it would be adjusted to compete with tin imports. So far the British government has shown no tendency to undercut the market and dispose of its stock. As other importers bring in supplies, however, the tin market is liable to show some of its prewar competitive dash and vigor.

# Cerro Bolivar
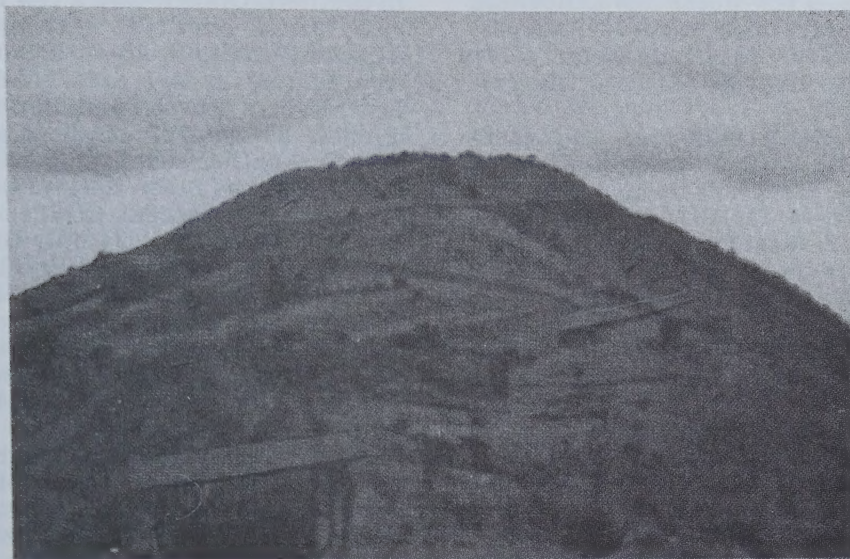


## Saga of an Iron Ore Crisis Averted

by T. W. Lippert
*Manager of Publications, AIME*

CUBA fancies herself the "pearl of the Antilles" and, by many, Jamaica is called "blessed." But far to the southward lies what is seemingly the Caribbean's most glittering jewel, the sparsely-settled, Spanish-speaking United States of Venezuela, indeed blessed by nature to a lavish degree. Not a large country, Venezuela is leaping from the donkey to the airplane under the impact of its natural wonders. Angel Falls, dwarfing Niagara and seldom seen by man, is hidden in the cold, primitive and unexplored Guiana highlands along the southeast border. A few hundred miles northwest are the low and torrid coastal plains from which gush unlimited black-gold streams of oil. About midway are the *Llanos*—low-lying, savanna-type grasslands, beneath which large deposits of bauxite are as yet barely touched by the explorer's diamond drill. And jutting starkly upward 2000 ft from a surrounding expanse of savanna is a small mountain (see front cover), 11 miles long and 1 mile wide. It is, or was, La Parida.

---

**Picture above shows the topmost tip of Cerro Bolivar. The road (for diamond drills) was blasted out of the richest of solid iron ore. Shed is a pumping station.**

---

This is the first disclosure that over half of La Parida is solid iron ore of almost unbelievable purity—by all sober estimate the richest and greatest iron deposit in the history of the world! The U. S. Steel Corp. has La Parida under denouncement for 100 yr, and its discovery was the terminal point of the most far-flung and greatest

of all ore searches, and also the quietest. Both the discovery and the plans being rushed forward for its development constitute a classic example of free enterprise at its very finest—daring, imaginative and responsible. Within a few years this little mountain will be exerting a profound influence on the American steel industry and the entire American economy. Its existence certainly brightens the long-term military potential of the United States. The only possible jarring note in as dramatic a record of geological derring-do as anyone could wish for—hardly worth a quibble perhaps—is that La Parida (in prim translation "a new mother"), after being delivered of her first ton of iron ore for experimental tests, has found herself both re-sexed and re-named Cerro Bolivar. To the midwives, a solid, masculine hero's name is none too fitting for a mountain soon to rank with Mesabi in the lexicon of steel.

These last few years, amid all the turmoil of postwar strikes, investigations, and insatiable demands for production, the steel industry has occasionally twisted around to stare uneasily at the six great Superior ore ranges. Like Alice in Wonderland, these ranges seemed to shrink and grow with disconcerting rapidity, depending on whether the reserves were being estimated by Mr. Barloon of Western Reserve University or Mr. Randall of Inland Steel Co. From out of the blue have come fitful showers of statements regarding Taconite, for the most part statements barren of any real substance. There were reports of Bethlehem opening a new ore pit in Chile, of Bethlehem and the U. S. Steel Corp. in Venezuela,

and of Republic in Liberia. Up in Labrador, Hanna-Hollinger have mixed a succession of ore discoveries and dramatic press relations with exemplary skill. And down near Trenton, N. J., the U. S. Steel Corp. a few weeks ago announced acquisition of 3800 acres of farm land—quite possibly for a 2 million-ton steel mill within a few years, not in perhaps 10 yr as has been the general press assumption.

These individual events may seem only casually related, the usual cut and thrust of economic enterprise. But just like beads on a string, they all fit together. And by far the biggest bead on the string is the U. S. Steel Corp.'s Cerro Bolivar. Within four years shipments into Birmingham, Youngstown, Pittsburgh and Trenton could be coming out at the rate of 10 million tons annually, to be stepped up later to 15 million tons, all the richest type of blast-furnace grade. And hard openhearth charge ore, a really scarce grade already 800,000 tons a year in short supply in the Pittsburgh area alone, is scattered in very generous lenses over U. S. Steel's eighteen denouncements and six concessions.

This article tells for the first time the story of Cerro Bolivar, a story of men and events which sometimes reaches into the suburbs of improbability. This article also tells of the other beads on the string, all components of the future iron ore supply of the United States—Taconite, Labrador, the various ore deposits around the periphery of the Atlantic Ocean, and of course the historic ore ranges of the Lake Superior area.

**Stretching across northern Minnesota,** in an extended sheet, 100 miles long and several miles wide, lies a primitive iron formation, Taconite, of which the Lake Superior iron ranges were formed. There is not one Taconite but many types of complex mixtures of hematite, magnetite and waste. At best it is one-third iron and two-thirds waste. Sprinkled here and there

in the Taconites, like rich raisins in a poor cake, are the high-grade ore pockets, the fabulously rich (at one time) Cuyuna, Mesabi and Vermillion ranges. The sheet of Taconite rises again in southern Ontario and a few more not-so-very-rich raisins stick out (Michipicoten, Gunflint, Atikokan ranges, *et al*) with Goulais the most recent finding in this area. (Algoma Steel Corp. just recently proved 50 million tons of magnetite minable by open-pit methods along the Goulais River.) Another short jump and there is a small rich outcrop at Steep Rock (Inland Steel is seeking additional deposits in this area), after which the Taconite falls away only to rise again along the far distant boundary line between Labrador and Quebec, which represents the last remaining large-sized explorable iron range in North America. Here the raisins pop out all over the place, relatively small pockets of rich ore outcropping over an area some 85 miles long and 15 miles wide. The best raisins are on the Hanna-Hollinger concession and their exploration has generated successive waves of publicity. This whole band of ore, from Fort Chimo on cold and desolate Ungava Bay down into Wisconsin, possesses iron formations of great similarity and was undoubtedly created in the same geologic age.

When Benjamin Franklin pressed down hard with his "strong red line" at the Treaty of Paris, it was Providence assisted by blind good fortune that set the ragged Canadian-American boundary line north of the Mesabi, Vermillion and four other fabulous iron ranges, which were discovered almost a hundred years later. Of late, with discovery of the Labrador pockets, historical justice at long last seems to be swinging a little toward a more equitable balance, but even so there is nothing in Labrador resembling the fabulous Hull-Rust pit at Hibbing, Minn.

Since the early 1900's over 80 pct of the nation's iron ore has come from the few pits in
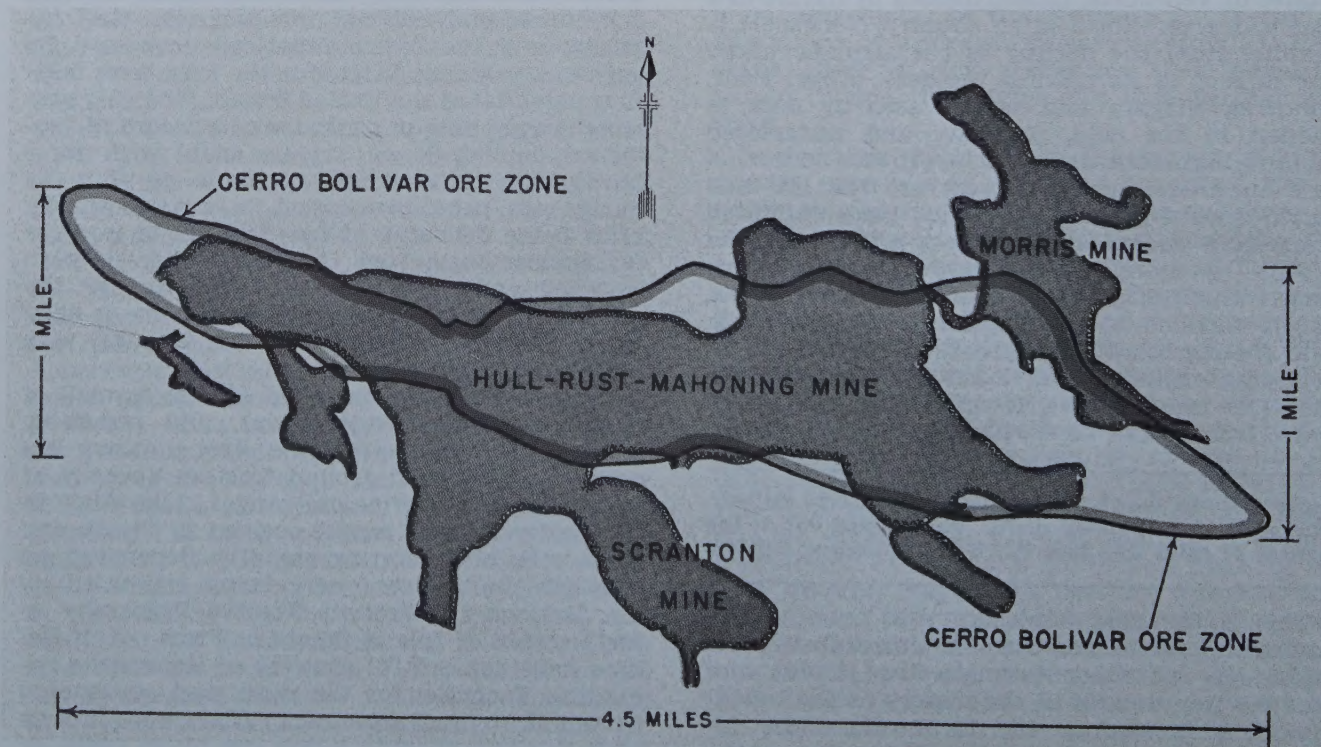


Cerro Bolivar compared in area with the champion of Lake Superior open pits, Hull-Rust-Mahoning.

the Lake Superior district. The country has been built and two world wars fought and won on the rich, easily-mined ore from these ranges, with the Hull-Rust pit carrying a large portion of the load. Since the ranges were first worked there has been available "unbounded" and "unlimited" iron ore, rich and for the most part open-pit. It is somewhat ironical to note that back in 1913 the U. S. Steel Corp. considered itself so burdened with iron ore that it hastened to rid itself of the "Hill Lease" containing well over 300 million tons. In the mid-1930's many steel companies chafed under the tax loads levied against their ore properties and foresaw no ore problem for their children or even their children's children. Even as late as 1939 many steel companies viewed ore reserves primarily as an *embarras de richesses,* but the U. S. Steel Corp. began shaking itself loose from the universal somnambulism and announced its willingness to sell ore in the open market. This historic move is a good case study of responsibility —it was a basic decision to share greater reserves with the remainder of the industry. Some 52 million tons of ore has been sold to all comers. If depletion and crises were to be the end result, at least everyone in the industry would approach that grim accounting at about the same time.

The second world war chopped 340 million tons of the highest quality reserves out of the pits, and a couple of years ago C. M. White, president of Republic, gloomily announced that no more wars were ever going to be fought off Superior's natural ores. He might just as gloomily have announced that there weren't many more years of peacetime prosperity left in the Superior pits. Nature's lush legacy had been spent, and many a directors' room echoed to grim forebodings, although on the surface the attitude was one of calm confidence. The safety of the country, the prosperity of the country and the preeminence of the American steel industry were approaching the cross-roads, and the disinclination to engage in barren controversy and discussion in public was based not on a Micawber-like attitude that "something will turn up," but genuine confusion as how to develop the technology and raise the great sums of money necessary to fend off the crisis.

The usable iron ores in the Lake Superior district, at present rate of consumption, will be totally exhausted in about 1963 for Independent companies and in about 1970 for the U. S. Steel Corp. And the assumption in some quarters that there are some hidden reserves being held back for tax reasons is a piece of dangerous wishful thinking.

As of Jan. 1, 1950, the natural iron ore reserves of the Lake Superior district amounted to 1290 million tons. Of this quantity the U. S. Steel Corp. held 690 million tons (53.5 pct). Among the Independents, National Steel is by far the best off, whereas one major steel company has less than 20 million tons in reserve and several others have less than 40 million tons each. An additional discouraging factor is that open-pit reserves (the easiest to skim off during a war) have fallen to 70 pct of the total reserves, and the industry must of necessity face up to more and more costly burrowing underground to get at their ore.

Some thirteen to fifteen years yet to prepare for total exhaustion might seem to many an outsider to present perhaps a rather reasonable breathing spell in which to somehow lick the problem. The task, however, is definitely not one for the next decade. It has demanded immediate solution. As a military compulsion alone some of the free-shipping ore remaining in several Superior pits should perhaps be frozen as a national emergency stockpile. With little over 1 billion tons up there, and conscious of the fact that nearly ½ billion tons were required in the last war, the situation becomes one that might adversely affect the life and future of each citizen. Further, if some optional source of metallics is to be devised, the tremendous capital investment required had better be scaled over as long an interval of time as possible, not come in one fell swoop. Even at best there will have to be some finger scratching along the bottom of the money barrels to carry the investments in prospect. Thirdly, and very important, indeed, steel companies must know where their metallics are coming from 15 yr hence in order to determine what equipment to build now and where to locate it. Costly ore boats cannot be constructed now only to have no cargo to haul before they have outlived their economic life. The same applies to blast furnaces, openhearth shops and rolling mills, which, if mislocated, could easily sink a steel company financially when the going got tacky.

**The only two ore options** available have been first, to devise some technically and economically practicable method of exploiting the huge Taconite deposits of the Superior region and, second, to go to foreign sources for ore. And, quite obviously, the Taconite challenge (Comparable in scope, complexity and cost with the war-time synthetic rubber program.) must be met, for a great nation like the United States with the world's largest steel industry can hardly risk drifting into a position of complete dependence on ore sources in foreign countries.

There's iron from which to make steel in the Taconites of Lake Superior—plenty of it, many billions of tons. This truism has led to a variety of public statements that the country has plenty of ore and that any concern is unwarranted. But the winning of usable iron from Taconite involves technical problems of such complexity that until very recently the huge sums of money required in capital investment and operation made a very large increase in the selling price of steel seem inevitable. It would be questionable whether the country's economy could stand such an added load, for industrial health over the past half century has been based in great part on the availability of large quantities of cheap steel.

Taconite is a mixture of hematite and magnetite crystals held in a matrix of rock which may be original or partly (or completely) decomposed. In most instances the waste accounts for about two-thirds of the total bulk, and since all the iron is usually not recoverable, it is necessary to mine close to 4 tons of material to get 1 ton of iron. There can be proportionally a little hematite and a lot of magnetite, or vice versa. The crystal size of either iron mineral can vary in any variety of combinations, and the proportion of ore to waste material can vary from infinitesimal to a rather respectable figure.

All pilot plants to date handling Taconite approach the problem in pretty much the same way. The Taconite is ground to a fineness dictated by the crystal size of the magnetite, and the magnetite is separated from the powder by passing over a drum or belt-type magnetic separator. The hematite goes along with the waste in the tailing. Then this powder must be reconstituted or agglomerated in some manner—nodulizing, sintering, pelletizing—to get a lump suitable for blast furnace charging containing about 63 pct iron. Obviously the most desirable type of Taconite should have, say, two-thirds of its iron in the form of magnetite and be characterized by relatively coarse crystals which would require grinding to much less fineness and make magnetic separation easier. Whether the Taconite has to be ground to 100 mesh or to 300 mesh, or whether the magnetite content is one-third the total iron or two-thirds, are the variables determining whether costs are to verge on the prohibitive or be modest enough to avoid serious increase in finished steel prices.

Fortunately, the eastern end of the Mesabi range has large deposits of Taconite which can be handled by the relatively cheap magnetite concentration process. The ore is hard and expensive to drill, but Minnesota has reduced taxes on this Taconite in order to encourage such operations. Michigan's Taconite, unfortunately, has hematite as the predominant iron-bearing mineral. Of course, this nonmagnetizable hematite can be reduced to magnetizable magnetite by heating and using reducing agents such as carbon monoxide. So far an operation of this complexity involves very discouraging cost factors.

Up on the ranges it is said that Taconite will be "manufactured" rather than mined. It is self-evident that the time, money, men and equipment necessary to drill and blast ore, grind it to a powder, extract one-quarter of the powder as a usable product, and then reconstitute this quarter into a lump form, are all on a far higher order than the conventional practice of having a steam shovel lift out great bites of hematite for direct shipment to blast furnaces. Furthermore, the problems involved in rapidly expanding Taconite concentrates during times of wartime national emergency are rather formidable, and may demand for minimum safety a number of standby plants or strategic stockpiles of concentrates.

At the very least, investment cost for Taconite concentrates will be well above $20 million per million tons of annual production of lump concentrates. This is investment cost alone which must be amortized and does not take into account day-to-day operating costs. If Taconites alone were to be depended upon to supplant the dwindling natural ores of the entire steel industry, some 52 million tons of capacity would be required in the next 15 yr. This would necessitate an investment of over $1.4 billion, a staggering sum which in final analysis would necessarily be borne in great part by steel consumers.

Even though the whole burden of future ore supply will not be thrown onto Taconite, a number of companies have attacked the problem with a zeal that mounts in direct proportion to the depletion of their natural ores. Within a few years the whole pace of Taconite exploitation must of necessity step up to a much faster tempo.

The Erie Mining Co. (Bethlehem, Youngstown and Pickands, Mather & Co.) began Taconite research some 10 yr ago and now is in the second year of operation of a 200,000-ton annual pilot plant at Aurora. From all information that can be gathered, the agglomeration of fine concentrates is presenting difficulties and there has been little or no production to date. Even so, this group of three companies now has plans in progress for a new plant of 2½ billion-ton annual capacity of lump concentrates.

Another combination, Reserve Mining Co. (Armco, Wheeling, Republic, and Cleveland-Cliffs) has acquired a 1½ billion-ton Taconite deposit, averaging 24 pct iron, at Babbitt, Minn. During the past 3 yr it has completed plans for a 10 million-ton capacity plant. Application was made for a $50 million loan from RFC to cover initial steps of constructing a 2½ million annual ton plant. The requested 30-yr loan was denied, and the RFC has suggested a 10-yr loan. This is a good example of the financing problems involved in shifting to Taconite—as yet RFC and the government is not conscious of the full seriousness of the situation.

Jones & Laughlin has completed a research laboratory for Taconite study at Ishpeming, Mich., and has acquired deposits of ore in Michigan and Ontario, Canada.

Cleveland-Cliffs has also completed a research laboratory at Ishpeming, Mich. This company plans to build a Taconite pilot plant in Michigan next year.

The U. S. Steel Corp. has Taconite reserves to produce some 300 million tons of concentrates in the western Gogebic Range in Wisconsin. However, much of the initial Taconite production will be based on the Minnesota ranges, and it is conservatively estimated that the district Taconite holdings will produce 1¼ billion tons of shipping lump concentrate, averaging 63 pct iron. The U. S. Steel Corp. definitely plans to have a pilot plant in operation by late 1952 turning out 500,000 tons of concentrates annually. This corporation has a very large laboratory at Duluth operating on Taconite research, and in late months officials are of the growing opinion that they have their problem pretty well licked. This is hopeful news, although it should be noted that large proportions of U. S. Steel's Taconite holdings are of the ideal type—large crystals and a very high proportion of magnetite.

In the next 20 yr it is to be expected that independent steel and ore companies must of necessity get into production some 17 million tons of Taconite concentrates. In the same period of time the U. S. Steel Corp. might well develop about 10 million tons of beneficiated Taconites, the exact capacity being dictated by cost relationships with Venezuelan ore imports delivered to various plants. Such an industry program, which cannot be avoided, will require new capital investment of well over $½ billion, and to manage such a sum will require some good profit years as well as a long series of special financings. It is certain that the growing dependence on Taconite will be reflected somewhat in finished steel prices. Until recently this figure looked as if it may be well over $4 a ton, although of late there is growing hope that when big production plants get into operation the
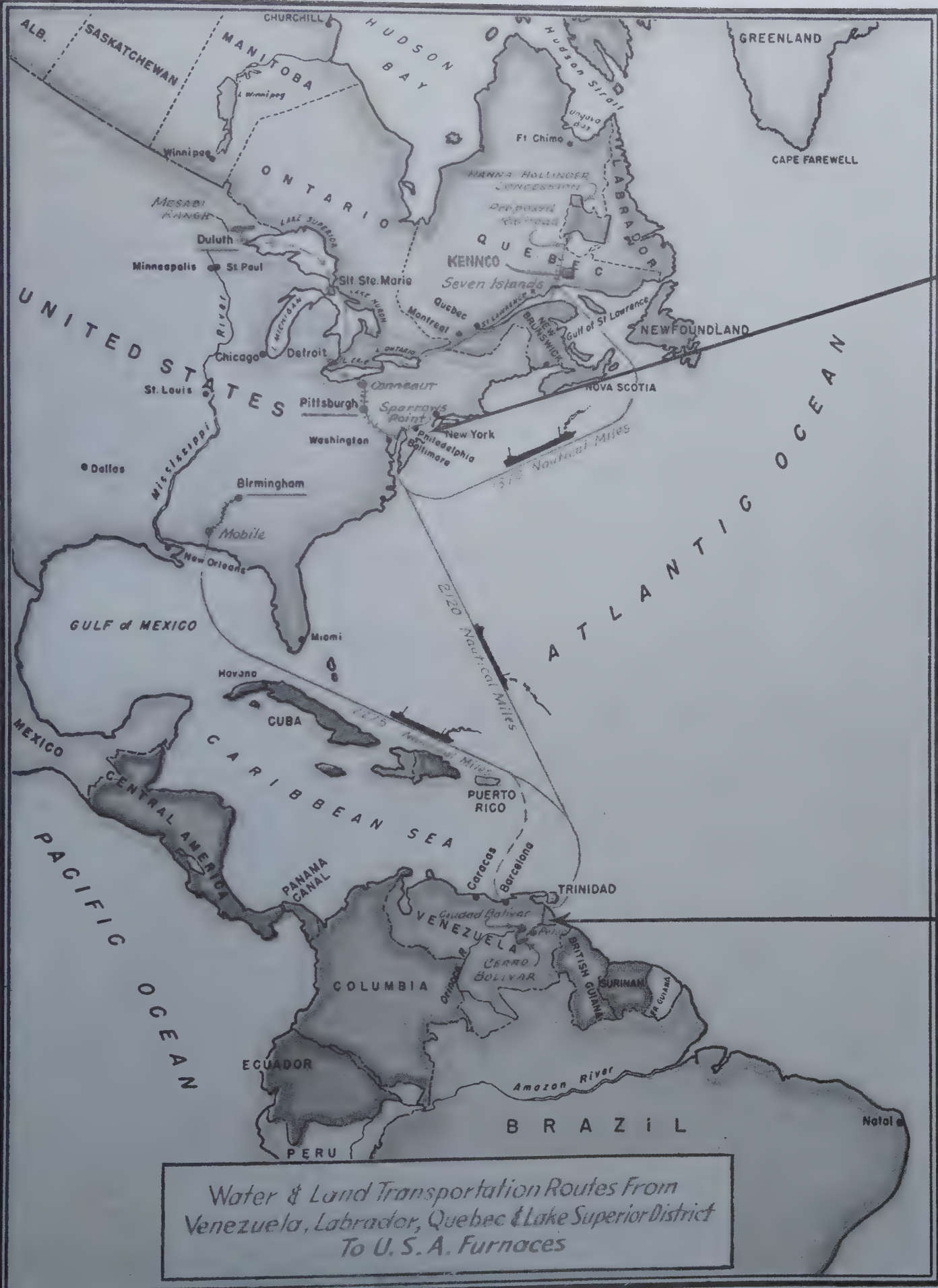
Water & Land Transportation Routes From Venezuela, Labrador, Quebec & Lake Superior District To U.S.A. Furnaces

## Pennsylvania / New Jersey map (top left)

Williamsport

Wilkes-Barre

P E N N S Y L V A N I A

Allentown

Reading

Harrisburg

Newark

NEW YORK

TRENTON

PHILADELPHIA

N E W   J E R S E Y

Wilmington

BALTIMORE

M A R Y L A N D

D E L

WASHINGTON

## Caption (top right)

✳ Location of U. S. Steel's projected eastern seaboard steel mill, to more economically service part of the 7 million ton annual finished steel market in that area. Assuming an annual 2 million ingot ton plant (3 blast furnaces; 16 openhearths; continuous hot and cold mills for plate, strip, sheet and tinplate; mills for wire, pipe and bars), the plant's completion would obviously coincide (before 1955) with availability of adequate Venezuelan ore. Giant ocean ore carriers would come directly to the plant (see map), barge trans-shipments would arrive from Baltimore via the C. & D. canal (map, dotted line). Quite possibly another "South Chicago" could rise on these flat New Jersey farmlands south of Trenton.

## Eastern Venezuela map (bottom)

To U.S.A.

To U.S.A.

C A R I B B E A N   S E A

PORT OF SPAIN

GUIRIA Tidewater Transfer Station

GOLFO DE PARIA

TRINIDAD

A T L A N T I C   O C E A N

GAS FIELDS

PTO DE LA CRUZ

BARCELONA

Barge Route to Transfer Station 200 Miles

Alternate River Routes

Ocean Vessel Route 26 Ft. Initial Draft 34 Ft. Ultimate Draft 170 Miles

Caño Monono

Caño Macareo

OIL & GAS FIELDS

Proposed Railroad to Tidewater Terminal 274 Miles

OIL & GAS FIELDS

Orinoco River

PIACOA

La Imperial

Transfer Station

PALUA

LA GRULLA

River

EL PAO

Orinoco River

Proposed Bridge

CIUDAD BOLIVAR

Rio Caroni

Proposed Railroad to River Terminal 91 Miles

ARIMAGUA 1-3

ALTAMIRA 1-8

CERRO BOLIVAR

RONDON 1-3

N

SCALE
10  5  0      10    20    30    40    50 MILES
10  5  0   10  20  30  40  50  60  70  80 KILOMETER.

Eastern Venezuela
Iron Ore Concessions

higher cost factors that must reflect down to the finished steel may be considerably less. In any case, Lake Superior Taconite concentrates will show up best competitively, vis a vis foreign ores, in the Lake Michigan and Erie consuming centers.

While the sharp-pencil experts in the back rooms worry the technology and economics of Taconite, a number of steel companies are reaching out into foreign countries to locate and acquire rich direct-shipping ores. While the problem for the nation as a whole is that of getting usable iron in any form and at any cost, the individual steel company has both that problem and also the one of competitive survival. And the individual plant's competitive survival will be based on cost of hot metal out of the blast furnace, vis a vis his competitors' costs in any particular district. In some instances the blast-furnace charge may be almost all Taconite concentrates, as, for instance, those plants bordering the Great Lakes to the west, such as Chicago and Detroit. Other plants may base their operations for the most part on foreign ores, such as plants in Birmingham and other Gulf areas, along the Eastern Seaboard up into the Northeast sections of the country. Still others, the great producing plants in the Pittsburgh, Youngstown, Cleveland, Wheeling area will likely fall back onto various combinations of Taconite concentrates and foreign ores.

It is probable that the rich Venezuelan ore discovered by the U. S. Steel Corp. will be available in almost any producing center at a better competitive price than units of iron from any other source. This great lode of ore which can practically be pushed onto railroad cars will be available to all who wish to buy. Further, this one body alone could supply the entire American steel industry all through the lifetime of children now being born. However, for reasons already mentioned—military, competitive, etc.—development of Cerro Bolivar will likely never rise beyond 15 million tons annually, although its price laid down in American steel centers will be a yardstick exerting great influence on iron from other sources.

For many years some iron ore has entered the United States from foreign countries—Bethlehem's large shipments from Chile and smaller deliveries from Cuba are the most conspicuous example. During the 1930's foreign ores and foreign finished steel were readily available at low prices, and some filtered throughout the eastern areas of the country. But they never got into the great midwest industrial areas primarily through inability to enter the Great Lakes without transhipment. Certain industrialists in the Great Lakes area based their opposition to the St. Lawrence Seaway on their desire to minimize foreign competition. Of late this opposition has ceased as a reflection of the imperative need to bring in foreign ores, particularly Labrador ores, as cheaply as possible.

Since Bethlehem has always been the most persistent of ore importers to feed its Sparrows Point, Md., plant, it might be of interest to review the foreign holdings of that company.

From Chile, Bethlehem imported 2.6 million tons of iron ore in 1948. This company recently has commenced expansion of its El Romeral iron mine as the result of a $2,750,000 credit from the Export-Import Bank for the Chilean Develop-

ment Corp. Estimated reserves in this area run to some 20 million tons of ore of 60 pct iron.

Bethlehem has for years also been in Cuba, bringing out small quantities of lateritic iron containing nickel and chromium. In general, Cuban laterites are not competitive with other ores, and persistent surveys by several companies have never uncovered any high-grade iron deposits of sufficient size to warrant interest as a dependable source of supply. Small deposits occur along the west coast of Pinar del Rio Province containing possibly 1 million tons of openpit ore averaging 55 pct dry iron and 10 pct silica.

The large deposits of lateritic iron ore containing nickel and chrome are in the Moa and San Felipe districts. U. S. Steel has some long-time holdings in this area, and there are other deposits which never have been denounced. Until an economic method is devised for extracting the nickel and chromium, these lateritic ores will not assume any importance. It might be of interest to note that Nicaro Nickel Co., financed during the war by the U. S. Government and directed by Freeport Sulphur Co., used these laterites from which to win nickel. This operation is now discontinued. For a few years some 3600 tons of ore carrying 30 pct iron was used daily. The iron was reduced to magnetite chemically and was wasted along with the chromium and tailing. There is quite a tonnage of iron lying down there with the tailing, and if some economical method could be devised to remove the chromium it would be possible to recover, through magnetic processes, a suitable ore for blast furnace use by agglomeration.

Bethlehem also held by far the best deposit of iron ore on the West Coast of Mexico, at Las Truchas. There is probably a large amount of open-pit ore in that holding, and Bethlehem first acquired possession by virtue of denouncements made prior to 1926. Bethlehem subsequently lost control of the deposit but re-acquired it under a special concession contract with the Mexican Government. It is believed that the contract has within the past several years been brought up for revision and perhaps has reverted to the original owners. Las Truchas has never been exploited and may never be until some company uses it for a hot-metal operation along the West Coast of the U. S.

Quite possibly Bethlehem's most interesting foreign holding is in Venezuela, where for the past ten years it has had a concession staked out at El Pao (see map). M. A. Hanna had been in and out of Venezuela for years and at one time had El Pao under option prior to Bethlehem's acquisition of the property. Hanna still has concessions next to El Pao. It would seem that M. A. Hanna Co. was singularly unimpressed with its Venezuela holdings even though their deposits, called Murcielago and Carambola, offered promise of possibly 10-20 million tons of open-pit ore. Bethlehem appeared satisfied with its El Pao holdings and showed little interest in the Represalia deposit, about 100 miles away and containing less than 5 million tons of ore, or other ore occurrences along a belt 100 miles long and situated between the Represalia and El Pao deposits.

Bethlehem's El Pao open-pit mine in Venezuela has reserves of at least 60 million tons, and

with an expenditure of some $50 million plus, this company hopes to be shipping out some 2.4 million tons annually by possibly late 1951. A lot of this ore is of the hard, crystalline type, open-hearth grade rather than blast furnace grade.

By late 1946 Bethlehem had practically completed its loading dock facilities at Palua near San Felix, at the confluence of the Orinoco and Caroni Rivers, and was building the railroad from Palua to the El Pao mine. By April of this year (1950) a transfer docksite will be finished and ready for operation at Puerto Hierro, east of Guiria on the north shore of the Gulf of Paria not far from Trinidad. They plan to get the ore out by using six barges each of 4000-ton capacity (300 x 50 x 6 ft) and a draft of 14 ft when full loaded. Two ocean-going tugs have been purchased and these tugs will haul two barges at a time from Palua down the Orinoco and the Cano Manamo past Pedernales (see map) and across the Golfo de Paria to the Puerto Hierro unloading station. There the ore will be loaded onto 26,000-ton ocean carriers—the specially designed Venore type. Bethlehem is also building several ships of 6000-ton capacity with a fully-loaded draft of 17½ ft for use on the same haul as the barges. Apparently the two methods of transportation are to be compared.

This shipping operation devised by Bethlehem is the most ingenious possible for the amount of ore they plan to move. The entry of U. S. Steel Corp. into the same area with a very much larger operation might, of course, influence future shipping plans. Certainly Bethlehem will finish its railroad to Palua near the confluence of the Orinoco, a distance of some 40 miles. However, if U. S. Steel or the government chooses to dredge the Orinoco for the largest of ore carriers, it would seem that Bethlehem also would bring its 25,000-ton Venore carriers right up to the railroad dock. However, if the Corporation elects to avoid river transportation and drive a railroad 274 miles across country to a tidewater terminal at Barcelona, then Bethlehem could possibly make some arrangement to use the same railroad or continue with its planned barge and transfer arrangement at Hierro. The Corporation's decision as regards railroad vs. river dredging probably will be reached before long.

Before describing in detail the U. S. Steel Corp.'s search for foreign ore and discovery of Cerro Bolivar, it might be best to cover two other foreign holdings—Liberia and Labrador.

African ores are becoming an increasingly important factor in the world markets. In Liberia various explorers were looking over ore showings there as long ago as 1938. There are occurrences of high-grade ore but the tonnages are in general too small to create a great deal of interest. Geologists from the U. S. Geological Survey examined the same area in 1944. Republic is now definitely planning to bring ore out of that country, probably for use in the Alabama area until the St. Lawrence Seaway permits shipment directly into Cleveland. Port facilities for loading ore are now being constructed at Monrovia, the capital city of Liberia. Republic has acquired majority interest in the Liberian Mining Co., controlling some 20 million tons of ore, and it is believed that the company plans to ship 500,000 tons annually, beginning sometime

in 1951. The development cost will be on the order of $8 million, of which one half the amount will be an Export-Import Bank credit.

**The Labrador iron ore** deposits have attracted a great deal of publicity during the past few years. As already pointed out, there is considerable ore of high quality up there, although as yet no definite plans are under way to get it out. There are some rather formidable obstacles facing open-pit mining operations and delivery of the ore over about 400-500 miles of tundra to a St. Lawrence River port. The railroad alone will cost more than $100 million, and at the mine the amortization of equipment must of necessity take into account use for only about half of each year. Personnel at the mine will also be somewhat of a problem, with the two possibilities of their being idle half the year or some provision made to bring them out for the non-mining period.

Without the St. Lawrence Seaway, the Labrador ore will likely not be competitive at most consuming centers with either other foreign ores or Superior Taconite concentrates. With the St. Lawrence Seaway, this ore should have a comparative cost factor through the Cleveland area and down into Youngstown.

By late 1946 it was already apparent that an important iron district would eventually be developed along the boundary line between Labrador and Quebec, primarily on concessions controlled by M. A. Hanna Co. and the Hollinger Consolidated Mines. The Labrador territory is part of Newfoundland, which is governed by a commission deriving its authority from the British crown. The Quebec area is under the Dominion of Canada.

This iron formation is part of a rock series occupying a trough which extends for about 350 air miles northward of the St. Lawrence River. Its northern extremity at an elevation of 125 ft is only about 60 miles from Fort Chimo, a tidewater port on the Koksoak River which enters Ungava Bay. Practically all known iron formations in this belt (see map) are now covered by exploration licenses or concessions, as follows, from north to south:

In Quebec

(1) Quebec-Labrador Development Co., Ltd.

(2) Fort Chimo Mines, Ltd. (Frobisher).

(3) Norancon Exploration (Quebec) Ltd. (Noranda, Anglo-Huronian & Conwest).

(4) Hollinger North Shore Exploration Co., Ltd. (Hollinger & Hanna).

In Labrador

(5) Labrador Mining & Exploration Co., Ltd. (Hollinger & Hanna).

(6) Norancon Exploration, Ltd.

(7) To the East of this iron formation belt Norancon has two concession areas in Labrador.

(8) Dome Exploration (Canada), Ltd., also has a concession area north of the Hamilton River bordering the Atlantic Ocean. No iron formation is expected to be found in this latter area.

(9) Kennco Exploration, Ltd. (Kennecott Copper Co. & N. J. Zinc Co.). A titaniferous magnetite deposit much further south (see

FOREIGN IRON ORE DEPOSITS
IN ATLANTIC AREA

map), about 50 miles north of Mingan on the north shore of the Gulf of St. Lawrence.

Kennco has disclosed the presence of some 50 million tons of reserves containing 35 pct titanium. To get the titanium this company has announced plans to spend $25 million to develop the deposit and another $15 million for an electric smelter of initial capacity of 1500 tons per day to be constructed at Sorel, Quebec, scheduled for operation by 1951. The by-product pig iron production might well range between 100-200,000 tons annually, analyzing 96.5-97 pct iron, 2 pct min C, 0.1 Si, 0.03 P, 0.10 or less S, 0.04 Mn, 0.2 Ti, 0.05 V and 0.05 Cr.

The Hanna-Hollinger concessions (Nos. 4 and 5 above) are the only ones on which important

explorations have been carried on. Some of the ore has been described as being physically like the harder ore of the Iron River district of Michigan, while other ore in the area has been compared with the Marquette range soft ore. In any event the ore will carry appreciable amounts of free moisture. In early 1946 there were reports that drill holes to a depth of 200 ft were still in frozen ground, thus indicating a nasty problem of handling frozen ore which would be gradually thawing en route to the furnaces. However, by early 1947 this possible difficulty was laid to rest when one exploratory tunnel, still in ore, penetrated 85 ft of ore under an ore cover of 70 ft without encountering any frozen ground except at the portal.

By early 1947 the Hanna-Hollinger geologists had discovered more than 25 ore bodies scattered over a length of 75 miles, with some of them ranging 1000 ft in width. By this time estimates were being made of a possible reserve tonnage sufficient to yield an annual production of 10 million tons for many years. Much of the ore showed an average 60 pct combined iron and manganese, with some showings containing up to 20 pct manganese. The group was granted a charter for the proposed Quebec North Shore & Labrador Railway Co., capitalized at $2 million. Financing of the remaining $100 million or so is as yet unresolved.

By late 1947 Hanna-Hollinger had discovered over 40 ore bodies and actual diamond drilling had proved tonnages in excess of 100 million tons. At this time it was estimated that further drilling would prove 300 million tons. Toward the end of 1948 over 44 separate ore bodies had been discovered with reserves of over 300 million tons indicated. In general the individual ore bodies are rather small and scattered over an area of 85 by 15 miles. The glacial-drift overburden is of the order of 16 ft.

A number of steel companies (Republic, Armco, National Steel, Wheeling and Youngstown) have joined with Hanna-Hollinger for several more years of exploratory work, and Republic has a one-year option for a quarter interest in this development. In view of the problems involved in building the long railroad to the St. Lawrence over very difficult terrain and delays certain to bedevil the St. Lawrence Seaway, it is likely that no large tonnages of Labrador ore will come out until the late 1950's. However, by 1960 these transportation problems will certainly have been rationalized and ore should be coming out at the rate of 10 million tons annually. To finance such a program will require a capital investment well over $175 million, exclusive of the lake vessels required to transport the ores from proposed railroad terminal at Seven Islands, Quebec, to the steel-producing areas.

The only other Labrador-Quebec concession given much exploratory attention has been the Fort Chimo area owned by Frobisher Exploration Co. It covers some 1000 sq miles and contains a length of about 35 miles of explorable iron formation located 100 miles north of the Hollinger holdings. It lies 100 miles southeast of Fort Chimo on Ungava Bay tidewater, the rail distance being about 150 miles with a drop of only 200 ft to this possible shipping port which is ice-free from four to five months of the year and lies 3000 miles from Baltimore. Late in 1946 the U. S. Steel Corp. was showing some interest in this concession, but a year later interest understandably waned as the Venezuela strike appeared to be of mother-lode proportions.

U. S. Steel's spectacular good fortune in Venezuela is the terminal point of a whole chain of encouraging and discouraging events leading back to Pittsburgh early in 1945. At that time, J. G. Munson, vice-president in charge of raw materials of the Delaware Corporation, along with B. H. Lawrence, then chief engineer, and R. E. Zimmerman, vice-president in charge of

Plan for initial development of Cerro Bolivar. The belt conveyor will generate enough electrical power to supply much of the area requirements.
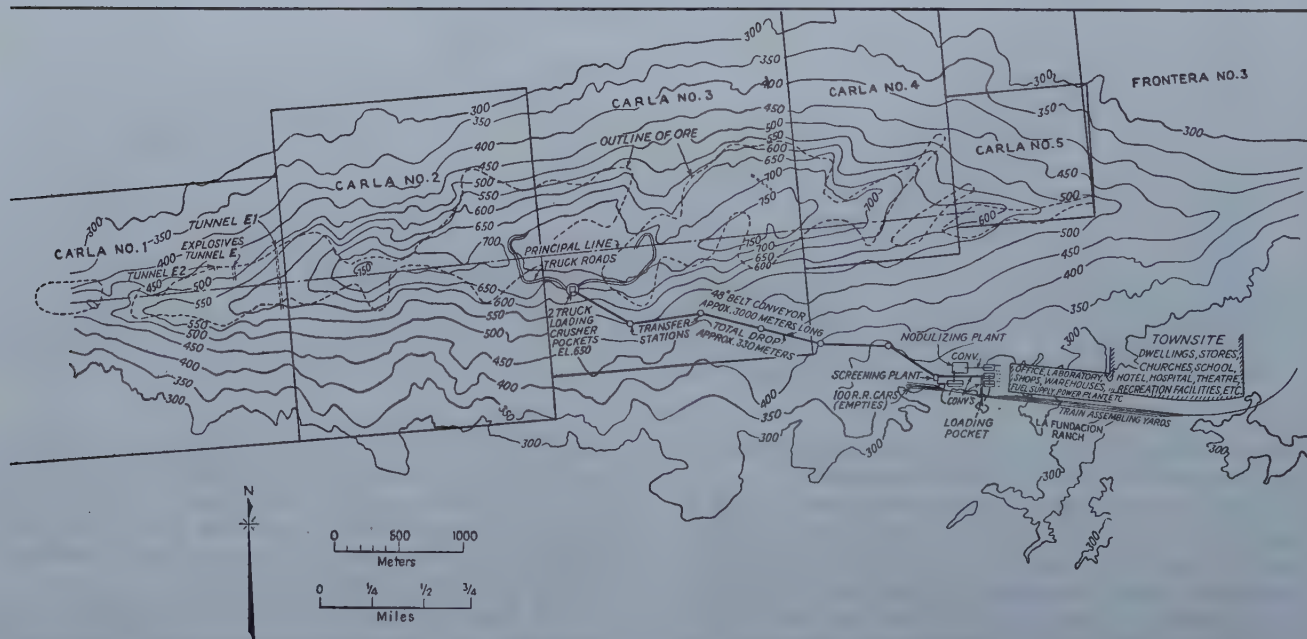
research, became convinced that the Corporation would soon have to earmark extremely large sums of money for Taconite plants if the future ore supply were to be assured. It occurred particularly to Mr. Munson that at least one more look should be taken at all the possible foreign ore sources around the entire periphery of the North and South Atlantic Oceans. This was a momentous decision, particularly so since the Corporation's files were crammed with tons of reports on the known deposits, some dating back to 1908. Even though the projected search would be the most detailed ever carried out and involve the expenditure of many millions of dollars, board-chairman Irving Olds and president B. F. Fairless likewise okayed the gamble, although the odds were very much that nothing new of interest would develop.

By early 1946 field forces were in Brazil, Venezuela, Honduras, Guatemala, Puerto Rico, Cuba, Mexico and Sweden. Hundreds of men were beating far back in the hinterlands following up every known showing of ore and tracing down every rumor of red earth. Before the entire search was concluded thousands of men became involved, many hundreds of ore bodies had been drilled and explored in the Agalteca deposit in Honduras; in various parts of Guatemala; at Mayagues and Jancos in Puerto Rico; various showings in Honduras; all around the vicinity of Tunki in Nicaragua; all the possibilities along the east coast of Mexico, and more than 40 deposits along the west coast; the well-known ore fields in Sweden; the Wabana Mines in Newfoundland; Little Whitefish Lake in Quebec; Texado Island, Iron Hill and Zeballos in British Columbia; the Marampa and Tonkolili deposits in Sierra Leone, West Africa; holdings owned by Cia. Espanola de Minas del Rif in Morocco; the Djebel Djerissa holdings in Tunisia; the Ouenza ores in Algeria; the Conakry ores in French Guiana; several ore possibilities in Alaska. The objective was to find an ore body, preferably in the Caribbean area, of sufficient quantity and quality to justify full-scale development over a period of many years. The cost of ocean freight would represent a large part of the delivered cost of any foreign ore because of the large investment in vessels of special design and the high cost of operation of merchant ships.

The rich ore deposits of Brazil were given another looking-over, hardly necessary inasmuch as the Corporation had periodically surveyed these ores ever since 1930. None the less careful new investigations were made of the Itabira district; Candu, Saraiva and Nhotin, near Bello Horizonte; Casa de Pedra, near Congonlias de Compa; Santa Maria, near Macapa on the north bank of the Amazon; Cera in the northeastern section; and Amapa, near the mouth of the Amazon. However, all this searching around was not in vain. An excellent manganese deposit was uncovered in the Urucum Mountain, 15 miles south of the city of Corumba in the State of Mato Grosso. Reserves of 27 million tons are indicated, of 46.4 pct Mn and 10.7 Fe. U. S. Steel plans to pull out 100,000 tons per year. There were some interesting findings in various countries, but, from the very first, the Orinoco iron ore district in Venezuela seemed to offer interesting possibilities for the discovery of commercial iron ore deposits reasonably accessible to river transportation and of sufficient size to justify utilization. Late in 1945 air observers started to work over the area adjacent to and south of the Orinoco River extending from Ciudad Bolivar towards the Atlantic Ocean, a distance of about 160 miles (see map).

A year later, toward the end of 1946, some ore holdings around Bethlehem's El Pao concession and the M. A. Hanna concession had been looked over by magnetic survey with nothing of consequence showing up. Field reports and the aerial observation had concentrated attention on Piacoa and an area northeast of Upata. It was soon determined that the Upata area had various high-grade bodies averaging 65 pct iron, but they were narrow and not sufficiently extensive to justify exploration for open-pit mining.

The Piacoa ore is located about 100 miles downstream on the Orinoco from Ciudad Bolivar and approximately 75 miles from the mouth of the river. Piacoa is an insular hill which is 2 miles away from the Orinoco River. It is 1½ miles long and rises 550 ft above the surrounding flat topography. Ore occurs in a ferruginous quartzite with a grade from 40-50 pct iron. The ore would have to be concentrated, although the concentration problems would not be difficult, requiring only grinding to 28-48 mesh to produce a concentrate of 60 pct iron or better. Oil is within 50 miles and gas 150 miles. Diamond drilling got well under way early in 1947. Quite obviously Piacoa was nothing to get really excited about.

It is to be noted from the map that all the area being worked over was south of the Orinoco, east of the Caroni (a tributary of the Orinoco) and toward the Atlantic Ocean. The Venezuelan government had all this territory listed as a Federal Reserve Zone on which concessions of only 40 yr were possible, and even they had a number of restrictions. Venezuela considered this area the only possible iron ore area, and for that matter so did Bethlehem and M. A. Hanna, both of whom had been over the ground pretty thoroughly. Some of the U. S. Steel Corp. men were discouraged, some resigned and the whole Venezuelan exploration began to sag.

At this point Mack C. Lake, a long-time M. A. Hanna geologist, was borrowed by the Corporation to take charge of the field work. Mr. Lake had been half-retired and was living in California when M. A. Hanna called him back to do consulting work on their new Labrador properties. He was loaned to the Corporation to do work for them only in Venezuela inasmuch as Hanna was rather convinced there was nothing more of consequence there. Mr. Lake and two young geologists on the field team, K. Burrell and F. Kilstead, conceived the idea of aerially photographing the area south of the Orinoco and *west* of the Caroni, an area open to denouncement, not particularly remote and generally considered of no promise by both the Venezuelan government and the other steel companies that had previously looked over the territory.

Christmas Day, 1946, Messrs. Burrell and Kilstead were in Pittsburgh giving S. G. Munson a sales talk on spending another $185,000. Mr. Munson took another momentous gamble, gave his permission, and shortly thereafter Fairchild

was hired to take the photographs and Venezuela had granted permission to bring them out of the country for piecing together and examination.

Examination of the photographs got the geologists interested in two small mountains or hills, known locally as La Parida and Arimagua. La Parida was located about 50 miles due south of Ciudad Bolivar and rises about 2000 ft above the surrounding savanna topography, and is about 11 miles long. Arimagua is about 30 miles east of La Parida, nearer the Caroni River. Neither mountain is particularly remote and they both appear on many an old map. Early in the year a field crew started in to look them both over, with S. G. Sargis (a magnetometer expert brought in from Geneva Steel) in charge of the geophysical work.

In April of 1947 the field party found huge outcrops of iron ore all over La Parida hill and slides exposing large expanses of iron ore at Arimagua. As Mr. Sargis worked over the deposits with his magnetometer he recorded extremely high readings, the highest responses ever recorded in the world! The excitement mounted. There was no doubt that a really enormous tonnage of iron ore was there and it appeared of sedimentary origin, and of a grade in excess of 60 pct iron.

When the word got back to the headquarters town of Ciudad Bolivar, Mr. Lake decided to pull in diamond drills from about everywhere. The important thing was to determine as quickly as possible whether the high surface grade extended down to any reasonable depth or whether the magnetometers were recording an enormous lump of poorer ore and Taconite. The two Longyear diamond drills at Piacoa were started on their way to La Parida, two others on their way from the United States were diverted and another drill in Honduras was called for. It was planned to get at least five drills working at La Parida.

It was also imperative to survey the area well by magnetometer to lay out the boundaries of denouncements. And quietly, too. For the area was outside the Federal Reserve Zone and open to anyone who filed first. By this time some of the news must have seeped out for a couple of local entrepreneurs started to look around in the same area. Everything went well, however, and the Corporation quietly filed its Carla, Arimagua and Rondon (other ore showings in same general area) denouncements, which were published in the Government Gazette. On April 11, 1947 Carla Nos. 1 to 5, totaling 11,330 acres were accepted by the government. On Sept. 1, Arimagua 1 to 3, totaling 2960 acres, were accepted. Rondon 1 to 3, totaling 3700 acres were not accepted until early in 1948.

**Drilling at La Parida** actually got underway in July 1947, with ten American drillers on the job working for the contractor, E. J. Longyear Co., and headed in the field by Mr. Axel Auguston. Mrs. Auguston (Betty) officiated as cook.

By late 1947 reports coming from the field indicated iron ore outcrops on La Parida every few hundred feet for a distance of at least 3 miles. It was exposed in slides for a height of 200 ft. It still seemed to be of sedimentary origin with some secondary enrichment of low-grade horizons. Evidence indicated that certain high-grade horizons had been hydrated near the surface, hence lowering the grade. The hydrated material appeared to contain nearly the theoretical maximum of iron. Six holes totaling 1545 ft had been drilled, indicating a dry analysis of 63.4 pct iron, phos content decreasing from 0.175 pct at surface to 0.048 pct at 380 ft. Likewise, the loss on ignition decreased from 12.1 pct to 1.2 pct at 380 ft. The general conclusion was that this ore was similar in type and mode of occurrence to the thin-bedded hard ores of the Minas Gerais region in Brazil.

By early 1948 Mr. Sargis had run magnetometer readings over Bethlehem's El Pao deposit to check his readings with known underground reserves. He was trying to verify his record readings at La Parida. The El Pao test confirmed his mathematics. Then the readings and calculations were sent to Dr. Louis Slichter (Sumner Slichter is his brother), Director of Geophysics at the University of California, for verification. His notation came back that everything was correct but perhaps someone had gotten the decimal points in the wrong place. But the decimal points definitely were in the right place and La Parida began to look more and more a champion.

By early 1948 La Parida had its name changed to Cerro Bolivar, and drillings had proven some 165 million tons of reserves. Seven diamond and two churn drills were operating, and 47 holes had been drilled to an aggregate depth of 11,436 ft. Moisture content of ore samples was 10 pct, indicating an average natural iron content of 56.7 pct. Most of the holes bottomed in quartzite, the average ore depth being 148 ft. The area covered by exploration was 18,000 ft long with an average width of 1200 ft. An exploratory tunnel had been driven, and the specific gravity of the ore was 12 cu ft per ton. A railroad survey was started, and river studies were planned to investigate dredging possibilities. Other ore showings in the Cerro Bolivar (La Parida) area—Arimagua, Rondon and Altamira—were given a quick look and estimates made that they also were large deposits, having perhaps an average dry analysis of 63.28 Fe, 0.113 P, 2.29 Si, 0.10 Mn, 1.53 alumina, 0.135 Ti, and 0.005 S; loss on ignition 5.31.

During the 1947-48 period also, interest had grown in a deposit at La Grulla, which was back over in the usual iron area east of the Caroni, in Federal Reserve territory, about 30 miles northeast of Bethlehem's El Pao mine, 30 miles south of the Orinoco River and 90 miles due east of Ciudad Bolivar. The ore seemed to be in relatively small bodies, but high grade. A concession was petitioned for, as the ore was hard and crystalline, of about 65 pct Fe with low-phos, and would make excellent lump ore. The individual ore bodies could, perhaps, be mined as a district, and reserves of 10 million tons were indicated. By late 1947 a magnetometer report over one deposit was on the order of the spectacular responses on La Parida hill. The high-grade ore showings on this deposit were very impressive, particularly when their extension in depth was indicated by the magnetometer interpretations. Several other deposits appeared connected as the result of geophysical work and there was some similarity between the magnetic responses and those at El Pao. By June 1947, five concessions

Sailing craft on the Orinoco near Palua. Venezuela hired ex-Maj. Gen. Tyler of U. S. Army Eng. to survey river with object of getting 35-ft. draft ocean ore carriers up the Orinoco as far as Palua.



Cerro Bolivar, the greatest and richest mountain of iron ore in the world, was discovered in April 1947. The explorer's camp shown here is perched on lumps of iron ore of almost maximum theoretical purity.



The "Spindle" anchored in the Orinoco at the headquarters town of Ciudad Bolivar. A barge-load of cargo has just been brought from the Piacoa camp.



Cerro Bolivar's climate is hospitable, the sunsets are stupendous, and the surrounding savanna terrain pleasing to the eye. This view north from Cerro Bolivar shows a road cut to bring in Longyear diamond drills.

were obtained in the La Grulla area. However, by late 1948 La Grulla began to be somewhat disappointing. In some places drillings showed that the hard, crystalline ore in outcrops did not extend more than a few feet below the surface. Further, some of the subsurface connections between surface outcrops did not appear to exist. However, drillings were continued.

In early 1949 over ½ billion tons were proved at Cerro Bolivar by drilling. La Grulla continued disappointing despite extensive drilling, with only 40 million tons proved up.

As of the present time, Mack C. Lake is in full charge of the Venezuelan operation for the Corporation, and has been made the first president of the newly-formed subsidiary, Orinoco Mining Co. R. J. Wysor, former president of Republic, has for some time been associated with Mr. Lake on the job as a consultant. Mr. Lake has set up offices at 25 Broadway and is energetically building up a staff. It is the intention to bring at least 10 million tons out annually by late 1953.

In the Cerro Bolivar area south of the Orinoco and west of the Caroni, U. S. Steel has 18 denouncements of 100 yr duration with probable reserves of the highest grades of iron ore greatly in excess of 1 billion tons. Some idea of the size of the Cerro Bolivar deposit can be obtained by comparing its linear dimensions with the world-famous Hull-Rust-Mahoning open pit at Hibbing, Minn. (see drawing) now scraped almost down to Taconite bottom. Cerro Bolivar alone contains more tonnage of iron than Hull-Rust ever produced or ever can produce.

There are other probable deposits in the Cerro Bolivar area but the Venezuelan government has closed the territory against further denouncements and only concessions of 40 yr may now be obtained.

U. S. Steel also has six concessions (La Grulla, etc.) in the usual area east of the Caroni and south of the Orinoco, which contains a wide variety of ores and respectable tonnages, although in no way comparable to Cerro Bolivar. These all are on the Federal Reserve and operation for a term of only 40 yr is possible.

The Corporation must soon make a decision on how it plans to bring its large tonnages at Cerro Bolivar out of the country. A railroad survey has been made straight across country from Cerro Bolivar to a tidewater terminal on the north coast near Barcelona, a distance of 274 miles (see map). This will require a bridge across the Orinoco at or near Ciudad Bolivar, about 4.5 miles in length including approaches. Pay load per train would be 10,000 tons and the annual tonnage 15 million tons. The total cost will be on the order of $113 million. At the Barcelona port there is excellent deep water so that the biggest ocean ore carriers can be brought in for loading.

Another alternative would be a railroad for 91 miles from Cerro Bolivar to a river terminal at the confluence of the Orinoco and Caroni Rivers. Then the Orinoco must be dredged to permit bringing up the ocean ore carriers to load at this terminal. The 91 miles of railroad would cost $51 million. The river survey contemplates a channel of 34 ft from the confluence of the Orinoco and Caroni, down the Orinoco and Macareo Rivers to a point

60 miles from tidewater, and from there a gradual deepening of the channel to 38 ft at sea level. To do this requires dredging 45,254,000 cu yd of bottom, at an estimated cost of $18 million. Annual maintenance would be $1.1 million. A combination 34-38 ft. channel would open up the river for even the enormous ocean carriers planned by the Corporation. The problem of dredging and maintaining a river of this size is a tremendous undertaking for a private company. In the United States the government would do the job although it has not yet been determined to what extent Venezuela will participate.

The distances to U. S. consuming centers by the various routes are as follows: Cerro Bolivar to Orinoco River port = 91 miles; Orinoco River port to tidewater = 170 miles; mouth of Macareo to Baltimore = 2280 miles; Baltimore to Pittsburgh (via B. & O. or Western Maryland) = 334 miles; mouth of Macareo to Mobile = 2460 miles; Mobile to Birmingham = 276 miles (rail) and 280 miles (water); Cerro Bolivar to Barcelona = 274 miles; Barcelona to Baltimore = 2190 miles; Barcelona to Mobile = 2190 miles.

A price comparison might now be in order, between U. S. Steel's Venezuelan ore, Labrador ore (assuming the St. Lawrence Seaway), Superior Taconite nodules and current non-bessemer ore shipments from the Mesabi. The following table has been constructed to this end, based on a variety of informed estimates. In the table L.E. = Lake Erie price (1949) based on $7.20 per ton for Mesabi non-bessemer ore.

| | Dry Iron | Nat. Iron | Phos. | Si₂O₂ | Mn | Nat. Mn | Moist | L.E. Price | 1949 Basis Per Unit Fe |
|---|---|---|---|---|---|---|---|---|---|
| Labrador Ores .. | 59.3 | 53.4 | 0.071 | 6.76 | 1.51 | 1.36 | 10.0 | $7.72 | 14.5¢ |
| Venezuelan Ores. | 63.8 | 59.0 | 0.113 | 2.29 | 0.10 | — | 8.75 | 8.54 | 14.5¢ |
| L. S. Taconite Nodules .... | 65.4 | 65.0 | 0.025 | 6.75 | 0.10 | — | 0.5 | 9.40 | 14.5¢ |
| Superior Natural Ores (1947). | 58.2 | 51.1 | 0.064 | 7.98 | 0.70 | — | 12.23 | 7.14 | 14.0¢ |

**It will be noted** that even at Lake Erie ports, Venezuelan ore shows an equivalent unit cost with Superior Taconite nodules and Labrador ore. Natural ore from Superior, however, shows up best of all, as might be expected. However, natural ore is a disappearing metallic which has no bearing on the economic relationship between future iron supplies.

Also to be considered is that the cost relationships in the table are modified by the iron units per ton of material passing through the blast furnace. Furnace operators have of recent years recognized that distinct savings in hot-metal costs are secured by using sized ores with larger proportions of coarser material in the form of concentrates or agglomerates. The higher grade ores produce less slag and thus require less coke and limestone. The coarser structure burdens usually reduce more rapidly, thus permitting larger metal production from the furnace; flue dust, with its content of fine ore, is also reduced. It is thus apparent that ores should be evaluated as to their effect on the cost of producing hot metal.

With this in mind, and thus allowing proper credit for structural and chemical characteristics, Venezuelan ores and Superior Taconite nodules improve slightly in cost factors.

From a hot-metal cost angle, and taking a rather brave shot into the 1960's, the Superior



Boccardo Hill, above Bethlehem's El Pao concession. Standing on lumps of 68 pct Fe (L to R) Jesus Lareto, Venezuelan Engineer; M. D. Meixel, El Pao foreman; Wm. Rankin, head of Bethlehem's Venezuelan operations; Mack C. Lake, the first president of U. S. Steel's Orinoco Mining Co.; and Mr. Boeckman, Esthonian engineer.



These men recorded the world's highest magnetometer readings. (L to R) Jose Ramon Zurita, Venezuelan trained to operate Tiberg magnetometer; Wm. Moyka; Sam Sargis, a magnetometer expert borrowed from Geneva Steel Co.; and Fred Wright.



Diamond drillers at fabulous Cerro Bolivar occupied these two tents surrounded by great chunks of iron ore.



Axel Auguston ran the field force of diamond drillers for E. J. Longyear Co. His wife Betty (right) cooked for the crew. Here she is with her helper before the dining hall at the Piocoa concession.

nodules should show up well at all the Lake consuming centers and down into the Youngstown area. Venezuelan ores will dominate the Gulf area, the East Coast, Pittsburgh and possibly work up into Youngstown. Labrador ores, via the St. Lawrence Seaway, will show up well in the Lake Erie consuming centers. Of course, the actual proportions of each metallic used at any producing point will be dictated in part by the type of material being developed by the particular companies.

By looking ahead to the late 1960's, it is possible to estimate that the steel companies other than U. S. Steel and Bethlehem most likely will be drawing ore from Labrador at the rate of 10 million tons annually, will have at least 17 million annual tons of Taconite-concentrate capacity in operation, be pulling a ½ million tons from Liberia, and be buying some 4 million tons of Venezuelan ore. Dependence on Lake Superior natural ores will have practically disappeared. The capital investment to finance such a program will exceed $600 million, exclusive of the lake vessels required for Labrador ore.

The U. S. Steel Corp.'s ore balance sheet in the late 1960's will probably show at least 15 million annual tons coming from Venezuela and 10 million annual tons from beneficiated Lake Superior Taconites. U. S. Steel definitely plans to pull 500,000 tons of Taconite nodules out by 1952. This will cost that Corporation in capital commitments a sum just about as much as for the other steel companies, $600 million plus.

The American steel companies, therefore, must get their hands on over $1.2 billion dollars to sink into new capital investment in the period up to 1965, and this staggering sum is in addition to the normal rebuilding of steel-producing facilities. It's going to take a lot of doing —some good profits and very friendly bankers! If the ore program is followed through, however, the drain on Superior natural ores will be lifted in time to retain possibly 500 million tons as a strategic stockpile. If there ever must be another war, just possibly it, too, will be fought in great part off that old standby—the Superior natural ores.

The next few years will see a dynamic stir in the steel industry having no equal for decades —certainly not since flat-rolled capacity fell before the onslaught of the continuous mill. But that was an intercompany competitive struggle, whereas today's ore program is a matter of company and country survival.

Certainly the U. S. Steel Corp. offices are already surging with plans to keep its construction program in balance. The Venezuelan ore fields will be mechanized as much as human ingenuity can devise, the railroad must be built or the Orinoco dredged to get the ore out, and a $50 million boat program must get under way to pick up the ore when it arrives at tidewater. It is planned to use giant ocean carriers, 45,000-ton jobs rivaling the battleship Missouri in size, to shave down transportation costs. (As comparison, one of the largest of Lake carriers, the Irving Olds, barely squeezes over the 26 ft sill at the Soo locks with 18,000 tons.) The first 2 million annual tons of Venezuelan ore should certainly go to Mobile and up the Warrior River to T. C. & I., where blast furnaces are

now literally agasping for rich ore. Production may rise there as much as 15 pct with the same furnaces. Over ½ million tons of hard ore and many millions of tons of blast-furnace grade will start coming into Baltimore (where already bulk unloading facilities are available) for rail shipment into Pittsburgh via the B. & O. and W. Md. And, most interesting, 1.5 million tons would go into the U. S. Steel Corp.'s Eastern steel mill, when built. For while the Corporation is designing all the equipment for Venezuela, it is also probably designing a large size steel mill for its site near Trenton, N. J. The total cost of such a manufacturing plant would run into some hundreds of millions of dollars.

It isn't necessary to be privy to U. S. Steel Corp. secrets to make some estimate as regards the Trenton plant. Press comment has been busily building the plant 10 yr from now, but obviously the desired planning would be to target its completion to coincide with adequate ore from Venezuela, and that certainly is before 1955.

The finished steel market in the Trenton-Philadelphia-Washington area is a lush one, some 7 million tons yearly, which holds up well even in hard times. It's a diverse market—over 1½ million tons of sheet and tin plate; 700,000 tons of wire; and 600,000 tons of plate. Bethlehem takes care of 40 pct of the market and most of the remainder comes in from U. S. Steel and other steel companies in Pittsburgh, Youngstown and Chicago. The Corporation can no longer afford not to replace wearing-out Pittsburgh tonnage with lower cost tonnage in the east to service this market.

A Trenton plant of 2 million annual ingot tons would require three blast furnaces, and, say, two openhearth shops of eight 150-ton furnaces each. The plant would run on strictly an ore burden with mill-return scrap. No bought scrap would be used. There would be at least one hot and one cold continuous mill, a wire mill, probably even pipe and bar mills. The whole thing would certainly be a long, level, straight-line affair, from blast furnaces to shipping dock, quite possibly the most beautifully designed integrated mill in the world. When both the Venezuelan ore and the finished steel market in that area are viewed together, it would be expected that by mid-1960 another "South Chicago" will have sprung up on the flat farmland beyond Trenton, N. J. The Delaware River already has a 41-ft channel up to Philadelphia, and the Army plans to scratch out a deep channel on up to Trenton, thereby permitting ocean ore carriers to dock alongside the steel mill (see map). Or, on occasion the ore can be barged from the unloading docks at Baltimore, through the C.&D. canal (dotted line, map), and thence to the steel mill.

For 60 yr the steel industry has viewed its ore problem with all the bland indifference of the heavily endowed. But with the endowment about gone, it is apparent from all the foregoing that the challenge has unleashed a great dynamic drive from Hibbing to Venezuela, from Labrador to Liberia, from Trenton, to Pittsburgh to Birmingham. It all involves enough imagination, ingenuity and romance to quicken the most sluggish pulse. Steel men are long going to remember the 1950's.

# aime NEWS

## Directors Face Deficit Problem at Dec. 7 Meeting

NO Board meeting being scheduled between that on Nov. 16 and that on Feb. 12 next, the Executive and Finance Committees met on Dec. 7 and Jan. 20 to consider routine matters. At the Dec. 7 meeting, with President Young presiding, the problem of how to meet the 1949 deficit was considered. It was finally voted to ask the Rocky Mountain Fund Committee for $7500 to finance the cost of Vol. 181 of the Transactions, covering metal mining, industrial minerals, mineral industry education, and geophysics; and to ask the Robert C. Gemmell Memorial Fund Committee for $6000 to cover the cost of publishing Vol. 183, on mineral beneficiation. The respective committees subsequently agreed to this use of accumulated interest in the funds, and the volumes will be issued under an imprint to credit the sponsors. The sum of $15,000 was appropriated from the Life Membership Fund, which is a portion of $59,000 that was set aside from surplus during the period 1927 to 1934 to finance service to Life Members of the Institute. Life members now number about 190 compared with some 390 at that time, so less income is required to meet the expense of supplying them with periodicals and carrying them on the rolls. The remainder of the deficit will be met out of the residue of some $46,000 left in the Special Fund for Publications, contributed some years ago to meet publication costs during periods of reduced income. The current levy on the fund will practically extinguish it for the time being until surplus can again be directed to its replenishment.

Authority was voted to engage an advertising salesman for the "Journal of Metals" and "Mining Engineering" in the territory centering in Chicago, and Joseph Halloran was subsequently engaged for the job.

Besides President Young, those present at the meeting included Donald H. McLaughlin, E. E. Schumacher, Erle V. Daveler, Clyde E. Weed, Andrew Fletcher, H. A. Maloney, and Edward H. Robie.

# The
# *Drift*
# of *Things*

as followed by *Edward H. Robie*

## Effect of Dues on Membership

Many AIME members have expressed an interest in whether or not the increased dues have been the cause of an abnormal number of resignations. It is, of course, too early to say with any definiteness, for as this is written, early in January, many members have only just received their bills for 1950, and a considerable number do not normally pay them for a month or two. They would not be likely to resign until faced with the stark necessity of writing out a check. Still, the data available at the end of the year show no cause for alarm, and certainly do not bear out the ideas expressed by the prophets of doom last spring who warned that the loss of members would more than balance any increase of income through the raising of dues.

To establish whether or not something is abnormal, one must first know what is normal, so let us go back to an average for the years 1946-1948 inclusive. In those three years, 0.9 percent of the enrolled members died; 1.1 percent resigned in good standing; and 2.3 percent were dropped for nonpayment of dues. In 1949, faced with an increase in the dues for the next three years, just exactly the same percentages died, resigned, and were dropped for arrears in dues. Without any unusual membership campaign, AIME membership—and all these data are exclusive of Student Associates—showed a greater net gain last year than it did in 1948, the respective figures being 687 and 580.

We have seen many of the letters of resignation, and the bulk of them seem to be in two categories: (1) those whose interests are no longer in the field of the Institute, or only partly so; and (2) members in foreign countries who have to pay what are often excessive sums in their own currency to secure American dollars. The Directors of the Institute are sympathetic to this latter group, and if any use could be made of foreign currencies would be glad to allow dues to be deposited in foreign countries, but unfortunately all the bills that the Institute incurs must be paid in American dollars.

In the data previously quoted, it is notable that more members are suspended for nonpayment of dues than resign. Many times these members later apply for reinstatement and are chagrined to find that they must pay up their arrears, or up to $20 thereof, in order to be reinstated. They perhaps regard AIME membership like a magazine subscription—if you don't want it any longer you just stop paying for it and ignore the numerous letters you receive from the publisher. The AIME is different. Members are in good standing for three months after their dues are payable—or until March 31. In that time they can resign, and should they later wish to apply for reinstatement there will be no new initiation fee or any arrears in dues to pay. But if Institute headquarters does not hear from you we assume you are on a safari, continue to keep your name on the rolls, print it in the Directory, and try to print enough extra copies of your favorite journal so that you can have the back numbers if you wish, when your check finally arrives. Members are not dropped until they have been in arrears for two years, and many pay their arrears in the second year.

## Professional Interests

Within the last two or three months all AIME members (exclusive of Student Associates) have received a card asking them to check (1) their major professional interest as expressed by the activities of one of the ten Divisions of the Institute; and (2) all Divisions in which they may have an interest. Some 9000 replies have now been tabulated, which represents more than half of the Institute membership, so should be a good sample, and we hasten to give readers the results to date:

### Major Technical Interest

| Division | Number | Percent of AIME | Percent of Branch |
|---|---|---|---|
| Mining, Geology, and Geophysics | 2380 | 26.6 | 57.5 |
| Minerals Beneficiation | 605 | 6.8 | 14.7 |
| Coal | 816 | 9.1 | 19.6 |
| Industrial Minerals | 339 | 3.8 | 8.2 |
| MINING BRANCH | | 46.3 | 100.0 |
| Extractive Metallurgy | 540 | 6.0 | 22.8 |
| Iron and Steel | 734 | 8.2 | 31.2 |
| Institute of Metals (physical met.) | 1083 | 12.1 | 46.0 |
| METALS BRANCH | | 26.3 | 100.0 |
| Petroleum (Division and Branch) | 2251 | 25.2 | 100.0 |
| Mineral Economics (no Branch affil.) | 138 | 1.5 | |
| Mineral Ind. Education (no Branch) | 56 | 0.6 | |
| Total | 8942 | 99.9 | |

## Desired Divisional Affiliations

| Division | Number | Percent of Total Selections | Percent of Members Replying |
|---|---|---|---|
| Mining, Geology, and Geophysics ......... | 4213 | 20.3 | 47.1 |
| Minerals Beneficiation | 2274 | 11.0 | 25.4 |
| Coal ................. | 1533 | 7.4 | 17.1 |
| Industrial Minerals ... | 2039 | 9.8 | 22.8 |
| MINING BRANCH | | 48.5 | |
| Extractive Metallurgy. | 1835 | 8.8 | 20.5 |
| Iron and Steel ....... | 1726 | 8.3 | 19.3 |
| Institute of Metals.... | 1978 | 9.5 | 22.1 |
| METALS BRANCH | | 26.6 | |
| Petroleum ........... | 2769 | 13.3 | 31.0 |
| Mineral Economics ... | 1527 | 7.4 | 17.1 |
| Mineral Industry Education .......... | 855 | 4.1 | 9.6 |
| | 20,749 | 99.9 | |

The foregoing data are based on returns from 55.2 percent of the Institute membership that had been received when the survey was made, so by simple arithmetic the officers of every Division can figure out just about how many AIME members are interested in their Division. For instance, 6.8 percent of Institute members are primarily interested in mineral beneficiation, but 25.4 percent are more or less interested. On the other hand, 25.2 percent of the membership is primarily interested in petroleum, but only 31.0 percent have any interest at all in that field, which would be expected.

### New Members

We fear this department is getting pretty statistical this month, but in connection with the foregoing data the Branch affiliation of those who applied for membership in 1949 is of interest. The number of applications for membership received from those who had not previously been members (excluding new Student Associates but including changes of status of Student Associate to regular grades of membership), plus reinstatements, was as follows:

| Branch | Total | Percent |
|---|---|---|
| Mining .................. | 471 | 41.4 |
| Metals ................. | 262 | 23.1 |
| Petroleum .............. | 404 | 35.5 |
| Total ................... | 1137 | |

Comparing the professional interests of the present total membership with those of the new applications, it is evident that the Petroleum Branch is growing much more rapidly than either the Mining or Metals Branches. Possible reasons for this are: (1) the petroleum industry is growing faster than the other branches of the mineral industry; (2) the AIME has less competition in the service it gives to the petroleum production industry than it has in the other fields; (3) petroleum men have more money than miners or metallurgists; (4) the service the AIME gives to members of the Petroleum Branch is more satisfactory than its service to the other Branches; or (5) the Petroleum Branch is more actively out for new members than the other groups. Whatever the reason, if the trend continues, the Petroleum Branch will before long boast of a third instead of a quarter of the Institute membership.

### A Job Well Done

Especially in view of what has just been said, it is with sincere regret that we must accept the resignation of William H. Strang as Executive Secretary of the Petroleum Division and Branch, Business Manager of the Journal of Petroleum Technology, and Assistant Secretary of the AIME. For much of the progress made by the Petroleum Branch, Bill has been responsible. Further, his relations with Institute headquarters have always been cordial and he has done much to advance the interests of the Institute as a whole. It is good to know that it was not because of dissatisfaction that he left the AIME to join the production division of the American Petroleum Institute in Dallas—it was just that he was offered a much better paid job. His new office will be in the same building as his present one.

### Newell Appleton Office Manager

A further step to promote efficiency in the New York office of the Institute was made at the beginning of the year in the naming of H. Newell Appleton as Office Manager. Thus is another of the recommendations of the Johnson Committee, made two years ago, being carried out. Mr. Appleton is thoroughly experienced in his new work, and is well known to a large number of AIME members who have seen him in action at many meetings, particularly annual meetings and those of the Metals Branch. He will have complete charge of the service departments at Institute headquarters, including purchasing, addressograph, receiving and shipping, orders, filing, change of address, membership, and the reception desk. In addition he will be convention manager and will have various staff duties in coordinating the work and promoting the efficiency of the line departments including the Secretary's office, the publications and accounting departments, and the work of the Mining, Metals, and Petroleum Branches. Before making the appointment the Secretary studied three volumes and numerous pamphlets on office management and we gather that it is a profession, like mining engineering, and one that has progressed rapidly in recent years. We have now turned these books over to Mr. Appleton, confident that he will fully live up to his new responsibilities. Which latter word reminds us of the nifty about the man who was applying for a job. His potential employer said to him, "For this job we want a responsible man." "That's me," replied the applicant. "Everywhere I've worked, when something went wrong, they told me that I was responsible."

# —Proposed for Membership—

**Arizona**

*Ajo*—Niemi, Alfred Edwin. (M).
*Flagstaff*—Riddell, Richard Drake. (C/S—J-M).
*Klondyke*—Fulmer, J. Walter. (C/S—J-M).
*Phoenix*—Dutton, Donovan Arnold. (C/S—J-M).
*Superior*—Sherman, Fred William, Jr. (C/S—J-M).
*Tucson*—Harshbarger, John William. (C/S—J-M). Williams, Seton Sawyer. (C/S—J-M).

**Alabama**

*Birmingham*—Pagel, Herbert Edwin. (C/S—J-M). Stevens, Edward Henry. (R, C/S—S-M).

**California**

*Bakersfield*—Hiatt, William N. (C/S—J-M).
*Bellflower*—Cox, Eugene Lee. (C/S—S-M).
*Glendora*—Mull, Bert Hathaway. (C/S—J-M).
*Hermosa Beach*—Pfaffman, George Arthur. (C/S—J-M).
*Huntington Park*—Hills, John Osmer. (C/S—J-M).
*La Jolla*—Jeffers, Alba William. (C/S—J-M).
*Long Beach*—Schaller, Herman Elliott. (C/S—J-M). Turner, Billy Jack, (C/S—S-J). Van Dyke, Gilbert Rusk, Jr. (C/S—J-M).
*Los Angeles*—Dale, Clarence Rae. (R—M). Lee, Francis Lincoln. (C/S—J-M). Stewart, Richard Malcolm. (C/S—J-M). Thomas, Gerald B., Jr. (C/S—J-M).
*Monrovia*—Houston, Fred Kennedy. (R—M).
*Monterey Park*—Barclay, Arthur Hugh, Jr. (R, C/S—J-M).
*Nevada City*—Metzger, Grant William. (C/S—S-AM).
*Palo Alto*—Nines, Charles Buford. (C/S—J-AM). Schellinger, (Alfred) Kenneth. (C/S—J-M).

*Pasadena*—Six, Clarence W. (AM). Sumner, Edwin Vose. (C/S—J-M). Terry, Paul Emmett. (M).
*Piedmont*—Hassan, Edward A., Jr. (C/S—J-M).
*Pomona*—Maak, Charles Henry. (C/S—J-M).
*San Jose*—Rose, R. Burton (C/S—J-M).
*San Marino*—Gates, Charles Fredrick. (C/S—J-M).
*South Pasadena*—Hester, Walter B. (C/S—AM-M).
*Taft*—Ganong, Richard Alonzo. (J).
*Whittier*—Ledbetter, Jerry Talbert. (C/S—J-M). Partridge, Padraic. (C/S—J-M).

## Colorado

*Golden*—Smith, Sigmund Levern. (C/S—J-M).
*Rico*—Hinckley, Sherman Bitner. (R, C/S—S-M).

## Connecticut

*Bloomfield*—Seltzer, David Donald (C/S—J-M).
*Fairfield*—Sistare, George Henry. (C/S—J-M).
*New Canaan*—Olmstead, Joseph Nye. (AM).
*Plantsville*—Mohr, James H. (C/S—J-M).
*Riverside*—Sibley, Arthur H. (AM).
*Stamford*—Haskell, Richard M. (M).
*Westport*—Foley, Rupert Merrick (M).

## Delaware

*Wilmington*—Peterson, Erle W. (C/S—J-M).

## District of Columbia

*Washington*—Ball, Douglas. (C/S—J-M). Graham, Gordon Marion. (C/S—J-M). Moyer, Forrest Theodore. (C/S—J-M).

## Florida

*Bartow*—McMullen, Donald Guy. (C/S—J-M).
*Brewster*—Barber, Elwood C. (M).
*Clearwater Beach*—Forth, Courtney Adolph. (C/S—J-AM).
*Lakeland*—Allen, Willie Alton. (M). Elliott, Fernley Harold. (M). Jones, Benjamin Pierce. (M). Uhland, H. E. (R—J).
*Mulberry*—Hatch, John Francis. (C/S—S-J). Icenogle, Karl Luster, Jr. (J).
*Pierce*—Wood, Allen Kelsey, Jr. (J).

## Georgia

*Augusta*—Berg, Eric Allan. (C/S—J-M).

## Idaho

*Kellogg*—Bacon, Charles. (C/S—J-M).
*Moscow*—Jackson, Frank Lee. (C/S—J-M). Scheid, Vernon Edward. (C/S—J-M).

## Illinois

*Aurora*—Molitor, Melvin Edward. (C/S—S-J).
*Benton*—Stephens, Robert Monroe. (C/S—S-J).
*Carmi*—Holz, Walter Ludwig. (C/S—J-M).
*Chicago*—Christon, Paul Charles. (C/S—J-M). Field, Elmer William. (C/S—J-M). Gordon, Paul. (C/S—J-M). Holtz, Richard Dean. (C/S—J-M). Lahr, Alvin Francis. (M). Pigott, John Robert. (C/S—J-M). Tokar, Floryan Joseph. (C/S—J-AM). White, Herbert A. (C/S—AM-M).
*Flora*—Grady, Guido Otto. (C/S—J-M).
*Hinsdale*—Jaicks, Frederick Gillies. (C/S—J-M). Schmidt, Donald Gray. (C/S—S-J).
*Maywood*—Molyneaux, Norman. (M).
*Mt. Vernon*—Atkinson, Jerrel Raymond. (M).
*Waukegan*—Lenz, William Henry. (C/S—J-M).
*West Chicago*—Kremers, Howard E. (M).

## Indiana

*Boonville*—McClevey, Robert A., Jr. (C/S—J-M).
*East Chicago*—McClure, Calvin Alexander. (M).
*Gary*—Brown, Joseph Andrew. (C/S—S-J).
*Logansport*—Lawrance, Robert Pryor. (M).

## Iowa

*Waterloo*—Schaffer, Harry John. (AM).

## Kansas

*Baxter Springs*—Powers, Harold Auburn. (C/S—J-M).
*Chase*—Rasmussen, Lyman Merrill. (C/S—S-AM).

## Kentucky

*Greenville*—Lamb, Charles Mitchell, Jr. (J).

## Louisiana

*Baton Rouge*—Manville, Mahlon Francis. (C/S—S-AM).
*Homer*—Van Horn, Harold Glen. (C/S—S-J).
*New Orleans*—Vitter, Albert Leopold, Jr. (C/S—J-M).
*Shreveport*—Morriss, Herbert Alexander, Jr. (C/S—J-M).

## Maryland

*Accokeek*—Harris, William James, Jr. (C/S—J-M).
*Arnold*—Ames, John Alfred. (J).

## Massachusetts

*Cambridge*—Wagner, Carl. (M). Walters, Stanley Hardy. (AM).
*New Bedford*—Knight, Stanley Storer. (C/S—J-M).
*Watertown*—Fayerweather, John. (C/S—S-J).

## Michigan

*Ann Arbor*—Ewing, John Frederick. (J).
*Negaunee*—Boyum, Burton Hill. (C/S—J-M).
*Port Huron*—Krupp, Roland Gerard. (C/S—J-M).

## Minnesota

*Coleraine*—Johnson, Everette Dan. (C/S—J-M). Lerohl, Iver Roger. (C/S—J-M).
*Marble*—Olson, Reuben Lester. (C/S—J-M).
*Minneapolis*—Sartell, Jack Albert. (J).
*North Hibbing*—Wood, Edwin Townsend. (C/S—S-J).

## Missouri

*Desloge*—Riley, Mard Edward. (C/S—J-M).
*Hayti*—Kidwell, Albert Laws. (C/S—J-M).
*Herculaneum*—Huddleston, Finis Samuel. (M).
*Rolla*—Winston, John Stanton. (C/S—S-M).

## Montana

*Butte*—Barrios, Alberto Hoeck. (C/S—S-M).
*Great Falls*—Eastman, Robert Allan. (C/S—S-J).

## Nevada

*Boulder City*—Jacobs, James Harrison. (C/S—J-M).
*Bristol Silver*—Werner, Donald G. (AM).
*Goldfield*—Hargrove, Frances Donald. (M). Hisle, William Hugh. (M).
*Round Mountain*—Pratt, Morton Edison. (C/S—J-M).
*Woodworth*—De La Mare, Grover Whitby. (C/S—J-M).

## New Jersey

*Avenal*—Stendahl, Gunnar D. (M).
*Morristown*—Hearn, Ira Kendell, Jr. (C/S—J-M). Hearn, Jane Kessler. (C/S—J-AM).
*Nutley*—Hawkins, Jesse Mills. (M).
*Perth Amboy*—Grodner, Abraham. (M).
*Ridgefield Park*—Adkins, Robert Charles. (AM).
*Upper Montclair*—Kuzmick, Jerome Florian. (M).
*Westfield*—Elliott, John Frank. (C/S—S-J).

## New Mexico

*Albuquerque.*—Hillyer, Larry DeWitt. (C/S—S-J). McCroden, Thomas James. (C/S—S-J).
*Carlsbad*—Arend, Carl A., Jr. (M). Greene, Lloyd Morris. (C/S—J-M). Jameson, Elmer Eugene, Jr. (C/S—J-M). Matheson, Robert K. (C/S—J-M). Murray, Jordan Stephens. (C/S—AM). Pressnell, Clarence Eugene. (M). Reeder, Robert Thomas. (C/S—S-J).
*Hurley*—Winn, William Howard. (C/S—J-M).
*Magdalena*—Matthews, Gilbert John. (C/S—J-M).

## New York

*Albany*—Platt, Douglas Howard. (M).
*Bayside*—Maloof, Samuel Barakat. (C/S—S-J).
*Brooklyn*—Miles, Frederick Victor. (C/S—S-J).
*Floral Park*—Besnette, Ulys Antoine. (R, C/S—J-M).
*Hempstead*—Carroll, John Marion. (C/S—S-AM).
*Kenmore*—Hibbard, David Sharpless. (C/S—J-M).
*New York*—Cudroff, Louis. (M). Dennis, Richard C. (R—M). Link, Walter Karl. (M). Rynalski, Augustyn T. (M). Sisto, Joseph A. (M). Skinner, Charles F. (C/S—J-M). Willner, Abner Robert. (C/S—S-AM).
*Scarborough*—Emison, John Clinton. (M).

## Ohio

*Cadiz*—Nelms, George Charles. (C/S—S-J).
*Canton*—Hontas James Peter. (C/S—J-M). Ludwig, Carl. (AM). Walther, Harry Fred. (M).
*Chesterland*—Mumma, Harries A., Jr. (C/S—J-M).
*Cleveland*—Irwin, J. Preston. (M).
*Columbus*—Jaffee, Robert I. (C/S—J-M). Pincus, Howard J. (C/S—S-J).
*Euclid*—Dennis, Howard J. (AM).

## Oklahoma

*Norman*—Schnee, Verne H. (R, C/S—AM-M).
*Oklahoma City*—Eyler, Albert Taylor, Jr. (R, C/S—S-M). Whiteley, Burton W. (C/S—J-M).
*Pauls Valley*—Hardebeck, Edward James. (C/S—S-J).
*Tulsa*—Chapman, Robert Bruce. (C/S—J-M). Culp, John Douglas. (C/S—J-M). Keller, Wallace O. (C/S—J-M). McMillen, Robert Edward. (C/S—J-M). Moore, John Isler, Jr. (C/S—J-M). Nedom, H. Arthur. (C/S—S-J).

## Oregon

*Albany*—Rasmussen, Robert Thorvald C. (C/S—J-M).
*Portland*—Dole, Hollis Mathews. (C/S—J-M).
*Troutdale*—Amos, Lloyd, Arthur. (M).

## Pennsylvania

*Beaver*—Peterson, Karl Freeman. (C/S—J-M).
*Bethlehem*—Good, Robert Charles, Jr. (C/S—J-M).
*Duquesne*—Wagner, George Edwin. (M).
*Ebensburg*—Jones, Sheldon, (C/S—J-M).
*Glenshaw*—Trout, Harry E., Jr. (C/S—J-M).
*Harrisburg*—Gray, Carlyle. (J).
*Holsopple*—Tomaszewski, John Martin. (C/S—S-J).
*Lebanon*—Dominguez, Ezequiel Chavez. (C/S—J-M).
*Mollenauer*—Popp, Victor T., Jr. (M).
*Nemacolin*—Core, Jesse Franklin. (C/S—J-M).
*New Kensington*—McClintock, Thomas Irvin. (M).
*Norristown*—Ellington, Thomas Settle. (M).
*Palmerton*—Held, Llewellyn John. (C/S—J-M).
*Pittsburgh*—Conroy, Edward Hubert, Jr. (AM). Haines, Harry William, Jr. (J). Lustman, Benjamin. (C/S—J-M). Peterson, John Louis. (R, C/S—S-M). Simnad, Massoud T. (J). Vonfeld, Jacques Martin. (C/S—J-M). Walmer, Charles Richard. (AM).
*Pleasant Hills*—Ogan, Albert C. (M).
*Punxsutawney*—Bullers, William Irvin. (C/S—J-M).
*Scottdale*—Anger, Earl Maxwell (AM).
*Secane*—Allshouse, Mervin Sorber, Jr. (M).
*Uniontown*—Oppermann, Albert J. (M).

## South Carolina

*York*—Beers, Seymour James. (C/S—J-M).

## Tennessee

*Copperhill*—Flournoy, Ezell. (M).

## Texas

*Beaumont*—Balch, Sinclair. (R, C/S—S-J).
*Bellaire*—Dumbauld, George Karl. (M).
*Chapman Ranch*—Davis, William Smith. (C/S—S-J).
*Dallas*—Dickson, William Preston. (J). Dyes, Alvin Berry. (J). Mozley, James Marshall. (J). Porter, Phil. (C/S—J-M).
*El Paso*—Butler, Howard Putnam. (C/S—S-J). Collins, Arthur Quinlan. (J).
*Encino*—Wright, Harold Thomas. (J).
*Falls City*—Upchurch,, Mack. (C/S—J-AM).
*Houston*—Blair, Philip Michael. (J). Bodin, Jean Alfred. (M). Evans, John Billy. (C/S—J-M). Laas, Charles William. (M). Nichols, James Bryant. (M). Rachford, Henry Herbert, Jr. (J).
*Kilgore*—McCray, John Lester. (C/S—J-M). Welch, Harlan E. (AM).
*Longview*—Miller, Herbert Dell. (R, C/S—S-M).
*Lubbock*—Nowlin, Roger Ernest. (C/S—S-J).
*Refugio*—Bankston, Ford Alfred. (C/S—J-M).
*San Antonio*—Andrews, Worth Briggs. (R—M).
*Tyler*—Stallings, Harold Owen. (C/S—S-J).
*Wichita Falls*—May, Donald Thomas. (M).
*Wickett*—Kennerly, Kenneth Spargur. (C/S—J-M).

## Utah

*Bingham Canyon*—Niemi, John Oscar. (M).
*Dragerton*—Ross, Marion Donald. (J).
*Salt Lake City*—Cassano, James. (R, C/S—S-M). Johnson, Earl Silver. (C/S—J-M). Prater, John Dingle. (C/S—J-M). Richards, William George. (C/S—J-M). Wilson, Robert Alexander. (C/S—J-M).
*Sunnyside*—Lackey, George Raymond. (J). McCourt, Thomas Raymond. (M).

## Virginia

*Big Stone Gap*—Meador, Harry Wallace. (M).
*Blacksburg*—Cooper, Byron Nelson. (M).
*Richlands*—Berube, Stephen Charles. (R, C/S—S-M).

## Washington

*Metaline Falls*—Land, Earl Fredrick. (C/S—J-M).
*Quincy*—Hughes, Charles Von Oden. (C/S—J-M).
*Richland*—Ward, Raymond. (C/S—J-M).
*Seattle*—Bethel, Horace L. (C/S—J-M). Magill, Elwin Arba. (C/S—J-M).
*Spokane*—Armstrong, John. (M).
*Tacoma*—Lloyd, Richard Hardy. (J).

## West Virginia

*Charlestown*—Gentry, William S. (M).
*Fairmont*—Sargeant, Harold Frederic. (M).
*Huntington*—Francis, David Livingston. (M).
*Morgantown*—Pursglove, Samuel Richard. (R—M).
*Omar*—Carter, Wade Howard. (M).
*Stotesbury*—Arnold, Alfred Cyrus. (C/S—J-M).

## Wisconsin

*Kenosha*—Doremus, George Edward, Jr. (C/S—J-AM).
*Milwaukee*—Swansen, Earl Edward. (C/S—S-J).
*Racine*—Osborne, Robert Vandervoort. (C/S—AM-M).
*West Allis*—Mariacher, Burt Charles. (C/S—J-M).

## Wyoming

*Casper*—Lambert, Joseph Gerrard. (J). Pallansch, Edward Peter. (C/S—S-M).

## Alaska

*Nome*—Lomen, Alfred J., Jr. (C/S—S-AM).

## British Columbia

*Alice Arm*—Rosen, Philip Edward. (C/S—S-J).
*Rossland*—Whiton, Leslie Victor. (R, C/S—J-M).

## Ontario

*Falconbridge*—Walton, Alan Kingsley. (C/S—J-M).
*Haileybury*—Atchison, Daniel W. (C/S—J-M).
*Owen Sound*—Fairfield, Herbert Holloway. (M).
*Sault Ste. Marie*—Barber, James Edgar. (C/S—J-M).
*Swastika*—McBean, John Williams. (C/S—J-M).
*Toronto*—Laird, Harry C. (C/S—J-M).

## Quebec

*Montreal*—Michaud, Joseph Marcel. (M). Weigel, Melvin Powell. (M).
*Nitro*—McIntosh, Jack Lorne. (C/S—J-M).

## Mexico

*Monterrey, Neuvo Leon*—Villareal, Eduardo Mauricio, Jr. (C/S—J-M).

## Nicaragua

*Siuna*—Plecash, John. (R, C/S—S-M).

## Cuba

*Pinar del Rio*—Sykes, Robert Edward. (C/S—S-J).

## Bolivia

*La Paz*—Matthieu, Willem. (J).

## Brazil

*Itabira, Minas Geraes*—Franca, Joao Mendes. (C/S—J-M).

## Chile

*Potrerillos*—Malcolm, John Baxter. (C/S—J-M).
*Rancagua*—Oram, Peter MacMillan. (C/S—S-J).

## Peru

*Casapalca*—Aimone, Francis Mario. (C/S—J-M). Goodman, Lyle Oral, Jr. (C/S—J-M).
*Yauricocha*—Allen, Kenneth Laidlaw. (J).

## Venezuela

*Jusepin*—Jones, Paul Robert. (C/S—J-AM).

## England

*Aldwick Bay*—Goulden, Charles Edward. (C/S—S-J).
*London*—Goodeve, Charles F. (M).
*Uddingston*—Ritchie, Alexander Malcolm. (M).

## Spain

*Murcia*—Dumas, Alexis Jacques. (J).

## Union of South Africa

*Maraisburg, Transvaal*—Margo, Eli. (M).

## India

*Delhi*—Sahai, Devi. (M).
*Rajasthan*—Sommerlatte, Herbert W. A. (R, C/S—AM-M).

## Japan

*Tokyo*—Yamada, Yukichi. (M).

## Victoria

*Melbourne*—Ritchie, John Gowar. (C/S—JFA-AM).

## Philippine Islands

*Baguio*—Dana, John Francis. (C/S—J-M). Farretta, Alvin Joseph. (C/S—J-AM)
*Rizal*—Boquer, Antonio Maria. (C/S—J-AM).

## ADDRESSES WANTED

| | |
|---|---|
| T. W. T. Atherton, (M'92) | W. Moore, (M'05) |
| S. K. Bradford, (M'02) | J. Morris, (M'98) |
| F. J. Dorion, (M'96) | A. H. Pogson, (R'28) |
| N. E. Franklin, (R'28) | J. W. Reno, (M'87) |
| R. Krahmann, (M'34) | G. A. Richard, (M'97) |
| E. A. Manners, (M'01) | W E. Richardson, (R'28) |
| G. McClurg, (R'28) | H. L. Rodgers, (R'28) |
| J. E. McDevitt, (M'26) | T. R. Starkey, (M'07) |
| H. S. Young, (M'03) | |

Effect of

# Melting Practice

# On Hydrogen

by Sam F. Carter

*T*HIS is the concluding portion of a two part article which presents a number of quanti-
tative hydrogen analyses of some electric arc-furnace steels with varied melting practices.
Last month the author reviewed past research contributions and described the experimental
methods used in this investigation and gave a discussion of results for carbon steels. Here,
this discussion is continued, along with an analytical study of evolved gases.

THE objective in heats C-17 and C-18 was a study of hydrogen pickup from newly lined ladles. Previous research has indicated that hydrogen is absorbed readily from wet ladles and sources of moisture contacting the steel in its finished and deoxidized condition. With the exception of wet ladles, hydrogen changes upon tapping have been controversial and evidence has been conflicting. Hare and Soler indicated decrease of hydrogen upon tapping. Wentrup and associates experienced an average increase from tap to ingot mold on acid-openhearth heats but a decrease on basic-openhearth heats. Of the heats studied by Sims and associates, roughly half showed no change or a slight loss upon tap-

ping while the other half showed increases of 0.05 to 0.16 R.V. It was inferred that inadequately dried ladles were the probable causes of the increases but only two newly lined ladles were specifically indicated.

Sam F. Carter, Junior Member AIME, is Assistant Melting Superintendent of American Cast Iron Pipe Co., Birmingham.

On heat C-5 an increase of 0.07 R.V. from a newly lined ladle has already been pointed out.

From this it appears that a physically wet ladle is not necessary for hydrogen absorption. In all probability the combined water in the clay is retained at a considerable temperature and can serve as a source of hydrogen. It was felt some quantitative correlation between ladle preheating and hydrogen pickup should be attempted. Principal objective was to determine if a "green" ladle could be given any preliminary treatment that would completely prevent hydrogen pickup. The next step would be to find the heating cycle that appears to be the best compromise between the cost of the absorbed hydrogen and the cost of ladle treatment.

The preheating schedules of three ladles were followed with pyrometers. Sufficient variety was chosen to give some indication of the most important qualification of preheating. Temperatures were plotted against times in fig. 5. All ladles were rammed from a mixture of one-third clay and two-thirds ganister. After air drying for several days each one was placed on a vertical heating wall.

Ladle I used on heat No. C-5 was brought up to 500° in 3 hr with a gas flame. Left overnight, the temperature reached 800°F by the 16th hour. A gas and air burner then was opened wide, heating the ladle in six more hours to its maximum temperature of 2380°F before it was tapped into. Hydrogen content increased from 0.25 to 0.32 R.V. for a 0.27 R.V. increase from this ladle lining.

Ladle II used on heat No. C-17 was heated for essentially the same period of time but at a much higher temperature level all the way. The cycle included: up to 1600° in 4 hr, 1600° to 2000° for 13 hr, from 2000° to a maximum of 2800°F in 5 hr. No increase of hydrogen was experienced from this ladle. Actually a decrease of 0.04 R.V. was realized, from 0.19 R.V. at tap to 0.15 R.V. in the ladle. Although the heating cycle was extremely severe and often could not be justified, it seems conclusive proof that hydrogen pick up from a new ladle can be prevented, at least on this type of steel.

Ladle III use on heat No. C-18 was given no gradual heating period. The temperature was pushed up to 2000°F in 1 hr and to 2400° in three more hours. A tap hydrogen of 0.09 R.V. increased only to 0.11 R.V. A 0.02 R.V. is a negligible increase, especially for such a low hydrogen content.

The data on these three ladles is summarized in table II.

The reason for the superiority of ladle II over the other two is obvious. However, the reason for ladle II experiencing less increase than I is not so readily apparent. The difference does not correlate with maximum temperature, total heating time, or area under the time-temperature curve. Time at high temperature (2000°F or higher) seems to be the only factor that can explain the relative position of these two ladles. This seems reasonable in view of the temperature required to remove combined water from clays.

Tap samples on these two heats provide some additional data on normal practice and the effect of the boil. Both heats melted similar charges and finished with short Mn-Si blocks. No additional source of moisture was present and atmospheric humidity was essentially the same. Because of a bridge in melting, C-17 experienced a relatively mild boil with a maximum rate of 0.78 pct C per hour. An ore down carbon of 0.27 pct was obtained and correspondingly high residual Si and Mn contents. However, a better melt on C-18 enabled the same ore addition to produce the most violent boil of this investigation, a maximum rate of 1.90 pct C per hour, an ore down carbon of 0.15 pct and the residuals were more nearly normal. Hydrogen contents at tap were 0.19 R.V. for the milder boil and 0.09 R.V. for the violent boil.

Since hydrogen pickup has been experienced on green ladles, the possibility of equal or greater absorption from a newly lined furnace hearth was considered. The acid furnace hearths are lined with the same rammed material as the ladles and given less preheating. Heat No. C-9 was produced on such a new hearth. A 2 pct ore addition generated a boil of normal violence and a low or-down carbon of 0.10 pct. The heat was blocked 5 min before tap with 0.40 pct Mn and 0.20 pct Si. Hydrogen content as melted was 0.14 R.V. The boil sample was inadequately killed with aluminum and analysis was not attempted. Tap sample was 0.17 R.V. and the ladle sample 0.13 R.V. Hydrogen content of this heat compares closely with others with similar practices. Very little, if any, increase can be attributed to the "green" hearth although moisture should have been present in greater amounts than in the ladles. The most likely explanation seems to be that the water was driven off during the melting and oxidation stages when the oxidized condition of the steel prevented absorption to any significant extent. Such a hearth might prove more detrimental to an alloy heat, a carbon heat with a less oxidized melt-down, or a different type of charge.

A survey of the carbon heats by groups provides some correlation trends between hydrogen content and general practice. A condensed summary is given in table III.

The hydrogen ranges of the four groups were as follows:

| Practice | No. Heats | Ladle B₂ |
|---|---|---|
| Vigorous boil; oxidized; short deox. time .............. | (7) | 0.11-0.18 R.V. |
| No boil; very oxidized throughout .............. | (4) | 0.12-0.27 R.V. |
| No boil; excess C but no deoxidizers; all dry......... | (3) | 0.12-0.21 R.V. |
| Early deoxidizer or reducing slag; long deox. time..... | (5) | 0.21-0.35 R.V. |

The highest hydrogen heats, as a group, were those deoxidized early or finished under reducing slags. The lowest group were those made by the currently normal practice of a vigorous boil, extended oxidizing period, and minimum deoxida-

tion period. Intermediate hydrogen concentrations were obtained from charges of rimmed steel not boiled but melted and kept very oxidizing.

In each of these groups, heats exposed to additional moisture or high atmospheric humidity were generally in the upper part of their respective ranges and slightly higher than drier heats. However, chemical condition of the steel seems to be a more dominant factor in absorption. Some of the oxidized heats absorbed less hydrogen when sprayed with water than was absorbed by some of the reducing heats from the natural humidity of the atmosphere.

The low hydrogens from the rimmed steel

charges without boiling suggests that all charges do not invariably melt high in hydrogen and require extensive elimination. However, on the basis of the experience of this investigation, rimmed steel scrap would be expected to melt lower in hydrogen than most other types. Such steel was originally produced under such oxidizing conditions that a very high hydrogen content as melted would have been prevented. The absence of deoxidizers plus the gas evolved would have carried away much of the hydrogen during solidification of the ingot. More hydrogen would be expected to have left the thin section plate over a period of years of service and another period of months on the scrap pile. This would leave relatively little hydrogen left in the scrap plate by the time it was charged into the furnace. Preheating prior to fusion by the arc might drive

out still more hydrogen if the moisture content of the surrounding atmosphere were not too high. The more deoxidized killed steel and cast-steel scrap would be expected to contain more hydrogen both because of the possibility of higher content as melted as well as proportionately less loss by natural ageing. Gates and risers of cast steel might be returned and charged for remelting within a few days after casting and before much hydrogen has been lost, especially from the heavier sections. Furthermore, if a deoxidized bath absorbs hydrogen more readily than an oxidized bath then a deoxidized charge would be expected to absorb hydrogen more readily in melting than an oxidized charge. For these reasons the make-up of the charge seems important. The experiences on these rimmed-steel charges should not be applied to charges made up of higher percentages of cast steel usually used, without some further investigations.

The practice that produced the lowest hydrogens under all conditions was a combination of a vigorous boil and an extended oxidized condition. Apparently, the boil functions principally in elimination and the prolonged oxidized condition in the prevention of absorption. Seven of such heats finished with ladle contents ranging 0.11 to 0.18 R.V. One of these melted a wet charge, one melted on a green hearth, and two were sprayed with water throughout. A vigorous boil seemed more effective in counteracting a moisture-saturated atmosphere than any other condition.

The characteristic of the boil that gave the best correlation with hydrogen content after the boil was violence of maximum rate of carbon elimination. Although the data is scant, the eight heats boiled against a continuous water spray should be a severe test for elimination effectiveness. In table IV all heats are arranged in the order of their maximum carbon elimination rate. Within the experimental limitations the hydrogen contents after the boil showed a definite decrease

#### TABLE III
#### Summary of Final Hydrogen Contents—Carbon Steels

| No. | Moisture | Atm.** | Characteristic of Practice | Hydrogen R.V. | |
|---|---|---|---|---|---|
|  |  |  |  | Tap | Ladle |
| | | | **Normal Practice. Vigorous boil. Short or no block** | | |
| C-18 | Dry | 88 | Violent boil; 8' Mn-Si block | 0.09 | 0.11 |
| C-1 | Dry | 52 | Late boil; 7' Mn-Si block | 0.13 | (−0.15) |
| C-17 | Dry | 80 | Mild Hi C boil; 10' Mn-Si block | 0.19 | 0.15 |
| C-2 | Damp chg. | 95 | Low C, ox. boil; 6' Mn-Si block | 0.21 | 0.15 |
| C-19 | New hearth | 58 | Low C, ox. boil; 5' Mn-Si block | 0.17 | 0.13 |
| C-3 | Wet spray | | Normal boil; 3' all Mn-Si | | 0.18 |
| C-4 | Wet Spray | | Mild, Hi C boil; 3' all Mn-Si | | 0.18 |
| | | | **No boil. Low-C charge. Very oxidizing throughout. No block** | | |
| C-5 | Dry | 60 | No boil; 3' all Mn-Si | (−0.10) | 0.12 |
| C-6 | Wet. Spray | | No boil; 3' all Mn-Si | 0.15 | 0.17 |
| C-7 | Wet Spray. Pole | | Ditto, but less oxidizing | 0.25 | 0.32* |
| C-8 | Wet hearth. Leak | | *Basic.* Mild boils; 3' all Mn-Si | | 0.27 |
| | | | **Cast irons from steel chg. No boil, no oxidation** | | |
| C-9 | Dry (basic) | 45 | Rim chg. Dead melt with C + Si | 0.12 | 0.13 |
| C-10 | Dry (acid) | 105 | Rim chg. Dead melt with C + Si | | 0.19 |
| C-11 | Dry (acid) | 72 | Kill chg. Dead melt with C + Si | | 0.21 |
| | | | **Earlier deoxidizer addition and/or reducing slag** | | |
| C-12 | Late leak | | 4140 steel. Boil. 10' Mn-Si block | 0.25 | |
| C-13 | Dry | 108 | Red. 2nd slag & block (*Basic*) | | 0.21 |
| C-15 | Early spray | 125 | Violent boil. Red. 2nd slag. | | (0.25-0.45) |
| C-16 | Early spray | 60 | Mild boil. Red. 2nd slag. | | 0.28 |
| C-14 | Wet. Spray | | Early Si block, very ox. slag. | | (0.19-0.30) |

* Indicates unusual increase in tapping from new lined ladle.
** Atmospheric moisture in grains per lb of dry air.

## TABLE IV
### Effect of Carbon Elimination Rate on Hydrogen Content

| No. | C Elim. per Hr, Pct | Min C & Residuals | Sources of Moisture | Melt | Hydrogen RV | |
| --- | --- | --- | --- | --- | --- | --- |
| | | | | | Boil | Tap |
| *Heats with Additional Sources of Moisture* | | | | | | |
| C-15 | 1.72 | Avg. | Wet chg. Spray | | 0.09 | |
| C-19 | 1.20 | Low | New hearth only | 0.14 | | 0.17 |
| C-14 | 1.09 | Low | Wet chg. Spray | 0.20 | (0.10-0.20) | |
| C-3 | 1.00 | Avg. | Wet chg. Spray | | | 0.18 |
| C-2 | 0.90 | Low | Damp chg. only | | (0.10-0.20) | 0.21 |
| C-16 | 0.60 | High | Damp chg. only | 0.22 | | |
| C-4 | 0.54 | High | Wet chg. Spray | 0.19 | 0.29 | |
| C-8B | 0.40 | Low | Wet hearth. Leak | | (0.19-0.37) | |
| C-6 | 0.16 | Low. Very ox. | Wet chg. Spray | | | 0.15 |
| C-7 | 0.16 | Low. Very ox. | Wet chg. Spray G. Pole | | | 0.25 |
| *Heats with no Additional Source of Moisture* | | | | | | |
| C-18 | 1.90 | Avg. | Dry. 88 grains per lb air | | | 0.09 |
| C-1 | 0.80 | Avg. | Dry. 52 grains per lb air | | (0.11-0.22) | 0.13 |
| C-11 | 0.78 | Hi | Dry. 80 grains per lb air | | | 0.19 |
| C-5 | 0.16 | Low. Very ox. | Dry. 60 grains per lb air | | | (0.10) |

with the increased violence of the boil. All five heats given what was considered a boil of normal violence (0.90 to 1.20 pct carbon eliminated per hr), experienced hydrogen contents in the middle teens after the boil. The three heats with what was considered mild boils for electric-furnace practice, (60 pct C per hr and less) were all well in the twenties. On the other hand the one heat with a very violent boil of 1.72 pct C per hour produced the lowest content of 0.09 R.V.

Two pairs of heats provides very good comparisons on boil violence. Heats Nos. C-15 and C-16 melted similar charges which were water sprayed throughout the oxidation period. After the boil the content of the mildly boiled heat (0.60 pct C per hr) was 0.22 R.V. and of the violently boiled heat (1.72 pct C per hr) was 0.09 R.V. On heats C-17 and C-18 no additional water was added and atmospheric humidity was similar. Boil samples were not analyzed but the tap samples should be indicative since melting practices were otherwise identical. C-17 with a rate of 0.78 pct C per hr ran 0.19 R.V. while C-18 with a boil rate of 1.90 pct C per hr ran only 0.09 R.V. From these results it appears that the internal pressure of a violent boil is the best means of forcing the hydrogen content of the metal to a low level in spite of a high moisture atmosphere. From all indications, with a high-hydrogen bath and a low-hydrogen atmosphere a mild boil might eliminate considerable hydrogen. However, with a higher hydrogen atmosphere in relation to the bath it appears that the violence of the boil becomes increasingly important if elimination is to be experienced.

Other factors such as minimum residuals, carbon content, FeO of the metal, FeO of the slag, etc. have an indirect effect on boil violence. These factors likewise have a considerable effect on the degree of oxidation previous to and subsequent to the boil and would conceivably effect the absorption tendency. Length of boil failed to improve the minimum hydrogen content. The lowest hydrogen of 0.09 R.V. was obtained after the shortest boil of only 8 min, but the most violent one. However, in as much as continued boiling denotes oxidizing conditions, reabsorption of hydrogen seems to be restrained. If the boil is prolonged at the expense of the deoxidation time then overall hydrogen content might be improved. On the other hand if the heat is simply prolonged for an extension of the boil it appears that hydrogen content might be higher than if the furnace had been driven harder, the same carbon eliminated in less time, and the heat tapped sooner.

Only three carbon heats on a basic lining is an insufficient number to compare a basic with an acid lining. However, these three heats were in line with the acid heats of comparable practice and exposure to moisture.

With the exception of the last three heats, nitrogen contents on these carbon steels were 0.003 to 0.005 pct.

### High Alloy Steel

In order to determine the hydrogen tendencies with large quantities of chromium and nickel alloys present, ten heats of austenitic heat- and corrosion-resistant compositions were investigated. Six were made on a basic lining and four on a similar furnace with an acid lining. Table V contains the data on these high-alloy steels.

Before the knowledge gained by the use of oxygen, it was thought that carbon could not be eliminated from charges high in Cr content by the usual boil. Consequently, the carbon specification determined the amount of return scrap used and the melting practice chosen.

One approach was to dead-melt a charge of maximum return scrap. Where lower carbons were required, it was necessary either to use all virgin alloys with no returns or to charge a small enough proportion of return scrap to permit a boil. Certain familiar disadvantages in cost or quality are associated with each method. Greater tendencies toward porosity have been experienced from certain practices and certain compositions. No actual hydrogen analyses have been found reported on such compositions that would indicate what quantities of hydrogen are contained or what concentrations begin to cause porosity. Austenitic compositions have not experienced the "flaking" tendency of carbon steels. However, on a heavy casting in our plant fine cracks were developed upon welding. These were not experienced after changing to a practice that produced a much lower final hydrogen.

Heat No. H-1 is a 25 pct Cr, 20 pct Ni austenitic heat-resisting composition made by a dead-melt

practice. In a basic-lined furnace 80 pct return scrap was melted with enough electrolytic nickel squares to complete the final 20 pct nickel. A 3 pct ore addition was charged with the scrap to supposedly oxidize the residual silicon, but no boil was produced. At 3100°F the Cr necessary to complete the composition was added as 70 pct ferrochromium. Two minutes before tap the necessary Mn and Si were added and the heat tapped at an optical temperature of 3250° into a used ladle. Hydrogen at melt was 1.00 R.V., 2 min before tap 0.96 R.V., and in the ladle 1.01 R.V.

On heat No. H-2 the charge and practice were identical and the absolute humidities similar. This heat was tapped into a newly lined ladle given a preheating somewhere between ladles II and III in fig 5, the best two in the ladle study.

Hydrogen content of this heat at melt was 0.64 R.V., at tap 0.73 R.V., and after tapping into a
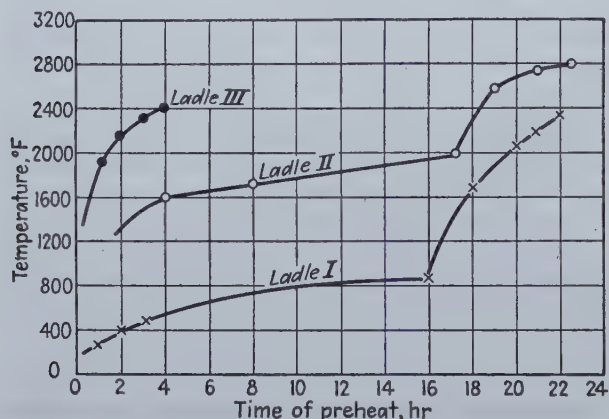


Fig 5—Heating schedules of newly lined ladles.

new lined ladle 0.86 R.V. According to the experience with other "green" ladles, this one should have caused little or no hydrogen pickup on mild-carbon steels. Nevertheless, a 0.13 R.V. increase was experienced on this high-alloy composition.

In order to investigate the segregation and effusion tendencies of this type of steel, a 4 in. block was cast in dry sand and specimens were cut from various depths. The sample from the center analyzed 0.84 R.V. which is a check with the 0.86 R.V. ladle sample. A sample from the outside edge ran 0.71 R.V. This indicates a very small loss, probably occurring at high temperature as the casting cooled. However, in comparison with carbon steels this is very little loss and a very stable and uniform concentration. Freezing directly to an austenitic form probably accounts for this uniformity.

From these two heats it became apparent that steels of this composition, when dead melted, tend to run several times higher in hydrogen than carbon steels. On high return charges the high hydrogen content was obtained from the charge or absorbed in melting with little change in the furnace after molten.

Another observation of practical significance was the fact that samples from these heats enclosed in glass tubes for weeks evolved no gas at room temperature in spite of their high hydrogen contents. Hot extraction required a longer period

at high temperature. This experience suggests that no hydrogen is lost from these steels by natural ageing and that elimination of hydrogen by low temperature heat treatment is impractical. This also indicates that these high final hydrogen contents would be retained in remelting. With repeated reuse of maximum return scrap hydrogen content would probably become cumulative unless counteracted by dilution or elimination.

The other extreme in-furnace practice is the more expensive use of all virgin alloy with no return scrap, typified by the next three heats in table V. These are low-carbon, corrosion-resistant compositions containing 18 pct Cr and 9 pct Ni. On acid heat No. H-3 a charge of low-carbon rimmed steel and electrolytic nickel squares were melted with 1 pct ore. No vigorous boil was obtained but some carbon was lost in the very oxidizing melt. With the C 0.07 pct and the temperature 3100°, the calculated amount of ferrochromium was added in two additions. Hydrogen content of the melt before the Cr was 0.22 R.V. After both Cr additions hydrogen at tap time had increased to 0.40 R.V., and after tapping into the used ladle 0.42 R.V. This was less than half the hydrogen contents of the high return heats but still higher than the highest of the carbon steels. The principal increase occurred after the Cr addition.

Heat No. H-4 was intended to check the effect of damp ferrochromium. With this exception the heat was identical with H-3. The first half of the FeCr was damp enough to "spit" when thrown into the molten bath. The second half was partially dried with a gas torch. Hydrogen content after half the Cr was 0.57 R.V. and after all the Cr and ready to tap, 0.66 R.V. Since atmospheric humidity was lower than on H-3, the 0.26 R.V. higher hydrogen can be attributed to the damp alloy.

H-5 was a basic steel made with all virgin alloy similar to the two previous heats with the exception of a double-slag process used to improve chromium recovery. The oxidizing slag was drained and a reducing slag of lime, Ca Si, and FeSi was added. The bath was given a preliminary deoxidation with Mn and Si before the Cr addition. Again at meltdown hydrogen content was only 0.13 R.V. in spite of the electrolytic nickel. After the two Cr additions under the reducing slag, hydrogen increased to 0.60 R.V. Although absolute humidity was only half, the basic reducing slag ran 0.20 R.V. higher than the acid oxidizing slag. After tapping into the ladle this heat increased from 0.60 to 0.79 R.V. No reason for the increase was observed.

H-6 was a 35 pct nickel cast iron made from steel scrap. This heat was studied because it provided an opportunity to separate the effect of nickel and chromium. Rimmed steel and electrolytic nickel squares were charged on top of 3½ pct fine graphite. In deadmelting, sufficient carbon was absorbed and the necessary silicon added 10 min before tap to product a type V Ni-Resist iron. Hydrogen content before the Si was 0.14 R.V. and from the ladle 0.09 R.V. The low content of the steel containing only Ni indicates

that Cr is the alloy responsible for the hydrogen absorption. When melted down with the charge in the absence of Cr, the high hydrogen content of electrolytic nickel is not absorbed. Whether the hydrogen escapes from the Ni at preheat temperatures or whether it was not absorbed due to the condition of the steel will require further research to determine. It is quite possible that Ni added to a deoxidized bath or one containing Cr might increase the hydrogen content. No gas was evolved at room temperature from this austenitic cast iron indicating that Ni is apparently the alloy responsible for the retention of hydrogen in the solid metal. This effect is probably a result of the austenitic condition.

The next four heats were directed toward finding some means of reducing the high hydrogen contents invariably obtained from melting large percentages of alloy returns. Heat No. H-7 was boiled with ore at high temperature. After melting a charge of 80 pct alloy returns a 3.2 pct ore addition was made at 3200°F (optical). At 3300°F a mild boil developed, eliminating 0.07 pct C over a period of 8 or 10 min. The supplementary Cr was then added. Hydrogen as melted and just before the boil was 0.96 R.V. The boil removed over half the hydrogen to a content of 0.40 R.V. which continued to drop to 0.36 R.V. at tap. Tapping into the ladle increased the content back to a final content of 0.48 R.V.

H-8 was a similar heat in a basic furnace. After the high-temperature ore boil and the Cr addition, a fine FeSi addition was made to the slag to reduce some Cr from the slag and decrease the high loss resulting from such oxidation. The hydrogen as melted was 1.26 R.V. at 2950°F. After heating to 3250° another sample ran 1.00 R.V. The boil again removed over half the hydrogen down to a content of 0.45 R.V. which continued the drop to 0.38 R.V. after the Cr addition. Ten minutes after the reducing agent had been added to the slag hydrogen had increased to 0.53 R.V. Tapping into the ladle produced a further increase to 0.81 R.V. The ladle had been used but the spout was freshly lined and not sufficiently heated. The hydrogen pickup in the furnace after the reducing agent was greater than that experienced on other heats left oxidizing.

Heat No. H-9 was given a similar boil but with oxygen instead of ore. A melt of 80 pct return in a basic furnace was heated to 3200°F. Oxygen was injected for 10 min for a total of 315 cu ft per ton. After a few minutes a mild boil developed that oxidized the carbon from 0.27 to 0.18 pct carbon. A 1 pct addition of fine calcium silicon was sprinkled over the slag to improve Cr recovery by reduction. Then the calculated Cr addition was made and the Mn and Si added 2 min before tap. Hydrogen content before the oxygen was 0.86 R.V., decreased after the oxygen boil to 0.57 R.V., and decreased further to 0.48 R.V. at tap. An increase to a final of 0.56 R.V. was experienced in tapping.

From these three heats it is evident that a late oxidation of carbon, whether induced by oxygen gas or solid iron oxide, is very effective in removing hydrogen. The advantages of oxygen in more positive carbon elimination and better Cr recovery are well known. No doubt still lower hydrogen contents could be obtained by boiling out more carbon with more oxygen or by charging a lower proportion of high Cr returns and thus obtaining more carbon elimination from the same quantity of oxygen. It seems quite possible that elimination of hydrogen might become an object of boiling such heats equal in importance to the removal of carbon. Further research should develop the most practical practice from the standpoint of hydrogen elimination, Cr recovery, and scrap utilization.

The last alloy heat investigated the possibility of removing hydrogen by flushing with argon gas. If such an inert gas could eliminate hydrogen like the carbon boils, the improved Cr recovery might justify the higher cost of the gas. Some hydrogen has been eliminated from the laboratory melts[28] and flushing induction furnace heats with argon has reportedly decreased the frequency of pinholes. The author was afraid to use argon in the ladle for fear of excessive temperature drop. None of the higher hydrogen return heats were in sight for the experiment, only low-C steels that required virgin alloys.

H-10 is such a heat very similar to H-5 but without the double slag. A charge of rimmed steel and nickel was melted in a basic furnace

## TABLE VI
### Summary of High Alloy Heats

| Heat No. | Type Lining | Moisture Atmosphere | Characteristic of Practice | Hydrogen R.V. | | | |
|---|---|---|---|---|---|---|---|
| | | | | Melt | Int | Tap | Ladle |
| 25 Cr-20 Ni steels. Maximum proportions of return. Dead melted | | | | | | | |
| H-1 | Basic | 62 | No boil | 1.00 | | 0.96 | 1.01 |
| H-2 | Acid | 70 | No boil | 0.64 | | 0.73 | 0.86* |
| 25 Cr-20 Ni Steels. Max. Proportions of return. Boiled | | | | | | | |
| H-7 | Acid | 70 | Boil ore. | 0.96 | 0.40 | 0.36 | 0.48 |
| H-8 | Basic | 40 | Boil ore. FeSi on slag | 1.26 | 0.38 | 0.53 | 0.81** |
| H-9 | Basic | 82 | Boil oxygen. CaSi on slag | 1.00 0.86 | | 0.57 0.48 | 0.56 |
| 18 Cr-9 Ni steels. Virgin alloys. Steel & Ni oxidized. Cr added later | | | | | | | |
| H-3 | Acid | 49 | No deox. Ox slag | 0.22 | | 0.40 | 0.42 |
| H-4 | Acid | 24 | Wet Cr. Ox slag. | | 0.57 | 0.66 | |
| H-5 | Basic | 20 | Deox. Reducing 2nd slag | 0.13 | 0.60 | | 0.79 |
| H-10 | Basic | 20 | Argon bubbled | | 0.60 | | 0.81** |
| 35 Per cent Ni Cast Iron | | | | | | | |
| H-6 | Basic | 68 | Steel + Ni + melted. Si added | | | 0.14 | 0.09 |

* Newly lined ladle.
** Newly lined or patched furnace spout.

# TABLE VII
## Analytical Data on Gas Evolved

| Sample No Heat No. Time | Evolution Time | Temp. | Total Gas, ml | CO₂ | O₂ | CO | N₂ | H₂ | H₂ Content of Gas, Pct | Rel. Vol. of Metal | Proport. of H₂ in Metal, Pct |
|---|---|---|---|---|---|---|---|---|---|---|---|
| | | | | Gasses Evolved, ml | | | |

| Sample No / Heat No. | Evolution Time | Temp. | Total Gas, ml | CO₂ | O₂ | CO | N₂ | H₂ | H₂ Content of Gas, Pct | Rel. Vol. of Metal | Proport. of H₂ in Metal, Pct |
|---|---|---|---|---|---|---|---|---|---|---|---|
| No. 4 36894 Tap | 52 days | Room | 0.42 | 0.00 | 0.00 | 0.00 | 0.08 | 0.34 | 81.0 | 0.060 | 39 |
| | 45 hr | 1925° | 1.52 | 0.00 | 0.00 | 0.76 | 0.17 | 0.51 | 33.6 | 0.089 | 59 |
| | | Residual Correction | | | | | | 0.02 | | 0.003 | 2 |
| | | Total | | | | | | 0.87 | | 0.15 | |
| No. 5 36894 Ladle | 52 days | Room | 0.67 | 0.00 | 0.00 | 0.00 | 0.08 | 0.59 | 88 | 0.101 | 58 |
| | 48 hr | 1925° | 2.23 | 0.04 | 0.00 | 0.80 | 0.97 | 0.42 | 19 | 0.072 | 41 |
| | | Correction | | | | | | 0.01 | | 0.001 | 1 |
| | | Total | | | | | | 1.02 | | 0.17 | |
| No. 18 36944 Si block | 26 days | Room | 1.43 | 0.00 | 0.00 | 0.00 | 0.08 | 1.35 | 94 | 0.235 | 80 |
| | 40 hr | 1925° | 1.10 | 0.00 | 0.00 | 0.68 | 0.08 | 0.34 | 31 | 0.059 | 20 |
| | | Correction | | | | | | 0.00 | | 0.000 | 0 |
| | | Total | | | | | | 1.69 | | 0.29 | |
| No. 22 56752 End boil | 19 days | Room | 0.93 | 0.00 | 0.00 | 0.25 | 0.00 | 0.68 | 73 | 0.115 | 40 |
| | 40 hr | 1925° | 2.37 | 0.00 | 0.00 | 1.44 | 0.00 | 0.93 | 39 | 0.158 | 54 |
| | | Correction | | | | | | 0.10 | | 0.017 | 6 |
| | | Total | | | | | | 1.71 | | 0.29 | |
| No. 24 56752 | 19 days | Room | 0.76 | 0.00 | 0.00 | 0.17 | 0.08 | 0.51 | 67 | 0.085 | 47 |
| | 40 hr | 1925° | 2.36 | 0.08 | 0.00 | 1.35 | 0.42 | 0.51 | 22 | 0.085 | 47 |
| | | Correction | | | | | | 0.06 | | 0.010 | 6 |
| | | Total | | | | | | 1.08 | | 0.18 | |
| No. 53 37038 Boil | 24 days | Room | 0.61 | 0.00 | 0.09 | 0.09 | 0.00 | 0.43 | 71 | 0.068 | 31.0 |
| | 1 hr | 1200° | 1.13 | 0.09 | 0.09 | 0.43 | 0.00 | 0.52 | 46 | 0.083 | 37.4 |
| | 70 hr | 1925° | 5.50 | 0.00 | 0.00 | 5.07 | 0.00 | 0.43 | 8 | 0.068 | 31.0 |
| | | Correction | | | | | | 0.01 | | 0.002 | 0.6 |
| | | Total | | | | | | 1.39 | | 0.22 | |
| No. 40 37027 Melt | 10 days | Room | 0.86 | 0.00 | 0.13 | 0.04 | 0.00 | 0.69 | 80 | 0.117 | 61.5 |
| | 15½ hr | 1200° | 0.69 | 0.00 | 0.17 | 0.09 | 0.00 | 0.43 | 62 | 0.073 | 38.5 |
| | 44 hr | 1925° | 0.43 | 0.00 | 0.00 | 0.43 | 0.00 | 0.00 | 0 | 0.0 | 0.0 |
| | | Correction | | | | | | 0.00 | | 0.0 | 0.0 |
| | | Total | | | | | | 1.12 | | 0.19 | |
| No. 37 56807 Ladle | 47 days | Room | 1.48 | 0.00 | 0.09* | 0.09 | 0.52* | 0.78 | 53 | 0.127 | 60.0 |
| | 15½ hr | 1200° | 0.68 | 0.00 | 0.00 | 0.34 | 0.00 | 0.34 | 50 | 0.055 | 26.2 |
| | 44 hr | 1925° | 1.98 | 0.09 | 0.00 | 0.86 | 0.86 | 0.17 | 9 | 0.029 | 13.1 |
| | | Correction | | | | | | 0.01 | | 0.002 | 0.7 |
| | | Total | | | | | | 1.30 | | 0.21 | |
| No. 8 36900 High-alloy | 20 days | Room | None | None evolved | | | | | | 0.000 | 0.0 |
| | 85 hr | 1025° | 9.06 | 0.08 | 0.00 | 2.12 | 1.78 | 5.08 | 56 | 0.850 | 98.7 |
| | | Correction | 0.13 | | | 0.03 | 0.03 | 0.07 | | 0.012 | 1.3 |
| | | Total | | | | | | 5.15 | | 0.86 | |

\* Indicative of air that leaked into tube.

\*\* Samples ranged in weight from 44.79 to 48.39 and calculated volumes from 5.71 to 6.15 ml.

and oxidized to 0.06 pct C. After deoxidizing with Mn and Si, the Cr was added in two additions. When about ready to top at 3200°F (optical), 212 cu ft (one tank) of argon was injected into the 2.3-ton heat. The gas was introduced through a refractory protected pipe near the bottom of the 14-in. bath and moved around considerably. After half the argon, the bath was sampled for hydrogen and a temperature reading taken, indicating a loss of 80°F. The second half of the tank was injected causing another 50°F drop. The heat was arced on 15 min to regain temperature, and tapped after the final Mn and Si addition. Hydrogen content after all Cr and before the argon was 0.60 R.V. This is identical with the same sample from H-5 which had a similar practice up to this point and the same absolute humidity. After one-half the argon, hydrogen content was 0.62 R.V., and after all the argon 0.60 R.V., indicating no elimination by the inert gas **under these conditions.** Hydrogen increased to 0.81 R.V. in tapping, apparently because of a green patch on the spout which could easily have escaped detection.

Such a purely mechanical flush would be expected to be less efficient in such a shallow bath than in a deeper ladle or induction furnace bath. However, argon could not be used in any other manner in the plant because of the temperature loss. Furthermore, had the hydrogen content been much higher and nearer the saturation point a greater inclination toward elimination might have been experienced. No doubt under some conditions hydrogen can be eliminated with argon. But an oxygen boil seems a more effective, less expensive and less complicated means of lowering hydrogen.

Nitrogen contents of these high alloy heats were 0.03 to 0.06 pct which is ten times the ranges of the carbon steels. The higher nitrogens were experienced on the dead-melt, high-return heats. Like hydrogen the lower nitrogens were obtained by boiling these heats or by the use of virgin alloys.

A condensed summary of the ten alloy heats is given in table VI.

The most apparent conclusions from the table are the high hydrogen contents of these steels, the variations possible, and the importance of melting practice. The highest contents near 1.00 R.V., resulted from dead melting high proportions of alloy return. Boiling these same charges easily

removed half the hydrogen. The use of virgin alloys, melting the Ni and adding the Cr, resulted in contents from 0.40 to 0.60 R.V. at tap. These heats experience a much greater tendency to increase in tapping all but two picking up 0.08 to 0.28 R.V. in the process. One 0.13 R.V. increase came from a thoroughly preheated new ladle that should have experienced no increase on carbon steels. Increases of 0.21 and 0.28 R.V. were apparently caused by new lined furnace spouts, suggesting that spouts and runners should receive the same attention as ladles. The other three were unaccounted for. This emphasizes the importance of steel composition and suggests that conditions that cause no absorption by carbon steels might produce considerable increases in alloy steels with greater affinity or capacity for hydrogen.

Although based on an insufficient number of tests, it appears that on high-alloy steels the basic heats are inclined to run slightly higher in hydrogen. In melting high return charges, the melt samples of the three basic heats averaged 1.00 R.V. while the two acid heats averaged 0.80 R.V. at melt. Absolute humidity averages were slightly in favor of the basic heats. On all three types of practice the lowest final hydrogen in each case was the one acid heat.

These results were limited to only a few of the alloy compositions. Similar quantitative data should be obtained on ferritic compositions of this alloy level, and intermediate alloy compositions.

### Analytical Study of Evolved Gas

The composition of the gas evolved as well as the rates of evolution are of some importance since they indicate how easily hydrogen might be driven from steel products before further processing. The progress of room temperature evolution of five typical samples is graphed in fig. 6.

The volumes are necessarily only relative and all are expanded by the reduced pressure of a 4- to 5-in. column of mercury but were corrected upon arrival at Battelle. Sample No. 4 might be followed as a typical example. This is a tap sample from heat No. 36894 with a total hydrogen content of 0.15 R.V. A sample weighing 44.79 gm with a calculated volume of 5.71 ml was floated up into an inverted mercury filled tube 3 min after casting.

After three days 0.35 ml of gas had displaced the mercury and collected in the tip of the tube. This volume increased to 0.50 ml after 12 days, and 0.80 ml after 40 days, after which it experienced no detectable increase in five more days and was stoppered for shipment. Compression of the rubber pad reduced the volume from 0.80 ml to 50 ml. After arriving at Battelle seven days later the corrected volume was found to be 0.42 ml. Table VII shows that this 0.42 ml of gas evolved from the metal specimen at room temperature was 81 pct hydrogen and 19 pct nitrogen. Vacuum extraction for 45 hr at 1925°F removed 1.52 ml more gas from the specimen. This high-temperature gas was found to be 50 pct carbon monoxide, 33.6 pct hydrogen, 11.2 pct nitrogen and 5.2 pct oxygen. Extrapolation based on reaction half-life periods indicated that 0.02 ml of hydrogen remained in the specimen. This made a total of 0.87 ml (STP) of hydrogen originally contained in the metal specimen as chill-cast. Hydrogen concentration in the metal calculated to be 0.00017 pct by weight or 0.15 Relative Volumes. Of this total hydrogen in the metal, 39 pct escaped in 52 days at essentially room temperature and pressure, 59 pct was vacuum-extracted in 45 hr at 1925°F, and a calculated 2 pct remained as residual.

The other samples followed a similar pattern. Sample No. 18 (from heat 36944 after Si block) evolved at room temperature the largest volume of gas and the largest proportion of its total hydrogen. Apparently, the fact that this sample was only silicon-killed accounts for its earlier and faster escape of hydrogen than the usual aluminum killed samples. Aluminum content seemed to have considerable effect on the rate and the proportion of the total hydrogen evolved at room temperature.

Three of the samples followed more closely for the first few hours indicated that a detectable bubble of gas collects in the top of the tube after 15 min and a measurable volume after one hour. Evolution curves of most of the samples flattened considerable after two days.



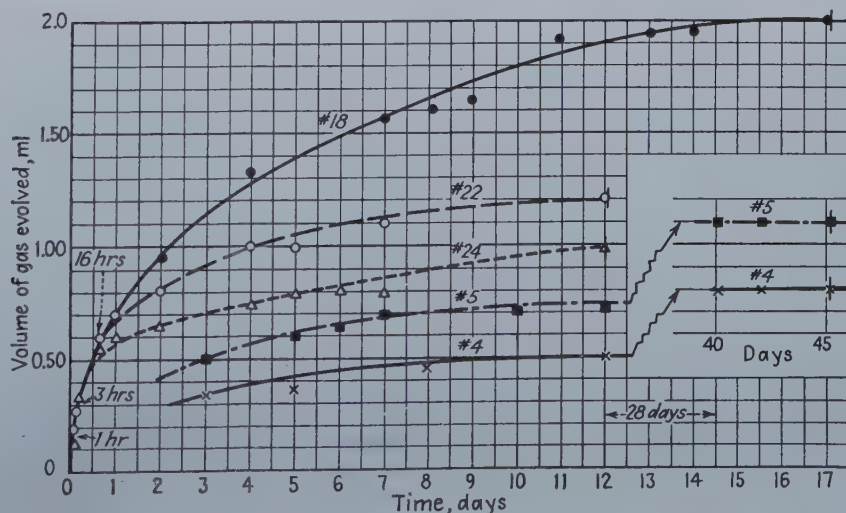Fig 6—Rate of gas evolution at room temperature.

## TABLE V
## High Alloy Steels

| Ht. No. / Lining / Type Steel | Atmos. Moisture, Grains Per Lb | Additional Sources Moisture | Charge and Furnace Practice | Approx. Composition As Melted, Pct | Carbon Drop Boil | No. | Sample Time Sample | Temp.* Deg. | Nitrogen Wt., Pct | Hydrogen Rel. Vol. |
|---|---|---|---|---|---|---|---|---|---|---|
| H-1  56817  Basic S  25 Cr-20 Ni | 62 | Dry | 80 pct Return + Ni. Dead melted with 3 pct Ore. Two additions 70 pct FeCr. Add Mn & Si. Tap CaSi. | 20 Cr  20 Ni  0.28 C | None | (48) | Melt | 2850 | | 1.00 |
| | | | | | | (49) | Mn & Si | 3200 | | 0.96 |
| | | | | | | (50) | Lad. U | 3250 | | 1.01 |
| H-2  36900  Acid S  25 Cr-20 Ni | 70 | New Ladle | 80 pct Return + Ni. Dead melted with 3 pct Ore. Two additions 70 pct FeCr. Add Mn & Si. Tap CaSi. | 18 Cr  20 + Ni  0.24 C | None | (6) | Melt | 2900 | | 0.64 |
| | | | | | | (7) | Tap | 3200 | | 0.73 |
| | | | | | | (8) | Ladle N | | 0.0572 | 0.86 |
| | | | | | | | Center | 4" Dry Sand Cstg. | | 0.84 |
| | | | | | | | Outside edge | 4" Dry Sand Cstg. | | 0.71 |
| H-3  56907  Acid S  18 Cr-9 Ni | 49 | Dry Chg. Alloys air dried | Rim Steel + Ni + 1 pct Ore. Melt to 0.07 C. FeCr added in two additions. Mn added. Tap CaSi. | 0 Cr  9 Ni  0.07 C | No boil  0.05 C/ melt | (108) | Melt | 3050 | 0.0067 | 0.22 |
| | | | | | | (109) | Tap | 3250 | 0.0380 | 0.40 |
| | | | | | | (110) | Lad. U | | 0.0351 | 0.42 |
| H-4  56901  Acid S  18 Cr-9 Ni | 24 | Dry Chg. Damp Cr. | Ditto. Damp FeCr. | 0 Cr  9 Ni  0.05 C | No. boil  0.07 C/ melt | (105) | Aft. ½ Cr | 3050 | 0.0226 | 0.57 |
| | | | | | | (106) | Tap | 3180 | 0.0332 | 0.66 |
| H-5  56839  Basic D  18 Cr-9 Ni | 20 | Dry | Rim Steel + Ni + Ore. Oxidized to 0.05 pct C. New reducing slag. Deox. FeCr added. | 0 Cr  9 Ni  0.05 C | No boil  0.07/ melt | (63) | Melt | 3050 | | 0.13 |
| | | | | | | (64) | Aft. all Cr | 3200 | | 0.60 |
| | | | | | | (65) | Lad. U | 3250 | 0.0242 | 0.79 |
| H-6  56821  Basic S  35 Ni Cast Iron | 68 | Dry Chg. | Rim Steel + Ni + Graphite. Dead melt. Add Si. Tap | 35 Ni  2.00 C | None | (46) | 10' Tap | 2850 | | 0.14 |
| | | | | | | (47) | Ladle U | | | 0.09 |
| H-7  56719  Acid S  25 Cr-20 Ni | 70 | Dry | 80 pct Return + Ni Melted. Boiled with 3.2 pct Ore at 3300°. FeCr added in two additions. Mn added. Tap CaSi. | 18 Cr  20 Ni  0.30 C | Boil  0.07 C/ 8 min | (9) | Bef. boil | 3200 | | 0.96 |
| | | | | | | (10) | Aft. boil | 3300 | | 0.40 |
| | | | | | | (11) | Tap | 3200 | | 0.36 |
| | | | | | | (12) | Ladle U | | 0.0373 | 0.48 |
| H-8  56833  Basic S  25 Cr-20 Ni | 40 | Slight leak on cooler. Green spout. | 70 pct Return + Ni melted. Boiled with 4 pct Ore. Fine FeSi on slag. FeCr added. Mn. Tap. | 18 Cr  20 Ni  0.25 C | Boil  0.06 C/ 12 min | (57) | Melt | 2950 | | 1.26 |
| | | | | | | (58) | Bef. boil | 3250 | | 1.00 |
| | | | | | | (59) | After boil | 3300 | | 0.45 |
| | | | | | | (60) | After Cr | 3200 | | 0.38 |
| | | | | | | (61) | Tap | 3300 | | 0.53 |
| | | | | | | (62) | Ladle U | | | 0.81 |
| H-9  56858  Basic S  25 Cr-20 Ni | 82 | Dry | 80 pct Return + Ni melted. O₃ added, (10 min 726 cu ft per 2.3 ton @ 100 psi) CaSi on slag. FeCr added. | 20 Cr  20 + Ni  0.27 C | Boil  0.09 C  12 min | (81) | Before O₂ | 3200 | | 0.86 |
| | | | | | | (82) | After O₂ | 3300 | | 0.57 |
| | | | | | | (83) | Tap | 3200 | | 0.48 |
| | | | | | | (84) | Ladle U | | | 0.56 |
| H-10  56863  Basic S  18 Cr-9 Ni | 20 | Green patch on spout. | Rim steel + Ni + 2½ pct Ore. Melt 0.06 C. Deox Mn + Si. Add Cr. Add argon (106 cu ft per 2.3 T in 5 min) Add more argon (106 cu ft per 2.3 T in 5 min) Regain temp. Add Mn. Tap. | 0 Cr  9 + Ni  0.06 C | No boil  0.06 C/ melt | (86) | Bef. argon | 3200 | | 0.60 |
| | | | | | | (87) | Aft. ½ argon | 3120 | | 0.62 |
| | | | | | | (88) | Aft. All argon | 3070 | | 0.60 |
| | | | | | | (89) | Ladle U. | 3300 | | 0.81 |

* Optical temperatures with 0.4 emissivity correction. In error according to emissivity variations of composition being read.

Three samples were given a 1-hr extraction at 1200° preliminary to the higher temperature treatment. One hour at this temperature removed 55 to 71 pct of the retained hydrogen. This was 24.7 to 38.4 pct of the total hydrogen. Two samples were given a 15½-hr extraction at 1200°F. On the melt sample (No. 40) all the hydrogen was removed, but on the ladle sample (No. 37) one third of the retained hydrogen or 13.8 pct of the total hydrogen was left. At this temperature the rate of evolution seems to be influenced considerably by the chemistry of the sample and not consistent enough to take advantage of the faster rate of evolution.

The high alloy sample (No. 36900) evolved no gas in 20 days at room temperature. An extended period of 85 hr at 1925° was needed to remove all the hydrogen but 1.3 pct left as residual. The gas evolved from this steel at 1925° was 56 pct hydrogen, 19.7 pct nitrogen, 23.4 pct carbon monoxide, 0.9 pct carbon dioxide, and no oxygen.

A sample of cast iron of 2.00 Si and 3.50 pct C content (not included in the table) evolved no gas at room temperature. One hour at 1200° extracted 83.6 pct of the total hydrogen while 45 hr at 1925° extracted 16 pct, and 0.4 pct was determined as correction. At 1200° hydrogen was 68 pct of the 3.22 ml evolved. At 1925° the 4.64 ml evolved was 88 pct carbon monoxide and only 9.1 pct hydrogen.

The free nitrogen evolved at room temperature and high temperature proved to be a variable fraction of the total content, which includes both free nitrogen and that stabilized by the formation of compounds. Aluminum content seemed to influence the proportion considerably. For instance, sample No. 22 in table VII being a boil sample was killed with a heavy aluminum addition that left a 0.24 pct Al residual. Total nitrogen of this sample was 0.00039 pct but no free nitrogen was evolved at room temperature or 1925°F. On the other hand the ladle sample from the same heat (sample No. 24 just below in table VII) contained only 0.052 pct Al from the regular ladle addition. This sample contained 0.0044 pct total nitrogen. Of this total 2.4 pct of it was evolved as free nitrogen at room temperature and 12.6 pct of it at the 1925° temperature, leaving 85 pct retained by the metal.

### Summary

Using simple equipment, samples of molten steel from the furnace were chilled, enclosed in gas tight tubes, and expressed to laboratory facilities for hydrogen analyses. Certain phases of furnace practice were deliberately exaggerated to emphasize their individual effects on hydrogen. In some cases moisture was deliberately made available to emphasize the susceptibility of the particular steel toward hydrogen absorption under the conditions prevailing.

The limited data obtained suggested certain relations and effects that should be confirmed by more quantitative data, further variation of certain variables and investigation of more types of steel. The following conclusions seemed to be suggested or confirmed.

(1)—The chemistry of the metal was found to have considerable effect on hydrogen absorption tendencies. Mild-carbon steels finished with hydrogen contents of 0.11 to 0.35 R.V. in spite of attempts to get higher. On the other hand austenitic Cr-Ni steels under more favorable moisture conditions ran over four times as high, ranging from 0.42 to 1.01 R.V. Conditions that contribute no hydrogen to one type of steel might cause considerable increases in another composition type.

(2)—The chemistry of the metal also seems to influence the ease of hydrogen escape from the solidified metal. Carbon-steel samples begin to give off part of their hydrogen at room temperature within a few minutes after casting and a considerable fraction after a few days. On the other hand several austenitic compositions have eliminated no hydrogen at room temperature and have required longer time at high temperatures. This difference would be important in determining the removal of hydrogen by heat treatment and the proportion retained in remelting charges of such steel.

(3)—A general effect of atmospheric humidity and excess moisture was apparent. In several cases where the practices were equivalent, slightly higher melt down hydrogens and final hydrogens were obtained from the higher moisture condition. However, the hydrogen equilibrium tendencies between the metal and the atmosphere can be influenced greatly by the chemistry of the metal and the sequence of operations. Hydrogen absorption has been resisted or limited to such an extent that some heats with a continuous spray of water finished lower than other heats exposed only to asmospheric moisture.

(4)—Final hydrogen seems to be the net result of five separate fractions

| I | II | III |
|---|---|---|
| $H_2$ from metal charge | $\pm$ $H_2$ absorbed or lost in melting | — $H_2$ eliminated by the boil or flush |

| IV | V | |
|---|---|---|
| $+$ $H_2$ absorbed in furnace in finishing | $+$ $H_2$ absorbed in tapping into ladle | = Final total hydrogen |

These phases are not equally important on all practices and all types of steel. In some cases hydrogen at melt is very high from I and II and no amount of care can produce a low hydrogen without an extensive elimination process represented by III. In other cases hydrogen content might be very low as melted in which case prevention of absorption in IV and V would be a more important objective than attempted elimination.

(5)—Because of maximum affinity for hydrogen in the ready-to-tap condition hydrogen increases from improperly dried ladles, spouts, etc. apparently ruin more heats than conditions within the furnace. Hydrogen pickup from a "green" ladle has been prevented but considerable preheating at high temperatures was required to

remove the combined water in clay refractories.

(6)—Under conditions of equivalent exposures, low-hydrogen heats were more inclined to absorb additional hydrogen than heats already high in hydrogen.

## Carbon Steels

(1)—With the acid-electric practice used by most foundries very low hydrogen contents of 0.11 to 0.15 R.V. in the ladle were experienced on foundry-grade carbon steel.

(2)—Such a practice consisting of an oxidizing melt, a boil of considerable violence, an oxidizing final slag, and a short deoxidation time seems to be surprisingly resistant to extremes in moisture exposure. With wet charges, "green" furnace hearths, and continuous water sprays commercially low hydrogen contents of 0.13 to 0.18 R.V. were still obtained and no pinholes encountered. Early exposures to moisture in the charge or during melting need not cause fear if followed by such a practice.

(3)—A rimmed steel charge with no boil, but very oxidizing conditions throughout, produced a low hydrogen content of 0.12 R.V. in the ladle. A similar heat continuously sprayed with water produced a reasonably low hydrogen of 0.18 R.V. This is considered evidence of the effectiveness of an extremely oxidized metal-slag-atmosphere system in resisting hydrogen absorption, at least when the source of hydrogen is moisture above the slag. This also indicates one case in which elimination is not so essential because of the low original hydrogen.

(4)—However, the average furnace charges would be expected to melt with enough hydrogen to require some elimination. The most consistent means found for obtaining a low hydrogen was maximum elimination by vigorous boiling followed by efforts to prevent reabsorption of hydrogen by maintenance of oxidizing conditions.

(5)—The factor that shows the most effect on elimination effectiveness was the violence of the boil. The concurrent state of oxidation seems influential, but not directly in the elimination process as much as in the prevention of hydrogen increases before and after the boil. Prolonging the boil does not seem to improve the effectiveness of the elimination but does seem to decrease the probability of reabsorption when extended at the expense of a shortened deoxidation period.

(6)—Further evidence was obtained that hydrogen is absorbed more readily after deoxidation. A leak after blocking, and a water spray after deoxidizer addition produced two hydrogen contents of 0.25 R.V. Reducing second slags produced the highest final hydrogen 0.21 to 0.35 R.V. Efforts toward perfectly dry materials and the absence of leaks should be concentrated on this period.

## High Alloy Steels

(1)—Ten heats of Cr-Ni steel ran 0.42 to 1.01 R.V., indicating an affinity or capacity for hydrogen increased several times over carbon steels by the alloys present. However, the critical concentration from the standpoint of porosity seems to be raised also since no gas porosity was found in these steels with such hydrogen contents.

(2)—No hydrogen was emitted from the chilled samples at room temperature and very little from the surface of a four inch casting in solidifying and cooling. The concentration at the center of such a section was practically identical with the ladle analysis. Virtually complete hydrogen retention would be expected in scrap remelting, requiring a very positive attack from the standpoint of melting practice.

(3)—Chromium seems to be the alloy that produces the affinity for hydrogen. The nickel content seems to be the cause of the strong retention of hydrogen probably because of its austenitizing influence and the resulting higher solubility. This would suggest less likelihood of porosity in the austenitic compositions but a greater buildup of hydrogen in return scrap.

(4)—Some of the lowest hydrogen contents were obtained by using all virgin alloy. By withholding the Cr, reasonably low hydrogen contents were obtained from the melt of rimmed carbon steel and nickel. Any elimination attempts at this point would have been superfluous. The most profitable objective was found to be the reduction of opportunities for absorption after the Cr addition, which accounted for over two-thirds of the hydrogen.

(5)—The highest hydrogen contents (0.86 and 1.01 R.V.) were obtained from dead-melting high proportions of high-alloy return. In this case the hydrogen was obtained at melt (from fractions I and II). Such heats seem destined for an equal or higher final content without an effective elimination procedure.

(6)—A carbon boil produced by either oxygen or ore at high temperatures proved very efficient in eliminating half or more of such high hydrogens. Relatively small carbon drops produced decreases of 0.96 to 0.36 R.V., 1.00 to 0.38 R.V. and 0.86 to 0.46 R.V.

(7)—Comparable effects of furnace practice were noted on both acid and basic linings. In each of three types of melting procedure used on these high-alloy heats the acid heats produced the lowest hydrogen content in each group.

(8)—Because of their greater affinity for hydrogen these high alloy compositions experienced much higher increases in tapping.

# Inductive Stirring in Arc Furnaces

by Sven Fornander

and

Folke Nilsson

## (4) The Reducing Period

THE effort of the steelmaker during the reducing period in the arc furnace has been aptly characterized as a battle against oxygen. If the oxygen content of the bath can be decreased, this will contribute substantially towards a quick desulphurization and towards a cleaner steel.

In the manufacture of constructional steels of the type made in the experimental heats one to four the following practice has been applied at Surahammar for a number of years. After "slag off" an aluminium addition of about 1 lb. per ton is made to the slag-free bath. Immediately afterwards the bulk of the silicomanganese is added as well as burnt lime, fluorspar, pulverized ferrosilicon and coke powder. Carbide slags are not used. A white slag is aimed at.

Sven Fornander is Research Manager of Surahammars Bruks AB, Surahammar, Sweden, and Folke Nilsson is General Manager, Hagfors Steelworks, Uddeholms AB, Uddeholm, Sweden.

Aluminium determinations made on mold samples, which are taken during the reducing period, show that the aluminium content of the steel bath has decreased to 0.002 pct Al already 30 min after the addition was made. The aluminium determinations were carried out by the Metallografiska Institute by means of a spectrographic method, which was developed there[7] and which has a good accuracy. It is improbable that an aluminium content as low as 0.002 pct would affect the properties of the finished steel. Therefore it can be said that by an aluminium deoxidation no new factor has been introduced in the steelmaking process, which could have an influence upon steel quality. The advantage of this practice is, that the deoxidation proceeds rapidly, at least in the beginning.

At the Uddeholm furnace all experimental heats were made without an early deoxidation. The practice applied was the same as that described by Marsh[8] and by Urban and Derge[9].

a—Deoxidation: Fig 15 shows the change with time of the oxygen content of the steel during the reducing period for the heats one to four. Each curve represents an average between two heats. It is obvious that the oxygen content of the steel decreases more rapidly in the heats made with inductive stirring. It can be seen from the curves that if it is intended to produce a steel of the type in question with a certain oxygen content before tapping, the time under reducing slag can be shortened by 30 to 40 min with the aid of the electric stirrer. For

This is the concluding portion of a two-part article. Last month the authors described the type of inductive equipment developed in Sweden to accelerate metallurgical reactions and speed the refining period. Herein are described factors developed during the reducing period, specific effects on refractory linings and economical aspects related to the use of the stirrer.
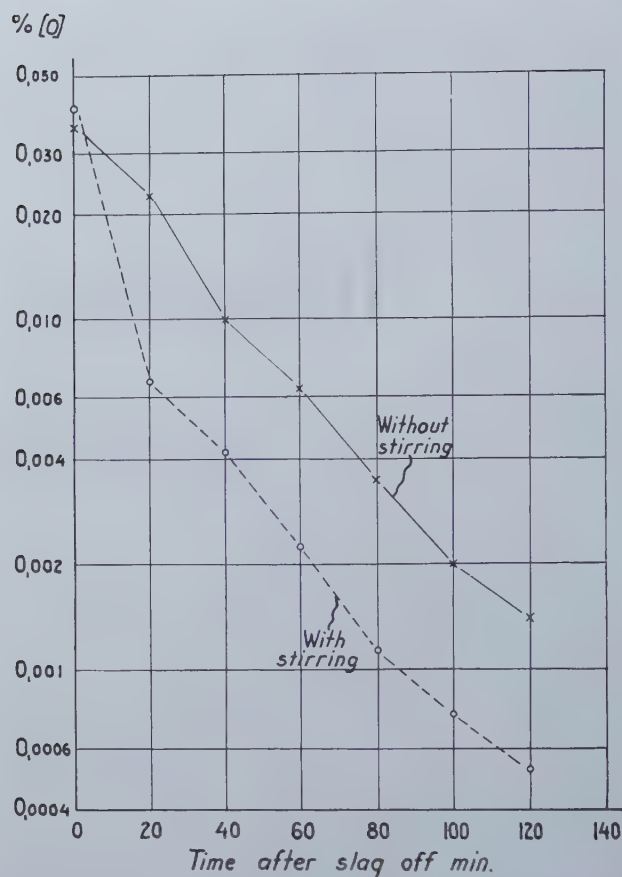


Fig 15—Deoxidation during reducing period, heats No. 1 to 4.

certain other types of steel the time saving is considerably greater, 1 hr or even more according to experience. It should perhaps be pointed out that the oxygen contents obtained in the steel bath just prior to tapping in the heats made with stirring are lower than any, which have been reported in the literature.

The experience gained at the Uddeholm furnace points in the same direction. Fig 16 shows the change with time of the oxygen content of the steel during the reducing period for four heats made with inductive stirring as well as for four additional heats, made in a conventional way for comparison. The diagrams cover the period of time from the end of slagging off to the last sample before the additions. As will be seen from the diagrams the oxygen contents at the end of slagging off were rather different in the different cases. All the heats in which the stirrer was used had lower oxygen contents towards the end, irrespective of whether the oxygen was higher or lower than in the comparable heats at the beginning.

To estimate the gain in time to be achieved by use of the stirrer only the heat pairs 5-6 and 12-13 are suitable. In heat No. 11 the oxygen content of the last sample is about 1/5 of that in the comparison heat No. 10. However, the oxygen contents at the beginning of the reducing period are so different that a comparison seems not to

be justified. In the heat pair 8-7 the reducing time was too short and the FeO content of the slag too high for conclusions to be drawn. From the diagrams the conclusion was drawn that the use of the stirrer permits a shortening of the reducing time by about 30 min if the deoxidation only is taken into account.

Reverting to the question of how the inductive stirring promotes a more rapid and complete deoxidation the following suggestions may be advanced. When the deoxidizing agents—aluminium, silicon and manganese—have been added to the steel bath, which contains oxygen, deoxidation products are formed. These consist mainly of oxides of Al, Si and Mn. If the deoxidation products are finely divided, it takes time before they are removed from the bath, as they rise to the surface only slowly to dissolve in the slag. As a result of the stirring during the reducing period, perpetually "new" parts of the steel bath come into contact with the lower surface of the slag layer. Until this aspect has been studied in detail it could be assumed that, during the first part of the reducing period, the deoxidation products stick to the slag. Thus the deoxidation products are continuously washed out from the steel by the slag.

As will be seen from fig 15 the deoxidation proceeds even after the effect of the deoxidizers has ceased, published investigations[13] showing that a
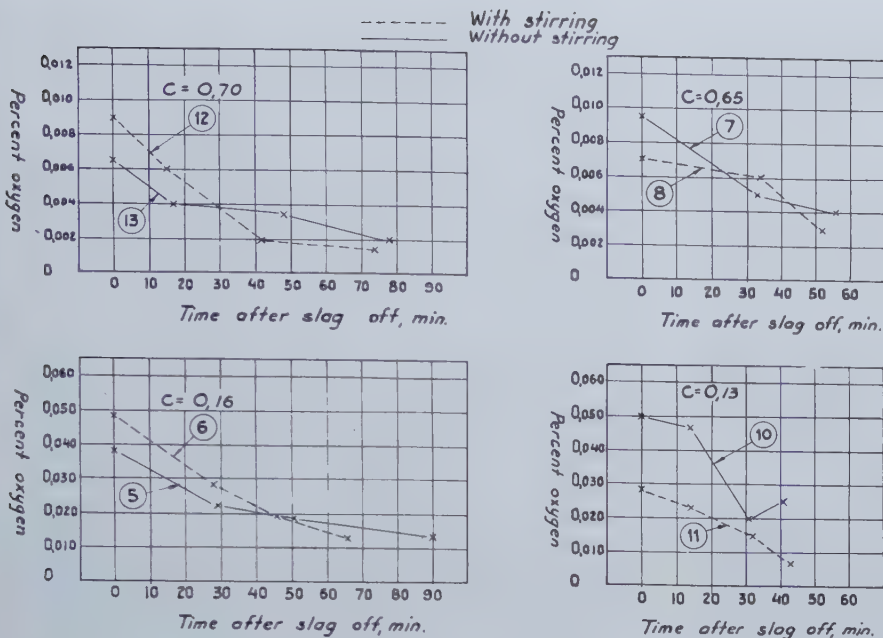
Fig 16—(Left) Deoxidation during reducing period, heats No. 5 to 13.

Fig 17—(Below) Desulphurization during reducing period, heats No. 1 to 4.

steel bath containing 0.3 pct Si and 0.7 pct Mn can hold about 0.010 pct 0 in solution. Fig 15 shows on the other hand that the oxygen contents obtained just prior to tapping are of the order of 0.001 pct 0. Therefore it is assumed that the deoxidation which occurs during the latter part of the reducing period takes place as a result of the following circumstances. The FeO activity of the steel bath, defined in the usual way, is of the order of 0.05 at 1600°C if the oxygen content is 0.010 pct 0. In the same circumstances

[7] G. Carlsson: "Spektralanalytisk bestämning av laga aluminiumhalter i stål" (Spectrographic Determination of Low Aluminium Contents in Steel), Jernkontorets Annaler 126, 1942, pp. 161/176.

[8] J. S. Marsh: "Slag-Metal-Oxygen Relationships in the Basic Open-Hearth and Electric Processes", Trans. A.I.M.E. 162, 1945, pp. 672/684.

[9] S. F. Urban and G. Derge: "Oxygen in Basic Electric-Furnace Baths", Trans. A.I.M.E. 172, 1947, pp. 196/211.

[10] D. A. Oliver and T. Land, "The Temperature Distribution in the Liquid Steel in Various Steelmaking Furnaces". Journ. Iron Steel Inst. 145, 1942, pp. 245/277.

[11] H. Pettersson: "Tillståndsdiagram för basiska stalslagger". (Phase Diagrams for Basic Steel Slags). Jernkontorets Annaler 132, 1948, pp. 42/56.

[12] A. L. Bradley, J. H. Chesters, J. M. Ferguson and R. J. Sarjant: "The Basic Open-Hearth Furnace". Iron Steel Inst., Spec. Rep. No. 33, London 1946, pp. 117/154.

[13] F. Koerber and W. Oelsen: "Grundlagen der Desoxydation mit Mangan und Silizium" (Fundamentals of the Deoxidation with Manganese and Silicon). Mitt. Kais.-Wilh.-Inst. Eisenforschg., Düsseld. 15, 1933, pp. 271/309.

the FeO content of the slag is low, about 1 pct. Although no investigations have been reported on the correlation between FeO activity and FeO content for slags of this kind it seems to be justifiable to assume that the FeO activity is low, of the order of 0.005. If there is to be an equilibrium between steel and slag, it is required that the

% [S]
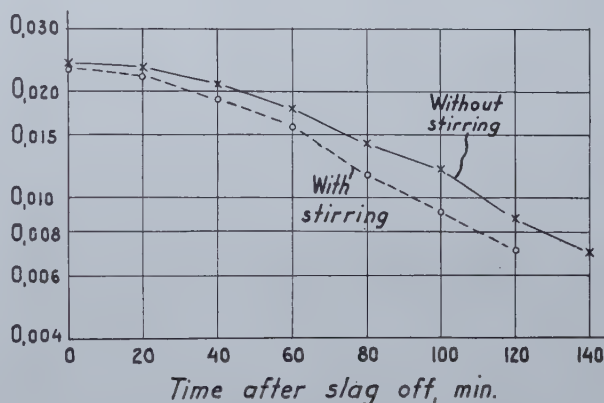


FeO activity is the same in both phases. As a result FeO has a tendency to escape from the steel bath and accumulate in the slag. In this case it is a question of a diffusion process which takes place in the surface of contact between slag and steel. The stirring can be said to enlarge this surface and for this reason a more effective deoxidation is obtained.

**b—Desulphurization:** Fig 17 shows the change with time of the sulphur content of the steel bath during the reducing period for the heats one to four. Desulphurization was good in both cases, when stirring was used and when it was not used. The rate of desulphurization is somewhat greater for the heats made with inductive stirring. The use of the stirrer has brought about a time saving of about 20 min. The remark above concerning oxygen is applicable to sulphur also: for certain other types of steel the time saving is greater, up to one hour.

Table VI shows the desulphurization obtained at the Uddeholm furnace. As will be seen from the table the stirrer brings about a more rapid desulphurization. Experiments on a somewhat larger scale than recorded in the table gave the following result. When stirring was not used the

refining time required to obtain an effective desulphurization amounted to 1½ hr. By use of inductive stirring the time could be shortened by 25 min.

**TABLE VI**
**Desulphurization at 15-Ton Furnace**

| Number of Heats | Stirring | Refining Time, Min. | Percent [S] | | Desulphurization, Pct S per hr |
|---|---|---|---|---|---|
| | | | At Slag Off | Prior to Tapping | |
| 6 | None | 89 | 0.029 | 0.020 | 0.006 |
| 6 | Inductive | 87 | 0.030 | 0.016 | 0.009 |

As to the reason why the inductive stirring promotes a quicker desulphurization the following circumstances should be taken into account. The desulphurization takes place according to the reaction

$$[FeS] + (CaO) = (CaS) + (FeO),$$
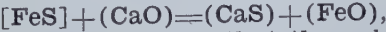
square brackets denoting that the substance is dissolved in the metal and parentheses that it is dissolved in the slag. According to this reaction the sulphur in the steel bath occurs as iron sulphide. This reacts with CaO in the slag, the reaction products being CaS and FeO, which are both in solution in the slag. Thus, the reaction

(1) During carbon refining the temperature is the same in different parts of the bath, and this is the case irrespective of whether the stirrer is used or not.

(2) Readings taken during the reducing period and without use of the stirrer showed a maximum temperature difference of 19°C between the surface and bottom layers of the bath.

(3) When the stirrer was used during the reducing period, no temperature difference was recorded between the surface and bottom layers.

In taking temperature readings at the 10-ton Surahammar furnace without use of the stirring coil it was difficult to obtain reliable results during the reducing period. The reason seemed to be that the pyrometer could not be kept steady during the measurement. Moving a short distance, say 2 in, would in some cases result in a change of the reading by 10° C or more. When the stirring current was switched on, it became easy to take readings, for the temperature was then the same in various parts of the bath.

A special technique was developed to measure the temperature of the slag. The hot junction of



Fig 18—Concentrations in surface and bottom layers of the steel bath.

takes place in the surface of contact between steel and slag only, this being the reason why the desulphurization in the arc furnace takes time. It is obvious that an inductive stirring makes it possible for the desulphurizing reaction to proceed faster, because it always brings new parts of the bath into contact with the slag, and probably causes a mild stirring in the slag layer itself.

**c—Temperature distribution:** British investigations carried out by Oliver and Land[10] have shown that in an arc furnace without stirring the temperature difference between various parts of the bath can amount to about 50° C in the reducing period. In these investigations specially designed pyrometers were used allowing temperature determinations to be made at various bath depths.

At the 15-ton Uddeholm furnace a fairly detailed investigation was made of the temperature distribution in the bath. The results obtained can be summarized thus:

the thermocouple was protected by two thin-walled silica sheaths, one inserted into the other. To make a determination the hot junction of the thermocouple is first immersed in the steel bath, the temperature of which is recorded. To attain temperature equilibrium a somewhat longer time is required than normally: about 30 sec as compared with about 15 sec. Then the silica sheaths are placed horizontally in the slag layer. After a further 15 sec the slag temperature is recorded. By the time the reading has been made, the outer silica sheath has usually dissolved in the slag layer, only the inner sheath remaining. Perhaps it should be added that measurements of this kind are not always successful.

The following series of measurements illustrate the importance of the inductive stirring for the heat transfer from the slag to the bath. During the whole experiment the power input to the 10-ton furnace was kept constant at 3500 kW. (The power input required to keep the bath at a constant temperature is approximately 800 kW).

Time,
min

0    Clear melt. Stirring current switched on 30 min previously. Bath carbon = 0.12 pct. Bath quiet; no boil.
12   Steel temperature = 1610°C. Slag temperature = 1636°C.
13   Stirring current switched off.
20   70 kg iron ore + 150 kg burnt lime added.
25   Weak boil.
30   Steel temperature = 1620°C. Slag temperature = 1722°C.

With this high power input to the furnace the difference between the temperatures of the slag and the steel was 26°C as long as the electric stirrer was in operation, and increased to 102°C 17 min after the stirring current had been switched off.

**d—Concentration distribution:** There is no reason to expect that the stirring would affect the distribution of the alloying elements in the steel bath during the carbon refining period. The bath is then homogeneous with respect to concentration and temperature.

During the reducing period conditions are different, and this is so especially shortly after alloy additions have been made. A study of these conditions was made at the Uddeholm furnace, see fig 18.

Heat No. 9 was made with inductive stirring. The concentrations of the alloying elements silicon and manganese are the same in the surface and bottom layers of the bath within 6 min of making the additions. Heat No. 11 was thoroughly rabbled by hand three times during the first 9 min after the addition, but in spite of this there are still large differences between the concentrations in the surface and bottom layers of the bath 12 min after the addition. In heat No. 10, which was neither stirred nor rabbled, the differences are larger still.

This experiment has been confirmed many times in everyday practice by both of the companies that took part in this investigation. It is obvious that inductive stirring affords an exceedingly good chance to obtain a homogeneous bath shortly after additions have been made. This property of the stirrer would be used to the greatest advantage in the manufacture of high-alloy steels, e.g. high speed steels and stainless steels.

**(5) The furnace lining:** According to the experience gained at Surahammar and at Uddeholm there is nothing which indicates that the life of the furnace bottom is affected by the electric stirrer, either favourably or unfavourably.

However, the investigations carried out by the two works have brought to the fore a question of great principal interest for steelmaking in the basic furnace, namely the role of the lining in the process. Some of the results obtained indicate that the lining gives off oxygen to the steel bath during the reducing period. The same hypothesis has previously been put forward by Marsh[8].

The phase diagrams for the systems composed of the oxides of iron and the basic oxides CaO and MgO are not known in detail[11]. However, it is obvious that a basic furnace lining can hold in solution at 1600°C a considerable amount of FeO, something between 10 and 30 pct[12]. Therefore the quantity of oxygen in form of FeO, which can be absorbed by a furnace bottom is many times greater than that dissolved in the steel.

Thus there is a good reason to study in rather more detail the effect of the furnace lining upon the course of the reactions taking place in the basic steel furnace. It is to be hoped that coming investigations will clarify this question.

**Economical aspects:** It will not be possible to make a generally applicable calculation of the savings which can be made by the installation of an electric stirrer. The profit obtained will depend upon the local conditions at the steelworks in question, and it can be stated only when these conditions are known.

At the two works which took part in this investigation experience has shown that the installation of the electric stirrer is well warranted from an economic point of view. In the authors opinion Dr. Dreyfus invention is one of the most valuable contributions made to the development of the arc furnace since its introduction in the steel industry 50 yrs ago. It is delicate to make predictions but it would not be surprising if the electric stirrer would in the future be regarded as the one device, which the arc furnace needed to allow it to compete successfully with other types of furnace as far as large-scale production of quality steels is concerned.

**Summary:** During 1½ yr operation of ASEA electric stirrers on arc furnaces the following information was gathered at two Swedish steelworks.

The inductive stirring has no influence upon carbon refining at high or medium carbon contents. In the production of low-carbon steels the stirring makes it possible to attain lower carbon contents. In spite of this the oxygen content of the steel is lower and the FeO content of the slag lower than in conventional practice.

The slagging-off operation is considerably facilitated by the stirring and can be carried out more effectively than in normal practice. Oxidizable impurities, e.g. phosphorus and chromium, can be removed effectively.

The reactions occuring between steel and slag during the reducing period are accelerated. Extremely low oxygen contents can be attained. The reducing time can be shortened.

The differences in temperature and concentration in the bath during the refining period are equalized by the inductive stirring. The heat transfer from the arcs to the steel bath is facilitated.

The installation of the stirrer is well warranted from an economic point of view.

# The Iron-Nitrogen System

by V. G. Paranjpe, Morris Cohen, M. B. Bever, and C. F. Floe

The iron-nitrogen system was investigated by X ray diffraction measurements and a controlled nitrogenizing method. The latter is an innovation and depends on the relation between the nitrogenizing power of an ammonia-hydrogen mixture and the nitrogen content of the iron-nitrogen alloy produced. Several heretofore controversial features of the iron-nitrogen phase diagram are clarified.

NITROGEN is becoming recognized as one of the important elements in ferrous physical metallurgy. Several investigations indicate that nitrogen plays a significant part in such phenomena as strain aging and temper brittleness. Nitrogen is known to be a powerful austenite stabilizer and may be a useful alloying element in stainless steels. The hardenability of steels has been found to be increased by nitrogen. The nitriding and carbonitriding pro-

V. G. PARANJPE, M. COHEN, M. B. BEVER, and C. F. FLOE are on the Staff, Department of Metallurgy, Massachusetts Institute of Technology, Cambridge, Mass.

This paper is based on a part of a thesis submitted by V. G. Paranjpe at the Mass. Inst. of Tech. in partial fulfillment of the requirements for the degree of Doctor of Science in Metallurgy, Sept. 1949.

cesses are examples of successful industrial application of nitrogen in ferrous materials. For a complete understanding of the various roles played by nitrogen in ferrous metallurgy a knowledge of the phase relations in the binary iron-nitrogen system is essential.

The literature contains a variety of iron-nitrogen phase diagrams. Those suggested by Fry,[1] Sawyer,[2] Epstein and his coworkers,[3, 4] Lehrer,[5] Eisenhut and Kaupp,[8] and Hägg[7, 8] differ significantly from one another. Moreover, the most recent of these investigations dates back about twenty years. A redetermination of the entire diagram, therefore, appeared desirable.

In addition to the published phase diagrams, investigations have been carried out on portions of the iron-nitrogen system. Bramley and Haywood[9] determined the composition and temperature of the iron-iron nitride eutectoid. The maximum solubility of nitrogen in $\alpha$ iron was investigated by Portevin and Seferian[10] and by Dijkstra.[11]

Several investigators have determined the crystal structure of the various iron-nitrogen phases. In fact, Eisenhut and Kaupp[8] and Hägg[7] based their entire phase diagrams on the results of such studies. Epstein[4] and Emmett[12] reported lattice-parameter measurements on the $\epsilon$ (hexagonal close-packed) phase. Osawa and Iwaisumi[13] also studied the change in lattice parameters of the $\alpha$, $\gamma'$ and $\epsilon$ phases with nitrogen content. Brill[14] and Hägg[7] showed that the $\gamma'$ phase has an ordered structure, and Hendricks and Kostings[15] suggested a structural relation between the $\epsilon$ and $\zeta$ phases. In a recent investigation Jack[16] carefully studied the super-lattice reflections from the $\gamma'$ and $\zeta$ phases.

## Experimental Procedure

A large variety of experimental methods has been used by previous investigators in studying the iron-nitrogen system. These methods include thermal analysis, microscopic examination, X ray diffraction, magnetic measurements, dilatometric analysis and anelastic experiments. Thermal analysis is of low accuracy in determining changes in the solid state. This accuracy is further decreased for iron-nitrogen alloys since composition changes will occur during heating or cooling unless extreme care is taken to use a proper atmosphere. Metallographic methods are of small value because homogeneous iron-nitrogen alloys of sufficient size can be produced only with great difficulty. The dilatometric method is open to the same objections as thermal analysis in that changes in composition may occur during heating and cooling. Lattice parameter measurements by X ray diffraction can be used satisfactorily for determining phase boundaries if cooling is fast enough to prevent structural changes.

In view of the limitations of the various other techniques two methods only were adopted in this investigation, (1) X ray diffraction measurements, and (2) a controlled nitrogenizing method. The second method is an innovation for investigating the iron-nitrogen system, and will be described at length.

**Materials:** All iron-nitrogen alloys were prepared from carbonyl iron powder of the analysis shown in table I. The average particle size was about 20
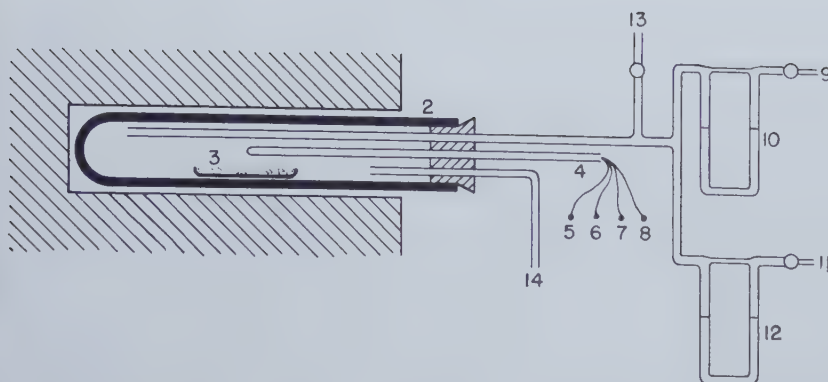
Fig. 1—Schematic diagram of the nitrogenizing equipment.

1 Furnace
2 Quartz chamber
3 Alundum boat
4 Thermocouple protection tube
5, 6 Control thermocouple
7, 8 Measuring thermocouple
9 Hydrogen inlet from tank
10 Hydrogen manometer
11 Ammonia inlet from tank
12 Ammonia manometer
13 Nitrogen inlet for flushing
14 Exhaust

microns. The carbon content was lowered to 0.010-0.015 pct by treatment with wet hydrogen prior to nitrogenizing.

**Table I. Chemical Analysis of Carbonyl Iron Powder**

| Constituent | Weight Pct |
|---|---|
| Carbon — before decarburization | 0.030 |
| Carbon — after decarburization | 0.010-0.015 |
| Copper | Nil |
| Chromium | Nil |
| Manganese | Nil |
| Molybdenum | Nil |
| Nickel | Nil |
| Nitrogen | 0.003 |
| Phosphorus | Nil |
| Silicon | 0.001 |
| Sulphur | Nil |

The nitrogenizing was carried out by the use of ammonia-hydrogen mixtures. The ammonia was at least 99.98 pct pure and the hydrogen analyzed less than 0.5 pct oxygen. The prepurified nitrogen used for flushing the nitrogenizing furnaces contained less than 0.001 pct each of hydrogen and oxygen.

**Nitrogenizing Procedure:** The procedure used for controlled nitrogenizing was evolved after many trials. The nitrogenizing equipment used is shown schematically in fig. 1.

A weighed amount (approximately 2 g) of carbonyl iron powder was spread uniformly in a new alundum boat. The boat was then inserted into the nitrogenizing chamber which was at the desired temperature. The nitrogenizing chamber was then sealed. Prepurified nitrogen was passed through the chamber during sealing and its flow was continued for about 5 min. The sample was first decarburized with wet hydrogen for about 6 hr. The controlled nitrogenizing treatment was then conducted by passing the desired ammonia-hydrogen mixture over the sample for 16 hr. At the end of this period, the ammonia-hydrogen mixture was shut off and the container was flushed for 1 min with prepurified nitrogen. The seal was then broken, with nitrogen still flowing, and the sample was quickly withdrawn and quenched into a beaker of cold water. This last step was carried out in less than 30 sec. The quenched samples were cleaned with alcohol and ether, dried and prepared for X ray and chemical analysis.

As shown in fig. 1 two chromel-alumel thermocouples were used, one for furnace control and the other for temperature measurement. The variation of temperature along the length of the alundum boat as determined by exploration was less than

0.5°C. The maximum deviation from the desired temperature in any series of experiments was found to be less than 2.0°C. This value includes all accidental changes in temperature.

**Chemical Analysis of Iron-Nitrogen Alloys:** The nitrogen content of nitrogenized samples was determined by the micro-Kjeldahl method. The results were found to be reproducible within about 10 pct of the nitrogen content for low nitrogen samples (up to 0.1 pct), and within about 1 to 5 pct of the nitrogen content for high-nitrogen samples (up to 11.2 pct nitrogen). The micro-Kjeldahl method was also compared with the vacuum fusion method and good agreement was found.

The hydrogen content of the nitrogenized alloys, determined by the method of Carney, Grant and Chipman,[17] was found to be negligible (approximately 5 parts per million by weight).

**X Ray Examination of Iron-Nitrogen Alloys:** The structures and lattice constants of the various iron-nitrogen phases were computed from Debye-Scherrer and Phragmen diffraction patterns. Cobalt K radiation was used because iron is known to be a filter for the $K_B$ radiation. The absorption-edge effect decreases the atomic scattering factor of iron and thus increases the relative contribution of the nitrogen atoms.

Samples used for X ray analysis were quenched from the nitrogenizing temperatures as previously described. The quenching rates employed were high enough to suppress structural changes during cooling with the exception of the martensite transformation in the $\gamma$ phase of low nitrogen content.

The disappearing phase method and the lattice parameter method were used to determine the phase boundaries from the results of X ray measurements. Preference was given to the results of the latter.

**Phase Boundary Determination by the Controlled Nitrogenizing Method:** This method consists in principle of nitrogenizing iron with a gas mixture of controlled "nitrogenizing power" and correlating the nitrogenizing power of the gas mixture with the nitrogen content of the iron-nitrogen alloy produced.

In the nitrogenizing of iron with mixtures of ammonia and hydrogen, the nitrogenizing power at a given temperature is governed predominately by the ratio of ammonia to hydrogen as suggested by the following equation:

$$NH_3 \text{ (gas)} = N \text{ (in an iron-nitrogen phase)} + 3/2\, H_2 \text{ (gas)}$$

When this reaction attains equilibrium, the nitrogen content of the iron-nitrogen phase is fixed by the nitrogenizing power of the gas mixture. The nitrogenizing power may be expressed in terms of the ammonia content of the nitrogenizing gas.

The scheme of determining the phase boundaries in the iron-nitrogen diagram by nitrogenizing with ammonia-hydrogen mixtures can be explained with the aid of fig. 2. Fig. 2a shows schematically a portion of the iron-nitrogen phase diagram, and fig. 2b shows the relation between the nitrogen content of iron-nitrogen alloys and the ammonia content of the nitrogenizing gas. The solid curve in fig. 2b pertains to equilibrium conditions. For a given temperature an increase in the ammonia content of the nitrogenizing gas causes a corresponding increase in the nitrogen content of the alloy. Thus the nitrogen concentration of the $\alpha$ phase increases steadily from 0 to A″ as the ammonia content of the gas increases from 0 to A′. When the ammonia concentration reaches the value A′ and the nitrogen content of the $\alpha$ phase becomes A″, the $\gamma'$ phase can exist together with the $\alpha$ phase. For this gas mixture the nitrogen content of the solid may, therefore, lie anywhere between A″ and B″ where B″ is the lower limit of the $\gamma'$ phase. (See fig. 2b.) A further increase of ammonia concentration produces only the $\gamma'$ phase. The nitrogen content of this phase increases with the ammonia concentration of the gas, until at an ammonia content C′, the $\gamma'$ phase having a nitrogen content C″ can co-exist with the $\epsilon$ phase of composition D″. A further increase of ammonia concentration only serves to enrich the $\epsilon$ phase in nitrogen.

A series of nitrogenizing experiments made at a temperature $T$, with progressively increasing ammonia concentrations in the nitrogenizing gas, yields data to plot the curve A-B-C-D-E. The points A, B, C and D where the curve is discontinuous determine the phase boundaries at that temperature.

Under practical nitrogenizing conditions, it is difficult to obtain the curve A-B-C-D-E, due to a side reaction

$$\text{NH}_3 \text{ (gas)} = \text{N}_2 \text{ (gas)} + 3/2 \text{ H}_2 \text{ (gas)}$$

The extent of this dissociation reaction depends upon temperature, flow rate of the gas mixture, and the catalytic conditions which prevail during a particular experiment. The composition of the nitrogenizing gas changes as it passes through the nitrogenizing chamber due to progressive dissociation of the ammonia. The gas phase in contact with the iron, therefore, contains less ammonia than the inlet mixture in proportion to the prevailing extent of dissociation. When the extent of ammonia dissociation is constant, the curve II in fig. 2b can be obtained. This curve is similar to curve I except that the ammonia concentration in the inlet gas required to produce a certain nitrogen content in the solid is higher. The discontinuities on curve II still represent the phase boundaries, as these are independent of the amount of dissociation and are dictated only by equilibrium relations of the co-existing solid phases. An increase in the extent of ammonia dissociation to a new constant value can only shift curve II vertically. This shift does not alter the nitrogen contents at the discontinuities.

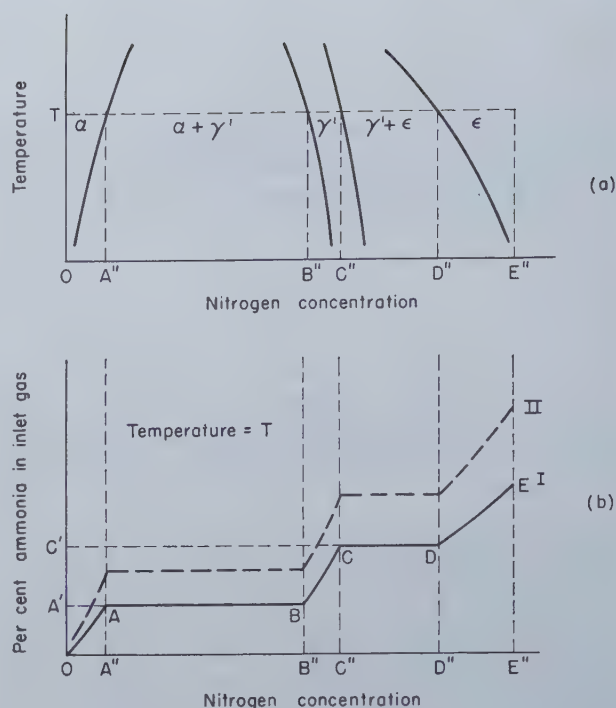A series of nitrogenizing experiments at a single



Fig. 2—Schematic diagram illustrating the principle of the controlled nitrogenizing method for phase boundary determination.

temperature gives the phase boundaries at that temperature. It is necessary to carry out similar sets of isothermal experiments in order to determine phase boundaries over a range of temperatures. This feature made the controlled nitrogenizing method tedious but its inherent dependability justified its use.

The controlled nitrogenizing method requires that the dissociation of ammonia be constant throughout an isothermal series of experiments and that equilibration be attained between the gas and solid phases. A considerable amount of experimentation was necessary to find the optimum operating conditions satisfying these requirements. Of the variables governing the degree of ammonia dissociation, temperature and flow rate were held constant without difficulty. The catalytic conditions in the nitrogenizing chamber depended on the nature and amount of various surfaces in contact with the gas mixture. Since quartz does not catalyze the dissociation reaction, it was used for the nitrogenizing chamber, the inlet and outlet tubes and the thermocouple tubes (fig. 1). A constant weight of iron powder was used because iron is known to catalyze the dissociation reaction. The alundum boat was contaminated with iron during nitrogenizing and was therefore renewed for every experiment. It was assumed that the catalytic conditions were held sufficiently constant by these precautions and the experimental results justified this assumption. A period of 16 hr was found to be adequate to attain equilibrium.

Some preliminary experiments were made to determine the best way of retaining the nitrogen content of the alloy when it was taken out of the nitrogenizing chamber for chemical analysis. Water quenching proved to be the best method.
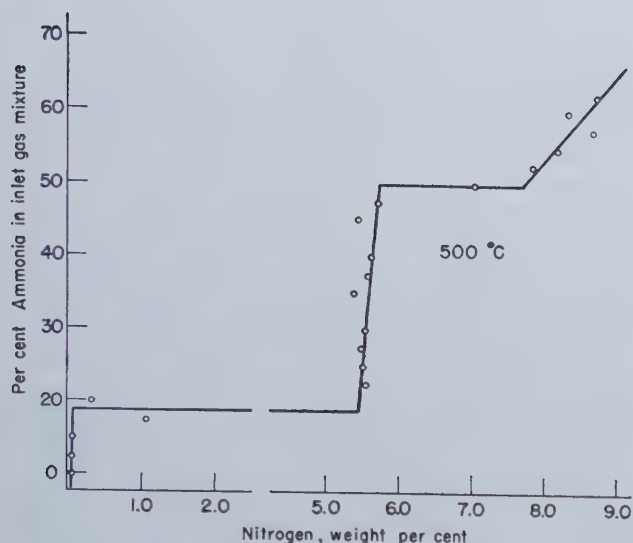
Fig. 3—Results of a typical series of controlled nitrogenizing experiments at 500°C.



Fig. 4—Solubility limit of nitrogen ferrite as a function of temperature.

Typical results of a series of nitrogenizing experiments at 500°C are presented in fig. 3. This plot of actual data resembles the schematic plot shown in fig. 2b. The phase boundaries were determined by the intersections of the horizontal two-phase lines with the sloping single-phase lines. For example, the $\gamma'$ curve intersects the $\alpha — \gamma'$ line and the $\gamma' — \epsilon$ lines (fig. 3) at 5.45 and 5.75 pct nitrogen respectively. These compositions therefore represent the boundaries of the $\gamma'$ phase at 500°C. The solubility limit in the $\alpha$ phase is similarly read as 0.05 pct nitrogen. This is the nitrogen content at which the $\alpha$ phase line intersects the horizontal $\alpha — \gamma'$ line. The lower limit of the $\epsilon$ phase is given by the point of intersection of the $\epsilon$ and $\gamma' — \epsilon$ lines at 7.7 pct nitrogen.

A similar series of experiments was also carried out at 500°C using a high-nitrogen alloy as the starting material. In this case equilibrium was approached from the high nitrogen side. The boundaries of the $\gamma'$ phase determined from the results of these experiments are in good agreement with those mentioned above. This fact shows that the controlled nitrogenizing method gives reliable results.

### Results and Discussion

The iron-nitrogen phase diagram was determined from the data obtained by X ray diffraction measurements and the controlled nitrogenizing method. The various iron-nitrogen phases will be described first in the order of their nitrogen contents. The constitution diagram combining these phases will then be presented. All results are discussed in the light of the work of other investigators.

**The $\alpha$ Phase (Nitrogen Ferrite):** The $\alpha$ phase has a body-centered cubic structure and contains small amounts of nitrogen in solution. This phase may be named nitrogen ferrite. The lattice parameter of nitrogen ferrite is affected only slightly by the amount of dissolved nitrogen. Experiments conducted to study the variation of lattice parameter with increasing nitrogen content did not show a consistent measurable change, even when the back reflection X ray technique was used. The lattice
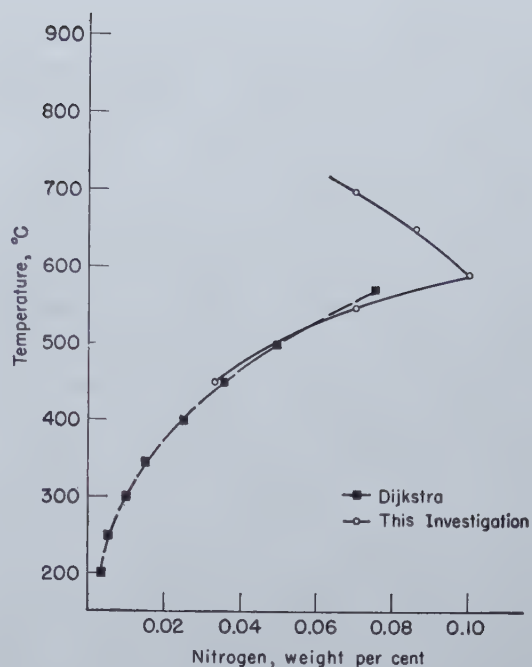
parameter method of phase boundary determination was therefore not applicable.

The solubility of nitrogen in the $\alpha$ phase was determined by the controlled nitrogenizing method. The results are plotted in fig. 4. Solubility limits determined by Dijkstra[11] are also shown for comparison. The agreement between the two sets of values is satisfactory. The small discrepancies may be attributed to differences in the techniques employed. In the present investigation, equilibration was carried out at the desired temperature, followed by quenching; for correct results it was sufficient to retain all nitrogen in the sample, but it was not necessary that the nitrogen remain dissolved in the $\alpha$ phase. In contrast, Dijkstra saturated

**Table II. Composition Limits of the $\gamma$ Phase (Nitrogen Austenite)**

| Temperature °C | Lower Limit (Weight Pct Nitrogen) | | Upper Limit | |
|---|---|---|---|---|
| 910 | 0.00 | $(\alpha-\gamma)$ | | |
| 700 | | | 2.70 | $(\gamma-\epsilon)$ |
| 675 | 1.40 | $(\alpha-\gamma)$ | 2.75 | $(\gamma-\epsilon)$ |
| 650 | 1.64 | $(\alpha-\gamma)$ | 2.80 | $(\gamma-\epsilon-\gamma')$ |
| 625 | | | 2.64 | $(\gamma-\gamma')$ |
| 590 | (2.35) | $(\alpha-\gamma-\gamma')$ | (2.35) | $(\alpha-\gamma-\gamma')$ |

Note: Values in parentheses were obtained by extrapolation.

**Table III. Composition Limits of the $\gamma'$ Phase (Fe₄N)**

| Temperature °C | Lower Limit Weight Pct Nitrogen | | Upper Limit | |
|---|---|---|---|---|
| 650 | 5.30 | $(\gamma-\epsilon-\gamma')$ | 5.6 | $(\gamma'-\epsilon)$ |
| 625 | | | | |
| 600 | 5.30 | $(\gamma-\gamma')$ | | |
| 590 | 5.30 | $(\alpha-\gamma-\gamma')$ | | |
| 550 | 5.45, 5.48 | $(\alpha-\gamma')$ | 5.70, 5.80 | $(\gamma'-\epsilon)$ |
| 500 | 5.45 | $(\alpha-\gamma')$ | 5.75, 5.80 | $(\gamma'-\epsilon)$ |
| 450 | 5.47 | $(\alpha-\gamma')$ | | |

all samples at 580°C, allowed precipitation to occur at successively lower temperatures and then measured only the amount of nitrogen retained in solu-

tion after quenching from the precipitation temperatures. Incomplete precipitation at low temperatures can account for high nitrogen values and accidental precipitation during quenching from high temperatures can explain the low values obtained by Dijkstra.

The solubility limits shown in fig. 4 are markedly lower than those reported by Eisenhut and Kaupp.[6] These investigators found an appreciable expansion of the ferrite cell with increasing nitrogen content and used this relation to determine the saturation limit. As already pointed out, the lattice parameter method was rejected in this investigation because no variation of the parameter on the nitrogen concentration of the $\alpha$ phase could be found. This is in accord with Hägg's results.[7] In view of the latter agreement the validity of the results of Eisenhut and Kaupp may be questioned. The maximum solubility at the eutectoid temperature found by Seferian[10] (0.14 pct nitrogen) is in fair agreement with the results reported here.

**The $\gamma$ Phase (Nitrogen Austenite):** The $\gamma$ phase, nitrogen austenite, has a face-centered cubic arrangement of the iron atoms and contains nitrogen in solution. Nitrogen austenite is stable above the eutectoid temperature (590°C). To prevent decomposition into pearlitic structures, all samples were water quenched from the nitrogenizing temperature. It was not possible, however, to preserve the low-nitrogen samples in a completely austenitic condition, because martensite formed during the quench. Samples containing more than 2.4 pct nitrogen remained completely austenitic. From this fact it may be concluded that the $M_s$ temperature for iron-nitrogen alloys of these compositions is below room temperature. Although samples analyzing less than 2.4 pct nitrogen contained martensite in addition to austenite, it was safe to assume that they were completely austenitic at the nitrogenizing temperature.

The lattice parameter of nitrogen austenite was found to increase with increasing nitrogen content. Fig. 5 summarizes the results of X ray diffraction measurements. The relation shown in this plot was used to determine the high-nitrogen boundary of the $\gamma$ field. The lower limit could not be determined by the lattice parameter method, since samples having these compositions contained only small amounts of nitrogen austenite. The controlled nitrogenizing method was, therefore, employed to find these values. The results are given in table II and are in good agreement with the findings of Lehrer[5] and Eisenhut and Kaupp.[6]

**The $\gamma'$ Phase (Fe$_4$N):** The $\gamma'$ phase has a face-centered cubic structure and exists over a very limited range of composition. X ray diffraction patterns of this phase with cobalt K radiation were found to contain several faint lines in addition to those normally belonging to a face-centered cubic structure. These additional lines were identified as superlattice reflections from the (100), (110), (210), (221), (310), (320), and (321) planes. Their relative intensities and spacings are in good agreement with Jack's work and confirm his interpretation of the ordered structure of the $\gamma'$ phase.

The lattice parameter of the $\gamma'$ phase was found to change from 3.78$_3$ kx units at 5.29 pct nitrogen

to 3.79$_8$ kx units at 5.71 pct nitrogen. Since this change was small, the lattice parameter method could not be used to determine the boundaries of the $\gamma'$ phase. The homogeneity limits were therefore determined by the controlled nitrogenizing method. The results are listed in table III.

**The $\epsilon$ Phase:** The $\epsilon$ phase has a hexagonal close-packed structure and exists over a wide range of nitrogen concentrations. The results of X ray diffraction measurements are summarized in fig. 6 which shows the dependence of the lattice parameters and the axial ratio on the nitrogen content above 7.3 pct nitrogen. Attempts to obtain similar data for lower nitrogen contents were unsuccessful, because homogeneous samples in this range could not be produced. At temperatures at which such samples are stable, the erratic nature of ammonia decomposition prevented adequate control of composition by nitrogenizing. An attempt to produce homogeneous low-nitrogen samples of the $\epsilon$ phase by decomposition of a high-nitrogen starting material failed owing to excessively high rates of decomposition.

The composition limits of the $\epsilon$ field were determined by the lattice parameter method. The results are presented in table IV. Owing to lack of experimental data for the low-nitrogen region, some values in this table were based on the extrapolated portions of the curve in fig. 6.

The controlled nitrogenizing method was also used to determine the lower limit of the $\epsilon$ phase at 450° and 500°C. The results obtained are included in table IV and are in good agreement with the results derived from lattice parameter measurements.

**The $\zeta$ Phase (Fe$_2$N):** The $\zeta$ phase which was originally found by Hägg[7] has an orthorhombic structure. Its unit cell dimensions were determined to be $a = 2.75$, $b = 4.82$, and $c = 4.43$ kx units, respectively. This phase which exists at nitrogen concentrations above 11.1 pct could be produced only by nitrogenizing at 450°C. Attempts to produce $\zeta$ at 475° and 500°C were unsuccessful.

The X ray technique used in this investigation was not accurate enough to warrant any interpretation of the atomic arrangement of the $\zeta$ phase. The diffraction patterns obtained by using cobalt K radiation were, however, in good agreement with the structure proposed by Jack.[16]

The lower limit of the $\zeta$ phase was found to be 11.1 pct nitrogen at 450°C which is also in good agreement with Jack's work. No evidence of an $\epsilon+\zeta$ field was obtained. Either this two-phase region is extremely narrow, or there is a continuous transition of the structure of $\epsilon$ into that of $\zeta$.

**The Iron-Nitrogen Phase Diagram:** The various single-phase regions described heretofore are fitted

### Table IV. Composition Limits of the $\epsilon$ Phase

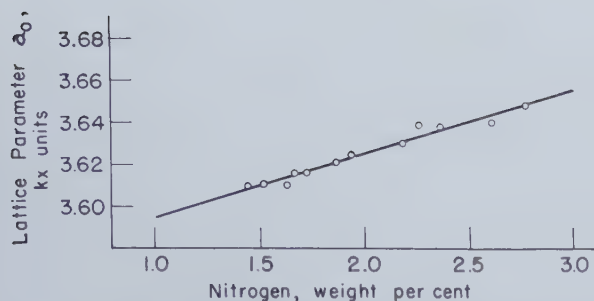| Temperature °C | X ray Method | | Controlled Nitrogenizing Method |
|---|---|---|---|
| 675 | 4.35 | $(\gamma$-$\epsilon)$ | |
| | 5.0 | $(\epsilon$-$\gamma')$ | |
| 650 | 4.5 | $(\gamma$-$\epsilon$-$\gamma')$ | |
| | 6.2 | $(\gamma'$-$\epsilon))$ | |
| 625 | 6.6 | $(\gamma'$-$\epsilon)$ | |
| 550 | 7.35 | $(\gamma'$-$\epsilon)$ | |
| 500 | 7.70, 7.75 | $(\gamma'$-$\epsilon)$ | 7.70 $(\gamma'$-$\epsilon)$ |
| 450 | 7.95 | $(\gamma'$-$\epsilon)$ | 7.95 $(\gamma'$-$\epsilon)$ |

**Fig. 5—Lattice parameter of nitrogen austenite as a function of nitrogen concentration.**

together to form the iron-nitrogen phase diagram shown in fig. 7. This diagram contains two eutectoids; the corresponding reactions involve the $\alpha$, $\gamma$ and $\gamma'$ phases and the $\gamma$, $\epsilon$ and $\gamma'$ phases.

The existence of the first eutectoid has been suggested by most previous investigators[1, 2, 3, 4, 5, 6, 7, 8, 9] and the eutectoid temperature is known fairly accurately. The most recent determinations by Lehrer[5] and Eisenhut and Kaupp[6] fix this temperature to be 590°C. Other determinations range from 580°C by Fry[1] to 608°C by Bramley and Haywood.[9] In the investigation reported here, no redetermination of this eutectoid temperature was undertaken and the value of 590°C was adopted. The eutectoid composition determined by the intersection of the extrapolated composition limits of the $\gamma$ phase (fig. 7) is 2.35 pct nitrogen. This value is in good agreement with the results of Lehrer[5] and Eisenhut and Kaupp[6] but differs from the values ranging from 1.5 to 1.8 pct nitrogen suggested by Fry,[1] Sawyer,[2] Epstein and coworkers[3, 4] and Hägg[7, 8]. This eutectoid reaction can therefore be stated:

$$\gamma_{2.35} \rightleftarrows \alpha_{0.10} + \gamma'_{5.30} \ (590°C)$$
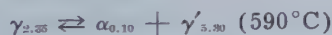
The subscripts indicate the nitrogen content in weight percent.

The existence of the second eutectoid reaction at 650°C was proposed by Lehrer[5] and was confirmed by the present research. It was found that iron-nitrogen alloys approximating the eutectoid compo-

sition quenched from 650° ± 2°C contained either $\gamma + \epsilon$ or $\epsilon + \gamma'$ or $\gamma + \gamma'$ depending on the exact quenching temperature and the composition of the alloy. These results show that the eutectoid temperature is 650°C. Eisenhut and Kaupp[6] proposed that a peritectoid reaction takes place at this temperature. Epstein[3, 4] reported the existence of thermal arrests at 660°C. The reaction temperature of 650°C is thus in good agreement with results of previous work.

Epstein did not find metallographic evidence of a eutectoid, and proposed a peritectoid in its place. The cogency of this negative reasoning may be questioned. Eisenhut and Kaupp also proposed a peritectoid reaction but their samples analyzing from 4.6 to 5.2 pct nitrogen and quenched from above 650°C contained $\gamma'$ as well as $\epsilon$ which is incompatible with the peritectoid reaction proposed by them. Their experimental results can, however, be explained by the eutectoid transformation at 650°C shown in fig. 7.

The lattice constants of the $\epsilon$ phase were found to have two different but constant values in the two two-phase fields: the low-nitrogen $\epsilon + \gamma$ field and the $\gamma' +$ low-nitrogen $\epsilon$ field. This fact is in accord with the existence of a homogeneous $\epsilon$ field between the two two-phase fields. Furthermore observations of relative intensities of the strongest diffraction lines from the $\epsilon$ and $\gamma$ or $\epsilon$ and $\gamma'$ phase mixtures showed that the amount of $\epsilon$ first increased and then decreased as the nitrogen content increased from 3.0 to about 5.2 pct nitrogen in samples quenched from slightly above 650°C. Similar variations in intensities were found in samples quenched from 660° and 675°C, but the nitrogen concentrations were slightly altered as shown in fig. 7. The shape of the low-nitrogen $\epsilon$ field is a further argument in support of the existence of the eutectoid. The eutectoid composition was fixed at 4.5 pct nitrogen, which is in agreement with Lehrer.[5] This eutectoid reaction can be stated:

$$\epsilon_{4.5} \rightleftarrows \gamma_{2.80} + \gamma'_{5.30} \ (650°C)$$

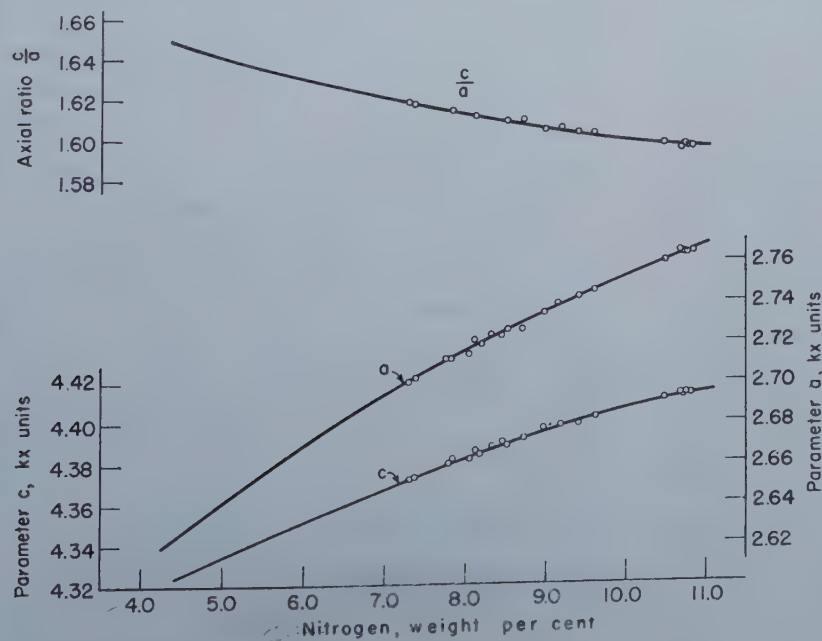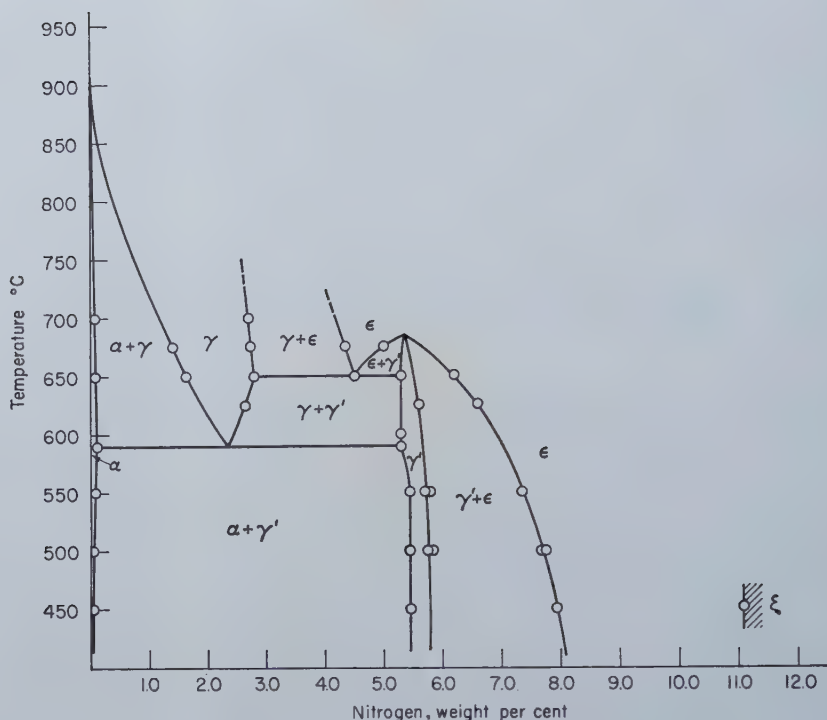The subscripts indicate the invariant compositions in weight per nitrogen.



**Fig. 6 — Lattice parameters and axial ratio of the ε phase as functions of nitrogen concentration.**

Fig. 7 — Iron-nitrogen phase diagram.

The phase diagram determined in this investigation resembles in general form that of Lehrer[5] more closely than any other published diagram. There are, however, a number of significant differences especially in the composition limits of the various phases.

It should be emphasized that the iron-nitrogen phase diagram differs in an important feature from the common metallurgical diagrams. The latter represent equilibrium relations at constant pressure while the iron-nitrogen phase diagram shown in fig. 7 is a projection of the various solid-phase equilibria in the temperature-pressure-concentration equilibrium diagram onto a temperature-concentration plane.

## Summary and Conclusions

1. A method for the determination of the phase boundaries in the iron-nitrogen system was developed. This method depends on the relation between the nitrogenizing power of an ammonia-hydrogen gas mixture and the nitrogen concentration of the iron-nitrogen alloy produced by nitrogenizing.

2. The following iron-nitrogen phases were found to exist in the temperature range from 450° to 700°C:

| Phase | Structure | Remarks |
|---|---|---|
| $\alpha$ | B.C.C.; $a_0$ = 2.86 kx units | Maximum solubility 0.10 pct nitrogen at 590° C |
| $\gamma$ | F.C.C.; $a_0$ = 3.61$_3$ kx units at 1.45 pct nitrogen to 3.64$_3$ kx units at 2.79 pct nitrogen | Maximum solubility 2.80 pct nitrogen at 650° C |
| $\gamma'$ | F.C.C.; a = 3.78$_3$ to 3.79$_3$ kx units | Homogeneity limit 5.30 to 5.75 pct nitrogen |
| $\epsilon$ | H.C.P.; c = 4.37$_3$ to 4.41$_1$ and a = 2.70$_2$ to 2.76$_1$ kx units | Very wide range of homogeneity, 4.35 to 11.0 pct nitrogen |
| $\xi$ | Orthorhombic a = 2.75, b = 4.82 c = 4.43 kx units | Lower homogeneity limit 11.1 pct nitrogen at 450° C |

3. The phase boundaries of the $\alpha$, $\gamma$, $\gamma'$, $\epsilon$, and $\zeta$ phases were determined.

4. Two eutectoid reactions were found to exist in the phase diagram:

$$\gamma_{2.35} \rightleftarrows \alpha_{0.10} + \gamma'_{5.30} \ (590°C)$$
$$\epsilon_{1.3} \rightleftarrows \gamma_{2.80} + \gamma'_{5.30} \ (650°C)$$
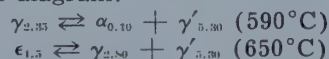
The subscripts show the invariant compositions in weight percent of nitrogen.

5. The iron-nitrogen phase diagram in the temperature range 450-700°C was constructed.

## References

[1] A. Fry: Stahl u. Eisen. (1923) 43, 1271.

[2] C. B. Sawyer: Trans. AIME (1923) 69, 798.

[3] S. Epstein, H. C. Cross, E. C. Groesbeck, and I. J. Wymore: Bur. of Stand. Jnl. of Res. (1929) 3, No. 6, 1005.

[4] S. Epstein: Trans. A.S.S.T. (1929) 16, 19.

[5] E. Lehrer: Ztsch. Elektrochemie (1930) 37, 460.

[6] O. Eisenhut and E. Kaupp: Ztsch. Elektrochemie (1930) 37, 392.

[7] G. Hägg: Nova Acta Regia, Soc. Sci. Upsaliensis, Series 4, 7, No. 1 (1929).

[8] G. Hägg: Ztsch. phys. Chemie (1930) 8, 455.

[9] A. Bramley and F. W. Haywood: Iron and Steel Inst., Carnegie Scholarship Mem. (1928) 17, 67.

[10] A. M. Portevin and D. Seferian: Iron and Steel Inst., Symp. on the Welding of Iron and Steel (1936) 2, 483.

[11] L. J. Dijkstra: Trans. AIME (1949) 185, 252. Jnl. of Metals, Mar. 1949, TP 2540.

[12] S. Brunauer, M. E. Jefferson, P. H. Emmett and S. B. Hendricks: Jnl. Amer. Chem. Soc. (1931) 53, 1778.

[13] G. Owasa and S. Iwaisumi: Ztsch. Krist. (1928) 69, 26.

[14] R. Brill: Ztsch. Krist. (1928) 68, 379.

[15] S. B. Hendricks and P. R. Kosting: Ztsch. Krist. (1930) 74, 511.

[16] H. K. Jack: Proc. Royal Soc. (1948) A 195, 34.

[17] D. J. Carney, N. J. Grant and J. Chipman: Trans. AIME 188. Jnl. of Metals, Feb. 1950.

A Study of the     # Iron-Chromium-Nickel Ternary System ———

THIS study of the ternary has been made as one phase of a metallurgical investigation which began nearly four years ago in the General Electric Company's Research Laboratory in Schenectady, N. Y. The objective of this program is the discovery of new metallurgical information which will lead to the development of better high-temperature materials. Combinations of the four pure base elements—iron, chromium, nickel, and cobalt—are being studied at the present time. It is essential in an investigation such as this to know as much as possible about the constitutional diagrams involved. The study of the iron-chromium-nickel system has been made to this end.

**Preliminary Explanation of Experimental Procedure:** In all, fifty-five alloys at steps of 10 at. pct were made for the investigation of this ternary. Several ternary alloys in the chromium rich corner had to be omitted because their extreme brittleness made testing impractical. All alloys were vacuum melted with hydrogen reduction and centrifugally cast. The apparatus and technique of this process has been described in detail by Nisbet.[1,2] The purity of the alloys prepared in this way is considered to be quite good.

Impurities are listed as follows:

|                 | Pct       |
|-----------------|-----------|
| Carbon          | 0.02      |
| Oxygen          | 0.02      |
| Nitrogen        | 0.005     |
| Magnesium       | 0.03–0.05 |
| Sulphur         | trace     |
| Hydrogen        | trace     |
| Phosphorous     | trace     |
| Silicon         | trace     |

After casting, all samples were given a homogenization treatment which consisted of holding

J. W. PUGH is Research Assistant and J. D. NISBET is Research Associate, Research Laboratory, General Electric Co., Schenectady, N. Y.

them for 15 hr at 1150°C (2100°F) and water quenching. Testing was begun with the samples in this condition.

The tests employed in the study of this system were (1) dilatometer, (2) hardness versus aging temperature, (3) tensile strength and elongation versus temperature, (4) microstructure analysis, and (5) electrical resistance versus temperature. Dilatometer tests were made at the rather rapid heating rate of 1093°C (2000°F) in one hour on a Bristol-Rockwell type instrument. Hardness data were taken on specimens cooled from 204°, 427°, 649°, 760°, 871°, 982°, and 1093°C under conditions which are thought sufficient to bring the specimens to equilibrium in all but the cases of the very sluggish transformations. Electrical resistance data for several specimens were taken for both heating and cooling conditions in a vacuum furnace especially designed for this work by D. W. Bainbridge, formerly of this laboratory. Provisions were made for heating and cooling standard specimens at a constant rate, while autographic records of resistance and temperature were made simultaneously. Micrographs of all the alloys were made in the quenched condition.

Some question may exist as to how such physical values as hardness, tensile strength, and elongation were interpreted to indicate a change in phase. Original data were recorded on physical property versus temperature graphs, each of which was made from the data of a single alloy (fig. 1a). From these, another series of graphs were plotted with the physical property as a function of composition for constant temperatures (fig. 1b). Sharp deviations in the slope of these composition versus hardness curves often indicate a change in phase.

The example of fig. 1 will serve to describe this experimental technique. The plotting of a single point from graph "a" to graph "b," and finally to the phase diagram "c," is illustrated. The location of the point on graph "b" is indicated as point (1). If all the alloys of the A-B binary system were solid solutions at temperature X, the hardness in this curve would be expected to rise at a fairly even rate as A is diluted with B to a maximum at some intermediate value between A and B, as

The iron-chromium-nickel ternary phase relationships in fifty-five alloys have been studied by means of hardness, elongation, tensile strength, dilatometer indications, and microstructure analysis. A comparison has been drawn between the conclusions reached and a composite picture of the ternary made from what were considered the best references on the subject. The diagrams presented represent a ternary picture which is regarded as a fairly accurate picture of the ternary situation.

## by J. W. Pugh and J. D. Nisbet

shown by the solid line, and then to be reduced in the same fashion as the amount of A dissolved in B is decreased as shown by the dotted line. This effect is in evidence from constituent A to about 60 pct B or to point (1) in fig. 1b. At point (1) the hardness suddenly rises very rapidly to point (2). Point (1) is chosen as the point at which the phase boundary exists for temp. X, and composition Y, because of the sudden rapid rise in hardness values at this point.

Physical properties do not always provide the best criterion for the determination of equilibrium diagrams. It is also true that equilibrium diagrams may not provide a means of accurately predicting physical properties. An improvement in the application of fundamental information to alloy design must come about through "physical property diagrams," or more specific relationship between physical properties and equilibrium. Therefore, an attempt was made in this survey to relate physical properties to the equilibrium diagram.

**The Iron-Chromium Binary:** The iron-chromium system presented here (fig. 2) is the result of a selection from the data of Adcock[3] and Wever and Jellinghaus.[4] A very limited amount of the data from the investigation at General Electric applies to this binary, but a dilatometer test of the alloy containing 10 pct chromium reveals the lower extremity of the gamma loop at 890°C. This location is in good agreement with previous investigations.

None of the samples was held at temperature long enough to permit the precipitation of sigma, the extremely hard, brittle intermediate constituent of this system. The sigma region of the binary presented here follows that of Wever and Jellinghaus.[4] Undoubtedly this sigma region is greatly expanded at lower temperatures as is suggested by Bradley and Goldschmidt,[5] who report evidence of a transformation to sigma at 75 pct chromium, and by Aborn and Bain,[6] who suggest that the two phase boundary be slanted in the direction of 20 pct chromium at room temperature. Hougardy[7] also states that this phase is much more extensive than the work of Wever and Jellinghaus indicates. There is certainly a need for a more comprehensive study of this phase using long holding times at temperature or mechanical working in order to enclose this

phase within boundaries which more accurately approach the equilibrium situation.

**The Iron Nickel Binary:** This diagram (fig. 3) was constructed from diagrams proposed by Merica[8] and by Hansen.[9] The position of the alpha plus gamma area at low temperatures in this system has long been a controversial subject. The characteristic "irreversability" or hysteresis of this transformation has resulted in two widely divergent sets of boundaries for this area. The two alpha plus gamma ranges, one of which is consistently obtained from cooling data while the other is obtained from heating data, probably indicate one equilibrium range which lies somewhere between the two. Since it has frequently been observed that there is considerably less resistance to the alpha to gamma transformation than there is to the gamma to alpha transformation, diagrams produced from heating data are very likely closer to true equilibrium than those produced from cooling data.[10]

Curiously, the data produced by the dilatometer tests place this region in about the position which might be predicted from Merica's diagram if we regard the region at higher temperatures as the most accurate.

The boundaries of the area beyond about 35 pct nickel have never been determined because at these compositions the increase in free energy when the alloy crosses thermally into the two phase region is insignificant compared to the resistance offered to the transformation. This increased resistance at higher nickel concentrations is caused by a decrease in the equilibrium temperature of the transformation and also the change in concentration. As indicated by Marsh,[10] the increase in resistance owing to the presence of a greater number of nickel atoms is probably caused by a low rate of diffusion since the atoms of iron and nickel are very similar in volume. For these reasons there seems little hope of completing an iron-nickel binary which very closely approaches equilibrium.

Two micrographs from this system are published here. The one of the 90 pct iron sample (fig. 17) shows areas of precipitated alpha which are relatively large and equiaxed when compared to the specimen at 80 pct (fig. 18) in which alpha has precipitated in the familiar Widmanstätten struc-
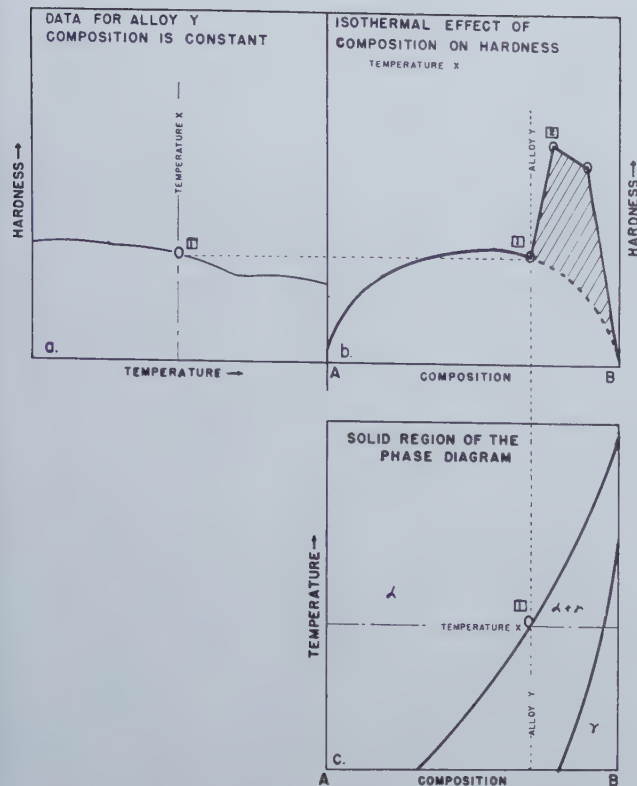
Fig. 1—Schematic representation of experimental technique in the use of physical properties to study phase changes.



Fig. 2—Selected from Wever and Jellinghaus[4] and Adcock.[3]

ture. These pictures reveal that the transformation is active enough at these low nickel compositions to cause alpha to precipitate on quenching, but at higher nickel contents the transformation does not take place with long holding times at temperature.

**The Chromium-Nickel Binary:** Data for the diagram presented here (fig. 4) were selected from the work of Hansen,[9] Matsunaga,[11] and Jenkins, Bucknall, Austin, and Mellor.[12] Data taken in this laboratory corroborate the limits of solid solubility indicated in this diagram.

Some of the micrographs taken of the alloys in this system are interesting. The one containing 90 pct chromium (fig. 19) reveals markings which appear similar to those speculated upon by Jenkins and his associates. The Jenkins paper suggested that the markings were caused by the precipitation of a compound containing nitrogen and it was thought that a comparison of several alloys containing varying amounts of nitrogen confirmed this theory. This photograph also shows a gamma precipitate (the light grey constituent) and the existence of gamma above 90 pct chromium is verified.

The micrograph (fig. 20) of a 60 pct chromium alloy quenched from 1150°C (2100°F) shows light primary alpha surrounding the darker, mottled eutectic. An examination of the chromium-nickel binary diagram shows that the solubility of gamma in alpha solid solution is decreased by diminishing temperature. This accounts for the occurrence of

precipitated gamma within the primary alpha.

The micrograph (fig. 21) of a 70 pct chromium alloy also quenched from 1150°C (2100°F) shows dark oxide inclusions and eutectic colonies in an unetched specimen.

An electrical resistance versus temperature test was made on a specimen containing 80 pct chromium with the hope that any change in structure other than the alpha to gamma transition might cause a break in the resistance curve. The curve which resulted from heating the specimen at the rate of 200°C per hr was difficult to interpret because the specimen both volatilized and oxidized to some extent in the vacuum which was provided by the testing apparatus. This effective diminishing of the conducting cross section tended to confuse the other factors of increasing temperature and phase change. However, two small breaks were observed in what was otherwise a fairly regular curve. The first break occurred at 722°C, while the second appeared at 1084°C. The latter is easily accounted for by the gamma to alpha transition, while the former may possibly account for the development of the extra precipitate suggested by Jenkins and his associates.[12] Fig. 22 is a micrograph of the alloy tested (Cr80, Ni20).

**The Iron-Chromium-Nickel Ternary:** The first comprehensive investigation of this ternary was by Bain and Griffiths[13] in 1927. This early investigation revealed the relative positions of the alpha, gamma,
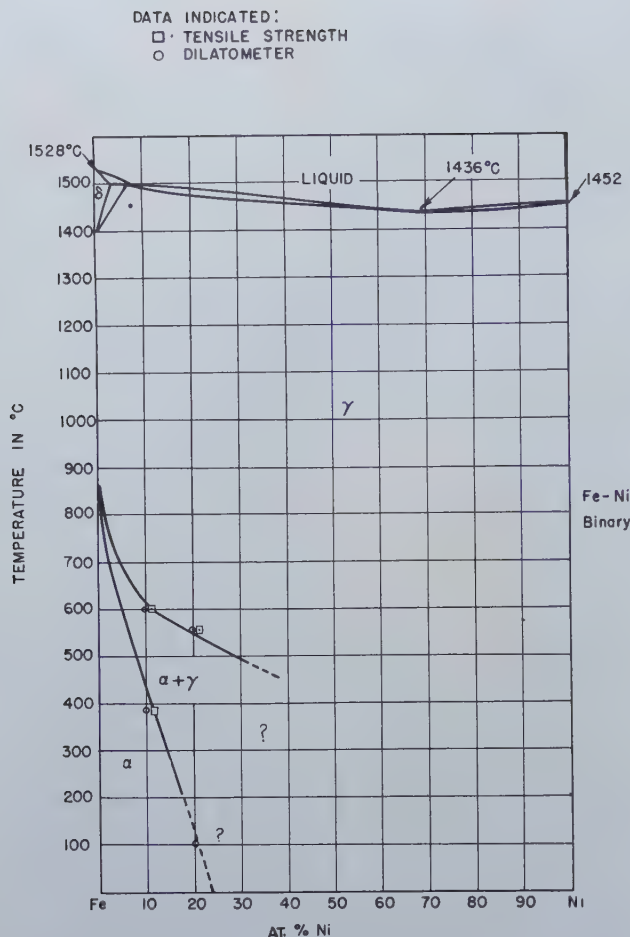
Fig. 3—Selected from Merica[8] and Hansen.[9]



Fig. 4—Selected from Hansen,[9] Matsunaga,[11] Jenkins, Bucknall, Austin, and Mellor.[12]

and alpha plus gamma phase fields on the iron side of the diagram and established the existence of the brittle constituent sigma (referred to by Bain and Griffiths as *B*). Since then, considerable experimentation has fairly well defined the ternary system. However, it is recognized that the exact equilibrium situation has only been approached and that in many instances the existing diagrams indicate phase changes in positions which are rather far removed from the true equilibrium positions. The two chief difficulties have been that of obtaining a sufficiently high degree of purity in the alloys and that of promoting the more sluggish transformations (notably the transformation to sigma).

The system has been studied in this case by first preparing a series of isothermal sections at selected temperatures and a series of nine constant-iron composition sections at intervals of 10 pct iron. The sections were constructed from a composite selection from the data of the following investigations: 1. Jenkins, Bucknall, Austin, and Mellor;[12] 2. Bradley and Goldschmidt;[14] 3. Schafmeister and Ergang;[15] and 4. Wever and Jellinghaus.[4] Data from the first reference were used chiefly in choosing the solidus and liquidus temperatures, while the other three, which for the most part are in fairly close agreement, were used in plotting the limits of solid solubility. A three-dimensional model of the system was constructed from these data using Plexiglass sheet for vertical sections of constant-iron composi-

sitions and for the three binaries, all of which were marked to show the phase changes. It was then possible to compare the data taken in our laboratories with that of the previous investigations.

Points plotted from hardness, tensile strength, and elongation data are taken from graphs made especially for this purpose with composition plotted against hardness, tensile strength, or elongation at constant temperatures. Points plotted from the data are in each case indicated in such a way as to show whether the source was dilatometer, hardness, tensile strength, or elongation. Dilatometer tests provide a very limited amount of information on this system owing to the temperature limitation (1093°C) of the instrument. Of the other tests, hardness is the most reliable and was put to the greatest use, but tensile strength and elongation were useful in corroborating changes indicated by hardness data.

An examination of fig. 5, 6, 7, and 8 will reveal that the data of this investigation were in close agreement with the reference investigators up to 50 pct iron. However, in a constant-iron plane at 50 pct iron there is a consistent difference which would enlarge the gamma region of solid solubility as indicated in fig. 9. This change disagrees specifically with a similar section published by Schafmeister and Ergang[15] who have placed the limit of solid solubility of gamma below 1000°C at about 22 pct nickel in this 50 pct iron section. Physical
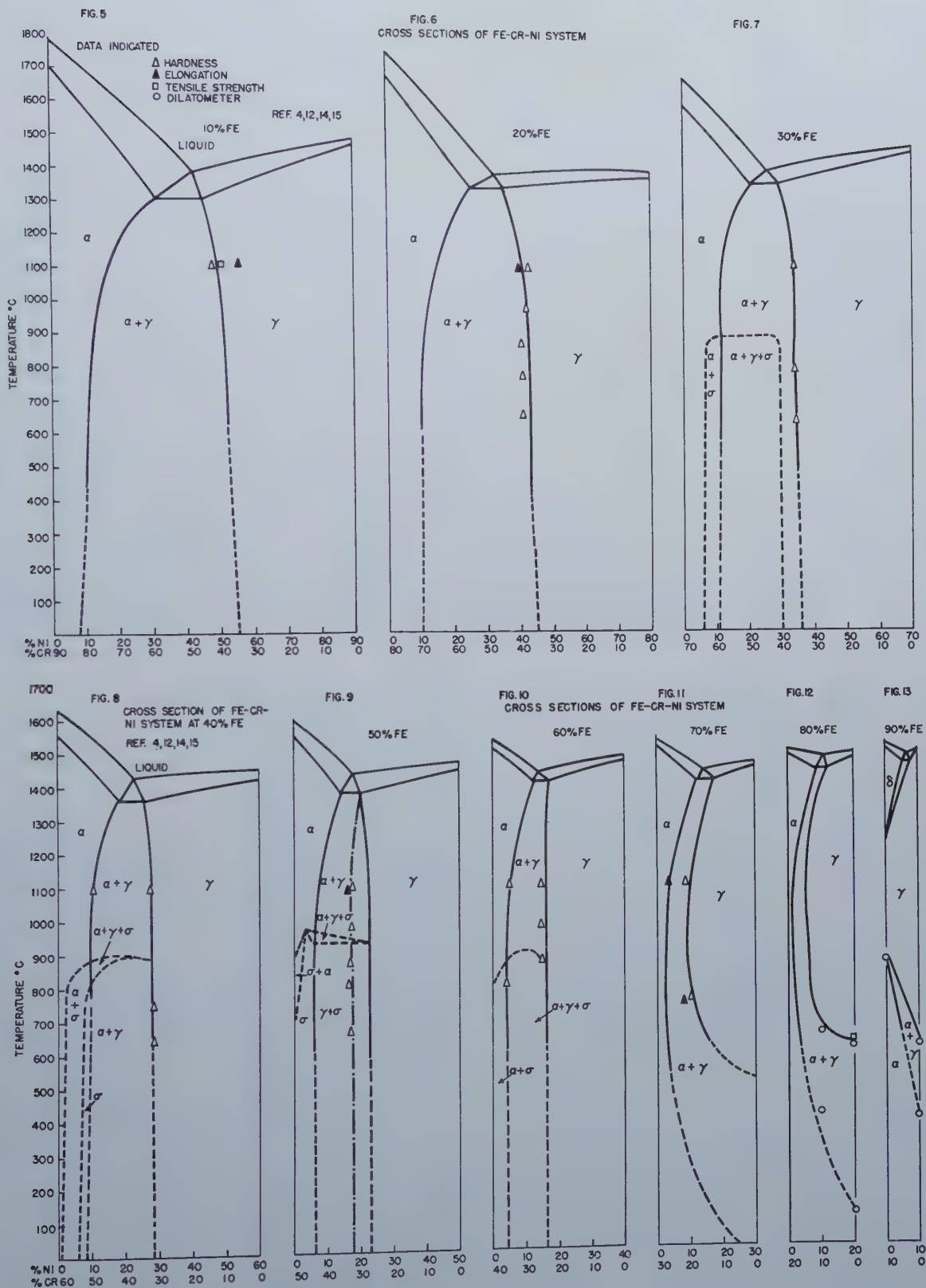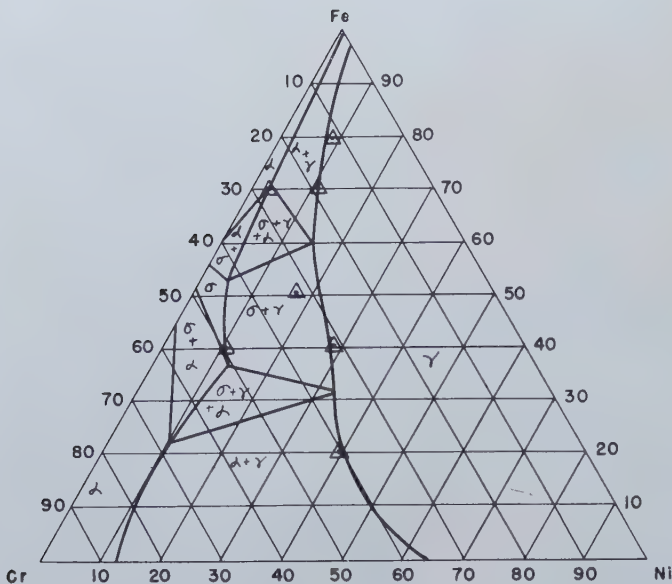
FIG. 5

DATA INDICATED

△ HARDNESS
▲ ELONGATION
□ TENSILE STRENGTH
○ DILATOMETER

REF. 4,12,14,15

10% FE
LIQUID

α

α + γ

γ

TEMPERATURE °C

%NI 0   10   20   30   40   50   60   70   80   90
%CR 90  80   70   60   50   40   30   20   10   0

FIG. 6
CROSS SECTIONS OF FE-CR-NI SYSTEM

20% FE

α

α + γ

γ

0   10   20   30   40   50   60   70   80
80  70   60   50   40   30   20   10   0

FIG. 7

30% FE

α

α + γ

γ

α + γ + σ

α + σ

0   10   20   30   40   50   60   70
70  60   50   40   30   20   10   0

FIG. 8
CROSS SECTION OF FE-CR-NI SYSTEM AT 40% FE
REF. 4,12,14,15

LIQUID

α

α + γ

γ

α + γ + σ

α + σ

α + γ

σ

TEMPERATURE °C

%NI 0   10   20   30   40   50   60
%CR 60  50   40   30   20   10   0

FIG. 9

50% FE

α

α + γ

γ

α + γ + σ

σ + α

σ    γ + σ

0   10   20   30   40   50
50  40   30   20   10   0

FIG. 10
CROSS SECTIONS OF FE-CR-NI SYSTEM

60% FE

α

α + γ

γ

α + γ + σ

α + σ

0   10   20   30   40
40  30   20   10   0

FIG. 11

70% FE

α

γ

α + γ

0   10   20   30
30  20   10   0

FIG. 12

80% FE

α

γ

α + γ

0   10   20
20  10   0

FIG. 13

90% FE

δ

γ

α + γ

α

0   10
10   0

Fig. 5-13

**Fig. 14—Fe-Cr-Ni isothermal section. 800°C.**
Ref. 4, 12, 14, 15.



**Fig. 15—Fe-Cr-Ni isothermal section. 400°C.**
Ref. 4, 12, 14, 15.



**Fig. 16—Fe-Cr-Ni isothermal section. 1100°C.**
Ref. 4, 12, 14, 15.

property data consistently indicate that this limit should be located at less than 20 pct nickel (fig. 9). Microstructure analysis substantiates the existence of this phase boundary below 20 pct nickel. A comparison of fig. 28 (50Fe, 10Ni, 40Cr) and fig. 30 (50Fe, 20Ni, 30Cr) reveals that the boundary of the two phase region falls some place between these adjacent alloys.

The section at 60 pct iron, which had to be constructed originally from published isothermal sections, is again in good agreement with the data taken in this laboratory as is indicated in fig. 10.

The section at 70 pct iron published here (fig. 11) differs considerably from the Schafmeister and Ergang section at this concentration, since these authors apparently have not allowed for a very extensive alpha plus gamma field in the iron-nickel binary. The data available on the alloys represented by this section are not very revealing, but the phase boundaries must be very nearly in the positions

indicated. If the 70 pct iron section as represented here is correct, the micrograph of fig. 23 (70Fe, 10Ni, 20Cr) might be expected to show a precipitation of alpha on quenching from 1150°C such as fig. 24 (80Fe, 10Ni, 10Cr) shows. The fact that this precipitation is not in evidence in the former micrograph may, however, be attributed to the same tendency for increasing resistance to transformation with decreasing iron content as was explained in the discussion of the iron-nickel binary. In this case the increase in chromium content must be held responsible. It seems logical to assume that the effect of additional chromium atoms would be similar to the effect of adding more nickel, since the chromium atom is also very similar in size to the iron atom and it is this similarity which impedes diffusion.

The section at 80 pct iron (fig. 12) has been adjusted at lower temperatures to fit the dilatometer data furnished by this laboratory and the situation presented in this diagram would seem to be the logical one. The micrograph of the alloy which is represented by the middle of this section (fig. 24) shows the expected alpha plus gamma Widmanstätten structure.

The 90 pct iron section (fig. 13) at low temperatures is also the result of dilatometer data; as it has been presented here it represents alpha plus gamma as a region almost triangular in shape and whose three vertices are points on the iron-nickel and iron-chromium binaries.

The shape of the alpha plus gamma region in the iron rich part of the diagram is quite odd. It is nearly impossible to visualize without the aid of a three-dimensional model. Beginning at the peritectic point (1500°C) in the iron-nickel binary, it bends down toward and touches the iron-chromium binary forming the gamma loop of that system (between 1400°C and 850°C). At still lower temperatures it sweeps back again toward the nickel-iron binary where it makes contact in the disputed alpha plus gamma region of that system. Never is this region common to both binaries at the same temperature and iron composition, but fluctuates from one to the other until the iron composition reaches
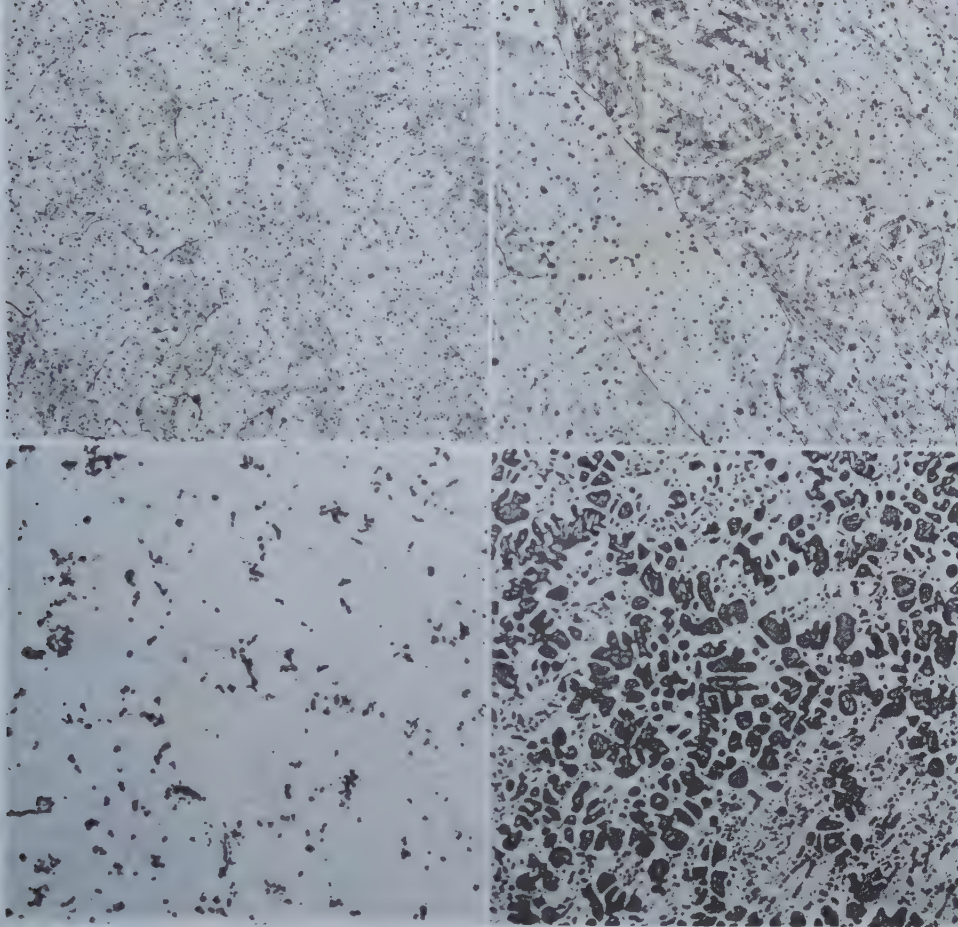
Fig. 17 (upper left)—
Composition: 90 Fe 10
Ni. Fig. 18 (upper
right) — Composition:
80 Fe 20 Ni. Fig. 19
(lower left) — Compo-
sition: 90 Cr 10 Ni. Fig.
20 (lower right) —
Composition: 60 Cr 40
Ni. Etchant: HCl +
$H_2O_2$.

Note: All micrographs are
of alloys held for 15 hr at
1150°C (2100°F) and
quenched.

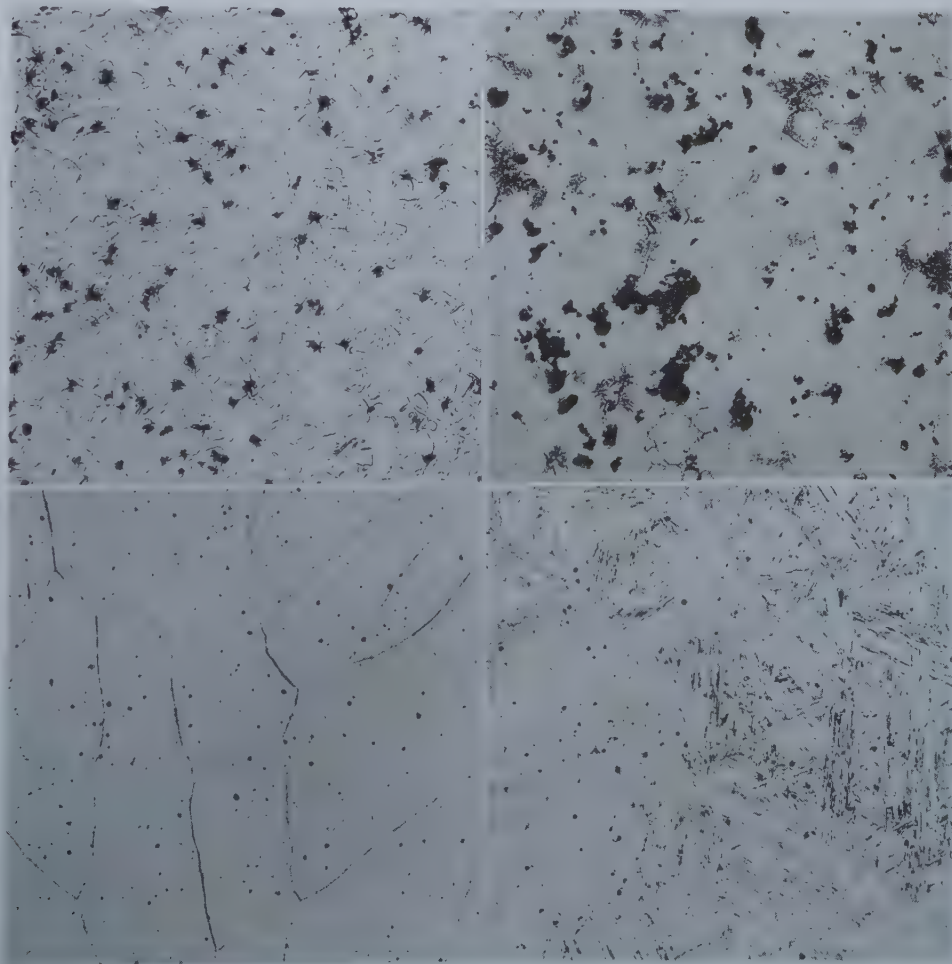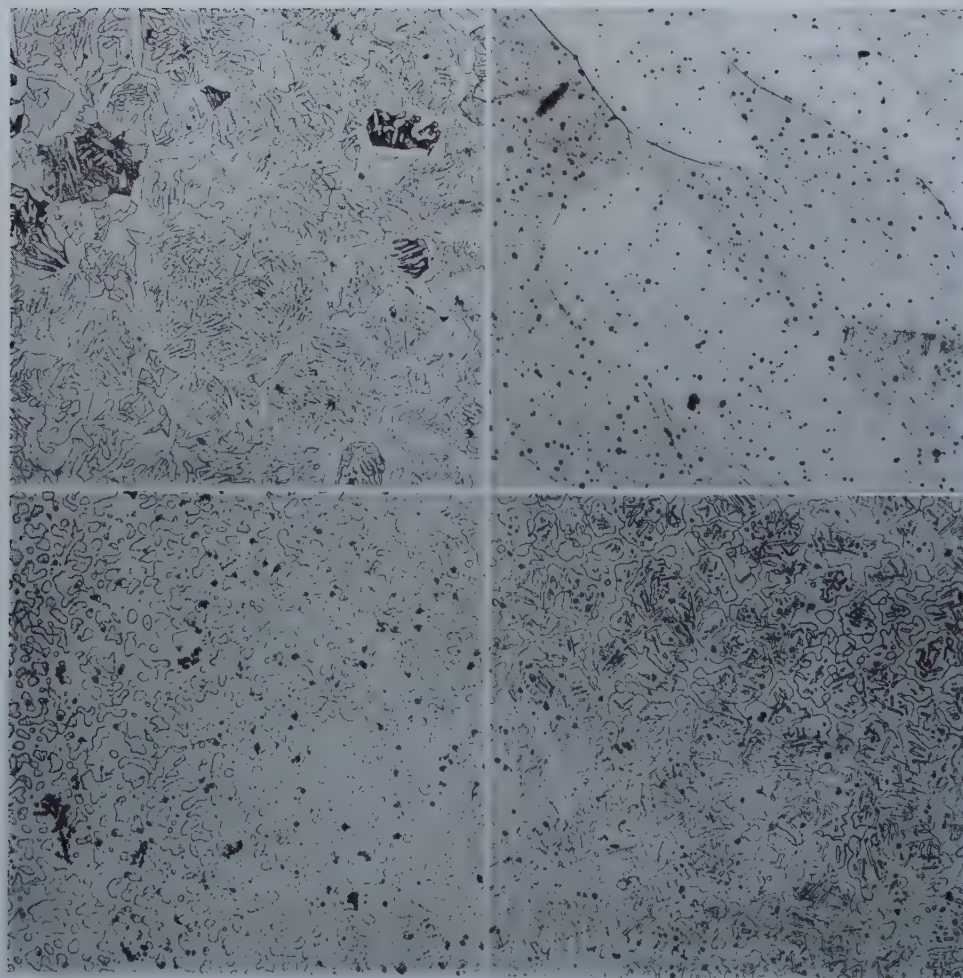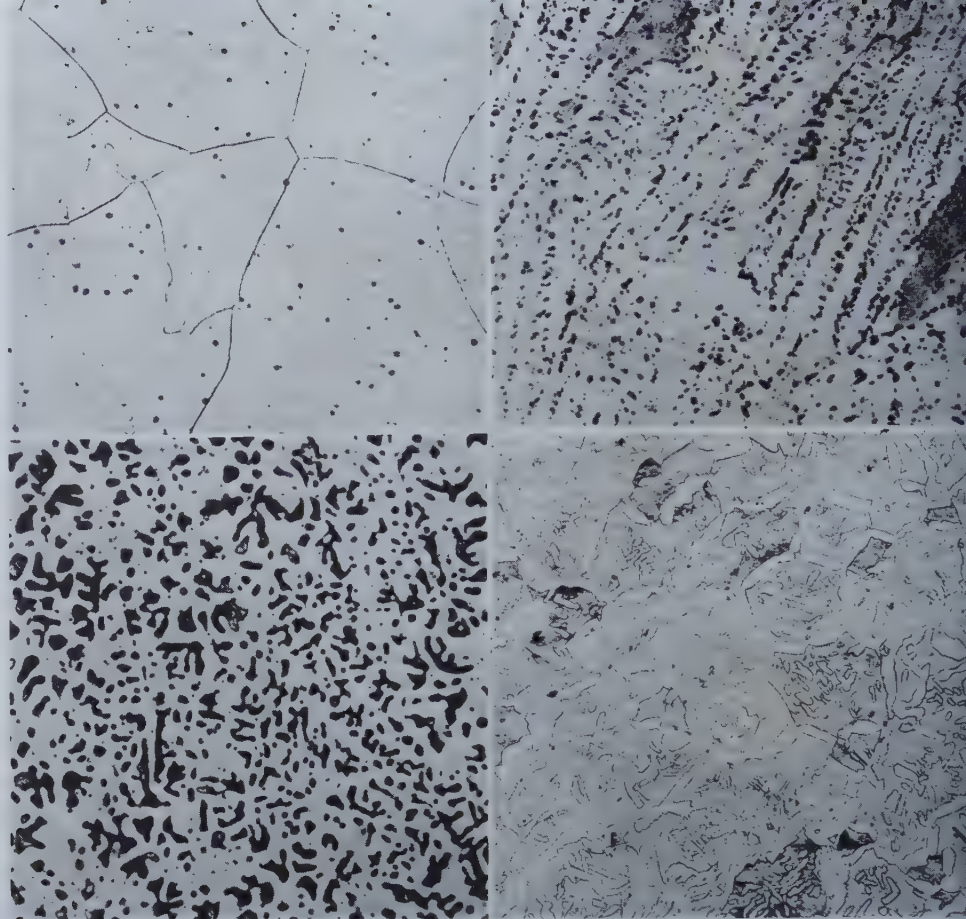Fig. 21 (upper left)—
Composition: 70 Cr 30
Ni. Fig. 22 (upper
right) — Composition:
80 Cr 20 Ni. Etchant:
HCl + $H_2O_2$. Fig. 23
(lower left) — Compo-
sition: 70 Fe 20 Cr 10
Ni. Etchant: Kahlings
Reagent. Fig. 24 (low-
er right) — Composi-
tion: 80 Fe 10 Cr 10
Ni. Etchant: Kahlings
Reagent.

Note: All micrographs are
of alloys held for 15 hr at
1150°C (2100°F) and
quenched.

Fig. 25 (upper left)—Composition: 30 Fe 30 Cr 40 Ni. Etchant: Marbles Reagent. Fig. 26 (upper right) — Composition: 30 Fe 40 Cr 30 Ni. Etchant: $(NO_2)_3$ $C_6$ $H_2$ OH + HCl. Fig. 27 (lower left)—Composition: 40 Fe 40 Cr 20 Ni. Etchant: $(NO_2)_3$ $C_6$ $H_2$ OH + HCl. Fig. 28 (lower right) — Composition: 50 Fe 40 Cr 10 Ni. Etchant HCl + $H_2$ $O_2$.

Note: All micrographs are of alloys held for 15 hr at 1150°C (2100°F) and quenched.

Fig. 29 (upper left)—Composition: 60 Fe 30 Cr 10 Ni. Etchant: HCl + $H_2$ $O_2$. Fig. 30 (upper right) — Composition: 50 Fe 30 Cr 20 Ni. Etchant: $(NO_2)_3$ $C_6$ $H_2$ OH + HCl. Fig. 31 (lower left) — Composition: 20 Fe 50 Cr 30 Ni. Fig. 32 (lower right) — Composition: 30 Fe 50 Cr 20 Ni.

Note: All micrographs are of alloys held for 15 hr at 1150°C (2100°F) and quenched.

something over 35 pct. At this point it presumably forsakes both binaries and expands to cover a vast range of temperature and intermediate compositions until it reaches the chromium-nickel binary.

The isothermal sections of fig. 14, 15, and 16 are published to indicate the differences in phase situation at the various temperatures.

Some of the micrographs of alloys which lie in this ternary alpha plus gamma region show interesting structures. Fig. 25 (30Fe, 30Cr, 40Ni) shows upon close examination what might be a minute quantity of precipitated alpha along crystallographic planes. This would infer that the alpha plus gamma region might be larger than previous investigation and our own hardness data (fig. 7) would indicate. This is a questionable region of the ternary. The alloy adjacent to this one (fig. 26—30Fe, 40Cr, 30Ni) shows a greater amount of precipitated alpha along the crystallographic planes.

Fig. 27 is a micrograph of an alloy (40Fe, 40Cr, 20Ni) which shows a typical eutectic structure occurring in this system.

Fig. 28 (50Fe, 40Cr, 10Ni) and fig. 29 (60Fe, 30Cr, 10Ni) present microstructures composed of white gamma crystals which precipitated from grey alpha solid solution along the alpha grain boundaries as well as within the alpha grains.

The microstructures of fig. 31 and 32 show the increase in structure coarseness with increasing iron content. Fig. 33 shows a microstructure typical of the nickel-rich gamma solid solution and fig. 34 shows an iron-rich gamma solution since the diffusion of atoms at this composition is too sluggish to permit alpha to precipitate.

## Summary

The constitutional diagram of iron-chromium-nickel alloys of a high degree of purity has been studied by hardness, elongation, tensile strength and dilatometric methods. The data collected in this way have verified much of the results of previous investigations. An enlargement of the gamma phase at 60 pct iron has been suggested on the basis of physical properties and a modification of many of the published diagrams in the iron rich corner has been made. Some of the most interesting of the micrographs of the fifty-five alloys tested are published and provide much interesting information about the system. While the extent of the sigma phase is probably considerably less than that of equilibrium and the alpha plus gamma region of the iron-nickel binary is rather ill defined, the diagrams presented here are believed to show a picture of the system which is as nearly accurate as is presently possible.

## References

[1] J. D. Nisbet: Producing High Purity Metals with Vacuum. *Iron Age*, June 19, 1947.

[2] J. D. Nisbet: Vacuum Melting Techniques. *Iron Age*, March 18, 1948.

[3] F. Adcock: Alloys of Iron Research. Part X—The Chromium-Iron Constitutional Diagram. *Jnl.* Iron Steel Inst. (1931) **124**, 99-149.

[4] F. Wever and W. Jellinghaus: Das Dreistoffsystem Eisen-Chrom-Nickel (The Iron-Chromium-Nickel System). *Mitt.* K.-W. Inst. Eisenforschung, (1931) **13**, 93-108.

[5] A. J. Bradley and H. J. Goldschmidt: X-Ray Investigation of Iron-Chromium-Nickel Alloys. *Jnl.* Iron Steel Inst. **144**, 273-283.

[6] R. H. Aborn and E. C. Bain: *Trans.* Am. Soc. Steel Treating, (1930) **18**, 837.

[7] H. Hougardy: Brittle Constituent in Chromium-Nickel-Iron Alloys. *Metal Progress* (1940) **37**, 64.

[8] P. D. Merica: Constitution of Iron-Nickel Alloys. *Metal Handbook,* (1939) 386-388.

[9] M. Hansen: Der Aufblau der Zweistofflegierungen (Constitution of Binary Alloys). Julius Springer, Berlin, 1936.

[10] J. S. Marsh: The Alloys of Iron and Nickel. **1**, New York: McGraw-Hill Book Co., 1938.

[11] B. Matsunaga: Japan Nickel Rev., **1**, 347.

[12] C. H. M. Jenkins, E. H. Bucknall, C. R. Austin, and G. A. Mellor: The Constitution of the Alloys of Nickel, Chromium, and Iron. *Jnl.* Iron Steel Inst., (1937) **136**, 187-222.

[13] E. C. Bain and W. E. Griffiths: An Introduction to the Iron-Chromium-Nickel Alloys. *Trans.* AIME (1927) **75**, 166-213.

[14] A. J. Bradley and H. J. Goldschmidt: *Jnl.* Iron Steel Inst. (1939) No. II p. 11.

[15] P. Schafmeister and R. Ergang: Das Zustandsschaubild Eisen-nickel-chrom (The Constitutional Diagram of Iron-Nickel-Chromium). *Archiv, f. d. Eisenhuttenwesen* (1939) **12**, 459-464.

# Effects of Three Interstitial Solutes (Nitrogen, Oxygen, and Carbon)

## on the Mechanical Properties of High-purity, Alpha Titanium

### by Walter L. Finlay and John A. Snyder

The effects of three interstitial solutes—nitrogen, oxygen, and carbon—on the mechanical properties of high-purity alpha titanium were determined on fusion-alloyed, annealed specimens in comparison with a substitutional solute, iron. A good correlation between bend ductility as well as the several microtensile properties and Vickers hardness was established for both the binary and ternary alloys of the interstitial solutes. In contrast to substitutional solutes, it was shown that the element with the lowest solubility had the greatest strengthening effect and this was discussed relative to the associated lattice parameter changes.

SEVERAL notable studies of the effects of substitutional solutes have been reported. Outstanding among these for its elucidation of general principles, is the summarized work of Hume-Rothery and coworkers.[1] For a systematic study of the effects of substitutional solutes on the mechanical properties of the solvent lattice, the work of Brick, Martin, and Angier[2] on copper; of Frye and coworkers[3, 4, 5] on copper and silver; and of Lacy and Gensamer[6] and of Austin[7] on iron may be mentioned.

Titanium is one of the few elements offering the possibility of a similar study of interstitial solutes since, unlike most metallic elements, it exhibits

W. L. FINLAY, Member, and J. A. SNYDER, Junior Member AIME are Supervisor and Research Metallurgist, respectively, Metals Research Unit, Remington Arms Co., Inc., Bridgeport, Conn.
New York Meeting, Feb. 1950.
TP 2759 E. Discussion (2 copies) may be sent to Transactions AIME before Apr. 1, 1950, and is scheduled for publication Nov. 1950. Manuscript received Oct. 18, 1949.

extended solid solubility for most of the interstitial solutes—hydrogen, boron, nitrogen, oxygen, and carbon. This paper reports a survey of the effects of dilute solutions of nitrogen, oxygen, and carbon on the mechanical properties of high-purity alpha titanium.

**Previous Work:** Van Arkel and De Boer showed[8] that high purity titanium was quite ductile and De Boer, Burgers and Fast established[9, 10] that not only were oxygen and nitrogen very soluble in

solid titanium but that, long before the limit of solid solubility of either had been reached, these interstitial solutes rendered the metal brittle. Their electrical resistance data as a function of
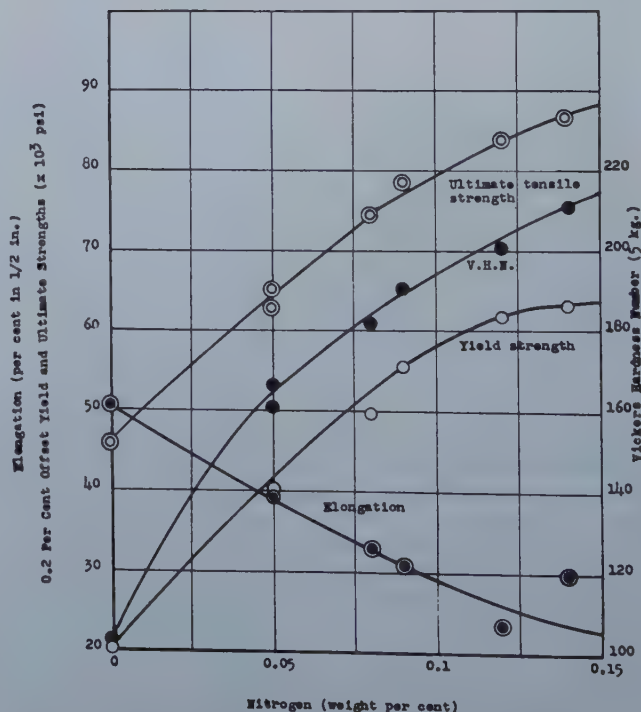


Fig. 1—Tensile properties and Vickers hardness of annealed, high-purity binary titanium nitrogen alloys.
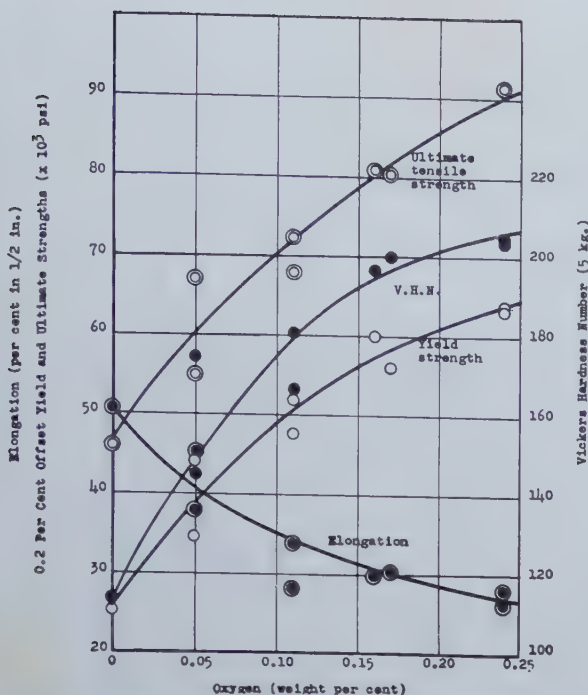
**Fig. 2—Tensile properties and Vickers hardness of annealed, high-purity binary titanium oxygen alloys.**

temperature showed that, with increasing contaminant, the alpha-beta transformation was both raised and spread over a temperature range. From this it may be inferred that the terminal alpha titanium solid solution in both binary alloys is formed by a peritectoid reaction. Ehrlich reported[11, 12] that the four binary systems of titanium with nitrogen, oxygen, carbon, and hydrogen were very similar and gave their maximum binary solid solubilities plus that of boron in titanium as:

| Element | Atomic Pct |
|---|---|
| Hydrogen | 33 |
| Oxygen | 30 |
| Nitrogen | 18 |
| Carbon | 8 |
| Boron | 7 |

Ehrlich gave no indication of the temperatures at which these maximum solubilities were obtained and it is believed that they can at best be considered only as approximations.

Fast concluded[10] that nitrogen had a more potent influence on the properties of titanium than did oxygen. Wartman, on the other hand, stated[13] that oxygen is the most important of all impurities in its effect on the mechanical properties of titanium. However, no quantitative data were presented by either investigator. The first report of such information was recently given[14] by Jaffee and Campbell. This work covered the effects in binary alloys of nitrogen, oxygen, and hydrogen on Vickers hardness, ultimate tensile strength, and percentage elongation.

## Experimental

**Outline of Investigation:** Titanium produced by the Van Arkel and De Boer process[8] involves the decomposition of titanium tetra-iodide on an incandescent filament and gives titanium of the highest purity obtainable.[15] Such titanium was employed throughout this investigation. As being prepared by the Battelle Memorial Institute for use in research programs sponsored by the Remington Arms Co., Inc., and others, this highest purity titanium has shown individual Vickers hardness readings as low as 60 and average Vickers hardnesses in the neighborhood of 70. In sharp contrast, commercial purity titanium has a Vickers hardness up to three times this minimum value.[16]

Battelle's best estimate[17] of the chemical composition of the iodide titanium prepared for alloy development work is as follows:

| | Standard Quality | Highest Purity |
|---|---|---|
| Raw material | 98.6 pct titanium | 99.8 pct iodide titanium |
| As-deposited hardness | 80-90 VHN | 70-80-VHN |
| Titanium | 99.85 | 99.95 |
| Nitrogen | 0.005 | 0.002 |
| Oxygen | undetermined | undetermined |
| Carbon | 0.03 | <0.03 |
| Iron | <0.04 | <0.02 |
| Aluminum | <0.05 | <0.03 |
| Silicon | <0.03 | <0.03 |

N.B.: 1. Both grades contain trace quantities of tungsten, molybdenum, lead, nickel and calcium.

2. Starting filament made of 99.8 pct titanium.

3. Based on Derge's results,[18] the oxygen content is believed to be approximately 0.01 pct in the
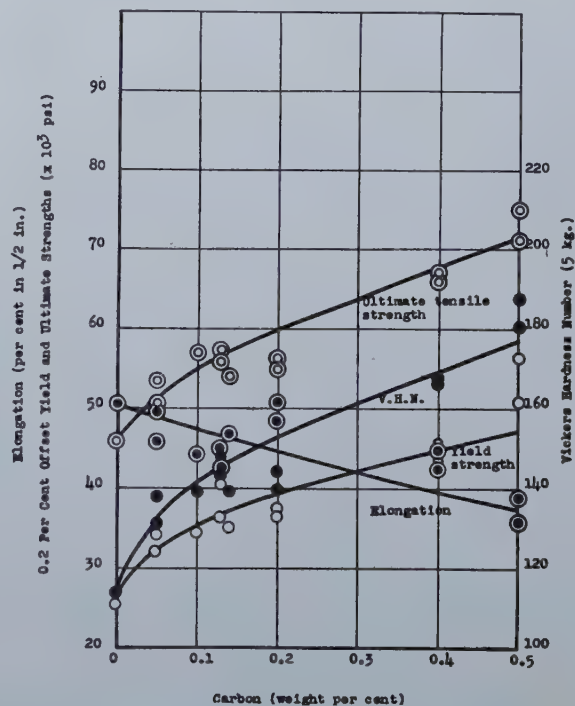


**Fig. 3—Tensile properties and Vickers hardness of annealed, high-purity binary titanium carbon alloys.**

standard quality and somewhat less than this in the highest purity grade.

Alloys and their unalloyed controls were prepared by fusion of as-deposited iodide titanium rod. Ingots approximately 10 g in weight were melted in purified argon in an electric arc furnace. In the case of alloys, the highest purity obtainable

element or titanium compound of the element, such as oxide, nitride, and carbide, was encapsulated in iodide titanium rod prior to melting. The cast ingots were cold rolled to 0.040 in. thick sheet, mechanically cleaned, 1000°C vacuum annealed, cold rolled to 0.020 in., and finally were annealed for one hour at 700°C in vacuum. For both the unalloyed titanium and its dilute binary and ternary alloys discussed in this paper, this treatment gave an annealed, equiaxed grain size of 0.020—0.025 mm av. diam. Several representative micrographs of these materials are presented in fig. 18-22. These were prepared according to the techniques recently[19] described by Finlay, Resketo and Vordahl.

**Microtensile Testing:** The scarcity and high cost of iodide titanium, particularly at the time when this investigation was undertaken, dictated the use of micrometallurgical procedures. Accordingly, equipment and techniques were established whereby accurate and reproducible tensile test results could be obtained on specimens having an overall length of 2¼ in. and gauge dimensions of 0.020 x 0.150 x 0.5 in. Yield and ultimate tensile strengths determined on microtensile and on standard A.S.T.M. sheet specimens of the same metal were found to agree closely; the microtensile elongation (over a ½ in. ga. length) was approximately five percentage points higher than the standard elongation (over a 2 in. ga. length) as was to be expected because of the proportionately larger effect which necking elongation has in the total ½ in. ga. length elongation. All microtensile results reported in this paper were on specimens whose longitudinal axis was parallel to the rolling direction; all the tensile data given are the average of three specimens.

**Hardness Testing:** Two 5-kg Vickers hardness determinations were made on each microtensile specimen. Thus, in general, each hardness figure
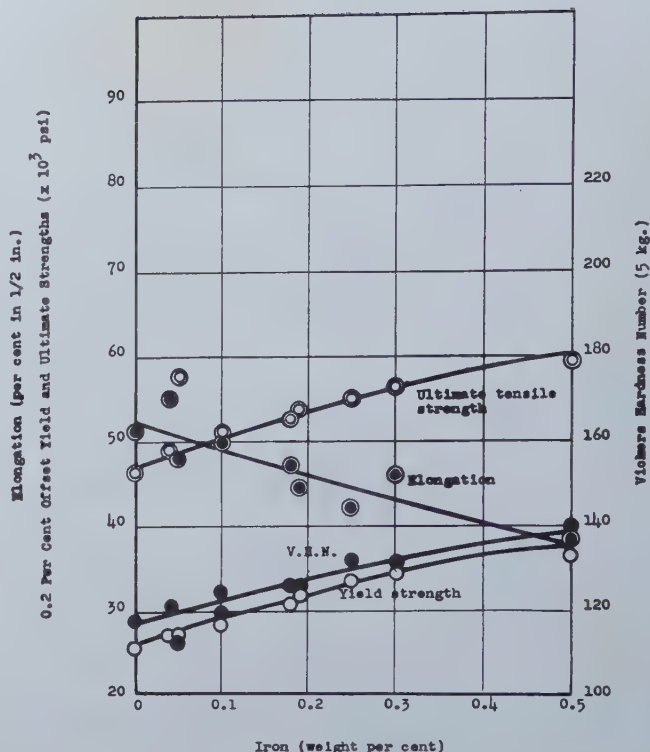


**Fig. 4—Tensile properties and Vickers hardness of annealed, high-purity binary titanium-iron alloys.**

packed structure. The conventional tensile test involves uniaxial stress during the period of uniform elongation and appreciable triaxiality during necking. With an 0.020 in. thick sheet specimen it is not feasible to determine reduction of area in the tensile test so that this index of reaction to triaxial stress was not available in this investigation. A sheet bend test, on the other hand, is quite convenient to conduct and, when a width-thickness
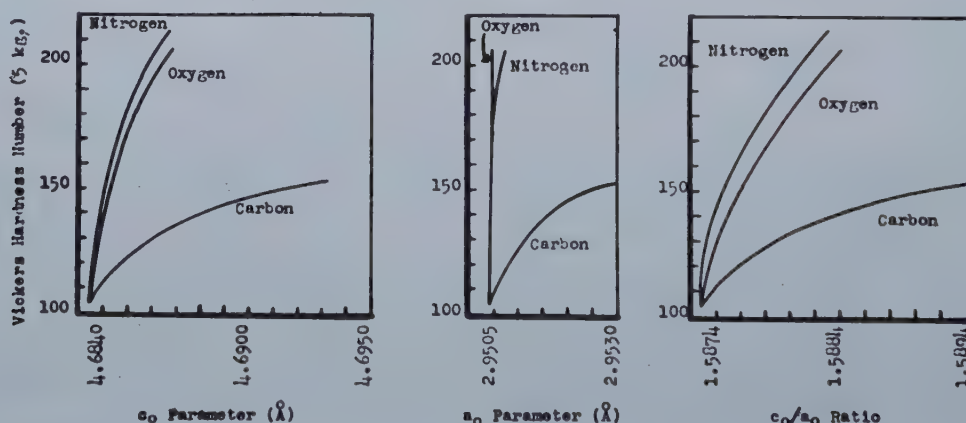


**Fig. 5—Correlation of Vickers hardness with the lattice parameters and $c_0/a_0$ ratios of annealed, high-purity, binary, titanium-base alloys containing nitrogen, oxygen and carbon.**

reported in this paper is the average of six hardness determinations.

**Bend Ductility:** The degree of axiality of the stress condition imposed by a given test is of particular importance in the case of alpha titanium because of the relatively few slip systems available for plastic deformation in its hexagonal-close-

ratio of eight or more is employed, considerable stress biaxiality is involved. Accordingly, a bend test was included in this investigation, employing specimens having dimensions of 0.020 × ⅜ × 2¼ in.

All the specimens involved in this study were found capable of being bent over a sharp (0.005 in.
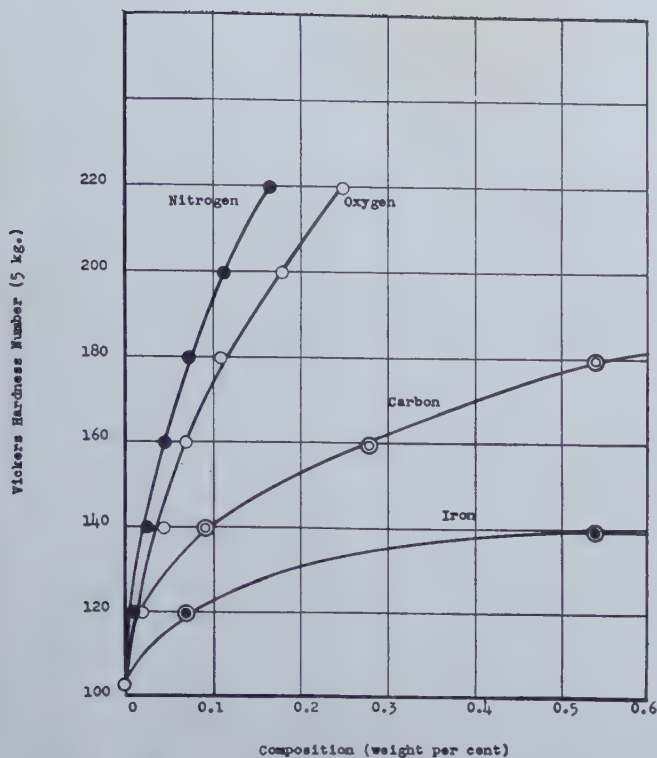
**Fig. 6—Relationship between Vickers hardness and composition by weight of annealed, high-purity, binary titanium-base alloys containing nitrogen, oxygen, carbon and iron.**
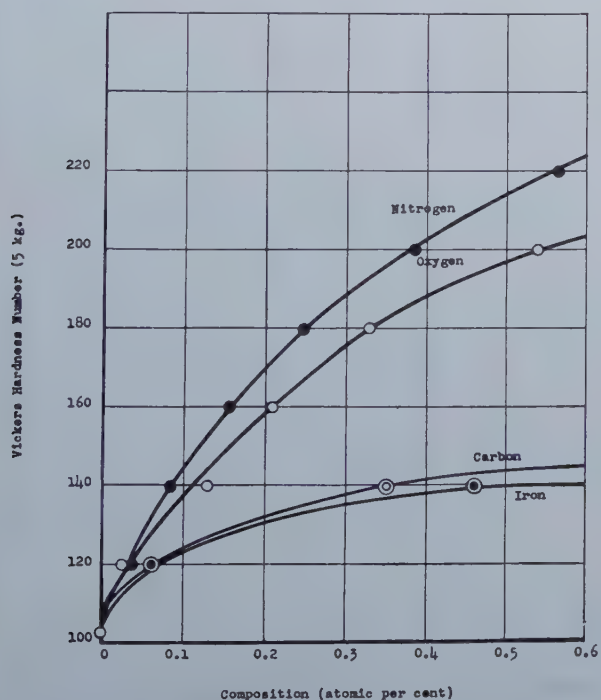


**Fig. 7—Relationship between Vickers hardness and composition by atomic percent of annealed, high-purity, binary, titanium-base alloys containing nitrogen, oxygen, carbon and iron.**

radius) wedge having an included angle of 75°, without any evidence of cracking. Specimens so bent were then folded flat on themselves (the 75°

included angle being thereby reduced to zero) and, if a particular specimen had not suffered cracking by then, it was opened out, by which action it was considered that the included angle decreased from zero to some negative value, e.g. to —180° if the specimen had been opened out flat. The bend ductility was taken as the angle at which the first evidence of cracking was detected.

**Reproducibility of Results:** A statistical analysis of the hardness, bend ductility, and microtensile properties of high-purity, unalloyed iodide titanium ingot melts made in the arc melting furnace during the period in which the melts involved in this study were made, showed the following rough screening differences for the various mechanical properties:

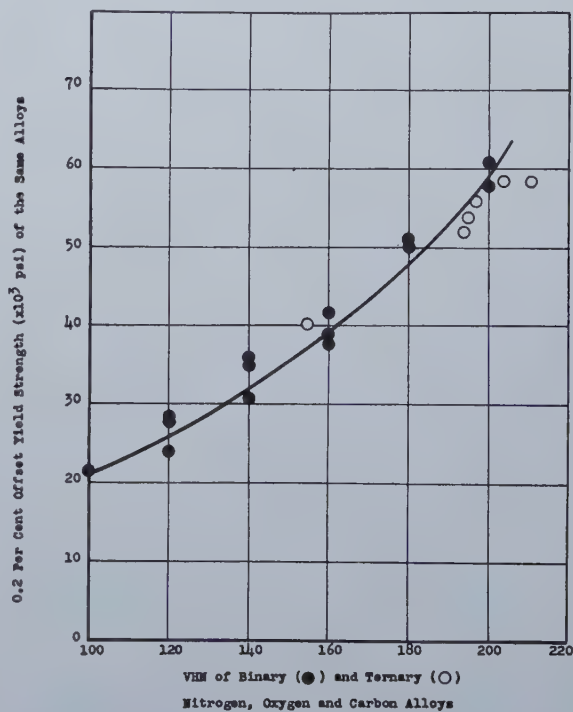| | |
|---|---|
| Bend Ductility | 60° |
| Hardness | 11 VHN |
| 0.2 pct Yield | 4,700 psi |
| Ultimate | 5,300 psi |
| Elongation (½ in.) | 10 pct |

These rough screening differences are triple the



**Fig. 8—Correlation of Vickers hardness with yield strength of annealed, high-purity, binary and ternary, titanium-base alloys containing nitrogen, oxygen and carbon.**

standard deviations and mean that if a sample has property values different from its reference base by more than the value given, then that sample is significantly different since, in even the borderline cases having differences just exceeding the values given, the probability of such a difference occurring by chance alone is only one in twenty.

**Properties of Unalloyed Base Material:** The average properties of the unalloyed iodide titanium employed in this investigation, in the form of 0.020 in. thick, annealed sheet with an 0.025 mm av. diam

grain size and fabricated from a fused, 10-g ingot were:

| | |
|---|---|
| Bend Ductility | —110° |
| Hardness | 103 VHN |
| 0.2 pct Yield | 21,400 psi |
| Ultimate | 46,000 psi |
| Elongation (½ in.) | 50 pct |

Because of the number of 10-g ingots involved, more than one iodide filament were used and this accounts for the variation in unalloyed properties shown in fig. 1-4. Both standard quality and highest purity iodide titanium grades were used, the latter for the lower alloy additions.

**Analysis of Chemical Composition:** It had fortunately been found, in melting gram quantities of pure iodide titanium in the arc furnace, that the furnace charge and the resulting cast ingot had the same weight within the accuracy of the analytical balance used, i.e. within 0.0002 g or, for the 10-g ingots involved, within 0.002 pct. When alloying



Fig. 10—Correlation of Vickers hardness with elongation of annealed, high-purity, binary and ternary, titanium-base alloys containing nitrogen, oxygen and carbon.
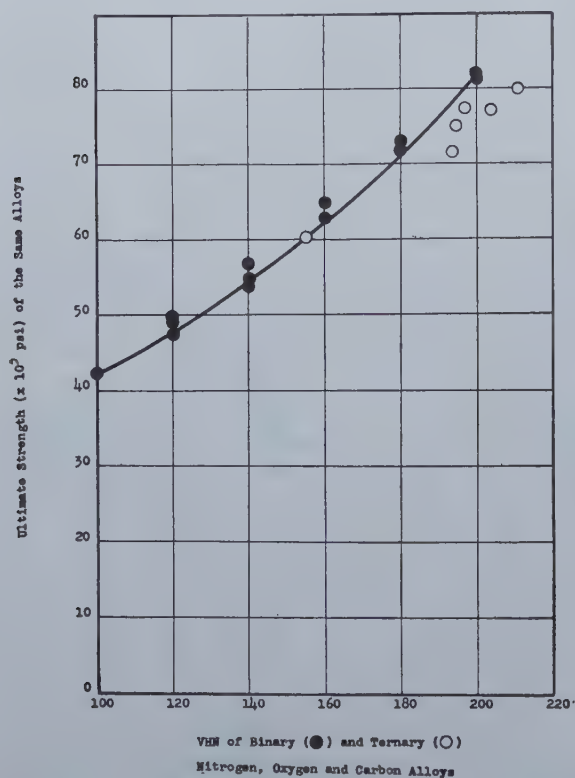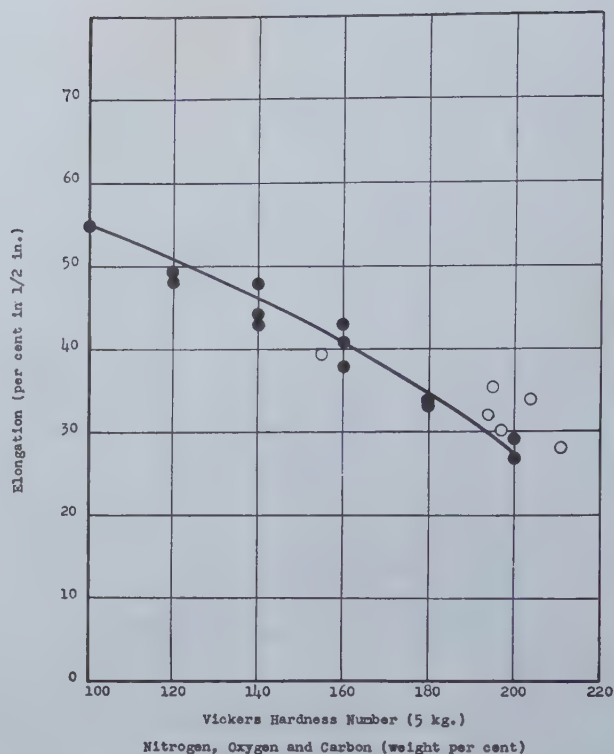


Fig. 9—Correlation of Vickers hardness with ultimate tensile strength of annealed, high-purity, binary and ternary, titanium-base alloys containing nitrogen, oxygen and carbon.

with titanium relatively nonvolatile metals, not only tungsten and molybdenum but also such elements as iron, aluminum, chromium, and copper, absence of a detectable weight change was also achieved. Chemical analyses of such ingots by standard wet procedures have checked the "weight analysis" within 0.02 pct.

The nonmetallic elements nitrogen, oxygen, and carbon offer the possibility of employing diffusion alloying as an alternative to fusion alloying. This procedure, however, is attended by its own problems, including those of holding thin, very highly
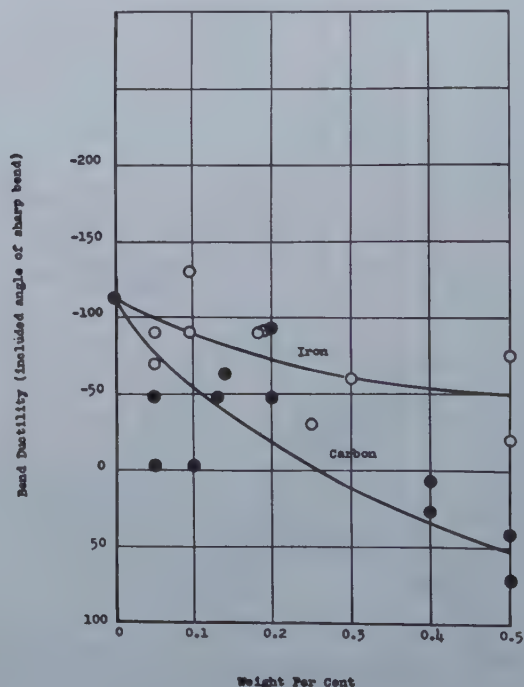


Fig. 11—Bend ductility of annealed, high-purity, binary titanium-base carbon and iron alloys.

reactive titanium sections for one or more hours above 1000°C without contamination, uncertainty whether homogeneity has been attained, poor control of grain size relative to the cold working and annealing practiced with fusion-alloyed specimens,

and the relatively slow diffusion rates of nitrogen and carbon in titanium.

In fusion alloying titanium oxide, nitride and carbide, a slight weight loss was incurred. This averaged 0.001 g in a 10-g charge for the dioxide and carbide, and approximately double this for the nitride. All this weight loss was ascribed to the loss of powdered compound and none to titanium metal. Thus the "weight analyses" of the ingots were arrived at. These were checked in a number of representative cases by chemical analysis. The latter agreed with the weight analyses within 0.03 pct for carbon, and within 0.02 pct for nitrogen.
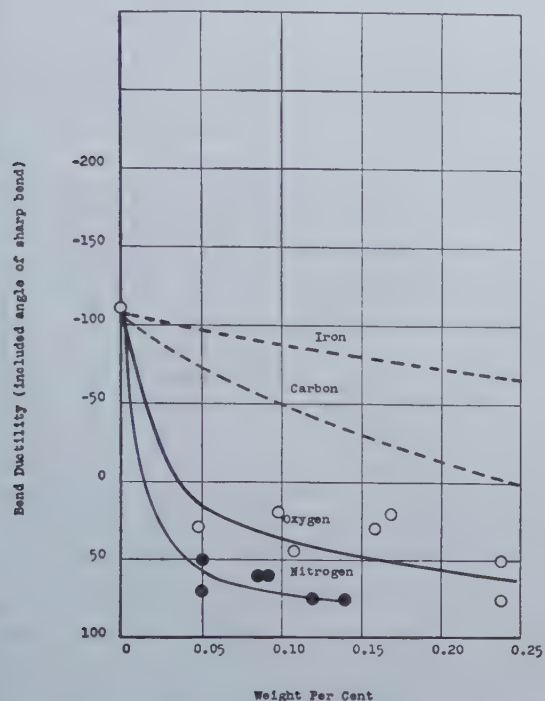


Fig. 12—Bend ductility of annealed, high-purity, binary titanium-base nitrogen, oxygen, carbon and iron alloys. Curves for last two from fig. 11.

One of the binary oxygen alloys was analyzed by Derge.[18] A difference of 0.03 pct was obtained between our weight analysis and his vacuum fusion analysis. This difference can, on the basis of other results obtained by Derge, be attributed to approximately 0.015 pct oxygen in the as-deposited iodide titanium filament and to a pickup of approximately 0.015 pct oxygen during arc fusion. These corrections were not made in the data reported in this paper.

### Results

Hardness and microtensile data on dilute binary alloys of three interstitial solutes, nitrogen, oxygen, and carbon, and of a single comparison substitutional solute, iron, are given in fig. 1-4. Relationships between Vickers hardness and composition for these four elements are shown in fig. 6 and 7. Bend ductility for these four elements is presented in fig. 11 and 12. Several typical micrographs are shown in fig. 18-22.

**Vickers Hardness—Tensile Properties Correlation:** Fig. 8, 9, and 10 were drawn from data derived from fig. 1-3 and show an excellent correla-

tion between Vickers hardness number and the three conventional tensile properties: (1) 0.2 pct Offset Yield Strength; (2) Ultimate Tensile Strength; and (3) Percent Elongation in ½ in. The points on these graphs were so close together for the binary alloys involving nitrogen, oxygen, and carbon that it was decided not to attempt to distinguish between them. Subsequently, similar data for ternary alloys involving these elements were plotted as open circles on these graphs and were found to fall within the band implied by the curve.

Fig. 11 and 12 show the relationships between bend ductility and the compositions of binary alloys based on nitrogen, oxygen and carbon. Fig. 13, derived from fig. 1-3 and fig. 11-12 shows the correlation between hardness and bend ductility of these alloys. Most of these derived data fall within a band 60° wide, representing the rough screening difference for bend ductilities at the 95 pct probability level.

Penetration hardness is well recognized as, at best, a complex criterion of the mechanical properties of a material, and any correlation with them must be carefully defined and probably should never be extrapolated. In the present case, the correlation has been established for fine-grained, equiaxed, annealed alpha titanium alloys involving nitrogen, oxygen, and carbon with hardnesses not appreciably exceeding 200 Vickers. Despite these delimitations, the correlation, while by no means
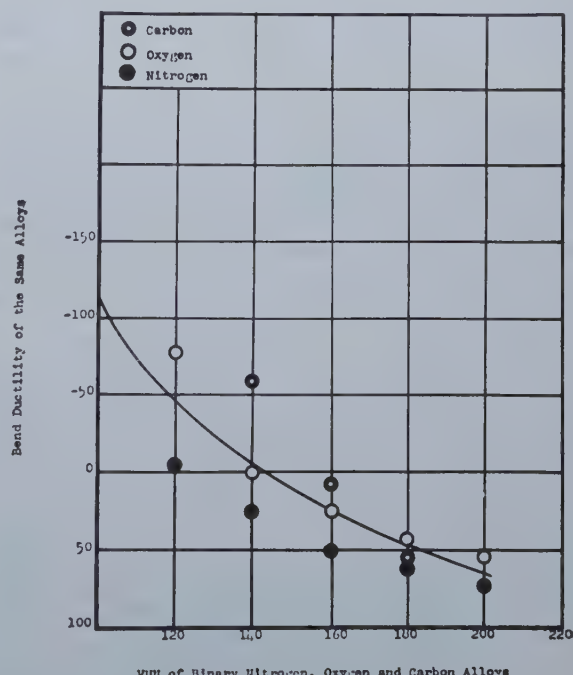


Fig. 13—Correlation of Vickers hardness with bend ductility of annealed, high-purity, binary, titanium-base alloys containing nitrogen, oxygen and carbon.

as extensive as the remarkable inter-relationships established for the tempered martensite structure by Janitzky and Baeyertz,[20] nevertheless is believed to be unusual.

**Binary Effects:** As a concomitant to the good correlation between Vickers hardness and microtensile properties, the outstanding effects of nitro-

gen and oxygen and the lesser effect of carbon are consistently exhibited by Vickers hardness, by yield strength, by ultimate strength, and by percent elongation.

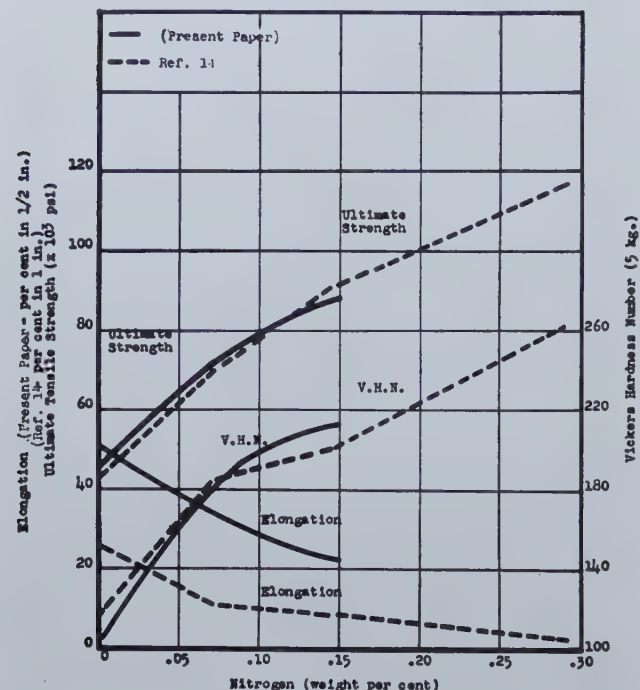Fig. 14, 15, and 16 compare the nitrogen and



Fig. 14—Comparison with Jaffee and Campbell[14] of the properties of annealed, high-purity titanium-nitrogen alloys.

oxygen data given by the present paper with those of Jaffee and Campbell.[14] These workers used iodide titanium as a base material and diffused oxygen and nitrogen into the solid titanium. They employed a 1 in. ga. length, which accounts for part, at least, of their consistently lower elongation

values. From fig. 14 and 16 it is seen that the data agree quite well for binary nitrogen. As can be seen in fig. 15, the binary oxygen alloys also exhibit good agreement up to 0.1 wt pct oxygen, beyond which point their data show higher hardnesses and lower ultimate tensile strengths than the authors'. The reason for this discrepancy is not known. One possible explanation which suggests itself, however, is that diffusion was not complete in their higher oxygen alloys so that their specimens had a harder case and a softer core than if they had been completely homogenized. In general, however, the close confirmation of the values obtained by the two different procedures is gratifying.

In connection with the scatter of the data in fig. 1-4, it is perhaps worth emphasizing the coupling of the uncertainty in the analyses (estimated to be about 0.03 pct) and the extraordinarily potent effects of nitrogen and oxygen on the mechanical properties of titanium. Less than 0.1 pct of these elements more than doubles the strength and halves the ductility of high-purity titanium. This is done, not by a multiplying factor such as is involved in the hardenability effect of boron in certain steels or in the grain boundary effect of bismuth in copper, but by simple solid solution. In any careful work with titanium and titanium-base alloys, therefore, the investigator must be ceaselessly vigilant against the accidental intrusion of these elements into his test material.

**Parameter-strength Correlation:** An interesting correlation between the lattice-expanding tendencies of nitrogen, oxygen and carbon and their effects on the mechanical properties of alpha titanium is shown in fig. 5. A similar effect has been shown[5] by Frye, Caum, and Treco for certain substitutional solutes in copper and silver. Data for fig. 5 were derived from fig. 6 of this paper and from the relationships between the lattice parameters and composition determined by Clark for carbon[21] and for



Fig. 15 — Comparison with Jaffee and Campbell[14] of the properties of annealed, high-purity titanium-oxygen alloys.
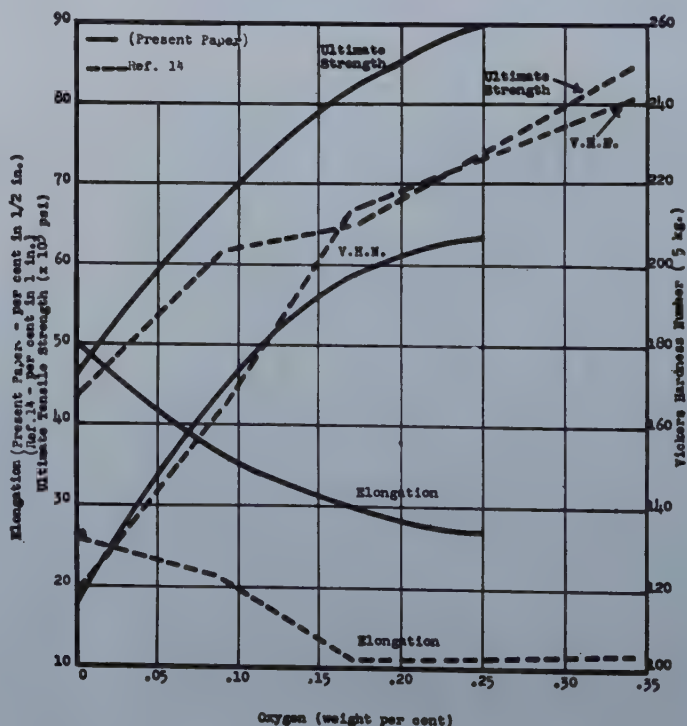
nitrogen and oxygen.[22] It is seen that the curves for oxygen and nitrogen almost coincide. It is something of an oversimplification to consider only the size factors of two solute atoms relative to their
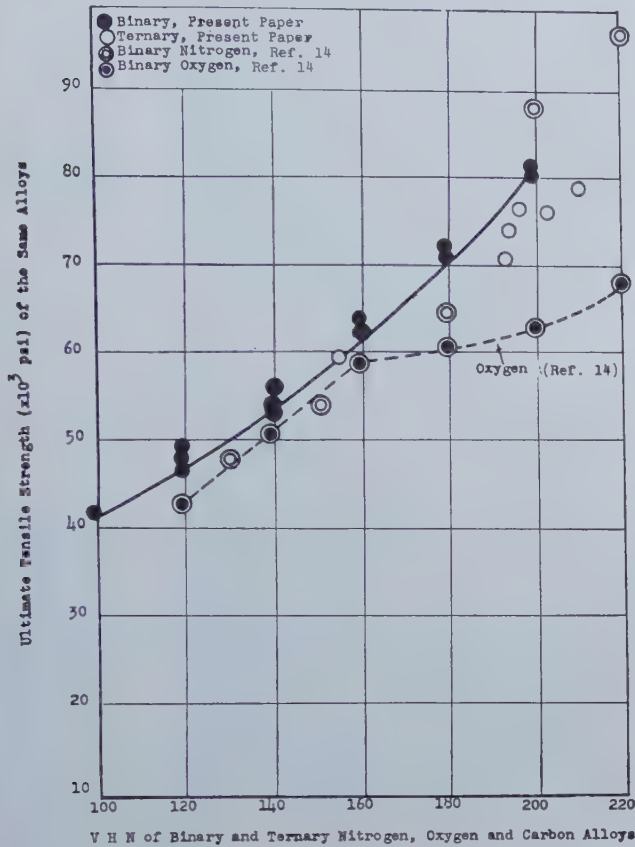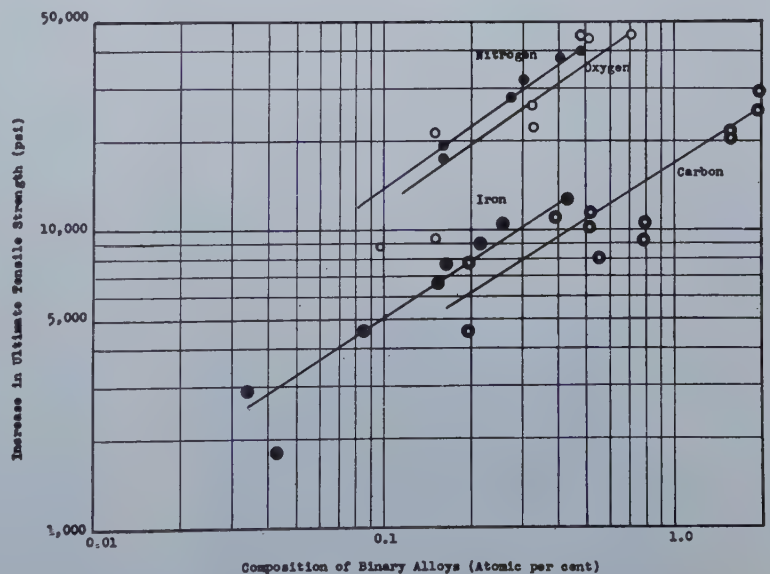
between mechanical properties, as epitomized by hardness, and the lattice parameters. With the lowest solubility, carbon has the lowest hardening effect despite having the greatest expanding effect on the lattice. This is contrary to the generalization which has been established for substitutional solutes in copper[2] and iron[6, 7], namely that the lower the parameter change effected by a solute the lower its hardening effect and the greater its solubility. Nitrogen, oxygen and carbon are, of course, interstitial solutes and this difference may be the basis on which the failure of the substitutional solute generalization to extend to the binary alloys under discussion may be explained. An opposite generalization for interstitial solutes, namely the greater the solubility the lesser the hardening effect, possibly cannot be made since nitrogen has a greater hardening effect on titanium than oxygen, yet is reported[12] by Ehrlich to have a greater solubility. A careful determination of the solubilities of nitrogen and oxygen would be of value in this regard. Another interstitial solute, hydrogen, appears to support the generalization for interstitial solutes since hydrogen has been shown[14] by Jaffee and Campbell to have a barely detectable hardening effect and is reported[12] by Ehrlich to have the highest solubility of any interstitial element.

It may appear surprising that carbon, with its greater expansion of the lattice than either oxygen or nitrogen, should effect less hardening. It will be noted from fig. 5, however, that carbon has a much more marked tendency than either nitrogen or oxygen to change the $c_0/a_0$ ratio towards the theoretical 1.63. Assuming the latter is associated with easier slip, one might envision that at least partial compensation for the lattice expansion is afforded

effects on the mechanical properties of a matrix lattice but perhaps oxygen and nitrogen are sufficiently alike in their interactions with the bonding electrons in the terminal alpha titanium solid solution to give rise to the correlation with the size effect shown by the parameter changes.

As shown in fig. 5, carbon exhibits, relative to nitrogen and oxygen, a quite different relationship

by closer approach to the $c_0/a_0$ ratio of hexagonally-close-packed spheres.

**Ternary Effects:** Several ternary alloys were made to secure some preliminary indication whether the simultaneous presence of two alloying elements from the group containing nitrogen, oxygen, and carbon gave mechanical properties which, on the basis of binary effects, were additive, more

Fig. 18—As-deposited, high-purity, iodide titanium. Light field illumination. "A" etch. 150X.
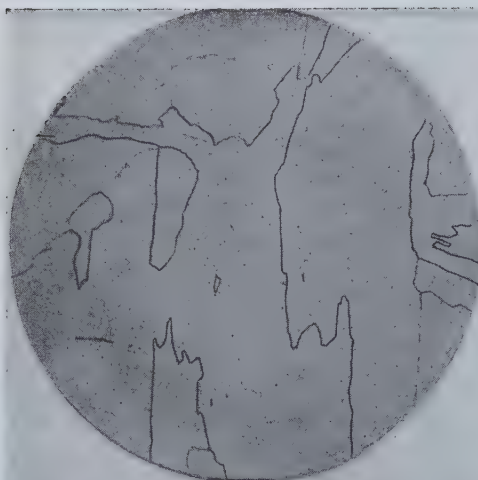
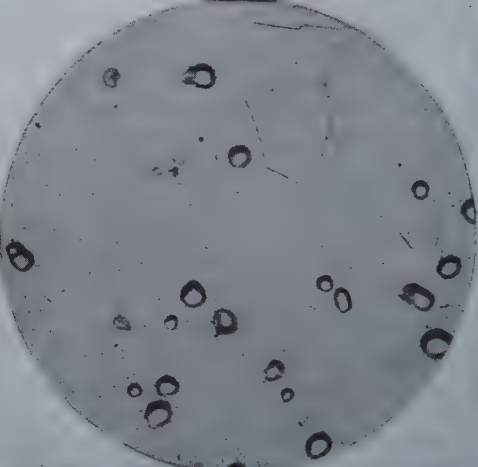Fig. 19—Same as Fig. 18, except dark field illumination.

Fig. 20—Ternary Ti-0.05 Nitrogen-0.07 Oxygen, 50 pct. Cold-rolled and annealed for one hour at 700°C. "B" etch. 600X.

Fig. 21—Binary Ti-0.4C, 50 pct. Cold-rolled and annealed for one hour at 700°C. "A" etch. 600X.

than additive or less than additive. Accordingly, the following additions were selected on the basis of their binary effects in giving a Vickers hardness in the neighborhood of 160:

| Nitrogen | 0.05 wt pct |
| Oxygen | 0.07 wt pct |
| Carbon | 0.20 wt pct |

Ternary additions were made by individual fusion for each addition; i.e. to make a ternary titanium-nitrogen-oxygen alloy, a titanium-nitrogen alloy



Fig. 22—Same as Fig. 21 except "B" etch.

was first melted and the TiO₂ was then melted into the binary titanium-nitrogen alloy. The following ingots were cast and tested:

| Code No. | Composition pct | VHN | Yield (psi) | Ultimate (psi) | Pct Elongation |
|---|---|---|---|---|---|
| 101-1 | 0.05 N 0.03 O | 211 | 58,800 | 80,000 | 28 |
| 101-2 | 0.05 N 0.03 O | 198 | 55,600 | 77,500 | 30 |
| 102-1 | 0.03 N 0.25 C | 194 | 52,000 | 71,900 | 32 |
| 102-2 | 0.05 N 0.20 C | 156 | 40,500 | 60,600 | 40 |
| 103-1 | 0.07 O 0.20 C | 204 | 58,800 | 77,100 | 34 |
| 103-2 | 0.07 O 0.20 C | 196 | 54,000 | 75,100 | 36 |

Fig. 8 through 10 show the relationship between Vickers hardness and microtensile properties by plotting the values in the foregoing tabulation as open circles. It is seen that these ternary values conform to the binary correlation.

Following the procedure of Lacy and Gensamer,[6] the log-log plot of ultimate strength increase versus composition in atomic percent shown in fig. 17 was drawn. The parallel, straight-line relationships established by Lacy and Gensamer for alloyed ferrites can perhaps be considered to hold for the four dilute titanium solid solutions considered in the present paper, although the scatter of experimental points is rather large. Moreover, the higher composition ranges of both the iron and the carbon

alloys are two-phase. However, it was felt worth-while as a first approximation to consider that the parallel, straight-line relationship existed and to employ the fig. 17 plot to express the concentration of all the elements in terms of equivalent concentration of one element, e.g. in terms of nitrogen. This is done in the following tabulation:

| Element | Atomic Pct to Increase Ultimate 15,000 psi | Equivalent Nitrogen Concentration (Atomic Pct) |
|---|---|---|
| Nitrogen | 0.115 | 1.00 |
| Oxygen | 0.140 | 0.82 |
| Iron | 0.57 | 0.20 |
| Carbon | 0.81 | 0.14 |

Employing the foregoing equivalent nitrogen concentrations, it is possible to compare the ultimate tensile strength of a particular ternary composition calculated on the basis of the addition of the binary effects with the experimentally observed ultimate tensile strength. This is done in table I.

**Table I. Comparison of Ultimate Tensile Strength with Experimentally Observed Ultimate Tensile Strength**

| Concentration Atomic Pct | Equiv. N. Concen. (At. Pct) | Total Equiv. N (At. Pct) | Calc. Ult. Strength (psi) | Obs. Ult. Strength (psi) | Difference |
|---|---|---|---|---|---|
| 0.17 N; 0.10 O | 0.17; 0.08 | 0.25 | 72,000 | 80,000 | 8,000 |
| 0.17 N; 0.10 O | 0.17; 0.08 | 0.25 | 72,000 | 77,500 | 5,500 |
| 0.11 N; 1.00 C | 0.11; 0.14 | 0.25 | 72,000 | 71,900 | —100 |
| 0.17 N; 0.80 C | 0.17; 0.11 | 0.28 | 74,000 | 60,600 | —13,400 |
| 0.20 O; 0.80 C | 0.16; 0.11 | 0.27 | 73,000 | 77,100 | 4,100 |
| 0.20 O; 0.80 C | 0.16; 0.11 | 0.27 | 73,000 | 75,100 | 2,100 |

The data in table I are relatively self-consistent with the exception of the two Ti-N-C alloys, the second of which has a considerably lower strength than would be expected from its analysis. The cause of this discrepancy is not known. From table I it would appear that, in dilute ternary alloys, the binary effects of nitrogen and carbon are somewhat less than additive, but that those of nitrogen and oxygen and of carbon and oxygen are somewhat more than additive. The paucity of the data, however, make these at most only preliminary indications.

## Summary and Conclusions

The effects of three interstitial solutes—nitrogen, oxygen, and carbon—on the mechanical properties of high-purity alpha titanium were determined on fusion-alloyed, annealed specimens in comparison with a substitutional solute, iron. A good correlation between bend ductility as well as the several microtensile properties and Vickers hardness was established for both the binary and ternary alloys of the interstitial solutes. Moreover, it was shown that, in contrast to the general principle established among substitutional solutes that the element with the lowest solubility has the greatest strengthening effect per unit concentration, the interstitial element with the lowest solubility of the three studied (carbon) has the lowest strengthening effect. In this regard attention was called to the fact that of the three, carbon had the most marked tendency to alter the axial ratio of its alloys to-

wards the theoretical 1.63 for the hexagonal-close-packed structure. Finally, a good correlation was shown between the amount of hardening and the amount of lattice parameter change effected by binary additions of nitrogen and oxygen.

## References

[1] W. Hume-Rothery: The Structure of Metals and Alloys. Inst. of Metals (London) Monograph I, Rev. 1947.

[2] R. M. Brick, D. L. Martin, and R. P. Angier: Effects of Various Solute Elements on the Hardness and Rolling Textures of Copper. Trans. ASM (1943) **31**, 675-695.

[3] J. H. Frye, Jr. and W. Hume-Rothery: Proc. Roy. Soc. (1942) **181A**, 1.

[4] J. H. Frye, Jr., and J. W. Caum: The Hardness of Certain Primary Copper Solid Solutions. Trans. AIME (1943) **152**, 75-82.

[5] J. H. Frye, Jr., J. W. Caum, and R. M. Treco: Hardness and Lattice Stress in Solid Solutions. Trans. AIME (1943) **152**, 83-89.

[6] C. E. Lacy and M. Gensamer: The Tensile Properties of Alloyed Ferrites. Trans. ASM (1944) **32**, 88-105.

[7] C. R. Austin: Effect of Elements in Solid Solution on Hardness and Response to Heat Treatment of Iron Binary Alloys. Trans. ASM (1943) **31**, 321-335.

[8] A. E. Van Arkel and J. H. de Boer: Ztsch. anorg. allg. Chem. (1925) **148**, 345.

[9] J. H. de Boer, W. G. Burgers, and J. D. Fast: Proc. Royal Acad. (1936) **39**, 515.

[10] J. D. Fast: Ductile Shaping of Zirconium and Titanium. Metallwiss. (1938) **17**, 459-462.

[11] P. Ehrlich: Ztsch. anorg. allg. Chem. (1941) **247**, 53-64.

[12] P. Ehrlich: Angew. Chem. (1947) **59A**, 163.

[13] F. S. Wartman: Production of Titanium Powder by the Bureau of Mines. Metal Prog. (1949) **55**, 188-190.

[14] R. I. Jaffee and I. E. Campbell: The Effect of Oxygen, Nitrogen, and Hydrogen on Iodide Refined Titanium. Trans. AIME (1949) **185**, 646-54. Jnl. of Metals, Sept. 1949.

[15] I. E. Campbell, R. I. Jaffee, J. M. Blocher, J. Gurland, and B. W. Gonser: Preparation and Properties of Pure Titanium. Trans. Electrochem. Soc. (1948) **93**, 6.

[16] C. I. Bradford, J. P. Catlin, and E. L. Wemple: Properties of Wrought Commercially Pure Titanium Prepared by Arc Melting and Casting. Metal Prog. (1949) **55**, 348-350.

[17] I. E. Campbell: private communication.

[18] G. Derge: Analysis of Oxygen in Titanium. Trans. AIME (1949) **31**. Jnl. of Metals, Jan. 1949.

[19] W. L. Finlay, J. Resketo and M. B. Vordahl: Some Introductory Notes on the Optical Metallography of Titanium. Titanium Symp., Amer. Chem. Soc., Atlantic City, Sept. 21, 1949.

[20] E. J. Janitzky and M. Baeyertz: The Marked Similarity in Tensile Properties of Several Heat Treated S.A.E. Steels. 1939 A.S.M. Handbook, 515-518.

[21] H. T. Clark, Jr.: private communication.

[22] H. T. Clark, Jr.: The Lattice Parameters of High Purity Alpha Titanium and the Effects of Nitrogen and Oxygen on Them. Trans. AIME (1949) **185**, 588-9. Jnl. of Metals, Sept. 1949.

Effect of Annealing in a Magnetic Field Upon

# Iron-Cobalt and Iron-Cobalt-Nickel Alloys

Prepared by Powder Metallurgy

by Joseph F. Libsch,

Eberhard Both,

George W. Beckman, Donald Warren and

Robert J. Franklin*

Iron-cobalt and iron-cobalt-nickel alloys prepared by powder metallurgy have been heat treated in a magnetic field. The 50 pct iron-cobalt alloy exhibits optimum magnetic properties and an essentially rectangular hysteresis loop when subjected to the best magnetic annealing cycle developed. Small amounts of nickel appear to be detrimental in the alloys studied.

BINARY and ternary alloys of iron, nickel and cobalt respond to annealing in a magnetic field by a characteristic change in the shape of their hysteresis loop.[1,2] An increase in retentivity and a decrease in coercive force produced by the magnetic treatment cause the hysteresis loop to approach the appearance of a rectangle.

Materials with a rectangular hysteresis loop have made possible the contact-rectifier[3] and have greatly improved the performance of pulse transformers[4] and magnetic amplifiers.[5] In the best material presently available for these applications, a 50 pct nickel-iron alloy,[6] the desired characteristics are achieved by aligning the preferred crystallographic directions of magnetization along the rolling direction of the tape.

The objective of the present study has been to produce rectangular hysteresis characteristics in materials with inherently high saturation. Iron-cobalt alloys, exhibiting saturation values up to 24,000 gausses[7] appeared to offer promise for the magnetic annealing technique, because they remain magnetic to very high temperatures,[8] exhibit favorable magnetostriction properties,[9] and show zero crystal energy at 42 pct cobalt.[10]

Among the ternary iron-cobalt-nickel alloys,[7,11] response to heat treatment in a magnetic field is unfortunately limited to alloys having rather low saturation values.[1] It appeared interesting nevertheless, to study a series of compositions connecting the optimum composition (50/50) of the binary

iron-cobalt system with the "Perminvar" composition (30 pct Fe, 25 pct Co, and 45 pct Ni).

Very recently, R. Smoluchowski and R. W. Turner,[12] have shown that under certain circumstances magnetic annealing can produce oriented recrystallization. A combination of this technique with the domain orientation utilized in the present study might well result in further improvements.

The advantages of the powder metallurgy technique in preparing magnetic alloys for study have

**Table I. Chemical Analysis of Powders Used in Preparation of Cores**

| Element | Type | C | P | S | Cu | Ni | Mn | Cr | Si | Fe |
|---|---|---|---|---|---|---|---|---|---|---|
| Iron Lot 1 | Electrolytic | 0.01 | 0.005 | 0.005 | 0.01 | 0.015 | 0.001 | 0.003 | 0.001 | balance |
| Cobalt Lot 1 | Reduced | | | | | | | | | |
| Lot 3 | | | | | | 0.42 | 0.28 | 0.01 | 0.43 | 1.20 |
| Lot 5 | | | | | | 0.42 | 1.1 | 0.018 | 0.35 | 0.75 |
| Lot 8 | | | | | | 0.53 | 0.09 | | 0.06 | 0.07 |
| Nickel | Carbonyl | 0.040 | | 0.001 | 0.004 | 0.50 99.92 | 0.09 | | | 0.025 |

**Table II. Screen Analysis of Powders Used in Preparation of Cores**

| Powder | 100/150 Mesh | 150/200 Mesh | 200/325 Mesh Pct | —325 Mesh Pct |
|---|---|---|---|---|
| Iron | | | | |
| Lot 1 | Trace | 22.4 pct | 29.5 | 48.4 |
| Lot 2 | Trace | 8.7 pct | 22.8 | 68.4 |
| Cobalt | | | | |
| Lot 1 | | | | |
| Lot 3 | Trace | Trace | 0.9 | 99.0 |
| Lot 5 | Trace | Trace | 1.1 | 98.8* |
| Lot 8 | Trace | Trace | 1 | 99 * |
| Nickel | 100 pct less than 6 microns | | | |

* Results of turbidimeter tests on Lots 5 and 8 cobalt powder showed a rather even distribution of 80 to 90 pct of each powder in the size range 9 to 37 microns.

**Table III. Composition and Sintered Density of Alloys**

| Pct Ni | Pct Fe | Pct Co | Density g per cc |
|---|---|---|---|
| **Series A** | | | |
| 10 | 50 | 50 | 7.88 |
| 20 | 45 | 45 | 8.09 |
| 30 | 40 | 40 | 8.15 |
| 40 | 35 | 35 | 8.23 |
| 50 | 30 | 30 | 8.28 |
| | 25 | 25 | 8.31 |
| **Series B** | | | |
| 10 | 55 | 45 | 7.85 |
| 20 | 50 | 40 | 8.01 |
| 30 | 45 | 35 | 8.06 |
| 40 | 40 | 30 | 8.17 |
| 50 | 35 | 25 | 8.17 |
| | 30 | 20 | 8.18 |
| **Perminvar** | | | |
| 45 | 30 | 25 | 8.23 |

been discussed by Rostoker[13] and are utilized in this study.

### Experimental Details

The experimental program required fabrication of test samples, performance of the magnetic anneal, and measurement of the consequent magnetic properties. Test samples were prepared from the elemental powders of iron, cobalt and nickel in the form of toroidal cores approximately 1⅞ in. od x 1 7/16 in. id x ¼ in. thick.

**Material:** High purity electrolytic iron powder from two lots having the chemical and screen analysis shown in tables I and II was selected for use.

Several lots of cobalt powder were used directly as supplied by the manufacturer. The cobalt powder was generally very fine and contained appreciable amounts of impurities as indicated in tables I and II. Toward the end of the study a limited amount of cobalt powder of special purity became available. This powder was very fine and was reported to contain 99.13 pct cobalt and 0.5 pct oxygen. Except where noted, the commercial cobalt powder was used in preparation of test cores.

**Preparation of Specimens:** Toroidal core specimens were prepared from the mixed elemental powders by the following sequence of operations:

1. Press mixed powders in die using pressure of 26 tons per in.² Die lubricant to be 3 pct stearic acid in carbon tetrachloride.
2. Pre-sinter green compact at 800-816°C for 10-25 min.
3. Machine to fit die, if necessary.
4. Repress compact at a pressure of 22 tons per in.² or 66 tons per in.²
5. Sinter compact at 1400-1430°C for a total time of 24 hr in atmosphere of purified dry elec-

trolytic hydrogen. Heating rate from 800° to 1400°C to be approximately 3°C per min.

The variations in the pre-sinter and repress operations correspond to changes made to facilitate production of the cores as the work progressed. These changes did not influence the final results obtained.

The apparatus used in fabricating the cores has been described by Rostoker.[18]

**Magnetic Anneal:** After fabrication and preliminary tests, toroidal cores were magnetically annealed in a stream of purified hydrogen. This was accomplished by heating the cores above their Curie points, and cooling in the presence of a magnetic field. Direct electric current was passed through a copper or platinum winding designed to develop a circumferential magnetic field of the desired magnitude. Optimum response in the magnetic anneal cycle generally involved an interruption in cooling at 900°C for 1½ hr and cooling to 230°C or below in the presence of the magnetic field.

The standard magnetic annealing treatment was therefore established as follows:

1. Heat cores above Curie temperature (1020°C) for 15 min.
2. Cool rapidly with magnetic field of 20 oersteds to 900°C.
3. Hold 1 to 1½ hr with magnetic field at 900°C.
4. Cool rapidly (23°C per min.) to 230°C or below in presence of magnetic field.

Except where noted, this standard magnetic annealing treatment was applied to all cores.

**Density Measurements:** Density determinations were made on all alloys using the weight in air-weight in water technique. Since the densities generally approached the theoretical value, the cores were not coated prior to immersion in water.

**Magnetic Testing:** The magnetic properties of the cores were determined by the standard ring method, employing a ballistic galvanometer and dc electric current. The ring dimensions were chosen in such a way as to make the radial thickness small with respect to the diameter.

The following magnetic properties were measured: (1) saturation at 100 oersteds, (2) retentivity or remanence after magnetization at 100 oersteds, and (3) coercive force. Because of extreme difficulty encountered in demagnetizing magnetic alloys cooled with a magnetic field, no attempt was made to measure permeability.[1]

**Variation in Magnetic Anneal Procedure for Iron-Cobalt-Nickel Cores:** The standard magnetic anneal procedure already described was used for all iron-cobalt cores. Iron-cobalt-nickel cores were annealed at the Signal Corps Engineering Laboratories, using a somewhat different procedure. This procedure consisted of heating in an atmosphere of purified electrolytic hydrogen to above the Curie temperature or the alpha-gamma transformation temperature of the individual cores in a magnetic field of 20 to 40 oersteds, increasing the field to 70-80 oersteds upon reaching maximum temperature; holding for 5 to 45 min and then cooling at 1.5 to 3°C per min to 500°C followed by continued cooling at approximately 20°C per min to below
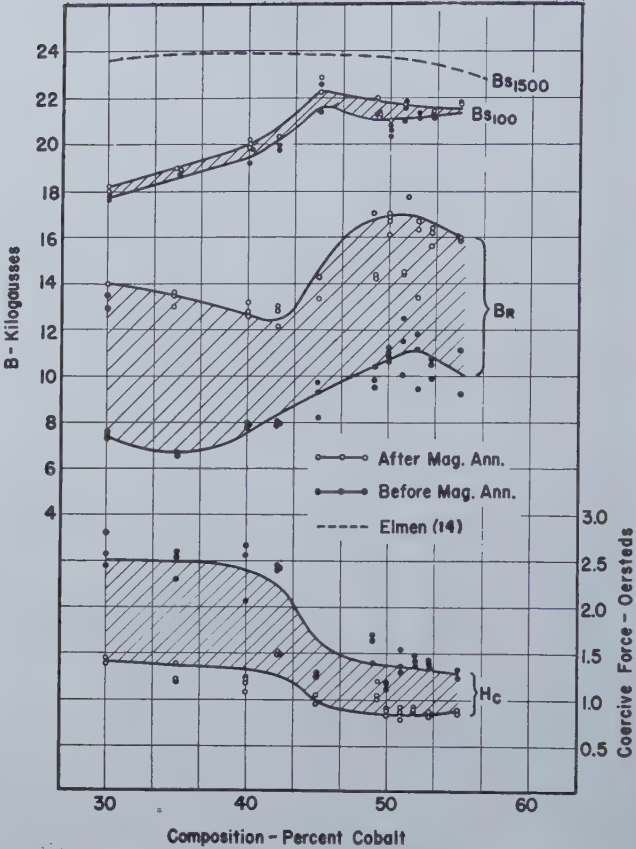


Fig. 1—Effect of Magnetic Anneal on the Magnetic Properties of Iron-Cobalt Alloys.
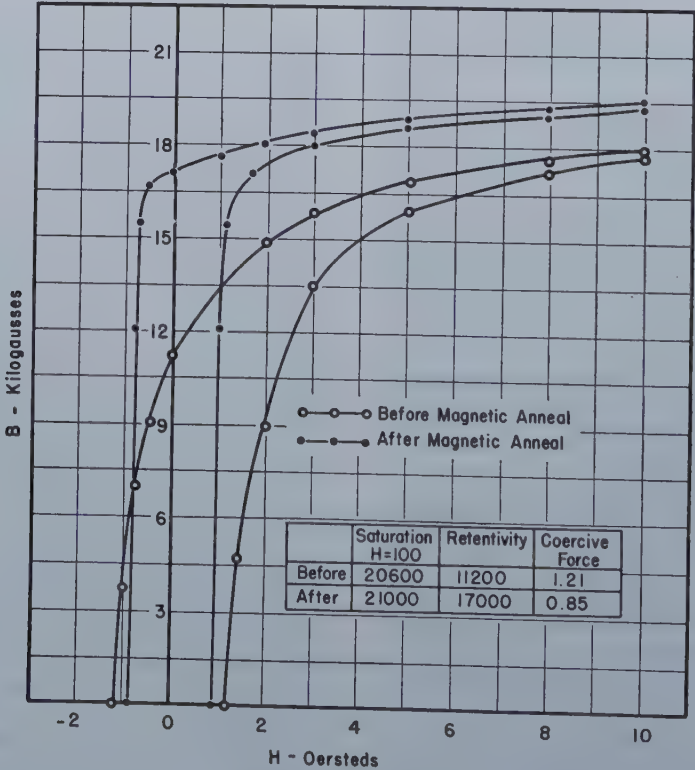


Fig. 2—Hysteresis Loops and Magnetic Properties of 50 pct Iron-50 pct Cobalt Alloy, Before and After Magnetic Annealing.
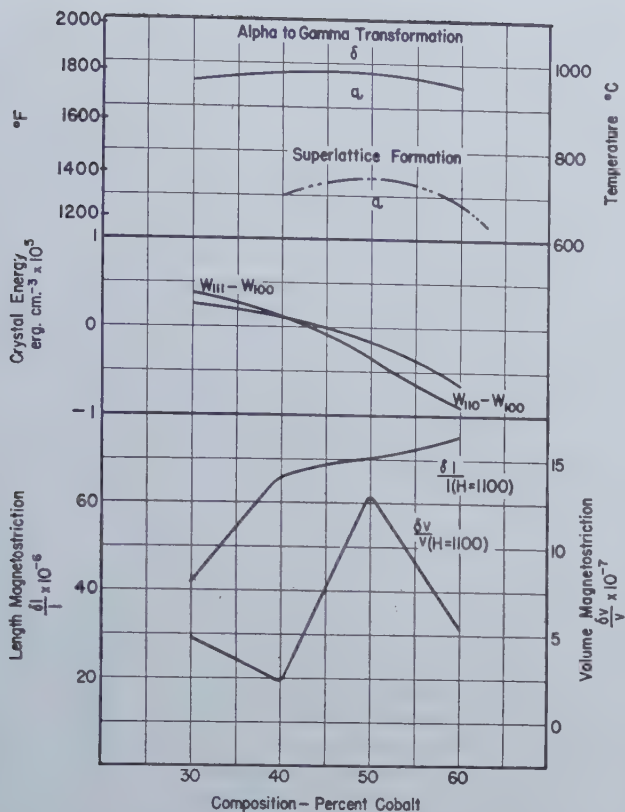
Fig. 3—Fundamental Literature Data
for Binary Alloys of Iron and Cobalt.

Magnetostriction — Masiyama[9]

Crystal Energy — Shih[10]

Alpha to Gamma Transformation
Superlattice Formation } Metals Handbook—1948[8]

100°C with the magnetic field. For the cores of the binary alloys, and the alloys containing 10 pct of nickel, the faster cooling rate was applied at 800°C rather than at 500°C.

### Experimental Results and Discussion

**Response of Iron-Cobalt Alloys to Magnetic Annealing:** Since the alloys of iron and cobalt containing approximately 30 to 55 pct cobalt possess the highest saturation values known for magnetic materials, binary alloys of iron and cobalt were prepared in this range of composition to determine the optimum magnetic properties and response to magnetic annealing.

The effect of composition on the magnetic properties of iron-cobalt alloys before and after magnetic annealing is shown in fig. 1. The properties plotted show the variation in the saturation induction measured at 100 oersteds, the retentivity, and the coercive force caused by the magnetic anneal. Magnetic saturation values given by G. W. Elmen[14]*

---
\* These values are credited to Elmen by Bozorth in ref. 14; they are somewhat at variance with those reported by Elmen in ref. 7.
---

for a field strength of 1500 oersteds are plotted for comparison.

The marked influence of magnetic annealing upon the magnetic properties of iron-cobalt alloys is clearly demonstrated by fig. 1. In general, magnetic annealing causes a large increase in retentivity, an insignificant increase in saturation (H = 100), and a decrease in the coercive force for the alloys studied. The optimum response to magnetic an-

nealing occurs at a cobalt concentration of approximately 50 pct.

The spread in experimental data for the alloys having a composition close to 50 pct iron-50 pct cobalt appears significant. Since almost no variation in magnetic properties occurred for alloys with lower cobalt concentrations, the spread noted for alloys containing approximately 50 pct cobalt appears due to the sensitive behavior of the latter alloys, rather than to any variation in processing variables. This sensitive behavior is most probably associated with the formation of the superlattice in this range of composition.

The 50 pct iron-50 pct cobalt alloy, after annealing, also shows the best magnetic properties characteristic of materials which develop a rectangular hysteresis loop, i.e., a high ratio of retentivity to saturation and a low coercive force. Fig. 2 shows typical hysteresis loops before and after magnetic annealing cores of a 50 pct iron-50 pct cobalt alloy prepared from commercial cobalt powder.

It is significant to note that the 58 pct iron-42 pct cobalt alloy shows the smallest increase in retentivity as the result of magnetic annealing. This result is surprising, since the 42 pct cobalt alloy was initially selected as the most promising for study after an analysis of the important parameters for optimum response to magnetic annealing. Fig. 3, for example, shows that the 42 pct cobalt alloy is magnetic to a very high temperature (980°C[8]); has a high linear magnetostriction value (67.0 x 10⁻⁶)[9] at room temperature and zero crystal anisotropy.[10]

Similar conditions in the iron-nickel system are associated with an excellent response to magnetic annealing.

Poor response to magnetic annealing in the 42 pct cobalt alloy, and optimum response in the 50 pct cobalt alloy are difficult to explain. A comparison of the magnetic constants for these two alloys shown in fig. 3, however, is interesting. The crystal energy of the 50 pct cobalt alloy is considerably greater than that of the 42 pct cobalt alloy. However, the abrupt increase in the volume magnetostriction at the 50/50 composition and the known presence of a superlattice formation in this range appear to be more than a coincidence, and seem to exert a controlling influence on the behavior of the iron-cobalt alloys in the magnetic anneal.

**Effect of Nickel on the Magnetic Properties of Iron-Cobalt Alloys:** Certain binary alloys of iron and nickel provide interesting magnetic characteristics and have achieved commercial prominence. A large number of these alloys respond to heat treatment in a magnetic field[1] and exhibit rectangular hysteresis loops and a low coercive force after magnetic annealing.

Since the binary alloys of iron and cobalt studied showed a comparatively high coercive force after magnetic annealing, it appeared desirable to determine the influence of nickel on the magnetic properties of iron-cobalt alloys.

Two series of iron-cobalt-nickel alloys were therefore fabricated, magnetically annealed, and tested (1) containing 0 to 50 pct of nickel and equal amounts of iron and cobalt and (2) containing 0 to 50 pct of nickel and an iron content exceeding the cobalt content by 10 pct. Table III gives the composition of the alloys prepared and their sintered density. In addition, cores corresponding to the commercial alloy Perminvar (30 pct iron, 25 pct cobalt, and 45 pct nickel) were prepared in an effort to confirm the response of this alloy to magnetic annealing. All iron-cobalt-nickel cores were fabricated in the standard manner except that they were repressed at 66 tons per in.[2] and sintered at 1375°C, rather than at 1400°C. Magnetic annealing and testing were conducted at the Signal Corps Engineering Laboratories in accordance with the technique already discussed.

The saturation induction, the retentivity and the coercive force before and after magnetic annealing are shown in fig. 4 for the series of iron-cobalt-nickel alloys containing equal amounts of iron and cobalt.

The data presented show a sharp decrease in saturation induction and in retentivity; and an exceedingly sharp increase in the coercive force as the nickel content is increased from 0 to 10 pct. While the coercive force decreases rapidly to a low value with a further increase in nickel content, the saturation and retentivity of the alloys containing more than 10 pct of nickel are considerably less than the saturation and retentivity of the 50 pct iron-50 pct cobalt alloy.

The primary influence of heat treatment in the magnetic field appears to be an increase in the retentivity. It is interesting to note from fig. 4 that this increase is pronounced for the alloys containing zero per cent nickel and 30 to 50 pct nickel, but

is very small for the alloy containing 45 pct iron, 45 pct cobalt and 10 pct nickel. The failure of iron-cobalt-nickel alloys containing 10 to 20 pct nickel to show appreciable response to magnetic annealing confirms the work of Bozorth and Dillinger.[1] It may be explained by the simultaneous presence of two phases for alloys of this composition when they are cooled to room temperature. The large coercive force also is the result of this fact.

The saturation induction, the retentivity and the coercive force before and after magnetic annealing are shown in fig. 5 for the series of iron-cobalt-nickel alloys in which iron exceeds cobalt by 10 pct. In general the effect of nickel in the iron-rich alloys is similar to its effect in the alloys containing equal amounts of cobalt and iron; although the minimum values of saturation induction and retentivity after magnetic annealing, and the maximum value of the coercive force occur at a somewhat higher nickel content, i.e., 20 pct nickel. This is most probably due to the location of the boundaries of the heterogeneous two phase field in the iron-cobalt-nickel system extending from the 78 pct cobalt point on the iron-cobalt side to the binary iron-nickel alloys with 20 to 30 pct nickel.

It is interesting to note in fig. 5 that the coercive force is a maximum after the magnetic anneal for the 20 pct nickel alloy. This observation is contrary to the decrease in coercive force resulting from the magnetic anneal experienced with all other iron-cobalt-nickel cores. The anomalous behavior of the 20 pct nickel alloy is most probably associated with the effect of heat treatment upon the development of the heterogeneous alloy containing two phases.

The magnetic properties before and after magnetic annealing of a Perminvar core prepared by powder metallurgy are given in table IV. This table also shows the approximate results obtained by Bozorth and Dillinger[1] by heat treating Perminvar in a magnetic field. The results are in fair agreement and confirm the response of this alloy to heat treatment in a magnetic field. The results also demonstrate that alloys prepared by powder metallurgy give results comparable to those prepared by conventional methods.

For the iron-cobalt-nickel alloys studied, the results presented demonstrate the undesirable influence of nickel upon the magnetic properties after heat treatment in a magnetic field. Unfortunately, a reduction in the coercive force is obtained only with nickel contents which cause a considerable decrease in the values of saturation and retentivity. Because of the sharp increase in coercive force with low nickel concentration, it appears that the presence of nickel as an impurity in the cobalt powder may be very detrimental.

**Influence of Variables in the Magnetic Anneal:** The influence of a number of variables in the magnetic annealing treatment was studied to determine an optimum cycle.

**Field Strength:** Experiments to determine the influence of field strength during cooling were conducted over a range of 1 to 20 oersteds, using a 50 pct iron-50 pct cobalt alloy. The subsequent tests conducted on iron-cobalt-nickel alloys, using a field strength of 70-80 oersteds during cooling, did not
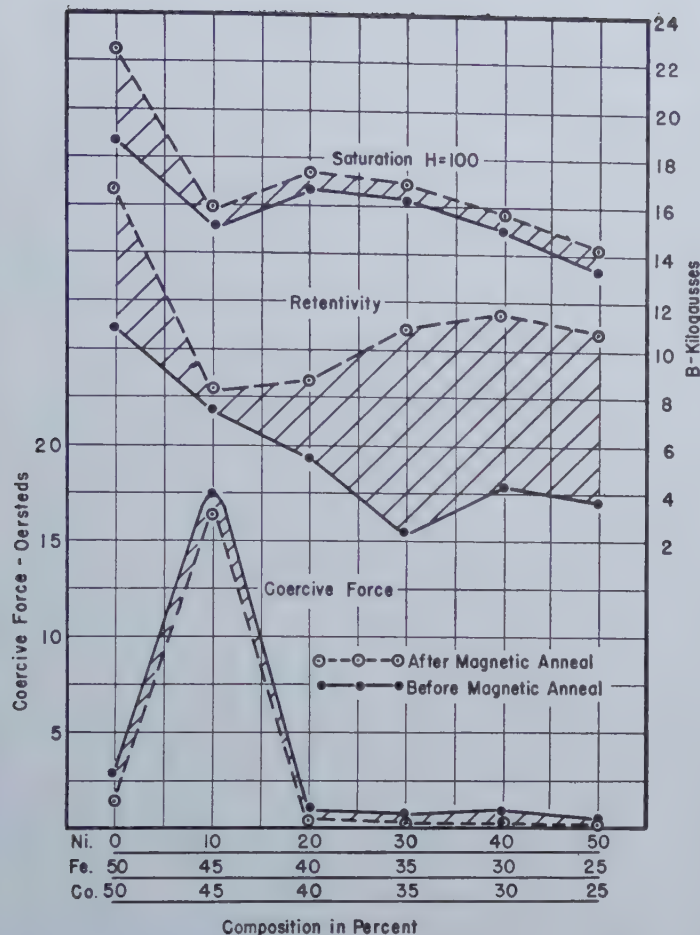
**Fig. 4—Influence of Nickel on the Magnetic Properties of Iron-Cobalt Alloys, Before and After Magnetic Annealing, pct Fe = pct Co.**

## Table IV. Magnetic Properties of Perminvar Core

| Properties | Before Magnetic Annealing | After Magnetic Annealing | |
| --- | --- | --- | --- |
| | | Present Study | Bozorth and Dillinger[1] |
| Saturation (H = 100) gausses | 15,200 | 16,350 | |
| Retentivity gausses | 4,000 | 12,850 | 13,500* |
| Coercive Force oersteds | 0.45 | 0.09 | 0.07* |

* Approximate values determined from graph presented by Bozorth and Dillinger.[1]

## Table V. Influence of Cooling Rates

| Cooling Rate | Magnetic Properties After Magnetic Anneal | | |
| --- | --- | --- | --- |
| °C per min | Saturation (H = 100) gausses | Retentivity gausses | Coercive Force oersteds |
| 3 | 20,750 | 16,400 | 1.09 |
| 23 | 20,700 | 16,900 | 0.94 |
| 48 | 20,900 | 17,000 | 0.88 |

appear to alter the conclusions reached from the experimental work using lower field strengths.

The influence of field strength on the retentivity and the coercive force after magnetic annealing is shown in fig. 6. Also plotted in this figure is the influence of field strength during magnetic annealing upon the ratio of retentivity to saturation in per cent. This ratio is an indication of the magnetic orientation achieved by magnetic annealing, and of the approach to a rectangular hysteresis loop. In these tests the cores were prepared from commercial cobalt powder, and were treated in accordance with the standard magnetic anneal cycle except that a slow cooling rate (3°C per min) was used to cool from the holding temperature of 900°C. Since subsequent experiments showed the beneficial effect of cooling more rapidly, particularly with respect to the coercive force, the properties shown in fig. 6 should not be considered optimum.

The rapid increase in retentivity upon cooling in a magnetic field as weak as 1 oersted is striking. It is also notable that the retentivity as well as the coercive force show little change as the field strength is increased from 10 to 20 oersteds. For this reason, all subsequent cores, except the iron-cobalt-nickel alloys, were cooled in a magnetic field of 20 oersteds.

It is interesting to note that Kelsall[1] also obtained excellent response to magnetic annealing for iron-nickel and iron-cobalt-nickel alloys using a field strength of one oersted. Apparently, only low field strengths are required to develop sufficient magnetostrictive stresses for good response to magnetic annealing in those alloys which do respond.

**Cooling Method:** The formation of a superlattice known to form in 50 pct iron-50 pct cobalt alloys under favorable conditions of cooling from above the $\alpha$–$\gamma$ transformation (see fig. 3), and the possible influence of the superlattice formation upon the magnetic properties, after magnetic annealing, made a study of the influence of cooling rate very desirable.

Three approximate cooling rates were used, (1) 3°C per min, (2) 23°C per min, and (3) 48°C per min, all cooling rates being determined over the temperature range 900 to 100°C. The influence of cooling rate may be seen by a comparison of magnetic properties after the magnetic anneal shown in table V. The results shown are an average of four cores heat treated in accordance with the standard magnetic anneal procedure described, except that the cooling rate was varied.

The principal effect of rapid cooling in the presence of a magnetic field is a decrease in the coercive force, without an appreciable change in the retentivity or saturation. This effect appears most pronounced when the cooling rate is increased from 3 to 23°C per min and seems less pronounced and consistent when it is increased to 48°C per min.

The decrease in coercive force resulting from a

### Table VI. Effect of Interrupting Cooling

| | Magnetic Properties | | | |
| | Cooling Rate 3° C per min | | Cooling Rate 23° C per min | |
| Time at 900°C (Hrs) | $B_R$ per $B_s$, Pct | $H_c$, oersteds | $B_R$ per $B_s$, Pct | $H_c$, oersteds |
|---|---|---|---|---|
| 1 | 82.6 | 0.94 | 84 | 0.84 |
| 0 | 79.9 | 1.06 | 80.9 | 0.97 |

### Table VII. Influence of Magnetic Field in Cooling

| Treatment | Magnetic Properties | |
| | $B_R$ per $B_s$, Pct | $H_c$, oersteds |
|---|---|---|
| Field Applied During Cooling 1020° to 900° C only | 71.1 | 1.17 |
| Field Applied During Cooling 1020° to 230° C | 80.9 | 0.97 |

more rapid cooling rate during magnetic annealing appears associated with the suppression of the superlattice which may form in the 50 pct iron-50 pct cobalt alloy. Actually, it appears doubtful whether cooling rates as high as 48°C per min would produce an appreciably disordered structure. Recently Goldman and Smoluchowski[15] have shown that a 50 pct iron-50 pct cobalt alloy may show slight ordering even after a quench in cold water. Unfortunately, any explanation for the behavior exhibited, based upon metallurgical effects such as a dispersed phase appear to require additional experimental work.

The effect of interrupting cooling to maintain a constant temperature of 900°C for 1 hr in the presence of the magnetic field before further cooling with the field is illustrated by the data tabulated in table VI. The holding period at 900°C causes a consistent though small increase in the ratio of retentivity to saturation, and a decrease in the coercive force. This effect appears to be associated with a metallurgical change and may well be attributed to an increase in grain size caused by the time of holding at a temperature just below the $\alpha \rightarrow \gamma$ transformation. Since these effects are beneficial, a holding period was included in the standard magnetic anneal procedure described.

The important influence of the magnetic field in cooling through the range of temperature 900° to 230°C is illustrated by the fact that 50 pct iron-50 pct cobalt cores cooled from 1020°C to 900°C with the magnetic field, and then to 230°C without the field gave decidedly inferior re-



Fig. 5—Influence of Nickel on the Magnetic Properties of Iron-Cobalt Alloys, Before and After Magnetic Annealing, pct Fe = pct Co + 10 pct.



Fig. 6—Effect of Field Strength During Magnetic Anneal on Magnetic Properties of a 50 pct Iron-50 pct Cobalt Alloy. Commercial Cobalt Powder. Furnace Cool (3°C per min) from Holding Temperature.
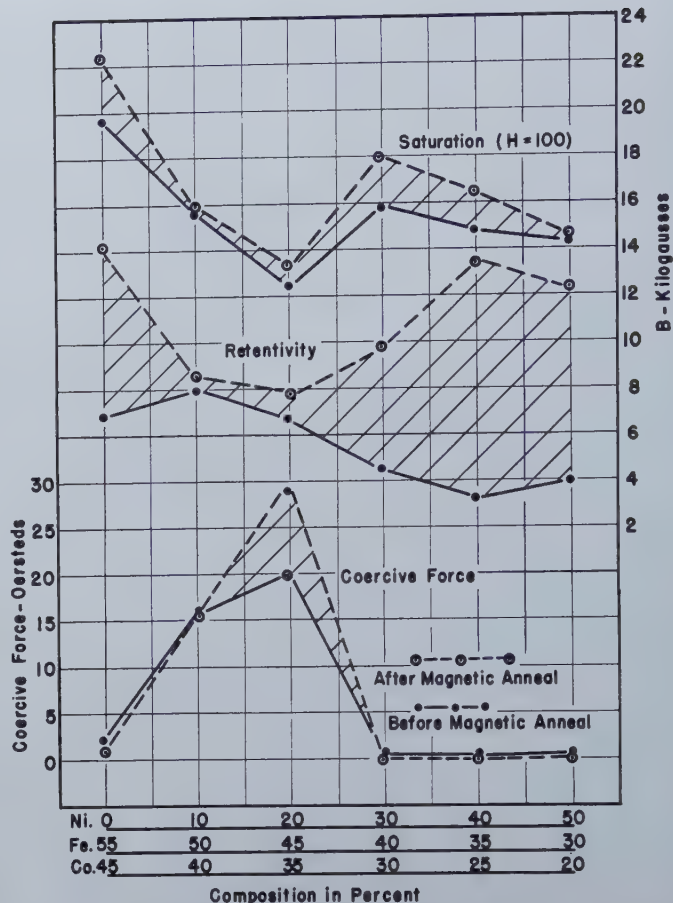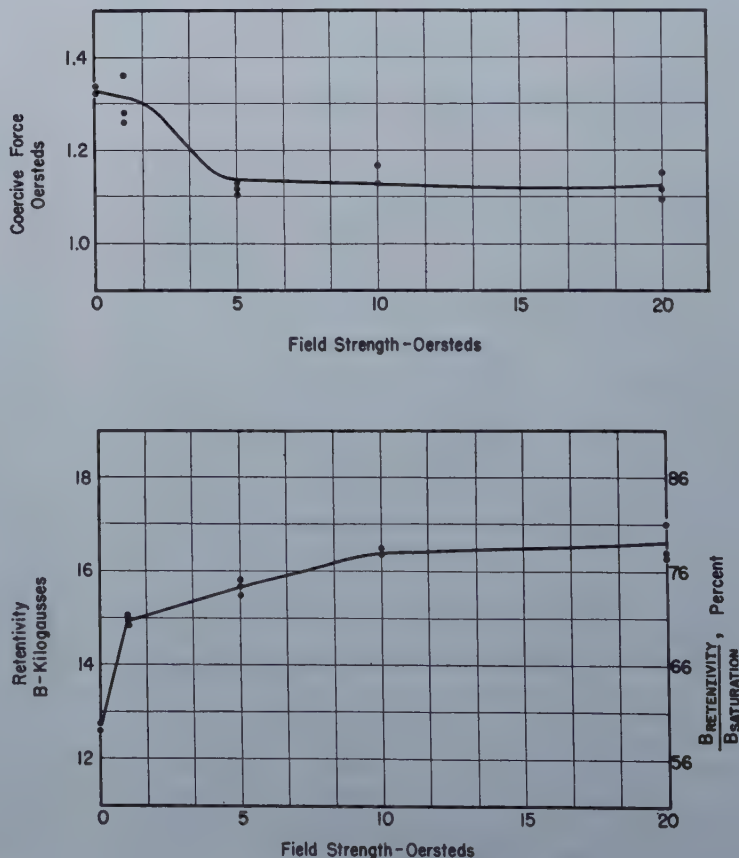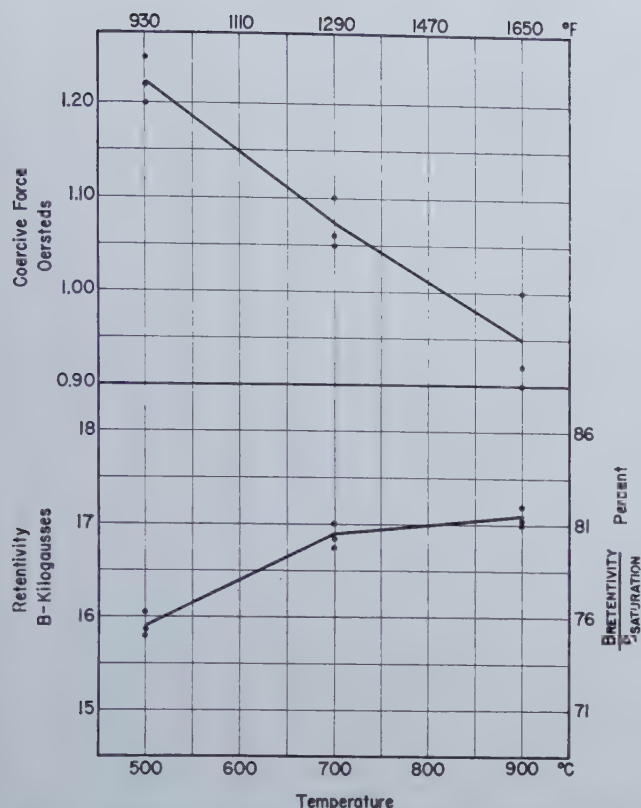
Fig. 7—Influence of Holding Temperature During Magnetic Anneal on Magnetic Properties, 50 pct Iron-50 pct Cobalt Alloy.

sults. This is illustrated in table VII. The ratio of retentivity to saturation is considerably lower and the coercive force appreciably higher for the core cooled without the magnetic field from 900°C.

The results presented in table VII agree with those of Bozorth and Dillinger,[1] who showed that maximum response in the magnetic anneal is associated with cooling in the presence of the magnetic field to a threshold temperature above which the alloy is plastic enough to be affected by the forces of magnetostriction.

**Holding Temperature:** Since the experiments concerning cooling method showed consistent improvement for a 1 hr holding period at 900°C with the magnetic field during cooling, additional experiments were conducted to determine the effect of other holding temperatures. The influence of a 1 hr holding period at various temperatures during the magnetic anneal upon the magnetic properties developed is shown in fig. 7 for a 50 pct iron-50 pct cobalt alloy. All cores were heat treated with the magnetic field in the standard manner, except that cooling was interrupted for a 1 hr period at the temperature shown.

The holding temperature appears to play a significant rôle in the ultimate properties to be derived from the magnetic anneal. The data indicate that the magnetostrictive forces are most effective at a temperature close to

**Fig. 8—Influence of Holding Time at 900°C During the Magnetic Anneal Upon the Magnetic Properties, 50 pct Iron-50 pct Cobalt Alloy.**

the transformation temperature where the increased plasticity allows optimum orientation of the magnetic domains. Since plasticity increases with temperature, the importance of a high Curie temperature is evident.

**Holding Time:** The influence of holding time at a temperature of 900°C while cooling with the magnetic field is shown in fig. 8. The results shown were obtained by using the same cores for each holding time. Between experiments the cores were heated above the $\alpha$-$\gamma$ transformation temperature, i.e., to 1020°C for 15 min and cooled slowly without the field to eliminate the effect of the previous magnetic anneal.

The data of fig. 8 show that little improvement is realized by increasing the time of holding with the magnetic field at 900°C beyond ½ hr. This is the anticipated behavior in the light of the good plasticity of the metal at higher temperature.

Although the results indicate that a holding period of 30 min was sufficient to develop optimum magnetic properties in cores repeatedly heat treated, subsequent work indicated that new cores magnetically annealed for the first time did not develop optimum response until the holding time was increased to 1½ hr. For this reason, 1½ hr was selected as the holding period at 900°C for the standard magnetic anneal procedure.

**Influence of Variables in Core Preparation:** The relative ease of preparing numerous new alloys of definite composition by the powder metallurgy technique is clearly demonstrated in this study. The ability to prepare cores directly, without resorting to fusion, hot working and cold working, or machining allows rapid study of alloy systems.

The magnetic properties produced in cores prepared by the powder metallurgy technique are in good agreement with those produced by fusion. This is illustrated in fig. 9. The somewhat lower values
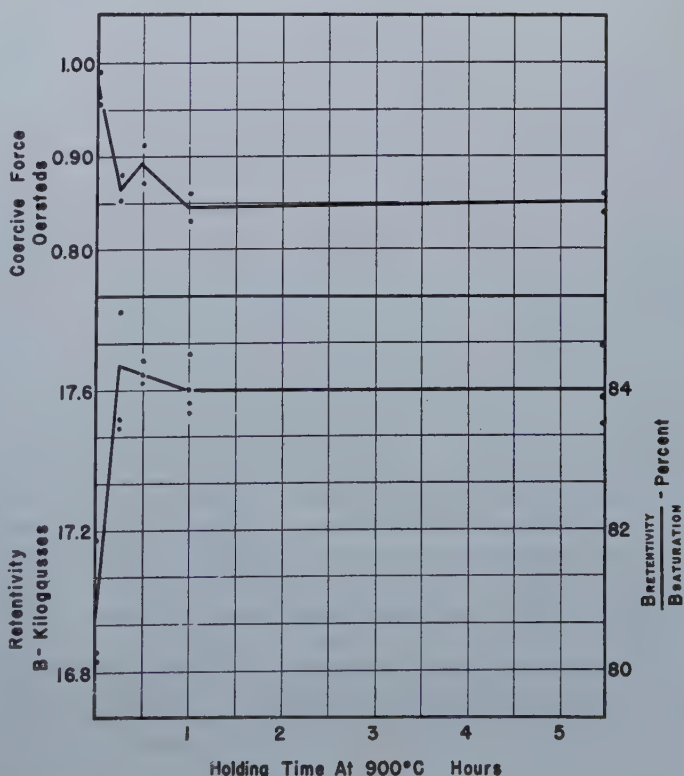
of saturation induction are probably the result of the lower density exhibited by the powder metallurgy alloys. In this respect, it may be noted that the maximum discrepancy in saturation occurs for those alloys which show the greatest difference in density between the fused alloy and the powder metallurgy alloy.

Since all of the alloys studied were prepared by the powder metallurgy technique rather than by fusion, no information was available concerning the influence of processing variables unique to powder metallurgy upon the magnetic properties of the alloys studied. Experiments were therefore conducted to determine the influence of different lots of commercial iron and cobalt powders, mixing time, repressing pressure and rates of heating and cooling, during sintering, upon the ultimate magnetic properties.

**Fabrication Variables:** The influence of different lots of commercial powder, mixing times from hand mixing to machine mixing for 72 hr, repressing pressures from (0 to 66 tons per in.²), and rapid vs. slow heating and cooling rates during sintering, upon the ultimate magnetic properties produced, was found to be insignificant in the range of variables studied. Small changes in magnetic properties caused by processing variables generally fell within the deviation expected for a single group of cores prepared in accordance with the standard procedure finally developed. The small effect of the processing variables studied upon the ultimate magnetic properties can be attributed to the long sintering treatment at a temperature just below the solidus for the alloys. All iron-cobalt alloys were sintered at 1400-1420°C for a total time of 24 hr. Such a sintering treatment would tend to mask the effects of other processing variables.

**Raw Material:** Although experiments showed little variation in the magnetic properties of cores produced from the different lots of commercial cobalt powder used in this investigation, the rather large amounts of impurities present in the commercial cobalt powder used (table I) suggested the possibility that purer cobalt powder might give better magnetic properties. The striking and detrimental influence of small amounts of nickel upon the coercive force of iron-cobalt alloys, appeared to strengthen this possibility.

Hysteresis loops and magnetic properties are shown in fig. 10 for a 50 pct iron-50 pct cobalt core prepared from the special cobalt powder reported to contain 99.13 pct nickel and 0.50 pct oxygen. The properties shown are the optimum achieved to date in this study. It will be noted by comparison with fig. 2 showing the typical magnetic properties for 50 pct iron-50 pct cobalt cores prepared with commercial cobalt powder, that the retentivity after magnetic annealing is appreciably higher, and the coercive force considerably lower for the core made with the special cobalt powder. Although the study to determine the influence of small amounts of impurity in iron-cobalt alloys upon the magnetic properties is in the initial stages, it is believed the improvement shown by cores made from the special powder is due to less impurities.

## Summary and Conclusions

Rectangular hysteresis loops have been developed for binary alloys of iron and cobalt prepared by
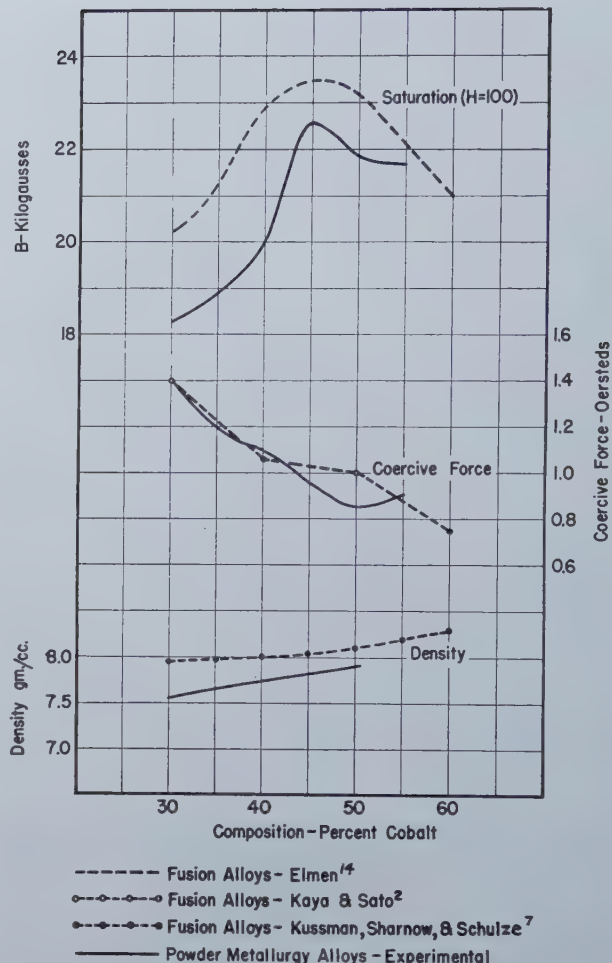


**Fig. 9—Comparison of Magnetic Properties for Alloys Prepared by Powder Metallurgy and by Fusion.**

powder metallurgy and annealed in a magnetic field. The pronounced influence of magnetic annealing on the ultimate magnetic properties produced in a 50 pct iron-50 pct cobalt alloy are shown in fig. 2 and 10.

Response to magnetic annealing and the ultimate magnetic properties are a function of the composition. The optimum retentivity and minimum coercive force after magnetic annealing occur at a cobalt concentration of approximately 50 pct.

The optimum magnetic properties of the 50 pct iron-50 pct cobalt alloy are: saturation (H = 100) equals 22,400 gausses, retentivity equals 19,000 gausses and coercive force equals 0.68 oersteds; and were obtained with a specially prepared cobalt powder. The 50 pct iron-50 pct cobalt composition coincides with a high α-γ transformation temperature, a high linear magnetostriction, and maximum volume magnetostriction, but not with minimum crystal anisotropy.

The addition of small amounts of nickel (0 to 10 pct) to iron-cobalt alloys with approximately equal amounts of iron and cobalt, causes a striking increase in the coercive force, and a sharp decrease in the retentivity and saturation. Although greater amounts of nickel (10 to 50 pct) cause a rapid decrease in the coercive force to a low value, the saturation (H = 100) and the retentivity of the iron-cobalt-nickel alloys after magnetic annealing remain considerably below those obtained for the 50 pct iron-50 pct cobalt alloy.

| | Saturation H=100 | Retentivity | H_c |
|---|---|---|---|
| Before | 22200 | 12600 | 1.145 |
| After | 22400 | 19000 | .68 |

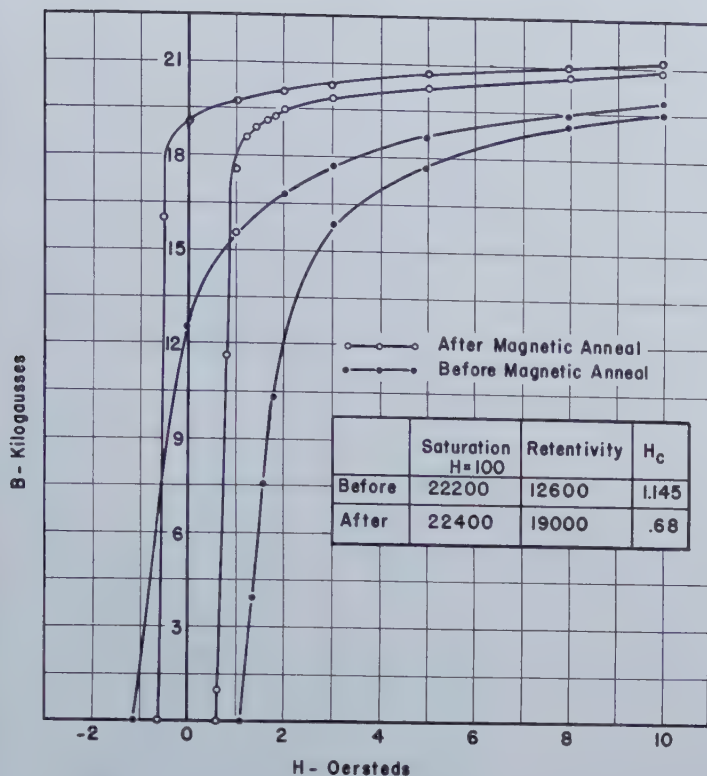Legend: ○——○ After Magnetic Anneal; ●——● Before Magnetic Anneal

Fig. 10—Hysteresis Loops and Magnetic Properties of 50 pct Iron-50 pct Cobalt Alloy Made from Specially Prepared Cobalt Powder, Before and After Magnetic Annealing.

The high coercive force, and the failure of iron-cobalt-nickel alloys containing 10 to 20 pct nickel to respond to magnetic annealing are associated with the heterogeneous two phase field known to exist for iron-cobalt-nickel alloys in this range of composition; and the results confirm those of Bozorth and Dillinger.[1] Likewise, the magnetic properties obtained in this study after magnetic annealing the alloy Perminvar (30 pct iron-25 pct cobalt-45 pct nickel) are in close agreement with those presented by Bozorth and Dillinger.[1]

Studies have been conducted to determine the influence of field strength, cooling method, holding temperature and holding time during cooling in a magnetic field upon response to magnetic annealing. Results of these studies indicate that cooling from above the $\alpha$-$\gamma$ transformation temperature in a magnetic field of 20 oersteds to 900°C, followed by a hold of 1½ hr at 900°C with the magnetic field, and then cooling at a rate of 20 to 25°C per min to below 230°C with the magnetic field provides an optimum response for the 50 pct iron-50 pct cobalt alloy.

Finally, the suitability and ease of powder metallurgy as a technique for preparation of numerous alloys for magnetic analysis has been demonstrated.

### Acknowledgment

### References

[1] G. A. Kelsall: *Physics.* (1934) **5**, 169-173.
J. F. Dillinger and R. M. Bozorth: *Physics.* (1935) **6**, 279-284.
R. M. Bozorth and J. F. Dillinger: *Physics.* (1935) **6**, 285-291.

[2] S. Kaya and H. Sato: *Proc.* Phys. Math. Soc. Japan, (3) (1943) **25**, 261-273.
[3] F. Koppelmann: *Elektrotech. Ztsch.* (1941) **62**, 3-20.
O. Jensen: *Trans.* Electrochem. Soc. (1946) **90**, 93-109.
O. Jensen: Naval Ordnance Lab. Magnetic Materials Symp., Washington, D. C., 1948, pp. 21-27.
[4] A. G. Ganz: AIEE *Trans.* (1946) **65**, 177-183.
[5] H. B. Rex: *Instruments,* (1947) **20**, 1102-1109 and (1948) **21**, 332, 352-362.
R. E. Morgan: *Elec. Engg.* (1949) **68**, 663-667.
[6] O. Dahl and F. Pawlek: *Ztsch. f. Phys.* (1935) **94**, 504-522.
J. L. Snoek: *Physica,* (4) (1935) **2**, 403-412.
E. Both: Naval Ordnance Lab. Magnetic Materials Symp., Washington, D. C., 1948, pp. 39-46.
G. W. Elmen and E. A. Gaugler: *Elec. Engg.,* (1948) **67**, 843-845.
E. A. Gaugler: *Prod. Engg.* (1949) **20**, 84-89.
J. H. Crede and J. P. Martin: *Jnl. Appl. Phys.,* (1949) **20**, 966-971.
[7] P. Weiss: *Trans.* Faraday Soc., (1912) **8**, 56.
G. W. Elmen: *Jnl.* Franklin Inst., (1929) **207**, 583-617.
A. Kussmann, B. Scharnow, and A. Schulze: *Ztsch. f. tech. Phys.,* (1932) **13**, 449.
[8] W. C. Ellis and E. S. Greiner: *Metals Handbook,* A.S.M., 1948, pp. 1191-1192.
[9] K. Honda and K. Kido: Sci. Rep. Tohoku Imp. Univ., (1) (1920) **9**, 221-231.
Y. Masiyama: Sci. Rep. Tohoku Imp. Univ., (1932) **21**, 394-410.
S. R. Williams: *Rev. Sci. Inst.,* (1932) **3**, 675-683.
[10] J. W. Shih: *Phys. Rev.,* (1934) **46**, 139-142.
[11] H. Masumoto: Sci. Rep. Tohoku Imp. Univ., (1) (1929) **18**, 195-229.
[12] R. Smoluchowski and R. W. Turner: *Jnl. Appl. Phys.,* (1949) **20**, 745-746.
[13] W. Rostoker: *Trans.* AIME (1949) **180**. *Metals Tech.,* Oct. 1948, TP 2437.
[14] G. W. Elmen: reported in Bell Telephone System Monograph B1445, by R. M. Bozorth.
[15] J. E. Goldman and R. Smoluchowski: *Phys. Rev.* (1949) **75**, 140-147.

The Extrusion of

# Powdered Magnesium Alloys

by R. S. Busk and T. E. Leontis

The direct extrusion of magnesium-alloy powder is described, and used to produce four new alloy types by controlled solid-state diffusion: (1) Use of steep alloy-gradients for control of grain size; (2) interference hardening; (3) control of stress-corrosion by cathodic protection; and (4) increase in extrudability.

WORK was initiated several years ago at The Dow Chemical Company to determine the applicability of powder metallurgy processes to magnesium and its alloys. Although it was found possible to apply the normal techniques of compacting and sintering, it was discovered early that the technique of extrusion offered special promise. This technique and the alloys produced were therefore studied extensively, and the present paper is a partial report of those studies. It is expected that a second paper will discuss more extensively some of the alloy systems simply mentioned here.

Although the literature on powder metallurgy is very extensive, there are only two articles dealing with magnesium[13, 14] and there is no reference to the direct extrusion of the powder of any metal without the preliminary step of compacting. Furthermore, no mention has been made of the possibility of designing alloys by the technique of powder extrusion, particularly alloys that cannot be made in any other way. Sauerwald[13] discusses the extrusion of magnesium and aluminum powder to produce alloys containing nonequilibrium phases, but again he emphasizes the importance of pre-compacting before extrusion.

There seems to be general agreement that some form of hot-pressing is essential to obtain in a compact the full theoretical density of the metal used.[1-6] The nearest approach to the technique of direct
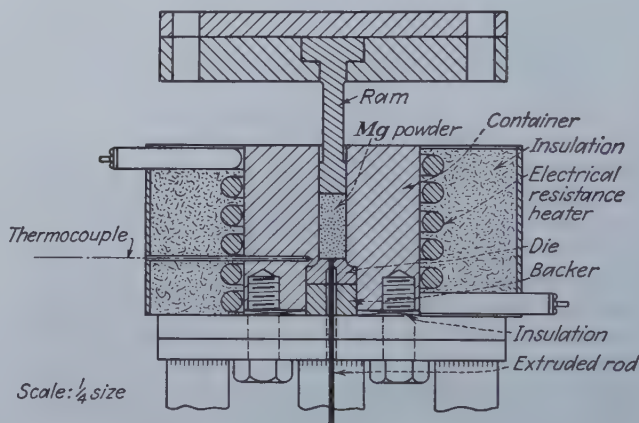
Fig. 1—Press and die for extruding powders.

powder extrusion is that of extrusion of pre-sintered compacts,[7-12] for which the best review through 1944 is that by Kieffer and Hotop.[11] Ensign[12] discussed a specialized technique of "extruding" already compacted and sintered gears for the purpose of sizing. Sauerwald[13] discussed the compacting and extrusion of magnesium and magnesium-aluminum alloy band-saw chips. The properties of the extruded compacts were found to be comparable with those of extrusions prepared from solid billets. He also extruded a compacted mixture of magnesium and aluminum powder and found the properties to be somewhat different from those obtained on an extrusion made from a cast billet of the same composition. The second reference dealing specifically with the powder metallurgy of magnesium is Stern's patent,[14] in which is described the extrusion of scrap chips and turnings following a hot-pressing and sintering step. Considerable emphasis in most of these articles is placed on the necessity of atmospheric protection to minimize the danger of oxidation.

## Experimental Procedure

The first experiments were made with the small extrusion press shown in fig. 1. With this press, billets of about ½ in. diam are used to produce wire
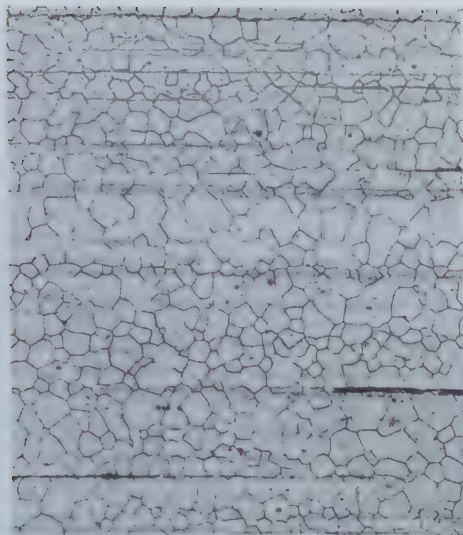
Fig. 2 (above)—Microstructure of A6 alloy extruded from billet.
Acetic-glycol etchant. 100X.

Fig. 3 (left)—Microstructure of A6 alloy extruded from machined chips.
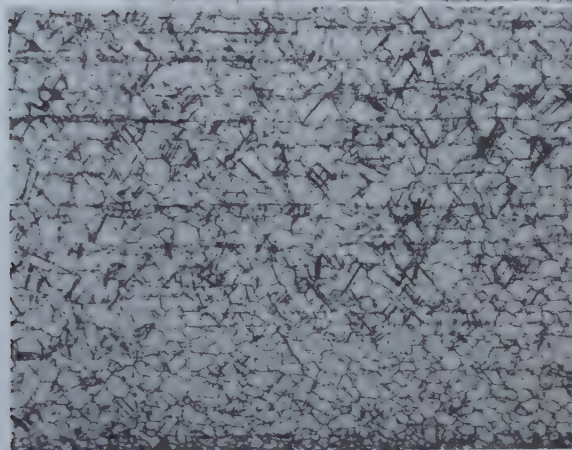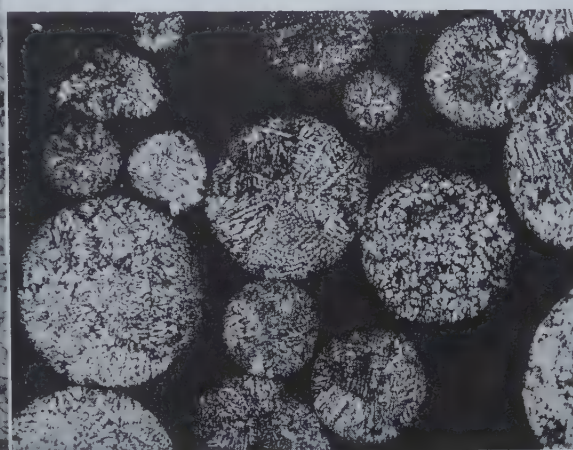Acetic-glycol etchant. 100X.

Fig. 4 (right)—Microstructure of as-atomized AZ31 alloy powder.
Acetic picral etchant. 100X. All micrographs reduced one fifth in reproduction.

of about 0.050 to 0.10 in. diam. On the basis of experience gained with this press, the major portion of the study made use of a 500-ton horizontal extrusion-press with a 3 in. diam container. The cold powder was introduced into the heated container, the ram advanced, and the powder extruded. There was no atmospheric protection, and the heat of the container was used to raise the temperature of the powder sufficiently to allow extrusion. The temperature rise occurred during the 15-30 sec needed to advance the ram prior to extrusion. Holding the powder at the container temperature for as long as 2 hr produced no change in the properties of the extrusion.

Two types of extrusion were made to study the extrudability and properties of alloys. Rod of ⅜ in. diam was extruded at a constant speed over a range of temperature to determine the pressure-temperature relationships for the alloy and the effect of temperature on the mechanical properties. Strip of ¾ x 1/16 in. section size was extruded at a constant temperature over a range of speeds. These two experiments gave the hot-short limit (lowest extrusion speed at which cracking occurs) and the mechanical properties as a function of speed. The compressive yield strength of strip is generally lower than that of rod and is, therefore, a more conservative measure of the properties representative of any given composition.

The mechanical properties determined were per-cent elongation, tensile yield strength (0.2 pct off-set), compressive yield strength (0.2 pct offset), and tensile strength (maximum load divided by original area). ASTM procedures were followed in all these tests.

### Results

The first experiment designed to establish the feasibility of powder-extrusion was made using machined chips. In particular, an extrusion from a billet and one from machined chips were compared directly. A 2-in. diam permanent-mold cast billet of Mg + 6 pct Al alloy was fully homogenized by soaking at 800°F. A slug ½ in. in diam by 2 in. long was machined from this billet and extruded into 0.050 in. wire, using the press shown in fig. 1. The chips obtained by machining the slug were then poured into the container and extruded into 0.050 in. wire, using identical extrusion conditions. The structures of these two extrusions are shown in fig. 2 and 3, and the properties are:

| Type Billet | Electrical Conductivity (95°F) Reciprocal Microhm-cm. | Tensile Properties 1000 psi | | |
|---|---|---|---|---|
| | | Pct E | TYS | TS |
| Solid | 0.0735 | 17.0 | 22.5 | 39.7 |
| Powder | 0.069 | 13.5 | 19.4 | 42.5 |

**Table I. 3 in. x ½ in. Rectangle Extruded from 4 in. Container at 700°F, 5 fpm**

(AZ31 Alloy)

| Type Billet | Longitudinal | | | | Transverse | | | |
| | 1000 psi | | | | 1000 psi | | | |
| | Pct E | TYS | CYS | TS | Pct E | TYS | CYS | TS |
|---|---|---|---|---|---|---|---|---|
| SHT D.C. Billet | 14 | 20 | 12 | 35 | 3 | 23 | 12 | 37 |
| As Cast D.C. Billet | 19 | 25 | 21 | 39 | 11 | 28 | 21 | 39 |
| Atomized Powder | 21 | 30 | 28 | 43 | 10 | 31 | 25 | 42 |

The two extrusions have similar microstructure, grain size, conductivity, and mechanical properties. The twinned structure seen in fig. 3 is there because the piece examined had been mechanically tested. It was on the basis of this experiment that it was decided that the extrusion of magnesium powder is feasible, and a study of the possibilities of this technique undertaken.

Four types of alloy behavior have been found, each dependent upon the powder process. It is the primary purpose of this paper to describe and illustrate these four types.

**Alloy Gradients:** The compressive yield strength of magnesium alloys is inversely related to grain size. It also has been shown[15] that the grain size of magnesium-alloy extrusions is influenced by the alloy gradients present in the billet. That is, the greater the coring, and the finer the scale over which the coring is distributed in the billet structure, the finer are the grains in the extrusion.

The atomizing process for manufacturing magnesium-alloy powder was, therefore, investigated to obtain as finely distributed coring as possible. This process consists of breaking a thin stream of molten metal into droplets with a stream of cold gas and quenching each droplet with the gas. The resultant powder consists of spherical particles having a cast structure with finely-distributed, highly-cored dendrites (fig. 4). This seems to represent the ultimate in the type of structure believed to result in fine grain extrusions, and this type of powder was, therefore, adopted for this study. AZ31* alloy was

---

* See Appendix for explanation of ASTM nomenclature.

---

atomized and extruded into 3 in. by ½ in. strip; with this strip both longitudinal and transverse properties could be studied. For comparison, a solution-heat-treated and an as-cast direct-chill billet were extruded to the same shape. The properties are shown in table I. The compressive yield strength rises markedly as the degree and distribution of coring increases. Furthermore, these data also show no adverse effect from the fibrous structure produced by extruding powder inasmuch as the properties are the same in both the longitudinal and transverse directions.

The microstructure of the atomized powder is shown in fig. 4 as compared with that of the as-cast and solution-heat-treated billets in fig. 5 and 6. Since the light microscope emphasizes the coring without clearly revealing the grain size of the atomized powder, fig. 7 is included. This is an electron microscope picture of as-atomized AZ31 alloy.
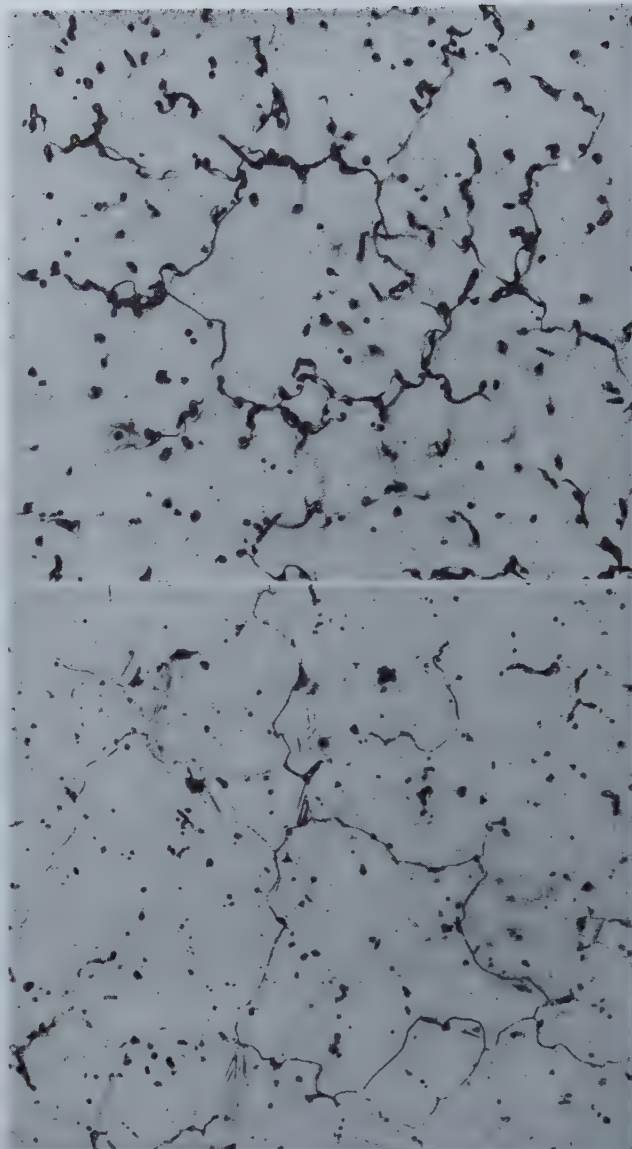


Fig. 5 (above)—Microstructure of direct chill AZ31 alloy billet.
As-cast condition. Acetic picral etchant. 100X.

Fig. 6 (below)—Microstructure of direct chill AZ31 alloy billet.
Solution heat treated condition. Acetic picral etchant. 100X

The fine grains are quite apparent. There is a sharp difference in the cast structure of the powder and that of the billet, and it is believed the differences in properties given are due to this difference in structure.

If the finer grains and higher strengths of extrusions from atomized powder as compared to those from billets are ascribable to the coring, a solution-heat-treatment of the powder would be expected to remove the coring and result in lower properties. Fig. 8-9 show the effect of heat-treatment on the microstructure of AZ31 atomized powder, and table II lists the effect of such heat-treatment on the properties. One hour at 500°F removes only some of the coring, whereas after 3 hr at 850°F, the structure is quite homogeneous. From table II, it is evident that the powder can be heated as long as 3 hr at 600°F without lowering the extrusion-

Fig. 7 — Electron micrograph of as-atomized AZ31 alloy powder.
Methyl iodide etchant.
7200X.

**Table II. Effect of Heat Treatment of AZ31 Powder Prior to Extrusion**

| Heat Treatment | | 3/8 in. Diam Rod (Ext. 5 fpm at 600°F) 1000 psi | | | | 3/4x1/16 in. Strip (Ext. 5 fpm at 650°F) 1000 psi | | | |
|---|---|---|---|---|---|---|---|---|---|
| Hours | Temp. °F | Pct E | TYS | CYS | TS | Pct E | TYS | CYS | TS |
| 0 | | 15 | 40 | 36 | 47 | 10 | 29 | 27 | 42 |
| 2 | 500 | 14 | 40 | 38 | 48 | 13 | 28 | 27 | 42 |
| 1 | 600 | 13 | 40 | 36 | 47 | 9 | 28 | 25 | 42 |
| 3 | 600 | 11 | 41 | 39 | 48 | 11 | 26 | 27 | 42 |
| 3 | 850 | 10 | 32 | 25 | 42 | 12 | 26 | 17 | 39 |

properties, but that a heat-treatment of 3 hr at 850°F results in a sharp decrease in compressive yield strength. The structure of the extrusions corresponding to fig. 8 and 9 is shown in fig. 10 and 11.

In view of the above experiments, it is of interest to compare directly the properties of alloys prepared by extruding atomized powder with extrusions from cast billets. This was done for three commercial alloys (AZ31, M1, ZK60) and one experimental alloy (AMZ111), and the data are given in table III. With similar extrusion conditions, the properties of the powder-extrusion are at least equal to, and usually much better than those of the billet-extrusion.

**Interference Hardening:** The use of powder allows the construction of alloys prohibited by the phase rule when the step of melting and casting must be used to obtain the total composition. Thus, co-extrusion of elements and subsequent diffusion result in the at least temporary appearance of every phase in the binary diagram. Proper control and distribution of these phases might be expected to produce unusual properties.

Normal precipitation- or age-hardening occurs when a supersaturated solid-solution is caused to precipitate its excess solute. This is normally accomplished by thermal control on alloy systems with greater solubility for the solute at elevated than at lower temperatures. If a third element could be introduced into the solid-solution that would result in lowering the solubility of the original solute, more copious precipitation and perhaps greater hardening would take place. This would be analogous to the "salting-out" effect in aqueous solutions. It should be possible also to find systems such that the addition of the third constituent would result in the precipitation of a compound completely insoluble in the solvent. This would be analogous to the precipitation of silver chloride by addition of sodium chloride to a water-solution of silver nitrate. Such a precipitate, since insoluble, would have only a small tendency to coalesce and would, therefore, retain any of its hardening effects even after extensive heat-treatment. This type of

### Table III. Comparison of As Extruded Properties of Alloys Extruded from Powder and from Permanent Mold Billets

| Shape | Extrusion Conditions Temp. °F | Speed Fpm | Powder 1000 psi Pct E | TYS | CYS | TS | Billet 1000 psi Pct E | TYS | CYS | TS |
|---|---|---|---|---|---|---|---|---|---|---|
| **AZ31** | | | | | | | | | | |
| Rod | 600 | 5 | 15 | 39 | 40 | 47 | 16 | 34 | 30 | 44 |
| | 700 | 5 | 15 | 36 | 36 | 45 | 15 | 34 | 25 | 45 |
| | 800 | 5 | 15 | 35 | 30 | 45 | 14 | 34 | 22 | 44 |
| Strip | 650 | 5 | 12 | 29 | 29 | 43 | 18 | 23 | 18 | 39 |
| | 650 | 15 | 12 | 25 | 18 | 39 | 16 | 25 | 15 | 38 |
| | 650 | 30 | 11 | 25 | 15 | 37 | 15 | 25 | 15 | 38 |
| **MI** | | | | | | | | | | |
| Rod | 600 | 5 | 14 | 44 | 38 | 48 | 25 | 27 | 23 | 39 |
| | 700 | 5 | 11 | 43 | 35 | 47 | 23 | 30 | 24 | 40 |
| | 800 | 5 | 13 | 43 | 28 | 47 | 14 | 33 | 19 | 43 |
| Strip | 650 | 5 | 6 | 34 | 33 | 43 | 23 | 16 | 16 | 33 |
| | 650 | 15 | 9 | 30 | 26 | 40 | 19 | 18 | 14 | 35 |
| | 650 | 30 | 8 | 28 | 19 | 40 | 18 | 18 | 14 | 35 |
| **AMZ111** | | | | | | | | | | |
| Rod | 600 | 5 | 12 | 40 | 41 | 48 | 19 | 37 | 31 | 45 |
| | 700 | 5 | 15 | 40 | 37 | 46 | 13 | 33 | 20 | 42 |
| | 800 | 5 | 12 | 38 | 34 | 46 | 11 | 32 | 16 | 40 |
| Strip | 650 | 5 | 5 | 37 | 36 | 45 | 10 | 29 | 19 | 40 |
| | 650 | 20 | 9 | 33 | 31 | 42 | 8 | 29 | 13 | 38 |
| | 650 | 40 | 8 | 32 | 24 | 39 | 9 | 28 | 13 | 38 |
| **ZK60** | | | | | | | | | | |
| Rod | 600 | 5 | 16 | 44 | 48 | 53 | 17 | 41 | 41 | 54 |
| | 700 | 5 | 17 | 41 | 43 | 51 | 14 | 40 | 34 | 51 |
| | 800 | 5 | 15 | 37 | 38 | 48 | 15 | 39 | 27 | 48 |
| Strip | 650 | 5 | 10 | 43 | 43 | 52 | 10 | 40 | 40 | 52 |
| | 650 | 20 | 6 | 37 | 37 | 47 | 13 | 38 | 36 | 49 |
| | 650 | 40 | 7 | 35 | 30 | 45 | Hot Short | | | |

reaction has been studied and the strengthening that sometimes occurs has been called "interference hardening."

Magnesium-zirconium alloys have been rather fully studied,[15] and the patent literature in particular is extensive.[16, 17] All the work to date shows that certain elements must be avoided when adding zirconium to magnesium, or compounds insoluble in the melt will form which will settle out, resulting in loss of zirconium. One of the most potent of these "interfering" elements is aluminum. From the previous discussion, it would be expected that addition of aluminum to a magnesium-zirconium alloy by solid-state diffusion might result in precipitation of an insoluble compound. This precipitation might be expected to have a strengthening effect similar to that induced by age-hardening.

The results of a study of the effect of the addi-

### Table IV. Effect of the Addition of Aluminum to Mg-Zr and Mg-Zr-Ce Alloys

| Alloy Type | Pct Zr | Pct Misch-metal | As Extruded Pct E | 1000 psi TYS | CYS | TS | HT 1 hr at 750°F Pct E | 1000 psi TYS | CYS | TS |
|---|---|---|---|---|---|---|---|---|---|---|
| KO | 0.33 | | 3 | 18 | 18 | 29 | 3 | 18 | 18 | 30 |
| KO + 12 pct Mg-Al eutectic | | | 1 | 34 | | 39 | 2 | 40 | 33 | 44 |
| EKOO | 0.48 | 0.17 | 1 | 45 | 35 | 47 | 3 | 38 | 33 | 41 |
| EKOO + 3 pct Al | | | 2 | 44 | 41 | 47 | 3 | 44 | 41 | 47 |
| EKOO + 12 pct Mg-Al eutectic | | | 1 | 41 | 42 | 46 | 2 | 41 | 38 | 43 |
| EKOO | 0.49 | 0.47 | 3 | 48 | 37 | 50 | 10 | 42 | 33 | 44 |
| EKOO + 3 pct Al | | | 3 | 46 | 46 | 50 | 6 | 45 | 46 | 50 |
| EKOO + 12 pct Mg-Al eutectic | | | 2 | 49 | 47 | 52 | 7 | 49 | 45 | 52 |
| 50EKOO/50M1 | 0.48 | 0.17 | 7 | 36 | 36 | 42 | 4 | 22 | 25 | 36 |
| 50EKOO/50M1 + 3 pct Al | | | 2 | 34 | 39 | 43 | 3 | 34 | 38 | 43 |
| 50EKOO/50M1 + 12 pct Mg-Al eutectic | | | 2 | 42 | 43 | 45 | 4 | 38 | 39 | 46 |
| 50EKOO/50M1 | 0.48 | 0.47 | 4 | 45 | 36 | 47 | 8 | 34 | 29 | 40 |
| 50EKOO/50M1 + 3 pct Al | | | | 44 | 40 | 46 | 5 | 39 | 38 | 45 |
| 50EKOO/50M1 + 12 pct Mg-Al eutectic | | | 5 | 47 | 47 | 49 | 7 | 46 | 42 | 52 |
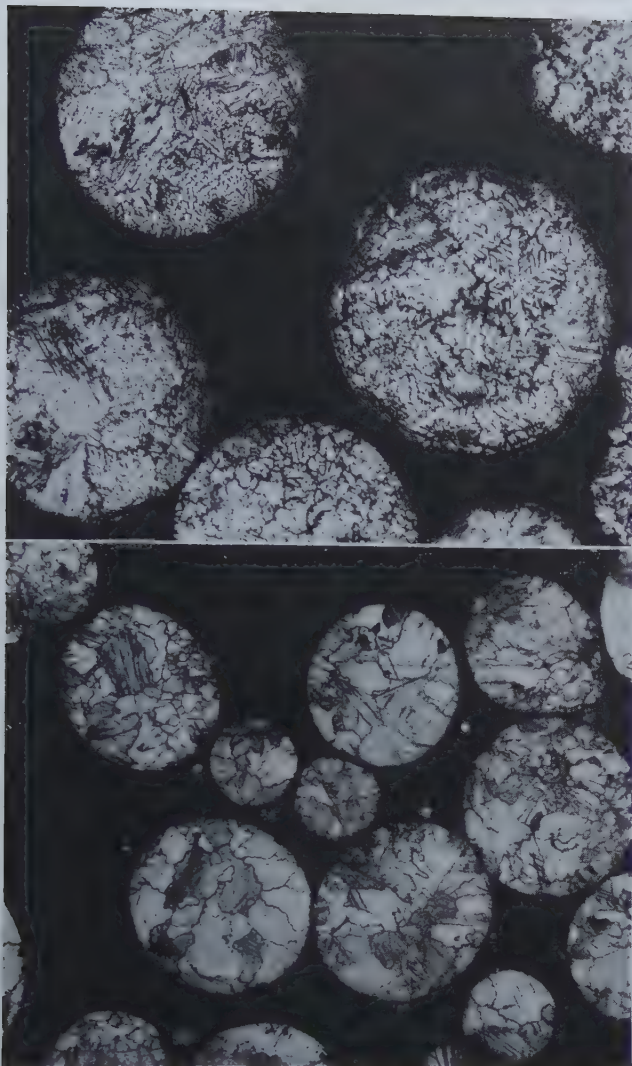
Fig. 8 (above)—Effect of 1 hr at 500°F on the structure of atomized AZ31 alloy powder.
Acetic picral etchant. 100X.

Fig. 9 (below)—Effect of 3 hr at 850°F on the structure of atomized AZ31 alloy powder.
Acetic picral etchant. 100X. Both micrographs slightly reduced in reproduction.

tion of aluminum to magnesium-zirconium alloys are given in tables IV and V. It was found that addition of mischmetal to the magnesium-zirconium alloy results in a general increase in the level of properties, and these data are also included in table IV. The aluminum was added by mixing the two powders (*magnesium-zirconium alloy* and *aluminum*) and extruding the mixture. The percent of addition refers to the percent of the aluminum in the mixture of alloy-powder plus aluminum.

The aluminum can be added in a number of forms including elemental aluminum, and aluminum alloy (e.g. 63S), $Mg_{17}Al_{12}$, $MnAl_4$, aluminum-magnesium (Mg + 64.3 pct Al) eutectic, and magnesium-aluminum (Mg + 32.2 pct Al) eutectic. Compounds do not extrude, but remain as hard lumps in the extrusion; aluminum and aluminum alloys result in a poor surface due to sticking and tearing. The use of the magnesium-aluminum eutectic is as effective as aluminum, but is less liable to sticking, and was, therefore, used more frequently.

Table IV shows that there is a marked increase in strength due to the presence of aluminum. This effect also persists after heating for one hour at 750°F. The effect of other heat-treatments is given in table V where it is apparent that a maximum combination of properties was obtained after heating for 16 hr at 600°F. Note that the properties are still high after as long as 300 hr at 750°F. This is remarkable for a magnesium-base alloy since 750°F is usually the solution-range and such long-time exposure usually results in marked grain coarsening and loss of strength.

The structure of this type of alloy is shown in fig. 12, 13, and 14. Fig. 12 is a micrograph of KO + 3 pct Al taken at 1000X in the as-extruded condition. The dark stringers are the magnesium-aluminum compound which has formed where the aluminum powder was included. There is a fine-grained layer immediately next to each particle of compound. Upon heat-treatment, most of the compound goes into solution and the area of extremely fine grains widens. There is some slight evidence of precipitation at the grain boundaries. Fig. 13 is an electron-micrograph of the mixture KO + 12 pct magnesium-aluminum eutectic in the as-extruded condition and fig. 14, in the heat-treated condition (1 hr at 750°F).

### Table V. Effect of Heat Treatment on the Properties of a Mg-Zr Alloy +Al

⅜ in. diam Rod Extruded at 5 fpm at 500°F

| Alloy Type | Pct Zr | Heat Treatment | | Pct E | 1000 psi | | |
| | | Hours | Temp. °F | | TYS | CYS | TS |
|---|---|---|---|---|---|---|---|
| KO | 0.43 | As Extruded | | 11 | 30 | 26 | 39 |
| | | 1 | 750 | 12 | 24 | 23 | 37 |
| KO + 12 pct Mg-Al eutectic | 0.43 | As Extruded | | 2 | 39 | 41 | 43 |
| | | 16 | 350 | 2 | 44 | 42 | 45 |
| | | 16 | 450 | 3 | 41 | 46 | 45 |
| | | 16 | 500 | 3 | 45 | 47 | 46 |
| | | 16 | 550 | 4 | 47 | 45 | 49 |
| | | 16 | 600 | 9 | 49 | 45 | 51 |
| | | 16 | 650 | 4 | 49 | 41 | 50 |
| | | 16 | 700 | 8 | 49 | 44 | 51 |
| | | 16 | 750 | 6 | 48 | 43 | 50 |
| | | 1 | 600 | 5 | 43 | 48 | 46 |
| | | 4 | 600 | 7 | 46 | 48 | 47 |
| | | 8 | 600 | 5 | 48 | 47 | 50 |
| | | 16 | 600 | 9 | 49 | 45 | 51 |
| | | 96 | 600 | 5 | 51 | 47 | 53 |
| | | 300 | 600 | 8 | 49 | 44 | 52 |
| | | 1 | 750 | 5 | 44 | 44 | 49 |
| | | 16 | 750 | 6 | 48 | 43 | 50 |
| | | 96 | 750 | 7 | 45 | 39 | 49 |
| | | 300 | 750 | 7 | 45 | 40 | 49 |

### Table VI. Properties of Mixtures of Ml and AZ31 Alloys

| | | Strip Extruded at 5 fpm — 650°F | | | |
| | | | 1000 psi | | |
| Pct AZ31 | Pct M1 | Pct E | TYS | CYS | TS |
|---|---|---|---|---|---|
| 0 | 100 | 1 | 26 | 26 | 37 |
| 20 | 80 | 2 | 29 | 30 | 40 |
| 25 | 75 | 3 | 29 | 29 | 40 |
| 40 | 60 | 3 | 30 | 31 | 41 |
| 50 | 50 | 7 | 35 | 31 | 44 |
| 60 | 40 | 5 | 33 | 29 | 43 |
| 100 | 0 | 10 | 31 | 32 | 44 |

### Table VII. The Properties and Stress Corrosion Resistance of AZ61 and 50Ml/50AZ61

**Stress Corrosion**

| | Days to Failure | |
| Stress 1000 psi | AZ61 | 50M1/50AZ61 |
|---|---|---|
| 30 | | 20 |
| 29 | | 16 |
| 26 | 13 | 63 |
| 24 | | 373 |
| 22 | | None for 400 |
| 20 | 16 | None for 400 |
| 16 | 49 | None for 400 |
| 14 | 18 | None for 400 |
| 12 | None for 400 | None for 400 |

**Mechanical Properties**

| Extrusion Conditions | | AZ61 | | | | 50M1/50AZ61 | | | |
| | | | 1000 psi | | | | 1000 psi | | |
| Temp. °F | Speed Fpm | Pct E | TYS | CYS | TS | Pct E | TYS | CYS | TS |
|---|---|---|---|---|---|---|---|---|---|
| Rod  600 | 5 | 13 | 36 | 33 | 48 | 16 | 38 | 37 | 47 |
| 700 | 5 | 11 | 35 | 26 | 47 | 12 | 37 | 33 | 47 |
| 800 | 5 | 17 | 33 | 22 | 46 | 12 | 36 | 29 | 46 |
| Strip  650 | 5 | 12 | 27 | 25 | 45 | 8 | 32 | 30 | 44 |
| 650 | 10 | 13 | 25 | 21 | 43 | 9 | 32 | 29 | 44 |
| 650 | 20 | 15 | 23 | 21 | 42 | 9 | 31 | 29 | 43 |

### Table VIII. Hot Short Limit of Co-Extrusions

| | Hot Short Limit* — Fpm | | |
| Alloy | No Mixture | With 50 Pct Ml | With 50 Pct AMZ210 |
|---|---|---|---|
| A6 | 65 | >80 | |
| AZ61 | 35 | >80 | |
| AZ63 | 15 | >40 | 50 |
| AZ80 | 10 | 40 | 25 |
| AZ92 | 5 | 7.5 | 7.5 |
| ZK60 + 0.5 Ca | 2 | 6 | |

\* Lowest extrusion speed at which cracking occurs



**Fig. 10 (above)—Microstructure of ⅜ in. diam rod of AZ31 alloy extruded from as-atomized powder.**

Acetic picral etchant. 100X.

**Fig. 11 (center)—Microstructure of ⅜ in. diam rod of AZ31 alloy extruded from powder heat treated at 850°F for 3 hr.**
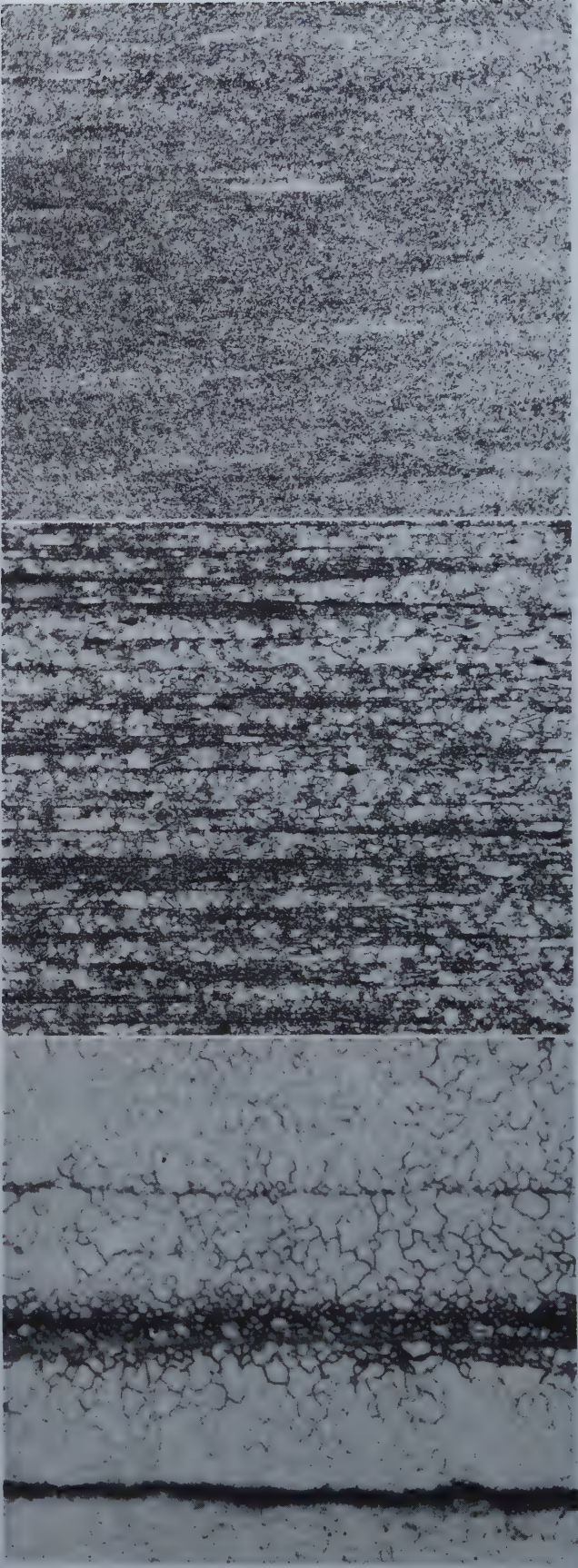
Acetic picral etchant. 100X.

**Fig. 12 (below)—Microstructure of ⅜ in. diam rod of KO + 3 pct Al.**

As-extruded condition. 10 pct HF etchant. 1000X.

## Table IX. Illustration of Property Effects by Design

| Alloy | Heat Treatment | Extrusion Speed, Fpm | Strip Extruded at 650°F | | | |
|---|---|---|---|---|---|---|
| | | | | 1000 psi | | |
| | | | Pct E | TYS | CYS | TS |
| ZK60 + 0.5 Ca | As Extruded | 1 | 6 | 53 | 50 | 56 |
| | 16 hr 350°F | 1 | 3 | 51 | 50 | 55 |
| | 1 hr 750°F | 1 | 13 | 35 | 34 | 45 |
| 50(ZK60+0.5 Ca) + 50 M1 | As Extruded | 5 | 12 | 44 | 41 | 49 |
| | 16 hr 350°F | 5 | 9 | 44 | 41 | 49 |
| | 1 hr 750°F | 5 | 17 | 26 | 26 | 40 |
| [50(ZK60+0.5 Ca) + 50 M1] + 12 pct Mg-Al Eutectic | As Extruded | 5 | 4 | 47 | 47 | 51 |
| | 16 hr 350°F | 5 | 3 | 46 | 48 | 52 |
| | 1 hr 750°F | 5 | 12 | 44 | 42 | 53 |

In fig. 13, a part of the eutectic can be seen lying next to an area of fine-grained matrix. The matrix itself is relatively clean. Fig. 14 shows the matrix grains after the aluminum has diffused throughout the alloy. There has been extensive precipitation. Electron-diffraction studies were made of this surface and the precipitating compound identified as probably $AlZr_3$.

**Stress-Corrosion:** As is common with most metals, certain magnesium alloys will stress corrode when subjected to sustained loads below the yield strength. AZ31 will sustain loads up to about 12,-000 psi when exposed to rural or seacoast atmosphere. Ml alloy, however, will sustain loads up to about 21,000 psi. One consequence of sensitivity to stress-corrosion is cracking due to locked-up stresses such as those in non-stress-relieved welds. Stress-relief of welds on AZ31 alloy is necessary to prevent stress-corrosion cracking. Ml alloy, however, can be welded without stress-relief and without danger of cracking.

It has been proposed[18] that an essential part of the stress corrosion mechanism is a difference in solution-potential between two parts of the microstructure, leading to galvanic attack. The stress acts to accentuate the effect and to widen cracks formed so as to expose fresh surfaces. If this basic idea is correct, making the susceptible alloy the cathode should stop the stress-corrosion. This can be done either by directly imposing a current by means of a battery, or by galvanically connecting the metal to a more anodic material.

Ml alloy is anodic to AZ31 alloy and is not susceptible to stress-corrosion. It was considered possible that extruding a mixture of Ml and AZ31 alloy would result in a fibrous structure with the Ml fibers protecting by galvanic current the AZ31 fibers.

Fig. 15 shows the microstructure of an extrusion from a powder mixture of 50 pct AZ31 + 50 pct Ml alloys. The dark stringers are Ml alloy, the light stringers, AZ31. Several such mixtures were extruded into strip and tested for stress-corrosion, with the results as shown in fig. 16. The specimens were spring-loaded in simple tension and exposed in a rural atmosphere; for details of the test see Loose and Barbian.[19]
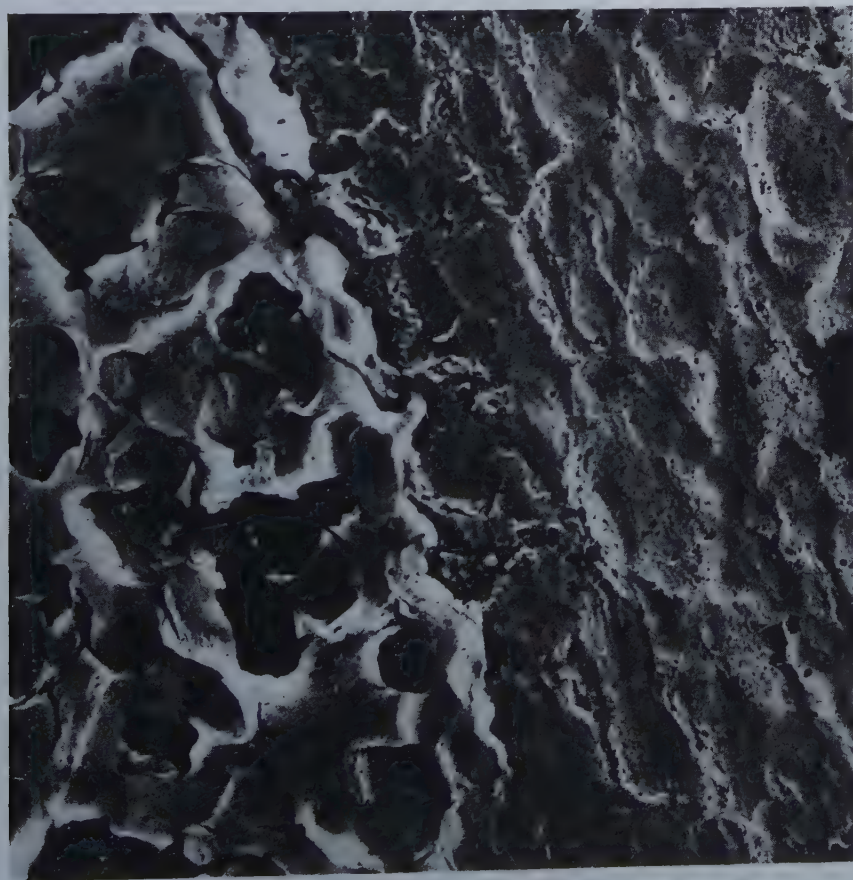
The data clearly show that, when AZ31 is diluted



Fig. 13 — Electron micrograph of ⅜ in. diam rod of KO + 12 pct Mg-Al eutectic.
As-extruded condition. Methyl iodide etchant. 13,500X.

with an equal quantity of Ml, the stress corrosion characteristics of the co-extrusion are similar to those of Ml alloy. The addition of 10 or 25 pct of Ml to AZ31 has little or no effect.

The mechanical properties of various mixtures of Ml-AZ31 alloys are given in table VI. The Ml alloy used in these series of tests contained no calcium. The lack of calcium accounts for the markedly lower strength properties and ductility than those given in table III where the Ml contains a nominal 0.10 pct calcium. The properties of the co-extruded alloys are not a linear function of composition, but, instead, become equal to those for AZ31 when only 40 pct AZ31 is present. It is believed that the non-linear character of the relation is due to some interference-hardening occurring between the aluminum of AZ31 and the manganese of Ml. This is possible since only a few tenths of one percent of manganese is soluble in the presence of 3 pct aluminum. Diffusion of aluminum into Ml or of manganese into AZ31 results in precipitation of a manganese-aluminum compound.

It, therefore, is possible to raise the stress corrosion limit of AZ31 alloy without sacrificing any strength by co-extrusion of equal quantities of Ml and AZ31 alloys.

There is some evidence that an alloy of the total composition Mg + 1.5 pct Al + 0.5 pct Zn + 1 pct Mn would not be any more sensitive to stress-corrosion than Ml. There could be some doubt whether the result reported for the 50Ml + 50AZ31 mixture is due to the galvanic protection proposed or simply to dilution. A 50/50 mixture of Ml and AZ61 was prepared and tested with results as shown in table VII. Although data are not available in this system for as long a time as with AZ31, the evidence is good that Ml is as effective in raising the stress-corrosion limit of AZ61 as of AZ31. The effect cannot, therefore, be ascribed to dilution.

The tensile properties shown in the same table illustrate again the interference-hardening reaction. The 50Ml/50AZ61 co-extrusion is stronger than either of the components. The data also show that the properties decrease less rapidly with increasing extrusion speed. This has been noted often and is probably due to the decreased tendency for coalescense exhibited by precipitation formed by interference, as discussed above.

**Hot Short Speed:** Many of the strong magnesium-base alloys contain enough alloying material to lower the solidus to such an extent that the alloys cannot be extruded at reasonable speeds without hot-shorting. This has been a severe limitation on the development of high-strength magnesium alloys. It has been found possible to eliminate this difficulty by co-extrusion with an alloy not susceptible to hot-shorting even at high speeds. Table VIII lists results obtained by co-extruding a few hot-short alloy types with Ml and AMZ210. In every case there is a significant increase in the hot-short limit of the mixture as compared to the single alloy.

### Summary

The technique of the extrusion of powdered magnesium alloys has been described. The importance of the use of atomized powder, a new mechanism termed "interference hardening," a method for combating stress-corrosion, and a method for increasing the hot-short speed of extrusions have also been discussed.

To summarize the ideas advanced in the paper,

Fig. 14 — Electron micrograph of ⅜ in. diam rod of KO + 12 pct Mg-Al eutectic heat treated, 750°F (1 hr). Methyl Iodide etchant. 10,000X.

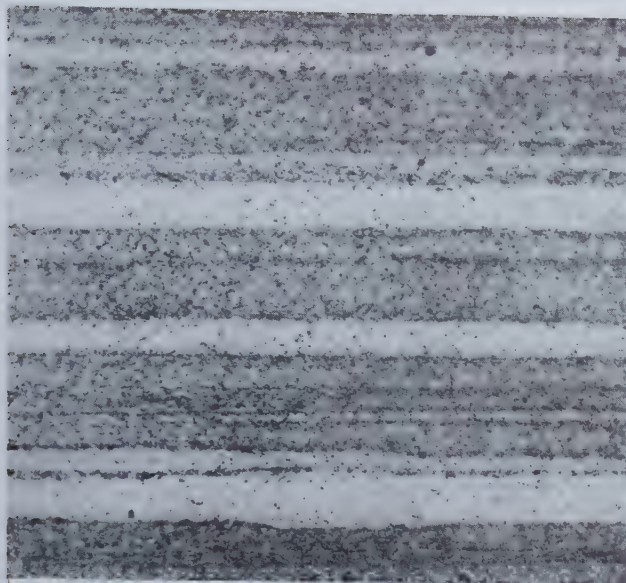**Fig. 15—Microstructure of ⅜ in. diam rod of 50Ml/
50AZ31 Co-extrusion.**

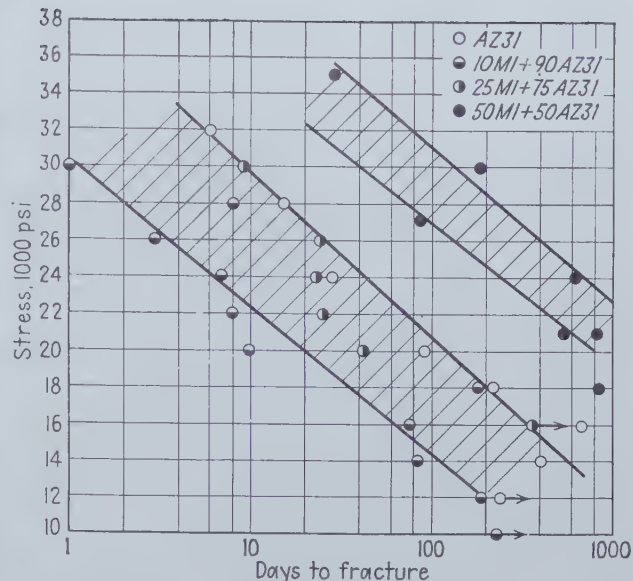Acetic picral etchant. 250X.



**Fig. 16—Stress corrosion of AZ31 alloy and Ml/AZ31
mixtures.**

AMZ111*   1 pct Al + 1 pct Mn + 1 pct Zn
AMZ210*   2 pct Al + 1 pct Mn + 0.5 pct Zn

* This composition is not designated according to the ASTM sys-
tem since three letters are used. However, for the purpose of this
paper the designation used is clearer.

and to illustrate what can be accomplished by com-
bining all the principles discussed, the data in table
IX are given. The alloy ZK60 + 0.5 pct Ca has
excellent mechanical properties, but it can be ex-
truded at only 1 fpm. Addition of Ml to this alloy
raises the permissable extrusion-rate to 5 fpm, but
the properties are significantly lower. However,
ZK60 + 0.5 pct Ca contains zirconium which can
be made to undergo an interference-hardening re-
action by addition of aluminum. Therefore, 12 pct
magnesium-aluminum eutectic was also added with
the results shown. The permissible extrusion-speed
is increased fivefold, a better combination of prop-
erties is obtained, and the alloy may be expected to
be no more sensitive to stress corrosion than Ml.

### Appendix

The ASTM nomenclature system for magnesium
alloys is designed to indicate the principle composi-
tion by the designation itself. The symbol for an
alloy contains, first, not more than two letters to
represent the principle alloying-ingredients listed
in order of decreasing total addition; second, num-
bers representing the amount of each constituent
assigned a letter, listed in the same order as the
letters. If a range of composition is specified for an
element the mean is used; if a minimum is specified,
the minimum is used to determine the symbol.
Compositions at 0.5 pct are rounded according to
standard ASTM procedure. The symbols for the
elements used for this paper are:

A—Aluminum
Z—Zinc
K—Zirconium
M—Manganese
E—Mischmetal

The nominal compositions of the alloys used are:

| ASTM Designation | Composition (Mg + ) |
|---|---|
| Ml | 1.2 pct Mn (minimum) + 0.10 pct Ca |
| KO | 0.5 pct Zr |
| AZ31 | 3 pct Al + 1 pct Zn + 0.2 pct Mn |
| AZ61 | 6 pct Al + 1 pct Zn + 0.2 pct Mn |
| ZK60 | 6 pct Zn + 0.7 pct Zr (minimum) |

### Bibliography

[1] C. G. Goetzel: Powder Metallurgy of Copper. *Metals
and Alloys*, (1940) **12**, 30, 154.
[2] W. D. Jones: Hot Pressing of Metal Powders. *Metal
Industry*, (London), (1940), **56**, 225.
[3] W. D. Jones: Powder Metallurgy—Techniques of
Hot Pressing. *Metal Industry*, (London), (1940), **56**,
69.
[4] O. H. Henry and J. J. Cordiano: Hot Pressing of
Iron Powders. *Trans.* AIME (1946), **166**, 520.
[5] G. J. Comstock and J. D. Shaw: New Developments
in Powder Metallurgy. *Iron Age* (May 22, 1947), **159**,
67.
[6] R. Kieffer and W. Hotop: Sintered Metals. *Metal
Industry*, (London), (1945), **66**, 342.
[7] W. D. Jones: Extrusion of Metal Powders. *Metal
Industry*, (London), (1940), **57**, 27.
[8] H. B. Duncan: U. S. Pat. 2,414,029, (1947).
[9] J. Tyssowski: The Coalescence Process for Pro-
ducing Semi-fabricated Oxygen-free Copper. *Trans.*
AIME, (1941), **143**, 335.
[10] F. G. Daveler and P. H. Aspen: Alloy Welding
Wire from Powder Metallurgy. *The Welding Journal*
(1945), **24**, 842.
[11] R. Kieffer and W. Hotop: Das Strongpressen in der
Fulvermetallurgie. *Metallwirtschaft* (1944), **23**, 379.
[12] E. E. Ensign: Ford Utilizes Extrusion Method for
Producing Metal Powder Gears. *Automotive Indus-
tries* (Aug. 15, 1947), **97**, 30.
[13] F. Sauerwald: Synthetic Light Metal Products.
*Archiv F. Metallkunde* (1947), **1**, 363.
[14] M. Stern: U. S. Pat. 2,358,667.
[15] J. P. Dean and G. Ansel: Some Effects of Zirconium
on Extrusion Properties of Magnesium-Base Alloys
Containing Zinc. *Trans.* AIME (1947), **171**, 286.
[16] F. Sauerwald, L. Holub and H. Eisenreich: Cana-
dian Pat. 416,168, (Nov. 2, 1943).
[17] Magnesium Elektron, Ltd.: British Pat. 511,137,
(Aug. 9, 1938).
[18] E. H. Dix: Electrochemical Theory of Stress Corro-
sion. *Trans.* AIME (1940), **137**, 11.
[19] W. S. Loose and H. A. Barbian: Stress Corrosion
Testing of Magnesium Alloys. Symposium on Stress
Corrosion Cracking, ASTM-AIME, (1945).

Kinetics of the

# Eutectoid Transformation

in Alloys of

# Iron and Nitrogen

## by B. N. Bose and M. F. Hawkes

Metallographic, X ray diffraction, and microhardness studies on an alloy of 2.35 wt pct nitrogen, balance iron are reported. This alloy is analogous to the eutectoid iron-carbon alloy with respect to transformation to "pearlitic" and "martensitic" structures. Isothermal transformation at all temperatures is slower in the nitrogen alloy, and the nitrogen austenite is far more stable with respect to transformation to martensite.

SINCE Davenport and Bain[1] introduced the isothermal transformation technique for the study of austenite decomposition in steels, a new field of investigation has opened up. Extensive research has been carried out on many different steels, but relatively little work has been done on eutectoid transformations in analogous alloy systems. The researches of Smith and Lindlief,[2] Mack,[3] and Klier and Grymko[20] on the beta-phase transformation in copper-aluminum alloys, of Hibbard, Eichelman, and Saunders[4] and Smith[5] on the kappa-phase transformation in copper-silicon alloys, of Chaudron and Forester[6] on the decomposition of "FeO," and of Wasserman[7] on similarities between the iron-carbon, copper-aluminum, copper-tin, and copper-beryllium systems essentially comprise the field.

The iron-nitrogen system, in view of its remarkable similarity to the iron-carbon system, is particularly attractive for the study of eutectoid decomposition. The present investigation is concerned with the study of isothermal transformation, proceeding by the familiar nucleation and growth processes, and of martensitic transformation characteristics of pure iron-nitrogen alloys. The kinetics of transformation and the morphology of the transformation products have been investigated, for these must be the factors determining the properties and behavior of the final product.

### The Iron-Nitrogen System

The binary iron-nitrogen phase diagram has been a matter of considerable disagreement among various investigators. However, the phase diagram according to Eisenhut and Kaupp[8] and Lehrer[9] is now considered essentially correct as reproduced in fig. 1. The important values, 2.35 pct nitrogen and 591°C, for the co-ordinates of the eutectoid point (obtained from this diagram and used in the re-

search to be described) were confirmed in a concurrent study of Paranjpe, Cohen, Bever and Floe.[21] The eutectoid decomposition involves the transformation of the $\gamma$ face-centered cubic interstitial solid solution of nitrogen in iron to the $\alpha$ body-centered cubic interstitial solid solution of nitrogen in iron and the $\gamma'$ nitride of iron. This nitride is essentially the compound $Fe_4N$; it also possesses a face-centered cubic lattice but a considerably larger one than the $\gamma$; the nitrogen atoms in $\gamma'$ are arranged in an ordered way in the centers of the unit cubes.[8, 10, 11] A martensitic structure has also been reported[8, 12] in iron-nitrogen alloys and was studied in the research to be described here.

### Materials and Methods

The specimens used in this investigation were prepared by nitriding "pure" iron. This iron was supplied by the Westinghouse Research Laboratories and is the product bearing their trade name "Puron"; it contains about 0.04 wt pct total impurities, the major portion of which is oxygen. Specimens were ribbons several inches long, a tenth of an inch wide, and 0.125 mm thick; this was the

B. N. BOSE was formerly Graduate Student in the Department of Metallurgical Engineering, and M. F. HAWKES, Member AIME, is Associate Professor of Metallurgical Engineering and Member of Staff, Metals Research Laboratory, Carnegie Institute of Technology, Pittsburgh, Pa.
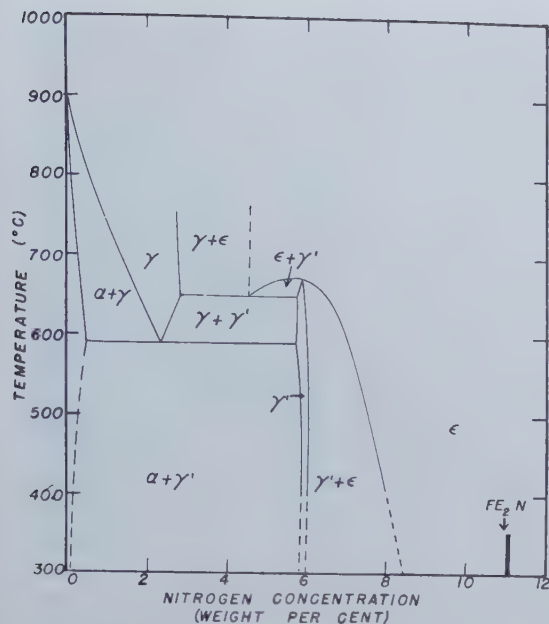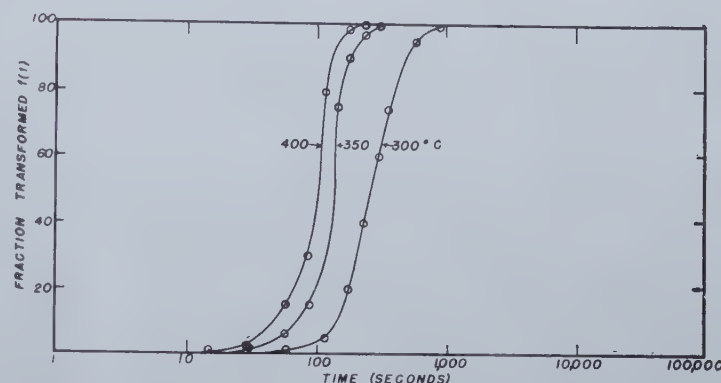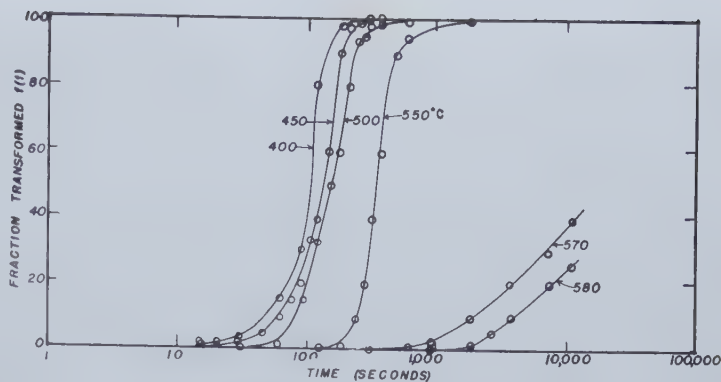
Fig. 1—The Iron-Nitrogen phase diagram.

Figs. 2 and 3 (right)—Isothermal reaction curves for Iron-Nitrogen eutectoid alloy.

480°C and 580°C curves are for lamellar transformation product only. (See text.)

maximum thickness that could be nitrided to give a uniform nitrogen concentration throughout.

It must be realized that in the iron-nitrogen system where one component is a gas, the equilibrium diagram (fig. 1) has significance only at a pressure corresponding to the vapor pressure of atomic nitrogen in the gaseous atmosphere surrounding the specimens used in the determination of the diagram. In other words, the diagram represents the iron-nitrogen system in equilibrium not at atmospheric pressure but at the very high pressure corresponding to the dissociation of ammonia.

Likewise in the studies reported here, the specimens were of necessity prepared and heat treated in an atmosphere consisting of a mixture of pure dry ammonia and hydrogen. It must also be remembered that the nitrogen concentration of the specimen is controlled directly not by the $NH_3$-$H_2$ ratio of the gas mixture entering the furnace but by the degree of dissociation of ammonia at the very surface of the specimen. This is in turn controlled empirically by the $NH_3$-$H_2$ ratio fed to the furnace, but the value of this ratio for a given nitrogen concentration in the specimen is affected by the various arbitrary dimensions of the specimen and furnace.

In practice the gas ratios varied but were always adjusted to give the desired nitrogen concentration in the specimen (usually 2.35 pct nitrogen by weight, the eutectoid concentration). The amount of nitrogen absorbed was measured by weighing the specimens in a semimicro balance before and after nitriding; previous to the latter weighing, the specimens were water quenched from the nitriding temperature. Analyses were also checked occasionally by means of the vacuum fusion method; good agreement was obtained.

Homogeneity of the specimens (with respect to uniform nitrogen concentration throughout the thickness) was obtained by continuing the original nitriding with constant $NH_3$-$H_2$ ratio until several weighings showed the desired value of nitrogen concentration and no change in that value. All later microscopic observations following isothermal transformation showed a uniform degree of transformation across the thickness of each specimen; in view of the pronounced effect of nitrogen concentration on rate of transformation to be described later, this is additional confirmation of the fact that the specimens were homogeneous.

The nitriding temperature used was 700°C; 3 to 4 hr at this temperature was sufficient to insure homogeneity; water quenching followed the nitriding. The specimens were reheated to 700°C for austenitizing in an $NH_3$-$H_2$ atmosphere suitable for maintaining the nitrogen concentration unchanged. Austenitizing times of from 3 to 30 min were used. This difference resulted in no variation in austenite grain size or degree of subsequent isothermal transformation; the austenite grains were rather uniform in size, averaging 0.06 mm in diam.

The heat treating arrangement consisted essentially of two electric resistance furnaces heating successive portions of a single silica tube through which the $NH_3$-$H_2$ atmosphere flowed. After austenitizing in the 700°C portion of the tube, the specimens were quickly pushed into the other zone of the tube maintained at the desired temperature of transformation within 2°C. Less than 10 sec was required for the specimens to cool from the austenitizing temperature to the temperature of transformation.

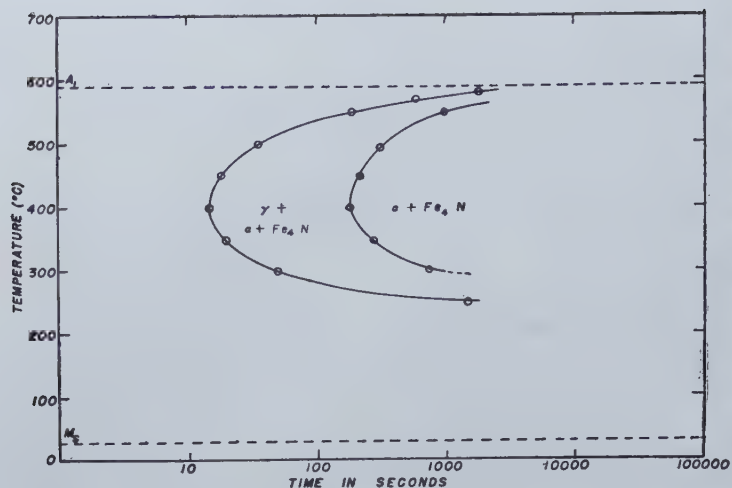Throughout the time of subcritical transformation, the $NH_3$-$H_2$ mixture was allowed to flow

Fig. 4—Isothermal transformation diagram for Iron-Nitrogen eutectoid alloy.



Fig. 5—Iron-Nitrogen eutectoid alloy, transformed 2 hr at 580°C.

(100 pct transformed) 1000X. Picral-nital etch.

through the silica tube in order to minimize loss of nitrogen from the specimen. Equilibrium was not attained, and it is probably not practical to attempt to attain it in view of the phase reactions occurring in the specimen during holding, the very high degree of ammonia dissociation necessary for equilibrium with $Fe_4N$, and the varying $NH_3$-$H_2$ ratio required at various temperatures of transformation. It is sufficient to say that with the gas ratios used, no loss of nitrogen was observed in any specimens for which results are reported later. This was checked by weighing every specimen after transformation. (Note in fig. 2 that transformation at 580° and 570°C could only be followed for about 10,000 sec before appreciable loss of nitrogen in the specimens occurred.)

Most of the experimental results reported here are based on microscopic analysis in conjunction with isothermal transformation experiments using the techniques described above. Some X ray diffraction studies were made, but these were undertaken primarily to supplement the microscopic work by identifying phases and more or less qualitatively estimating the progress of reactions. Microhardness measurements have also been made to supplement the metallographic and X ray diffraction studies. Except for the study of martensitic transformation, the isothermal transformation technique has been used to study both kinetics and morphology.

## Kinetics of Transformation and Morphology

Isothermal reaction curves for the eutectoid iron-nitrogen alloy (2.35 pct nitrogen) at various sub-critical temperatures are presented in fig. 2 and 3. They are similar in form to the reaction curves obtained for nucleation and growth processes in other systems, notably the isothermal decomposition of eutectoid steel. These curves have been summarized in the customary "T-T-T" diagram reproduced in fig. 4, using 1 pct and 99 pct as the criteria for the beginning and the end of reaction. The resulting curves have the familiar C-shape similar to the isothermal transformation diagram for eutectoid iron-carbon alloys. The highest temperature of reaction studied was 580°C, about 10° below the eutectoid; the transformation at this temperature
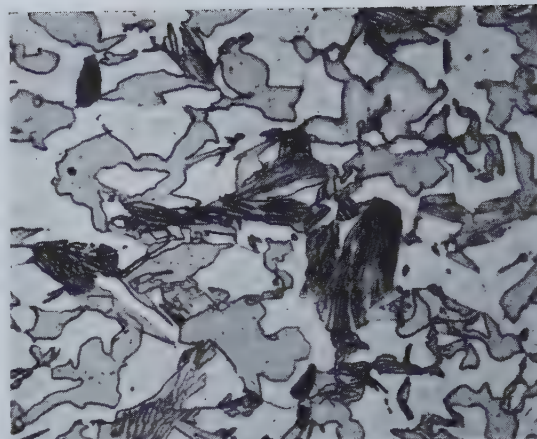
starts in about 30 min. It was not possible to study the transformation at any higher temperatures because the rate of reaction is quite slow and there is a pronounced tendency for the specimen to decompose with loss of nitrogen at these high temperatures; the loss of nitrogen was appreciable before any detectable eutectoid transformation occurred.

At 580°C, as also at the next lower temperature investigated, 570°C, the transformation resulted in a lamellar structure as well as irregular massive precipitates of ferrite and nitride ($Fe_4N$). In estimating the amount of transformation at these temperatures, for fig. 2-4, only the lamellar structure has been taken into consideration. It is difficult to distinguish microscopically the massive transformation product from the untransformed matrix; quantitative estimation is practically impossible although qualitative estimation was obtained by X ray means. It may be noted, however, that both types of structure appear to start forming at about the same time.

The fastest rate of reaction occurs at about 400°C where the reaction starts in 15 sec and is completed in 4½ min. At lower temperatures, the rate of reaction again decreases until at temperatures below 250°C, it is so slow that the beginning of transformation cannot be detected even after 12 hr at 150°C. No evidence for a second "knee" in the T-T-T curve was obtained. The martensite transformation will be discussed in a later section.

The morphological features exhibited by the iron-nitrogen system are rather interesting. Just below the eutectoid temperature, at 580°C, a lamellar structure, very similar to iron-carbon pearlite is formed. In addition to this lamellar structure, the eutectoid alloy at this temperature also gives rise to a transformation product consisting of irregular masses of ferrite and nitride. These two transformation products are shown in fig. 5. X ray diffraction studies also indicate that at this temperature the entire specimen is converted into ferrite and nitride ($Fe_4N$) in 2 hr although only less than half of the specimen shows lamellar structure.

At 570°C, the transformation is essentially the same as at 580°C; the lamellar structure is again observed, and, as expected, it has a finer inter-lamellar spacing. The irregular massive precipitates
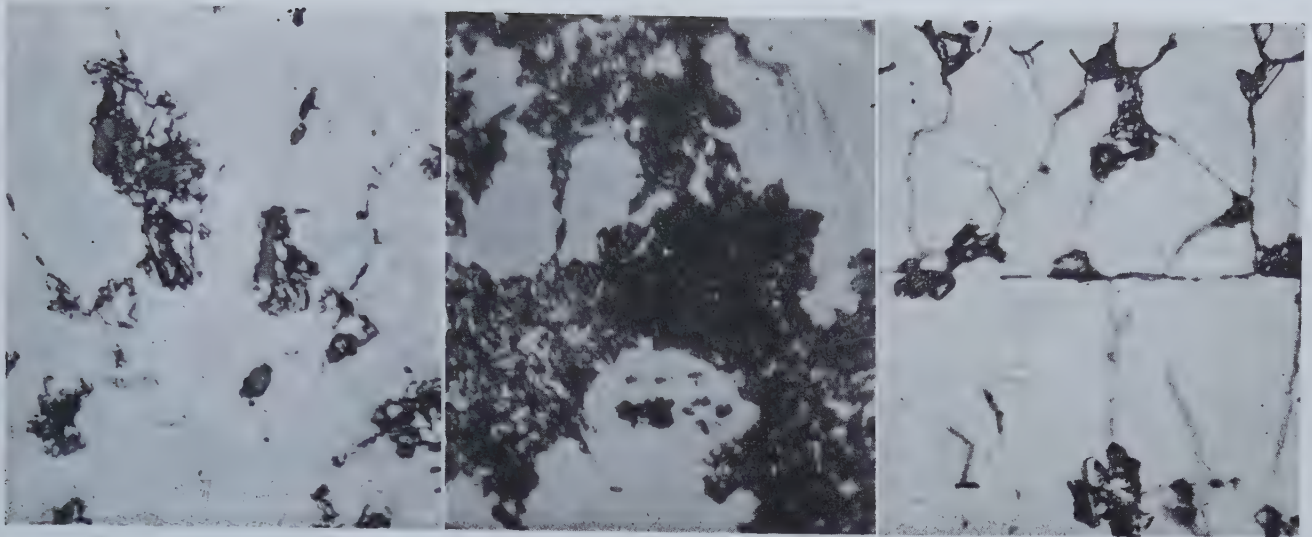
Fig. 6 (left)—Iron-Nitrogen eutectoid alloy, transformed 4 min at 550°C. 1000 X. Fig. 7 (center)—
Iron-Nitrogen eutectoid alloy, transformed 6 min at 550°C. 1000 X. Fig. 8 (right)—Iron-Nitrogen
eutectoid alloy, transformed 3 min at 550°C followed by 45 sec at 400°C. 1000 X.
All specimens etched in picral-nital solution.

still form, and the entire specimen presents a "jumbled" structure.

At lower temperatures, such as 550°C, well defined lamellar structure is no longer discernible, and the formation of massive precipitates has also practically stopped. Down to this temperature, the rate of nucleation is relatively slow. Only a small number of nuclei form, effectively at random, and grow to large size, showing the group nodule type of transformation as discussed by Hull and Mehl,[13] in the case of iron-carbon alloys. Fig. 6 and 7 show stages in the progress of transformation at 550°C.*

---

* Partial transformation only is depicted in fig. 6-11. The light etching background was untransformed austenite at the end of the stated time of isothermal holding. On subsequent quenching to room temperature, less than half of this austenite transformed to martensite. See later discussion.

---

That nucleation starts essentially at the grain boundaries, is revealed in fig. 8, which shows partial transformation at 550°C followed by a small amount of transformation at 400°C to bring out the austenite grain boundaries.

As the reaction temperature is lowered further to 500°C, nucleation starts rapidly at and forms an envelope around the grain boundaries. Growth then occurs radially towards the center. The progress of transformation at 500°C is depicted in fig. 9 and 10. The behavior thus continues to be strikingly similar to the morphological characteristics of iron-carbon alloys studied in detail by Hull and Mehl.[13] As the reaction temperature is further lowered to 400°C, the structure continues to be essentially the same, though becoming progressively finer and less resolvable under the microscope.

As the reaction temperature is further lowered below 400°C, that is below the knee of the isothermal transformation diagram, a distinct change in the microstructure of the products is observed, as seen in fig. 11; the structure becomes lighter etching and completely unresolvable. Although the transformation does not show any structural similarities to bainite, it seems highly probable that in the iron-nitrogen system as in the iron-carbon system, a fundamental change in the mechanism of transformation occurs at the knee of the isothermal

diagram. This is further suggested by hardness measurements of the products of transformation at different temperatures, as will be seen presently.

### Rates of Nucleation and Growth

From the foregoing discussion and from examination of the structures developed at various reaction temperatures, the following qualitative statements may be made. The rate of nucleation is quite slow at temperatures immediately below the eutectoid and increases rapidly as the transformation temperature is lowered. The rate of growth also increases somewhat with decrease in reaction temperature but not nearly so rapidly as the rate of nucleation. The ratio of the rates of nucleation and growth thus increases rapidly with decreasing temperature. These relationships cause the formation of group nodules at higher transformation temperatures and pronounced grain boundary transformation at relatively lower temperatures.

Actual measurement of the rates is extremely difficult in view of the fact that at the highest transformation temperatures studied, the nucleation and growth of the normal eutectoid product is interfered with by the simultaneous formation of irregular massive precipitates, whereas at somewhat lower temperatures, the transformation product has pronounced tendency to form in chains along grain boundaries. There is also the difficulty of distinguishing very small nuclei from inclusions and other imperfections. Owing to these difficulties, no attempt was made to measure accurately the rate of nucleation.

The rate of growth, however, has been measured at two temperatures, 580° and 550°C, using the technique developed by Hull, Colton, and Mehl.[14] This consists in examining partially reacted specimens in which nodule impingement has not occurred, and plotting maximum nodule radius against time of transformation. When rate of growth is constant, as it usually is, the plot gives a straight line, the slope of which is the rate of growth.

At 580°C, the maximum nodule radius has been plotted as indicated above, ignoring the interfer-
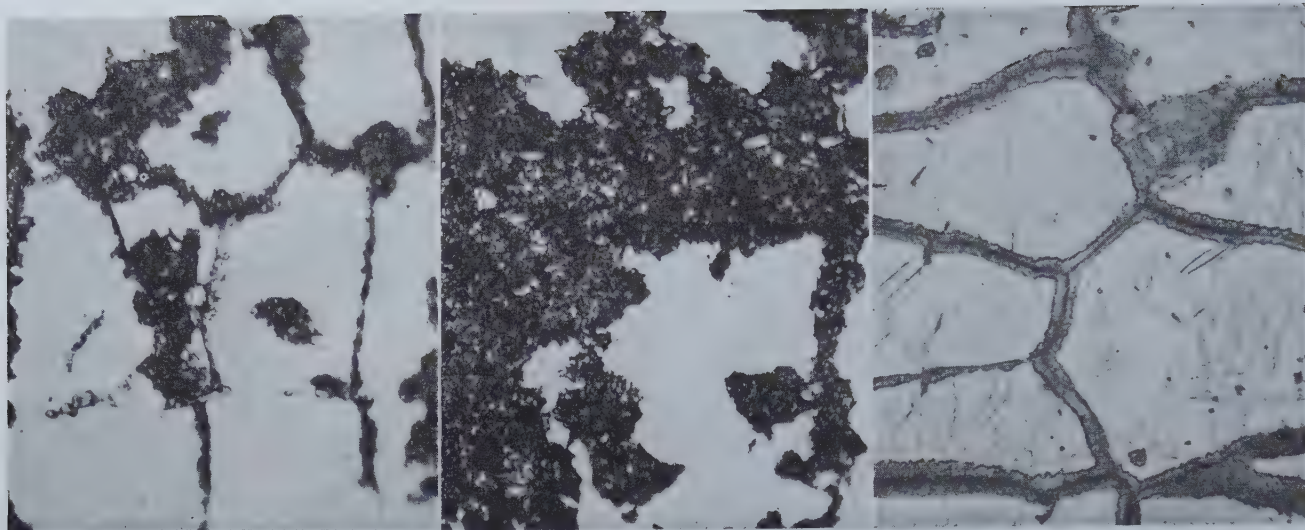
Fig. 9 (left)—Iron-Nitrogen eutectoid alloy, transformed 1 min 45 sec at 500°C. 1000 X. Fig. 10 (center)—Iron-Nitrogen eutectoid alloy, transformed 3 min 30 sec at 500°C. 1000 X. Fig. 11 (right)—Iron-Nitrogen eutectoid alloy, transformed 1 min 30 sec at 350°C. 1000 X.
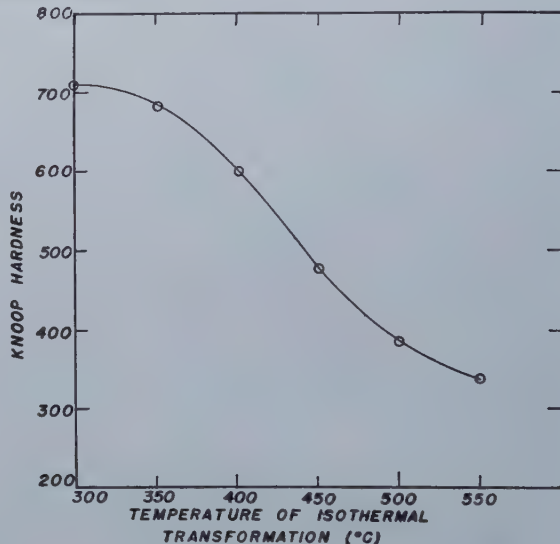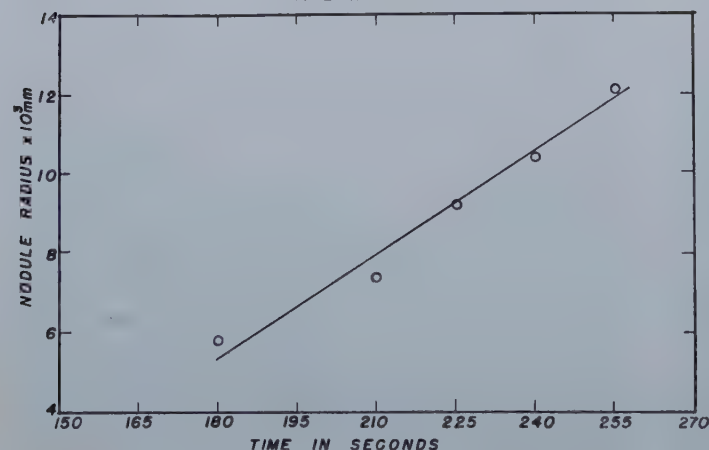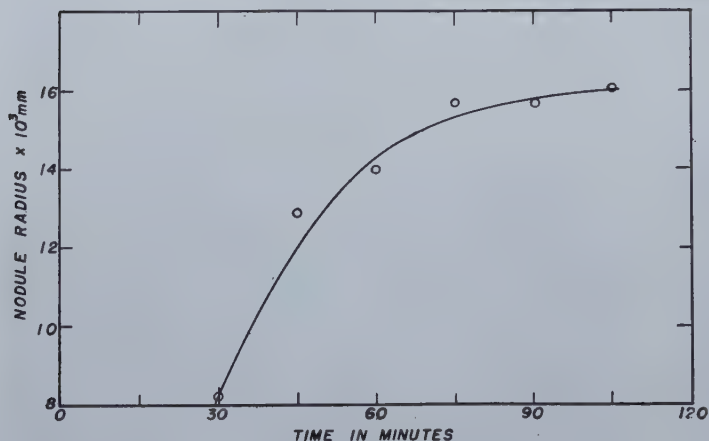All specimens etched in picral-nital solution.



Fig. 12 (left above)—Growth curve; 580°C.

Fig. 13 (left below)—Growth curve; 550°C.

Fig. 14 (above)—Microhardness of the products of isothermal transformation of eutectoid Iron-Nitrogen alloy at various temperatures.

ence due to the blocky precipitates. The result is shown in fig. 12. It will be noticed that although there is a straight portion to begin with, the curve flattens out with time indicating hindrance in growth, presumably due to the massive precipitates. The initial rate of growth is found to be $4.2 \times 10^{-6}$ mm per sec. At 550°C, the reaction is relatively free from the massive precipitation observed at higher temperatures, and also from the pronounced grain boundary precipitation occurring at lower temperatures. The maximum nodule size plotted against

time gives more nearly a straight line (fig. 13), and the rate of growth is found to be $8.7 \times 10^{-5}$ mm per sec.

### X ray Diffraction Studies

Powder photograms were taken with specimens transformed at various temperatures for various lengths of time. Cobalt $K_a$ radiation with iron filter was used. The observed lattice parameter of the phases are as follows:

| | |
|---|---|
| $\gamma$ | $a_0 = 3.637$ A° |
| $\gamma'$ (Fe$_4$N) | $a_0 = 3.786$ A° |
| $\alpha$ (ferrite) | $a_0 = 2.863$ A° |
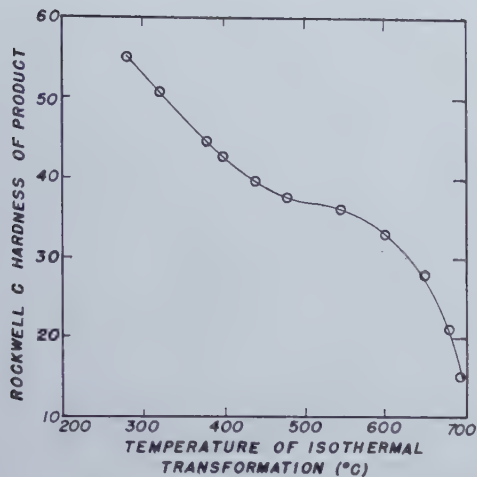
Fig. 15—Hardness of the products of isothermal transformation of eutectoid Iron-Carbon alloy at various temperatures. Davenport and Bain.[1]
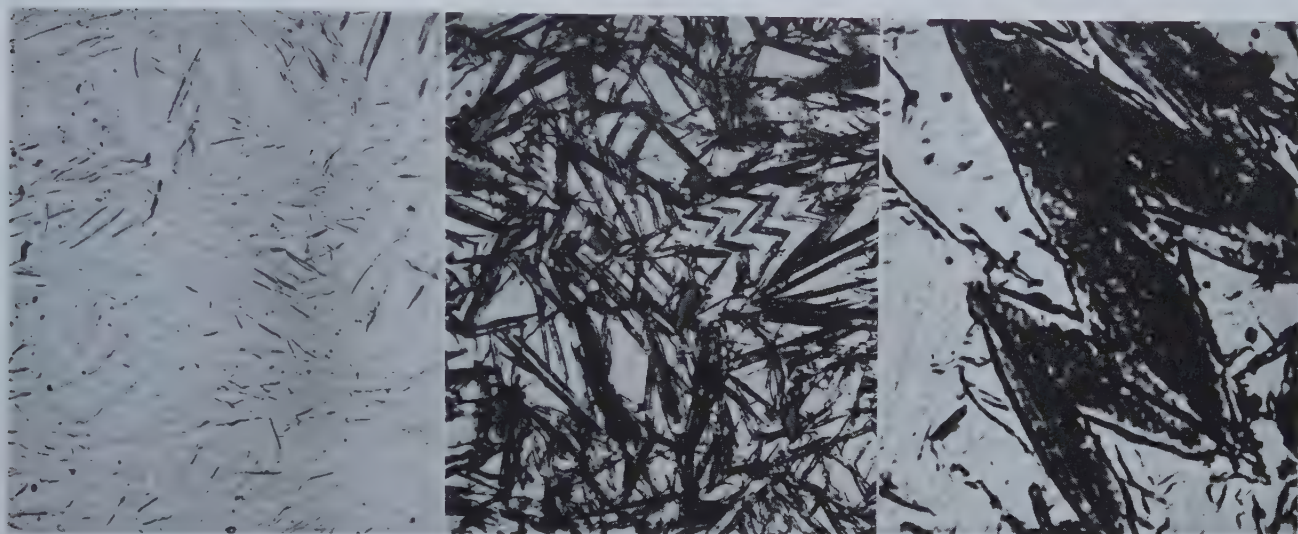


Fig. 16 (left)—Martensite in eutectoid Iron-Nitrogen alloy, as quenched in liquid Nitrogen. 750 X.
Fig. 17 (center)—Martensite in eutectoid Iron-Nitrogen alloy, quenched in liquid Nitrogen then tempered 30 min at 225°C. 750 X. Fig. 18 (right)—Same as fig. 17. 2000 X.

The light etching matrix phase in all three micrographs is retained gamma. All specimens etched in picral-nital solution.
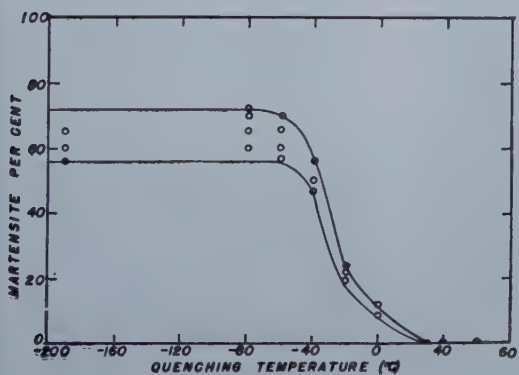


Fig. 19—Martensite transformation in eutectoid Iron-Nitrogen alloy as a function of quenching temperature.
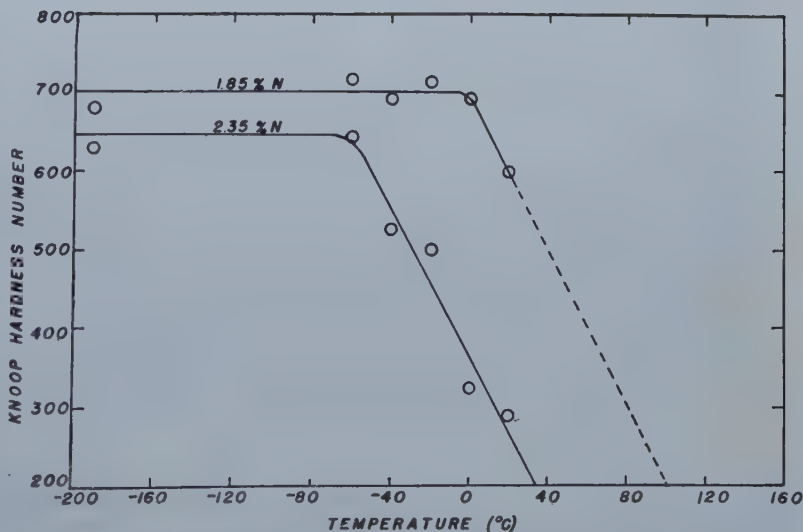


Fig. 20—Microhardness of Iron-Nitrogen alloys quenched to various temperatures.

Fig. 21—Isothermal transformation diagram (50 pct transformation) for Iron-Nitrogen alloys:

eutectoid (2.35 pct N), hypo-eutectoid (1.85 pct N), and hyper-eutectoid (2.55 pct N).
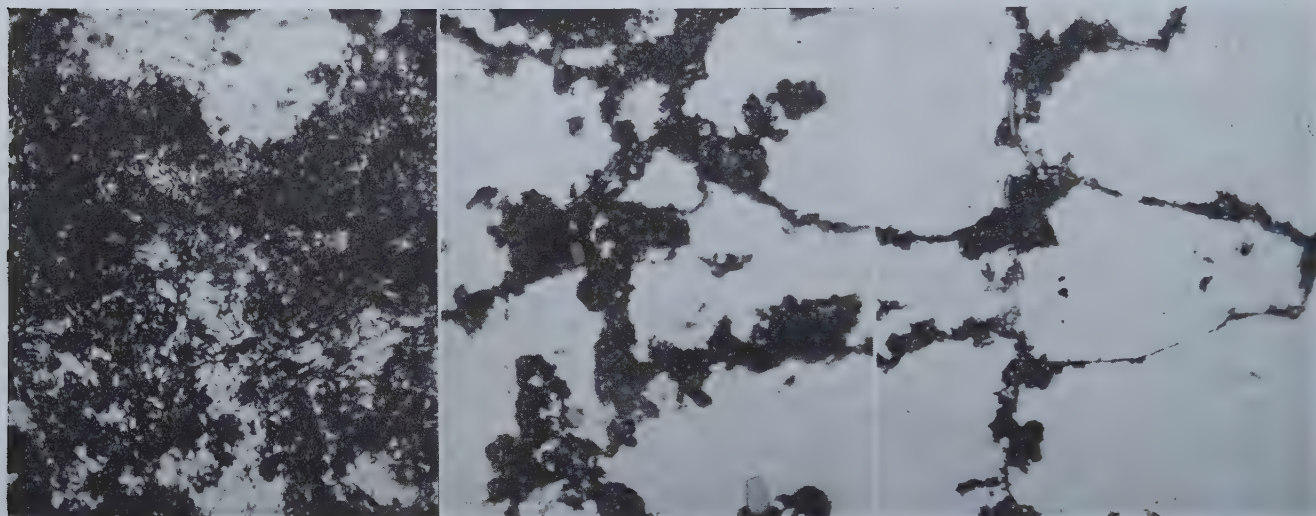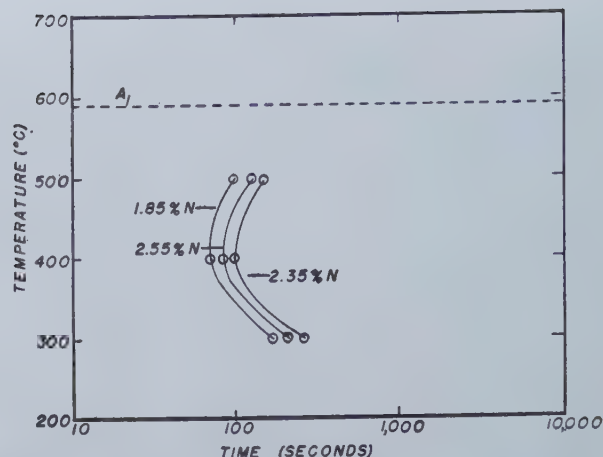


Fig. 22 (left)—Hypo-eutectoid Iron-Nitrogen alloy (1.85 pct N) transformed 100 sec at 500°C. 1000 X.
Fig. 23 (center)—Hyper-eutectoid Iron-Nitrogen alloy (2.55 pct N) transformed 100 sec at 500°C.
1000 X. Fig. 24 (right)—Eutectoid Iron-Nitrogen alloy (2.35 pct N) transformed 100 sec at 500° C. 1000 X.

All specimens etched in picral-nital solution.
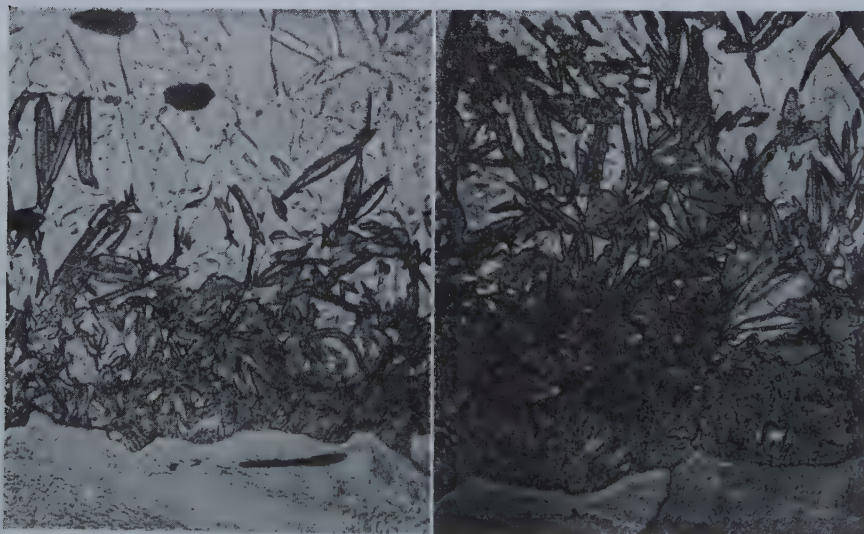


Fig. 25 (left)—Iron-Nitrogen alloy with progressively decreasing nitrogen concentration from 2.6 pct N, corresponding to the top of the micrograph, quenched to 60°C, then tempered 30 min at 225°C. 750 X.

Picral-nital etch.

Fig. 26 (right)—Iron-Nitrogen alloy with progressively decreasing nitrogen concentration from 2.6 pct N, corresponding to the top of the micrograph, quenched to —20°C, then tempered 30 min at 225°C. 750 X.

Picral-nital etch.

A specimen transformed for 2 hr at 580°C is found to consist entirely of ferrite and nitride (Fe₄N), although only less than half of the product appears lamellar in structure, the rest consisting of irregular massive precipitates mentioned earlier. As the transformation progresses, the gamma lattice parameter appears to retain constancy, indicating that the gamma phase does not change in composition during the progress of the transformation.

Both above and below the knee of the reaction curve, the transformation consists of ferrite and nitride (Fe₄N) as shown by X ray diffraction, so

that crystallographically, the products of transformation above and below the knee are identical, in spite of their microstructural difference.

## Microhardness Measurements

Microhardness measurements were made by means of a Tukon Tester, using a load of 500 g for most of the experiments. Untransformed gamma, much of which is retained on quenching to room temperature, has a Knoop hardness* of 290. The

* For the relationship between Knoop hardness and Rockwell hardness, see ref. 15 and 16.

hardness increases on transformation into ferrite and nitride ($Fe_4N$), presumably due to the dispersed hard nitride particles.

The hardness of the completely transformed product at various temperatures is shown in fig. 14. It will be noticed that the trend is the same as would be expected from the microstructures; that is, as the transformation temperature decreases, the structure becomes finer and the hardness increases. Also, with decrease in transformation temperature, the product becomes more brittle. For the sake of comparison, the change of hardness with the isothermal transformation temperature for an eutectoid iron carbon alloy, as obtained by Davenport and Bain,[1] is reproduced in fig. 15. The similarities between fig. 14 and 15 are quite obvious; in both cases, there is increase in hardness with decrease in transformation temperature. There is, however, one significant difference between the two curves. In the case of the iron-nitrogen alloy, the hardness curve shows a maximum slope at a temperature of about 400°C which corresponds to the knee of the isothermal transformation diagram. In the case of the iron-carbon alloys also, the hardness curve shows a marked change in slope at the temperature of the knee, about 550°C; but in this case, the slope at this temperature is at a minimum, and for a certain temperature range, there is hardly any change in hardness as the transformation temperature is decreased. However, the changes in slope of the hardness curves at the temperature of the knee, though in the opposite direction in the two systems, may both indicate a fundamental change in the mode of transformation in this temperature range.

## Martensite Transformation in the Iron-Nitrogen System

Fry[12] first reported a microstructure similar to that of martensite in rapidly cooled iron-nitrogen alloys. Eisenhut and Kaupp[8] observed that iron-nitrogen alloys quenched from the gamma phase contained a body-centered tetragonal structure. These authors found the axial ratio of the body-centered tetragonal iron-nitrogen martensite to be 1.06 for 0.8 pct nitrogen and stated that the axial ratio decreases with lower nitrogen concentration.

In the course of the present investigation, the above findings have been essentially confirmed and extended. It has been found that an eutectoid iron-nitrogen alloy when quenched to subzero temperatures undergoes martensitic transformation and produces the structures shown in fig. 16 in the as-quenched state and fig. 17 after quenching and tempering at 225° for 30 min. Fig. 18 shows the

tempered martensite at a higher magnification. It will be noticed that the martensite in this alloy forms as well-defined plates with prominent midribs very similar to the structure observed in high carbon steels. Also, as in steel, the iron-nitrogen martensite etches dark as a result of tempering. This permits the use of the technique developed by Greninger and Troiano[17] for metallographic study of the progress of martensite transformation. The amount of martensite formed as a function of quenching temperature is shown in fig. 19.* The

* The results show considerable scatter and are presented in the form of a band in fig. 19.

$M_s$ temperature for the eutectoid alloy is found to be 35°C. It will be noticed that the form of the curve in fig. 19 is typical of the martensite transformation curves in steel or in other systems. The amount of martensite at first increases with decrease in the quenching temperature, but the transformation apparently stops at a temperature of about —70°C and no additional martensite is formed even on quenching to the temperature of liquid nitrogen, although a considerable amount of austenite is still retained untransformed. The iron-nitrogen system thus presents an extreme case of the phenomenon of stabilization and retention of austenite. In accordance with Cohen's theory,[18] it would appear that in this system, the supply of available nuclei which may transform into martensite is very limited, so that the loss of those consumed during the progress of the transformation seriously affects further reaction. In other words, it may be considered as a case of pronounced self-stabilization.

X ray diffraction studies were undertaken to determine the structure of quenched specimens. The eutectoid alloy quenched to room temperature consisted almost entirely of the face-centered cubic gamma phase; the eutectoid alloy quenched to —80°C showed the body-centered tetragonal martensitic structure, together with a considerable amount of the untransformed gamma. The axial ratio for the body-centered tetragonal martensite in this alloy was found to be 1.09, the c and a axes being respectively 3.100 A° and 2.844 A°. The gamma phase had $a_0 = 3.637$ A°. An hypo-eutectoid alloy (1.85 pct nitrogen) showed much weaker lines of the gamma phase indicating that the amount of retained austenite was less, although an appreciable amount still existed. The axial ratio for this alloy was found to be 1.07 with the c and a axes respectively 3.045 A° and 2.846 A°. The gamma in this case had $a_0 = 3.616$. The transformations in hypo-eutectoid alloys are further discussed in the following section. For the X ray diffraction work reported here, the experimental set up was the same as reported earlier in connection with the studies on isothermal transformation. The semi-circumference of the film was 17.87 cm. Cobalt K alpha radiation and an iron filter were used.

Microhardness measurements were made on the quenched specimens. The duplex structure obtained on quenching in liquid nitrogen showed a Knoop hardness number of approximately 640. The hardness number for a specimen quenched to room temperature and consisting essentially of untransformed gamma was 290. Hardness measurements

were made on a series of specimens quenched to various subzero temperatures and then brought back to room temperature. The results are shown in fig. 20. It will be noticed that although there is considerable scatter in the measured values on account of duplex structure, the curve shows the true trend of the variation of hardness with quenching temperature. The hardness of the quenched specimens showed a small increase on tempering at 225°C. This may be due to isothermal transformation of gamma into ferrite and nitride (Fe₄N) occurring during tempering.

## Transformations in Hypo- and Hyper-Eutectoid Iron-Nitrogen Alloys

The isothermal transformation of two alloys with 2.55 pct and 1.85 pct nitrogen respectively were studied at three different temperatures, namely, 500°, 400°, and 300°C. The time for 50 pct transformation of these alloys, together with the same for the eutectoid alloy, is shown in fig. 21. The curves show the familiar C shape; the hypo-eutectoid alloy shows a much faster reaction rate, while the hyper-eutectoid alloy also shows a somewhat faster rate as compared with the eutectoid alloy. The transformation products obtained with the three alloys for the same length of time at 500°C are shown in fig. 22-24.

No pro-eutectoid constituents were observed either in the hypo or in the hyper-eutectoid alloys at the temperatures studied; the "pearlite interruption" apparently sets in at an early stage, so that no pro-eutectoid rejection is discernible.

An alloy with 2.55 pct nitrogen did not show any measurable difference from the eutectoid alloy with 2.35 pct nitrogen as regards the M$_s$ point and the course of martensite transformation, probably because the compositions are not far removed from each other. With a hypo-eutectoid alloy containing 1.85 pct nitrogen, metallographic study was found to be difficult. The quenched and tempered specimens did not show well defined martensite plates as in the case of the eutectoid alloy. The difficulty was probably enhanced due to relatively rapid isothermal transformation of the untransformed gamma into ferrite and nitride during tempering. The microstructures shown in fig. 25 and fig. 26 are, however, instructive. The specimens concerned had a gradient of nitrogen concentration, the maximum at the top of the figures was about 2.6 pct with progressively decreasing nitrogen content until at the bottom there was practically pure iron. The specimen in fig. 25 was quenched to 60°C then tempered at 225°C and finally quenched to room temperature. The one in fig. 26 was quenched to —20°C, then tempered at 225°C and cooled back to room temperature. From both figures, it is quite obvious that the M$_s$ point is raised and the martensite transformation progresses further as the concentration of nitrogen is decreased. The same effect is confirmed by the X ray diffraction studies mentioned earlier. It was pointed out that an alloy of 1.85 pct nitrogen quenched to —80°C shows much weaker lines of retained gamma than the eutectoid alloy. However, even in the hypo-eutectoid alloy an appreciable amount of gamma remains untransformed. The effect of nitrogen concentration on the martensite transformation in iron-nitrogen alloys thus

appears to be similar to that of carbon and other alloying elements in steel with the exception of cobalt and aluminum.

It has also been pointed out that the axial ratio of martensite in the 1.85 pct nitrogen alloy has been found to be 1.07; the axial ratio for the eutectoid alloy was found to be 1.09. There are not enough data available to show the effect of nitrogen content over an appreciable range on the lattice parameters of martensite. However, Eisenhut and Kaupp[8] found the axial ratio for an alloy of 0.8 pct nitrogen to be 1.06. Recently, Jack[19] has reported the axial ratio to be 1.08 for an alloy containing 2.19 pct nitrogen. The results of the present investigation, together with those of Eisenhut and Kaupp and of Jack, are presented in fig. 27. It is seen that the effect of nitrogen concentration on the axial ratio of martensite is quite similar to that of carbon in iron-carbon alloys. This, however, is not surprising for the martensite in both systems consists of an interstitial solid solution.

Microhardness measurements were also made on a series of specimens of the 1.85 pct alloy. The results are shown in fig. 20. It is seen that the hardness of the specimen quenched to liquid nitrogen is somewhat higher than that of the corresponding specimen of eutectoid composition, presumably due to a higher martensite content in the hypo-eutectoid alloy. A rough measure of the M$_s$ temperature for the hypo-eutectoid alloy can be obtained by extrapolating the hardness curve to the value corresponding to untransformed gamma, which, in the case of the eutectoid alloy, was found to be 290 Knoop. The M$_s$ temperature for 1.85 pct nitrogen is thus found to be approximately 85°C.

## Summary and Conclusions

The transformations in iron-nitrogen alloys have been found to be very similar to those of iron-carbon austenite. The time temperature transformation diagram for the eutectoid iron-nitrogen alloy has a simple C shape as does that of the iron-carbon eutectoid alloy. Isothermal transformation at temperatures very close to the eutectoid produces a lamellar pearlitic structure. Along with the lamellar product, transformation to irregular massive precipitates of ferrite and nitride occurs simultaneously. At somewhat lower temperatures, the massive precipitates are no longer observed, and the structure becomes finer and less resolvable under the microscope. Group nodule transformation is observed at higher temperatures and is gradually replaced by predominantly grain boundary transformation as the temperature is lowered. At the knee of the T-T-T curve, the microstructures show a distinct change; this, together with the marked change in the slope of the hardness versus temperature curve, strongly suggests a fundamental difference in the mechanism of transformation above and below the knee as in the case of iron-carbon alloys.

Accurate determination of the rates of nucleation and growth is difficult in this system. It is observed, however, that both rates increase with decreasing temperature, the rate of nucleation at a much faster pace than the rate of growth. The ratio of rate of nucleation to rate of growth thus increases with
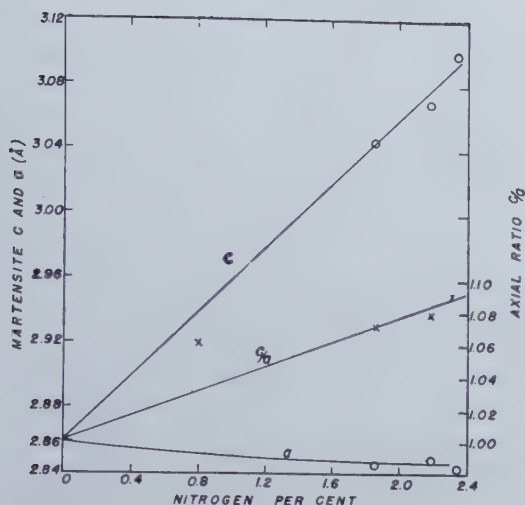
**Fig. 27—Variation of lattice constants of Iron-Nitrogen martensite with nitrogen concentration.**

Data for 0.8 pct nitrogen from Eisenhut and Kaupp.[8]
Data for 2.19 pct nitrogen from Jack.[19] Remaining
data from the present investigation.

decreasing temperature. The rate of growth at 550°C has been found to be $8.75 \times 10^{-5}$ cm per sec.

X ray diffraction studies confirmed the phases formed on isothermal transformation to be ferrite and $\gamma'$ ($Fe_4N$). The final products of transformation above and below the temperature of the knee are found to be crystallographically identical. The composition of the austenite is found to remain constant during the progress of the isothermal transformation.

The products of transformation have increasing hardness and decreasing ductility with decreasing temperature of reaction. The hardness versus temperature curve shows a marked change in slope at the temperature of the knee.

Iron-nitrogen alloys also undergo martensitic transformation. The microstructure and the crystal structure of iron-nitrogen martensite are found to be very similar to those of iron-carbon martensite. Both also show similar behavior on tempering. The $M_s$ point of the eutectoid iron-nitrogen alloy is 35°C. The iron-nitrogen alloys exhibit an extreme case of the phenomenon of stabilization and retention of austenite. The body-centered tetragonal iron-nitrogen martensite has an axial ratio of 1.09 when the nitrogen concentration is 2.35 pct.

Studies on hyper- and hypo-eutectoid iron-nitrogen alloys show that deviation from eutectoid composition in either direction increases the rate of isothermal transformation. Two alloys of nitrogen concentration, 1.85 and 2.55 pct respectively, were studied. In neither case was pro-eutectoid precipitation observed on isothermal transformation at 500°, 400°, and 300°C.

With regard to the martensitic transformation, it is observed that the $M_s$ temperature is raised and the martensite transformation progresses further as the nitrogen content is decreased. The axial ratio of the body-centered tetragonal martensite also decreases with decreasing nitrogen concentration. The effects of nitrogen are thus very similar to those of carbon.

**References**

[1] E. S. Davenport and E. C. Bain: The Transformation of Austenite at Constant Subcritical Temperatures. *Trans.* AIME (1930) **90**, 117.

[2] C. S. Smith and W. E. Lindlief: A Micrographic Study of the Decomposition of the $\beta$-Phase in the Copper-Aluminum System. *Trans.* AIME (1933) **104**, 69.

[3] D. J. Mack: The Isothermal Transformation of an Eutectoid Aluminum Bronze. *Trans.* AIME (1948) **175**, 240. *Met. Tech.* Sept. 1947. TP 2242.

[4] W. R. Hibbard, G. H. Eichelman, and W. P. Saunders: The Kappa Eutectoid Transformation in the Copper-Silicon System. *Trans.* AIME (1949) **180**, *Met. Tech.* Sept. 1948. TP 2441.

[5] C. S. Smith: The $\alpha$-Phase Boundary of the Copper-Silicon System. *Jnl.* Inst. of Metals (1928) **40**, No. 2, 359.

[6] G. Chaudron and H. Forester: Etude de la Decomposition due Protoxyde de fer. Anomalies de Dilitation Correlatues de son Instabilite. *Comptes Rend.* (1924) **178**, 2173.

[7] G. Wasserman: Umwandlungen in Eutectoid Legierungen. *Ztsch. f. Metallkunde* (1934) **26**, 256.

[8] O. Eisenhut and E. Kaupp: Das System Eisen Stickstoff. *Ztsch. f. Electrochemie* (1930) **36**, 392.

[9] E. Lehrer: Magnetische Untersuchungen über das System Eisen Stickstoff. *Ztsch. f. Electrochemie* (1930) **36**, 460.

[10] A. Osawa and S. Iwaizumi: X-Ray Investigation of Iron and Nitrogen Alloys. *Ztsch. f. Kristallog.* (1928) **69**, 26.

[11] G. Hägg: X-Ray Studies on the Nitrides of Iron. *Nature* (1928) **121**, 826; *Ztsch. f. Phys. Chem.* (1930) **8**, 455.

[12] A. Fry: Stickstoff in Eisen, Stahl und Sonderstahl. *Stahl u. Eisen* (1923) **43**, 1271; *Kruppsche Monatshefte* (1923) **4**, 138.

[13] F. C. Hull and R. F. Mehl: The Structure of Pearlite. *Trans.* A.S.M. (1942) **30**, 381.

[14] F. C. Hull, R. A. Colton, and R. F. Mehl: Rate of Nucleation and Rate of Growth of Pearlite. *Trans.* AIME (1942) **150**, 185.

[15] D. L. Martin and F. E. Wiley: Induction Hardening of Plain Carbon Steels. *Trans.* A.S.M. (1945) **34**, 351.

[16] V. E. Lysaght: Microhardness Testing of Materials. *Materials and Methods* (Oct. 1945) **22**, 1079.

[17] A. B. Greninger and A. R. Troiano: Kinetics of the Austenite to Martensite Transformation in Steel. *Trans.* A.S.M. (1940) **28**, 537.

[18] M. Cohen: Retained Austenite. *Trans.* A.S.M. (1949) **41**, 35.

[19] K. H. Jack: Binary and Ternary Interstitial Alloys. Paper presented at the International Union of Crystallography, Boston (July, 1948).

[20] E. P. Klier and S. M. Grymko: The Transformation in $\beta$-Cu Al Alloys. *Trans.* AIME (1949) **185**, 611. *Jnl. of Metals*, Sept. 1949.

[21] V. G. Paranjpe, M. Cohen, M. B. Bever, and C. F. Floe: The Iron-Nitrogen System. *Trans.* AIME (1950) **188**. *Jnl. of Metals*, Feb. 1950. TP 2794.

# The Effect of Carbon

# on the Activity of Sulphur in Liquid Iron

## by J. P. Morris and R. C. Buehl

A study has been made of the equilibrium conditions in the reaction between hydrogen gas and dilute solutions of sulphur in liquid iron-carbon alloys. The equation for the reaction may be written as follows:

$$S \text{ (in liquid Fe-C alloy)} + H_2 \text{ (gas)} = H_2S \text{ (gas)}.$$

The carbon content of the metal has a decided influence on the equilibrium conditions. At constant temperature and constant $H_2S$ concentration in the gas phase, the sulphur content of the metal at equilibrium decreased as the carbon content was increased. At 1600°C and with 2.3 pct carbon in the metal, the activity coefficient of sulphur was twice that for sulphur dissolved in pure iron; and at carbon saturation it was more than six times as great.

The effect of temperature on the reaction is small. At 4.35 pct carbon, the relation between the equilibrium constant and temperature may be expressed as follows:

$$\log K = \frac{-450}{T} - 1.74.$$

ACTIVITY values for sulphur dissolved in liquid iron and slags as functions of composition and temperature are needed in applying thermodynamics to sulphur-control problems in iron- and steel-making. The purpose of this investigation was to determine the effect of carbon on the activity of sulphur in the metal phase. The method employed was the same as that used in an earlier investigation[1] concerning the effect of silicon on sulphur activity in liquid iron. A study was made of the conditions of equilibrium in the reaction between hydrogen gas and sulphur dissolved in iron-carbon alloys. The chemical equation for this reaction can be written as follows:

$$S \text{ (in liquid Fe-C alloy)} + H_2 \text{ (gas)} = H_2S \text{ (gas)}.$$
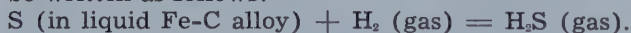
It was found that the activity coefficient of sulphur in liquid iron increases as the carbon content increases. At 2.3 pct carbon and 1600°C, the activity coefficient of sulphur is twice its value in carbon-free iron, and at carbon saturation it is more than six times as great. The effect of temperature on sulphur activity was found to be small.

Previous work on the reaction between hydrogen gas and sulphur dissolved in liquid iron has been reported by several investigators[2,3,4] but only recently have studies been made of the effect of alloying elements. Silicon[1] is known to have a pronounced influence on the activity of sulphur in iron, its effect being similar to that shown by carbon as described in the present report. Kitchener, Bockris, and Liberman[5] recently have published a preliminary report of their work on the effect of carbon on sulphur activity in iron. Their experiments were made at 1570°C and carbon saturation in the melt. Under these conditions they found that the activity coefficient of sulphur was approximately doubled by the presence of carbon. This is a much smaller effect than that found in the present work.

**Experimental Method:** The apparatus and procedure were essentially the same as those used in the earlier investigation of the effect of silicon on sulphur activity.[1] Briefly, the method was as follows: A molten iron-carbon alloy was brought to equilibrium at constant temperature with a mixture of $H_2$ and $H_2S$ of constant composition by bubbling the gas through the metal. Samples of the melt were

*J. P. MORRIS is Associate Chemist, Minerals Division, Metallurgical Branch, and R. C. BUEHL, Member AIME, is Supervising Engineer, Minerals Division, Metallurgy of Steel Section, Bureau of Mines, Pittsburgh, Pa.*
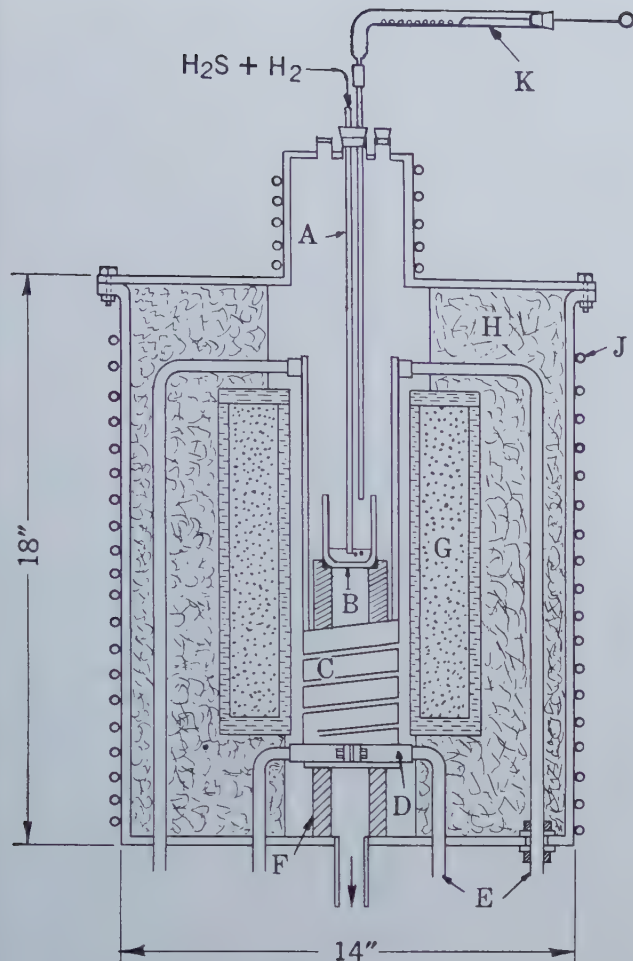
**Fig. 1—Furnace arrangement.**

A—gas bubbling tube. B—crucible and melt. C—spiral graphite heating element. D—water-cooled copper contact clamp. E—water-cooled electrical leads. F—graphite support for crucible. G—insulating jacket (graphite filled with lamp black). H—insulating brick. J—cooling coil for steel shell. K—pusher device for adding graphite pellets to melt.

taken for analysis periodically during the test. Equilibrium was assumed to have been attained when the sulphur content of the liquid metal reached constant value. Thermal diffusion in the gas mixture was eliminated by conducting the gas at high velocity directly into the metal through a small bore alumina tube.

For making the melts, an Arsem-type carbon-resistor furnace was used. The arrangement within the furnace is shown in fig. 1. Temperature control was manual; but because of the high heat loss to the water-cooled contacts in comparison to the loss through the refractories, the furnace reached a steady state rapidly, and a constant temperature could be maintained easily by occasional adjustment of a rheostat. Temperature measurements were made with a disappearing-filament-type optical pyrometer. Consistent optical readings were obtained by sighting on the bubble tube at the point of immersion in the metal. The emissivity correction was determined by making simultaneous measurements with the optical pyrometer and with a platinum-platinum rhodium thermocouple immersed in the metal and protected by a sintered alumina sheath. Temperature measurements are believed to be accurate within ±10°C.

The gas bubbling tube shown at A in fig. 1 was

made of high-purity alumina sintered to a dense, translucent structure and was impervious to gas. It was 24 in. long and 0.33 in. od, and had a 0.10-in. bore. Alumina tubes were used for bubbling in all experiments except E-93. In this test, run at 1800°C, a graphite tube was used because of excessive reduction of aluminum into the melt at this temperature.

Crucibles were of two types: graphite crucibles for melts to be saturated with carbon, and sintered-alumina crucibles for melts of lower carbon content. Both were made of high-purity materials. The crucibles were 1.75 in. od, 1.50 in. id, and 2.50 in. high.

The gas mixtures were prepared as used by introducing a stream of hydrogen sulphide into a jet of hydrogen in a special mixing bulb.[1] Each gas was metered separately before mixing, using capillary-type flowmeters with butyl phthalate manometers. The rate of hydrogen flow was approximately 1050 ml per min in each test. The flow was controlled by means of a pressure regulator on the cylinder and a manually operated needle valve mounted beside the flowmeter. Precise control of the hydrogen sulphide flow was more difficult than that of the hydrogen because of the very small rate, but was accomplished satisfactorily by means of a needle valve supplied by a cylinder filled with hydrogen sulphide to a pressure of 5 to 15 lb. The two flowmeters were used only to keep the rates of flow constant, the actual ratio of $H_2S$ to $H_2$ being determined in each experiment by analysis.

In carrying out an experiment a charge of 50 to 70 g of electrolytic iron and enough high-purity graphite to give the desired carbon content were melted and brought to the operating temperature with the hydrogen flowing. When using a graphite crucible, electrolytic iron saturated with carbon was used for the charge to prevent excessive attack on the crucible. Next, the $H_2S$ flow was started; the tip of the gas-bubbling tube was immersed in the liquid metal and enough FeS was added to the melt to bring the sulphur content near to the expected equilibrium value. The latter step was necessary in most experiments to shorten the time needed for attaining equilibrium. An experiment usually lasted 6 to 7 hr, equilibrium being attained in the first 3 hr in most tests. Samples of the liquid metal for analysis were taken at intervals of about 1 hr.

Metal samples were obtained by applying suction to a refractory tube or steel tube dipped momentarily into the melt. Four-hole refractory thermocouple tubing has been very satisfactory for this purpose. In practice, a 3-in. length of the refractory tube was cemented to a 2-ft length of steel tubing. With high-carbon melts, steel sampling tubes were used successfully. These tubes were made by drilling one or more holes lengthwise through a 2.5-in. length of 3/8-in.-diam steel rod. The holes were 3/32 to 1/8 in. in diam at the lower end and tapered to facilitate removal of the sample. To prevent sticking, the tubes were given a light wash with fine alumina powder suspended in alcohol.

**Loss of Carbon:** In experiments run in alumina crucibles, carbon in the melt reacted with the crucible, causing a drop in carbon content and contamination of the melt by aluminum. An attempt to

offset the loss of carbon by adding a small amount of methane to the gas mixture was unsuccessful because the methane attacked the bubble tube, causing it to disintegrate.

The problem of loss of carbon was solved by adding graphite to the melt at short, regular intervals. The additions were made without opening the furnace by using the device shown at $K$ in fig. 1. The horizontal tube was charged with a weighed quantity of graphite pellets of uniform size, and one or more of these were pushed at intervals into the vertical tube leading into the crucible. The rate of addition needed was determined by experiment, the loss of carbon being greater the higher the temperature and the higher the carbon content of the melt. By this procedure, the carbon content of the melt could be maintained constant within 0.10 pct carbon for the duration of an experiment.

The extent of aluminum contamination in the melts is shown in table I. When a graphite crucible was used, the aluminum pickup resulted from reaction with the bubble tube and sampling tubes. Contamination of the melts by silicon ranged from 0.01 to 0.09 pct.

**Methods of Analysis:** Metal samples were analyzed for sulphur and carbon by standard gravimetric procedures. Whenever possible, an entire sample from one hole of a sampling tube was used for an analysis to eliminate errors due to segregation.

Gas samples were taken in a cylindrical bulb of 1,839 ml capacity placed in the gas line between the mixing unit and the furnace. The analysis was made by displacing the gas in the bulb with nitrogen, absorbing the hydrogen sulphide in ammoniacal hydrogen peroxide, and precipitating the sulphur as barium sulphate.

Gas compositions are expressed as the ratio of the partial pressure of $H_2S$ to the partial pressure of $H_2$. At high temperatures, this ratio very nearly equals the molar ratio. A correction has been made for the dissociation of $H_2S$ into $H_2$, $S_2$ (gas), and S (gas). No correction was made, however, for the reaction between the gas mixture and carbon in the melt to form gases such as $CH_4$, $C_2H_2$, and $CS_2$.

Calculations show that the formation of $CH_4$ and $C_2H_2$ would have a negligible effect on the $H_2S : H_2$ ratio in the gas mixture. The effect of $CS_2$ formation is greater, but still small at the temperatures and $H_2S$ concentrations used in most of the experiments. The majority of the tests were run at 1600°C or below and at an $H_2S : H_2$ ratio in the neighborhood of 0.00255.

At this gas composition and with a melt saturated with carbon, the formation of $CS_2$ at 1600°C would lower the $H_2S : H_2$ ratio by about 3 pct, assuming that equilibrium in regard to $CS_2$ were attained. This represents the maximum error for this temperature and gas composition, since, at a lower concentration of carbon in the metal, less $CS_2$ would be formed. For the same $H_2S : H_2$ ratio, the maximum errors at 1200°, 1400°, and 1800°C are, respectively, 0.2, 1, and 8 pct. Data used in these calculations were from Basic Open Hearth Steel-making[6] and K. K. Kelley.[7] To calculate the extent of $CS_2$ formation for the melts not saturated with carbon, it would be necessary to know the activity coefficient of carbon at each concentration and temperature involved.

### Experimental Results

The experimental data are given in table I. Experiments were run at 1200°, 1415°, 1600°, and 1800°C and at $H_2S : H_2$ ratios ranging from 0.00242 to 0.00752. In column 6 the carbon contents shown are the actual values obtained by analysis. The values for metal saturated with carbon agree closely with published data on the solubility of carbon in iron.

The extent of aluminum contamination in the melts is shown in column 7. At 1200° and 1415°C, the aluminum pickup was small. This is in agreement with the observation that the rate of carbon loss was much less at these temperatures than at 1600°C. An experiment run at 1600°C with 2 pct aluminum in the melt, but no carbon, indicated that aluminum affects the activity of sulphur in iron in the same direction as carbon but to a much smaller degree. It is likely, therefore, that the equilibrium sulphur values obtained were somewhat too low in those tests in which the aluminum contents were high. Thus, in test E-63 with 2.33 pct aluminum in the metal, the sulphur content at equilibrium was 12 pct lower than in test E-73, which was run at the same carbon content but with only 0.30 pct aluminum in the metal. Test E-63, however, was the only experiment run at such a high aluminum content, and the effect of aluminum contamination in the other tests should be much smaller.

### Table I. Experimental Results

| Test No. | Crucible | Temp. °C | Time, hr | $\dfrac{H_2S}{H_2}$ x 10³ | Carbon, pct | Aluminum, pct | Initial sulphur, pct | Sulphur at equilibrium, pct |
|---|---|---|---|---|---|---|---|---|
| E-47 | Al₂O₃ | 1600 | 7.1 | 2.44 | 1.70 | | 0.75 | 0.59 |
| E-50 | Al₂O₃ | 1600 | 7.3 | 2.42 | 2.75 | 0.49 | 0.50 | 0.42 |
| E-52 | Al₂O₃ | 1600 | 7.1 | 2.43 | 0.01 | 0.14 | 0.95 | 0.97 |
| E-58 | Al₂O₃ | 1600 | 5.1 | 2.46 | 2.82 | 0.62 | 0.35 | 0.41 |
| E-59 | Al₂O₃ | 1600 | 5.7 | 2.49 | 0.98 | 0.42 | 0.60 | 0.73 |
| E-61 | Al₂O₃ | 1600 | 7.2 | 2.52 | 1.97 | 0.76 | 0.48 | 0.55 |
| E-62 | Al₂O₃ | 1600 | 4.1 | 2.55 | 3.84 | 0.78 | 0.28 | 0.29 |
| E-63 | Al₂O₃ | 1600 | 4.4 | 2.59 | 5.24 saturated* | 2.33 | 0.20 | 0.14 |
| E-73 | graph. | 1600 | 7.3 | 2.63 | 5.30 saturated | 0.30 | 0.00 | 0.16 |
| E-74 | Al₂O₃ | 1600 | 7.5 | 4.93 | 2.20 | | 0.95 | 1.10 |
| E-75 | Al₂O₃ | 1600 | 7.0 | 5.09 | 0.01 | 0.17 | 1.90 | 2.15 |
| E-76 | graph. | 1600 | 7.2 | 5.09 | 5.32 saturated | 0.37 | 0.00 | 0.31 |
| E-77 | Al₂O₃ | 1600 | 7.0 | 5.12 | 4.02 | | 0.45 | 0.57 |
| E-78 | graph. | 1600 | 4.7 | 7.52 | 5.30 saturated | 0.30 | 0.25 | 0.48 |
| E-65 | Al₂O₃ | 1415 | 6.8 | 2.62 | 4.17 | 0.16 | 0.38 | 0.29 |
| E-70 | Al₂O₃ | 1415 | 7.6 | 2.67 | 2.07 | | 0.42 | 0.64 |
| E-71 | graph. | 1415 | 7.2 | 2.64 | 4.83 saturated | 0.05 | 0.10 | 0.21 |
| E-68 | Al₂O₃ | 1210 | 7.0 | 2.65 | 4.10 | | 0.20 | 0.32 |
| E-91 | graph. | 1200 | 6.7 | 2.45 | 4.35 saturated | 0.02 | 0.14 | 0.27 |
| E-93 | graph. | 1800 | 6.0 | 2.51 | 5.90 saturated | 0.22 | 0.00 | 0.11 |

* Run in alumina crucible with excess of graphite floating on surface of melt.
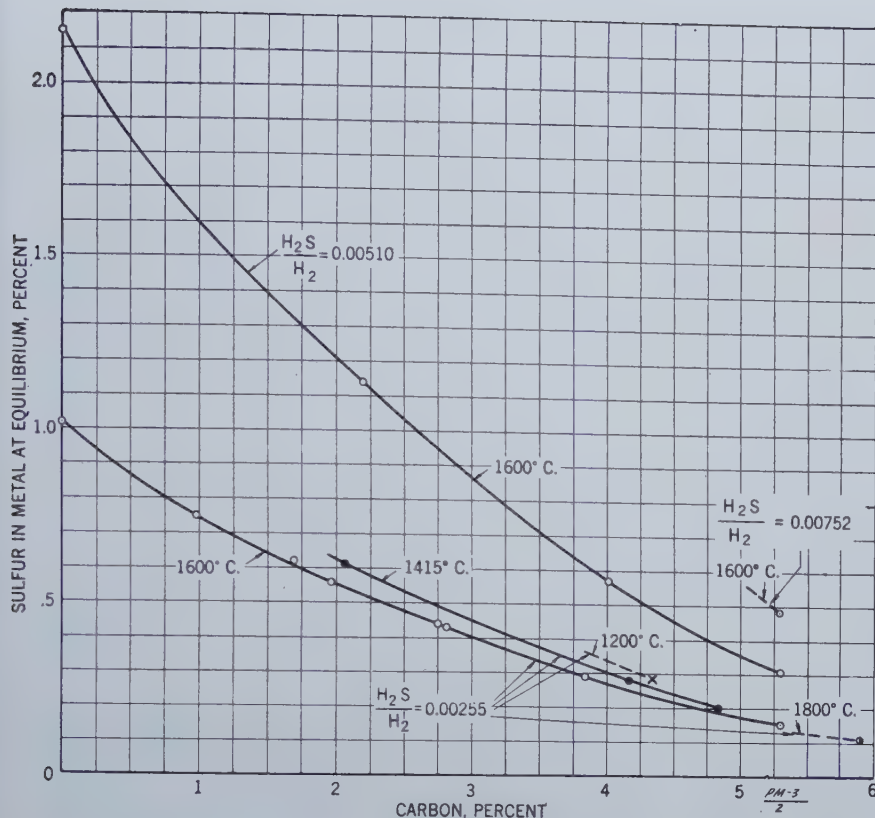
**Fig. 2—Variation in equilibrium sulphur content of metal with carbon content, temperature, and H₂S-H₂ ratio.**
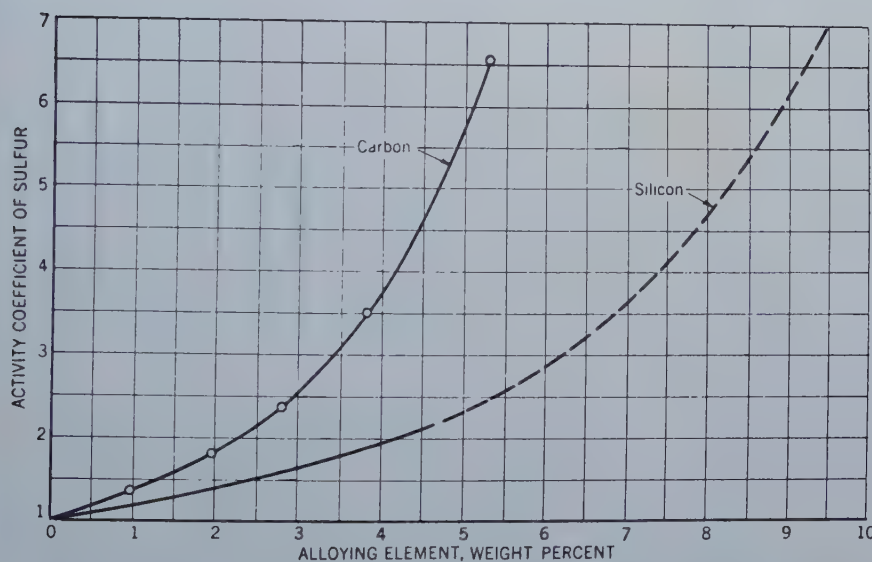


**Fig. 3—Effect of carbon content and silicon content on activity coefficient of sulphur in iron at 1600°C.**

Concentration expressed in weight percent.

melt was the same, regardless of the direction of approach.

In a number of the experiments, the initial and final sulphur concentrations were far enough apart to permit study of the reaction rates. Analysis of the data indicated that the rate of reaction was very rapid, and that virtually all of the H₂S available reacted with the melt; that is, at any given time the H₂S concentration of the outgoing gas was very near to equilibrium with the metal. Therefore, the rate of change of percent sulphur in a melt at any time depended only on the rate of H₂S input, weight of the melt, and distance to final equilibrium.

The experimental results are shown graphically in fig. 2 as a plot of the percentage of sulphur in the metal at equilibrium versus the carbon content for several gas compositions and temperatures. For the purpose of plotting, the results of tests run at H₂S : H₂ ratios between 0.00242 and 0.00267 have been recalculated to a basis of 0.00255 by assuming a linear relationship between H₂S concentration in the gas and sulphur content of the melt. Also, the results of test E-74 have been extrapolated to the higher gas ratio used in tests E-75, E-76 and E-77.

The curves in fig. 2 show that at constant gas composition and temperature, the sulphur content of the melt at equilibrium falls rapidly with increasing carbon content. The effect of temperature at a gas ratio of 0.00255 is shown by the lower group of curves. In the high-carbon range, the actual change in percentage of sulphur with change in temperature at a constant carbon content is small. Of more practical importance is the effect of temperature at carbon saturation. In this case the change in percentage of sulphur with change in temperature is greater because of the combined effect of temperature on sulphur activity and carbon solubility.

The relation between carbon content and activity coefficient of sulphur in dilute solutions of sulphur in iron at 1600°C is shown in fig. 3 and 4. The points on the curves were calculated from the results of experiments E-52, E-58, E-59, E-61, E-62, and E-73,

The last two columns in the table give the initial and equilibrium sulphur contents of the melts and show the direction of approach to equilibrium. In the paper on the effect of silicon on sulphur activity[1] it was shown that the final sulphur content of the
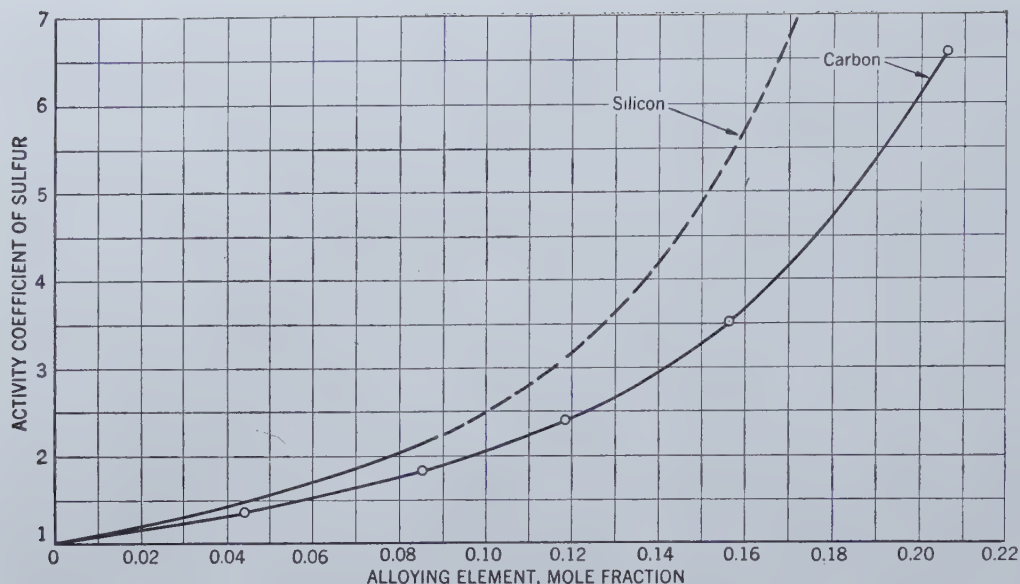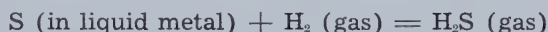
**Fig. 4—Effect of carbon content and silicon content on activity coefficient of sulphur in iron at 1600°C.**
Concentration expressed in mol fraction.

using the following relations:

$$\text{S (in liquid metal)} + \text{H}_2 \text{ (gas)} = \text{H}_2\text{S (gas)}$$

$$K = \frac{p_{\text{H}_2\text{S}}}{p_{\text{H}_2} \times a_s}$$

and $a_s = \gamma_s \times$ pct S,

where $a_s$ and $\gamma_s$ are the activity and activity coefficient of sulphur, respectively. The standard reference state for sulphur was taken to be a 1 pct solution of sulphur in pure iron, making $K$ equal to 0.00251, according to the results of test E-52. This value for $K$ agrees closely with that found in the earlier work on the effect of silicon[1] and also checks well with the results of a recent investigation by Sherman, Elvander, and Chipman[8], who used a technique quite different from that used in our work.

The values for $\gamma_s$ calculated in this manner apply only to dilute solutions of sulphur where the activity coefficient is approximately constant. In both pure iron and iron-carbon alloys, $\gamma_s$ tends to decrease as the sulphur content increases. In pure iron this decrease becomes appreciable above 1 pct sulphur.[1] In iron saturated with carbon, the results of experiments E-73, E-76, and E-78 shown in fig. 6 indicate that $\gamma_s$ is approximately constant up to 0.48 pct sulphur, which is the highest concentration studied.

For comparison with the effect of silicon, the relation between silicon content and activity coefficient of sulphur[1] is also shown in fig. 3 and 4. On a weight percent basis, carbon has a much greater effect than silicon. However, when the concentration of alloying element is expressed in mol fraction, the effect of silicon is greater than that of carbon.

One experiment of an exploratory nature was run at 1600°C to determine the effect of carbon and silicon when present together in the melt. In this test the addition of 1.40 pct silicon to a melt containing 4.0 pct carbon increased the activity co-

efficient of sulphur from 3.75 to 5.08. This increase is about the same as would have resulted from adding 1.4 pct silicon to an iron-silicon melt in which $\gamma_s$ was initially 3.75, that is, adding 1.4 pct silicon to iron containing 7.15 pct silicon.

In fig. 5, a plot of log $K$ against $1/T$ is shown for the reaction:

$$\text{S (in liquid Fe containing 4.35 pct C)} + \text{H}_2 \text{ (gas)} = \text{H}_2\text{S (gas)}$$
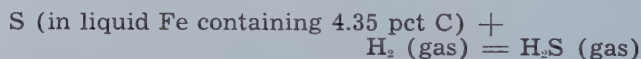
$$K = \frac{p_{\text{H}_2\text{S}}}{p_{\text{H}_2} \times \text{pct S}}$$

At 4.35 pct carbon in the metal, values of $K$ at three temperatures can be calculated from the data in fig. 2. In drawing the straight line through the points, more weight was given to the determinations at 1200° and 1415°C than at 1600°C because errors due to $CS_2$ formation and aluminum contamination are smaller at the lower temperatures. Corrections for these two errors should bring the point at 1600°C



**Fig. 5—Equilibrium between hydrogen, hydrogen sulphide, and sulphur dissolved in liquid iron containing 4.35 pct carbon.**

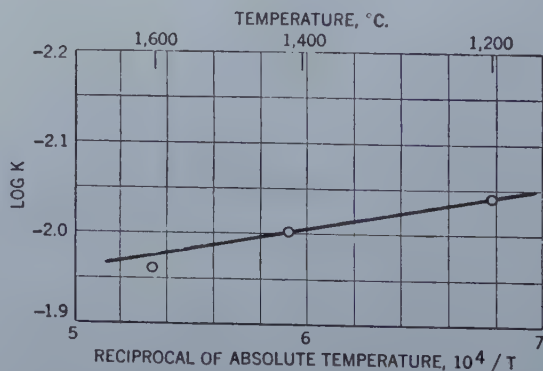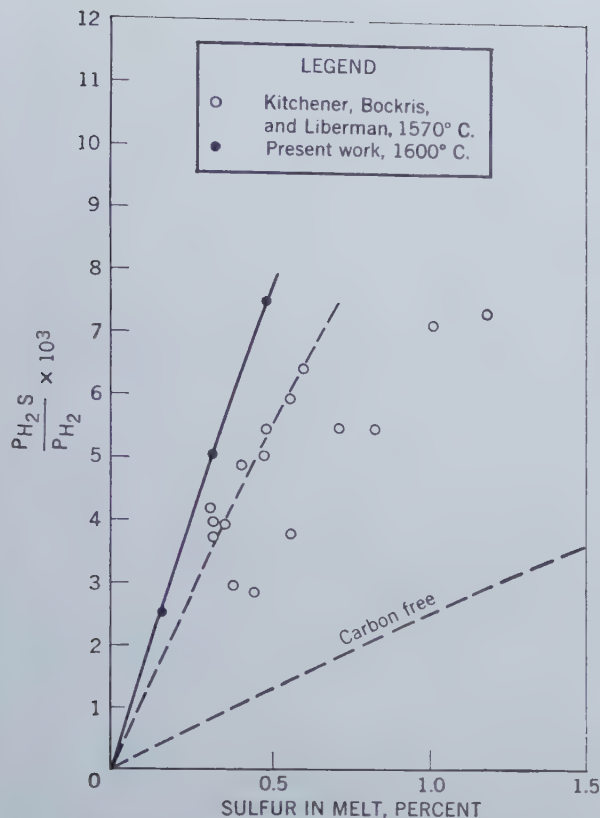**Fig. 6—Comparison of results of present work with those of Kitchener, Bockris, and Liberman for the activity of sulphur in iron saturated with carbon.**

*(Figure legend:)*
LEGEND
○ Kitchener, Bockris, and Liberman, 1570° C.
● Present work, 1600° C.

*(Figure axes:)* $\frac{P_{H_2S}}{P_{H_2}} \times 10^3$ (vertical); SULFUR IN MELT, PERCENT (horizontal); "Carbon free" line labeled.
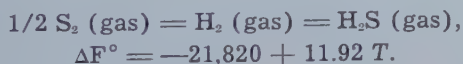
more into line with the other two. The straight line may be represented by the equation:

$$\log K = -\frac{450}{T} - 1.74$$

From this equation we obtain the free-energy change of the reaction:

$$\Delta F^\circ = 2,060 + 7.96\ T$$

The free energy of formation of $H_2S$ is given by the following equation[6]:

$$1/2\ S_2\ (gas) = H_2\ (gas) = H_2S\ (gas),$$
$$\Delta F^\circ = -21,820 + 11.92\ T.$$

Combining this free-energy equation with the previous one, we get the free energy of solution of sulphur in the liquid alloy:

$$1/2\ S_2\ (gas) = S\ (in\ liquid\ Fe\ containing\ 4.35\ pct\ C),$$
$$\Delta F^\circ = -23,880 + 3.96\ T.$$
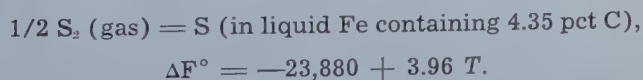
A comparison between the results of this investigation and those of Kitchener, Bockris, and Liberman[5] for the activity of sulphur in iron saturated with carbon is given in fig. 6. The experimental data for the present work were taken from tests E-73, E-76, and E-78. The wide spread in the results of Kitchener, Bockris, and Liberman indicates that some of their work was subject to large experimental errors. Their results seem to fall into two groups. The group of nine points at the left agrees better with the results of this investigation, but the

difference in the two curves is still rather large. The difference of 30°C in temperature between the two sets of data would account for only a small part of the discrepancy.

## Conclusions

The experimental data have shown that carbon has a decided influence on the activity of sulphur in dilute solutions of sulphur in liquid iron. At a given percentage of sulphur in the metal, the activity of sulphur is greater the higher the carbon content. Between zero carbon and carbon saturation the increase in sulphur activity is more than sixfold at 1600°C. This fact indicates that in slag-metal relationships and in other reactions involving sulphur in liquid iron, the alloy content of the metal is a very important factor. For example, the greater efficiency of desulphurization in the blast furnace as compared to that in the open hearth is due in considerable part to the higher level of sulphur activity in blast-furnace metal as a result of the higher carbon and silicon contents.

The activity of sulphur dissolved in a liquid iron-carbon alloy increases with a rise in temperature. The temperature effect is rather small, however, except at carbon saturation, where a rise in temperature is accompanied by an increase in the carbon content of the metal and by a rise in sulphur activity resulting from the carbon increase. This indirect effect of temperature on sulphur activity may be largely responsible for the relationship that exists in the blast furnace between temperature and sulphur content of the metal. With a rise in temperature, the carbon plus silicon content of the metal increases causing a corresponding increase in the activity coefficient of sulphur and a greater tendency for the sulphur to pass into the slag.

### References

[1] J. P. Morris and A. J. Williams, Jr.: The Effect of Silicon on the Activity of Sulphur in Liquid Iron. *Trans.* Amer. Soc. for Metals (1949) **41**, 1425-1439.

[2] John Chipman and Ta Li: Equilibrium in the Reaction of Hydrogen with Iron Sulphide in Liquid Iron and the Thermodynamics of Desulphurization. *Trans.* Amer. Soc. for Metals (1937) **25**, 435-465.

[3] E. Maurer, G. Hammer, and H. Möbius: The Equilibrium between Iron and Hydrogen Sulphide. *Archiv. Eisenhüttenwesen* (1942) **16**, 159-165.

[4] J. White and H. Skelly: The Determination of the Equilibrium Constant of the Reaction between Molten Iron and Hydrogen Sulphide. *Jnl.* Iron and Steel Inst. (1947) **155**, 201-212.

[5] J. A. Kitchener, J. O'M. Bockris, and A. Liberman: The Activity of Sulphur in Liquid Iron: The Influence of Carbon. Discussions of the Faraday Soc., No. 4, 1948.

[6] Basic Open Hearth Steelmaking. AIME, New York, 1944.

[7] K. K. Kelley: Contributions to the Data on Theoretical Metallurgy. U. S. Bur. of Mines, Bull. 406 (1937).

[8] Charles W. Sherman, Hans I. Elvander, and John Chipman: The Thermodynamic Properties of Sulphur in Molten Iron-Sulphur Alloys. *Trans.* AIME (1950) **188**, 334. *Jnl. of Metals*, Feb. 1950. TP 2773.

The Vapor Pressure and Thermodynamic Activities of

# Zinc in Solid Alpha Brasses

## by A. W. Herbenar, C. A. Siebert, and O. S. Duffendack

The vapor pressures of zinc over solid alpha brasses were determined for six alloys ranging in composition from approximately 5 to 30 pct zinc. The absorption spectra method was utilized for obtaining the vapor pressure data. Activities and activity coefficients are given for zinc for the six alloys investigated.

IN metallurgical problems involving the study of equilibrium in binary systems, the existence of an additional vapor phase, due to the presence of a volatile component in the alloy, has often been neglected. This is well indicated by the modified form of the phase rule, usually accepted in condensed systems in which pressure is not considered as a degree of freedom. In many cases the vapor pressure of the volatile component is exceedingly small and for all purposes can be considered negligible, in which case this form of the phase rule is applicable. However, alloys containing Hg, Cd, Zn, or Mg, tend to show very marked equilibrium vapor pressure, even in the solid state, and therefore present cases where the modified form of the phase rule no longer holds true.

A quantitative determination of the vapor pressure of zinc in alpha brasses is not only of practical interest because of the loss of zinc in the processing of these alloys, but also of theoretical interest in that such measurements provide a means of applying the principles of theoretical physics and physical chemistry to problems of applied metallurgy.

A number of investigators have reported vapor pressure measurements of zinc in alpha brasses. Hargreaves[1] made extensive measurements which were used by Birchenall and Mehl[2] and Guttman[3] for the determination of activity coefficients of zinc in alpha brasses. Hargreaves[1] used a differentially heated quartz tube and measured the condensation

A. W. HERBENAR is District Metallurgist, Ohio Crankshaft, Tocco Division. C. A. SIEBERT, Member AIME, is Professor of Metallurgical Engineering, University of Michigan. O. S. DUFFENDACK is Director of Research, North American Philips Corporation.

temperature at one end corresponding to the temperature of the heated brass at the other end.

Birchenall and Cheng outlined the condensation method of obtaining vapor pressure of zinc and Cd over some of their silver alloys.[4]

The primary object of the present investigation was to increase the range and accuracy of the vapor pressure data for the alpha brasses.

**Preparation of Alloys:** Six alloys were prepared from Bunkerhill zinc and O.F.H.C. copper, both of 99.99 pct purity. The cast ingots were annealed for 24 hr at 550°C, scalped, cold rolled 40 pct and annealed for 50 hr at 550°C. The annealed bars were then surface ground and degasified for 30 min at approximately 550°C in an induction heated vacuum furnace. The surface of the bars was removed before milling the bars into relatively fine chips for chemical analysis and samples for the equilibrium cell. The analyses of the six alloys are given in table I.

**Experimental Method:** The vapor pressure of zinc over the various alloys at a number of temperatures was determined from absorption spectra data. The spark source was produced by means of a high tension discharge between two electrodes of pure zinc. The design of the absorption vessel is shown in fig. 1. The vessel was constructed of transparent quartz which transmits the whole of the visible spectrum and the ultraviolet down to a wave length of 2000 Å. The thickness of the vapor space was set at 0.8 mm so as to permit a relatively wide range of measurements without altering the vapor space, and thereby necessitating recalibration of the vessel. The furnace used for heating the absorption vessel consisted of a split wound furnace as shown in fig. 2. The spectrograph used in obtaining the transmitted zinc spectra was a double prism type especially designed for a region of 2500-3500 Å. A step diaphragm used in conjunction with a tungsten filament provided the necessary intensity patterns required for calibration of the photographic plates.

Table I. Analyses of Alloys

| Alloy | Pct Cu | Pct Zn |
|---|---|---|
| A | 94.65 | 5.35 |
| B | 88.95 | 11.05 |
| C | 83.82 | 16.18 |
| D | 80.01 | 19.99 |
| E | 75.97 | 24.03 |
| F | 71.05 | 28.95 |

This pattern was photographed on each plate in addition to the zinc spectra. The line densities were measured with a Moll type microphotometer. Fig. 3 shows the experimental setup, where $A$ is the spark source, $B$ is the furnace with the absorption vessel enclosed, and $C$ is the spectrograph.

The absorption vessel was calibrated using pure zinc and the 3035 Å and 3076 Å resonance lines of the zinc spectrum. The 3035A line showed no tendency for absorption and was used as an internal standard. The vapor pressure data for liquid zinc were taken from Overstreet's spectroscopically determined free energy values for zinc vapor. The equation used for determining the vapor pressure of saturated zinc vapor at any desired temperature was:

$$\ln p = \frac{-15{,}540}{T} - 3.04 \log T - 0.138 \times 10^{-3} T + 29.38 \quad (p \text{ in mm}) \quad [1]$$

**Results:** The line density data for pure zinc, and the step bands corresponding to a given photographic plate are given in table II in terms of galvanometer deflections recorded by the microphotometer. The plate calibration was obtained by plotting the density of the step bands against the values 0., 1.40, 2.03, 3.38, and 5.21 corresponding to a logarithmic (base 1.5) variation of the steps on the calibrating diaphragm. The values of the logarithms of the relative intensities of the pairs of spectral lines were obtained by applying their measured densities to the calibration curve for any corresponding plate. The last column of table II shows these values as obtained from the calibration curve. The line intensity ratios, and vapor pressures calculated from the vapor pressure equation, for a given temperature are shown in table III.

The absorption law may be represented by the following equation:

$$-\log \frac{I_{3076}}{I_{3035}} = K \frac{p}{T} d$$

when $K$ = absorption coefficient
$p$ = pressure
$T$ = absolute temperature
$d$ = thickness of absorbing space

A plot of log intensity ratio vs. $\frac{p}{T}$ should result in a straight line relationship if Beer's absorption law is valid for this case. A plot of the data of table III as shown in fig. 4 demonstrates a linear relationship for the calibration curve.

The vapor pressure data for the solid alloys were obtained in much the same manner as were the calibration data. This consisted in photographing the spectrum at a series of temperatures for each alloy, measuring the density of the lines on a calibrated

## Table II. Line-Density Data for Zinc

| Plate | T°C | No. | $D_{3076}$ | $D_{3076}$ | $D_{3035}$ | $D_{3035}$ | log $\frac{I_{3076}}{I_{3035}}$ |
|---|---|---|---|---|---|---|---|
| 1 | 453 | 1 | 46.70 | 46.70 | 46.75 | 46.75 | 0.04 |
| 1 | 453 | 2 | 46.80 | 46.85 | 46.90 | 46.90 | 0.06 |
| 2 | 481 | 1 | 45.85 | 45.80 | 45.90 | 45.90 | 0.06 |
| 2 | 481 | 2 | 45.75 | 45.80 | 45.85 | 45.85 | 0.07 |
| 2 | 513 | 3 | 45.95 | 45.95 | 46.10 | 46.15 | 0.13 |
| 2 | 513 | 4 | 46.15 | 46.15 | 46.30 | 46.40 | 0.15 |
| 2 | 542 | 5 | 46.30 | 46.30 | 46.65 | 46.65 | 0.26 |
| 2 | 542 | 6 | 46.35 | 46.40 | 46.70 | 46.75 | 0.26 |
| 3 | 576 | 1 | 44.70 | 44.70 | 45.40 | 45.40 | 0.50 |
| 3 | 576 | 2 | 44.75 | 44.75 | 45.50 | 45.45 | 0.51 |
| 3 | 607 | 3 | 44.95 | 45.00 | 46.20 | 46.25 | 0.80 |
| 3 | 607 | 4 | 44.85 | 44.85 | 46.10 | 46.10 | 0.89 |
| 3 | 639 | 5 | 44.10 | 44.20 | 46.25 | 46.30 | 1.53 |
| 3 | 639 | 6 | 44.20 | 44.25 | 46.30 | 46.40 | 1.52 |
| 4 | 667 | 1 | 42.80 | 42.85 | 46.10 | 46.10 | 2.36 |
| 4 | 667 | 2 | 43.10 | 43.10 | 46.35 | 46.40 | 2.34 |
| 4 | 699 | 3 | | | 46.25 | 46.25 | |
| 4 | 699 | 4 | | | 46.30 | 46.30 | |
| 4 | 730 | 5 | | | 46.80 | 46.80 | |
| 4 | 730 | 6 | | | 46.75 | 46.75 | |
| 5 | 745 | 1 | | | 45.85 | 45.80 | |
| 5 | 745 | 2 | | | 45.70 | 45.70 | |
| 6 | 709 | 1 | | | 45.95 | 45.95 | |
| 6 | 709 | 2 | | | 46.10 | 46.10 | |
| 6 | 681 | 3 | 41.45 | 41.45 | 45.50 | 45.55 | 2.93 |
| 6 | 681 | 4 | 41.65 | 41.60 | 45.70 | 45.70 | 2.93 |
| 6 | 652 | 5 | 43.10 | 43.15 | 45.75 | 45.75 | 1.88 |
| 6 | 652 | 6 | 43.10 | 43.10 | 45.75 | 45.75 | 1.86 |
| 7 | 620 | 1 | 43.95 | 44.00 | 45.40 | 45.40 | 1.12 |
| 7 | 620 | 2 | 43.90 | 43.85 | 45.30 | 45.30 | 1.12 |
| 7 | 590 | 3 | 45.55 | 43.50 | 46.35 | 46.40 | 0.65 |
| 7 | 590 | 4 | 45.25 | 45.25 | 46.10 | 46.10 | 0.65 |
| 7 | 559 | 5 | 46.30 | 46.35 | 46.80 | 46.80 | 0.36 |
| 7 | 559 | 6 | 46.25 | 46.25 | 46.75 | 46.70 | 0.37 |
| 8 | 524 | 1 | 44.60 | 44.65 | 44.85 | 44.90 | 0.18 |
| 8 | 524 | 2 | 44.70 | 44.75 | 44.95 | 44.95 | 0.17 |
| 8 | 492 | 3 | 46.25 | 46.20 | 46.30 | 46.35 | 0.09 |
| 8 | 463 | 4 | 46.60 | 46.65 | 46.70 | 46.70 | 0.08 |
| 8 | 463 | 5 | 46.25 | 46.25 | 46.30 | 46.30 | 0.05 |
| 8 | 463 | 6 | 46.45 | 46.43 | 46.50 | 46.50 | 0.05 |
| 9 | 444 | 1 | 44.25 | 44.20 | 44.25 | 44.30 | 0.04 |
| 9 | 444 | 2 | 44.40 | 44.45 | 44.40 | 44.40 | 0.06 |

**Step Bands**

| | | | | | | |
|---|---|---|---|---|---|---|
| Plate 1 | 40.00 | 41.30 | 42.05 | 43.80 | 45.00 | 46.20 |
| Plate 2 | 39.90 | 41.20 | 42.05 | 43.85 | 45.05 | 46.30 |
| Plate 3 | 38.00 | 41.15 | 42.05 | 43.90 | 45.20 | 46.50 |
| Plate 4 | 39.80 | 41.20 | 42.05 | 43.95 | 45.20 | 46.50 |
| Plate 5 | 39.90 | 41.25 | 42.10 | 43.95 | 45.15 | 46.45 |
| Plate 6 | 39.80 | 41.15 | 41.90 | 43.75 | 45.00 | 46.30 |
| Plate 7 | 39.90 | 41.20 | 42.00 | 43.70 | 44.85 | 46.05 |
| Plate 8 | 39.90 | 41.90 | 41.95 | 43.75 | 44.95 | 46.20 |
| Plate 9 | 39.80 | 41.10 | 41.95 | 43.75 | 44.95 | 46.20 |

## Table III. Summarized Vapor Pressure Data for Liquid Zinc

| T°C | T°K | (av) log $\frac{I_{3076}}{I_{3035}}$ | ln $P_{mm}$ | $P_{mm}$ | $\frac{P_{mm}}{T°K}$ |
|---|---|---|---|---|---|
| 453 | 726 | 0.050 | —0.86 | 0.42 | 0.00058 |
| 481 | 754 | 0.065 | —0.13 | 0.88 | 0.00117 |
| 513 | 786 | 0.140 | 0.62 | 1.86 | 0.00237 |
| 542 | 815 | 0.260 | 1.26 | 3.53 | 0.00433 |
| 576 | 849 | 0.505 | 1.95 | 7.05 | 0.00831 |
| 607 | 880 | 0.895 | 2.55 | 12.80 | 0.01455 |
| 639 | 912 | 1.525 | 3.11 | 22.50 | 0.02468 |
| 667 | 940 | 2.350 | 3.58 | 35.90 | 0.03820 |
| 699 | 972 | | 4.09 | 60.00 | 0.06174 |
| 730 | 1003 | | 4.54 | 94.10 | 0.09372 |
| 745 | 1018 | | 4.76 | 117.00 | 0.11489 |
| 709 | 982 | | 4.37 | 79.50 | 0.08014 |
| 681 | 954 | 2.930 | 3.81 | 45.30 | 0.04747 |
| 652 | 925 | 1.870 | 3.34 | 28.25 | 0.03054 |
| 620 | 893 | 1.120 | 2.79 | 16.23 | 0.01820 |
| 590 | 863 | 0.650 | 2.23 | 9.30 | 0.01078 |
| 559 | 832 | 0.365 | 1.61 | 5.00 | 0.00602 |
| 524 | 797 | 0.175 | 0.87 | 2.39 | 0.00299 |
| 492 | 765 | 0.085 | 0.13 | 1.14 | 0.00149 |
| 463 | 736 | 0.050 | —0.60 | 0.55 | 0.00075 |
| 444 | 727 | 0.050 | —0.84 | 0.43 | 0.00058 |

Fig. 1—Transparent quartz absorption vessel.
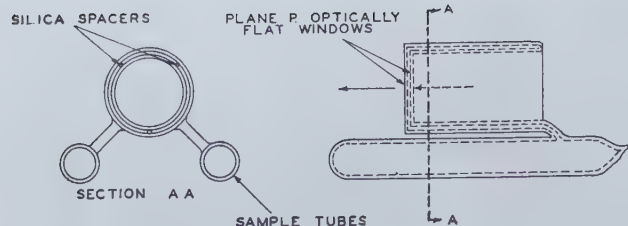


Fig. 2—Heating furnace.

plate, and finally obtaining the log intensity ratios from the calibration curve. Values of $p/T$ corresponding to the log intensity ratio at a definite temperature were obtained from the absorption curve. Since the temperature is known, the pressure which represents the equilibrium vapor pressure of zinc in the solid alloy can be calculated.

The summarized vapor pressure data for the six alloys investigated, including the log intensity ratios, values of $p/T$, and the calculated vapor pressures are given in tables IV through IX.

**Table IV. Summarized Vapor Pressure Data for Alloy A**
**(94.65 pct Cu 5.35 pct Zn)**

| $T°C$ | $T°K$ | (av) log $\frac{I_{3076}}{I_{3085}}$ | $\frac{1}{T°K}$ x $10^4$ | $\frac{P_{mm}}{T°K}$ | $P_{mm}$ | ln $P_{mm}$ |
|---|---|---|---|---|---|---|
| 815 | 1088 | 0.080 | 9.19 | 0.00145 | 1.58 | 0.46 |
| 858 | 1131 | 0.165 | 8.84 | 0.00280 | 3.17 | 1.15 |
| 902 | 1175 | 0.310 | 8.51 | 0.00515 | 6.05 | 1.80 |
| 952 | 1225 | 0.595 | 8.16 | 0.00965 | 11.83 | 2.47 |
| 970 | 1243 | 0.700 | 8.05 | 0.01140 | 14.16 | 2.65 |
| 928 | 1201 | 0.445 | 8.33 | 0.00725 | 8.70 | 2.16 |
| 878 | 1151 | 0.220 | 8.69 | 0.00370 | 4.26 | 1.45 |
| 823 | 1096 | 0.095 | 9.12 | 0.00165 | 1.81 | 0.59 |

**Table V. Summarized Vapor Pressure Data for Alloy B**
**(88.95 pct Cu 11.05 pct Zn)**

| $T°C$ | $T°K$ | (av) log $\frac{I_{3076}}{I_{3085}}$ | $\frac{1}{T°K}$ x $10^4$ | $\frac{P_{mm}}{T°K}$ | $P_{mm}$ | ln $P_{mm}$ |
|---|---|---|---|---|---|---|
| 759 | 1032 | 0.090 | 9.69 | 0.00160 | 1.65 | 0.50 |
| 796 | 1069 | 0.170 | 9.35 | 0.00285 | 3.05 | 1.12 |
| 844 | 1117 | 0.360 | 8.95 | 0.00595 | 6.65 | 1.89 |
| 889 | 1162 | 0.655 | 8.60 | 0.00105 | 12.44 | 2.54 |
| 925 | 1198 | 1.035 | 8.35 | 0.00170 | 20.12 | 3.00 |
| 950 | 1223 | 1.335 | 8.18 | 0.02165 | 26.47 | 3.28 |
| 894 | 1167 | 0.695 | 8.57 | 0.01130 | 13.19 | 2.58 |
| 865 | 1138 | 0.475 | 8.79 | 0.00780 | 8.87 | 2.18 |
| 822 | 1095 | 0.250 | 9.13 | 0.00415 | 4.55 | 1.51 |
| 786 | 1059 | 0.145 | 9.44 | 0.00245 | 2.60 | 0.96 |

**Table VI. Summarized Vapor Pressure Data for Alloy C**
**(83.82 pct Cu 16.18 pct Zn)**

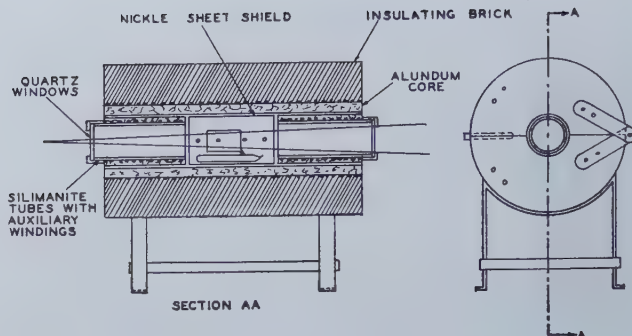| $T°C$ | $T°K$ | (av) log $\frac{I_{3076}}{I_{3085}}$ | $\frac{1}{T°K}$ x $10^4$ | $\frac{P_{mm}}{T°K}$ | $P_{mm}$ | ln $P_{mm}$ |
|---|---|---|---|---|---|---|
| 702 | 975 | 0.065 | 10.25 | 0.00120 | 1.17 | 0.16 |
| 748 | 1021 | 0.155 | 9.79 | 0.00260 | 2.66 | 0.98 |
| 789 | 1062 | 0.300 | 9.41 | 0.00500 | 5.31 | 1.67 |
| 830 | 1103 | 0.555 | 9.07 | 0.00905 | 9.98 | 2.30 |
| 878 | 1151 | 1.080 | 8.69 | 0.01750 | 20.14 | 3.00 |
| 922 | 1195 | 1.855 | 8.37 | 0.03025 | 36.14 | 3.56 |
| 943 | 1216 | 2.410 | 8.22 | 0.03910 | 47.51 | 3.86 |
| 909 | 1182 | 1.605 | 8.46 | 0.02595 | 30.67 | 3.42 |
| 859 | 1132 | 1.055 | 8.84 | 0.01720 | 15.20 | 2.72 |
| 802 | 1075 | 0.365 | 9.30 | 0.00605 | 6.51 | 1.87 |
| 759 | 1032 | 0.185 | 9.69 | 0.00316 | 3.20 | 1.16 |
| 714 | 987 | 0.085 | 10.13 | 0.00150 | 1.48 | 0.39 |

**Table VII. Summarized Vapor Pressure Data for Alloy D**
**(80.01 pct Cu 19.99 pct Zn)**

| $T°C$ | $T°K$ | (av) log $\frac{I_{3076}}{I_{3085}}$ | $\frac{1}{T°K}$ x $10^4$ | $\frac{P_{mm}}{T°K}$ | $P_{mm}$ | ln $P_{mm}$ |
|---|---|---|---|---|---|---|
| 703 | 976 | 0.100 | 10.24 | 0.00175 | 1.71 | 0.54 |
| 749 | 1022 | 0.235 | 9.78 | 0.00395 | 4.04 | 1.40 |
| 793 | 1066 | 0.455 | 9.38 | 0.00750 | 8.00 | 2.08 |
| 811 | 1084 | 0.600 | 9.22 | 0.00980 | 10.63 | 2.36 |
| 843 | 1116 | 0.950 | 8.96 | 0.01545 | 17.24 | 2.85 |
| 889 | 1162 | 1.690 | 8.60 | 0.02725 | 31.69 | 3.46 |
| 929 | 1202 | 2.800 | 8.32 | 0.04540 | 54.57 | 4.00 |
| 903 | 1176 | 2.045 | 8.50 | 0.03330 | 39.18 | 3.67 |
| 865 | 1138 | 1.265 | 8.79 | 0.02050 | 23.32 | 3.15 |
| 822 | 1095 | 0.705 | 9.13 | 0.01150 | 12.60 | 2.53 |
| 764 | 1037 | 0.290 | 9.69 | 0.00480 | 4.98 | 1.61 |
| 723 | 996 | 0.145 | 10.04 | 0.00245 | 2.44 | 0.89 |

**Table VIII. Summarized Vapor Pressure Data for Alloy E**
**(75.97 pct Cu 24.03 pct Zn)**

| $T°C$ | $T°K$ | (av) log $\frac{I_{3076}}{I_{3085}}$ | $\frac{1}{T°K}$ x $10^4$ | $\frac{P_{mm}}{T°K}$ | $P_{mm}$ | ln $P_{mm}$ |
|---|---|---|---|---|---|---|
| 646 | 919 | 0.110 | 10.37 | 0.00195 | 1.88 | 0.63 |
| 689 | 962 | 0.350 | 9.74 | 0.00575 | 5.90 | 1.78 |
| 753 | 1026 | 0.705 | 9.34 | 0.01155 | 12.37 | 2.51 |
| 797 | 1070 | 1.345 | 8.96 | 0.02185 | 24.39 | 3.19 |
| 843 | 1116 | 2.540 | 8.58 | 0.04120 | 48.00 | 3.87 |
| 933 | 1206 | 2.930 | 8.49 | 0.04750 | 55.95 | 4.02 |
| 904 | 1177 | 1.940 | 8.74 | 0.03165 | 36.21 | 3.59 |
| 871 | 1144 | 0.985 | 9.16 | 0.01600 | 17.47 | 2.86 |
| 819 | 1092 | 0.445 | 9.61 | 0.00730 | 7.60 | 2.03 |
| 767 | 1040 | 0.195 | 10.09 | 0.00325 | 3.22 | 1.17 |
| 718 | 991 | 0.070 | 10.56 | 0.00145 | 1.37 | 0.31 |

**Table IX. Summarized Vapor Pressure Data for Alloy F**
**(71.05 pct Cu 28.95 pct Zn)**

| $T°C$ | $T°K$ | (av) log $\frac{I_{3076}}{I_{3085}}$ | $\frac{1}{T°K}$ x $10^4$ | $\frac{P_{mm}}{T°K}$ | $P_{mm}$ | ln $P_{mm}$ |
|---|---|---|---|---|---|---|
| 642 | 915 | 0.070 | 10.93 | 0.00125 | 1.14 | 0.13 |
| 687 | 960 | 0.175 | 10.42 | 0.00295 | 2.83 | 1.04 |
| 714 | 987 | 0.320 | 10.13 | 0.00530 | 5.23 | 1.65 |
| 752 | 1025 | 0.535 | 9.75 | 0.00875 | 8.97 | 2.19 |
| 783 | 1056 | 0.855 | 9.47 | 0.01395 | 14.73 | 2.69 |
| 809 | 1082 | 1.265 | 9.24 | 0.02050 | 22.19 | 3.10 |
| 858 | 1131 | 2.440 | 8.84 | 0.03960 | 44.78 | 3.80 |
| 871 | 1144 | 2.915 | 8.74 | 0.04730 | 54.12 | 4.06 |
| 823 | 1096 | 1.555 | 9.13 | 0.02510 | 27.50 | 3.31 |
| 797 | 1070 | 1.080 | 9.34 | 0.01750 | 18.74 | 2.93 |
| 768 | 1041 | 0.685 | 9.61 | 0.01115 | 11.60 | 2.45 |
| 727 | 1000 | 0.350 | 10.00 | 0.00515 | 5.75 | 1.75 |
| 670 | 943 | 0.125 | 10.61 | 0.00215 | 2.03 | 0.71 |

**Fig. 3—Experimental setup.**
A—spark source.  B—furnace with absorption vessel enclosed.
C—spectrograph.

**Activities and Activity Coefficients:** The activities and activity coefficients for zinc in the six alloys studied are given in table X, employing pure liquid zinc as the reference state. These values differ somewhat from those shown by Birchenall and Mehl[2] due to a difference in vapor pressure values reported in this investigation and those of Hargreaves used by Birchenall and Mehl for their calculations.

## Summary

1. Data are presented of the vapor pressure of zinc over solid alpha brasses of six compositions.

2. The absorption spectra method was utilized for obtaining the vapor pressure data.

3. Activities and activity coefficients for zinc in alpha brasses were calculated for the six alloys investigated.

## References

[1] R. Hargreaves: Inst. of Metals (1939) **64**, 115.
[2] C. E. Birchenall and R. F. Mehl: *Trans.* AIME (1947) **171**, 143. *Metals Tech.*, June 1947.

[3] L. Guttman: *Trans.* AIME (1948) **175**, 178.
[4] C. E. Birchenall and C. H. Cheng: *Trans.* AIME (1949) **185**, 428. *Jnl. of Metals*, July, 1949.

### Table X. Activities and Activity Coefficients of Zinc in Alpha Brasses (with respect to Liquid Zinc)

| T°C | Alloy A | B | C | D | E | F |
|---|---|---|---|---|---|---|
| 650 | α<br>γ |  |  |  |  | 0.0417<br>0.1468 |
| 675 |  |  |  |  | 0.0311<br>0.1323 | 0.0511<br>0.1801 |
| 700 |  |  | 0.0167<br>0.1053 | 0.0227<br>0.1164 | 0.0356<br>0.1514 | 0.0538<br>0.1895 |
| 725 |  |  | 0.0179<br>0.1130 | 0.0263<br>0.1348 | 0.0395<br>0.1678 | 0.0584<br>0.2058 |
| 750 |  | 0.0119<br>0.1108 | 0.0198<br>0.1250 | 0.0299<br>0.1528 | 0.0425<br>0.1809 | 0.0642<br>0.2261 |
| 775 |  | 0.0121<br>0.1118 | 0.0227<br>0.1434 | 0.0332<br>0.1702 | 0.0468<br>0.1988 | 0.0697<br>0.2457 |
| 800 | 0.00431<br>0.0828 | 0.0131<br>0.1219 | 0.0251<br>0.1585 | 0.0349<br>0.1787 | 0.0502<br>0.2134 | 0.0761<br>0.2681 |
| 825 | 0.00539<br>0.1034 | 0.0144<br>0.1337 | 0.0272<br>0.1719 | 0.0393<br>0.2010 | 0.0552<br>0.2445 | 0.0828<br>0.2917 |
| 850 | 0.00633<br>0.1216 | 0.0160<br>0.1484 | 0.0291<br>0.1839 | 0.0422<br>0.2162 | 0.0583<br>0.2480 | 0.0889<br>0.3132 |
| 875 | 0.00695<br>0.1334 | 0.0175<br>0.1620 | 0.0324<br>0.2045 | 0.0447<br>0.2287 | 0.0641<br>0.2724 | 0.0958<br>0.3374 |
| 900 | 0.00762<br>0.1463 | 0.0188<br>0.1740 | 0.0353<br>0.2229 | 0.0490<br>0.2510 | 0.0686<br>0.2918 |  |
| 925 | 0.00854<br>0.1639 | 0.0202<br>0.1876 | 0.0386<br>0.2437 | 0.0525<br>0.2687 |  |  |
| 950 | 0.00930<br>0.1784 | 0.0214<br>0.1987 |  |  |  |  |
| 970 | 0.00955<br>0.1833 |  |  |  |  |  |
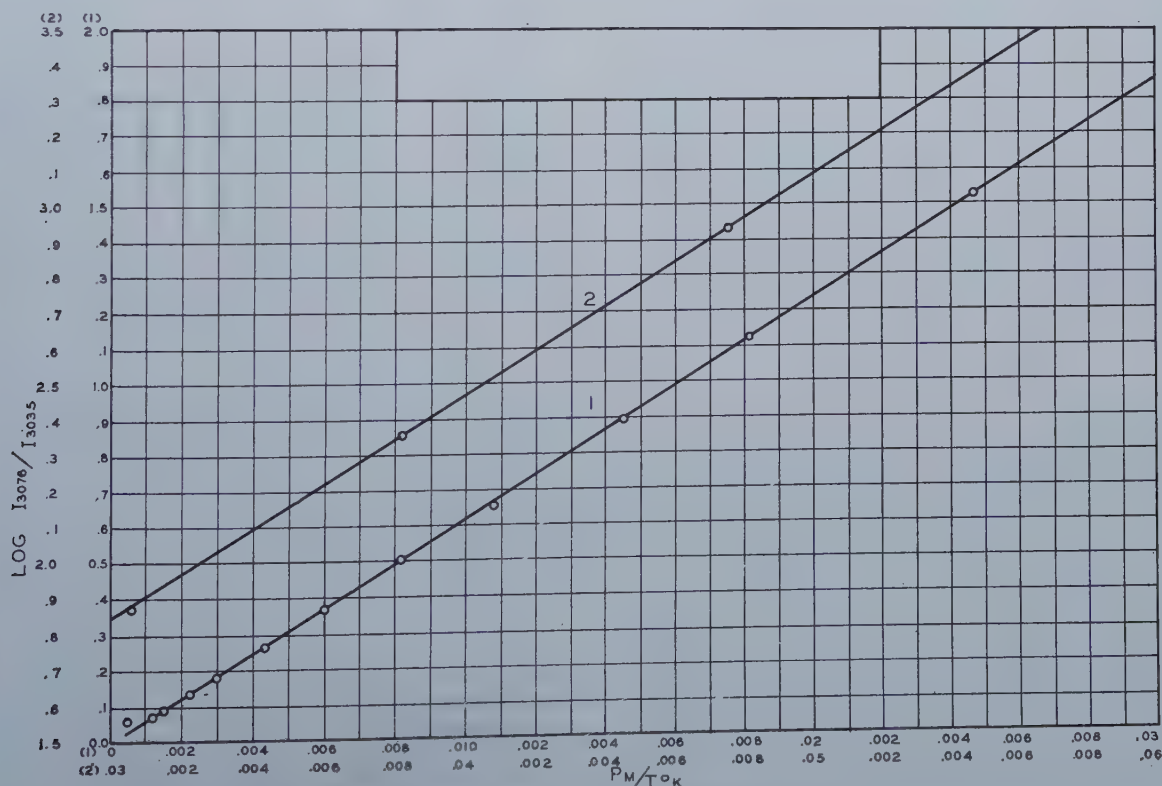


**Fig. 4—Calibration curve for absorption vessel.**

# The Thermoelastic Effect

## in Iron and Nickel as a Function of Temperature

●

## by Roberto Rocca and M. B. Bever

The adiabatic thermoelastic temperature change was determined as a function of temperature and stress in nickel and Armco iron. The results are in agreement with an equation first derived by Lord Kelvin. Near the Curie temperature the thermoelastic effect changes appreciably. Calculations confirm that the thermal expansion coefficient of iron decreases in the vicinity of the Curie temperature as predicted by the theory of ferromagnetism.

THE adiabatic elastic deformation of a body is accompanied by a change in temperature. This phenomenon is known as the thermoelastic effect. Under adiabatic conditions the temperature of a metal bar is decreased by an elastic elongation and is increased by an elastic compression. All materials which elongate on heating behave in this manner. The sign of the thermoelastic temperature change is reversed for the few materials which have a negative coefficient of thermal expansion.

The following equation for the thermoelastic effect can be derived from fundamental thermodynamic theorems, as shown in the Appendix:

$$dT_s = - \frac{\alpha_l}{c_\sigma{}'} \; T \; d\sigma_s \qquad [1]$$

In this equation, $T$ is the absolute temperature, $S$ is the entropy, $\alpha_l$ is the coefficient of linear thermal expansion, $c_\sigma{}'$ is the heat capacity per unit volume at constant stress and $\sigma$ is the stress (positive in tension). Eq 1 can be applied to small, but finite changes in stress in the following form:

$$\Delta T_s = - \frac{\alpha_l}{c_\sigma{}'} \; T \; \Delta\sigma_s \qquad [2]$$

The sign of the temperature change $\Delta T$ is opposite to that of the change in stress $\Delta\sigma$ for materials which have a positive coefficient of thermal expansion.

Eq 2 has been verified for many different materials and stresses at room temperature. No previous publication appears to have been devoted to an investigation of the thermoelastic effect over a range of temperatures.

## Review of Literature

Lord Kelvin (W. Thomson) presented a general theory of the thermoelastic effect in 1851[1] and later applied it to a solid, subject to an arbitrary system of stresses[2]. His analysis was based on a cycle of isothermal and constant-strain transformations and led to Eq 2 above. Even today, one of the clearest expositions of the thermoelastic effect is found in Lord Kelvin's article on elasticity in the Ninth Edition of the Encyclopedia Britannica (1878).

Gibbs[3] analyzed the general equilibrium conditions for strained elastic solids. His treatment emphasized the role of energy and entropy in thermoelastic phenomena.

Even before the development of the theory, Weber[4] (1830) observed the thermoelastic effect in solids. He noted that a change in the stress applied

to a wire was followed by a transitory period during which the vibrational frequency of the wire differed from the frequency characteristic of the new stress. Weber reasoned that the transient change in acoustical pitch was produced by a thermal effect. He attempted to calculate the magnitude of this effect from the observed changes in vibrational frequency.

Lord Kelvin's formula was first verified by Joule[5, 6] (1857-59) who employed a variety of materials, including iron, wood and rubber. Joule used various thermocouples, but did not establish the correlation between galvanometer deflections and temperature changes with absolute accuracy. The deviation of the observed from the calculated values of the thermoelastic effect was ±8 pct.

Edlund[7] (1861) experimented with wires of various metals, employing crystals of antimony and bismuth as a thermocouple, but only correlated galvanometer deflections with changes in load. Apparently unaware of Lord Kelvin's papers, Edlund based the analysis of his results on Clausius' principle of the equivalence of heat and work. In 1865 Edlund[8] published further experiments in an attempt to confirm Lord Kelvin's formula, but the observed temperature changes amounted to about half of the theoretical values. Edlund considered that the balance was accounted for by "internal work". Various attempts by others[9, 10, 11] to explain this discrepancy were unsuccessful.

Haga[12] (1882) measured the coefficient of thermal expansion and the heat capacities of the materials used in his thermoelastic experiments. The difference between observed and calculated values amounted to about 2.5 pct for steel and 0.25 pct for nickel-silver wire.

Wassmuth[13, 15] (1888 and later) attached six thermocouples connected in series to six equally loaded samples in order to obtain increased sensitivity. He also measured the thermoelastic effect in torsion or bending[14, 16] and determined the temperature dependence of Young's modulus and of the torsional modulus by thermoelastic measurements[17, 18].

Turner[19] (1902) attempted to use the thermoelastic effect for the determination of stresses in large-scale elements of engineering structures. He showed that this effect can serve as a criterion for limiting the elastic range. Coker[20] and Coker and McKergow[21] (1904) explored the applicability of the thermoelastic effect to engineering measurements and to the determination of the yield point. Coker[20] analyzed the distribution of stresses in the cross-section of a loaded beam in this manner. Rasch[22] (1908) used the thermoelastic effect with fair success to determine the yield point of metals.

Compton and Webster[23] (1915) devised a temperature-measuring system many times more sensitive than a thermocouple by determining the change in electrical resistance of a wire specimen. Their investigation verified Lord Kelvin's formula with an average accuracy of 0.07 pct.

In recent years the study of the thermoelastic effect has been confined mainly to rubber. In the field of metals, Tammann and Warrentrup[24] (1937) thoroughly investigated the temperature changes associated with elastic and plastic deformation. They observed that in low-carbon steels Lord Kelvin's formula was followed up to the yield point, where a sharp reversal in the direction of the temperature change indicated the occurrence of plastic deformation. For unannealed copper and nickel the reversal was more gradual, so that no yield point could be assigned to them.

The thermoelastic effect is now recognized as an important factor in the phenomenon of internal friction in polycrystalline materials. The pertinent theory was developed by Zener[25]. Temperature changes have been observed during loading of specimens in high-temperature creep tests[26].

### Experimental Procedure

The apparatus used in the experiments reported here is shown schematically in fig. 1. The specimen S was a tensile test specimen measuring between grips 1 in. (nickel) or 1½ in. (iron); the diameter was 0.250 in. (nickel) or 0.245 in. (iron). The specimen was fastened to the frame F through the rod R and its upper end was connected to a lever BC by means of which various loads could be applied. The connection AB between the specimen and the lever was made by a system of links, details of which are included in fig. 1. These links, together with the fact that the distance AB from the specimen to the lever was 2½ ft, permitted the specimen to align itself so that the state of stress approached pure tension. The lever had its fulcrum
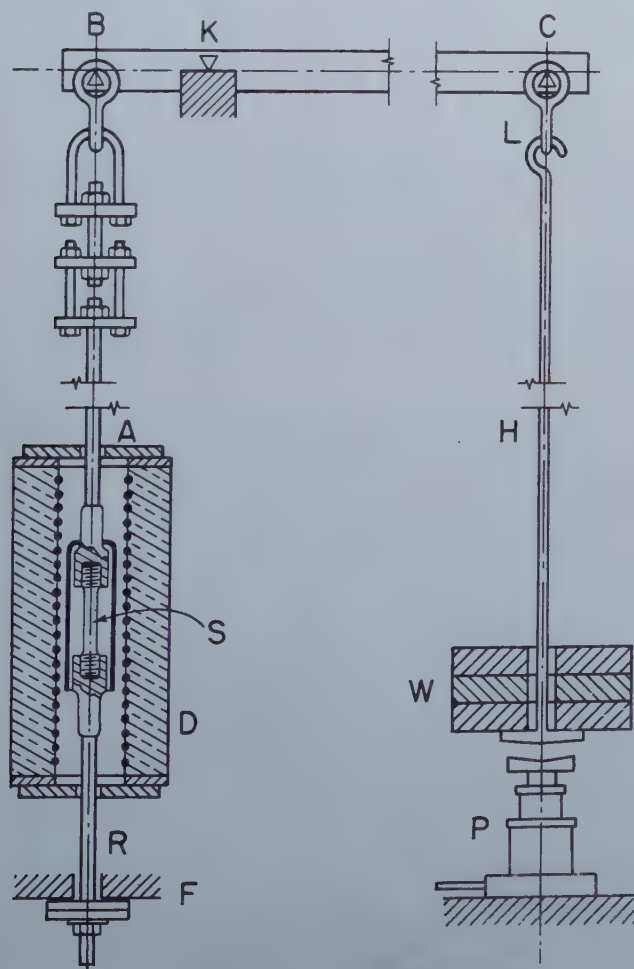


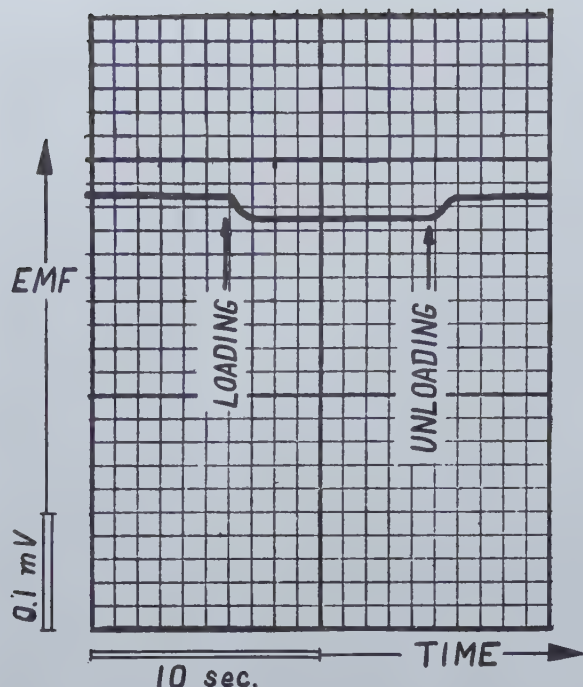**Fig. 1—Schematic diagram of apparatus.**

Fig. 2—Typical record of loading and unloading cycle.

at the knife edge $K$, resulting in a lever ratio of ten to one.

The load consisting of the hanger $H$ and the weights $W$ could be raised or lowered by means of a hydraulically operated platform $P$, whereby the hanger was engaged and disengaged at the point $L$. The center of gravity of the connecting system $AB$ and lever $BC$ was to the right of the knife-edge $K$. The specimen was under slight tension even when the load was not applied.

The specimen, surrounded by a sleeve of temperature-resistant metal was enclosed in a resistance furnace $D$. A thermocouple was placed inside the sleeve and was connected to an automatic temperature regulator. The specimen temperature was measured by a second thermocouple made by spot welding two thermocouple wires to a circumference of the specimen at an angular separation of approximately 90°. The electromotive force was recorded by a Leeds & Northrup Speedomax recording potentiometer. This instrument had a full scale of 2 mv and a potentiometer was put in series with it to measure higher electromotive forces. A chromel P-constantan thermocouple was used because it gave the largest electromotive force of any of the generally available couples. The thermocouple was calibrated at four temperatures in the range of 100-660°C.

The specimen was brought to a desired temperature level for each set of determinations. The power input was then adjusted to result in a very slow temperature decrease amounting to less than 1°C per min. This slight temperature drift standardized the thermal conditions and particularly the temperature gradient existing between furnace and specimen. It also eliminated any mechanical slack in the recording instrument which would have interfered with the accurate measurement of the temperature

decrease caused by loading. All temperature levels were chosen so that they would be read in the same part of the scale, in order to keep as constant as possible inaccuracies inherent in the instrument.

The technique of loading and unloading was standardized and each of these operations required less than 2 sec. The hydraulic platform, however, was manipulated so as to avoid impact or appreciable kinetic effects. The load was removed again after about 10 sec. An example of a typical record is shown in fig. 2. At each temperature level three cycles of loading and unloading were completed at intervals of less than 20 sec. It was possible to make three sets of measurements with different loads during such a short time that the temperature level changed by less than 2°C.

The potentiometer records were measured on a reading instrument originally designed for X ray diffraction films. Its vernier scale could be read to 0.02 mm. The readings were always made on the same edge of the recorded line and the probable positioning error was ±0.02 mm. The probable maximum reading error therefore was ±0.03 mm.

The lag of the instrument was an important factor in determining the probable errors. It was found that the slight temperature drift maintained during the experiment did not register continuously on the record, but in minute steps, presumably because the instrument had to reach a certain degree of electrical unbalance before responding. The maximum error introduced from this source is estimated as 0.08 mm. Adding this figure to the reading error the maximum total error inherent in the method of measuring temperatures was ±0.11 mm of scale corresponding to a temperature interval of approximately ±0.012°C. This error is believed to be larger than the errors introduced by mechanical inaccuracies inherent in the system of loading. An error affecting only the values for iron above about 500°C will be mentioned later.

## Experimental Results

The thermoelastic temperature change was measured on specimens of nickel and Armco iron.
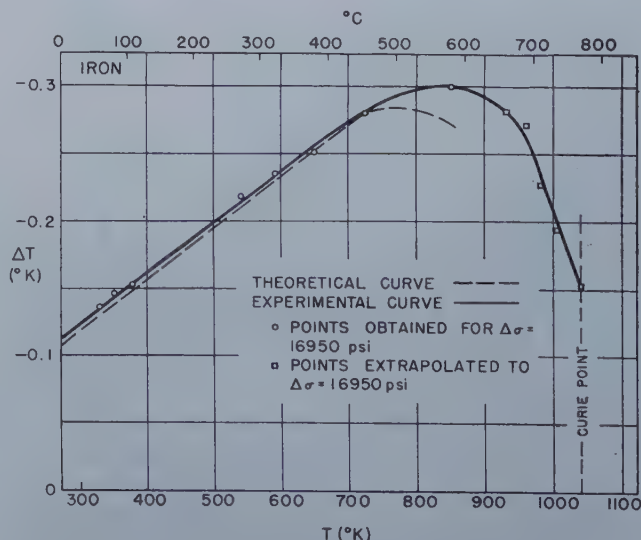


Fig. 3—The thermoelastic temperature change in Armco iron as a function of temperature.
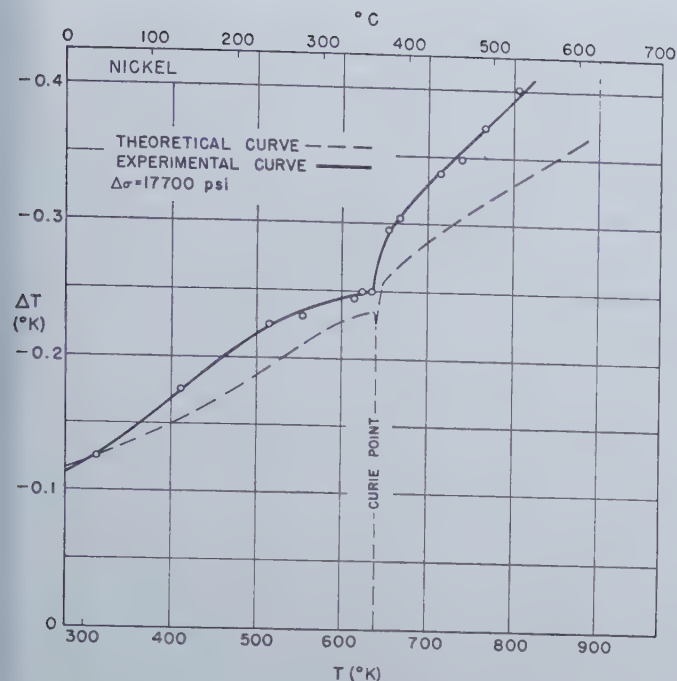
Fig. 4—The thermoelastic temperature change in nickel "L" as a function of temperature.



Fig. 5—The thermoelastic temperature change in Armco iron at different temperatures as a function of the change in stress.

Nominal compositions of these metals are given in table I. The results of the experiments are presented in fig. 3 to 6. The points plotted are averages of three determinations except in a few cases where an uncertain reading was rejected because it could be traced to faulty technique.

**Table I. Nominal Compositions of the Materials Employed**

|  | C | Mn | Si | S | Cu | P | Fe |
|---|---|---|---|---|---|---|---|
| Armco Iron (specified maxima) | 0.02 | 0.03 | 0.01 | 0.03 |  | 0.006 | bal. |
| Nickel "L" 99.4 pct Ni + Co | 0.01 | 0.20 | 0.15 | 0.005 | 0.05 |  | 0.1 |



Fig. 6—The thermoelastic temperature change in nickel "L" at different temperatures as a function of the change in stress.

Fig. 3 shows the thermoelastic temperature change in Armco iron as a function of temperature while fig. 5 shows the same effect as a function of change in stress. Corresponding data are given for nickel in fig. 4 and 6. In fig. 3 and 4 theoretical values of the thermoelastic effect, calculated by Eq 2, have also been entered. The data required for these calculations have been taken from the literature[27, 28, 29] for the pure metals.

According to Eq 2 the thermoelastic temperature change is directly proportional to the absolute temperature, the coefficient of thermal expansion and the change in stress, and is inversely proportional to the volume heat capacity. At any temperature the thermoelastic effect is an approximately linear function of the change in stress. The observed values follow this linear relation very closely, as shown in fig. 5 and 6. For equal changes in stress the effect is a function of the temperature; the nature of this function is determined by the manner in which the
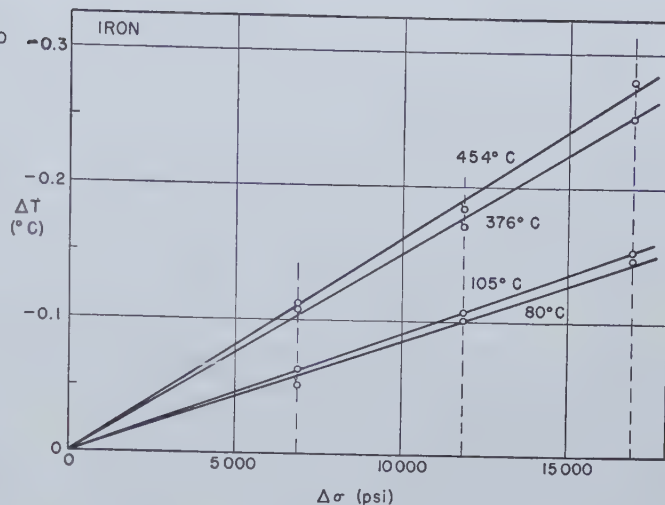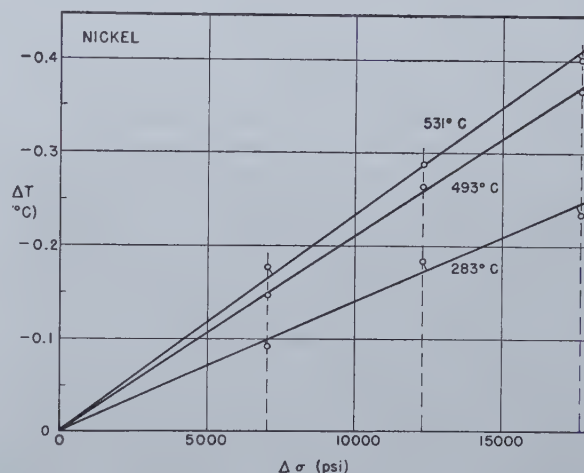
heat capacity and the thermal expansion coefficient change with temperature.

According to Grüneisen's theory[30] of thermal expansion the ratio of the heat capacity to the expansion coefficient is proportional to the compressibility. This ratio may be considered constant over a wide temperature range, but increases slightly at elevated temperatures. The thermoelastic effect should therefore be an approximately linear function of temperature, although increasing deviations from linearity must be expected as the temperature is raised. For a ferromagnetic metal the assumptions of Grüneisen's theory are not valid in the temperature range in which the metal loses its ferromagnetism. Consequently the thermoelastic effect is not a simple function of temperature in this range and a sharp discontinuity may be expected at the Curie point.

The thermoelastic temperature change observed in iron between 50°C and approximately 450°C
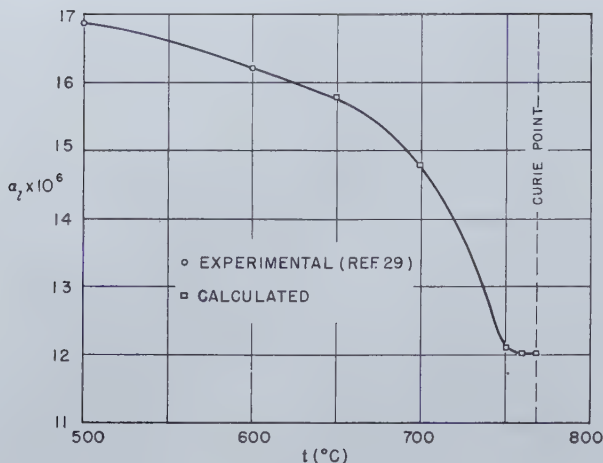
Fig. 7—The thermal expansion coefficient of iron as a function of temperature calculated from the thermoelastic effect.

agrees well with the curve calculated from Lord Kelvin's equation. It also is a linear function of temperature in accordance with Grüneisen's theory. Above about 450°C, the calculated and experimental curves show the effect of the gradual loss of ferromagnetism. The calculated curve is not carried beyond 600°C as the values of the expansion coefficient are uncertain above this temperature.[29] It has been deduced from general considerations, however, that the thermal expansion coefficient of α-iron decreases in the vicinity of the Curie point[31]. Reliable data for the heat capacity are available and show a large increase near the Curie temperature[29]. The thermal expansion coefficient and the heat

capacity thus combine to reduce substantially the thermoelastic temperature change, as confirmed by the experimental results presented in fig. 3.

Fig. 3 shows an excess of the observed over the calculated values at temperatures above 450°C. This excess is explained by a decrease in the cross-section of the specimen which resulted in an increase in the stress. One reason for the reduction of the effective cross-section at elevated temperatures was slight scaling of the iron specimen. A small amount of plastic deformation also occurred in a few instances above 650°C. Such plastic deformation could be prevented by reducing the load. Points obtained with reduced loads are included in fig. 3



Fig. 8—Record of a loading and unloading cycle showing interference by plastic deformation.
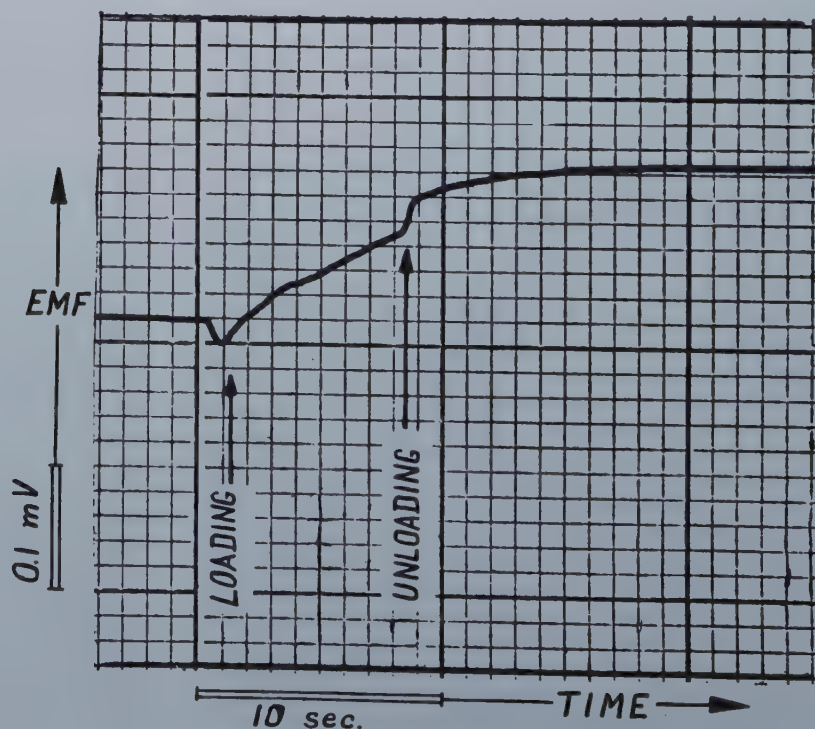
after extrapolation to the original load by Eq 2. Above the Curie temperature of iron it was not possible to make dependable measurements even with the smallest practicable load. After the completion of the experiment the total reduction in the cross-section of the iron specimen due to scaling and plastic deformation was found to be about 15 pct. This figure included a small amount of reduction which had taken place above the Curie point. It is concluded that the error in the observed thermoelastic temperature changes of iron increased gradually above 450°C to a maximum of about 15 pct at the Curie point.

Values of the thermal expansion coefficient of iron were calculated from the observed thermoelastic temperature changes by Eq 2. In these calculations, corrections for the change in cross-section, increasing from 9 pct at 600°C to 15 pct at the Curie point, were made. After these corrections the total error in the calculated thermal expansion coefficients is estimated to be less than 10 pct. The thermal expansion coefficients shown in fig. 7 decrease as the Curie point is approached in accordance with the theory of ferromagnetism[31].

For nickel the calculated and observed values of the thermoelastic temperature change coincide only at room temperature, but differ as the temperature is raised. This difference cannot be explained by a change in cross-section. The nickel specimen did not scale and its diameter remained unchanged during the entire experiment. The temperature records also did not show a single indication of plastic deformation. Nix and McNair[28] have found that the expansion coefficient of ferromagnetic metals is very sensitive to small amounts of impurities at elevated temperatures. The discrepancies between the calculated and experimental curves in fig. 4 may be chiefly due to this cause. Both curves, however, agree in that the decrease in the thermoelastic effect near the Curie temperature is small, especially when compared to iron. In iron the expansion coefficient decreases near the Curie point and thus reinforces the effect of the heat capacity, while in nickel the expansion coefficient increases and thus counteracts the effect of the heat capacity.

In the few instances in which incipient plastic deformation of the iron specimen occurred an initial temperature drop on loading was followed by a rise in temperature as shown in fig. 8. The former was due to the thermoelastic effect while the latter was caused by plastic deformation. The superposition of these two phenomena interfered with the evaluation of the thermoelastic effect so that the few observations of this type were rejected. After unloading in the plastic range the temperature continued to rise slightly for a short period. This phenomenon may be explained by the fact that plastic deformation generates heat in active slip-regions which are distributed over the cross-section. This heat reaches the thermocouple after some delay. A small amount of plastic deformation resulting from the stress relief after unloading in the plastic range may also contribute to this heat evolution.

## Summary

The thermoelastic effect was determined experimentally as a function of temperature in nickel and

Armco iron. Tensile stresses of various magnitudes were employed.

At all temperatures the experimental results were in agreement with an equation first derived by Lord Kelvin from thermodynamic postulates. The magnitude of the thermoelastic effect was found to change appreciably near the Curie temperature. It was possible to confirm by calculation that the thermal expansion coefficient of iron decreases in the vicinity of the Curie temperature as predicted by the theory of ferromagnetism.

## Acknowledgments

## References

[1] W. Thomson (Lord Kelvin): *Trans.* Roy. Soc. Edinb. (1853) **20**, 261; Coll. Works, Cambridge (1882) **1**, 174.

[2] W. Thomson (Lord Kelvin): *Quart. Jl. of Math.* (1857) **1**, 55; Coll. Works, Cambridge (1882) **1**, 291.

[3] J. Willard Gibbs: *Trans.* Conn. Acad. (1876-78) **3**, 343; Coll. Works, New York (1928) **1**, 184.

[4] W. Weber: *Pogg. Ann. der Phys.* (1830) **20**, 177.

[5] J. P. Joule: *Proc.* Roy. Soc. (1857) **8**, 355.

[6] J. P. Joule: *Phil. Trans.* (1859) **149**, 91.

[7] E. Edlund: *Pogg. Ann. der Phys.* (1861) **114**, 1.

[8] E. Edlund: *Pogg. Ann. der Phys.* (1865) **126**, 539.

[9] P. de Saint Robert: *Atti* Acad. Sc. Torino (1868) **3**, 201; also *Ann. de chim. et de phys.* 4th ser. (1868) **14**, 229.

[10] R. Rühlmann: Handbuch der mechanischen Wärmetheorie. Wien (1876), 529.

[11] G. R. Dahlander: *Pogg. Ann. der Phys.* (1872) **145**, 147.

[12] H. Haga: *Ann. der Phys. u. Chem.*, N.F. (1882) **15**, 1.

[13] A. Wassmuth: Sitz. Ber. Wien Akad. (1888) **97**, 2a, 52.

[14] A. Wassmuth: ibid. (1889) **98**, 2a, 1393.

[15] A. Wassmuth: *Ann. der Phys.* (1903) **11**, 146.

[16] A. Wassmuth: *Ann. der Phys.* (1904) **13**, 182.

[17] A. Wassmuth: Sitz. Ber. Wien Akad. (1906) **115**, 2a, 223.

[18] A. Wassmuth: ibid. (1907) **116**, 2a, 1245.

[19] C. A. P. Turner: *Trans.* Am. Soc. Civ. Eng. (1902) **48**, 140.

[20] E. G. Coker: *Trans.* Roy. Soc. Edinb. (1904) **41**, 229.

[21] E. G. Coker and C. M. McKergow: Can. Roy. Soc. Proc. and Trans. 2nd ser. (1904) **10**, III, 5.

[22] E. Rasch: Sitz. Ber. Akad. d. Wiss. Berlin. (1908) **1**, 210.

[23] K. T. Compton and D. B. Webster: *Phys. Rev.* (1915) **5**, 159.

[24] G. Tammann and H. Warrentrup: *Ztsch. f. Met.* (1937) **29**, 84.

[25] C. Zener: *Phys. Rev.* (1937) **52**, 230 and (1938) **53**, 90.

[26] N. E. Hamilton: Unpubl. research, Mass. Inst. of Tech.

[27] C. Sykes and H. Wilkinson: *Proc. Phys. Soc.* (1938) **50**, 834.

[28] F. C. Nix and D. McNair: *Phys. Rev.* (1941) **60**, 597.

[29] *Metals Handbook.* Am. Soc. f. Met., Cleveland, O. (1949) 426-427.

[30] E. Grüneisen: *Handbuch der Phys.*, Berlin (1926) **10**, 21.

[31] W. Shockley: Bell Syst. *Tech. Jl.* (1939) **18**, 718.

## Appendix

In deriving an equation for the thermoelastic temperature change associated with an adiabatic elastic deformation of a bar of unit cross-section the following quantities and symbols will be used:

$l$ : length of the bar

$\sigma$ : axial stress (positive in tension)

$T$ : absolute temperature

$c_\sigma$ : specific heat at constant stress

$d_o$ : density in the standard state

$c_\sigma'$ : volume heat capacity $= c_\sigma d_o$

$\alpha_l$ : coefficient of linear thermal expansion $= \dfrac{1}{l_o}\left(\dfrac{\partial l}{\partial T}\right)_\sigma$

$S$ : entropy of the bar

$Y$ : Young's modulus $= 1 / \dfrac{1}{l}\left(\dfrac{\partial l}{\partial \sigma}\right)_T$

$\nu$ : Poisson's ratio.

Subscript $_o$ refers to room temperature.

Since $S = S(T, \sigma)$ and $dS$ is a perfect differential,

$$\left(\frac{\partial T}{\partial \sigma}\right)_S = -\frac{(\partial S/\partial \sigma)_T}{(\partial S/\partial T)_\sigma} \qquad [1]$$

For axial deformation, one of the Maxwell relations takes the following form:

$$\left(\frac{\partial S}{\partial \sigma}\right)_T = \left(\frac{\partial l}{\partial T}\right)_\sigma = \alpha_l \, l_o \qquad [2]$$

For the entropy of the entire bar having unit cross-section it follows from defining equations that:

$$\left(\frac{\partial S}{\partial T}\right)_\sigma = \frac{1}{T} c_\sigma \, d_o \, l_o \qquad [3]$$

Substituting Eq 2 and 3 into 1 and rearranging:

$$dT_S = -\frac{\alpha_l}{c_\sigma d_o} T \, d\sigma_S \qquad [4]$$

In applying Eq 4 it is necessary to know the stress $\sigma$ at the temperature $T$. This stress is related to the stress at room temperature by the equation

$$\sigma = \frac{\sigma_o}{1 + 2\,\overline{\alpha_l}\,(T-T_o)} \qquad [5]$$

where $\overline{\alpha_l}$ is the mean coefficient of linear expansion. Since $\overline{\alpha_l}$ is of the order of $10^{-5}$, and $(T-T_o)$ of the order of $10^2$, this correction can be omitted.

A correction term due to the contraction in the cross-section under load is expressed by the equation

$$\sigma = \frac{\sigma_o}{1 - 2\,\nu\sigma/Y} \qquad [6]$$

This correction may be ignored, since $\nu \cong 0.25$ and $Y \cong 10^7$ psi. Eq 4 may therefore be applied in the following form to a reversible adiabatic deformation:

$$dT = -\frac{\alpha_l}{c_\sigma\,d_o} T \, d\sigma_o \qquad [7]$$

In integrating Eq 7, $\alpha_l$ and $c_\sigma$ may be treated as independent of the temperature $T$ in the very small interval $\Delta T$. Since $\Delta \sigma$ may be of considerable magnitude, however, it is necessary to evaluate the dependence of $(\alpha_l/c_\sigma)$ on $\sigma$ as follows:

$$\left[\frac{\partial}{\partial \sigma}\left(\frac{\alpha_l}{c_\sigma}\right)\right]_S = \left[\frac{\partial}{\partial \sigma}\left(\frac{\alpha_l}{c_\sigma}\right)\right]_T + \left[\frac{\partial}{\partial T}\left(\frac{\alpha_l}{c_\sigma}\right)\right]_\sigma \cdot \left(\frac{\partial T}{\partial \sigma}\right)_S \qquad [8]$$

Developing the first term of the right side of Eq 8:

$$\left[\frac{\partial}{\partial \sigma}\left(\frac{\alpha_l}{c_\sigma}\right)\right]_T = \frac{1}{c_\sigma}\left(\frac{\partial \alpha_l}{\partial \sigma}\right)_T - \frac{\alpha_l}{c_\sigma^2}\left(\frac{\partial c_\sigma}{\partial \sigma}\right)_T \qquad [9]$$

$$\left(\frac{\partial \alpha_l}{\partial \sigma}\right)_T = \frac{1}{l_o}\left[\frac{\partial}{\partial \sigma}\left(\frac{\partial l}{\partial T}\right)_\sigma\right]_T = \frac{1}{l_o}\left[\frac{\partial}{\partial T}\left(\frac{l}{Y}\right)\right]_\sigma = \frac{\alpha_l}{Y} + \frac{l}{l_o}\left(\frac{\partial (1/Y)}{\partial T}\right)_\sigma \qquad [10]$$

From Eq 3:

$$\left(\frac{\partial c_\sigma}{\partial \sigma}\right)_T = \frac{T}{d_o l_o}\left[\frac{\partial}{\partial \sigma}\left(\frac{\partial S}{\partial T}\right)_\sigma\right]_T = \frac{T}{d_o l_o}\left[\frac{\partial}{\partial T}\left(\frac{\partial S}{\partial \sigma}\right)_T\right]_\sigma \qquad [11]$$

Substituting Eq 2 into 11:

$$\left(\frac{\partial c_\sigma}{\partial \sigma}\right)_T = \frac{T}{d_o l_o}\left[\frac{\partial}{\partial T}(\alpha_l \cdot l_o)\right]_\sigma = \frac{T}{d_o}\left(\frac{\partial \alpha_l}{\partial T}\right)_\sigma \qquad [12]$$

Substituting Eq 10 and 12 into 9 and combining with 8:

$$\left[\frac{\partial}{\partial \sigma}\left(\frac{\alpha_l}{c_\sigma}\right)\right]_S = \frac{1}{c_\sigma}\left[\frac{\alpha_l}{Y} + \frac{l}{l_o}\left(\frac{\partial (1/Y)}{\partial T}\right)_\sigma - \frac{T\alpha_l}{c_\sigma\,d_o}\left(\frac{\partial \alpha_l}{\partial T}\right)_\sigma\right] + \left[\frac{\partial}{\partial T}\left(\frac{\alpha_l}{c_\sigma}\right)\right]_\sigma \cdot \left(\frac{\partial T}{\partial \sigma}\right)_S \qquad [13]$$

Numerical values may be substituted into Eq 13 and the assumption may be made that the second derivative of $(\alpha_l/c_\sigma)$ with respect to $\sigma$ is negligibly small compared to the first derivative. In this manner it is found that the change of the ratio $(\alpha_l/c_\sigma)$ for the maximum load is less than 2.5 pct in the entire temperature range investigated. Hence this correction can also be omitted and Eq 7 can be integrated, for a small interval $\Delta T$:

$$\Delta T = -\frac{\alpha_l}{c_\sigma d_o} T\Delta\sigma_o = -\frac{\alpha_l}{c_\sigma'} T\Delta\sigma_o \qquad [14]$$
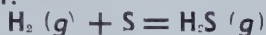
Thermodynamic Properties of

# Sulphur in Molten Iron-Sulphur Alloys

by Charles W. Sherman,

Hans I. Elvander and

John Chipman

To determine the thermodynamic properties of sulphur dissolved in liquid steel, the equilibrium in the reaction:

$$H_2 (g) + \underline{S} = H_2S (g)$$

was reinvestigated for the temperature range of 1530-1730°C and sulphur concentrations up to 4.8 pct.

The free energy change in the above reaction was established as a function of temperature. Values of the activity coefficient of sulphur were determined. The effect of silicon on the activity coefficient of sulphur was computed from the data of Morris and Williams. Using these coefficients it is shown that other recent data on the same reaction are in good agreement with the present results.

THE pronounced and usually deleterious effects of sulphur on all ferrous metals and the resultant necessity for its control in metallurgical processes have stimulated many investigations of the system iron-sulphur. The data required for thermodynamic study of the behavior of sulphur in molten iron and steel include the activity and free energy of the dissolved sulphur and its heat of solution. Such data are also of theoretical interest since there is all too little information available concerning solutions of nonmetallic solutes in metallic solvents.

It was the purpose of this investigation to attack the problem very directly by a study of equilibrium at several temperatures in the reaction

$$H_2 (gas) + \underline{S} = H_2S (gas) \qquad [1]$$

$$K_1 = p_{H_2S} / p_{H_2} \cdot a_s$$

where the sulphur is present in the liquid iron in amounts up to several percent by weight. Such a method of attack is not new since several careful studies have already been reported. It is planned, however, to extend the study to other metallic solvents and particularly to determine the effects of the various alloying elements on the activity of sulphur in liquid iron. This paper presents the results on molten iron-sulphur alloys containing up to 4 pct sulphur in the temperature range 1530°-1730°C.

## Literature Review

The significant researches on dilute molten solutions of sulphur in iron include those of Chipman

and Ta Li,[1] Maurer, Hammer and Möbius,[2] White and Skelly,[3] Kitchener, Bockris and Liberman,[4] and Morris and Williams.[5]

Chipman and Ta Li used the induction furnace in the temperature range 1513°-1640°C and studied melts containing 0.3-1.2 pct sulphur in the iron. A preheated mixture of $H_2S$ and $H_2$ was passed over the surface of a small pool of metal maintained at constant temperature. The metal was cooled rapidly and analyzed. The advantages of the induction furnace, the easy handling and the good stirring effect, are to a great extent offset by the steep temperature gradient in the system, which promotes thermal diffusion. This effect is especially serious when such a heavy gas as hydrogen sulphide is mixed with hydrogen, the gases near the hot surface becoming richer in the lighter gas. It now seems probable that in this instance the preheating of the gas was insufficient to prevent appreciable error from this source.

Maurer, Hammer and Möbius were chiefly concerned with melts that approached FeS in composition. By passing hydrogen over FeS at varying flow rates and analyzing the exit gas for $H_2S$, they were able to extrapolate to zero gas velocity to obtain the equilibrium constant. They reported only one melt which fell within the range studied in this investigation.

White and Skelly used a resistance-wound furnace to investigate the temperature range 1555°-1600°C. Small iron beads weighing about one gram were placed on an alumina tray and put in a closed reaction chamber of alumina. By taking the average value of in-going and out-going $H_2S/H_2$ ratio and by picking the three runs giving the lowest values, they obtained an equation for the temperature dependence of the equilibrium constant. The narrow temperature range and high silicon contents, sometimes as much as 2.6 pct Si, leave the equation in reasonable doubt.

Kitchener, Bockris and Liberman have reported on a preliminary study of the effect of carbon on the activity of sulphur. Indirect estimates of the influence of carbon on the activity of sulphur were reviewed. Direct measurements were made on the iron-sulphur equilibrium for melts saturated with graphite. Preliminary results indicated that saturation of the melt with carbon approximately doubles the sulphur activity at 1560°C.

Morris and Williams conducted a very careful investigation of the effect of silicon on the activity of sulphur in iron at 1615°C. In order to study the effect of silicon these authors redetermined the equilibrium constant for the pure iron-sulphur system at 1615°C. They used a graphite-spiral-heated furnace. Thermal diffusion was avoided by bubbling the $H_2S$-$H_2$ gas mixture through the melt. Duplicate iron samples were taken with a two-bore refractory thermocouple tube by immersion in the melt and drawing up of a sample in the holes. Melts containing silicon were compared with the pure iron melts. Silicon was found to have a marked effect on the activity coefficient of sulphur.

The quantitative results found in these investigations will be discussed when comparison is made with the results of this research.

## Description of the Method

The essential features of the method used by
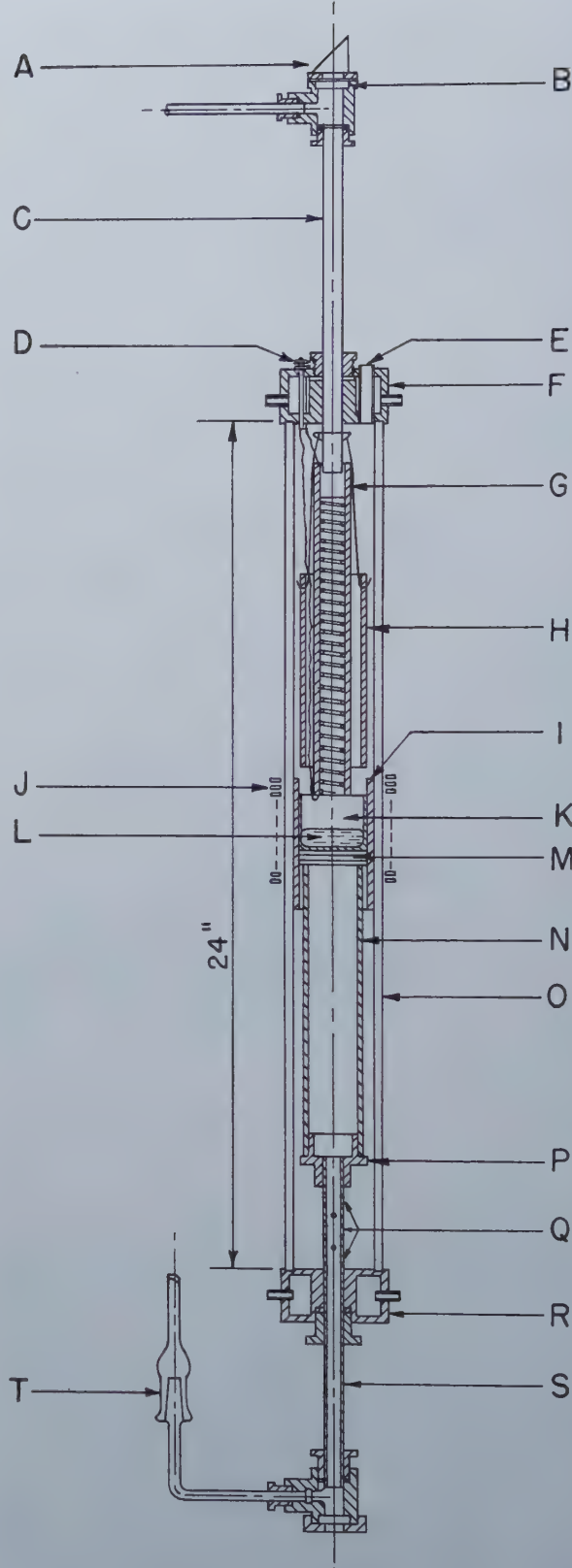


**Fig. 1—Induction Furnace for Equilibrium Measurements.**

A — Glass prism 38.5 x 38.5 mm
B — Glass-window 1.8 mm
C — Pyrex tubing 13.5 x 11 mm
D — Terminals for the preheater
E — Sampling opening
F — Water-cooled brass head
G — Preheater
H — Radiation shield, alundum
I — Heat insulation, alundum 4.5 mm
J — Induction coil
K — Crucible
L — Melt
M — Alundum discs
N — Supporting tube, alundum
O — Quartz tube 69 x 60 mm
P — Supporting disc, stainless steel
Q — Holes for gas outlet
R — Brass head
S — Stainless steel tube 14.2 x 11.2 mm
T — Ground glass joint

Chipman and Ta Li have been retained in the present work. A prepared mixture of hydrogen and hydrogen sulphide was conducted over molten iron at constant temperature until equilibrium was reached. Instead of cooling the entire melt, however, samples for analysis were obtained during the run by solidification in small-bore silica tubes.

Fig. 1 shows the pertinent parts of the furnace assembly. Induction heating was used because of its several advantages for this type of study. The melt is constantly stirred throughout the run, exposing new metal surface to the gas continually. The refractories used do not reach the high temperatures found in resistance type furnaces.

The gas preheater tube was made of pure alumina and wound with 0.025 in. molybdenum wire. Silica in this portion of the system was found to be objectionable because of its tendency to be transferred to the melt by the gas passing through the preheater.

The crucibles holding the melt were made of high purity alumina in the following manner: Alumina powder, grain size 220 mesh, was dry ground for 24 hr in a steel ball mill, after which water was added and the pulp passed through an electromagnetic separator to remove any iron particles. The pulp was treated with hydrochloric acid four times with settling and decantation after each wash. Water was added in each wash until the leach solution reached a pH of 3-4. The material was then slip cast into plaster molds. After drying in air 24 hr, the crucibles were prefired at 1000°C and finally fired at 1800°C to a dense, translucent, white body. These crucibles endured molten iron at 1725°C in an atmosphere of hydrogen and hydrogen sulphide during a 12-hr run without being affected. The wall of a crucible after such a run contained less than 0.005 pct S.

Temperatures were measured by sighting a disappearing-filament optical pyrometer on the melt. The optical system consisted of a prism, a glass window and a gas column 55 cm in length. Calibration of the system was made against the melting point of electrolytic iron at 1535°C in a hydrogen atmosphere. The true temperature was read from the calibration chart of Dastur and Gokcen,[6] which
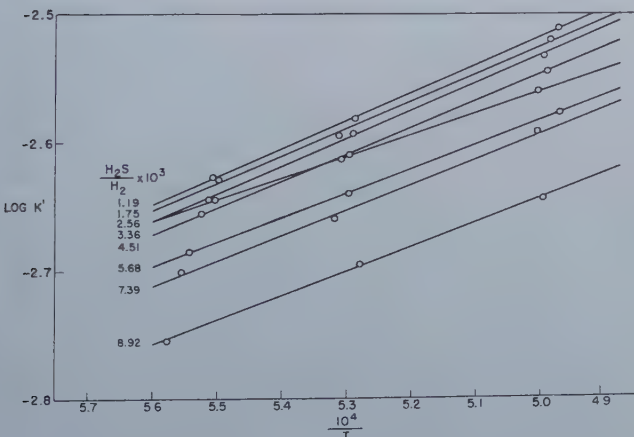
### Table I. Comparative Reproducibility of Gas Analyses

| | Method No. 1 (CdS Precipitation) g $H_2S/2$ l | Method No. 2 (Ascarite Absorption) g $H_2S/2$ liters |
|---|---|---|
| Gas No. 1 | 0.0008 | 0.0016 |
| | 0.0012 | 0.0015 |
| | 0.0016 | 0.0016 |
| | 0.0015 | 0.0015 |
| | 0.0012 | 0.0016 |
| | 0.0013 | 0.0016 |
| | 0.0009 | |
| | 0.0014 | |
| | 0.0016 | |
| Gas No. 2 | 0.0017 | 0.0018 |
| | 0.0015 | 0.0017 |
| | 0.0018 | 0.0018 |
| | 0.0015 | 0.0017 |
| | 0.0016 | 0.0019 |
| | 0.0018 | |
| | 0.0016 | |

was determined under similar experimental conditions.

The melt was sampled by dipping a quartz tube through the opening in the upper brass end of the furnace and drawing up a sample of approximately 6 cm length. The entire piece was analyzed. As a precautionary measure, the quartz tube was flushed with hydrogen to prevent oxidation of the sample by air.

Thermal diffusion was eliminated by vigorous preheating of the gas and by adding a heavy inert gas, argon, to the mixture. The preheater tube has a hot zone about 10 in. long where the wall was maintained at the same temperature as that of the melt. The flow of argon was controlled by a simple capillary flowmeter. The usual argon flow rate during a run was about 500 ml per min.

The hydrogen-hydrogen sulphide mixtures were prepared by evacuating a tank that had been saturated with hydrogen sulphide, introducing a small amount of pure $H_2S$ and then filling with hydrogen. The mixtures were allowed to come to equilibrium for at least three days and then analyzed before, during and immediately after a run. The composition did not change. The flow of this gas mixture into the system was controlled by a simple flowmeter that had been calibrated with pure hydrogen. The usual flow rate for this mixture during a run was approximately 500 ml per min.

A representative run was carried out as follows: Approximately 175 g of electrolytic iron were melted down under an atmosphere of hydrogen. The optical pyrometer was checked at the melting point. The argon and hydrogen-hydrogen sulphide mixtures were then introduced into the system. The power was increased until the melt was at the desired temperature. After the melt had been at constant temperature for an hour, the first metal sample was taken and analyzed for sulphur. At hourly intervals the melt was sampled and analyzed until three successive samples gave identical results. The melt was then considered at equilibrium with the gas. The gas was then analyzed for $H_2S$ and $H_2$ by taking three samples as described in methods of analysis. The run was terminated at this point, or a new run could be started by simply changing the temperature and repeating the process described above.

**Methods of Analysis:** Former investigators have relied on some variation of the standard volumetric



**Fig. 2—Experimental Values of Log K′₁, Where**

$$K'_1 = \frac{p_{H_2S}}{p_{H_2} \cdot \% \, S}$$

Numbers indicate ratio $H_2S$: $H_2 \times 10^3$ in entrant gas.

**Table II. Checks on the Method for Metal Analysis**

| Steel No. 1 | Pct S |
|---|---|
| National Bureau of Standards No. 129a Recommended value for S = 0.273 pct | 0.274 0.273 0.274 0.273 0.273 0.273 |

| Steel No. 2 | Pct S |
|---|---|
| National Bureau of Standards No. 123 Recommended value for S Combustion = 0.133 pct HCl volumetric = 0.126 pct | 0.126 0.126 0.126 0.126 0.126 |

method for determining sulphur in iron.[7] This procedure involves the precipitation of a metal sulphide (CdS, ZnS, etc.) in an alkaline solution and subsequent titration with standard iodine or potassium iodate in conjunction with sodium thiosulphate. This method was used to obtain the preliminary values shown in fig. 6.

As pointed out by Morris and Williams[5] who preferred a gravimetric method, this procedure has been shown by Lundell, Hofman and Bright[8] to be of doubtful accuracy when used with varying weights of sample. The precipitation of CdS is shown by the same authors to suffer from an additional degree of variability. The precipitate is photosensitive and exposure to sunlight in varying degrees leads to erroneous results unless a very rigid analytical technique is employed.

The analysis of $H_2S$ and $H_2$ gas mixtures can be performed in a manner similar to that used for the metal samples. When the sulphur sought for is already in the form of $H_2S$, the determination is the same as described above with precipitation of a sulphide and titration with a standard iodine solution. The hydrogen is measured in a suitable collection flask of known volume.

After the first few results were obtained in this study, it was felt that an improved method of analysis for both metal and gas samples was desirable. The following method proved to be satisfactory:

*Gas Analysis:* The mixtures that were passed over the melt contained three different gases: $H_2S$ in amounts up to 1 pct, $H_2$ and argon. The exact percentage of argon was not required but an approximate value was necessary in order to compute the extent of dissociation of $H_2S$ at elevated temperatures. This could be obtained with sufficient accuracy from the rate of flow.

The prepared mixture of $H_2S$ and $H_2$ was analyzed before admixture of argon. Most acidic gases are readily absorbed on sodium hydroxide-impregnated asbestos (trade name Ascarite, Caroxite, etc.). Ascarite absorption of $CO_2$ is very satisfactory in the conventional combustion method for carbon in steel. Its use was also found very satisfactory for $H_2S$. The change in weight of an absorption bulb can be attributed directly to $H_2S$ when a suitable drier such as anhydrone has been included in the bulb to trap the water of reaction.

Table I includes values for two different tanks of $H_2S$-$H_2$ mixtures, where the $H_2S$ had been determined by the cadmium acetate volumetric

method and by a gravimetric method using Ascarite absorption. The values for the CdS precipitation are reported in grams per two liters of gas mixture so that they may be compared directly with the Ascarite absorption values where 2-liter gas samples were used. Actually the low percentages of $H_2S$ in the gases necessitated taking a 13.6 liter sample to precipitate CdS in amounts enough to titrate, an additional disadvantage of the volumetric method. It can be seen that the deviation is much less for the Ascarite absorption even though a much smaller sample was used.

The necessary equipment for the Ascarite method includes tank, reducing valve, drying tower, nesbitt bulb, and hydrogen collection flask of known volume.

When using this method, the drying tower must be saturated with $H_2S$ before use and the absorption bulb should be primed by running some of the gas mixture through it so that the bulb contains an atmosphere of pure hydrogen.

*Metal Analysis:* At first, it was felt that analysis of metal samples could be performed quite satisfactorily using the combustion method.[7] This was found to be true; the combustion method has been used to check most of the values reported. However, an additional point should be considered. When possible, the gas samples and metal samples should be analyzed by similar procedure to reduce the effect of inherent errors.

The analysis of the gas samples reported in table I involved a comparison of two analytical methods on a gas whose composition was not known exactly. This did not establish the validity of the method. A standard reference of known value was needed.

In the conventional volumetric method of analysis for sulphur in iron, the samples are dissolved in HCl with the evolved gases passing through an absorbing solution where a sulphide is precipitated. Ascarite absorption may be substituted for the ab-
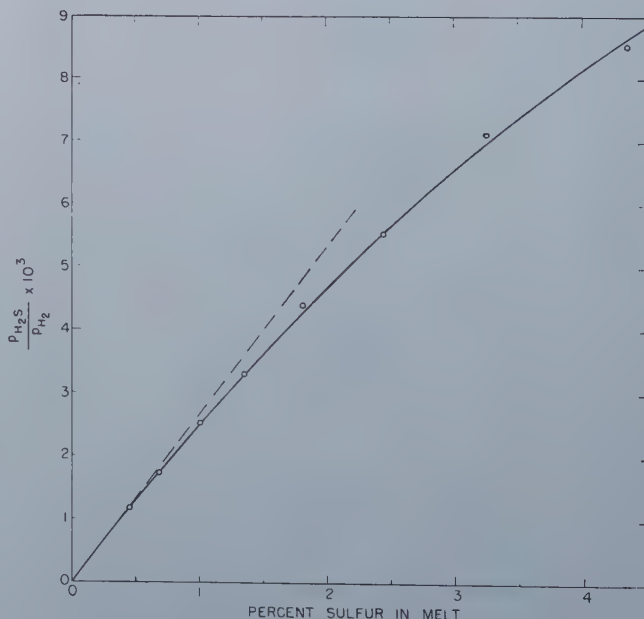


**Fig. 3—Equilibrium at 1600°C.**
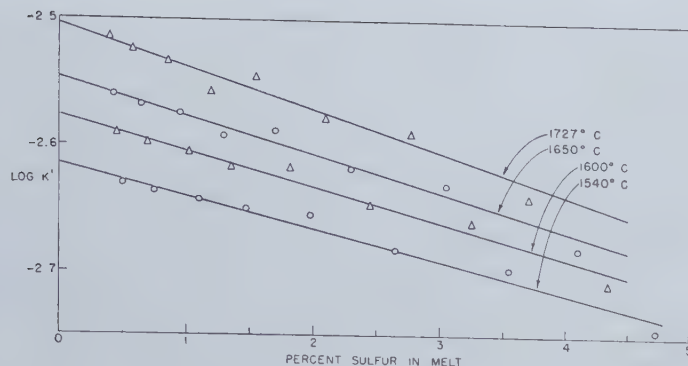The broken line represents Henry's law.

Fig. 4—Apparent Equilibrium Constant at Four Temperatures.

$$K'_1 = \frac{p_{H2S}}{p_{H2} \cdot \% \, S}$$

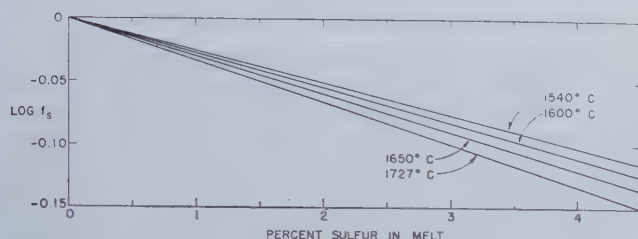Extrapolation to 0% S gives the value of log $K_1$.



Fig. 5—Logarithm of the Activity Coefficient as a Linear Function of Concentration.

sorbing solution providing certain precautions are observed. The HCl treatment of metal samples releases the sulphur in iron as $H_2S$ and in addition $H_2O$ and HCl are carried over through the train and must be eliminated before the absorption bulb. The absorption of HCl must take place in a medium which does not absorb $H_2S$. Very dilute HCl was found to do this admirably. The solution must be changed when the HCl concentration becomes too high but usually performs very satisfactorily for at least ten determinations. The water is absorbed by anhydrone in a drying tower. The whole system is kept closed and the reaction products flushed through the apparatus with an inert gas such as nitrogen.

Table II includes the results for two Bureau of Standards high-sulphur steel samples analyzed in this manner. The usefulness of this method lies in the fact that it can be performed with the minimum of attention and is quite convenient to use when analyzing furnace samples before the run has been completed. There is therefore less chance of terminating a run before equilibrium has been reached, which might occur when metal samples are not analyzed until later.

### Results and Calculations

Equilibrium runs were made at three different temperature levels, approximately 1530°, 1610°, and 1725°C with sulphur contents in the melt varying between 0.4 and 4.8 pct. The results of these runs are recorded in table III. The values of the gas analyses are reported both as determined at room temperature and as corrected for dissociation of hydrogen sulphide at high temperatures.

The $H_2S/H_2$ ratios were corrected by using the known thermodynamic data for the following reaction which represents the only important dissociation of $H_2S$ at the temperatures in question:

$$H_2 \, (g) + 1/2 \, S_2 \, (g) = H_2S \, (g) \qquad [2]$$
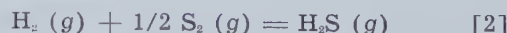
To determine the equilibrium constant, the standard free energy change for this reaction at each temperature must be computed. This may be done conveniently by determining $\Delta F°$ at 298° K and then using data of Kelley[9] to obtain the increments in enthalpy and entropy above 298° K. The heats of formation and entropies of the three gases at 298° K are:

| | $\Delta H°_f$ (Kcal per mol) | S° (cal per deg mol) |
|---|---|---|
| $H_2S$ | 4.815 | 49.15 |
| $H_2$ | 0 | 39.211 |
| $S_2$ | 31.02 | 54.42 |

The heat of formation of $H_2S$ and the entropy of hydrogen were taken from the data of the National Bureau of Standards[10] and the remaining values from Kelley.[11] The result, which is applicable in temperature range of these experiments, is:

$$\Delta F° = -RT \ln K = -21,680 + 11.81T \quad [2a]$$

$$K_2 = p_{H2S}/p_{H2} \times p_{S2}^{1/2} \, ; \quad \log K_2 = 4740/T - 2.582$$

As an example of the computation, the ratio in a given run of argon: hydrogen:hydrogen sulphide was 1092:1000:2.94, the total pressure being 1.019 atm. The temperature was 1900° K and accordingly

### Table III. Experimental Results

| Run | Temp. °C | $p_{H2S} \times 10^3$ | $p_{H2}$ | Pct S | $\frac{p_{H2S}}{p_{H2}} \times 10^3$ (corr.) | $K'_1 \times 10^3$ | log $K'_1$ |
|---|---|---|---|---|---|---|---|
| P-1 | 1546 | 1.71 | 0.470 | 1.46 | 3.60 | 2.46 | —2.609 |
| P-2 | 1661 | 1.49 | 0.516 | 1.11 | 2.82 | 2.54 | —2.595 |
| P-3 | 1599 | 1.52 | 0.516 | 1.23 | 2.91 | 2.36 | —2.627 |
| P-4 | 1718 | 1.46 | 0.516 | 0.96 | 2.74 | 2.86 | —2.544 |
| P-5 | 1731 | 1.16 | 0.482 | 0.78 | 2.35 | 3.02 | —2.520 |
| P-6 | 1780 | 1.50 | 0.392 | 1.08 | 3.60 | 3.33 | —2.478 |
| P-7 | 1799 | 1.79 | 0.492 | 1.09 | 3.41 | 3.13 | —2.504 |
| S-1 | 1543 | 0.599 | 0.503 | 0.50 | 1.18 | 2.36 | —2.627 |
| S-2 | 1618 | 0.598 | 0.502 | 0.45 | 1.18 | 2.62 | —2.582 |
| S-3 | 1738 | 0.596 | 0.501 | 0.38 | 1.17 | 3.08 | —2.511 |
| S-4 | 1546 | 0.896 | 0.512 | 0.74 | 1.74 | 2.35 | —2.629 |
| S-5 | 1609 | 0.884 | 0.505 | 0.68 | 1.73 | 2.54 | —2.595 |
| S-6 | 1733 | 0.882 | 0.504 | 0.57 | 1.72 | 3.02 | —2.520 |
| S-7 | 1541 | 1.30 | 0.507 | 1.12 | 2.54 | 2.27 | —2.644 |
| S-8 | 1617 | 1.28 | 0.500 | 0.99 | 2.52 | 2.55 | —2.593 |
| S-9 | 1729 | 1.30 | 0.509 | 0.85 | 2.49 | 2.93 | —2.533 |
| S-10 | 1544 | 1.69 | 0.503 | 1.46 | 3.32 | 2.27 | —2.644 |
| S-11 | 1611 | 1.69 | 0.502 | 1.35 | 3.30 | 2.44 | —2.613 |
| S-12 | 1725 | 1.69 | 0.502 | 1.18 | 3.25 | 2.75 | —2.561 |
| S-13 | 1537 | 2.24 | 0.497 | 2.01 | 4.44 | 2.21 | —2.656 |
| S-14 | 1615 | 2.28 | 0.506 | 1.79 | 4.40 | 2.46 | —2.609 |
| S-15 | 1731 | 2.32 | 0.515 | 1.51 | 4.31 | 2.85 | —2.545 |
| S-16 | 1531 | 2.81 | 0.496 | 2.71 | 5.58 | 2.06 | —2.686 |
| S-17 | 1615 | 2.85 | 0.501 | 2.41 | 5.51 | 2.29 | —2.640 |
| S-18 | 1739 | 2.89 | 0.510 | 2.02 | 5.36 | 2.65 | —2.577 |
| S-19 | 1527 | 3.75 | 0.507 | 3.63 | 7.22 | 1.99 | —2.701 |
| S-20 | 1607 | 3.74 | 0.507 | 3.25 | 7.12 | 2.19 | —2.660 |
| S-21 | 1725 | 3.76 | 0.509 | 2.69 | 6.89 | 2.56 | —2.592 |
| S-22 | 1520 | 4.48 | 0.503 | 4.94 | 8.69 | 1.76 | —2.754 |
| S-23 | 1621 | 4.51 | 0.505 | 4.21 | 8.50 | 2.02 | —2.695 |
| S-24 | 1729 | 4.49 | 0.503 | 3.61 | 8.20 | 2.27 | —2.644 |

the value of $K_2$ was 0.82. Solution of the $K_2$ equation yields a relative figure of 0.026 for $S_2$ on the above scale. The corrected ratio of $p_{H_2S}/p_{H_2}$ is therefore $(2.94 - 2 \times 0.026)/1000$ or $2.89 \times 10^{-3}$. Values of the corrected ratio are given for each experiment in table III.

Using the corrected $H_2S$-$H_2$ ratios and the value for sulphur in the metal, it is possible to determine for each heat a value of $K'_1$ defined as:

$$K'_1 = \frac{p_{H_2S}}{p_{H_2} \cdot \% \underline{S}}$$

This is not the true equilibrium constant of the reaction. Observed values of log $K'_1$ of the S-series experiments are plotted against the reciprocal of the absolute temperature in fig. 2. The results for each given series using a constant gas composition are tied together by a straight line. Graphical interpolation on these straight lines has been used to obtain values of $K'_1$ at selected temperatures. Since the sulphur content and the corrected gas ratio are not constant during a series but vary with temperature in a regular manner, the percentage of sulphur and the ratio $p_{H_2S}/p_{H_2}$ associated with each value of $K'_1$ have been obtained also by interpolation.

The experimental results, interpolated to a temperature of $1600°$, are shown in fig. 3. It is evident that the gas ratio is not quite a linear function of sulphur concentration, although the first three points fall nearly on a straight line. The ratio represented by $K'_1$ is therefore not quite constant and it becomes necessary to introduce an activity coefficient in defining the true equilibrium constant.

The data at four selected temperatures are shown in fig. 4 in which values of log $K'_1$ at each temperature are plotted against the weight percent of sulphur. At each temperature the points are adequately fitted by a straight line, the maximum deviation being of the order of 0.01 in log $K'_1$.

In order to establish an equilibrium constant for the reaction we shall define the activity of sulphur
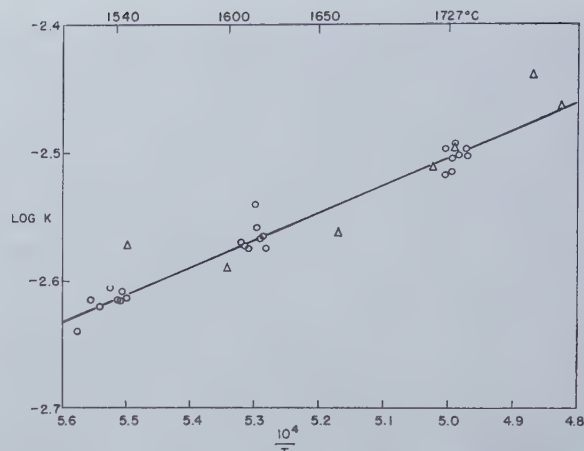


Fig. 6—Plot Containing All Experimental Values of Log $K_1$ as Function of $1/T$.
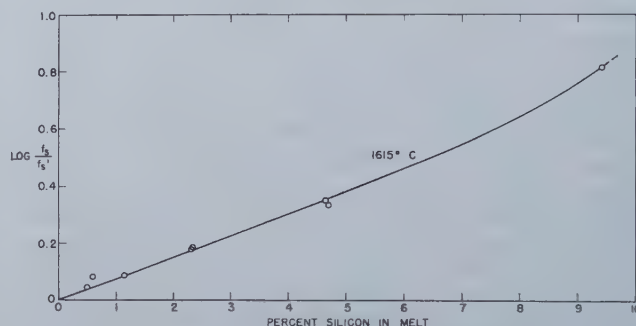$\Delta$ = preliminary runs;   O = improved technique.



Fig. 7—Effect of Silicon on Activity Coefficient of Sulphur.
(Data of Morris and Williams.)

in the melt on the same scale that we have used for its concentration, making $a_8 = \% S$ in the infinitely dilute solution. Further we define the activity coefficient $f_8$ as the ratio $a_8 / \% S$, its value being unity at infinite dilution. The equilibrium constant is then:

$$K_1 = \frac{p_{H_2S}}{p_{H_2} \cdot a_8} = \frac{p_{H_2S}}{p_{H_2} \cdot f_8 \cdot \% \underline{S}}$$

Values of $K_1$ at each temperature are given by the intercept of the line at 0 % S.

It is evident that log $f_8$ = log $K'_1$ — log $K_1$. Values of log $f_8$ are shown in fig. 5 as straight lines parallel to the lines of fig. 4. It is noteworthy that the line of highest temperature has the highest slope, indicating the greatest deviation from ideality. This unexpected result arises from the manner in which the lines of fig. 4 have been drawn, each line representing the points at one temperature without regard to the slopes of the other lines. Actually a system of parallel lines would have represented the data almost as well. For this reason the temperature effect denoted by the lines of fig. 5 is not firmly established by the data and should be regarded as tentative.

It is now possible with the aid of activity coefficients from fig. 5 to compute a value of the equilibrium constant for each datum of table III. These are

## Table IV. Data of White and Skelly, Corrected

| | 1555° C | | | | | | | |

| Run | $\frac{H_2S}{H_2} \times 10^3$ (in) | Pct S | Pct Si | $K'_1 \times 10^3$ | log $K'_1$ | log $f'_8$ | log $f_8^{Si}$ | log $K_1$ |
|---|---|---|---|---|---|---|---|---|
| II-3 | 7.12 | 3.41 | 1.12 | 2.09 | —2.680 | —0.089 | 0.084 | —2.675 |
| B-2 | 3.42 | 1.16 | 2.08 | 2.95 | —2.530 | —0.030 | 0.156 | —2.656 |
| B-3 | 3.42 | 1.12 | 2.02 | 3.05 | —2.516 | —0.029 | 0.150 | —2.637 |
| C-1 | 4.83 | 1.66 | 1.65 | 2.91 | —2.536 | —0.043 | 0.123 | —2.616 |
| C-3 | 4.83 | 1.34 | 1.52 | 3.60 | —2.444 | —0.035 | 0.112 | —2.521 |
| D-1 | 2.04 | 0.56 | 1.74 | 3.64 | —2.439 | —0.015 | 0.130 | —2.554 |
| E-1 | 3.15 | 1.13 | 2.10 | 2.79 | —2.554 | —0.030 | 0.159 | —2.683 |
| E-3 | 3.15 | 1.15 | 1.99 | 2.74 | —2.562 | —0.030 | 0.150 | —2.682 |

| | 1578° C | | | | | | | |

| I-1 | 7.10 | 2.09 | 2.04 | 3.40 | —2.469 | —0.056 | 0.153 | —2.566 |
| I-3 | 7.10 | 2.27 | 1.99 | 3.13 | —2.504 | —0.061 | 0.150 | —2.593 |
| J-1 | 8.73 | 3.47 | 1.63 | 2.52 | —2.599 | —0.094 | 0.122 | —2.627 |

| | 1600° C | | | | | | | |

| F-1 | 5.58 | 1.62 | 2.23 | 3.45 | —2.462 | —0.049 | 0.168 | —2.581 |
| F-3 | 5.58 | 1.71 | 2.25 | 3.26 | —2.487 | —0.051 | 0.170 | —2.606 |
| G-1 | 8.83 | 3.65 | 1.53 | 2.42 | —2.616 | —0.110 | 0.113 | —2.619 |
| G-3 | 8.83 | 3.47 | 1.63 | 2.55 | —2.593 | —0.104 | 0.122 | —2.611 |
| H-1 | 7.63 | 2.94 | 1.38 | 2.59 | —2.587 | —0.088 | 0.103 | —2.606 |
| H-3 | 7.63 | 3.09 | 1.34 | 2.47 | —2.607 | —0.093 | 0.100 | —2.614 |

shown in fig. 6. The straight line represents our best value for the equilibrium constant of the reaction and from it the following equations result:

$$H_2\ (g) + \underline{S} = H_2S\ (g) \qquad [1]$$
$$\log K_1 = -2150/T - 1.429$$
$$\Delta F° = +9840 + 6.54T$$

The latter may be combined with the equation for dissociation of $H_2S$ to give the following for the free energy of solution of gaseous sulphur ($S_2$) in liquid iron:

$$\tfrac{1}{2}\ S_2\ (g) = \underline{S}; \qquad [3]$$
$$\Delta F° = -31{,}520 + 5.27T$$

## Comparison with Other Investigations

Before the results of this research can be compared with those of previous investigators, some method must be used to eliminate the effect of the third element such as silicon which was present as an impurity in the work of Chipman and Ta Li and of White and Skelly. This element was added by Morris and Williams in amounts up to 9 pct and from their results its effect on the activity of sulphur may be computed.

In the iron-sulphur binary system, it has been shown that sulphur has an activity coefficient less than unity (fig. 5). With the information gained in the study of the binary system it is possible to attack ternary systems in a similar manner.

In any solution containing iron, sulphur and silicon the activity coefficient of sulphur is $f_s$ as previously defined. We shall use the symbol $f'_s$ to represent its activity coefficient in a pure iron-sulphur alloy containing the same percentage of sulphur. The ratio of these two in the ternary we shall call $f_s^{s1}$ The equilibrium constant of the $H_2S$ reaction with the ternary alloy is then:

$$K_1 = \frac{p_{H_2S}}{p_{H_2} \cdot f_s^{s1} \cdot f_s' \cdot \%\ S}$$

The data of Morris and Williams lead to the values of $f_s^{s1}$ shown in fig. 7.

It is now possible, with the information at hand, to apply corrections to part of White and Skelly's work. Since they did not analyze all their heats for silicon, only the portion that were analyzed can be recalculated. By substituting the proper $f_s'$ and $f_s^{s1}$ from fig. 5 and 7 for each heat, the resultant equilibrium constant is a true K. Table IV is a compilation of their data at 1555°, 1578°, and 1600°C. The true K is calculated simply from the relationship:

$$\log K_1 = \log K'_1 - \log f_s^{s1} - \log f'_s$$

The work of the several investigators is summarized in fig. 8. The values for $K_1$ have been calculated for each heat in the manner described above. The line drawn is that of fig. 6. The new data are markedly lower than those of Chipman and Ta Li which are believed to have suffered from errors of thermal diffusion. The agreement with the three other investigators is excellent.

## Summary

To determine the thermodynamic properties of sulphur dissolved in liquid steel, the equilibrium in the reaction:

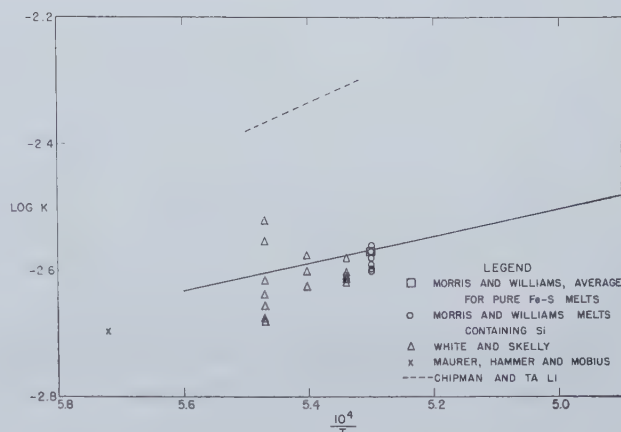$$H_2\ (g) + \underline{S} = H_2S\ (g) \qquad [1]$$

Fig. 8—Comparison of All Published Data.
Solid line represents authors' results.

was reinvestigated at temperatures up to 1730°C and sulphur concentrations up to 4.8 pct.

The ratio $p_{H_2S}/p_{H_2} \cdot \%\ S$ is not a true constant. To obtain the equilibrium constant, values of this ratio were extrapolated graphically to zero sulphur concentration. Values of the activity coefficient $f_s$ were determined.

The free energy change in the above reaction was established as a function of temperature.

From the similar work of Morris and Williams, the effect of silicon on the activity coefficient of sulphur has been determined. The results are used to obtain values of the equilibrium constant from their data and from those of White and Skelly. These two sets of data are shown to be in excellent agreement with those of this investigation.

## Acknowledgment

## References

[1] Chipman and Ta Li: Trans. Amer. Soc. for Metals (1937) 25, 435.

[2] Maurer, Hammer and Möbius: Arch. Eisenhuttenw. (1942) 16, 159.

[3] White and Skelly: Jnl. Iron & Steel Inst. (1947) 155, 201.

[4] Kitchener, Bockris and Liberman: Discussions, Faraday Soc., No. 4 (1948), 49.

[5] Morris and Williams: Trans. Amer. Soc. for Metals (1949) 41, 1425.

[6] Dastur and Gokcen: Trans. AIME 185, 665. Jnl. of Metals, Oct. 1949. TP 2693.

[7] "A.S.T.M. Methods of Chemical Analysis of Metals", Amer. Soc. for Test. Mat. (1946).

[8] Lundell, Hoffman and Bright: Chemical Analysis of Iron and Steel. John Wiley and Sons (1931).

[9] Kelley: U. S. Bur. Mines Bull. No. 476 (1949).

[10] Tables of Selected Values of Chemical Thermodynamic Properties. U. S. Dept. of Comm., Nat. Bur. of Stand. (1949).

[11] Kelley: U. S. Bur. Mines Bull. No. 406 (1937).

# The Manganese Equilibrium

## Under Simple Oxide Slags

### by John Chipman, John B. Gero and Theodore B. Winkler

New experimental data are presented on the manganese equilibrium in liquid steel under simple slags consisting of the oxides of iron and manganese with small amounts of impurities. The new data lead to values of $K_{Mn}$ which are significantly higher than those of Körber and Oelsen and in general somewhat above those of other investigators.

Thermodynamic calculation from published data at lower temperatures gives results which agree fairly well with the experimental data.

The distribution of oxygen between these slags and the liquid metal conforms to the solubility curve of Taylor and Chipman.

IN the basic open hearth process the reaction of manganese in the bath with iron oxide in the slag attains a condition very closely approximating true equilibrium, and the distribution of manganese between slag and metal during the refining period is determined by the factors which control this equilibrium condition. For this reason a number of investigators have studied this reaction both in the laboratory and under various conditions of furnace operation.

The principle reaction and its equilibrium constant are:

$$FeO \text{ (in slag)} + \underline{Mn} = MnO \text{ (in slag)} + Fe \text{ (liq.)}$$

$$[1]$$

$$K_{Mn} = \frac{(MnO)}{(FeO)_t \, [\% \, Mn]}$$

The symbols in parentheses represent activities of the two oxides in the slag which, in the simple slags consisting almost wholly of the two oxides, may be assumed equal to the respective mol fractions. The symbol $(FeO)_t$ is used to denote the total iron oxide computed as FeO; or it is the sum of the mol fraction of FeO plus twice that of $Fe_2O_3$.

Early attempts to obtain laboratory data on this reaction suffered from failure to appreciate the great speed of the reaction. When slag and metal are cooled slowly together, the equilibrium shifts with temperature and the final compositions correspond to equilibrium at the freezing point rather than at bath temperature. The early work of Oberhoffer and Schenck[1] and of Tammann and Oelsen[2] apparently suffered from this source of error. In most of the other published laboratory investigations[3,4,5] this error was not present but other uncertainties have existed, notably dependence upon optical temperature measurements and exposure to atmospheric oxidation.

JOHN CHIPMAN, Member AIME, is Professor of Metallurgy, and J. B. GERO is Graduate Student, Dept. of Metallurgy, Mass. Inst. of Tech. T. B. WINKLER is Engineer, Research Dept., Bethlehem Steel Co., Bethlehem, Pa.

## Table I. Experimental Data

| Sample Number | Temp. °C | Steel Analysis, Pct | | Slag Analysis, Pct | | | | | |
|---|---|---|---|---|---|---|---|---|---|
| | | Mn | O | FeO | $Fe_2O_3$ | MnO | MgO | $SiO_2$ | CaO |
| E-32-1 | 1655 | 0.065 | 0.209 | 76.94 | 4.15 | 13.86 | 3.84 | 1.16 | 0.32 |
| 4 | 1640 | 0.144 | 0.156 | 65.51 | 4.53 | 26.94 | 1.50 | 0.88 | 0.18 |
| 13 | 1620? | 0.160 | 0.175 | 66.21 | 4.12 | 26.92 | 1.85 | 0.56 | 0.08 |
| 15 | 1680? | 0.190 | 0.221 | 65.09 | 4.14 | 25.89 | 3.44 | 1.46 | 0.32 |
| 17 | 1690? | 0.250 | 0.180 | 56.30 | 3.26 | 36.07 | 2.37 | 1.74 | 0.40 |
| 20 | 1610 | 0.220 | 0.139 | 57.83 | 4.41 | 33.01 | 1.82 | 2.52 | 0.32 |
| E-38-4 | 1630 | 0.172 | 0.161 | 60.73 | 4.28 | 29.08 | 2.62 | 2.00 | 0.67 |
| 6 | 1672 | 0.211 | 0.194 | 60.26 | 3.57 | 29.58 | 3.55 | 2.16 | 0.59 |
| 8 | 1730+ | 0.234 | 0.225 | 58.56 | 3.25 | 30.86 | 4.83 | 1.60 | 0.43 |
| 10 | 1738 | 0.314 | 0.225 | 58.81 | 2.97 | 30.84 | 4.96 | 1.74 | 0.43 |
| 12 | 1689+ | 0.224 | 0.206 | 58.76 | 3.91 | 28.43 | 3.94 | 1.52 | 3.25 |
| 14 | 1583 | 0.132 | 0.138 | 59.17 | 4.12 | 26.49 | 2.90 | 2.66 | 3.56 |
| D-65-2 | 1603 | | 0.229 | 86.89 | 5.69 | | 1.32 | 2.28 | 0.37 |
| 4 | 1635 | | 0.280 | 86.09 | 5.47 | | | | |
| 6 | 1743 | 0.38 | 0.178* | 55.14 | 1.93 | 38.10 | 0.62 | 1.84 | 0.47 |
| 8 | 1750 | 0.42 | | 55.43 | 1.95 | 37.40 | | | |
| 10 | 1723 | 0.32 | 0.215* | 55.85 | 2.47 | 36.36 | | | |
| 12 | 1637 | 0.23 | 0.181 | 56.73 | 2.83 | 35.32 | | | |
| 14 | 1615 | 0.20 | 0.166 | 57.07 | 3.15 | 34.66 | | | |
| 16 | 1587 | 0.17 | 0.147 | 57.81 | 2.99 | 33.61 | 1.12 | 3.64 | 0.50 |
| 26 | 1598 | 0.18 | 0.128* | 56.38 | 2.55 | 36.03 | 0.10 | 1.64 | 1.24 |
| 28 | 1597 | 0.182 | 0.126 | 55.70 | 2.86 | 38.02 | | | |
| 30 | 1633 | 0.26 | 0.165 | 52.18 | 2.36 | 39.27 | | | |
| 32 | 1638 | 0.27 | 0.167 | 52.28 | 2.44 | 39.25 | 1.45 | 2.66 | 1.94 |
| 34 | 1706 | 0.29 | 0.258 | 59.27 | 2.57 | 33.40 | 1.18 | 1.30 | 0.77 |
| 36 | 1718 | 0.30 | 0.264 | 59.64 | 1.98 | 33.59 | | | |
| 38 | 1697 | 0.24 | 0.233 | 59.69 | 2.40 | 32.85 | | | |
| 40 | 1646 | 0.21 | 0.189 | 59.77 | 3.34 | 31.95 | | | |
| 42 | 1630 | 0.17 | 0.176 | 59.83 | 3.69 | 31.25 | | | |
| 44 | 1568 | 0.118 | 0.138* | 61.61 | 3.43 | 29.34 | 0.66 | 3.00 | 1.02 |
| 46 | 1580 | 0.096 | 0.128 | 65.42 | 1.27 | 27.91 | | | |

* Oxygen analysis based on single determination.

## Table II. Equilibrium Constants

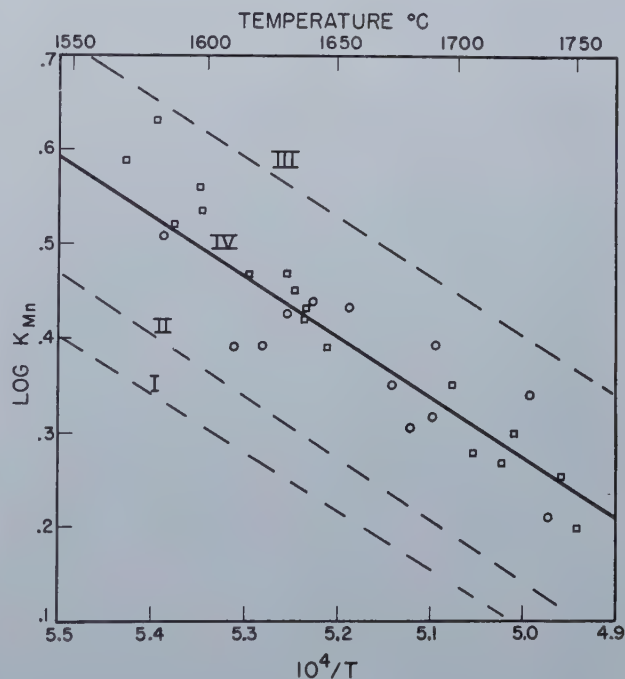| Number | Temp. °C | $K_{Mn}$ | $K \pm_{Mn}$ | $L_O$ |
|---|---|---|---|---|
| E-32-1 | 1655 | 2.70 | 2.84 | 0.255 |
| 4 | 1640 | 2.73 | 2.90 | 0.215 |
| 13 | 1620? | 2.41 | 2.55 | 0.221 |
| 15 | 1680? | 2.01 | 2.12 | 0.315 |
| 17 | 1690? | 2.47 | 2.60 | 0.297 |
| 20 | 1610 | 2.47 | 2.64 | 0.214 |
| E-38-4 | 1630 | 2.67 | 2.83 | 0.239 |
| 6 | 1672 | 2.24 | 2.36 | 0.298 |
| 8 | 1730+ | 2.18 | 2.29 | 0.365 |
| 10 | 1738 | 1.62 | 1.70 | 0.365 |
| 12 | 1689+ | 2.07 | 2.20 | 0.327 |
| 14 | 1583 | 3.24 | 3.45 | 0.211 |
| D-65-6 | 1743 | 1.79 | 1.84 | 0.297 |
| 8 | 1750 | 1.58 | 1.63 | |
| 10 | 1723 | 1.99 | 2.06 | 0.349 |
| 12 | 1637 | 2.62 | 2.74 | 0.287 |
| 14 | 1615 | 2.93 | 3.07 | 0.260 |
| 16 | 1587 | 3.31 | 3.47 | 0.229 |
| 26 | 1598 | 3.44 | 3.59 | 0.203 |
| 28 | 1597 | 3.62 | 3.71 | 0.206 |
| 30 | 1633 | 2.82 | 2.95 | 0.285 |
| 32 | 1638 | 2.70 | 2.81 | 0.290 |
| 34 | 1706 | 1.90 | 1.97 | 0.399 |
| 36 | 1718 | 1.85 | 1.91 | 0.411 |
| 38 | 1697 | 2.24 | 2.32 | 0.356 |
| 40 | 1646 | 2.45 | 2.57 | |
| 42 | 1630 | 2.94 | 3.12 | 0.276 |
| 44 | 1568 | 3.91 | 4.09 | 0.259 |
| 46 | 1580 | 4.43 | 4.46 | 0.198 |
| | | | | 0.182 |



Fig. 1—The Manganese Equilibrium Constant.

Circles, data from Heats E-32 and E-38 (1941). Squares, data from Heat D-65 (1949). Line I, equation of Körber and Oelsen (1932). Line II, average equation of Chipman (1934). Line III, calculated from low-temperature data. Line IV, present best average, Eq 8.

## Experimental Study

During the course of our laboratory investigation of the phosphorus equilibrium[6] a considerable number of samples were obtained which were essentially free from phosphorus and silicon. In two heats which were made in new crucibles the slag consisted of the oxides of iron and manganese along with minor amounts of magnesia and other impurities. The data on these two heats, E-32 and E-38, have been published but have not previously been used to obtain values of $K_{Mn}$.

Fig. 2—Distribution of Oxygen between Liquid Fe-Mn Alloys and Simple FeO-MnO Slags.

Circles, Heats E-32 and E-38. Squares, Heat D-65. Crosses, manganese-free points from D-65. The line represents data of Taylor and Chipman on solubility of oxygen in iron.
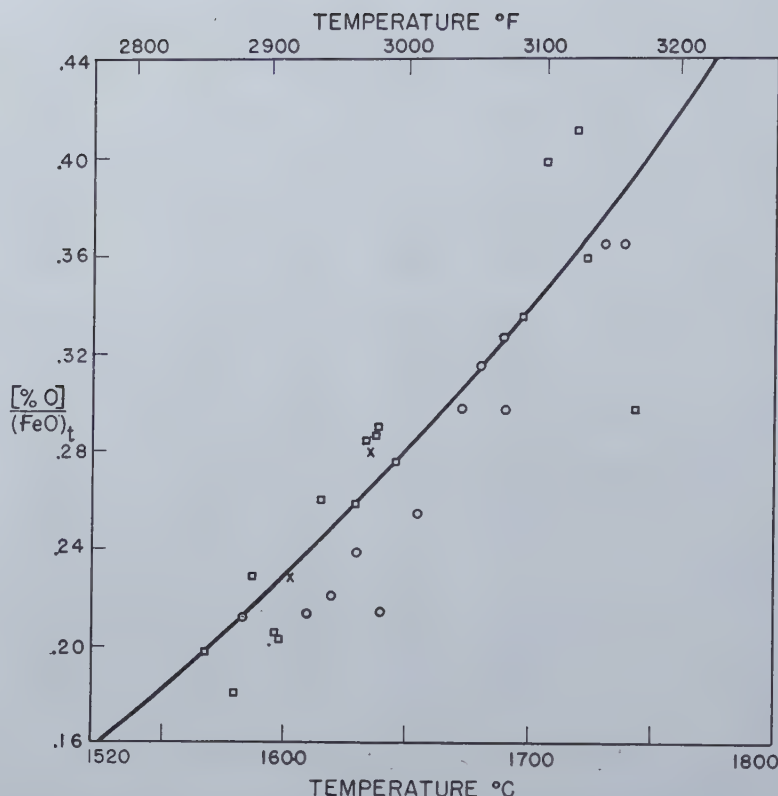
Another heat, D-65, was made and sampled by essentially the same technique the details of which have been described previously[6], the only change being elimination of vacuum melting. Sixty-five pounds of Armco ingot iron was melted in an open, magnesia-lined induction furnace. An atmosphere of hydrogen was then maintained over the melt for an hour to bring the carbon content below 0.01 pct. The bath was then exposed to air for 25 min to remove hydrogen, the electrodes were put in place and the furnace was operated from this point on in an atmosphere of nitrogen. Ferric oxide was added to form the first slag and two pairs of slag and metal samples were obtained. Electrolytic manganese and manganese dioxide were added and sampling was continued over a period of several hours. Samples were obtained by dipping steel molds into slag or metal respectively, the power being turned off momentarily. Molds for metal sampling were in the form of split cylinders ½ in. id and 1¼ in. od, 2 in. long. Slag molds were slightly larger. Temperatures were taken by tungsten-molybdenum thermocouples encased in silica tubes. This led to a slight increase in silica content of the slag which was offset by occasional additions of the other components. Slags taken before and after these additions were analyzed completely, all others for iron and manganese oxides only. Estimates of impurities in the other samples may be obtained by interpolation. The thermocouples were from an entirely different lot from those used in E-32 and E-38 and were independently calibrated.

The experimental results are given in table I.

Values of $K_{Mn}$ obtained from all three heats are assembled in table II. In fig. 1 the logarithm of $K_{Mn}$ is plotted against the reciprocal of absolute temperature. For comparison the results of two previous studies are shown as broken lines. The lowest represents the data of Körber and Oelsen[4] which, up to the present time, have been regarded as affording the most reliable values of the constant. The second is the best average value selected by one of the authors[7] to represent all data available in 1934. The new data are substantially different from those of Körber and Oelsen. They are in somewhat better agreement with the results of Krings and Schackmann.[5]

The distribution coefficient for oxygen defined as

$$L_o = [\% \text{ O}]/(\text{FeO})_t \qquad [2]$$

is also tabulated. Here $(\text{FeO})_t$ is the mol fraction of total iron oxide corrected for impurities by assuming that all acidic components form compounds with the basic oxides. In these slags the correction is quite small. Values of $L_o$ are shown by the points in fig. 2. The line represents the solubility of oxygen in liquid iron under pure iron oxide slags determined by Taylor and Chipman[8]. The agreement indicates that the distribution of oxygen between slag and metal is unaffected by manganese within the limited composition range that can be covered by the experimental method employed. It confirms Körber's conclusion that the solubility of MnO in the bath is small.

### Thermodynamic Calculations

The data shown in fig. 1 are not sufficiently accurate to establish the relationship between $K_{Mn}$ and temperature. The scatter of points would permit representation of the average result by a line of almost any slope. This slope, however, can be calculated from other data. Southard and Shomate[9] have measured the heat of formation of MnO and its heat content up to 1300°C. Kelley, Naylor and Shomate[10] have established the heat content of the metal up to high temperatures. Similar data for
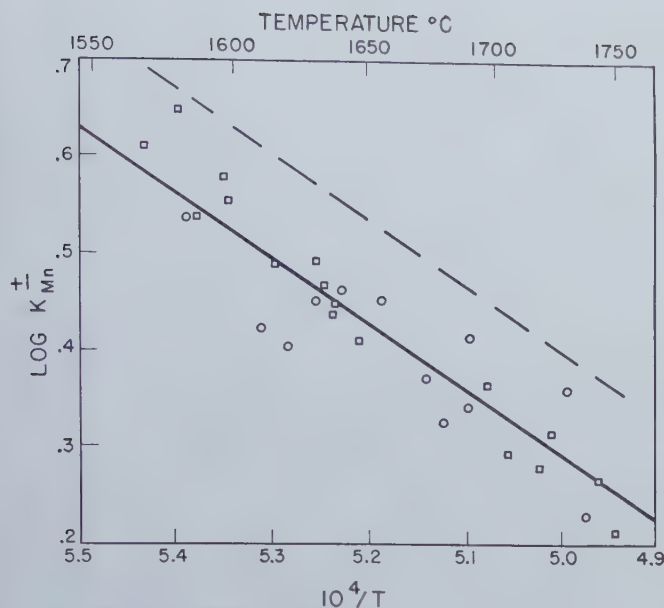
**Fig. 3—The Manganese Equilibrium Constant in Terms of the Ions.**

Circles, Heats E-32 and E-38. Squares, Heat D-65. Broken line, calculated; solid line, best experimental average using calculated slope, Eq 13.

oxygen have long been available. Likewise the entropies of the same substances are known and these data have also been assembled by Southard and Shomate. For the reaction of liquid manganese with oxygen to form solid MnO their data lead to the equation*:

---
* Note the adjusted Eq 14 discussed later.
---

$$Mn \ (liq.) + 1/2 \ O_2 \ (g) = MnO \ (s);$$
$$\Delta F° \ (calc.) = -97,000 + 20.9T \qquad [3]$$
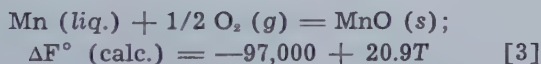
Since the estimated change in heat capacity is less than 1 cal, this equation may be used throughout the range of steelmaking temperatures.

The heat of fusion of MnO is unknown. It is estimated by comparison with that of FeO for which Darken and Gurry[11] find 8600 cal. The melting points of FeO and MnO are respectively 1643 and 2058°K. If the heat of fusion of like substances is proportional to the melting temperature, that of MnO is about 10,700 cal. This enables us to write the equation:

$$MnO \ (s) = MnO \ (liq.); \Delta F° = +10,700 - 5.2T \quad [4]$$

The free energy of the liquid iron oxide phase in equilibrium with iron has been redetermined very recently by Dastur and Chipman[12] who write the following equation for the free energy per gram atom of oxygen:

$$xFe \ (liq.) + 1/2 \ O_2 \ (g) = Fe_xO \ (in \ sat. \ liq.); \quad [5]$$
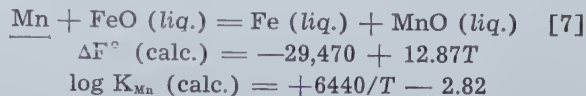$$\Delta F° = -56,830 + 11.94T$$
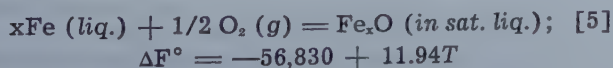
According to Darken and Gurry the value of $x$ at 1600°C is 0.988. The error involved in using the above equation for the free energy of FeO or of

(FeO)$_t$ is of the order of magnitude of $RT \ln 0.988$ or about 45 cal, This can be ignored.

Assuming ideality of the solution of manganese in liquid iron, its free energy[13] is:

$$Mn \ (liq.) = \underline{Mn}; \Delta F° = -9.11T \qquad [6]$$

The four equations (3, 4, 5 and 6) may now be combined to give the free energy change in reaction (1) and a calculated equation for $K_{Mn}$.

$$\underline{Mn} + FeO \ (liq.) = Fe \ (liq.) + MnO \ (liq.) \quad [7]$$
$$\Delta F° \ (calc.) = -29,470 + 12.87T$$
$$\log K_{Mn} \ (calc.) = +6440/T - 2.82$$

The line corresponding to this calculated equation is shown as line III of fig. 1. The agreement with the experimental results is better than is usually to be expected in such calculations. The best values for the manganese constant are represented by line IV which is drawn parallel to line III through the average of the experimental points. The equation of this line is:

$$\log K_{Mn} \ (exp.) = +6440/T - 2.95 \qquad [8]$$

**Ionic Calculation:** The slight uncertainty introduced by applying the free energy of Fe$_x$O to an equilibrium constant involving (FeO)$_t$ can be avoided by placing all calculations on an ionic basis. The reaction and its equilibrium constant then become:

$$Fe^{++} + \underline{Mn} = Mn^{++} + Fe \ (liq.) \qquad [9]$$
$$K^{\pm}_{Mn} = \frac{a_{Mn}{}^{++}}{a_{Fe}{}^{++} \cdot \% \ Mn}$$
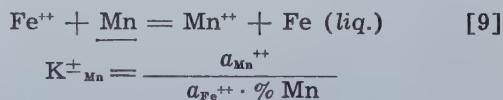
Values of this constant in these simple oxide slags are the same as would be obtained for the ordinary $K_{Mn}$ if only *ferrous* oxide rather than (FeO)$_t$ were employed. These are shown in the fourth column of table II.

In the calculation of the ionic $K^{\pm}_{Mn}$, Eq 3 and 4 are applied to the ions Mn$^{++}$ and O$^{--}$ as being identical with MnO. In the ferrous case, however, Eq 5 is eliminated in favor of a corresponding equation involving Fe$^{++}$. This is obtained from the calculations of Chipman and Chang[14] whose Eq 4 follows:

$$Fe \ (liq.) + \underline{O} = Fe^{++} + O^{--} \qquad [10]$$
$$K = \frac{a_{Fe}{}^{++} \cdot a_o{}^{--}}{\% \ O}$$
$$\log K = +6000/T - 2.57$$
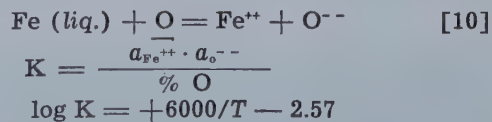
This equation also represents fairly accurately the oxygen distribution data of the present experiments. From it the free energy change of Eq 10 is:

$$\Delta F° = -27,450 + 11.75T$$

We must combine with this another equation from Dastur and Chipman[12]:

$$1/2 \ O_2 = \underline{O}; \Delta F° = -27,930 - 0.57T \qquad [11]$$
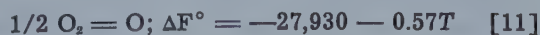
Now bringing together Eq 3, 4, 6, 10 and 11 we have:

$$Mn + Fe^{++} = Mn^{++} + Fe \ (liq.) \quad [12]$$
$$\Delta F^\circ = -30{,}920 + 13.63T$$
$$\log K^{\pm}_{Mn} \ (calc.) = +6760/T - 2.98$$

The line representing this equation is the broken line of fig. 3. The parallel solid line gives our best representation of the data. Its equation is:

$$\log K^{\pm}_{Mn} \ (exp.) = +6760/T - 3.09 \quad [13]$$

**Adjustment:** Eq 8 and 13 differ from the corresponding calculated values by only 0.13 and 0.11 units in log K. The calculated values may be brought into agreement with the observed by an appropriate small adjustment in one of the equations employed. It seems best to make this adjustment by altering Eq 3 so as to obtain full agreement with Eq 13. This is done by numerically increasing the entropy term $4.575 \times 0.11$ or 0.50 units. The adjusted equation is:

$$Mn \ (liq.) + 1/2 \ O_2 \ (g) = MnO \ (s) \quad [14]$$
$$\Delta F^\circ = -97{,}000 + 21.40T$$
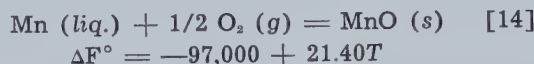
It is evident that the same adjustment is required in Eq 7 and 12 to yield the experimental Eq 8 and 13.

**Manganese Deoxidation:** The maximum content of dissolved oxygen which may be present in equilibrium with slags containing only the oxides of iron and manganese is readily obtained from values of $K_{Mn}$ and $L_o$. From Eq 1 and 2 we have:

$$\% \ O = L_o/(1 + K_{Mn} \ [\% \ Mn]) \quad [15]$$

Using the value of $L_o$ from solubility measurements[8] and of $K_{Mn}$ from Eq 8 we obtain the results shown by the solid lines of fig. 4. These lines and their dotted extensions represent metal compositions in equilibrium with liquid slags containing only the oxides of iron and manganese. On account of uncertainties as to the exact form of the phase diagram for the system FeO-MnO, the exact point at which the solid oxide phase appears is somewhat uncertain. The breaks shown in the curves correspond to points read from the liquidus line of Hay, Howart and White[15]. The broken lines representing equilibrium with solid oxide were not determined experimentally but were computed on the assumption of a constant value of $K_{Mn}$ in the solid solution. Needless to say, their positions are not accurately known.



Fig. 4—Limiting Oxygen Content of Fe-Mn Alloys under Slags Containing only FeO and MnO.

conclusion that the solubility of MnO in the bath is small.

## Summary

New experimental data are presented on the manganese equilibrium in liquid steel under simple slags consisting of the oxides of iron and manganese with small amounts of impurities. The new data lead to values of $K_{Mn}$ which are significantly higher than those of Körber and Oelsen and in general somewhat above those of other investigators.

Thermodynamic calculation from published data at lower temperatures gives results which agree fairly well with the experimental data. An adjusted equation is derived for the free energy of MnO.

The distribution of oxygen between these slags and the liquid metal conforms to the solubility curve of Taylor and Chipman. This confirms Körber's
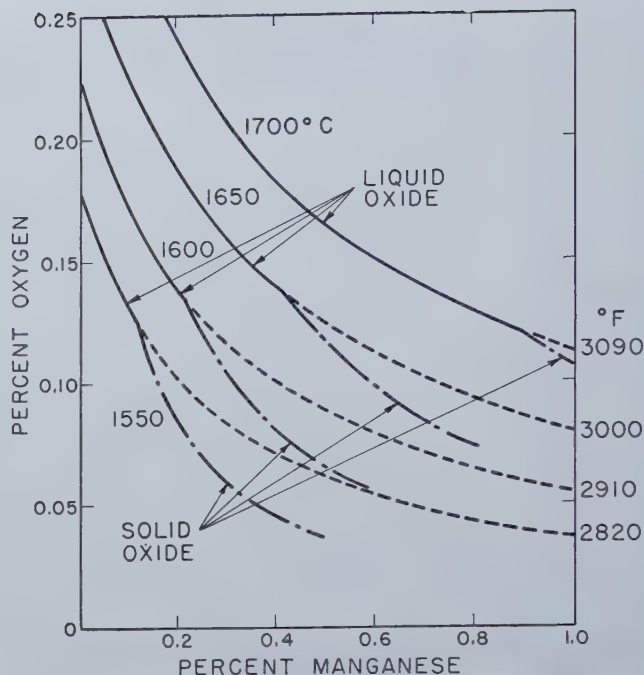
### References

[1] P. Oberhoffer and H. Schenck: *Stahl u. Eisen* (1927) **47**, 1526.

[2] G. Tammann and W. Oelsen: *Archiv. Eisenhuttenwesen* (1932) **5**, 75.

[3] C. H. Herty, Jr.: *Trans.* AIME (1926) **73**, 1107.

[4] F. Körber and W. Oelson: Mitt. Kais. Wilhelm Inst. Eisenforsch., Dusseldorf (1932) **14**, 181. Also F. Körber: *Stahl u. Eisen* (1932) **52**, 133.

[5] W. Krings and H. Schackmann: *Ztsch. anorg. allgem. Chemie* (1931) **202**, 99; (1932) **206**, 337.

[6] T. B. Winkler and J. Chipman: *Trans.* AIME (1946) **167**, 111.

[7] J. Chipman: *Trans.* A.S.M. (1934) **22**, 385.

[8] C. R. Taylor and J. Chipman: *Trans.* AIME (1943) **154**, 228.

[9] J. Southard and C. H. Shomate: *Jnl.* Am. Chem. Soc. (1942) **64**, 1770.

[10] K. K. Kelley, B. F. Naylor and C. H. Shomate: The Thermodynamic Properties of Manganese. U. S. Bur. Mines Tech. Paper 686 (1946).

[11] L. S. Darken and R. W. Gurry: *Jnl.* Am. Chem. Soc. (1946) **68**, 798.

[12] M. N. Dastur and J. Chipman: *Trans.* AIME (1949) **185**, 441. *Jnl. of Metals,* Aug. 1949. TP 2661.

[13] Basic Open Hearth Steelmaking, AIME (1944) 480.

[14] J. Chipman and L. C. Chang: *Trans.* AIME (1949) **185**, 191. *Jnl. of Metals,* Feb. 1949. TP 2529.

[15] R. Hay, D. D. Howart and J. White: *Jnl.* West Scot. Iron Steel Inst. (1933-34) **41**, 97.

# Some Effects of Phosphorus and Nitrogen

## On the Properties of Low Carbon Steel

### by G. H. Enzian

Study of the effects of simultaneous small variations in phosphorus and nitrogen contents on the properties of low carbon steel show that these two elements have concomitant effects. The amounts of both elements present must be known to evaluate properly the significance of a change in either.

THE effects of phosphorus and nitrogen on the properties and behavior of low carbon steels are important considerations to both the manufacturer and the user of such material. For one thing, these two elements are the principal points of distinction between the chemical compositions of Bessemer and open-hearth grades. Further, open-hearth steels themselves may vary considerably in nitrogen content depending on the raw materials and practice used. In addition, appreciable amounts of rephosphorized open-hearth steels are being used at the present time in some low alloy, high strength grades and in certain other cases. For these and other reasons, it was felt desirable to obtain more complete knowledge of the effects of simultaneous small variations in phosphorus and nitrogen content on such properties of low carbon steel as tensile strength, impact toughness, sensitivity to cold work, and strain aging. A long range investigational program designed to furnish such information, was carried out, and the present paper summarizes some of the data currently obtained.

### General Discussion

The strengthening effect of relatively small amounts of phosphorus in steel has been recognized, and to some extent utilized, for many years. A number of investigators have pointed out, from time to time, that under proper conditions of control, phosphorus can be a useful alloying element in low carbon steels.[1-3] Nevertheless, in spite of the volume of data on the subject, the use of phosphorus for this purpose has always been handicapped by widespread feeling that its presence makes the steel brittle, difficult to cold work, and unreliable at low temperatures. This belief on the part of some steel users is not entirely justified in many cases, and often stems from early experience with acid Bessemer steels which have appreciably higher phosphorus (and nitrogen) contents than basic open-hearth grades.

Nitrogen in steel, and its effect on properties, has also received considerable attention in the literature.[4] In 1906, Braune[5] ascribed the brittleness of Bessemer rails to the nitrogen content, and proposed a schedule of nitrogen limits for steels for various uses. This was one of the first papers to recommend directly the use of nitrogen content as a quality control measure, but it did not meet with much favor or support; as a matter of fact, the Jernkontoret was rather sharply criticized for publishing the paper. In the intervening years a number of papers have been published on the subject of nitrogen in steel. As a result, it is now generally recognized that nitrogen can have an important effect on the properties and behavior of steel and that the presence of this element should be considered in any systematic study of factors affecting steel quality.

In 1932, Graham[6] introduced the concept that the quality of various steels could conveniently be evaluated and compared in terms of "sensitivity", which was defined as "the characteristic reaction rate of a piece of steel toward brittleness or hardness." This concept formed the basis for a broad research program into factors causing variations in the quality of commercial steels. At an early stage of this work, it became apparent that the observed effect of either phosphorus or nitrogen on the sensitivity of steel depended, in no small measure, on how much of the other of these two elements was also present. Indeed, the combined effect of phosphorus and nitrogen in steel may often be more important than the specific effect of either. With a few exceptions, it is not possible to predict accurately the effect on steel properties of a change in the amount of either phosphorus or nitrogen in the steel without also specifying the approximate amount of the other element.

It seems desirable, at this point, to discuss briefly the distinction between strain-sensitivity and strain aging as used in this paper. In the early stages of its development, the work-brittleness test[7] (which will be described in more detail later) was used
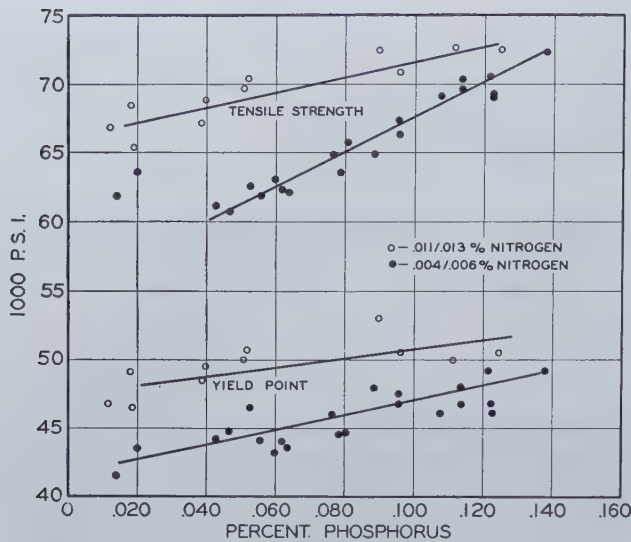
Fig. 1—Effect of Phosphorus on tensile properties.

Note that the effect of increasing phosphorus content on tensile properties is somewhat more pronounced in the low (0.004/0.006 pct) than in the higher (0.011/0.013 pct) nitrogen steels.
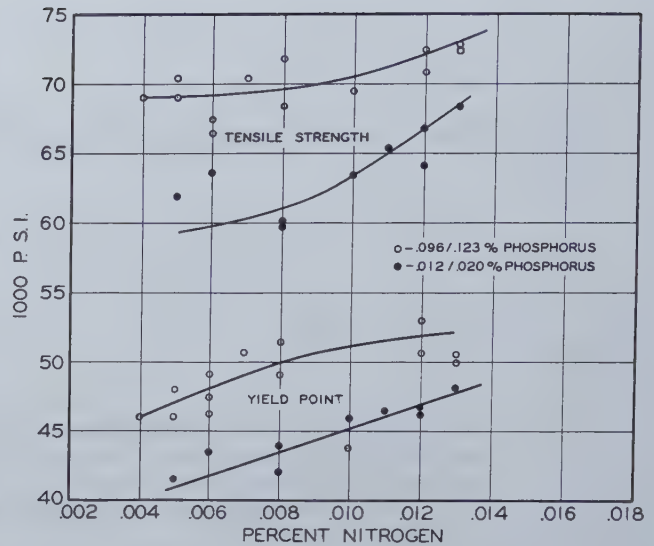


Fig. 2—Effect of Nitrogen on tensile properties.

The effect of nitrogen on tensile properties is similar to that of phosphorus but there is considerable scatter of the individual values.

## Table I. Work-Brittleness Test Results

| Heat No. | P | $N_2$ | Izod Impact—Ft-lb Percent Cold Work | | | | | |
|---|---|---|---|---|---|---|---|---|
| | | | 0 (Unstressed)* | 0.7 | 2.6 | 4.5 | 6.3 | 8.7 |
| A-636 | 0.018 | 0.008 | 97 | 92 | 86 | 79 | 70 | 22 |
| A-637 | 0.018 | 0.008 | 101 | 96 | 92 | 73 | 18 | 8 |
| A-638 | 0.012 | 0.010 | 101 | 100 | 93 | 79 | 11 | 5 |
| A-639 | 0.012 | 0.012 | 102 | 92 | 35 | 25 | 5 | 5 |
| A-640 | 0.018 | 0.013 | 102 | 90 | 26 | 5 | 5 | 5 |
| A-642 | 0.012 | 0.012 | 98 | 92 | 32 | 26 | 13 | 5 |
| A-653 | 0.063 | 0.004 | 100 | 97 | 88 | 81 | 26 | 16 |
| A-654 | 0.043 | 0.005 | 98 | 96 | 88 | 80 | 74 | 17 |
| A-654-2 | 0.053 | 0.005 | 97 | 96 | 88 | 84 | 79 | 28 |
| A-655 | 0.052 | 0.004 | 98 | 98 | 90 | 84 | 51 | 20 |
| A-657 | 0.083 | 0.004 | 99 | 98 | 90 | 20 | 8 | 6 |
| A-658 | 0.096 | 0.007 | 82 | 65 | 29 | 23 | 10 | 3 |
| A-660 | 0.138 | 0.004 | 50 | 33 | 3 | 4 | 4 | 2 |
| A-661 | 0.019 | 0.011 | 102 | 95 | 81 | 27 | 21 | 5 |
| A-662 | 0.040 | 0.012 | 82 | 51 | 29 | 19 | 15 | 4 |
| A-663 | 0.090 | 0.012 | 77 | 38 | 13 | 8 | 3 | 3 |
| A-664 | 0.051 | 0.011 | 84 | 34 | 21 | 3 | 3 | 3 |
| A-666 | 0.099 | 0.010 | 54 | 34 | 20 | 9 | 3 | 3 |
| A-667 | 0.096 | 0.006 | 79 | 54 | 22 | 7 | 8 | 3 |
| A-669 | 0.123 | 0.008 | 34 | 15 | 3 | 3 | 3 | 3 |
| A-671 | 0.096 | 0.012 | 50 | 32 | 7 | 6 | 3 | 3 |
| A-673 | 0.112 | 0.013 | 35 | 11 | 3 | 3 | 3 | 3 |
| A-684 | 0.052 | 0.011 | 72 | 41 | 25 | 10 | 3 | 3 |
| A-685 | 0.122 | 0.006 | 58 | 25 | 6 | 4 | 4 | 3 |
| A-688 | 0.014 | 0.005 | 95 | 95 | 83 | 79 | 73 | 70 |
| A-691 | 0.020 | 0.006 | 94 | 85 | 83 | 72 | 70 | 22 |
| A-692 | 0.123 | 0.004 | 50 | 29 | 3 | 4 | 2 | 2 |
| A-693 | 0.105 | 0.008 | 68 | 71 | 32 | 6 | 6 | 3 |
| A-694 | 0.117 | 0.013 | 42 | 30 | 4 | 4 | 3 | 3 |
| A-696 | 0.039 | 0.012 | 97 | 100 | 32 | 21 | 19 | 8 |

* Unstressed Izod value average of three tests.

to obtain a measure of the susceptibility of a steel to cold-work embrittlement. Specimens were normally tested within a few hours after the cold working operation, although on some occasions a day or two might elapse before testing. As work on the general subject of the effects of cold deformation progressed, it became apparent that an appreciable amount of strain aging might take place with some steels before the specimen could be tested after cold working. Therefore, to minimize variations due to differences in strain-aging rates in different steels, it was felt desirable to subject all tests to an accelerated aging treatment. Thus, the test actually shows the extent of embrittlement resulting from the combination of cold working plus strain-aging embrittlement induced by different amounts of straining. For convenience, however, it has been customary to use the less cumbersome term, "strain-sensitivity", in referring to this behavior.

A test for aging capacity should be used in conjunction with the work-brittleness test in order to obtain an indication of the role of strain aging in the strain-sensitivity of a steel. For example, if the work-brittleness test results on a steel show sensitive behavior and the aging test does not indicate appreciable strain aging, it is then apparent that the embrittlement obtained was due primarily to the effect of cold working. If the test results show both sensitive behavior and high aging capacity, the observed embrittlement must be considered to be the result of both the cold working operation and the effects of strain aging. Although it appears possible that a non-aging steel might be relatively sensitive to cold work, no indications have been

found which would support the possibility of an aging steel being insensitive.

## Material and Methods

To obtain material with varying phosphorus and nitrogen contents but having a uniform history insofar as steelmaking and processing practices were concerned, a number of 25-lb induction furnace heats of the following general ranges of chemical composition were prepared:

**Composition**

| Series | C | Mn | P | S | Si | N$_2$ |
|---|---|---|---|---|---|---|
| P (low N$_2$) | 0.13/0.16 | 0.50/0.60 | Varying 0.015/0.120 | 0.025 max | 0.15 max | 0.004/0.006 |
| PN (high N$_2$) | 0.13/0.16 | 0.50/0.60 | 0.015/0.120 | 0.025 max | 0.15 max | 0.011/0.013 |
| N (low P) | 0.13/0.16 | 0.50/0.60 | 0.015/0.020 | 0.025 max | 0.15 max | Varying 0.004/0.013 |
| NP (high P) | 0.13/0.16 | 0.50/0.60 | 0.095/0.120 | 0.025 max | 0.15 max | Varying 0.004/0.013 |

The heats were made in acid crucibles and the desired phosphorus and nitrogen contents were obtained by blending selected open-hearth and Bessemer scrap. The only additions made to the heats were small amounts of ferromanganese to meet the carbon and manganese specifications, and sufficient ferrosilicon to assure sound ingots in the 3x3 in., big-end-up, hot top molds. It was originally intended that the ranges of phosphorus and nitrogen contents to be studied would encompass the variations normally encountered in low carbon, Bessemer, open-hearth, and duplex steels. This was accomplished reasonably well with the exception of Bessemer-range nitrogen content. It will be noted that the upper nitrogen limit in these induction furnace heats was 0.013 pct; this is somewhat below the normal range of 0.012 to 0.020 pct nitrogen for Bessemer steel. The reason for this limitation is loss of nitrogen in remelting high nitrogen scrap. It was observed that when melting scrap containing less than about 0.008 pct nitrogen there was a tendency for a nitrogen pick-up. With scrap containing more than about 0.012 pct nitrogen, some nitrogen was lost in making the heat. This behavior has been observed by others and has recently been noted by Dickie.[8]

The ingots were rolled in a laboratory mill to 1⅛ in. square bars which were cropped at top and bottom, cut in half and identified as top or bottom sections. These lengths were rolled to ⅝ in. square bars and normalized at 1650°/1675° F before testing.

The composition of the material tested was determined on drillings from the ingot approximately 1½ in. below the hot top portion.

The relative aging susceptibility of the various steels was measured by the increase in tensile strength at 500°F over the room temperature strength. Similar "blue heat" tests have been used by a number of investigators as a rapid means of obtaining an index of strain aging capacity. It has been observed that, with aging steels, the tensile strength at "blue heat" temperatures (400°-500°F) increases appreciably whereas in non-aging or "stabilized" steels, the tensile strength remains substantially unchanged or shows a slight decrease from the room temperature value.[9] This behavior has been explained on the basis that at the elevated testing temperature, strain aging takes place during

the test and the test specimen increases in hardness and strength as it is deformed. The choice of 500° F for the test temperature was an approximation and was selected for convenience.

The strain-sensitivity of the steels was determined using the work-brittleness test in the manner described in a previous paper.[10] Briefly, the test consists of cold drawing a round bar, tapered from 0.450 to 0.475 in. diam, through a 0.450 in. die. The drawn bar, with varying amounts of cold work (0 to about 10 pct reduction in area) along its length, is at 450°F (230°C), and broken in an Izod machine.

Impact toughness was determined using round Izod specimens broken at room temperature in the course of the work-brittleness studies. The amount of material available was insufficient for detailed study of the low temperature impact behavior of these steels.
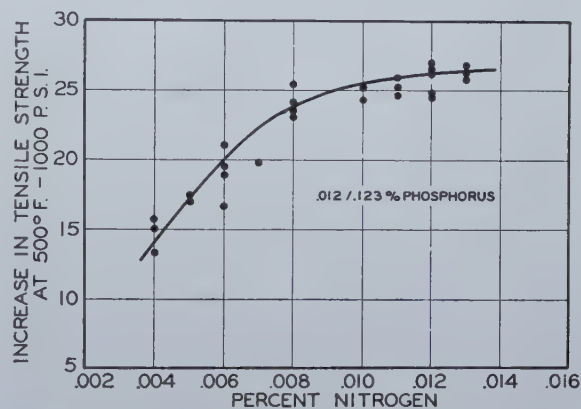


Fig. 3—Effect of Nitrogen on aging behavior.

The change in aging characteristics with change in nitrogen content is most marked below about 0.008 pct nitrogen. Note that data for both high and low phosphorus steels are included in this graph.

Tests were made on top and bottom sections of the heats and check analyses for phosphorus and nitrogen were run for each test. In the case of tensile tests for aging behavior, two specimens were machined from a single short length, one for room temperature testing and the other for testing at 500° F. Millings for check analysis were obtained from material between the two specimens. In the work-brittleness tests, millings were usually taken from that portion of the specimen which was gripped in pulling it through the die and which was between the cold drawn part of the test and the unstressed, or standard, Izod specimen. When additional tests were made on any of the heats, millings for analysis were taken from the broken specimens.

## Test Results

**Tensile Properties:** In order to present the test data conveniently, the heats were grouped into high and low nitrogen, and high and low phosphorus categories and the results have been plotted graphically.

Fig. 1 shows the effect of phosphorus in low (0.004/0.006 pct) and high (0.011/0.013 pct) nitrogen steels. It will be noted that, in general, increasing phosphorus increased the yield point and tensile strength of both the low and high nitrogen steels.
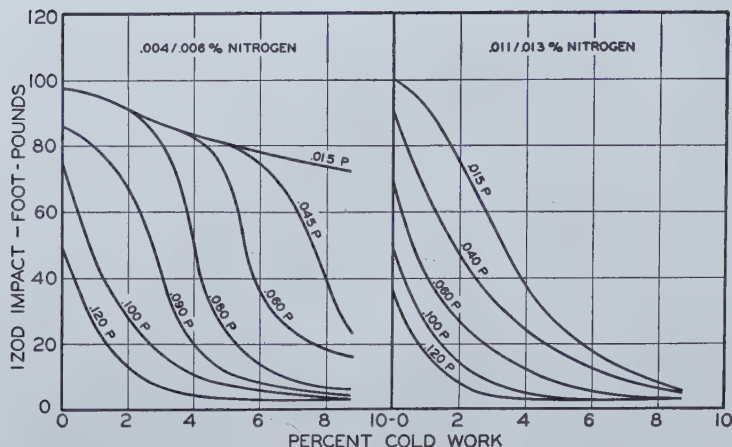
**Fig. 4—Effect of Phosphorus on work-brittleness test behavior.**

Variations in phosphorus from 0.015 to 0.120 pct resulted in a greater change in the reaction of the low nitrogen steels to cold work than similar phosphorus variations in the higher nitrogen material.
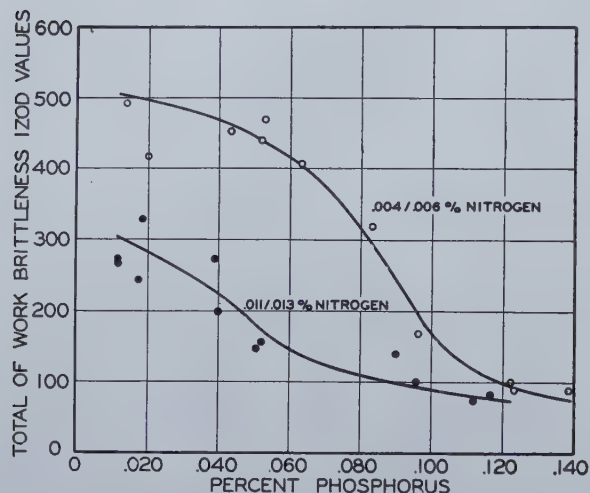


**Fig. 5—Effect of Phosphorus on strain sensitivity.**
These data show that the change in strain-sensitivity with change in phosphorus content, particularly below about 0.120 pct phosphorus, is more marked in low than in high nitrogen steels.

However, it is interesting that in the low nitrogen steels, a definite effect of the phosphorus on the tensile strength was not apparent for amounts less than about 0.050 pct. In the higher nitrogen steels, the data show a progressive increase in tensile properties with phosphorus over 0.020 pct. It is also interesting that, in the low nitrogen steels especially, phosphorus had a greater effect on the ultimate strength than on the yield point. Variation in phosphorus had little effect on the elongation and

reduction in area values for these steels, and the results have not been plotted.

The effect of nitrogen on the tensile properties of low (0.012/0.020 pct) and high (0.096/0.123 pct) phosphorus steels is shown in fig. 2. In general, nitrogen affects these properties in a manner similar to phosphorus. Although the data are limited, the results indicate that variation in nitrogen content in low phosphorus steels results in a somewhat greater change in the yield and tensile strengths than similar nitrogen variations in high phosphorus steels. Apparently, when appreciable amounts of phosphorus are present, the effect of nitrogen on tensile properties is largely overshadowed by the influence of phosphorus. As was the case with phosphorus, variations in nitrogen content had little effect on elongation and reduction in area values.

**Aging Behavior:** Study of strain-aging susceptibility, based on the increase in tensile strength at "blue heat" over the room temperature strength, indicates that phosphorus does not noticeably affect this behavior of steel, the general level of the increase being essentially independent of variations in phosphorus from about 0.012 to 0.120 pct.

The effect of nitrogen on the increase in tensile strength at 500°F is shown graphically in fig. 3; data for both high and low phosphorus steels have been included. Changes in nitrogen content up to about 0.008 pct were accompanied by pronounced changes in aging characteristics but beyond that amount, the increase per unit of nitrogen change became progressively less. These results appear particularly significant since they indicate that

**Fig. 6—Effect of Nitrogen on work-brittleness test behavior.**

In the low phosphorus steels, variation in nitrogen from 0.004 to 0.014 pct changes the reaction to cold work over a wider range than similar nitrogen variations in the high phosphorus material.
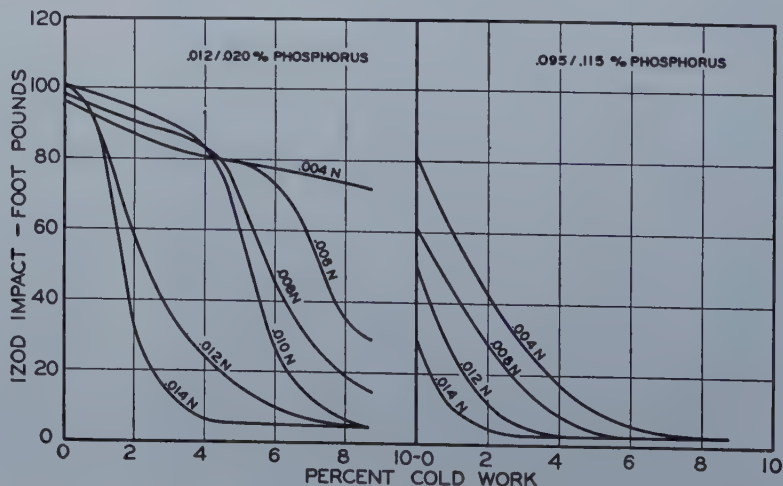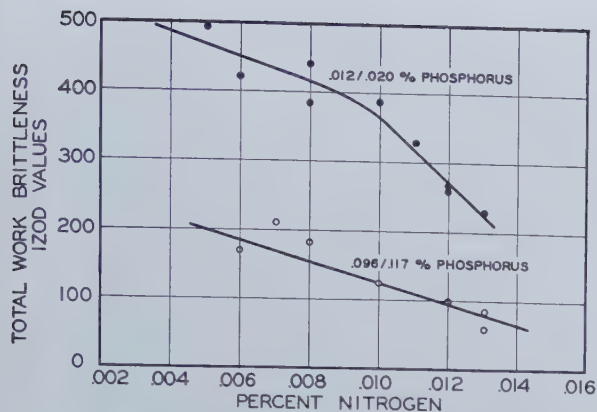
**Fig. 7—Effect of Nitrogen on strain sensitivity.**
In low phosphorus steels the effect of nitrogen on sensitivity is more pronounced when present in amounts greater than about 0.010 pct. Variation in nitrogen content within the limits studied, affects this behavior of high phosphorus steels relatively little.



**Fig. 8—Effect of Phosphorus on Izod impact.**
The amount of phosphorus needed to cause a decrease in Izod toughness depends on the amount of nitrogen present.



**Fig. 9—Effect of Nitrogen on Izod impact.**
The effect of change in nitrogen between 0.005 and 0.013 pct on Izod toughness is dependent on the phosphorus content.

minor variations in the nitrogen content of low nitrogen open-hearth steels result in a greater change in aging susceptibility than similar variations in steels containing nitrogen contents in excess of 0.010 pct.

**Strain-sensitivity:** The work-brittleness test results are listed in table I. Because of the confusing maze of curves which would be obtained if an attempt were made to plot each test, the results were summarized and the effect of phosphorus is shown, schematically, in fig. 4. It is seen in the figure that any generalization on the effect of phosphorus on strain-sensitivity must be qualified according to the nitrogen content of the steel. It will be noticed that with 0.004 to 0.006 pct nitrogen, variation in phosphorus from 0.015 to 0.120 pct resulted in a change in strain-sensitivity covering the full range from exceptionally insensitive to very sensitive behavior. On the other hand, the higher nitrogen steels, even those of low phosphorus content, seemed to be inherently sensitive to cold working, and the change in sensitivity with change in phosphorus covered a somewhat narrower range than was the case with lower nitrogen content.

In order to illustrate the effect of varying phosphorus on strain-sensitivity in a more quantitative manner, the Izod values obtained at each percentage of cold work used in the test, including the unstressed value, were totalled for each work-brittleness test. This method gives a relative measure of the area under the work-brittleness curve and provides a convenient index for expressing the test results as a single number. It is apparent that an insensitive steel will have a high total and a sensitive steel will be low.

The data in table I were totalled in this manner and the effect of phosphorus is shown in fig. 5. This figure shows somewhat more clearly that, in the low nitrogen steels, the change in sensitivity with increasing phosphorus is gradual up to about 0.080 pct and becomes more rapid between 0.080 and 0.120 pct phosphorus. The sensitivity of the higher nitrogen steel is equivalent at 0.015 pct phosphorus to that of the low nitrogen steel with about 0.080 pct phosphorus. At about 0.120 pct phosphorus, the low and the high nitrogen steels are equally sensitive.
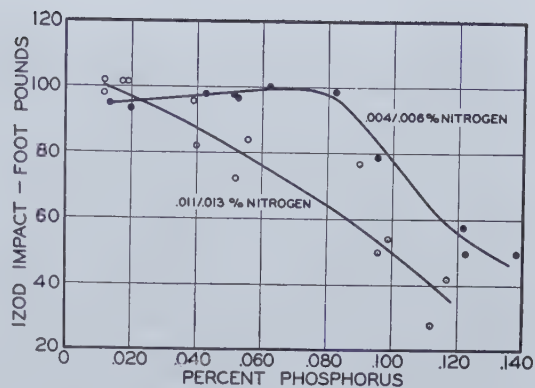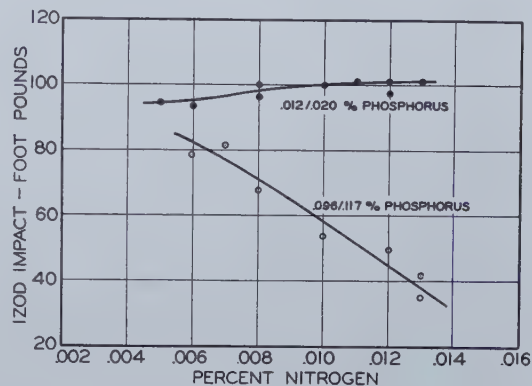
The effect of nitrogen on the work-brittleness of

low and of high phosphorus steels is shown in fig. 6. It is seen that the change in sensitivity with increasing nitrogen covers a wider range in the low phosphorus steel than in the higher phosphorus material. The effect is shown graphically by plotting the total of the work-brittleness Izod values for each specimen against nitrogen in fig. 7. It will be noted that, in the low phosphorus range, the change in sensitivity with increasing nitrogen is not very great up to about 0.009 pct nitrogen. With higher nitrogens, however, the effect is more pronounced, and a difference of 0.001 pct in the nitrogen content results in a marked difference in strain-sensitivity. With phosphorus between 0.096 pct and 0.117 pct, variations in nitrogen content produce a less pronounced change in sensitivity to cold working than in the low phosphorus steels. It would appear from the figure that a high phosphorus steel with 0.004 pct nitrogen is, roughly, equivalent in sensitivity to a low phosphorus steel with about 0.013 pct nitrogen.

**Impact Toughness:** The effect of phosphorus on room temperature Izod toughness is shown in fig. 8. Although it is generally considered that phosphorus contributes to the embrittlement of steel, the amount of phosphorus necessary to cause a drop in impact toughness can be seen to depend on the nitrogen content. With nitrogen in the range of 0.004 to 0.006 pct, phosphorus did not become an embrittling agent until a content in excess of about 0.080 pct was reached. On the other hand, with a nitrogen content of 0.011 to 0.013 pct, the Izod impact toughness fell off continuously with increasing amounts of phosphorus.
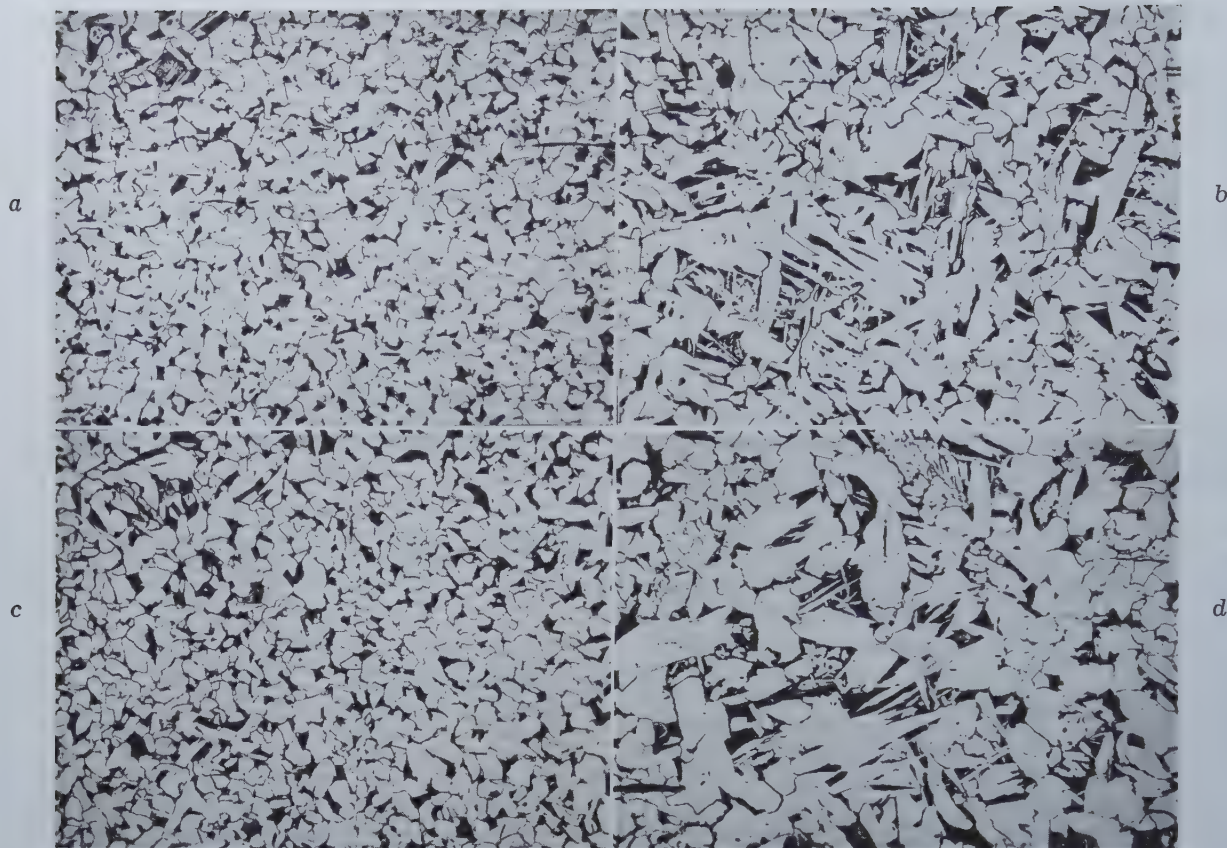
Fig. 10—Effect of Phosphorus and Nitrogen on microstructure.

*a.* Heat A-691: 0.020 pct phosphorus; 0.006 pct nitrogen. *b.* Heat A-685: 0.122 pct phosphorus; 0.006 pct nitrogen. *c.* Heat A-642: 0.012 pct phosphorus; 0.012 pct nitrogen. *d.* Heat A-694: 0.125 pct phosphorus; 0.012 pct nitrogen. Micrographs 100X; etched 4 pct Nital. Normalized 1650°/1675°F. Note the apparent effect of phosphorus on grain coarsening; no noticeable effect of nitrogen. *a* and *c:* low phosphorus. *b* and *d:* high phosphorus. *a* and *b:* low nitrogen. *c* and *d:* high nitrogen.

The presence of appreciable amounts of nitrogen also is generally assumed to result in brittleness of steel, but it was found that the effect of nitrogen, in this respect, depends a great deal on the phosphorus content. This can be seen in fig. 9 where it is shown that, when the amount of phosphorus present was low, increasing nitrogen contents up to about 0.013 pct actually raised the Izod value of these steels. But with steels containing phosphorus within the usual Bessemer range, increasing amounts of nitrogen resulted in a continuous decrease in Izod toughness.

**Microstructure:** Micrographs illustrating the extremes of phosphorus and nitrogen combinations used in this study are shown in fig. 10. All samples were normalized at 1650° to 1675°F. There was no indication of phosphorus banding in any of the samples examined. This may be due to the very rapid rate of freezing obtained in the 3x3 in. molds which, together with the silicon-killed practice, tended to minimize segregation. The only noticeable effect of either element on microstructure was the higher percentage of Widmanstätten structure in the high phosphorus steels. The low phosphorus steels contained only traces of this structure, and no differences in structure due to nitrogen were noted. These results would seem to indicate an effect of phosphorus on grain coarsening, but this possibility has not been thoroughly explored.

**Effect of Deoxidation Practice:** The steels used in the present study were silicon-killed in order that sound ingots would be obtained from the small induction furnace heats. Before concluding, it seems appropriate to mention briefly some of the effects of deoxidation practice on the properties under consideration. This subject has been discussed in more detail in a previous paper,[10] where it was shown that the effect of nitrogen on the strain-sensitivity of undeoxidized (rimmed) steels is, in general, applicable to silicon-killed material, but not always to steels killed with aluminum. When properly made, aluminum-killed steels, whether open-hearth or Bessemer, are insensitive to cold work as measured by the work-brittleness test.[10-12] This effect of aluminum on strain-sensitivity has been associated with the formation of aluminum nitride.[10] However, it still is not known whether the aluminum nitride contributes to insensitivity merely by rendering the nitrogen inactive or whether the presence of the aluminum nitride is actually beneficial.

The effect of aluminum killing on the sensitivity of a low phosphorus steel high in nitrogen could be explained rather easily on the basis of the nitrogen being rendered inactive. Low phosphorus steels are insensitive to cold work when the nitrogen content is low (fig. 6 and 8). Thus, an aluminum-killed, low phosphorus steel high in nitrogen (such as heat E in fig. 2 of the paper by Work and Enzian[10]) has strain-sensitivity characteristics similar to the same steel with low nitrogen content. Application of this reasoning to the high phosphorus steels is hampered by the fact that even with the lowest nitrogen con-

tent available for study (about 0.004 pct), silicon-killed, high phosphorus steels are rather sensitive to cold working (fig. 6 and 7), whereas a similar steel, when aluminum-killed, is insensitive. It may, of course, be possible that a high phosphorus steel containing no nitrogen would be insensitive to cold working even though not aluminum-killed. This is an interesting possibility, but one that requires rather severe extrapolation of the lower curve of fig. 7 which the available data do not appear to justify. Therefore, although the present evidence is admittedly indirect, it seems reasonable to suspect that the effect of aluminum-killing on the properties of low carbon steels probably goes somewhat beyond mere "fixation" of the nitrogen.

It should be mentioned that other deoxidizers, notably titanium and vanadium and some other less commonly used elements, will, under proper conditions, produce results similar to those observed with aluminum. It is known that these elements can also form stable nitrides in steel, and, in this respect, behave similarly to aluminum. Further work on the subject is currently in progress and, with the recent development of an analytical technique which permits determination of the form of nitrogen in steel,[13] it is hoped that these studies will soon lead to a better understanding of the role of nitrogen in steel and the mechanism of control of properties by deoxidation.

## Discussion of Results

Before discussing the results of the present study, it might be interesting to review Stromeyer's[14] observations of forty years ago on the effects of phosphorus and nitrogen in steel. After testing 26 different "qualities" of steels for susceptibility to notch brittleness and aging, Stromeyer, in 1909, concluded: "Nitrogen is a far more dangerous impurity than even phosphorus, and as its determination is a relatively simple matter, no investigation which deals with a steel failure can be considered complete if the percentage of nitrogen has not been determined." In the light of present knowledge, this is, indeed, sage advice even though it has received general acceptance only in recent years. In 1910, Stromeyer simplified some of his previous calculations and reached the more specific conclusion that, by weight, nitrogen was five times as effective as phosphorus in its effect on brittleness.

In a recent study of the properties of a modified, low nitrogen, basic Bessemer steel, Dickie[8] concluded that the basis suggested by Stromeyer was "as good as any, assuming, of course, no fixation of the nitrogen." He reported that the relative merits of the steel in relation to work-hardening susceptibility could be determined using the index (P + 5N) × 1000. He further concluded that the maximum index for capped steel for tube-making is 80. The question of the validity of this empirical quality control index is not within the scope of this paper. However, it should be pointed out that in neither of these references was conclusive evidence provided to support the basic generalization that "nitrogen is five times as effective as phosphorus."

The results obtained in the present investigation indicate that any generalization as to the relative effectiveness of either phosphorus or nitrogen on the properties of low carbon steels would be valid only over a limited range of composition.

The absence of an effect of phosphorus, between 0.012 and 0.120 pct, on aging behavior is of particular significance. For a considerable period of time, it had been felt that strain-sensitivity and strain aging were merely different manifestations of the same basic behavior. However, the present tests indicate that the effect of phosphorus is primarily that of embrittlement by cold working rather than by strain-age embrittlement and that nitrogen in certain forms causes both strain aging and embrittlement during deformation.

The observed differences in the effects of phosphorus and nitrogen, depending on the amount of each present, are of direct practical significance. For example, dephosphorization of Bessemer steel accomplishes relatively little from the standpoint of sensitivity, when the nitrogen content is high. On the other hand, an equal amount of phosphorus reduction in low nitrogen material produces a marked improvement in sensitivity. These results indicate that appreciable quality advantages could be realized from the development of blowing practices to produce low nitrogen Bessemer steel having a phosphorus content less than about 0.080 pct. The same data can also be used to show that rephosphorizing open hearth grades to phosphorus contents higher than about 0.070 pct results in an abrupt increase in sensitivity. These phosphorus changes likewise have significant effects on the tensile properties. With low nitrogen content, appreciably greater softening is obtained per unit of phosphorus removed than in high nitrogen steel. Similarly, in rephosphorizing open-hearth steel, the tensile strength increases rapidly above about 0.060 pct phosphorus.

The data show that reduction of the nitrogen content of acid Bessemer steel can be expected to produce a relatively slight improvement in sensitivity as compared to the advantage gained in a basic practice. It is also shown that the nitrogen content of duplex practice open-hearth steels is a significant factor, although the change in sensitivity with a given increment in nitrogen is less pronounced below about 0.010 pct nitrogen than above. From the standpoint of strain aging behavior, however, the most significant range is below about 0.009 pct nitrogen.

Deoxidation with aluminum and certain other elements has been shown elsewhere to alter the effects of phosphorus and nitrogen observed in silicon-killed, capped, and rimmed steels. Little work has been done on determining the extent to which aluminum deoxidation restrains the embrittling effects of other elements such as arsenic. It should also be mentioned that variations in the amounts of carbon, manganese, sulphur, etc. present may have some influence on the effects of phosphorus and nitrogen. As more work is done in this field, certain aspects of inter-relationships between constituents become clearer, but at the same time new questions arise. Further study is indicated to explain more fully the various factors affecting brittleness in mild steel.

## Summary and Conclusions

Study of the tensile and impact properties, sensitivity, and strain aging of a number of induction furnace heats containing varying amounts of phosphorus and nitrogen has brought to light several interesting and important facts concerning these

two elements in low carbon steel. Although the effect of one in the absence of the other has not been determined, there are indications that phosphorus and nitrogen exert additive effects and, with the exception of strain aging behavior, the relative amounts of both elements must be considered in evaluating either. In the case of strain aging, phosphorus apparently contributes so little that the aging behaviors of high and low phosphorus steels with the same nitrogen contents are virtually indistinguishable.

Based on the results of this study, it may be concluded that, from a practical standpoint:

1. Nitrogen variations in low phosphorus steel have a greater effect on its properties than similar variations in high phosphorus material.
2. Phosphorus variations in low nitrogen steel produce a greater change in properties than similar variations with high nitrogen contents.
3. Deoxidation with aluminum, and certain other elements, alters the above observations. Thus, the degree of nitrogen "fixation" is of importance and must be known for intelligent evaluation of steel quality based on chemical composition. Recent developments in the field of analytical chemistry indicate that such determinations are now within the realm of practicability.

**Acknowledgment**

**References**

[1] Report of the Joint Committee on Investigation of the Effect of Phosphorus and Sulphur in Steel: *Proc. A.S.T.M.* (1934) **34**, Part 1, 113.

[2] H. W. Gillett: Metals and Alloys, (1935) **6**, 280, 307.

[3] C. H. Lorig and D. E. Krause: Metals and Alloys (1936), **7**, 9, 51, 69.

[4] Sixth Report on the Heterogeneity of Steel Ingots (1935), 121. Bibliography on Nitrogen in Iron and Steel, 1887-1934.

[5] H. Braune: Jernkontorets Annaler (1906) **59**, 565.

[6] H. W. Graham: Yearbook, Amer. Iron and Steel Inst. (1932), 59.

[7] H. W. Graham and H. K. Work: *Proc. A.S.T.M.* (1939), **39**, 571.

[8] H. A. Dickie: *Jnl.* of The Iron and Steel Inst. (1948) **159**, No. 4, 360.

[9] R. L. Kenyon and R. S. Burns: *Proc. A.S.T.M.* (1934) **34**, Part 2, 48.

[10] H. K. Work and G. H. Enzian: *Trans.* AIME (1945) **162**, 723.

[11] H. W. Graham and S. L. Case: U. S. Pat. 2,174,740 (Oct. 1939).

[12] E. C. Wright: *Trans.* AIME (1944) **158**, 107.

[13] H. F. Beeghly: The Determination of Aluminum Nitride Nitrogen in Steel. Paper presented at 116th Meeting of the Amer. Chem. Soc., Sept. 19, 1949.

[14] C. E. Stromeyer: *Jnl.* of The Iron and Steel Inst. (1909) **79**, No. 1, 404; (1910) **81**, No. 1, 679.

# Special Mounting Techniques

## by Earl C. Roberts

TO facilitate some recent microscopic investigations it was necessary to devise special mounting techniques for the polishing of two quite different metallographic specimens. These techniques are extremely simple and are submitted for whatever value they may be to other investigators.

The first specimen mount proved very satisfactory for the study of untempered martensite. Since it was undesirable to heat the specimen, lucite or bakelite mounting materials could not be used in the conventional manner. A cold mount was made by drilling a hole of the same diameter as the specimen in a cylindrical piece of polystyrene then pressing the steel specimen into the hole on an ordinary vise. A prefabricated disk of lucite should work equally well. The only precautions necessary are that the hole be drilled out cleanly and the piece

*EARL C. ROBERTS, Junior Member AIME, is Research Assistant in Metallurgy, Massachusetts Institute of Technology.*

*Technical Note No. 34 E. Manuscript received Nov. 23, 1949.*

of steel be pressed into the plastic uniformly, otherwise the mount will crack.

The second type of mount was required for the study of slag specimens by reflected light. Mounting these specimens in bakelite and then attempting to rough finish the surfaces on graded emery papers resulted in a considerable amount of chipping and breaking out of the slag particles. This made further satisfactory polishing almost impossible. It was found, however, that if the bakelite-mounted specimen was first rough finished to a point where a good specimen surface became visible, the interstices in the specimen surface could be filled and the polishing completed. This filling was accomplished by placing a small amount of lucite powder in the bottom of the steel specimen mold then reinserting the bakelite-mounted specimen on top of the lucite powder. Reheating the mold to the proper temperature and applying the required pressure resulted in the formation of a thin disk of lucite on the bottom of the bakelite specimen. By carefully grinding the lucite away a uniform surface including the slag specimen was obtained and further polishing was unhampered by slag disintegration.

# Microstructure of Iron Silicon Alloys

## As Developed by the

## Powder Metallurgy Process

### by R. Wachtell

This paper attempts to present, by means of a succession of micrographs, a literal picture of a portion of the diffusion process occurring in iron-silicon powder compacts. It discusses the metallographic characteristics of Fe-Si alloys (especially in the 6 pct Si range), compounded by the powder process, and describes various misleading pseudomorphic structures encountered in microscopic investigation. An etch is described which indicates Si content within certain rather wide ranges.

IN order to study better the phenomena at work in various phases of diffusion of the Fe/Si system when compounded and alloyed by powder metallurgy methods, several attacks have been planned. Electrical, hardness and other measurements have been discussed elsewhere.[1,2] The metallographic phenomena will be considered here.

Concerning the metallography of the ferrosilicon alloys, some initial discussion is in order. As this laboratory discovered to its chagrin, there are many traps that lie in wait for even the experienced metallographer when he deals with alloys of high silicon content. Chief of these is probably the anomalous behavior of these materials under conventional etching techniques.

We have before us, for instance, Corson's paper[3] of 1928, wherein is mentioned and illustrated (probably for the first time) the peculiar "barley shell"

---

R. WACHTELL is associated with American Electro Metal Corporation, Yonkers, N. Y.

---

structure sometimes found in these alloys. Again in 1941[4] the same author reports the structure in 5-14 pct silicon irons. Houghton and Becker mention its presence[5] but make only tentative effort to explain it. In 1943, Hurst and Riley[6] discussed the "barley shell" and declared it to be a false structure, resulting from the peculiar and characteristic film-forming propensities of the alloy. At about the same time, Wrazej[7] proved correct the contentions of Hurst and Riley, establishing pretty well the mechanisms of formation and identifying the constituents involved.

Hurst and Riley[6] also describe in their paper (1943) a "cracked film" structure, also a pseudomorph, the precise nature of which they do not suggest. Careful examination of such a film reveals that it not only cracks but begins to curl away from the

surface of the metal and peel, much in the manner of flaking paint. The careful microscopist will be able to focus on the topmost edge of the flake, and, by optical sectioning, follow it down to the metal surface. We have been able, by oblique illumination of such specimens, to observe the raised segment of the film, the shadow that it casts, and the mating segment on the metal into which it fits. As late as 1946, Hurst and Riley[8] found occasion to correct misinterpretation of this "cracked film" structure in a work by others on a 12 pct Si/Fe alloy.

The "barley shell" and "cracked film" pseudomorphs are not the only ones encountered in studies of these materials. A third pseudomorph, which may, however, have some structural significance is a fine striation of the surface. Closely spaced and parallel striae extend entirely across single grains. Each grain shows a different direction for the striae, and different closeness of the spacing. The regularity of this structure, and the fact that the striae do not cross from one grain to another, suggest that the structure is a film cracking controlled in some way by the crystal plane orientation of the surface being etched.

In general it is wise for the metallographer dealing with these alloys to cultivate a feeling of uncertainty not only of the more complex questions of interpretation, but also of the basic question of whether that which he sees is indeed a true representation of the structure. We have taken, as a first test of the validity of a structure, its reproducibility "in situ" after repolishing and re-etching of the samples. Thus we knew the "barley shell" to be false (fig. 1) even before encountering the definitive works on the subject.

**The Metallography of Silicon Diffusion in Laminate Bars:** As a first step in the study of the metallography of the diffusion process, we have pressed a series of laminate bars. These bars, or "sandwiches" as we have termed them, were pressed with covering layers of iron powder, and a "filler" of the Fe/Si master alloy under study. Bar dimensions were approximately ½ x 3 x ¼ in. The total
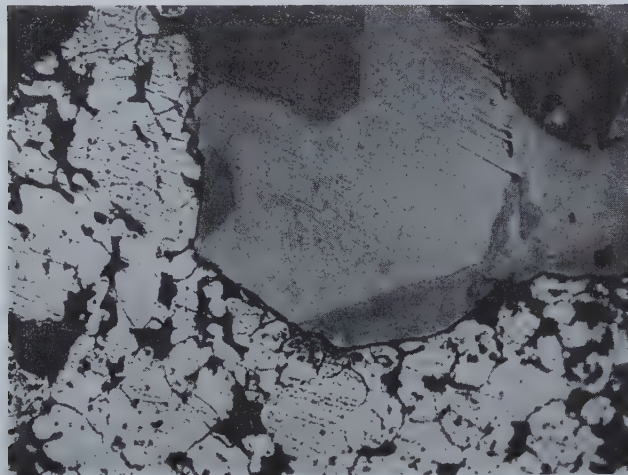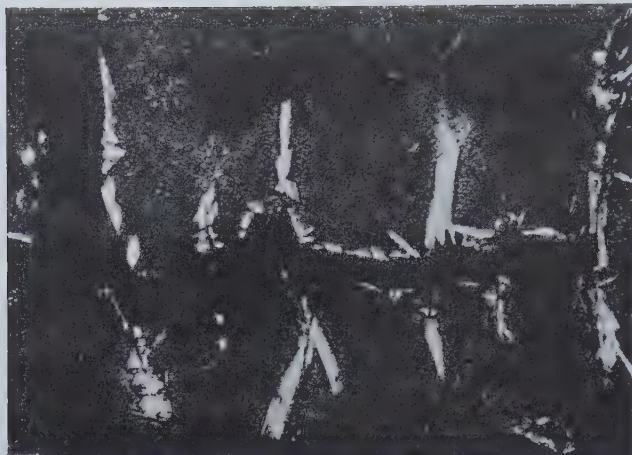
**Fig. 1 (top)—10 pct Silicon-Iron alloy homogenized by 9 hr of sintering at 1180°C.**

Iron fluoride crystals which constitute the "barley shell" pseudomorph nucleate first at any surface discontinuity. Grain boundaries, cracks, pores, etc. are therefore preferred sites. If etching is continued, the entire surface is covered with "barley shell". Re-etching after a re-polish results in different crystal deposit patterns. X300. Etchant: 15 pct HF, 15 pct HCl, 70 pct Picral.

**Fig. 2 and 3—Diffusion process in laminate bar 75/25 Fe/Si master alloy, end composition 10 pct Si.**

Fig. 2 (center)—Interface of master alloy powder with iron powder. Condition: As hot pressed (1080°C). X500. Picral etch.

Fig. 3 (below)—Interface of same laminate bar shown in fig. 2 after sintering 25 min at 1180°C. X300. Picral etch.
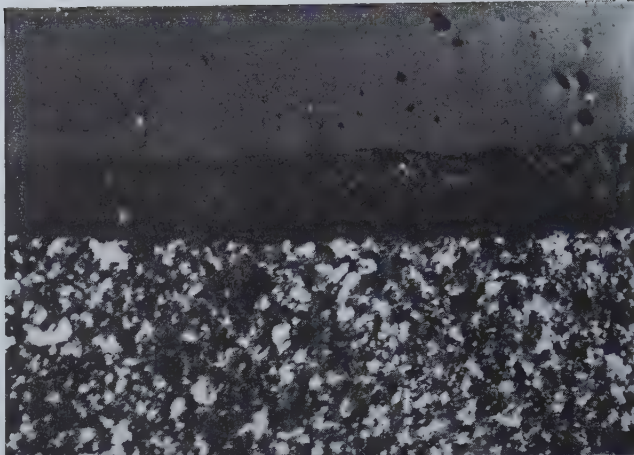


**Fig. 4 and 5—Diffusion process in laminate bar 75/25 Fe/Si master alloy, end composition 10 pct Si.**

Fig. 4 (above)—Interface of laminate bar showing the effect on the pearlite of diffusing silicon. The specimen shown is the same one illustrated in fig. 3 (hot pressed, plus 25 min sinter). X100. Nichols partly crossed. Picral etch.

Fig. 5 (below)—The same laminate shown in fig. 2, 3, 4 after an additional 9 hr of sintering at 1180°C. An interface no longer exists. The entire compact presents this uniform substantially single phase ferritic structure.

amounts of powder used were adjusted to yield a final analysis of given type. Some specimens were hot pressed (1080°C), some cold pressed, and all were sintered for varying lengths of time. After each of the sintering stages, a segment of the bar was removed for microexamination, and the balance of the bar returned for further sintering. The types of material used are listed in table I.

Let us consider the microstructure developed in these laminate bars. Fig. 2 shows the interface of a hot pressed bar compounded of 75/25 ferrosilicon master alloy. The lack of diffusion between the iron grains and the large ferrosilicon particle is quite evident. Fig. 3 shows this interface after a 25 min sinter at 1180°C. The initial site of the iron powder within the compact is outlined by the extent of its characteristic porosity, which persists to the line of the more completely densified zone at the upper portion of the figure. Above this densified zone (and out of the field of this figure) is a zone of unconsolidated individual Fe/Si powder particles. An interesting, albeit confusing, element is added to the picture in the form of carbon incorporated either in the powders themselves, or picked up from the graphite dies during hot pressing. Fig. 3 shows clearly the pres-
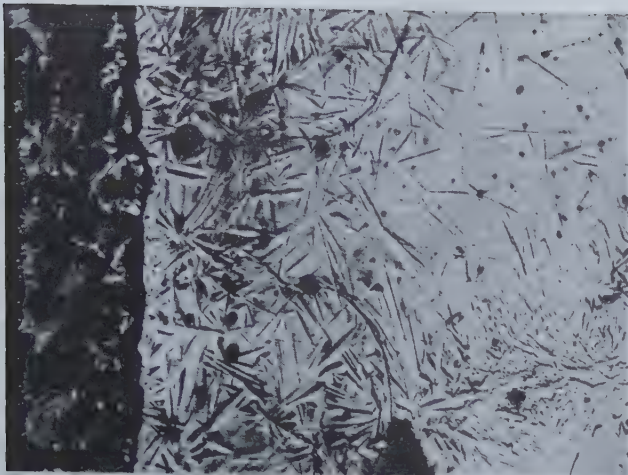
**Fig. 6 and 7—The "Barley Shell" etch as used to indicate Silicon diffusion in Iron.**

Fig. 6 (above)—The effect of the "Barley Shell" etch when applied to the specimen illustrated in fig. 3, 4.

Fig. 7 (below)—The effect of the "Barley Shell" etch on that zone of the same laminate (fig. 3, 4, 6) but at the interface with unconsolidated and undiffused master alloy particles at the center of the bar.

**Fig. 8 and 9—Diffusion process in 6 pct Silicon-Iron compacts, as hot pressed from Iron and 75/25 Fe/Si master alloy powders.**

Fig. 8 (above)—The dark areas in this micrograph are pearlite colonies, the lamellae unresolved at the low magnification used. The light areas are diffusing Fe/Si particles. X100. Alcohol/Iodine etch.

Fig. 9 (below)—The specimen of fig. 8 etched with the "Barley Shell" etch. The pearlite colony has been severely attacked, and no detail remains. X500. Etchant: 15 pct HF, 15 pct HCl, balance 4 pct Picral.

ence of pearlite in the iron powder. It also shows clearly its absence from the densified zone, the area immediately below it, and its progressive elimination from the zone of partial diffusion adjacent to the iron powder. Taking advantage of the behavior of pearlite in polarized light, the micrograph in fig. 4 has been taken (nichols crossed), showing the dramatic effect on the pearlite of the advancing silicon layer. Ihrig[9] has shown that carbon rejected by the iron as it absorbs silicon (during siliconizing) piles up in the zone under the silicon boundary, and gives analyses of turnings to demonstrate this. This pattern of pearlite buildup is plainly visible in the laminates after longer sintering times.
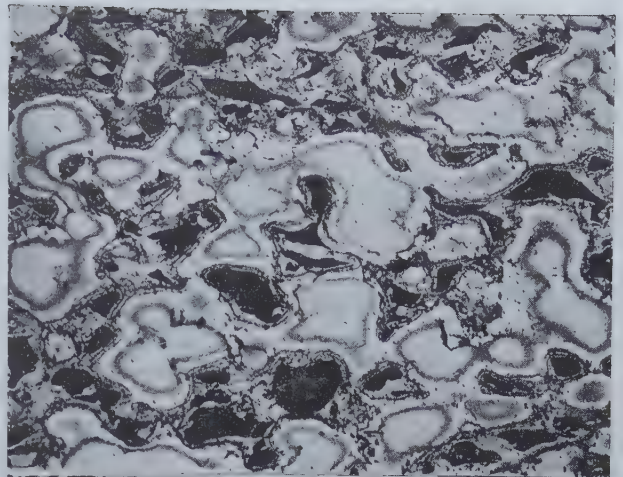
The cold pressed specimens show, after 25 min sintering, a similar pattern to the as hot pressed compacts. After long sintering (9 hr) even the laminate bars present a large grained substantially single phase structure (fig. 5) throughout.

In tracing the pattern of diffusion, a use has been found for the "barley shell" structure of Corson. This hinges upon the fact that the "barley shell" can be produced, according to Corson, at from 5-14 pct Si, and most easily forms at from 8-10 pct Si. Thus, although Wrazej has produced these markings on pure iron, by etching with 1:1 HF and saturated picral, we find, with Corson, a strong difference in the tendency to form "barley

**Table I. Types of Material Used**

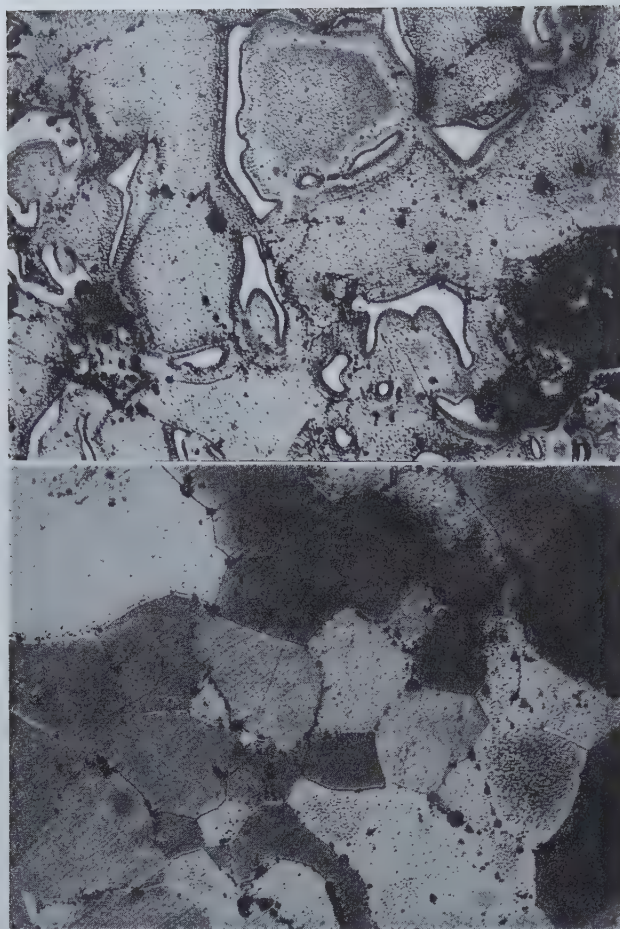| | Typical Analysis, Pct | | | | | | | | |
|---|---|---|---|---|---|---|---|---|---|
| Powder Employed | Fe | Mn | Ni | Cr | C | Al | Ca | Si | Wt. Loss in $H_2$ |
| Electrolytic iron<br>Fe-Si (85/15)<br>Fe-Si (75/25)<br>Silicon | Bal.<br>83.1<br>74.0<br>0.82 | 0.6 | 0.3 | 0.2 | 0.004<br>0.70<br>0.03<br>0.10 | 0.3<br>0.75 | trace<br>0.25 | 15.4<br>25.2<br>97.6 | 0.65 |

**Fig. 10 and 11—Structures of 6 pct Si. Compacts hot pressed from Iron and 75/25 Fe/Si master alloy powders, and sintered for varying times.**

Fig. 10 (above)—After a 25 min sinter at 1140°C, the structures shown in fig. 8, 9, are altered to that shown above. The carbide-like phase forms a grain boundary constituent in most of the compact, some graphite appears, and only occasional patches of pearlite may be found. X500. Picral etch. Fig. 11 (below)—After a total of 12 hr of sintering, the intergranular phase (fig. 10) is virtually eliminated from the microstructure. X500. Picral etch.

**Fig. 12 (above)—6 pct Silicon alloy as hot-pressed from pre-homogenized powder.**

X500. Picral etch.

**Fig. 13 (below)—Hot pressed (upper), and hot pressed plus a 25 min sinter at 1180°C (lower) compacts.**
These are compounded of pure Fe and pure Si, end composition 50 pct Fe, 50 pct Si. X100. Picral etch.

shell" markings, depending on the Si content present. Fig. 6 and 7, are micrographs of the diffusion zone of the same laminate illustrated in fig. 3 and 4 after etching with a "barley shell" producing etch. The abrupt cessation of the barley shell where the diffusion zone contacts the unconsolidated master alloy powder (fig. 7) is plainly evident, especially in the small particle in the middle of the field. A compact compounded with 85/15 master alloy shows the barley shell even in the undiffused Fe-Si powder at the center of the laminate. Therefore we may say that this etch* delineates barley shell in a range

_____
* The etch used in producing these structures consisted of 15 pct HF, 15 pct HCl, balance 4 pct picral.

of Si composition whose upper limit is above 15 pct Si, but lower than 25 pct Si, and whose lower limit lies below 6 pct Si.

Interpretation of the structures observed must be conditioned by several factors. If the implications of Ihrig's data regarding carbon migration may be accepted at face value, then the structures obtained will be substantially carbon-free where the diffusing silicon has pushed the carbon back (or perhaps more correctly, has permitted the diffusion to pro-
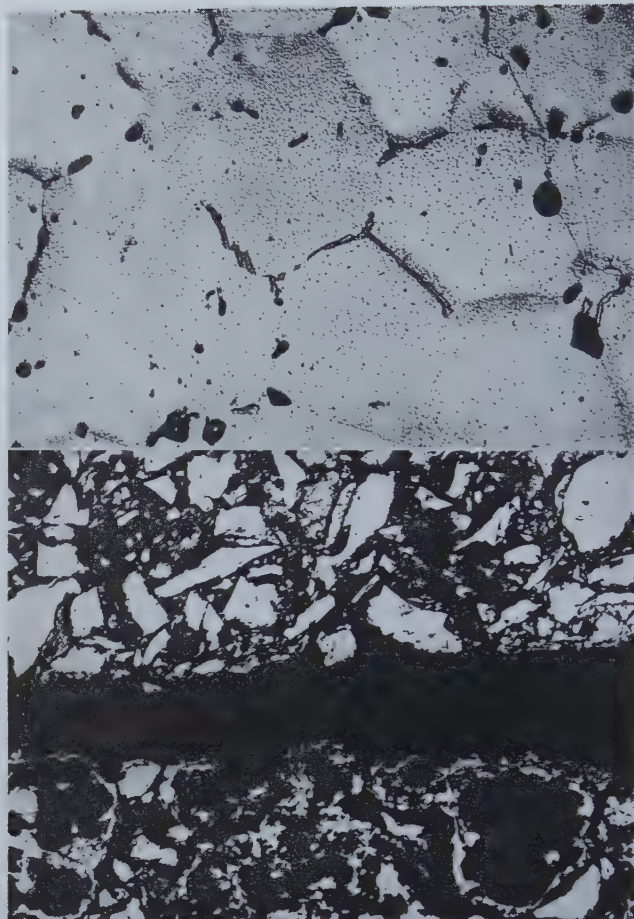
ceed only in one direction because of the low carbon solubility in the silicon-containing areas). Yensen[10] gives a solubility limit (in ferrite) of 0.007 pct for carbon in alloys of 4.7 pct Si and above; a value perhaps not inconsistent with Ihrig's 0 pct, probably analyzed by cruder methods.

Under these circumstances, with carbon largely eliminated as an interfering phase, one may follow the iron-silicon binary with reasonable security.* The system, up to about 15 pct Si, falls within the single phase ($\alpha$) (ferritic) region.

_____
* When we speak of the iron-silicon system, the terms are not nearly so rigid and well determined as one might expect for a relatively common and much-used alloy. There is still considerable variation in thought as to what constitutes the correct constitution diagram, especially at high silicon content (over 15 pct in Si content). There is general agreement, however, that the gamma loop is closed at about 4 pct Si, and that a single phase ($\alpha$) structure obtains to about 15 pct. Some workers show an ordered structure (superlattice) occurring in the $\alpha$ region at about 12.5 pct Si, a contention with which we are in agreement.

In a private communication, Dr. J. T. Norton has informed us that he finds unmistakable evidence of ordering in an X ray study of 12.5 pct Si samples, in confirmation of resistance data and hardness changes as developed by Glaser and Corson. In addition, the work of Farquhar, Lipson and Weill[11] establishes ordering, first visible in their X ray pattern at about 6.7 pct of Si.

In the "sandwiches", therefore, we have, adjacent to the 75/25 master alloy, a region of silico-
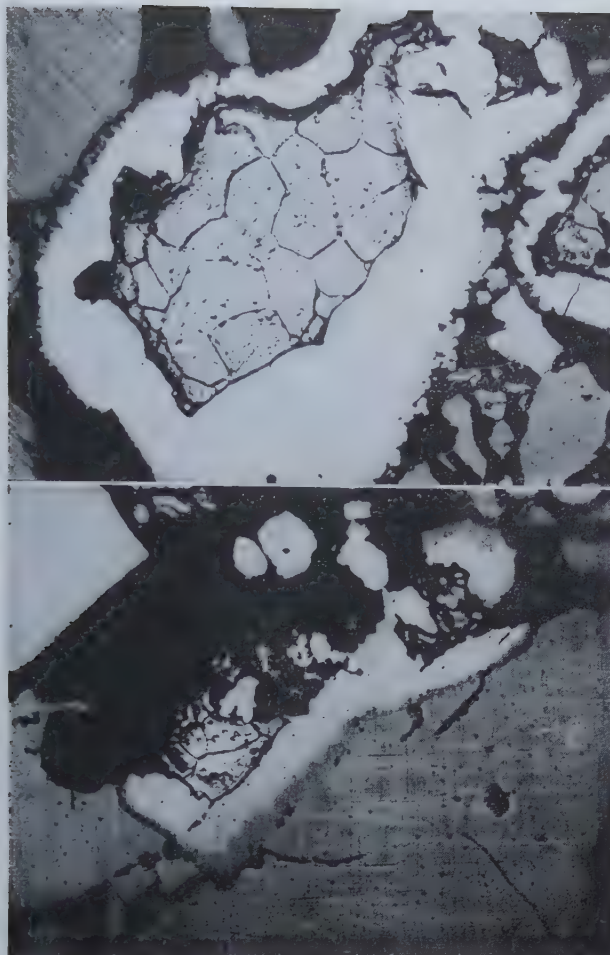
Fig. 14 and 15—Diffusion of Iron and Silicon in
hot pressed compacts of pure Fe and pure Si, end
composition 50 pct Fe, 50 pct Si.

Fig. 14 (above)—Diffusion of Si into Fe particle. X500. Picral
etch.

Fig. 15 (below)—An exceptional case, in which the diffusion
zone is intact and grades continuously from pure Si (lower
right) to relatively pure Fe at the center. X500. Picral etch.

ferrite varying from about 15 pct Si, at its upper
point to about 4.7 pct at that point in the structure
(fig. 3), where the secondary phase (carbide?) be-
gins to appear. At about 4 pct Si, again according
to Yensen,[10] carbon goes into solution up to about
0.02 pct; from 0.02 to about 0.10 pct it is precipitated
as carbide. It appears to be the area of carbide pre-
cipitation occurring at 3.7 to 4 pct Si content, that is
outlined in the zone of fig. 3 under discussion. No
graphite has been observed along the diffusion
line of the laminates. Presumably the high solubility
of carbon in the pure iron is responsible for its
absence.

**The Metallography of Silicon Diffusion in Com-
pacts of Mixed Powder:** An essential difference
occurs in the diffusion process where the powders
have been mixed in the conventional manner, rather
than pressed as laminates. Here, as Si diffusion oc-
curs, the carbon migration can proceed only inward
into the iron grain, since each iron grain is more or
less isolated from its neighbors. Fig. 8 and 9 show the
structure developed in a 6 pct Si alloy, compounded
of 75/25 master alloy powder, in the "as hot pressed"
condition. Considerable diffusion, it will be seen,
has already occurred. This is a situation which did
not occur in the laminate illustrated. It will be
seen in fig. 2 that the hot pressed laminate shows

no diffusion of Si into the iron powder. Although the
precise reason for this is not entirely understood
at this time, one explanation suggesting itself is
that temperature control during hot pressing (man-
ual, with the aid of an optical pyrometer sighted
upon the outside of the graphite die), is sufficiently
inexact to permit moderate fluctuation of the press-
ing temperature from specimen to specimen. This
would be very important where hot pressing is in
the region of formation of a liquidus, which, in a
master alloy of 75/25, would be reached at about
1190-1200°C. This does not seriously alter the
micromechanics of the diffusion process, but simply
retards it. Thus a specimen which has failed to
diffuse in hot pressing will reach the condition nor-
mally associated with that state after about 25 min
of initial sintering time.

At higher magnification the rejection of carbon as
pearlite in the center of the iron particles is easily
seen. Etching with barley shell-producing etch gives
the results shown in fig. 9. The original Fe-Si grains
are reduced to about 15-20 pct Si, the areas im-
mediately surrounding the pearlite colonies have
too little Si to yield a barley shell, i.e., between 5
and 0 pct Si — probably from 3.5-4 pct, since traces
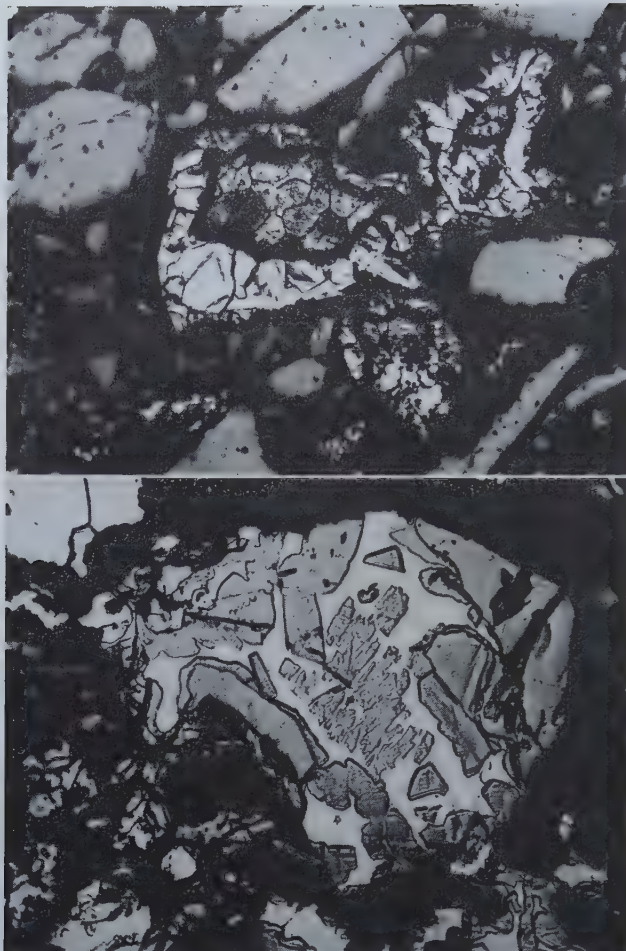of carbide appear.

Fig. 16 (above)—The result of application of the
"Barley Shell" etch to diffusion structures in hot
pressed pure Fe/Si mixtures.
(See fig. 14). X300. Etchant: 15 pct HF, 15 pct HCl, balance
4 pct Picral.
Fig. 17 (below)—A 25 min sinter produces this
effect in the hot pressed compacts of pure Si/Fe
mixtures.
X500. Picral etch.

It can be seen readily that continuing diffusion of
silicon will cause precipitation of carbide and/or
graphite in a site roughly along the axis of the exist-
ing pearlite colonies. This does in fact occur. Fig.
10 is a micrograph illustrating the microstructure
of the same compact after a 25 min sinter at 1140°C.
An intergranular carbide-like phase is abundant,
forming a grain boundary constituent in much of
the specimen. Some graphite is also present, and
scattered remnants of pearlite colonies can be ob-
served.

A few words of comment must be devoted to the
"carbide-like phase" mentioned. Hurst and Riley[12]
discuss a "cementite-like phase" occurring in higher
silicon (10-15 pct) cast irons, which, to judge from
their photographs, (their fig. 2), strongly resembles
the phase here under discussion. Hurst and Riley
report that an alkaline picric acid etch failed to
blacken their "carbide" phase, thus confirming a
prior observation of Kriz and Poboril,[13] who sug-
gested that perhaps silicon in solution in the carbide
phase had modified its behavior toward the etch.
Our own test indicated that the "carbide" phase in
fig. 10 darkens when etched with the alkaline sodium
picrate etch. Some minimal silicon content may be

necessary to confer upon the carbide the etch resist-
ance discussed above. Such an assumption seems not
unreasonable. Anomalous behavior (for a carbide)
was observed in testing the hardness of this con-
stituent. Tests with an Eberbach microhardness
tester, using a 27 g load, indicate a hardness aver-
age of $VPN_{25}$ 325 for observations on different car-
bide particles. Avery[14] has reported microhardness
values for a number of different types of carbide,
the lowest value reported being $VPN_{25}$ 885. This
great difference in hardness must necessarily cast
some doubt on the identification (admittedly incom-
plete) of this phase as a carbide phase, or at least
invests it with some unusual properties for a carbide.

Further sintering of this compact produces a
structure as shown in fig. 11. Substantially a single
phase alpha (ferritic) structure is attained. Porosity
and inclusions (mostly oxides and silicates) persist
to some degree. It is interesting to note that if a
fully diffused compact is crushed and then re-hot-
pressed, a compact immediately results which com-
pares favorably in microstructure with those of long
time sintering. Fig. 12 shows a 6 pct Fe/Si alloy
made from such a pre-homogenized powder in the
"as hot pressed" condition. There remains a small

amount of "carbide" phase, but the structure is, again, predominantly single phase alpha. It is of some significance that resistivity measurements[1, 2] made upon such compacts give values identical with those found in mixed powder compacts sintered for 12 hr or more.*

The implications are, of course, that with some refinement of technique it may be possible to hot press these alloys without the need for long homogenizing treatment, and the virtually unavoidable difficulties of shrinkage and other dimensional changes which accompany such a process may be eliminated. All alloys discussed are quite brittle, and present no problem in pulverizing.

Certain interesting phenomena were observed in hot pressing powders compounded of pure silicon and pure iron. Compacts made from these powders are prone to "blow up" in initial sintering, even after hot pressing. Fig. 13 incorporates two specimens mixed from pure Si and pure Fe powders, end composition 50 pct Si. The specimen on the top is in the "as hot pressed" condition; the specimen on the bottom is shown after 25 min of sintering at 1180°C. The "blowing up" effect is plainly visible in the microstructure, especially the formation of characteristic blisters — several of which are plainly visible, in section, in the micrograph.

The diffusion of pure Si into Fe can be observed in studies of these compacts. Fig. 13 (upper) shows an area in the hot pressed specimen including silicon grains, iron and iron/silicon diffusion zones. The specimen has been etched in picral, and the iron powder has been most heavily attacked. The silicon particles may be identified by their characteristic angular contour, as well as their resistance to etching. That area of the iron grains into which Si has diffused is also resistant to etch attack, but the rounded outline of the iron particle persists. Fig. 14 illustrates the case of an iron particle, partly diffused with Si. An Si particle may be observed in the upper portion of the micrograph and the contact zone is visible between it and the iron particle. The separation between these two particles at a point of obvious prior contact is a typical feature. The Si particles are themselves quite hard and brittle, averaging about VPN$_{27}$ 1000, and the high silicon iron is likewise extremely brittle, despite its much lower hardness (VPN$_{27}$ 400-500). It may be that the slight movements resulting from mounting pressures, or movement in cooling resulting from differences in coefficient of expansion are responsible for the general separation of the Si particles from the iron. Considerable search of the field disclosed a particle in which such separation had not occurred. Fig. 15 illustrates this particle and the appearance of the diffusion zone. Application of the "barley shell" producing etch produces the structures shown in fig. 16. The previously unattacked white zones in contact with the iron particles develop the structures characteristic of the 5-15 pct Si range. Here an interesting question arises. According to the Iron-Silicon Phase diagram, as shown by Greiner, Marsh and Stoughton,[15] at least five phases exist (at room temperature) across the field from 100 pct Si

to 100 pct Fe, and, according to the Metals Handbook (1948 ed.), four.[16] As we are told by the studies of Rhines[17] and others, we should discern each of these phase changes in diffusion zones which, after all, extend in concentration from 100 pct Si to at least moderately low Si content in the center of the Fe particle.

This is not the case. Examination of fig. 14 and 15 discloses no such zones, but only the original Si particle, the white diffusion zone adjoining it (5-15 pct Si in Fe?) and the purer iron core. We do not attempt any explanation of this phenomenon at this time.

After sintering for 25 min at 1180°C, however, a complex structure does begin to develop within the powder particles. Fig. 17 shows a particle after such treatment. Three, possibly four, phases may be identified in the micrograph. These probably consist of the epsilon, eta, zeta, and theta regions, since the iron present will probably have picked up sufficient Si to be removed from the alpha phase region. We are again using the diagram of Greiner, Marsh and Stoughton.

## Conclusions

We have endeavored to provide, in this paper, a literal picture of some of the processes occurring during the diffusion of iron, iron/silicon, and silicon as compounded by the powder metallurgy process. The specimens utilized are in most cases identical with specimens used by Glaser in his studies of the resistances of these alloys[1, 2], and these writings may be consulted by those interested in the relation of the electrical properties to the metallographic state.

## Acknowledgment

## References
[1] F. W. Glaser: *Trans.* AIME (1949) **185**, 475. *Jnl. of Metals,* Aug. 1949.
[2] F. W. Glaser: Powder Met. Bull. 4, 1, 19 (Jan. 1949).
[3] M. G. Corson: *Trans.* AIME (1928) **80**, 259.
[4] *Iron Age,* Aug. 8, 1941, pp. 45-49.
[5] *Jnl.* of the Iron and Steel Inst. (1930) **1**, 1322.
[6] "A Note on Microstructure of High-Silicon Acid-Resisting Iron": *Jnl.* Iron and Steel Inst. Dec. 1944, p. 1221.
[7] W. J. Wrazej: *Jnl.* Iron and Steel Inst., Dec. 1944, p. 227.
[8] *Metal Progress:* Jan. 1946, **49**, 96.
[9] *Metal Progress:* Apr. 1938, **33**, 367.
[10] T. D. Yensen: *Trans.* A.I.E.E. (1924) **43**, 145.
[11] M. C. M. Farquhar and A. R. Weill: *Jnl.* Iron and Steel Inst. Oct. 1945.
[12] J. E. Hurst and R. V. Riley: *Jnl.* Iron and Steel Inst. (1944) **149**, No. 1.
[13] A. Kriz and F. Poboril: *Jnl.* Iron and Steel Inst. (1930) No. II, 191; (1932) No. II, 323.
[14] H. S. Avery: Hard Surfacing by Fusion Welding. Amer. Brake Shoe Co. N. Y. (1947) p. 14.
[15] E. S. Greiner, J. S. Marsh and B. Stoughton: Alloys of Iron and Silicon. McGraw-Hill, N. Y., 1933, p. 111.
[16] Metals Handbook. A.S.M., Cleveland, 1948, p. 1217, 1254.
[17] F. N. Rhines: Powder Met. Bull. (1948) **3**, 2, 28.

The Use of

# Radiocalcium to Study the Distribution of Calcium

Between Molten Slags and Iron Saturated with Carbon

by

W. O. Philbrook,

Kenneth M. Goldman and

Martha M. Helzel

Radioactive calcium has been used to learn whether calcium can be detected in iron saturated with carbon after it has been melted under $CaO$-$Al_2O_3$-$SiO_2$ slags similar to those used in the iron blast furnace. It was hoped that the radioactive tracer technique might make possible a general study of steelmaking reactions in which calcium or calcium oxide are involved. No calcium could be found in the metal under conditions which were favorable for the reduction of calcium, and it has been concluded that the calcium content of the iron was less than $6 \times 10^{-5}$ pct. Some of the problems encountered have been instructive with regard to pitfalls and limitations of tracer methods.

RADIOACTIVE calcium has been used to learn whether calcium can be detected in iron saturated with carbon after it has been melted under $CaO$- $Al_2O_3$- $SiO_2$ slags similar to those used in the iron blast furnace. It was hoped that the radioactive tracer technique might make possible a general study of steelmaking reactions in which calcium or calcium oxide are involved. No calcium could be found in the metal under conditions which were favorable for the reduction of calcium, and it has been concluded that the calcium content of the iron was less than $6 \times 10^{-5}$ pct. Some of the problems encountered have been instructive with regard to pitfalls and limitations of tracer methods.

Calcium oxide occurs in almost all iron- and steelmaking slags, and it is essential to the success of all commercial basic steelmaking processes. Calcium alloys are sometimes used in the deoxidation of steel and for the innoculation of gray iron. The element calcium is therefore almost as ubiquitous in the steel industry as are carbon and oxygen, but calcium has been thought to be completely immiscible with iron in both the liquid and the solid states.[1] It does not seem entirely unreasonable to suppose, however, that some low concentration of calcium might exist in *liquid* iron under a basic slag with other conditions being favorable, just as silicon and other elements can be introduced into iron by reduction of their oxides from slags under appropriate

circumstances. The radioactive tracer technique offered a more sensitive method than chemical analysis of testing this supposition.

The reasons for interest in this investigation were strong enough to justify a recognized risk of failure. On the theoretical side, information on the distribution of calcium between liquid iron and a slag and the rate at which the equilibrium distribution is approached would contribute strongly to the general theory of slag-metal interface reactions. Furthermore, any evidence on the presence of calcium in liquid iron might provide a vital clue to the mechanism of the desulphurization of iron by slags. All of the reactions which have been proposed to explain desulphurization postulate that the sulphur ultimately becomes fixed in the slag as calcium sulphide, but the mechanism by which sulphur
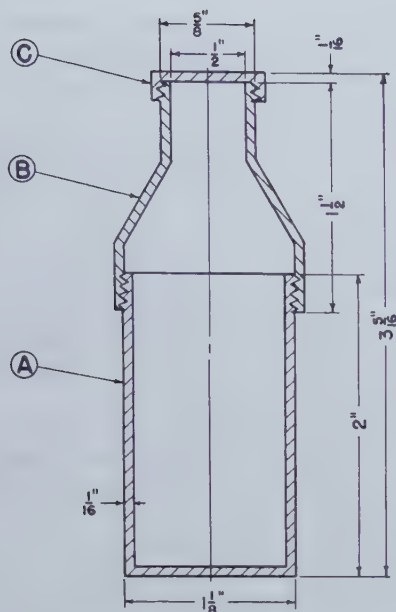
**Fig. 1—Aluminum weighing bottle-funnel combination.**

reaches this final state is still imperfectly understood. It would be interesting to know whether there is any reasonable probability that calcium sulphide could be formed by direct reaction in the metal phase.

From the steelmaker's standpoint, a direct determination of the calcium deoxidation constant (if one can truly be written) and the manner in which it is influenced by temperature and by the composition of the slag or reaction products would be of practical utility. The only datum which is now available to indicate the relative deoxidizing power of calcium is a theoretical value calculated by Chipman[2] of $10^{-8}$ pct oxygen in steel in equilibrium with calcium vapor at 1 atm. pressure.

In order to learn whether calcium could or could not be detected in iron with sufficient sensitivity to be useful, the first experiment was planned to be a simple slag-metal exchange reaction under conditions favorable to a high calcium recovery in the metal. The radiocalcium was introduced as CaO into a slag of the $CaO-SiO_2-Al_2O_3$ system (similar to blast furnace slags) of about the highest CaO content which would give a fluid slag at temperatures close to 1600°C (2900°F). The slag was allowed to react with liquid iron in a graphite crucible under an inert (helium) atmosphere to provide strongly reducing conditions. Since the sensitivity of the tracer method proved to be inadequate even for favorable conditions, it was impossible to extend the study toward more acid slags and toward oxidizing conditions as had been planned. No attempt has been made to determine a true solubility by holding the iron in equilibrium with calcium vapor.

Early experiments, designated as Series I in this paper, were complicated by the presence of a trace (estimated as a few parts per million) of radiophosphorus, $P^{32}$, in the irradiated unit of calcium carbonate[3a]. After elaborate procedures had been developed to eliminate spurious counts from the $P^{32}$, no radioactivity attributable with certainty to $Ca^{45}$ could be detected in the iron. In order to verify

the work, the experiments of Series II were conducted in a similar manner but using a high specific activity separated isotope unit[3b] of $Ca^{45}$ which was verified to be free of $P^{32}$.

## Experimental Methods and Equipment

**Radiocalcium:** Radioactive calcium-45 has a half-life of 180 days and emits only beta radiation (electrons) having a maximum energy of 0.25 Mev[3a]. The first source of $Ca^{45}$ was an irradiated unit containing approximately 0.8 mc of $Ca^{45}$ in 25 g of $CaCO_3$ target material. The unit of radiocalcium for Series II experiments contained 0.9 mc of $Ca^{45}$ as $CaCl_2$ in a few ml of solution, with a specific activity of 26 mc per g of calcium. This was converted to calcium oxide, with the addition of inactive calcium, as will be described later.

**Special Precautions for Radioactive Experiments:** Information on the safe handling of radioactive isotopes is now easily available.[4] The precautions for this investigation included the use of protective coveralls, surgeon's gloves and caps, and air-line respirators. All of the melting work, sample preparation, and chemical manipulations were carried out under enclosed high-velocity hoods, and samples were cut and filed under kerosene to control dust. In order to minimize the possibility of contamination by dusting during the mixing of the radioactive calcium carbonate with other slag constituents, the weighing bottle-funnel shown in fig. 1 was constructed. After thorough mixing of the slag constituents in the closed container, the long neck *B* was inserted into the crucible to transfer the contents with a minimum of manipulation and dust hazard. Prior to experiments with radioactive materials, several rehearsals or "cold runs" were made using exactly the procedures and precautions that were intended for the "hot runs" in order to foresee and eliminate as far as possible any serious experimental difficulties or health hazards which might interfere with the active runs.

Radioactive counting methods are described later.

**Melting Apparatus:** The melting equipment was the simple induction furnace setup shown schematically in fig. 2. The graphite crucible was 1 in. in inside diam and 3¾ in. deep with ¼ in. wall. It was suitably insulated and enclosed in a fused silica tube with ends sealed so that a helium atmosphere could be maintained. Temperature was measured by means of an optical pyrometer.

**Experimental Procedure, Series I:** The metallic charge of 20 g of ingot iron was premelted to saturate it with carbon and allowed to freeze in the crucible. Powdered slag constituents sufficient to form the amount and composition of slag shown in table I were added by means of the mixing container previously described, and the metal and slag were then melted. Starting time was taken when the slag reached the desired temperature.

After the melt had been held at temperature for the desired length of time (see table I), the crucible was quickly lifted from the furnace and dropped into a hole in a block of copper, which cooled it about 500°C in the first minute. The rapid freezing was done to minimize migration of calcium from the metal during cooling and freezing. The crucible was then broken away, the slag separated from the top of the ingot, and the metal was carefully cleaned by

Fig. 2—Schematic diagram of melting apparatus.

(11) SIGHTING WINDOW
(12) GAS OUTLET
(13) WATER COOLED TOP
(10) FUSED SILICA TUBE, GAS INLET
(1) FUSED SILICA TUBE, 2" I.D., 24" LONG
(9) SIGHTING HOLE FOR TEMPERATURE MEAS-UREMENT WITH L & N OPTICAL PYROMETER
(2) ALUNDUM THIMBLE
(3) GRAPHITE POWDER
(4) GRAPHITE CRUCIBLE
(6) SLAG
(5) ARMCO IRON
(7) INDUCTION COIL
(8) A-20 BRICK
(14) STEEL BOTTOM, CEMENTED TO SILICA TUBE
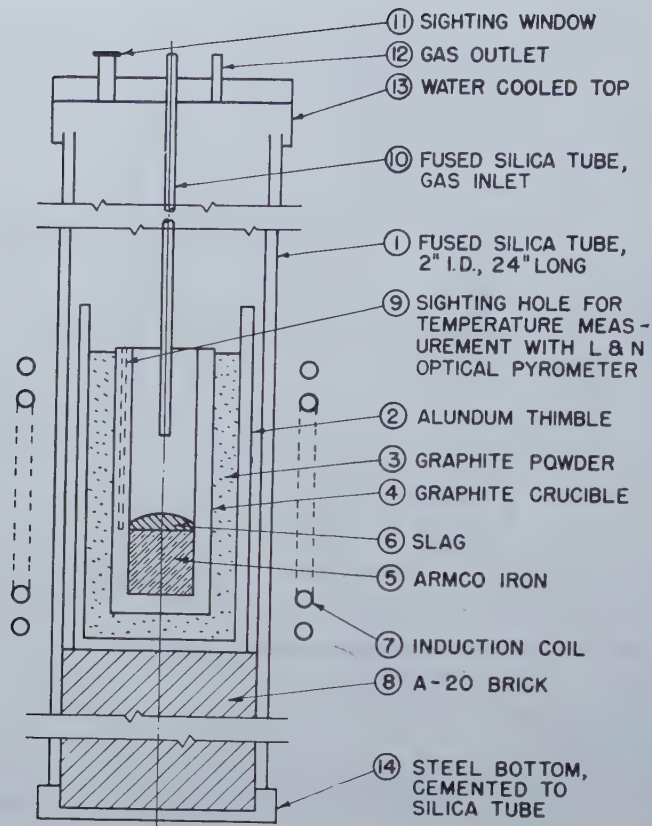
filing all surfaces to avoid contamination of metal samples by slag particles.

Filings taken from the first ingot, T-1, had a specific activity of 55 counts per min per mg of iron, which was several orders of magnitude greater than anticipated. A contact exposure of a photographic film against a flat section produced uniform darkening of the emulsion with no evidence of segregation. To check these observations, the active slag from heat T-1 was melted over a new bath of iron to make ingot T-2, which showed an activity of only 6.4 c/m/mg. A third melting of the same slag over new iron produced ingot T-3 having an activity of only 0.5 c/m/mg. These results were entirely anomalous if the activity were due to Ca-45, but as the counting data became available, the recorded activity was found to be consistent with the 14.3 day half-life and 1.7 Mev maximum energy of $P^{32}$. The chemical behavior of the activity was also consistent with the known behavior of phosphorus in slag-metal systems under reducing conditions, both in heats T-1 to T-3 where the activity entered the metal, and in heat T-4 where the activity from ingot T-1 failed to partition with a new, inactive slag. A demonstration that the 14-day radioisotope could be separated from the radiocalcium carbonate by precipitation (with phosphate carrier) as ammonium phosphomolybdate served as the final confirmation that the high counts of the first two ingots came, not from $Ca^{45}$, but from a minute amount of $P^{32}$ which had been in the irradiated unit as it came from Oak Ridge.

After the phosphorus contamination had been removed from the active slag by the first two extractions with molten iron (heats T-1 and T-2), any $Ca^{45}$ which might have been reduced and have entered the iron was present in too low a concentration to yield a positive count above "background." It then became necessary to separate the calcium from the large bulk of iron in order to concentrate the radioactivity to a high enough specific activity to be measurable. This was done by adding a small amount of ordinary calcium to a solution of the iron from ingot T-3 to serve as a carrier to precipitate the minute amount of calcium which might have been dissolved in the iron. The details of the separation are given in a later section. The radioactivity of the calcium precipitate from this separation was so close to the background level that it was uncertain whether any activity really was present.

In order to make a check run, a new and more basic slag was purified by two extractions with molten iron to remove $P^{32}$, heats T-5 and T-6. This slag was then held at 1550°C for 90 min over a new iron melt in heat T-7. A calcium separation from this ingot gave a faint count which seemed to be originating from a trace of $P^{32}$ rather than from $Ca^{45}$.

These results from Series I experiments were not conclusive so it was decided to repeat the experiment under more favorable conditions. A new allocation of radiocalcium was obtained and found to be free of troublesome impurities. Even though pilot tests had proved it to be reliable, the involved wet chemical separation of calcium from large amounts of iron was the cause of some misgivings, and it was believed that it could be replaced by the extraction of the calcium from the iron in the molten condition by a second, acid slag from which the calcium could easily be recovered by conventional slag analysis and counted. The calcium content of the metal could then be calculated because most of the $Ca^{45}$ atoms

Table I. Summary of Data

| Series | Expt. No. | Temp. °C | Time min | Al$_2$O$_3$ | CaO | SiO$_2$ | MgO | Wt. Slag g | Wt. Active CaCO$_3$, g | Wt. Iron g | Iron | Slag | Zero Time | Remarks |
|--------|-----------|----------|----------|-------------|-----|---------|-----|------------|------------------------|------------|------|------|-----------|---------|
| | | | | Slag Composition pct by wt. | | | | | | | Specific Activities d per min per mg | | | |
| I | T-1 | 1530 | 30 | 19.0 | 36.6 | 44.4 | | 5 | 3.27 | 20 | 55 | 66,000 | 3/17/47 | ⎫ |
| | T-2 | 1530 | 30 | Slag from T-1 | | | | | | 20 | 6.4 | 72,600 | 3/17/47 | ⎬ —P$^{32}$ found in iron ingot. |
| | T-3 | 1530 | 30 | Slag from T-2 | | | | | | 20 | 0.5 | 68,000 | 3/17/47 | ⎭ |
| | T-4 | 1540 | 30 | 20 | 38 | 42 | | 6.7 | | 21.1 | 55 | 0 | 3/17/47 | Fe ingot from T-1 used. |
| | T-5 | 1560 | 30 | 15 | 48 | 37 | | 6 | 5.15 | 20 | | | | ⎫ —Purification runs to |
| | T-6 | 1540 | 60 | Slag from T-5 | | | | | | 20 | | | | ⎬ remove P$^{32}$ from slag. |
| | T-7 | 1550 | 90 | Slag from T-6 | | | | | | 20 | | 54,300 | 6/28/47 | Ca separated from Fe ingot. Trace of P$^{32}$ still present. |
| II | T-8-1 | 1600 | 60 | 15 | 49 | 36 | | 10 | 5.11* | 106 | 0 | 736 | 9/16/48 | 1 pct S added to iron. |
| | T-8-2 | 1300† | 60 | 21 | 6 | 50 | 23 | 10 | | 106 | 0 | 0 | | |
| | T-9-1 | 1600 | 60 | 15 | 49 | 36 | | 22 | 10* | 106 | 0 | 3980 | 10/17/48 | |
| | T-9-2 | 1600 | 60 | 21 | 1 | 54 | 24 | 10 | | 106 | 0 | 0 | 12/13/48 | |

\* Wt. CaO in which active Ca$^{45}$ was contained.
† Approximate temperature; heat went out of control because fumes caused false optical pyrometer readings.

from the metal would be found in the second slag.

**Experimental Procedure, Series II:** 1. *Melting with radioactive (basic) slag:* The high specific activity calcium chloride obtained from the Atomic Energy Commission contained only about 35 mg of total calcium in solution. To aliquots of this solution were added amounts of CaCO$_3$ sufficient to provide the weights of CaO needed for the slag as indicated in table I. The calcium was precipitated with an excess of ammonium oxalate at pH4, and the calcium oxalate was dried and ignited to CaO at 1000°C.

The experimental procedure was the same as that described for Series I heats except that a considerably larger iron ingot was made (see table I) to increase the total quantity of calcium in the metal. No radioactivity could be detected on the surface of the cleaned ingot by counting with the monitoring probe.[5]

2. *Melting with an inactive (acid) slag:* The cleaned ingot was remelted under a slag containing 54 pct SiO$_2$, 21 pct Al$_2$O$_3$, 24 pct MgO, and 1 pct CaO; the melt was held at 1600°C for 1 hr under a helium atmosphere. The crucible was then removed from the furnace and the slag and metal were separated mechanically. The CaO was recovered from the slag by conventional chemical methods. This separated CaO was then counted for radioactivity. To check the validity of the assumption that practically all radiocalcium would be in the second slag, a chemical separation was also performed on the final ingot to recover the calcium in the event that it had remained in the iron.

**Chemical Separation of Calcium from Iron:** A number of experiments were necessary in the development of a satisfactory chemical separation of a possible trace of calcium from the gross mass of iron. Attempts to remove large quantities of iron by continuous extraction with isopropyl ether proved unsatisfactory owing to the difficulty of controlling conditions. The separation of the iron with cupferron[6] gave satisfactory results. The method was tested for recovery of inactive calcium as follows:

1. One-half gram of Bureau of Standards No. 55b ingot iron and 15 mg of carrier Ca as CaCO$_3$

were dissolved in HCl, and the solution was adjusted to 1.5 to 2 normal. One-half gram of iron was found to be the maximum quantity that can be handled conveniently as iron cupferrate.

2. Iron was precipitated as iron cupferrate by the addition of fresh 6 pct cupferron solution.

3. The iron cupferrate was removed by successive extractions with chloroform.

4. Excess cupferron in the aqueous solution was destroyed by successive evaporations with HNO$_3$ and HCl.

5. Calcium in the aqueous solution was precipitated with an excess of ammonium oxalate at pH4, and the precipitate was ignited at 1000°C to calcium oxide.

The added calcium was recovered from the iron with a yield of 96 pct, thus establishing the feasibility of the cupferron-oxalate method. A series of tests by the same procedure proved that 5 mg of carrier calcium per 0.5 g aliquot of iron was the minimum addition which could be recovered with sufficiently quantitative and consistent results.

A third series of tests demonstrated that radiocalcium was recovered by the cupferron method. Calcium 45 in the amount of 50 or 300 d per min was added to control samples containing 0.5 g of iron, 5 mg of calcium, and 5 mg of phosphorus as phosphate to serve as "holdback" for P$^{32}$. Separation of ammonium phosphomolybdate prior to precipitation of calcium oxalate resulted in low and erratic recoveries of calcium. When no phosphate separation was made, the recovery of carrier calcium was 92 to 100 pct and the CaO residues counted with a half-life of 180 days and with disintegration rate equivalent to the added activity. No evidence of P$^{32}$ activity was found either in calcium or phosphorus precipitates in these experiments because of the minute portions of the irradiated unit employed. Supporting data are omitted for the sake of brevity, but the control tests proved that the method was capable of recovering small amounts of radiocalcium from iron with good efficiency.

For calcium separation in an actual analysis, a metal sample of 5 g was dissolved in HCl and divided into 0.5 g aliquot portions; 5 mg of Ca was added

to each aliquot and the iron was removed by cup-ferron as described above. All aliquot portions were combined after the iron was separated and before the calcium was precipitated.

**Radioactivity Counting Procedures and Calculations:** Metal samples were prepared by filing, and slag samples were crushed to pass a 100-mesh sieve. A weighed amount of material, about 100 mg of slag or 200 mg of metal, was mounted in an aluminum counting plate of conventional design having a depression $5/8$ in. in diam x 1/16 in. deep. The counting was done with a commercial, bell-type Geiger-Müller tube having a 3 mg per sq cm mica window about 1⅛ in. in diam. The counts were recorded on a commercial 64-scaler circuit and mechanical counter.

It was found early in the investigation that all counts should be made with the same counting chamber and scaler because there was a considerable variation between counts of the same sample on two different circuits, in spite of corrections based on the same radiation standard, whereas counts on the same scaler were internally consistent with a coefficient of variation of about 4 pct. All calculations in this work are on a relative rather than absolute basis, so it is sufficient that the data be internally consistent; the absolute accuracy need not be known.

Our experience with $P^{32}$ and difficulties of a similar nature with another irradiated unit have demonstrated very forcibly the necessity of adhering to the practice of identifying positively the radioisotope responsible for a measured activity to avoid false interpretation of counts which might originate from radioactive impurities. This is done by determining both half-life and absorption curves. Reference to tables of isotopes[7] in conjunction with observed chemical behavior of the isotope in question will usually suffice to establish identity fairly conclusively.

The counts as read from the scaler must be corrected for the following variables:

1. The background count originating from cosmic radiation, natural radioisotopes in the materials of construction, or contamination.
2. Efficiency of collection by the G-M tube, or "geometry" of the counter.
3. Decay of the isotope with time.
4. Absorption of radiation by the cellophane, air, mica window, and intentionally interposed absorbers between the sample and the inside of the G-M tube chamber.
5. Self-absorption within the sample.

All of these corrections, in the order named above, are combined in the following equation:

$$N_o = \frac{(C_t - C_b)}{A} \cdot \frac{S_o}{S_t} \cdot e^{\lambda t} \cdot e^{ay} \cdot \frac{2\alpha}{(1 - e^{-ax})} \qquad [1]$$

where:

$N_o$ = Absolute activity of the sample, d per min per mg at zero time.
$A$ = Area of sample effectively covered by counter, cm².
$C_t$ = Recorded counts per min.
$C_b$ = Background count, averaged from "blank" counts taken shortly before and after sample count.

$S_o$ = Actual disintegration rate of radioactivity standard, d per min.
$S_t$ = Recorded counts per min from standard, average of counts taken immediately before and after sample count.
$\lambda$ = Decay constant for the isotope being counted, fraction disintegrating per unit time.
$t$ = Time of measurement after zero time ($\lambda$ and $t$ in consistent units).
$\alpha$ = Absorption coefficient for the radiation being counted, cm² per mg.
$y$ = Thickness of absorbers between sample and inside of G-M tube (air, window, absorber plates, etc.), total mg per cm².
$x$ = Thickness of sample, mg per cm².
$l_o$ = Range of beta particles in matter (usually measured in aluminum), mg per cm².

For samples thicker than the range of the beta particles emitted, $x > l_o$, $(1 - e^{-ax}) \rightarrow 1$ and Eq 1 simplifies to:

$$N_o = \frac{2}{A} (C_t - C_b) \cdot \frac{S_o}{S_t} \cdot e^{\lambda t} \cdot \alpha e^{ay} \qquad [2]$$

Eq 1 and 2 are approximately valid, within 2 to 5 pct, for most beta emitters. Henriques et al.[8] give a simple derivation of the portion of Eq 1 which corrects for self-absorption, and Glendenin[9] gives a good discussion of the approximations inherent in such calculations of beta particle absorption.

### Data and Results

The more important data have been collected in table I. Detailed decay and absorption data used to establish the identity of the isotopes are not recorded in full. Slag samples exhibited half-lives of 168-190 days and half-thicknesses of about 6.5 to 7 mg per sq cm, in satisfactory agreement with data recorded in the literature[10,7,8] for $Ca^{45}$. Calcium activity was so strong in the slag samples that it completely masked the phosphorus activity, but some of the metal samples, as previously noted, displayed energies of about 14.8 ± 0.7 day half-life and 100 mg per cm² half-thickness, compared with the reported values[11] of 14.3 days and 110* mg per cm² for $P^{32}$.

* Estimated from maximum energy value of 1.7 Mev by methods of Glendenin.[9]

The results of the experiments of Series I are doubtful because of the presence of $P^{32}$ as an impurity, and these heats T-1 to T-7 will not be discussed further.

The experiments of Series II yielded no indication of calcium in the iron. The initial slag for heat T-8-1† had an activity of 6480 c per m, correspond-

† The initial metal of heat T-8-1 contained about 1 pct sulphur, and the apparatus was modified somewhat so that the experiment would concurrently serve another purpose irrelevant to this study. These circumstances are reported for accuracy of record, but they probably are not significant to this work.

ing to an absolute activity of 736 d per m per mg of slag. When no activity could be detected either in the second slag or in the final ingot from T-8-2, the experiment was repeated at a five-fold increase in the level of activity of the initial slag. Slag T-9-1 had an activity of 41,700 c per min, corresponding to an absolute activity of 3980 d per min per mg. Again no positive count was obtained either from slag T-9-

2 or by a chemical separation of calcium from the final ingot.

Since no positive count has been detected from Series II experiments, an indirect argument has been adopted to estimate the limit of detection. Suppose there had been enough $Ca^{45}$ in slag T-9-2 to yield a count capable of detection by the counting circuit, say 6 counts per min. From this value, the corresponding calcium content in the iron can be calculated. Since, in fact, no count was obtained, then the actual calcium content of the iron must have been lower than this limit of detection.

The basic assumptions in the calculation of this minimum amount of detectable calcium are as follows:

1. Some small amount of calcium will be reduced from the initial $CaO-SiO_2-Al_2O_3$ slag and enter the metal.
2. The ratio of radioactive $Ca^{45}$ atoms to the total Ca atoms in the iron will be the same as the corresponding ratio in the original radioactive slag.
3. In the second heat, the portion of the experiment in which an acid slag is melted over the iron ingot, Ca atoms in the metal will exchange with Ca atoms in the slag, and, because of the extremely high distribution ratio of Ca in slag to Ca in iron, practically all of the $Ca^{45}$ atoms will in time be found in the second slag, from which they can be recovered and counted.

The following counting and decay data for the counting setup used in the experiments and for $Ca^{45}$ are necessary for substitution in Eq 1:

$A$ = Area scanned by counter = 2 sq cm for sample mounts used.

$S_o/S_t$ = Efficiency correction factor of counter = 6 for these experiments.

$t_{1/2}$ = Half-life for $Ca^{45}$ = 180 days[3b].

$\lambda$ = Decay constant = 0.693/180 = 0.00385 per day, $2.67 \times 10^{-6}$ per min.

$\alpha$ = Absorption coefficient = 0.10* $cm^2$ per mg for $Ca^{45}$.

---

* Based on half-thickness of 7 mg per cm² estimated from initial slope of absorption curve for $Ca^{45}$ of Solomon and Glendenin[10], which is in good agreement with our observed $x_{1/2}$ = 6.5 to 7 mg per cm².

---

$x$ = Thickness of samples = wt. in mg ÷ 2 sq cm.

$y$ = Total thickness of external absorbers = 6.3 mg per cm² for these experiments.

$l_o$ = Range in aluminum = 64 mg per sq cm[10] for $Ca^{45}$.

It is assumed that $(C_t-C_b)$ must equal or exceed 6 counts per min to be considered a positive count; this is three times the standard deviation of 2 c per m for background counts in our laboratory and therefore represents a 99.7 pct probability that the count is significant and not due to chance fluctuations.

The calculation, which is essentially a material balance, was made in the following way for experiment T-9:

1. From the weight, CaO content, and measured specific activity of slag T-9-1 (see table I) and the decay constant given above for $Ca^{45}$, it was calculated that the ratio of total Ca atoms to $Ca^{45}$ atoms in slag T-9-1 was $3.0 \times 10^9$ at zero time.
2. By means of Eq 1 it was calculated that $2.1 \times 10^{-14}$ g of $Ca^{45}$ (referred to zero time) would

have been needed in the 102 mg of CaO extracted from T-9-2 to have produced a significant count of 6 c per min above background (uncorrected, 23 days after zero time, corresponding to actual conditions under which the CaO residue was first counted). This, from step 1, would have required that $(2.1 \times 10^{-14})$ $(3.0 \times 10^9)$ = $6.3 \times 10^{-5}$ g of total Ca be received by the slag from the ingot.

3. Since the ingot from T-9-1 weighed about 110 g (106 g Fe + approx 4 g C), the percentage of calcium in the iron ingot required to give a significant count from slag T-9-2 was $\dfrac{6.3 \times 10^{-5}}{110}$

$\times 100 = 6 \times 10^{-5}$ pct Ca = 0.00006 pct Ca.

Because of the low precision of the absorption coefficient for $Ca^{45}$ and the approximations inherent in Eq 1, the reliability of this estimate is no better than ± 20 pct.

Similar calculations carried through for the wet separation of calcium from ingots T-3 and T-7 indicate that $5 \times 10^{-5}$ pct Ca should have given a positive count. Had the calcium content of the iron been as high as $1 \times 10^{-4}$, it could certainly have been detected; a content as low as $5 \times 10^{-5}$ pct would probably have been detected. The calcium content of liquid iron saturated with carbon under blast furnace type slags must therefore be exceedingly low.

## Discussion of Results

Although most of the original plans of this investigation had to be abandoned because of our inability to detect any calcium in the iron, one pertinent conclusion can be drawn. It may be noted that the carbon-saturated iron, slag compositions used, and the temperature level of these experiments represent conditions fairly comparable with those in the hearth of the iron blast furnace, even though the atmosphere above the melt was predominantly helium rather than CO plus $N_2$. The fact that the calcium content of the metal was so vanishingly small seems to preclude the possibility that any sort of association of calcium with sulphur within the metal phase can contribute significantly to the mechanism of desulphurization in the blast furnace (or in oxidizing steelmaking processes).

A spectrographic method for the determination of calcium in steel has recently been described by Carlsson.[12] The limit of detection claimed for his method is 0.0001 pct Ca, of the same order of magnitude as calculated for the radioactive technique described in this paper. It should be emphasized, however, that the two results are not necessarily comparable since the investigations were done under entirely different conditions. Carlsson's data apply to the calcium content of commercial steels analyzed by spectrographic methods. Although Carlsson reports results for both "acid soluble" and "acid insoluble" calcium, it is conceivable that the acid soluble calcium might have existed in the steel in easily soluble inclusions rather than as a true alloy of calcium. The data presented here apply to the calcium content introduced into carbon-saturated ingot iron by melting under a reducing slag, as determined by the radioactive tracer technique.

The sensitivity of the radioactive tracer method could theoretically be improved by several orders of magnitude by a corresponding increase in the

specific activity of the original slag. The only limitation is the number of millicuries of high specific activity Ca[45] which can be handled safely and which can be justified on the basis of availability and cost. It seems doubtful, however, that the calcium content of the metal would be sufficiently above the threshold of detectability to make possible the conduct of experiments such as were outlined in the introduction and thus justify the time and expense of further research of this nature.

The results presented here pertain only to the experimental conditions described; they do not purport to relate to the solubility of calcium in pure iron in equilibrium with pure calcium vapor or liquid. The radioactive tracer technique would be applicable to a study of true solubility of Ca in iron, but the problems of apparatus would be considerably more complicated than for the present study.

## Summary

1. An attempt has been made by a radioactive tracer technique to determine the calcium content of carbon-saturated iron melted in graphite under a comparatively basic slag of the $CaO$-$SiO_2$-$Al_2O_3$ system in a neutral atmosphere of helium at about 1600°C, these conditions being the most favorable for reducing calcium from the slag which could be handled conveniently in the laboratory.

2. Two methods have been used in order to concentrate for counting purposes the minute amount of calcium which might have been introduced into the iron. These methods were (1) a wet chemical separation of calcium from iron after the addition of small amounts of carrier calcium, and (2) an extraction of calcium from liquid iron by an acid slag low in CaO, followed by separation and counting of the CaO from the second slag.

3. Both methods have failed to detect the presence of any calcium in the iron under experimental conditions outlined. The limit of detection has been calculated as approximately 0.00006 pct Ca, so that any calcium present in iron under reducing conditions similar to those in the iron blast furnace is presumed to be lower than this limit of detection.

4. It seems evident from this result that no direct reaction or association between calcium and sulphur dissolved in molten iron can contribute significantly to desulphurization in the blast furnace.

5. While it is theoretically possible to increase the sensitivity of the tracer technique by several orders of magnitude, it is probable that the calcium content of iron would, at best, be so close to the threshold of detection as to preclude any useful experiments concerning the influence of slag composition or oxygen level on the calcium content of liquid iron under steelmaking conditions.

6. The data presented herein do not relate to the true solubility of calcium in iron, nor do they give any direct information on the total calcium content which might be obtained in steel by the addition of calcium-bearing deoxidizers or from fortuitous inclusions.

7. This paper illustrates techniques for handling low-energy radioactive tracers in high-temperature metallurgical experiments and gives examples of radiochemical calculations; our experience emphasizes the necessity for identifying the isotope responsible for observed radioactivity to avoid false interpretation of activities originating from unsuspected impurities.

## References

[1] M. Hansen: *Aufbau der Zweistofflegierungen.* Berlin: Julius Springer, 1936; photolithoprint reproduction by Edwards Brothers, Inc. (1943), p. 396.

[2] John Chipman: Application of Thermodynamics to the Deoxidation of Liquid Steel. *Trans.* Amer. Soc. for Metals (1934) **22**, 385.

[3a] U. S. Atomic Energy Commission: Radioisotopes Catalogue and Price List No. 2. Effective March 1, 1947; revised September, 1947, Item No. 13A, p. 16.

[3b] *Ibid:* Item S-5, p. 12.

[4] U. S. Dept. of Commerce: Safe Handling of Radioactive Isotopes. Nat'l. Bur. of Standards Handbook 42, Sept. 1949.

[5] Claude Schwob and Raymond Nether: A Monitoring Probe for Radiochemistry Laboratories. *Science,* Oct. 3, 1947, **106**, 327.

[6] G. Frederick Smith: Cupferron and Neo-Cupferron. (Columbus, Ohio: G. Frederick Smith Chemical Co., 1938).

[7] Glenn T. Seaborg and I. Perlman: Table of Isotopes. *Rev. Modern Physics* (1948) **20**, No. 4, 585. See also: G. Friedlander and M. L. Perlman: Chart of the Isotopes. Gen. Elec. Res. Lab., 1948.

[8] F. C. Henriques, Jr., G. B. Kistiakowsky, Charles Margnetti, and W. G. Schneider: Radioactive Studies, Analytical Procedure for Measurement of Long-Lived Radioactive Sulphur, S-35, etc. *Ind. and Eng. Chem., Analytical Ed.* (1946) **18**, 349-353.

[9] Lawrence E. Glendenin: Determination of the Energy of Beta Particles and Photons by Absorption. *Nucleonics* (1948) **2**, 12-32.

[10] A. K. Solomon and L. E. Glendenin: Range and Energy of Beta-Radiation from Calcium-45. *Phys. Rev.* (1948) **73**, 415-416.

[11] K. Siegbahn: The Disintegration of Na-24 and P-32. *Phys. Rev.* (1946) **70**, 127.

[12] C. Georg Carlsson. Kalcium I Stal. *Jernkontorets Annaler* (1948) **132**, 221-236.

# Measurement of Relative Interface Energies
# in Twin Related Crystals

## by C. G. Dunn, F. W. Daniels, and M. J. Bolton

The nature of boundaries in twin related grains of silicon iron is investigated
and the relative interface energy of the {112} twin is determined. The effect of
boundary orientation on boundary energy is treated briefly. Mathematical and experi-
mental techniques are discussed in detail.

IN recent papers on interface energies in metals[1, 2] the concept of an equilibrium of forces has been used in the measurement of interfacial tensions. Mathematically the equilibrium of three forces is given by the relations:

$$\frac{\gamma_{12}}{\sin \theta_3} = \frac{\gamma_{23}}{\sin \theta_1} = \frac{\gamma_{13}}{\sin \theta_2} \qquad [1]$$

where the $\gamma$'s are the interfacial tensions (interface energies per unit area) of three phases or grains meeting at angles $\theta_1$ $\theta_2$ and $\theta_3$ ($\gamma_{12}$ relates to the 1-2 boundary formed by grains 1 and 2; $\gamma_{23}$ to the 2-3 boundary, etc.). If these relationships are valid, one can calculate relative values of the interface energies from measured boundary angles on specimens which have been brought to equilibrium.

Since Eq 1 may be derived through a mathematical process of minimizing the grain boundary energy under the restriction that the $\gamma$'s be independent of boundary orientation,[2] the concepts of surface tensions and equilibrium of forces are not particularly essential. To deal with the general case involving dependence of boundary energy on boundary orientation, it becomes desirable to drop certain concepts formerly held (namely that energy per unit area is identical with force per unit length or surface tension) and to use the energy concept alone. It is appropriate, therefore, to use $E$ in place of $\gamma$ in deriving and using the more general equations that express the anisotropic nature of the grain boundary energy.

Herring[3, 4] recently has derived the required general equations using the principle of minimization of energy. Specifying the boundary orientations in terms of angles ($\phi$) measured with reference to

crystal axes within the grains, Herring's equations take the form

$$E_{23} + E_{31} \cos \theta_3 + E_{12} \cos \theta_2 - \sin \theta_3 \frac{\partial E_{31}}{\partial \phi_{31}}$$
$$+ \sin \theta_2 \frac{\partial E_{12}}{\partial \phi_{12}} = 0 \qquad [2]$$

where the partial derivatives are measured in the direction of counterclockwise rotation of the boundaries. Eq 2 implies that an infinitesimal displacement of the triple point along the 2-3 boundary produces no change in the boundary energy. Similar equations apply for infinitesimal displacements along each of the other two boundaries. From such equations Herring obtains the following general relationship

$$\frac{E_{12}}{(1 + \epsilon_1 \epsilon_2) \sin \theta_3 + (\epsilon_2 - \epsilon_1) \cos \theta_3} =$$
$$\frac{E_{23}}{(1 + \epsilon_2 \epsilon_3) \sin \theta_1 + (\epsilon_3 - \epsilon_2) \cos \theta_1} =$$
$$\frac{E_{13}}{(1 + \epsilon_1 \epsilon_3) \sin \theta_2 + (\epsilon_1 - \epsilon_3) \cos \theta_2} \qquad [3]$$
$$\text{where} \quad \epsilon_1 = \frac{1}{E_{23}} \frac{\partial E_{23}}{\partial \phi_{23}}$$

and $\epsilon_2$ and $\epsilon_3$ have similar expressions.

It is apparent that Eq 3 reduces to Eq 1 when the $\epsilon$'s vanish. Eq 3 also reduces to Eq 1 when the $\epsilon$'s are all equal.

Shockley and Read[4] have pointed out one limitation to these equations. When $E$ plotted versus $\phi$ appears as an energy cusp, as their theory requires, for example, for the energy near a twin boundary position, then Eq 3 (and therefore Eq 1 also) no longer applies if one boundary is in the minimum energy position. One of the equations of form Eq 2, however, applies if the infinitesimal displacement is along the boundary associated with the energy cusp.

From the foregoing treatment it will be apparent that equilibrium angles alone are not sufficient in general for calculating relative interface energies.

C. G. DUNN, Member AIME, is Research Physicist, and F. W. DANIELS and M. J. BOLTON are Metallurgists, General Electric Co., Pittsfield, Mass.

Consequently, calculations made on the implicit assumption of zero ε's must be held questionable. Nevertheless, such questionable calculations can be of value in ascertaining more fully the nature of the problem of grain boundary energies.

In the present investigation, which is primarily concerned with determining a relative value of the {112} twin boundary energy and in observing boundary relationships in special 3-grain groups, the experimental work was completed prior to receiving knowledge of this concurrent basic mathematical development. In the analysis and treatment of results obtained, the new concepts prove to be of inestimable value.

Past investigations on twin boundaries have indicated that the amount of energy associated with a twin boundary is low, particularly in the face-centered cubic lattice. Smith[1] from measurements on the shapes of grain and twin boundaries in face-centered cubic metals estimated a value less than



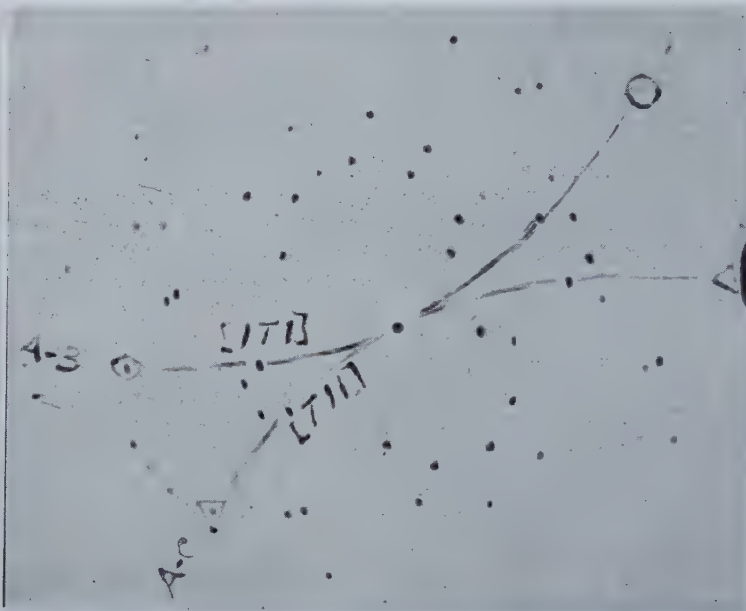Fig. 1—Original sample before cutting to obtain specimen G. Etched. (Natural size) (top left)

Fig. 2—Stereographic projection showing orientation relationships of grains in specimen G. (bottom)
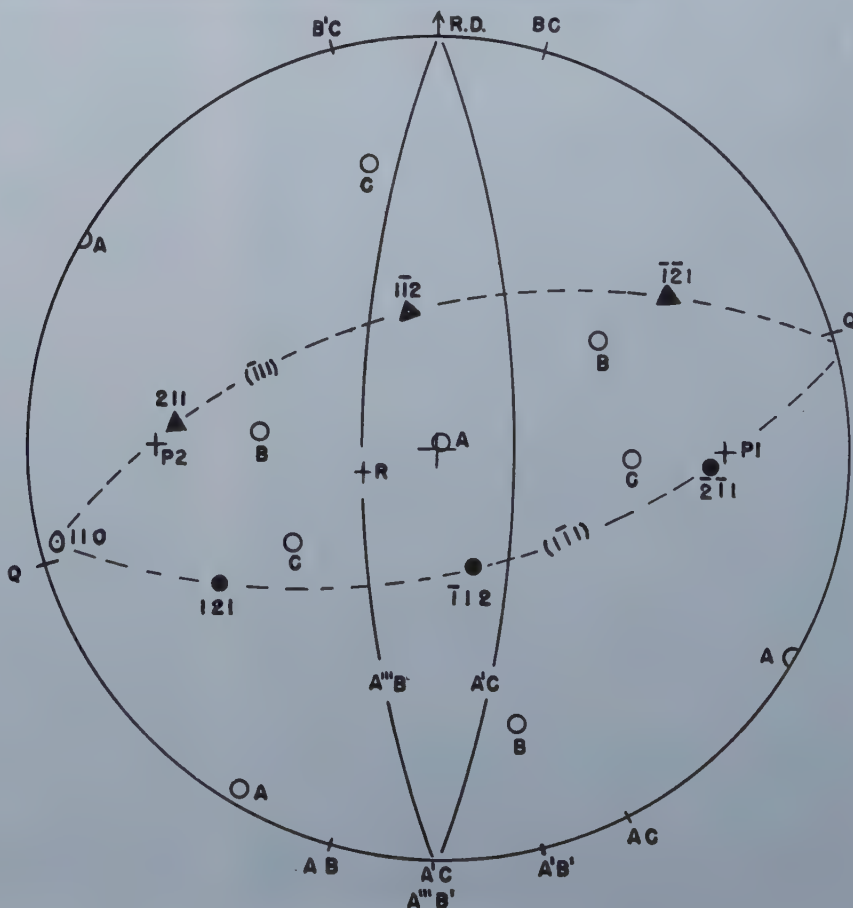
Fig. 3—Laue photograph of grains A″, B′, and C. (top right)

one-tenth that for a grain boundary. Lacombe[5] noted a marked dependence of rate of boundary etching on orientation of the boundary between twin grains of aluminum. The attack of a {111} twin boundary was negligible compared with that of the boundary departing appreciably from the twin composition plane, indicating an effect of boundary orientation on boundary energy. McKeehan[6] and Preston[7] from considerations of the distances between atoms for twinned lattices concluded that the lowest energy forms would be the {111} twin plane for a face-centered cubic metal and the {112} twin plane for a body-centered cubic metal. Preston further concluded that the latter type twin would have a higher boundary energy than the former because of stresses due to atoms lying closer together than normal. Dunn and Lionetti[8] investigated the dependence of relative grain boundary energy on difference in orientation in crystals of silicon ferrite and observed an effect of lowered energy for "near twin" orientations. Since the boundaries were far from real twin planes, their results give no quantitative information on the energy of the {112} twin boundary.

In the present investigation, experiments were made on sheet specimens of silicon iron containing one or more 3-grain groups. These experiments will be reported in two parts: (1) 3-grain groups with two sets of twin related grains and (2) 3-grain groups with one set of twin related grains.

## 3-Grain Groups with Two Sets of Twin Related Grains

**Specimens:** Since annealing twins form under favorable conditions during the recrystallization of fine grained silicon ferrite (this fact apparently has not been reported previously), finding a suitable group of twins in recrystallized sheet specimens was not difficult. Thus specimen G, the outlined portion in fig. 1, was found in a sheet sample of 3.5 pct silicon iron that had been recrystallized by a strain-anneal method starting with a reoriented seed crystal[9] (note twisted region at extreme bottom in fig. 1). Growth of the seed crystal produced grain A, which twinned at a number of isolated points during growth to produce all the other grains. Because of preferred growth characteristics, only two of the four possible twins of A formed during recrystallization. These twins are identified B and C and are given prime marks according to location. Each 3-grain group therefore contains the letters A, B, and C.

In fig. 2 the same letters refer to the position of cube poles of the corresponding grains. Grain A has a (001) plane almost in the plane of the sheet and grains B and C have {221} planes approximately in the plane of the sheet.

Along the B′C boundary, which extended a length of almost 6 in. in the uncut specimen, there were over one hundred small isolated areas of orientation A formed by B′ or C twinning back to A, presumably during the original growth process. These small crystals occurred only on the underneath side of the specimen, but strangely none occurred along the BC boundary. The cut specimen G contained one of these island grains, called A″, and part of another, A‴. A transmission Laue photograph of grain A″, which naturally also included grains B′ and C, is shown in fig. 3. Com-

parison of this Laue pattern with those taken separately for grains A, B, and C showed that the photograph consisted of the patterns of the three grains A, B, and C. Because of twin relationships, the patterns have common zones and common Laue spots. The common [1$\bar{1}$1] zone for twins A and B and the [$\bar{1}$11] zone for twins A and C, which appear in the photograph as hyperbolas, contain also common {112} Laue spots and these are shown inclosed by circles and triangles.

A much larger type of island grain, but of orientation B, can be seen as a white grain along the AC boundary in fig. 1, but this grain will not be considered in terms of possible 3-grain groups.

**Annealing Methods:** In order to promote the motion of grain boundaries towards minimum energy positions, it was necessary to anneal repeatedly the sample at high temperature until the grain boundaries' angles became constant. During anneals, protection was provided by encasing the sample within two concentric silicon iron boxes which were in turn placed within a tightly welded steel box equipped with a gas inlet and outlet. Before introducing the gas into the welded box, the gas was passed through a purification train consisting of a deoxo catalyzer, an activated alumina drier, a magnesium chip furnace (600°C), and two towers of phosphorous pentoxide. The atmosphere used was hydrogen at the lower temperatures and argon at the higher temperatures. The dewpoint of the gas in either case was approximately —90°F.

**Results:** During the first anneal the small island grain of orientation B, along the AC boundary, completely disappeared. The other island grains will be mentioned later. Old and new boundaries in the ABC group may be seen in the photograph shown in fig. 4. The old boundaries show because the surface of the specimen was etched prior to the anneal and the new boundaries show because of thermal etching during the anneal. The relative positions of these boundaries indicate that grain A grew at the expense of grains B and C with a reduction in length of the BC boundary. This same type of movement can be seen more strikingly, however, for island grain A‴ shown in fig. 5. Here the fine line is well in advance of the dark line of the old boundary.

Angles were measured and the sample was then given an anneal for 48 hr at 1400°C. Fig. 6 shows a photograph of island grain A″ taken after the surface was given a metallographic polish and etch. On comparison with other grain boundary angles in the specimen, it was observed that the angles for A‴ and A′ were the same as those shown for A″ in the figure. At a magnification of 500 diam, one angle in each of these 3-grain groups was 180 degrees and this is also clearly evident for the groups at both ends of island grain A″ shown in fig. 6. A photograph of a cross section of grain A‴, sectioned in the direction indicated in fig. 2 and 4 by the line QQ, is shown in fig. 7. The direction R was located along the line QQ in fig. 2 according to the angle of tilt of the A‴B′ plane which is given in fig. 7.

Directions of boundaries in the surface at the meeting point of grains are also indicated in fig. 2 along the basic circle (for example: B′C, BC, etc.), and these define the surface angles between boundaries. The straight sides of grain A″ (A″B′ and

$A''C$ in fig. 6) were found to be parallel to within two degrees and also to coincide in direction with the $A'C$ boundary of the $A'B'C$ group and the $A'''B'$ boundary of grain $A'''$. Two directions, $A'C$ and $R$, therefore, determine the plane for the actual grain boundary $A'''B'$; and this plane has the pole $P1$, which is indicated in fig. 2. Similarly—but without making any cross section cuts since $A'$ passed completely through the specimen—the $A'C$ plane was determined from surface measurements on the specimens. This plane and its pole $P2$ are indicated in fig. 2.

Poles of possible {112} twin planes for grains $A$ and $B$ and grains $A$ and $C$ are plotted in fig. 2, the former by black circular dots and the latter by black triangular dots. Also plotted is a pole of a (110) plane which is common to all three grains $A$, $B$, and $C$.

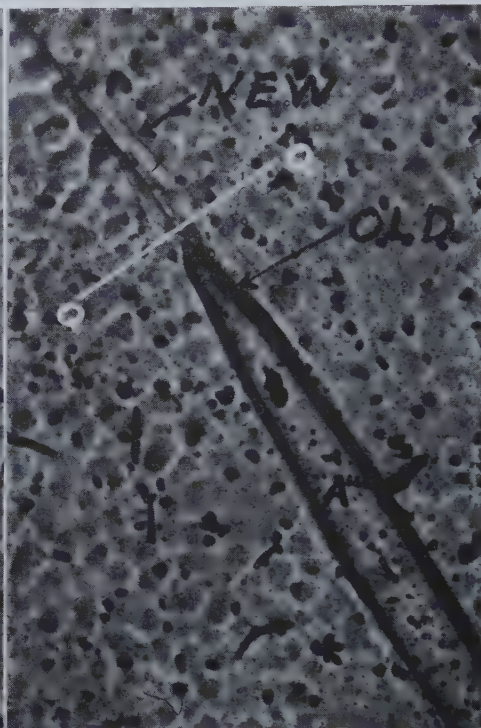The reduction in length of the $BC$ boundary was further confirmed from direct measurements of the



Fig. 4 (left)—
Specimen G in
vicinity of
grains
A, B, and C.

As annealed 14
hr at 1400°C.
X100.

Fig. 5 (right)—
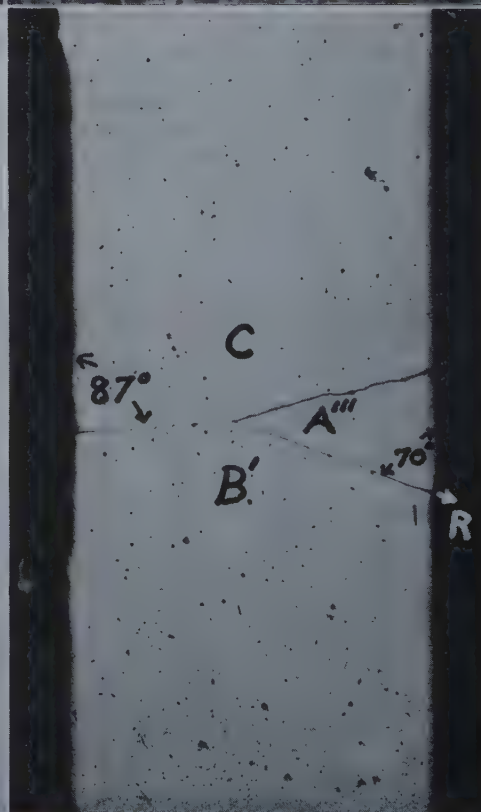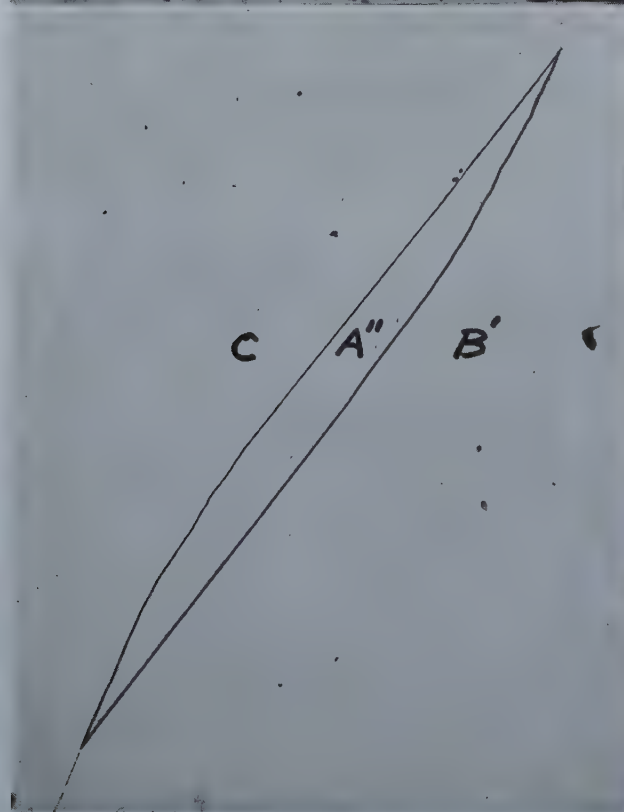Grain A''' in
specimen G.

As annealed 14
hr at 1400°C.
X75.

Fig. 6 (left)—
Grain A'' in
specimen G.

Annealed 48 hr
at 1400°C.
Nital etch. X60.

Fig. 7 (right)—
Cross section of
specimen G.

Nital etch. X100.

position of boundaries before and after a final twelve hour 1300°C anneal.

**Analysis and Discussion of Results:** The locations of $P1$ and $P2$ relative to poles of {112} twin planes indicate that the boundaries $A'''B'$ and $A'C$ are within five degrees of real twin boundaries. An experimental error of two or three degrees could be expected in the measurements, so the nearness to real twin planes is significant. If grain $A$ were exactly in the (001) orientation, the poles of the planes $(\bar{2}11)$ and (211) would lie on a diameter in fig. 2, and traces of the twin planes in the (001) surface would be parallel. This explains the near parallelism of the observed twin boundaries in grain $A''$. Acute angles at the ends of island grain $A''$ are practically equal (value of about 15°) and are the same as that in the $A'B'C$ group and in the island grain $A'''$. Analyses also show that the 180° angle occurred opposite the boundary $AC$ in the $ABC$ group. This was not particularly clear in fig. 4, but became clearer upon subsequent annealing. Further, the surface direction of the boundary $AC$ as shown in fig. 2 indicates that this boundary also could be a real twin boundary if the plane were tilted properly (note position of $\bar{1}21$ pole). The acute angle in the $ABC$ group, however, remained at about 43° during the anneals.

The direction of the boundary $AB$ is about right for a possible correlation with a {112} plane in the lattice of grain $B$ alone (the {112} pole required is not given in fig. 2). This possibility together with the $AC$ twin boundary may be the reason for the constant 43° angle in this group of grains. On the other hand, directions of the type $A'B'$, which together with a twin boundary are responsible for the surface angles of 15°, seem to correlate only with the (110) plane (the pole of this plane is

shown tilted 1.5° to the surface in fig. 2). The $B'C$ boundary tilts 87° to the surface (see fig. 7) and nearly coincides with the (110) plane. The $A'''C$ boundary, also shown in fig. 7, is probably in the transition region between the end of the grain and the twin boundary and is, therefore, not near enough the end of $A''$ to have much significance on this question of the (110) type boundary. Nevertheless the angle that would be made in the surface by the (110) plane and the (211) plane, for example, would be about 18.5° and this is not far from the observed 15° angle (within the specimen these planes would meet in a $[\bar{1}11]$ direction and at an angle of 30°). Also the direction of the junction line $[\bar{1}11]$ would lie at an angle of about 55° to the vertical and in the (110) plane. Measurements on the $A'B'C$ common boundary gave a value of 62° for its tilt from the vertical and this direction was also properly located to lie near the $[\bar{1}11]$ direction. These data, although strongly suggestive of the (110) plane being active, are not sufficiently accurate to prove the point. They do indicate, however, some tendency to a preferred crystallographic boundary arrangement in addition to that of the {112} twin boundary of which more will be mentioned later.

Some conclusions regarding the value of twin boundary energy can be drawn from the data if we assume that the change in type of surface—{221} to {100}—provides no appreciable driving energy. First we note that growth of island grains such as $A''$ represent an increase in boundary area—in fact the increase in the twin boundary area is more than twice the decrease in the second-order twin boundary area, because the twin boundaries are tilted more from the vertical than is the second-order twin boundary $B'C$. Applying the principle of diminishing energy to this case of increasing boundary area gives

$$E_t < 0.46\ E_s \qquad [4]$$

where $E_t$ is the energy per unit area of twin boundary, $E_s$ is the energy for the second-order twin boundary, and tilt-angles of 22° have been used for each twin plane.

Eq 3 cannot be used on specimen G because each 3-grain group contains a {112} twin boundary—an energy cusp boundary as pointed out in the introduction in reference to the theoretical work of Shockley and Read. Because of unique crystallographic and geometrical configurations for each 3-grain group, it appears that one or both of the non-twin boundaries are also of the energy cusp type. If so, the situation means that no equation of the type of Eq 2 applies because any infinitesimal displacement of the triple point produces more than a zero increase in boundary energy.
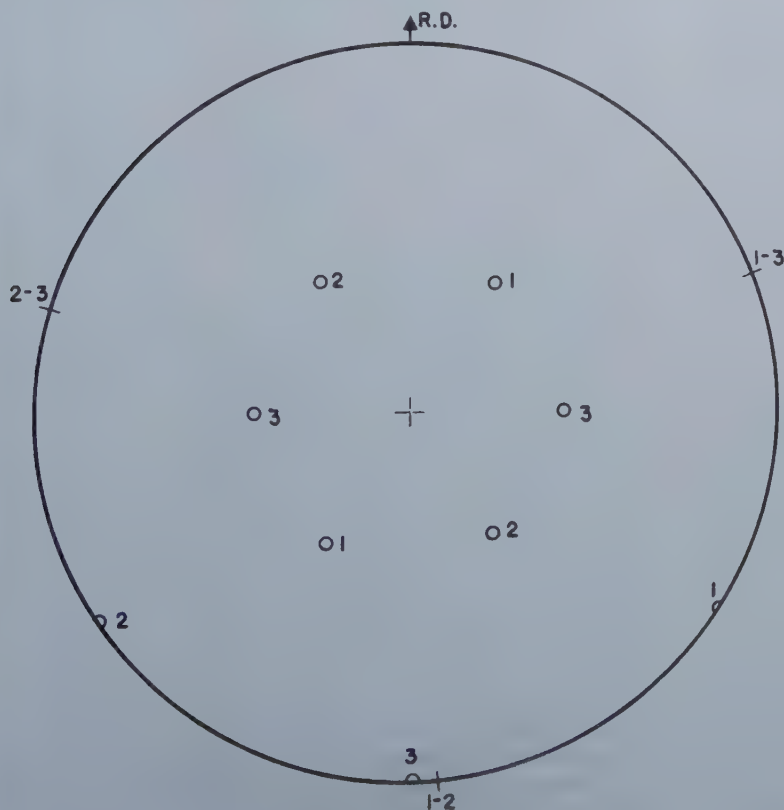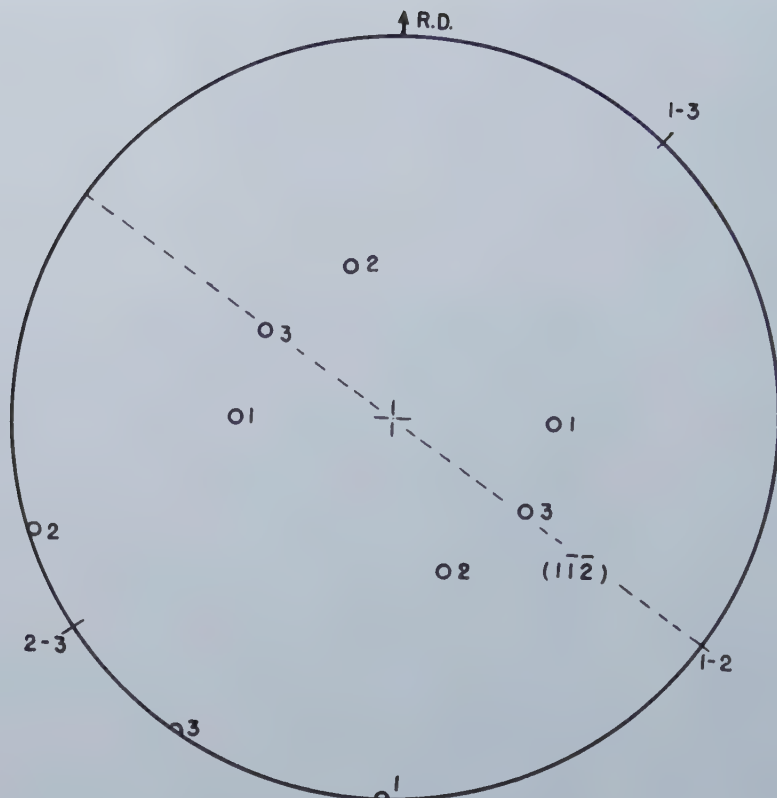


Fig. 8—Stereographic projection showing orientations and boundaries of grains in specimen Q1.

Fig. 9—Stereographic projection showing orientations and boundaries of grains in specimen T1.

Quantitatively the only result obtainable from the data is that expressed in Eq 4 which of course sets an upper limit to the {112} twin boundary energy in terms of $E_{s}$. Qualitatively a twin boundary energy appreciably above zero in value is not inconsistent with the observed 180° angle if non-twin boundaries are associated with energy cusps.

The data show also that a grain boundary in a sheet specimen may deviate from perpendicularity with the surface and thereby reach a lower energy position for the entire boundary. As a result we may obtain, as in the present experiment, a common junction line tilted as much as 60° to the surface. Although apparent, it is important to point out that the present results show the existence of boundaries which are far from their minimum area positions and hence are themselves evidence for an appreciable effect of boundary orientation on boundary energy.

### 3-Grain Groups with One Set of Twin Related Grains

**Specimens:** A method of producing 3-grain specimens with grains in predetermined orientations was described in earlier papers.[2, 8] This method was also used in the preparation of the present specimens. In specimen Q1 each grain had the (110) plane in the plane of the sheet and the [001] direction as shown in fig. 8, grains 1 and 2 being approximate twins. During preparation of this specimen, the boundary orientation of grains 1 and 2 was controlled as closely as possible, resulting in an approximate {112} twin boundary for these near twin grains.

In order to produce grains in exact twin orientation with each grain having the (110) plane in the plane of the sheet, recourse was made to the phenomenon of twinning by stimulated nucleation.[9]

Requirements considered necessary for a successful application of this phenomenon were: (1) a matrix of fine grains which would support growth of a single grain after the matrix was strained a small amount, and (2) a matrix which would support growth of a twin grain preferentially to that of the starting grain. Since the desired orientations were (110) in the plane of the sheet, the problem was to prepare a material that would support growth of the (110) [001] orientation preferentially over the twin orientation 70°32′ away without losing the ability to support growth of this latter orientation. Cold rolled silicon iron, which develops a sharp (110) [001] texture by selective grain growth,[10] would be unsuitable for the present purpose because of its narrow range of orientations for permissible grain growth.

A satisfactory material was made by cold rolling a hot rolled band from a thickness of 0.1 in. to 0.030 in., decarburizing at 850°C to a final carbon content of about 0.004 pct, cold rolling from a thickness of 0.030 in. to 0.025 in., annealing a short time at 800°C, and finally straining 2.5 pct in tension. Instead of starting the growth of two reoriented seed grains as is normally done in the preparation of a 3-grain specimen, the present method consisted in starting the growth of one grain having the (110) plane parallel to the sheet and the [001] direction 70.5° from the rolling direction.

During a short anneal in a gradient temperature furnace, two new grains in the (110) [001] orientation were obtained as the result of twinning. These grains grew adjacent to the mother crystal. As expected, however, the boundaries of the twin grains were not straight like those in copper, but were irregular in shape as a result of anisotropic growth in the strained matrix. To complete the sample

another grain, after reorientation, was grown from the opposite end until it met the three grains previously formed. This sample was then cut into two 3-grain specimens called T1 and T2.

The orientation of the boundaries between the twin grains in these specimens was nearly ideal for an attempt to make them coincide with specific crystallographic planes. This could be done by causing the open ends of the boundaries to move a small amount. Notches for this purpose, therefore, were made in specimen T1 (see fig. 11) in such a way that the boundary between grains 1 and 2 would tend to move towards coincidence with a common {112} plane during subsequent annealing. Similarly the 1-2 boundary in specimen T2 was cut in the hope that it would form on a {111} type plane and thus produce {111} twins in silicon iron. Fig. 9 and 10 give the orientations of the grains in each of these specimens. It will be noted that the groups are identical except for reversal in the notation for grains 1 and 2.

Annealing at high temperatures, as described in the first section of this paper, was carried out to equilibrate the grain boundaries. Annealing schedules were as follows:

Q1: (1) 24 hr at 1200°C, (2) 8 hr at 1400°C, (3) 10 hr at 1400°C, (4) 48 hr at 1400°C, (5) 47 hr at 1400°C, all in an atmosphere of argon.

T1 and T2: (1) 12 hr at 1300°C, (2) 5 hr at 1200°C, (3) 10 hr at 1300°C, (4) 12 hr at 1300°C, (5) 4 hr at 1200°C, and (6) 47 hr at 1400°C, all in argon except the 1200°C anneals which were run in pure dry hydrogen to effect additional purification of the samples.

Structures: The changes in the grain boundaries of specimens T1 and T2 produced by annealing at high temperatures are shown by the photographs in fig. 11 and 12 taken before and after anneals.

A significant change in specimen T1 is the early straightening of portions of both parts of the 1-2 boundary to coincide with the {112} twin boundary (such behavior was not noted in specimen Q1 for the "near twin" grains). Interesting also is the removal of the edge grain during the last anneal and the register of a twin boundary through thermal etching.

The 1-2 boundary of specimen T2 did not straighten even with extra notching, which was employed in an attempt to put the boundary in the desired {111} orientation. Also, the junction line failed to reach perpendicularity with the sheet, but consistently remained tilted 5 to 10°.

The micrograph shown in fig. 13 gives the final grain configuration of specimen T1 after polishing and etching (reversed in photographing). Difficulties were encountered in disclosing the twin boundary without overetching the other boundaries. The angle opposite the twin boundary ($\theta_s$) is 167° and this was reached early in the anneals. The other two angles, however, continued to change in the anneals, $\theta_1$ increasing about 10° after the first anneal to a value of 82° and $\theta_2$ decreasing about 10° to a value of 111°.

The directions of the final grain boundaries for specimens Q1, T1, and T2 are given in fig. 8, 9, and 10 respectively. The 1-2 boundary of Q1 is about 4° from an approximate {112} twin plane for grains 1 and 2 (such a plane would lie halfway between the [001] directions of these grains). The 1-2 boundary of T1 (see fig. 9) coincides with the ($1\bar{1}2$) twin plane within an experimental error of 1°; so {112} twins were obtained in this specimen. In specimen T2, however, {111} twins were not ob-
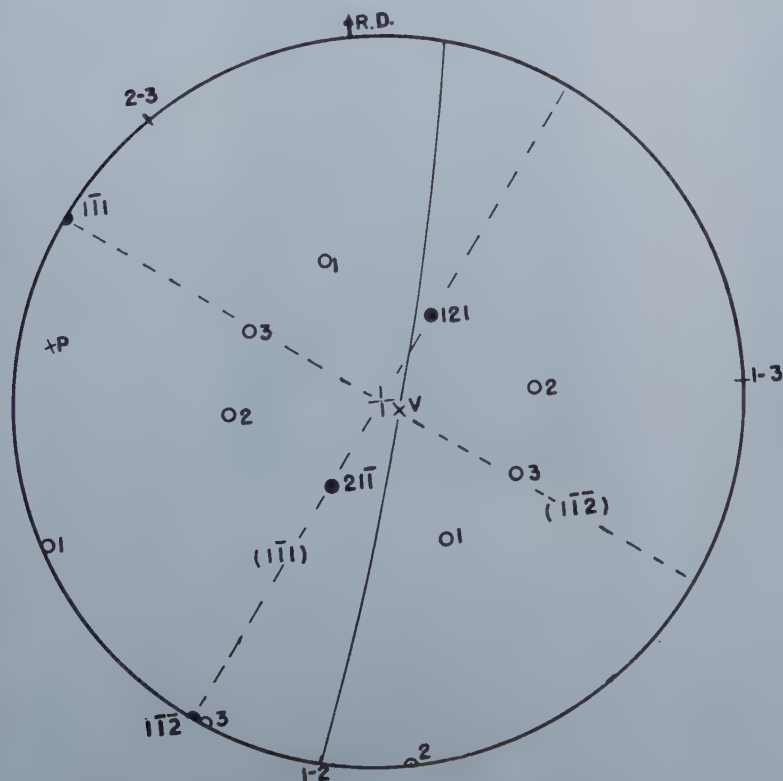


Fig. 10—Stereographic projection showing orientations and boundaries of grains in specimen T2.

Fig. 11—Specimen T1.

A. Original specimens. Etched. X7.5.
B. After 12 hr at 1300°C. Etched.
X7.5.

Fig. 12—Specimen T2.

C. After fifth anneal. Hydrogen
etch. X7.5.
D. After final anneal. Thermal etch.
X7.5.

**Fig. 13—Specimen T1 after final anneal.**
Nital etch.  X500.

tained because the 1-2 boundary of the twin grains (see fig. 10) is 21° from the $(1\bar{1}1)$ plane. The solid line passing through $V$, the common junction line, gives the orientation of the 1-2 boundary, and the normal to this boundary is the point $P$. All three poles of possible {112} twin planes—and these apply also to specimen T1—lie in the $(1\bar{1}1)$ plane as shown. Only the $(1\bar{1}\bar{2})$ pole falls anywhere near a position which would represent a plane perpendicular to the sheet (this is the one obtained in specimen T1). Although the $(1\bar{1}1)$ plane is also perpendicular to the sheet, the 1-2 boundary is removed from it both azimuthally and by tilt.

**Discussion of Results:** From the nature of the data and expected energy cusps, an equation of the form of Eq 2 should be employed for specimens T1 and Q1. The required equation is

$$E_{12} + E_{23} \cos \theta_2 + E_{13} \cos \theta_1 + \epsilon_2 E_{13} \sin \theta_1 - \epsilon_1 E_{23} \sin \theta_2 = 0 \quad [5]$$

with the $\epsilon$'s introduced explicitly. (To agree with the notation of Shockley and Read, we should think of the present specimens turned over so that the sequence of grains 1, 2, 3, is counterclockwise and, therefore, in the direction of increasing $\phi$). We believe that $\epsilon_1$ and $\epsilon_2$ may be neglected for specimens T1, Q1, and T2. Making these assumptions we obtain

$$E_{12} + E_{23} \cos \theta_2 + E_{13} \cos \theta_1 = 0 \quad [6]$$

In order to obtain $E_{12}$ relative to $E_{23}$ and $E_{13}$, we shall set $E_{23}$ and $E_{13}$ both equal to 1, which seems reasonable according to the curve of fig. 10 of ref. 2.

The 1-2 boundary in specimen T2, however, is not in a minimum energy position, so Eq 3 can be used with $\epsilon_1$ and $\epsilon_2$ set equal to zero, it being remembered that the 2-3 and 1-3 boundaries of specimen T2 are the same as those of T1 except for boundary orientation. As in specimen T1 we set $E_{23}$ and $E_{13}$ both equal to 1. Substituting in Eq 3 gives

$$\frac{E_{12}}{\sin \theta_3} = \frac{1}{\sin \theta_1 + \epsilon_3 \cos \theta_1} = \frac{1}{\sin \theta_2 - \epsilon_3 \cos \theta_2} \quad [7]$$

This equation and the equation of definition of $\epsilon_3$

determine $E_{12}$, $\epsilon_3$ and $\dfrac{\partial E_{12}}{\partial \phi_{12}}$ for specimen T2.

The equilibrium angles are the angles between the grain boundary directions. These directions as given in fig. 8, 9, 10 were determined relative to the direction R. D. by direct measurement of the specimens at a magnification of 200 diam with a microscope attachment for reading angular positions. The equilibrium angles and the calculations made with them using Eq 6 for Q1 and T1 and Eq 7 for T2 are given in table I.

**Table I. Equilibrium Angles and Relative Grain Boundary Energies of Specimens Q1, T1, and T2**

| Specimen | Equilibrium Angles | | | Relative Energies | | | | |
|---|---|---|---|---|---|---|---|---|
| | $\theta_1$ | $\theta_2$ | $\theta_3$ | $E_{12}$ | $E_{13}$ | $E_{23}$ | $\epsilon_3$ | $\dfrac{\partial E_{12}}{\partial \phi_{12}}$ |
| Q1 | 107 | 111 | 142 | 0.65 | 1 | 1 | | |
| T1 | 82 | 111 | 167 | 0.22 | 1 | 1 | | |
| T2 | 102 | 131 | 127 | 0.86 | 1 | 1 | 0.26 | 0.22 |

Of major interest in these results is the relatively low value of the {112} twin boundary energy as given by the figure 0.22 in the table. Whether or not this energy is too high, the removal of the edge grain in specimen T1 by grain boundary movement may be taken as evidence in favor of a value appreciably above zero (the driving energy for similar boundary movements recently has been discussed[11]). The thermal etching of the twin boundary is also evidence of grain boundary energy.

Another interesting result is the fact that the value of $E_{12}$ for a "near" {112} twin boundary is much larger than $E_{12}$ for an exact twin boundary. The value of 0.65 of Q1 is not strictly comparable with the value 0.22 of T1 because of no common reference points, but the magnitude of the difference justifies the conclusion that boundary energy increases rapidly with departure from the twin condition—a result that is in agreement with the theoretical predictions of Shockley and Read.[4] There are two features to the theoretical predictions: (1) a rapid increase in energy with departure from the twin orientation and (2) a rapid increase in energy with departure of the boundary from the twin plane, the orientations remaining in a twin relation. This latter effect provides a reasonable explanation of the rapid straightening of the 1-2 boundary of specimen T1, which occurred during annealing. Since the area $A$ of a boundary alters only to a small degree toward the end of a straightening process, the total boundary energy (product of $E$ and $A$) decreases mainly because $E$ itself decreases as the boundary approaches the minimum point of an energy cusp.

Finally the results obtained on specimen T2 are interesting for two reasons. First the results show the existence of a relatively high energy (namely, 0.86) in a grain boundary of twin oriented grains. Secondly it can be seen that estimates of the grain boundary orientation effect (i.e. values of $\epsilon$ and $\dfrac{\partial E}{\partial \phi}$) can be made using Eq 3 if the $\epsilon$'s and $E$'s of two boundaries are known.

A rough curve of $E$ versus $\phi$ for the boundary between twin related grains may be drawn from the data on orientation relationships and the $E$ and $\epsilon$

values of table I. Such a curve rises rapidly near the {112} twin boundary and slowly at a point 70° away. Qualitatively this result is in agreement with a {112} cusp predicted[4] for twin related grains.

An energy cusp is expected for certain symmetrical arrangements of the lattices of two grains relative to the boundary between them[4] and both {112} and {111} twins have the symmetrical relationship. Whether or not a drop in energy occurs when the boundary approaches the orientation of the {111} common plane cannot be determined from the present data. Since energy changes rapidly near a cusp position, it probably would be necessary to put the grain boundary within 5 or 10° of a cusp position before the boundary would move by itself to the minimum energy configuration. Consequently failure to make {111} twins in specimen T2 may be due mainly to the fact that the boundary was never brought near enough the "cusp position."

### Comments on Energy Cusp Boundaries

When two grains are related exactly according to some simple crystallographic law as, for example, "twin related," the possibility exists for low energy boundaries and energy cusps for certain orientations of the boundary. The orientation of a boundary may be described in terms of the crystallographic plane of each lattice which coincides with the boundary. We therefore shall indicate in the following such boundaries by attaching subscripts 1 and 2 to the crystallographic notations, these subscripts referring to the two lattices respectively.

In the case of twin grains of silicon iron (a BCC lattice), the present data are in agreement with a $\{112\}_1$, $\{112\}_2$ energy cusp boundary. Results on specimen G indicate (1) a possible $\{110\}_1$, $\{110\}_2$ energy cusp boundary and (2) a $\{112\}_1$, $\{552\}_2$ low energy boundary. The behavior of the 1-2 boundary in specimen T2, however, puts doubt on the $\{112\}_1$, $\{552\}_2$ possibility. The point P, the pole of the 1-2 boundary, is 6° from the correct point which lies on the basic circle and 19°28′ from the pole of the (111) plane. It would be expected that the 1-2 boundary if only 6° away would have moved into coincidence with a minimum energy position, and also would have formed a straight line in the surface of the specimen. Actually these changes did not occur.

Shockley and Read[4] predict energy cusps in twin related grains for (1) $\{111\}_1$, $\{111\}_2$; (2) $\{110\}_1$, $\{114\}_2$; and (3) $\{112\}_1$, $\{112\}_2$ boundaries.

In the case of second-order twins, the data for specimen G suggest an energy cusp for a $\{110\}_1$, $\{110\}_2$ boundary. Theory[4] also indicates energy cusps for $\{114\}_1$, $\{114\}_2$ and $\{221\}_1$, $\{221\}_2$ boundaries. Grains in these configurations could be called {114} and {221} twins respectively. The $\{110\}_1$, $\{110\}_2$ configuration, however, does not satisfy the reflection law which is definitive for twins.

Because of these interesting possibilities an investigation has already been started at this laboratory to determine the existence of various energy cusp boundaries. In such work it has been found convenient to use 2-grain specimens. 2-grain specimens also offer the possibility of studying quantitatively "the effect of boundary orientation on boundary energy" because the mathematical relationships involved are relatively simple.

### Summary and Conclusions

An investigation of energy in twin boundaries has been undertaken. Silicon ferrite specimens containing twin related grains were prepared using the phenomenon of "annealing twin formation." In the study of changes that took place during specimen preparation and during subsequent annealing, the following points of interest were noted:

1. On annealing one specimen consisting of twin related grains, it was found that a combination of two twin boundaries and one second-order twin boundary was unstable because of low energy in the twin boundaries. Under these conditions the total grain boundary area increased as the system moved to lower energy. Although constant angles were obtained for the specimen, it was concluded that none of the equilibrium equations could be used to calculate relative interface energies.

2. It was found possible (a) to make exact twin oriented grains having the (110) plane in the plane of the sheet and (b) to vary the boundary orientation over wide ranges. An attempt to make {112} twins in this manner proved successful; a similar attempt to make {111} twins, however, was not successful.

3. Using specimens as indicated under (2), (a) a {112} twin boundary with an energy between one-fifth and one-fourth that of ordinary boundaries was found, (b) boundary energy increases rapidly with deviation from a twin condition, (c) depending on orientation of the boundary, high as well as low boundary energy occurs in twin related grains, and (d) a {112} twin boundary like any other boundary will thermally etch at high temperatures producing a visible groove that coincides with the position of the boundary.

### References

[1] Cyril Stanley Smith: Grains, Phases and Interfaces: An Interpretation of Microstructures. *Trans.* AIME (1948) **175**, 15. *Metals Tech.*, June 1948. TP 2387.

[2] C. G. Dunn and F. Lionetti: The Effect of Orientation Difference on Grain Boundary Energies. *Trans.* AIME (1949) **185**, 125. *Jnl. of Metals*, Feb. 1949, TP 2517.

[3] C. Herring: Surface Tension as a Motivation for Sintering. To be published.

[4] W. Shockley and W. T. Read: Dislocation Models of Crystal Grain Boundaries. To be published.

[5] P. Lacombe: "Sub-boundary" and Boundary Structures in High Purity Aluminum. Bristol Conf. on Strength of Solids (1947). The Phys. Soc. London (1948).

[6] L. W. McKeehan: The Formation of Twin Metallic Crystals. *Nature* (1927) **119**, 120, 392. See also: Twinning in Ferrite. *Trans.* AIME (1928) **78**, 453.

[7] G. D. Preston: The Formation of Twin Metallic Crystals. *Nature* (1927) **119**, 600.

[8] C. G. Dunn: Controlled Grain Growth Applied to the Problem of Grain Boundary Energy Measurements. *Trans.* AIME (1949) **185**, 72. *Jnl. of Metals*, Jan. 1949, TN 9.

[9] W. G. Burgers and W. May: Auslosungskrystalle und Zwillingsbildung in Rekrystallisierten Aluminium. *Rec. Trav. Chim.* (1945) **64**, 5-19.

[10] C. G. Dunn: Recrystallization Textures. Phila. Seminar on the Cold Working of Metals, Oct. 1948. Sponsored by the Amer. Soc. for Metals.

[11] C. G. Dunn, F. W. Daniels, and M. J. Bolton: On the Problem of Grain Boundary Movement. *Trans.* AIME (1949) **185**, 708. *Jnl. of Metals*, Oct. 1949, TN 25.

# Behavior of Pores

## during the

# Sintering of Copper Compacts

## by F. N. Rhines, C. E. Birchenall, and L. A. Hughes

STUDIES upon the sintering of metal powders, in the solid state, have led to the proposal that the surface energy of the powder particles provides the driving force that causes points of contact between pairs of particles to grow into broad welds which isolate the residual vacant space into pores that tend to spheroidize and gradually to diminish in total volume.[1] Investigators differ with regard to the mechanism of the movement of the metal, under the influence of surface energy, to accomplish these changes. One school asserts that there is a mass movement of the metal, referred to as a "viscous flow," while the other school prefers to view the movement as a self diffusion process, wherein individual atoms are transferred without disturbance of the basic pattern of the crystal lattice. Extensive experimental studies upon the sintering of copper, conducted recently by A. J. Shaler,[2] have been in-

terpreted by their author as support for the viscous flow mechanism of transport, the theory of which was developed originally by J. Frenkel.[3] Duplicating a portion of this work with minor changes, G. C. Kuczynski[4] is led to the alternate view, namely, that the initial stages of sintering, at least, proceed as a self-diffusion process. Both of these investigations were designed to deal with an isolated unit of sintering, i.e., with the shrinkage of a single pore, or with the growth of a single point weld. It remains to ascertain the behavior of a typical metal powder compact composed of a large number of particles of varying size and sintering to a body with a multiplicity of pores. The observation of density changes alone during sintering is not sufficient in such a case; it is essential to know how the internal geometry of the compact changes. This has been the object of the present investigation, the results of which are used to support the self-diffusion mechanism of sintering.

The present studies consist in the measurement of the number of pores as a function of size and time at temperature during the sintering of a copper compact made from a commercial copper powder lightly pressed and sintered in several different atmospheres. A brief survey was made also of the change in shape of the pores, under the influence of the same variables. All of this was done by direct observation with the microscope. Densities were measured on the same sample. It is found that, while the compact is exhibiting an overall shrink-

F. N. RHINES, Member AIME, is Professor of Metallurgy and Member of Staff and C. E. BIRCHENALL is Member of Staff, of the Metals Research Laboratory, Carnegie Institute of Technology. L. A. HUGHES was formerly Laboratory Assistant in the Metals Research Laboratory, Carnegie Institute of Technology. Currently, Materials Engineering Division of the Westinghouse Electric Co., Pittsburgh, Pa.

age in volume, the pores exhibit progressive growth with a decrease in their total number, the reduc-

**Table I. Particle Size Analysis of the Copper Powder**

| Mesh Size | Pct by Weight |
|---|---|
| 150 | 0.1 |
| 200 | 7.5 |
| 250 | 11.1 |
| 325 | 20.4 |
| 40 | trace |
| 20 | 29.6 |
| 10 | 21.4 |
| 5 | 7.8 |
| —5 | 2.0 |

tion in number being accomplished by the disappearance of pores of smaller size. The critical size, below which all pores shrink and disappear,

becomes larger as sintering progresses. It is noteworthy also that all porosity soon disappears from the immediate neighborhood of the external surface of the compact. As has been observed by previous investigators, the pores change in shape from a highly complex form towards more or less equiaxed shapes. All of these changes proceed much more rapidly as the temperature is raised.

### Experimental Procedure and Results

All of the compacts used in these studies were made from a single lot of reduced oxide copper powder, the particle size analysis of which is presented in table I.

Upon receipt, this powder was carefully blended by hand "rolling" and was sealed in small glass vessels until the moment of its use. While a special effort

**Table II. Pore Counts in Surface Area of 0.0293 sq cm**
**Hydrogen Treatment**

| Temp. °C | Time (Hr) | Pore Size Equivalent to Square with Side of Length (mm) | | | | | | | | |
|---|---|---|---|---|---|---|---|---|---|---|
| | | 0.034 | 0.025 | 0.017 | 0.012 | 0.009 | 0.006 | 0.004 | 0.003 | smaller |
| 800 | 1 | 0 | 0 | 0 | 18 | 41 | 361 | 677 | 1496 | 1798 |
| 800 | 10 | 0 | 0 | 1 | 17 | 33 | 421 | 566 | 1370 | 1695 |
| 800 | 100 | 0 | 2 | 5 | 24 | 53 | 291 | 568 | 1423 | 1730 |
| 800 | 1000 | 0 | 2 | 5 | 27 | 61 | 302 | 548 | 1339 | 1638 |
| 900 | 1 | 4 | 9 | 16 | 51 | 163 | 545 | 803 | 1654 | 1255 |
| 900 | 10 | 0 | 7 | 27 | 61 | 256 | 399 | 651 | 1423 | 953 |
| 900 | 100 | 1 | 4 | 69 | 199 | 371 | 765 | 1263 | 850 | 743 |
| 900 | 1000 | 3 | 18 | 65 | 316 | 925 | 1085 | 872 | 757 | 639 |
| 1000 | 1 | 0 | 15 | 65 | 413 | 1397 | 2987 | 2340 | 1415 | 1189 |
| 1000 | 10 | 7 | 21 | 73 | 221 | 683 | 1208 | 1645 | 1024 | 674 |
| 1000 | 100 | 7 | 44 | 93 | 293 | 769 | 824 | 514 | 392 | 314 |
| 1000 | 1000 | 24 | 49 | 113 | 241 | 357 | 272 | 133 | 66 | 39 |

**Table III. Pore Counts in Surface Area of 0.0293 sq cm**
**Vacuum Treatment**

| Temp. °C | Time (Hr) | Pore Size Equivalent to Square with Side of Length (mm) | | | | | | | | |
|---|---|---|---|---|---|---|---|---|---|---|
| | | 0.034 | 0.025 | 0.017 | 0.012 | 0.009 | 0.006 | 0.004 | 0.003 | smaller |
| 800 | 1 | 0 | 3 | 17 | 149 | 233 | 374 | 685 | 1431 | 2206 |
| 800 | 10 | 0 | 0 | 9 | 47 | 94 | 129 | 320 | 1196 | 2163 |
| 800 | 100 | 0 | 33 | 89 | 181 | 318 | 677 | 878 | 807 | 1500 |
| 800 | 1000 | 0 | 8 | 101 | 145 | 307 | 536 | 750 | 1360 | 1450 |
| 900 | 1 | 1 | 14 | 15 | 59 | 99 | 226 | 680 | 1515 | 1867 |
| 900 | 10 | 2 | 7 | 14 | 34 | 98 | 243 | 731 | 1486 | 1686 |
| 900 | 100 | 4 | 3 | 23 | 54 | 130 | 283 | 568 | 1270 | 1122 |
| 900 | 1000 | 5 | 13 | 87 | 194 | 327 | 347 | 627 | 1270 | 1301 |
| 1000 | 1 | 0 | 6 | 32 | 74 | 145 | 221 | 351 | 805 | 1509 |
| 1000 | 10 | 1 | 10 | 34 | 185 | 435 | 866 | 1464 | 2096 | 1424 |
| 1000 | 100 | 3 | 12 | 40 | 123 | 181 | 425 | 923 | 1044 | 833 |
| 1000 | 1000 | 5 | 17 | 56 | 133 | 306 | 590 | 1243 | 1101 | 865 |

**Table IV. Pore Counts in Surface Area of 0.0293 sq cm**
**Argon Treatment**

| Temp. °C | Time (Hr) | Pore Size Equivalent to Square with Side of Length (mm) | | | | | | | | | | | |
|---|---|---|---|---|---|---|---|---|---|---|---|---|---|
| | | 0.096 | 0.068 | 0.048 | 0.034 | 0.025 | 0.017 | 0.012 | 0.009 | 0.006 | 0.004 | 0.003 | smaller |
| 800 | 1 | 0 | 0 | 0 | 0 | 0 | 0 | 5 | 119 | 589 | 1135 | 1753 | 1894 |
| 800 | 10 | 0 | 0 | 0 | 0 | 0 | 0 | 14 | 169 | 715 | 1026 | 1482 | 1681 |
| 800 | 100 | 0 | 0 | 0 | 0 | 1 | 41 | 138 | 297 | 581 | 1152 | 1533 | 1599 |
| 800 | 1000 | 0 | 0 | 0 | 0 | 4 | 28 | 80 | 207 | 486 | 842 | 1384 | 1594 |
| 900 | 1 | 0 | 0 | 0 | 0 | 1 | 3 | 209 | 618 | 1100 | 1224 | 1294 | 1358 |
| 900 | 10 | 0 | 0 | 0 | 0 | 6 | 79 | 175 | 498 | 743 | 1296 | 1435 | 1338 |
| 900 | 100 | 0 | 0 | 0 | 2 | 18 | 65 | 139 | 270 | 792 | 1267 | 1118 | 1039 |
| 900 | 1000 | 1 | 10 | 17 | 55 | 172 | 264 | 284 | 454 | 440 | 352 | 292 | 243 |
| 1000 | 1 | 0 | 0 | 0 | 0 | 0 | 6 | 104 | 503 | 620 | 1361 | 1605 | 1908 |
| 1000 | 10 | 0 | 0 | 0 | 0 | 0 | 8 | 53 | 464 | 746 | 1331 | 1844 | 1577 |
| 1000 | 100 | 0 | 0 | 0 | 0 | 3 | 172 | 210 | 553 | 676 | 672 | 718 | 687 |
| 1000 | 1000 | 0 | 0 | 0 | 1 | 9 | 28 | 152 | 647 | 862 | 673 | 604 | 542 |
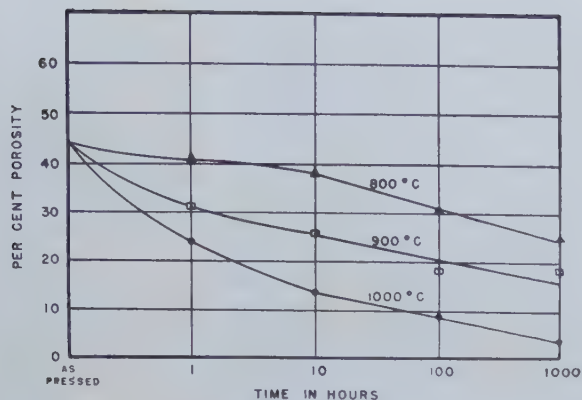
Fig. 1 (left)—Change in density of samples sintered in hydrogen.

Fig. 2 (below)—Change in density of samples sintered in vacuum.
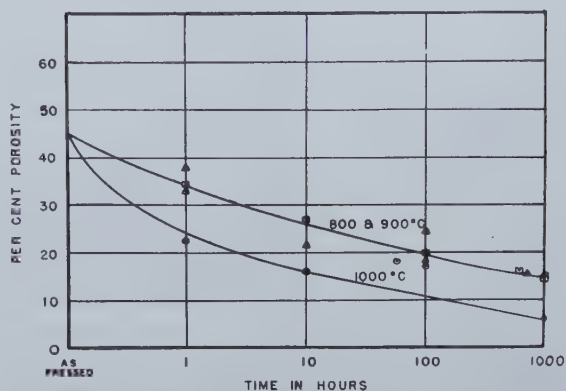


was made to secure powder of high chemical purity, it is evident from the microstructure of the sintered compacts that this powder contained a small amount of nonmetallic impurities in addition to the expected surface film of copper oxide. Cylindrical compacts 0.876 in. in diam and approximately 0.4 in. high were pressed, without lubricant from about 30 g of powder, in a double acting steel die, at a unit pressure of 12,700 psi.

Sintering treatments were conducted in thermostatically controlled electric resistant furnaces wherein the heating chamber consisted of a horizontal silica tube. The samples were set on edge in alumina lined boats which were introduced into the furnace before heating and were removed only after the furnace had cooled to room temperature. About a half hour was usually required for the furnaces to reach the control temperature and a maximum of about 10 hr for cooling. The atmospheres used were: tank hydrogen, dried by passing through calcium chloride, high purity tank argon, and a moderate vacuum in which the atmosphere consisted of somewhat less than 1 mm pressure of air (i.e., the vacuum produced continuously by a laboratory type vacuum oil pump). Schedules of the heat treatments run are included in tables II, III and IV. No less than four and often as many as twelve check samples were treated under each set of conditions.

Density measurements were made by weighing in water and air. A thin paraffin coating was applied to each sample to prevent entrance of water into the pores during the test. The results of the density measurements are presented in fig. 1, 2, and 3, wherein the average per cent porosity of the as-pressed samples is indicated at the left edge of each graph, and the curves record the variation of density with time under each of the conditions of sintering. Each plotted point represents an average of at least 4 and at most 12 separate tests.

Pore counts were made directly with a microscope, using a grain size measuring eye-piece. The latter is a device which superimposes upon the image of the specimen a selection of eight squares of descending size, see tables II, III, and IV. With this equipment, the number of pores in each of nine size ranges (12 for the argon treatments) was counted in a specified area of surface. Each pore was identified as such and distinguished from inclusions by applying the focusing test and was then matched in total cross-sectional area to one of the comparison squares.

This method of size classification, although leaving much to be desired, was adopted only after several other optical and X ray procedures had been tried. It ignores both the shape of the cross section of the pore and the depth, but it does yield a measurement that is proportional to the true pore size for any established shape. Since the shape changes proceed more slowly than the volume changes, this measurement is capable also of revealing pore volume changes in a semiquantitative way.

Under these circumstances any attempt to achieve a high degree of precision in the size classification may appear pointless. It remains desirable, however, to insure that all measurements be comparable and, to this end, the procedures used in preparing the polished surfaces and in counting were carefully planned and standardized. Chief among the precautions taken was a system of polishing the specimens in groups, in polishing clamps, with regrouping and repolishing, after counting a first time, so as to detect any variation in the pore count that might arise through inadvertent deviations from the prescribed polishing procedure. Ordinary polishing techniques were employed, using the sequence of smoothing on fine emery paper, followed by rough polishing with 600 grit alundum and finishing with Fisher No. 3 levigated alumina on a Gamal cloth. Prior to counting, the samples were lightly etched with a dichromate reagent, in order to remove flow and to reveal the grain boundaries. This treatment did not noticeably enlarge the pores; indeed, it appears that the pore size has been underestimated rather than the reverse; see typical structures in fig. 4, 5, 6 and 7.

On each sample the pore count was made along

two traverses wherein all pores coming within the field of view were counted throughout the length of the traverse. These traverses were made perpendicular to the flat surface of the cylindrical specimen, one being close to the external surface and the other close to the center line of the specimen. Since each specimen was polished and measured twice, there were four sets of counts which were added to give the total pore count, see tables II, III and IV. The total area over which the count was made was approximately 3 sq mm.

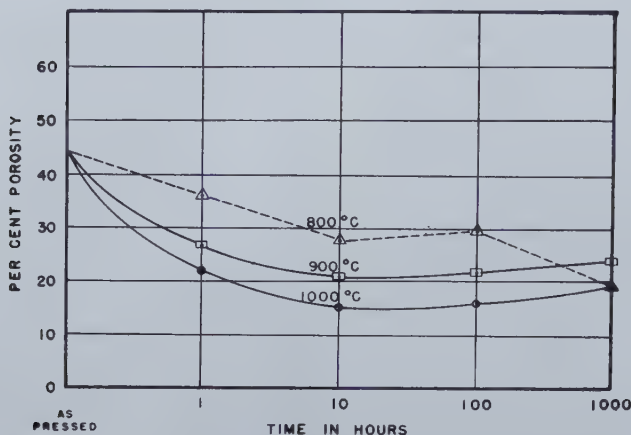For the study of the change in shape of the pores during sintering, observations were made on enlarged micrographs of typical areas in each of the specimens. The measurement here consisted in a planometric measurement of the area of each pore and a linear measurement of its perimeter. These two measurements were converted to a ratio, namely: the perimeter divided by 2 $\pi$ times the radius of a circle of area equal to that of the pore cross-section. About 50 pores were so measured on each specimen and the shape factor ratios presented in table V represent the average of this number of observations. The only clear trend exhibited in this table is that shown in hydrogen sintering at 1000°C (a most favorable case), where the shape factor progresses regularly toward unity (spherical). It is to be understood that the shape factors of the pores in a given sample deviated greatly from the mean.

### Discussion of the Observations

A clear qualitative impression of the volume changes that are being experienced by the pores during sintering may be had by reference to fig. 8, a schematic representation of results for a single temperature from table II. Here it is apparent that the pore count reaches a maximum for some intermediate pore size and that the size corresponding to this maximum increases with time of sintering, while the height of the maximum is decreasing. This means that, individually, each pore, larger than the minimum size, grows for a time and then shrinks to ultimate disappearance. On the average, those pores that are larger than the size at the maximum count are growing, while those smaller than this are shrinking. No change in the total volume of porosity need occur, only a growth of the larger pores at the



Fig. 3—Change in density of samples sintered in argon.

### Table V. Average Shape Factors*

| Treatment | Time | | | |
|---|---|---|---|---|
| H₂, °C | 1 | 10 | 100 | 1000 hr |
| 800 | 1.50 | 1.32 | 1.26 | 1.22 |
| 900 | 1.40 | 1.30 | 1.27 | 1.22 |
| 1000 | 1.42 | 1.26 | 1.23 | 1.17 |
| Vacuum (low air pressure) | | | | |
| 800 | 1.30 | 1.34 | 1.30 | 1.30 |
| 900 | 1.25 | 1.25 | 1.26 | 1.26 |
| 1000 | 1.25 | 1.25 | 1.25 | 1.30 |
| Argon | | | | |
| 800 | 1.22 | 1.28 | 1.21 | 1.24 |
| 900 | 1.22 | 1.32 | 1.36 | 1.22 |
| 1000 | 1.19 | 1.32 | 1.22 | 1.26 |

* Note—The shape factor is the ratio of the measured perimeter of the pore section divided by 2 $\pi$ times the radius of the circle of the equivalent area. For a circular cross-section the factor would be 1.00

expense of the smaller ones. A net reduction in the total pore volume may, on this basis, be regarded as the "growth" of the space outside the bounding surfaces of the sample. That this is probably the true mechanism of total volume shrinkage, after the pores have become isolated, is indicated by the additional observation that there is always a region next to the external surface where no pores are present.

Attention is directed to the fact that the pore count curves in fig. 8 progress rather steeply downward from their maxima toward the smallest pore size observed. This suggests that the number of submicroscopic pores is small; their volume would make a negligible contribution to the total volume of porosity in the sample. It suggests also that the velocity of shrinkage of the pores becomes very high as their size becomes very small. While this condition is most evident in the case of the samples sintered in hydrogen at 1000°C (fig. 8 and table II), it appears to be general for all conditions of sintering, with the exception that the existence of a maximum pore count at some submicroscopic pore size must be taken on faith in some of the series sintered at the lowest temperature.

Turning to the opposite ends of the pore count curves, fig. 8, it is seen that there is an actual increase in the number of pores of the larger sizes as sintering proceeds. In most cases, long sintering induces the appearance of pores of larger size than any found at shorter times, see tables II, III and IV. There is little difference in this respect between the samples sintered in hydrogen and those sintered in vacuum, but the growth of the largest pores becomes exaggerated and the density begins to decrease upon sintering in argon for long times at 900°C, see table IV and fig. 3. From this it may be concluded that there is a definite effect of entrapped gas upon the growth of pores; hydrogen, which diffuses rapidly through copper has no more effect than a low air pressure, but argon, which diffuses very slowly, tends to expand the pores. The absence of a marked effect of this kind, when sintering in argon at 1000°C suggests that the faster diffusion of this gas at the higher temperature permits

Fig. 4—Micro-
structure of Cu
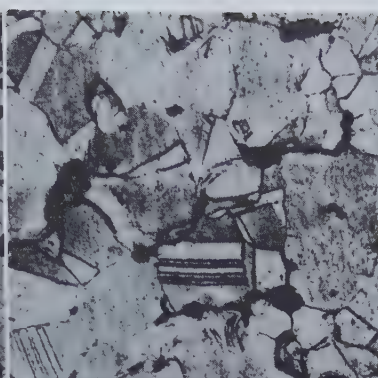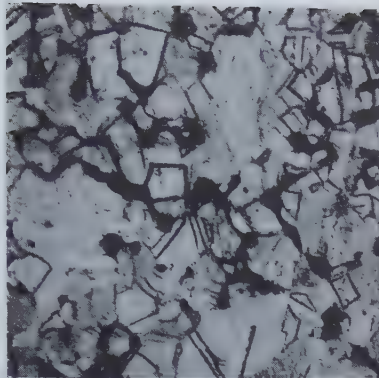compact sintered
1 hr at 1000°C
in hydrogen.

Fig. 5—Same:
10 hr at 1000°C
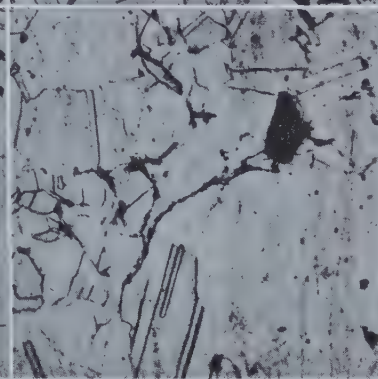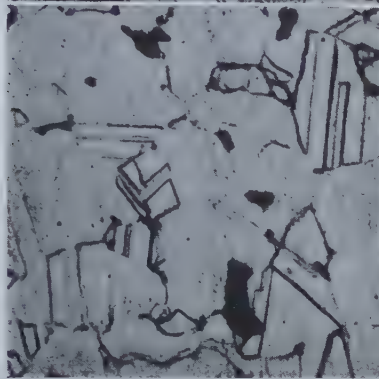in hydrogen.

Fig. 6—Same:
100 hr at 1000°C
in hydrogen.

Fig. 7—Same:
1000 hr at 1000°C
in hydrogen.

better escape through the external surface at a rate such as to avoid any large increase in pressure within the pores. Density measurements still indicate an increase in total porosity.

The presence of an oxide coating might be expected to interfere with either surface diffusion or vapor transport of metal to alter the pore shape, see table V. Only in the presence of hydrogen, which reduces copper oxide at the sintering temperature, was regular variation in the shape factor found and the trend toward unity (spherical form) was most clearly apparent here at the highest temperature, where the process is expected to be most rapid. The erratic behavior of the shape factor in vacuum and argon sintering is doubtless to be associated with the interference of unreduced copper oxides and other foreign matter. While the shape factor used in this instance is admittedly a crude and rather insensitive measure of shape, the fact that the values obtained were often erratic, indicates that a more sensitive expression of shape would offer no advantage.

Efforts by earlier investigators to fit curves of density versus time of sintering to some mathematically simple form have been consistently disappointing and no simple form is apparent in the curves presented in fig. 1, 2 and 3. Neither is there any simple function apparent in the progressive change of the pore count with time of sintering. This may mean that the progress of sintering is dependent upon two or more processes that operate under different sets of laws, such as a mechanism of metal transport, perhaps simple in itself, but operating within a geometrical pattern that changes concurrently in a less simple way, with a superimposed effect of gas pressure varying in yet another manner.

In order to analyze the volume changes that are

observed, it is desirable to find a precise means for describing the shape, size and quantity of porosity. The total volume of porosity, thus described, should be equal to that computed from the measured density. No satisfactory solution to this problem has been found, because of the almost infinite variety and complexity of the pore shapes. As an approximation it may, of course, be assumed that the true pore shapes are effectively equivalent to certain simple geometrical forms; thus it might be assumed, for example, that they are equivalent to cylinders, parallelopipeds, tetrahedra, or spheres. When such assumptions are made their reasonableness can be tested by computing the density from the pore counts (considering all pores counted to have the assumed form) and comparing with the measured density; some comparisons of this kind are presented in table VI.

The column headed "Cylindrical," table VI, gives values of density computed from pore counts upon the assumption of cylindrical pores all lying perpendicular to the plane of observation and extending through the thickness of the sample. Close agreement between the measured density and the density thus computed is shown under conditions of sintering in hydrogen at 1000°C for times in excess of 100 hr and less than 1000 hr. The prediction of a density lower than that measured at 1000 hr indicates that the pores are equivalent in shape to some form midway between a cylinder and a sphere. The overestimation of the density, upon this assumption, at the shorter sintering times, however, is disturbing, because it is difficult to conceive of a geometrical form that would yield a smaller cross-sectional area-to-volume ratio than does a cylinder cut perpendicular to its axis. This can mean only that the experimental method of classifying the

pores in size ranges has resulted in an underestimate of their true cross-sectional area that is the greater the more irregular the outline of the pore, i.e., the shorter the sintering time and the lower the sintering temperature.

### Table VI. Comparison of Measured with Computed Density

Treatment (in $H_2$)

| °C | Hr | Measured Density | Computed Density | |
|---|---|---|---|---|
| | | | Cylindrical | Spherical |
| 800 | 1 | 5.29 | 8.76 | 8.84 |
| 1000 | 1 | 6.77 | 7.83 | 8.85 |
| | 10 | 7.82 | 8.24 | 8.88 |
| | 100 | 8.09 | 8.29 | 8.88 |
| | 1000 | 8.52 | 8.39 | 8.89 |

Density values computed upon the assumption that the pores are all spherical are given in the 5th column of table VI. This represents the other extreme in which the ratio of cross-sectional area to volume is the smallest that can be had and should be expected to overestimate the density until the spheroidization of the pores reaches perfection. This condition is approached most closely by hydrogen sintering for 1000 hr at 1000°C, but that it was not actually reached was shown in table V. Some of the divergence between the computed and measured density at short times and low temperatures of sintering must be ascribed to experimental error as in the case of cylindrical pores. The method used for computing the volume of spherical pores from estimates of the cross-sectional area is the same as that proposed by Scheil[5] for determining true grain size from measurements made upon a flat surface. The number of pores per cubic centimeter, used in plotting fig. 8, was also computed by this method.

### Conclusions From the Data

Despite the uncertainties that are introduced by the lack of an adequate means for measuring and expressing the true pore shapes there are a number of qualitative conclusions, cited above, that seem firm. These may be summarized as follows:

1. The total number of pores decreases progressively during sintering at all temperatures.
2. The average pore size existing in the compact increases with time of sintering.
3. There is, for each condition of sintering, a pore size which occurs in maximum number in the size scale, and this maximum shifts towards larger pore size as sintering proceeds.
4. Late in the sintering process there exist pores which are larger than any present at the beginning of sintering.
5. Pores are absent from a region adjacent to the external surface of the specimens.
6. The rate of change of pore count increases rapidly with rising temperature.
7. The progression of the pore counts in samples heat treated in vacuum approximates that in samples heat treated in hydrogen except that there is much more scatter in the observations (possibly due to the presence of a larger quantity of nonmetallic inclusions).
8. There is a positive decrease in the density of samples sintered in argon for a long time at 900°C, and this decrease is associated with the appearance of some pores which are much larger than are seen in any of the other samples.
9. The pore shape changes gradually from very complex forms toward a roughly equiaxed form, but the latter condition is attained only very approximately even at the longest times of sintering and at the highest temperatures used in this work.

Somewhat less direct, and therefore less firm, conclusions that have been proposed are:

10. Densification is ascribable to the loss of internal void space to the outside surface.
11. The presence of hydrogen, which diffuses rapidly, has little effect upon the rate of change of pore size, but argon, which diffuses slowly, can have a marked effect.
12. Densification begins long before the pores break up into discrete units and continues to progress rather more rapidly than does spheroidization.

### Diffusion Theory of Sintering

A satisfactory theory of the sintering process must contain in it an explanation of the phenomena described in the experimental part of this paper. In particular, it must agree with the firm conclusions arrived at, and if possible with those inferred from it. Such a theory must also be consistent with the fundamental aspects of the metallurgical science upon which it is based. In constructing a mechanism, it is desirable not only to identify the driving forces which produce the changes to be described, but specifically to relate these to the atomic processes which are involved. Other theories dealing with the process of sintering such as those described by Shaler and Frenkel, based on a viscous flow process, are not in themselves a mechanism but merely establish the surface tension as the driving force of the process and attempt to explain the phenomena by analogy with other processes also driven by surface tension, whose mechanisms are equally in doubt. A specific atomic mechanism will be proposed here.

In describing the observations contained in the experiments recorded, one must provide for the transport of copper atoms from pore to pore and from one part of a pore to other parts in order to account for the change in size and shape of the void spaces in the copper powder compact. One of the characteristic features involved is that transport must occur between pores which are separated by solid copper in the annealed condition; that is, the matrix of the copper is not subject to mechanical strain or cold work in the latter parts of the sintering process. To account for transport under this condition one must choose between diffusional and plastic flow mechanisms. The reasons for choosing the former will be discussed later.

In accounting for the change of shape of pores, there are four possible mechanisms available. These include the two just stated for transport between pores, that is, body diffusion and plastic flow, and in addition, transport within the confines of a single pore space may take place by migration along the

surface of the metal, that is, surface self diffusion, or by transport through the vapor phase. It is possible of course that some or all of these processes occur simultaneously. Calculations to be given will demonstrate that the vapor transport mechanism appears able to account for the spheroidization observed in these experiments at the highest temperatures during the early stages. It is possible that as the temperature is lowered some other process becomes relatively more important.

Admitting the surface energy as the driving force of the sintering reaction and considering the mode of communication between two isolated pores, it is desirable to consider the relative energies of formation of the lattice site vacancies of diffusion theory and the dislocations of plastic flow theory. Huntington and Seitz[6] estimated the energy to form a unit lattice vacancy in copper to be 1.5-1.8 electron volts while Koehler[7] estimates the energy to form an isolated dislocation in copper as 3.16 electron volts per atomic distance along its length. It is obvious from this that the energetic picture greatly favors the lattice vacancy as the transport unit in moving copper from one pore to another in the absence of external forces. For this reason the vacancy diffusion mechanism will here be considered the only means of transport of copper atoms between disconnected pores.

For the spheroidization process, the plastic flow mechanism will again be eliminated, because of the high energy required to initiate a dislocation. The body diffusion process also seems likely to be considerably slower than surface diffusion or vapor transport. A simple calculation shows this to be the case with respect to vapor transport. In addition Langmuir[8] in comparing the surface and body diffusion of thorium in tungsten indicates that surface diffusion is much faster than body diffusion. Recent experiments by Nickerson and Parker[9] tend to support this view. They have measured the rate of surface self diffusion of silver in the range of 200° to 350°C. Over this range they find surface self diffusion to be relatively rapid, with an activation energy of about 10 kcal per mol, much lower than that for body self diffusion in silver.[10] A calculation of the rate of vaporization at the highest temperature in this range, 350°, indicates that it would take several years for the surface atoms of the silver crystal to vaporize. However, the heat of vaporization is considerably higher than the activation energy for self diffusion, and it is possible at higher temperatures that vapor transport could become much more important than surface self diffusion in transporting atoms from one point to another within a single channel. The recent studies by Kuczynski[4] of the rate of increase in diameter of the weld between spherical particles of copper and silver and plates of like material lead to inferred rates of body and surface diffusion. His equation for surface self diffusion of copper indicates the activation energy to be equal to that for volume diffusion. On the basis of the more direct measurements of Nickerson and Parker, it seems likely that this may be in error and that Kuczynski may have overestimated the role which surface self diffusion plays in spheroidization. In the absence of an adequate description of the geometry of his experimental setup, it is impossible to estimate the contribution which vapor transport might make to the growth of these regions.

## Spheroidization

As a simple model of the spheroidization process, consider a tube whose cross-section is a three-cusped hypocycloid. This figure is shown in fig. 9a. The cross-sectional area is taken to be $1.96 \times 10^{-7}$ sq cm, which is reasonably typical of the sample treated for 1 hr at 1000°C in hydrogen. The radius of the equivalent circle is $2.5 \times 10^{-4}$ cm. If the cross-section is now deformed to remove the sharp corners by transport of copper from the convex surfaces, a new cross-section with a shape similar to that shown in fig. 9b will result. The radius of curvature of the corners will be about $4.5 \times 10^{-5}$ cm. If these figures represent the cross-section of a tube 1 cm long, $7.0 \times 10^{-9}$ cc or about $6.26 \times 10^{-8}$ g must be removed from each space and deposited in the adjoining corner.

From the measured vapor pressure of copper, determined by Harteck[11] and by Marshall, Dornte and Norton,[12] it is possible to calculate the rate of evaporation and condensation from the kinetic theory of gases. When this is done as shown in the footnote*

---

* The kinetic theory of gases gives the maximum rate of vaporization or condensation by $G = \alpha (M/2\pi RT)^{1/2}p$, where $G$ is the mass of metal vaporized per unit area per unit time, $M$ is the molecular weight, $p$ is the vapor pressure, and $\alpha$ is the accommodation coefficient which is taken to be unity. Harteck and Marshall, Dornte and Norton find the vapor pressure of copper to be $6.8 \times 10^{-5}$mm Hg at 1000°C. Vaporization can occur at a rate of $7.9 \times 10^{-6}$ g per cm$^2$ x sec. However, there is a greater area for vaporization than condensation so the pressure will be nearly the equilibrium value, and transport will be determined by the rate of condensation in the sharp corners. These will be progressively blunted and the back pressure over them will build up from zero (for infinitely small radius of curvature) according to the Kelvin

equation $\ln p_1/p_2 = -\frac{2\gamma M}{\rho RT}\left\{\frac{1}{r_1} - \frac{1}{r_2}\right\}$, symbols defined for Eq 1

in the text. Roughly, the condensation rate for the case above should average about $1.1 \times 10^{-8}$ g per hr or $2.8 \times 10^{-7}$ g in 25 hr, the time required to produce the change of shape factor in the powder compact corresponding to that of our model. The fact that the estimated rate is high by a factor of four is not significant in view of the approximations.

---

it is evident that enough copper may be transported by this mechanism to change the shape factor of the section shown in fig. 9 by an amount equivalent to that observed for the shape factors of the pore cross-sections for samples sintered in hydrogen at 1000°C. This rate is much greater than the transport by volume diffusion. Surface self diffusion measurements are not available for comparison, and it is possible that some contribution arises from this source. It appears, however, that at 1000°C vapor transport is sufficient, in itself, to account for the rate of spheroidization observed. As the vapor pressure decreases very rapidly with temperature, this may not be the case at lower temperatures. When high back pressures exist in the pores as may be the case when sintering occurs in argon, or when the surfaces may be covered with an oxide film such as could occur when reducing atmospheres are not present, that is in either argon or the "vacuum" used here, it is likely that vaporization would be greatly reduced. In the latter case surface diffusion should be similarly affected. This is in accord with the failure to observe marked changes in shape factors in the argon and vacuum sintered samples.

## Growth of Pores

The present treatment must be regarded as a first approximation since the assumptions necessary to analyze the data and to solve the model permit only a semiquantitative comparison. The assumptions

and steps in the procedure will first be outlined to give an overall picture, after which the reasons will be given.

The basic process is regarded as one of the "vaporization" of lattice site vacancies from the pores in accordance with the long recognized principle that vapor pressures are higher over smaller droplets. Rapid establishment of vacancy concentration equilibrium in the immediate neighborhood of each pore leads to concentration gradients with the high ends near small pores and the low ends near large pores or external surfaces. The flow of vacancies along the gradient builds up higher concentrations near large pores and external surfaces followed by condensation thereupon, while evaporation must continue from the small pores to maintain their equilibrium atmosphere. The net result is the elimination of the smaller pores and the growth of their near neighbors at their expense. Some intermediate size will be static. Condensation of vacancies at the external surfaces accounts for the decreased density of the specimen.

In order to facilitate calculation the distribution of irregular channels was replaced by a random distribution of spheres whose total volume equalled that determined experimentally for the compact by density measurements. The relative populations of the various sizes were taken to be those obtained by applying the Scheil table to the cross-section counts. It is probable that this is a reasonable assumption from a qualitative point of view since a rambling pore is likely to interact with various neighboring pores at different parts of its extremities like nearly independent pores of differing radii of curvature. However, it is unlikely that quantitative agreement can be expected from such an assumption.

Further, it was necessary to assume nearly steady state flow along a linear gradient between pores. Each pore was assumed to interact with only a limited number of neighbors though all were affected by the external surfaces. These conditions were achieved in a somewhat artificial manner to be described, but it is not thought that these approximations are serious in view of the degree of uncertainty introduced by replacing the true pores by a sphere distribution. The authors do not wish to gloss over the assumptions introduced nor slight the effect they are likely to have on the quantitative results. The general qualitative behavior of the model is fixed by the mechanism assumed, and it should come as no surprise that the mechanism, chosen to fit experience, should endow the mathematical model with properties of the real system.

The Kelvin equation relates the vapor pressure of a droplet of radius of curvature, $r$, to its vapor pressure, $p$, the absolute temperature, $T$, and the surface tension, $\gamma$, by:

$$\ln p^2/p_1 = \frac{2\gamma M}{\rho RT}\left(\frac{1}{r_2} - \frac{1}{r_1}\right) \qquad [1]$$

where $M$ is the molecular weight, $\rho$ the density, and $R$ the gas constant. We may replace the pressure by the concentration of holes in the lattice. If we take a flat surface for reference $\left(\frac{1}{r_o} = 0\right)$ the equation becomes:

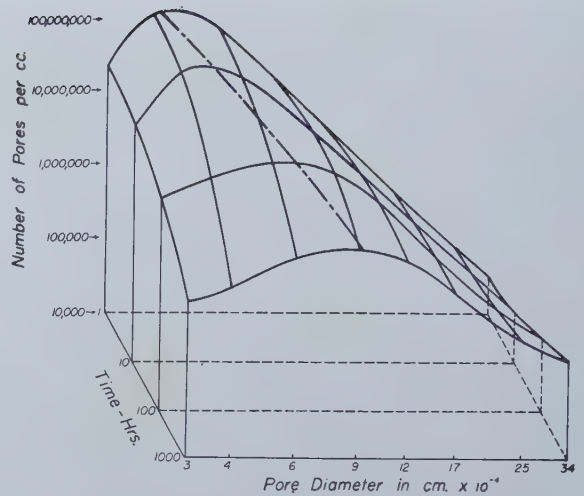$$\ln c/c_o = \frac{2\gamma M}{r\rho RT} \qquad [2]$$



Fig. 8—Space diagram showing the population distribution of pores of various sizes as a function of time at 1000°C in hydrogen.

The dash-dot curve traces the pore size at which the largest number of pores is found at each time interval.

In our calculations the surface tension values for solid copper determined by Udin, Shaler and Wulff[13] were employed.

In order to estimate $c_o$, it was assumed that the thermal energy of the crystal could be assigned to the lattice sites according to a Boltzmann distribution. The fraction of the sites, $f$, having an energy greater than $\epsilon$, the energy necessary to form a vacancy in a copper lattice, were assumed to exist as vacancies. The quantity $\epsilon$ was taken to be 39.7 kcal per mol following the procedure of Glasstone, Laidler and Eyring[14]. This value falls in the range prescribed by Huntington and Seitz. The results were:

$$T°C : 700, \qquad 800, \qquad 900, \qquad 1000,$$

$$f : 1.2\text{x}10^{-9},\ 8.0\text{x}10^{-8},\ 3.9\text{x}10^{-8},\ 1.5\text{x}10^{-7}.$$

If these calculations are correct, the equilibrium lattice is so dilute in holes that their interaction with each other may be neglected.

Consider a small sphere surrounded by a larger one concentrically, with equilibrium vacancy concentrations $c_1$ and $c_2$ at their respective surfaces. As the sizes of the spheres change, $c_1$ and $c_2$ will also change. Instantaneously the gradient may be approximated by $\frac{c_1 - c_2}{\Delta x}$, where $\Delta x$ is the distance between the surfaces. The rate of diffusion of vacancies $g$, is equal to the negative of the gradient times $D_h$, the diffusion coefficient for vacancies in copper, or:

$$g = -D_h \frac{\Delta c}{\Delta x} \qquad \frac{\text{holes}}{\text{cm}^2 \times \text{sec}} \qquad [3]$$

If the volume of a unit hole is $v_o$ the number of these in a spherical pore is $N_h = \frac{4}{3}\frac{r^3}{v_o}$, where $r$ is the radius of the pore. The rate of loss of holes $\frac{dN_h}{dt}$ is proportional to $g$, indeed:
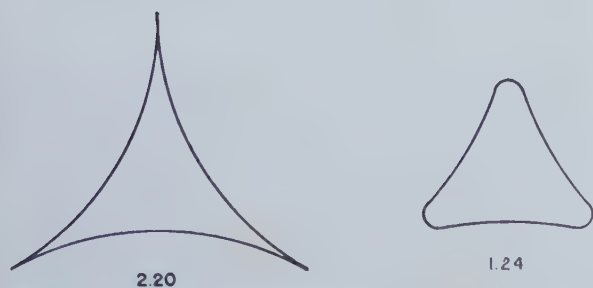
2.20          1.24

**Fig. 9—Schematic representation of a pore before (left) and after (right) a limited time of sintering.**
Numbers below each sketch are the shape factors; compare with table V.

$$g = \frac{1}{4\pi r^2} \frac{dN_h}{dt} = \frac{1}{v_o} \frac{dr}{dt} \quad [4]$$

$$\frac{dN_h}{dt} = \frac{4\pi r^2}{v_o} \frac{dr}{dt} \quad \text{and} \quad [5]$$

$$\frac{dr}{dt} = -v_o D_h \frac{\Delta c}{\Delta x} \quad [6]$$

It is easy to solve this simple case exactly. Applying this to the case of a single pore near an external

**Table VII. Diffusion Coefficients for Vacancies in Copper**

| T°C | $D_{Cu}$ | $D_h$ |
|---|---|---|
| 700 | $6.0 \times 10^{-12}$ | $5.0 \times 10^{-3}$ |
| 800 | $6.0 \times 10^{-11}$ | $7.5 \times 10^{-3}$ |
| 900 | $4.0 \times 10^{-10}$ | $1.0 \times 10^{-2}$ |
| 1000 | $2.0 \times 10^{-9}$ | $1.3 \times 10^{-2}$ |

surface shows that the smaller sizes would disappear quickly at these temperatures, but that the largest pores would persist for very long times, under the influence of high temperature. In the body of the sample, where most of the transfer of vacancies must be from pore to pore, this simple geometry is not adequate and it becomes necessary to consider the transfer between a pore and its system of neighbors. Before proceeding with this more complex analysis, however, it is necessary to evalu-

ate $D_h$, the coefficient of the diffusion of vacancies.

It is generally regarded that self diffusion in copper occurs by a vacancy mechanism. If this mechanism is entirely responsible for self diffusion, the vacancies, being present in very small amount, must move much more rapidly than copper atoms, on the average, in order to accomplish the necessary transport. Indeed the ratio of the number of holes to copper atoms must be equal to the ratio of the diffusion coefficient of copper atoms to the diffusion coefficient of holes.

The ratio of the number of holes to copper atoms is the quantity $f$ given above. Selecting reasonable values of the copper self diffusion coefficient from the four sets of data, permits the computation of the hole diffusion coefficients given in table VII.

It is now desirable to set up a more complicated model for comparison of its behavior with that of the experimental compacts. Taking the sphere distribution obtained from the Scheil[5] table, and correcting it to give the experimental density, a random dispersion in the sample is assumed. Average distances between pores of any two sizes are obtained by arranging the total of the two sizes simultaneously on a simple cubic lattice and using the lattice parameter as the average distance between pores. There will be six neighbors at distance a and eight at $\sqrt{2a}$. The proportion of total solid angle cut off by the cross-section of pores surrounding a central pore is inversely proportional to the square of the distance between, and the diffusion gradient varies inversely as the distance, so the resultant effect on flow is the inverse of the cube of the distance. The pores at distance $\sqrt{2a}$ and more distant pores should contribute enough to make 9 a good approximation of the coordination number of the central pore. This must be weighted by the ratio of the number of pores of the second size to the total number of pores of both sizes. Finally the calculation must be carried out for all pairs of sizes.

Allowance must also be made for the nearly plane exterior surfaces of the sample. The average distance from a pore to its nearest surface is 0.173cm. As a rough approximation it was considered that the whole pore distribution was concentrated at this distance and all lost vacancies to the exterior. Neglecting the screening effect of pores on each other

**Table VIII. Rate of Change in Number of Pores**

| Time in Hr Size‡ | 800°C | | | | 900°C | | | |
|---|---|---|---|---|---|---|---|---|
| | 1 | 10 | 100 | 1000 | 1 | 10 | 100 | 1000 |
| 1 | $-1.02 \times 10^9$ | $-1.02 \times 10^9$ | $-6.16 \times 10^8$ | $-4.80 \times 10^6$ | $-5.18 \times 10^8$ | $-4.97 \times 10^8$ | $-1.64 \times 10^8$ | $-8.04 \times 10^7$ |
| 2 | $3.47 \times 10^7$ | $2.54 \times 10^7$ | $1.57 \times 10^7$ | $1.13 \times 10^7$ | $-1.62 \times 10^6$ | $-8.19 \times 10^6$ | $-3.41 \times 10^6$ | $-2.60 \times 10^6$ |
| 3 | $1.66 \times 10^6$ | $1.68 \times 10^6$ | $8.78 \times 10^5$ | $7.30 \times 10^5$ | $1.82 \times 10^6$ | $8.97 \times 10^5$ | $-4.61 \times 10^5$ | $1.25 \times 10^5$ |
| 4 | $3.25 \times 10^5$ | $4.10 \times 10^5$ | $6.93 \times 10^4$ | $1.18 \times 10^5$ | $3.38 \times 10^5$ | $2.76 \times 10^5$ | $1.88 \times 10^5$ | $1.41 \times 10^5$ |
| 5 | $4.10 \times 10^4$ | $2.14 \times 10^4$ | $1.46 \times 10^4$ | $2.03 \times 10^4$ | $8.40 \times 10^4$ | $7.60 \times 10^4$ | $6.50 \times 10^4$ | $5.01 \times 10^4$ |
| 6 | $2.61 \times 10^4$ | $4.14 \times 10^3$ | $4.86 \times 10^3$ | $4.26 \times 10^3$ | $2.60 \times 10^4$ | $2.57 \times 10^4$ | $2.40 \times 10^4$ | $1.59 \times 10^4$ |
| 7 | | $1.01 \times 10^3$ | $2.15 \times 10^3$ | $1.27 \times 10^3$ | $1.01 \times 10^4$ | $1.02 \times 10^4$ | $9.20 \times 10^3$ | $4.62 \times 10^3$ |
| 8 | | $4.41 \times 10^2$ | $1.12 \times 10^3$ | $8.30 \times 10^2$ | $4.75 \times 10^3$ | $4.80 \times 10^3$ | $3.65 \times 10^3$ | $1.75 \times 10^3$ |
| 9 | | | $6.04 \times 10^2$ | $3.02 \times 10^2$ | $2.49 \times 10^3$ | $2.52 \times 10^3$ | $1.56 \times 10^3$ | $7.37 \times 10^2$ |
| 10 | | | $3.78 \times 10^2$ | $1.93 \times 10^2$ | $1.55 \times 10^3$ | $1.53 \times 10^3$ | $6.48 \times 10^2$ | $4.08 \times 10^2$ |
| 11 | | | $2.74 \times 10^2$ | $1.54 \times 10^2$ | $1.23 \times 10^3$ | $1.03 \times 10^3$ | $2.88 \times 10^2$ | $2.25 \times 10^2$ |
| 12 | | | $2.85 \times 10^2$ | $1.67 \times 10^2$ | $1.48 \times 10^3$ | $9.11 \times 10^2$ | $1.68 \times 10^2$ | $1.85 \times 10^2$ |
| density (calc.) | $2.9 \times 10^{-9}$‡ | $2.3 \times 10^{-9}$ | $1.7 \times 10^{-9}$ | $1.3 \times 10^{-9}$ | $6.2 \times 10^{-9}$ | $4.7 \times 10^{-9}$ | $2.3 \times 10^{-9}$ | $1.7 \times 10^{-9}$ |
| density (meas.) | $4.2 \times 10^{-9}$ | $4.2 \times 10^{-7}$ | $4.2 \times 10^{-8}$ | $4.2 \times 10^{-8}$ | $8.4 \times 10^{-6}$ | $7.8 \times 10^{-7}$ | $6.1 \times 10^{-8}$ | $5.0 \times 10^{-9}$ |

• Pores per hr   † cc per sec x cc
‡ The number listed is a coefficient which when multiplied by 0.000125 gives the pore radius in cm.

may tend to give high results, but irregularities in shape leading to quicker dissipation of pores at points of high curvature seem to overbalance this. From Eq 5:

$$\frac{dN_i}{dt} = \frac{4\pi r_i^2}{v_o} \frac{dr_i}{dt},$$ where $N_i$ is the number of unit holes leaving spheres of size $r_i$ per unit time. From Eq 6.

$$\frac{dN_i}{dt} \cdot = -4\pi r_i^2 N_i D_h \frac{\Delta c}{\Delta x} \qquad [7]$$

By introducing $N_i$, the number of pores of radius $r_i$, Eq 7 now gives the rate of loss of vacancies from all pores of that size.

An area factor must then be applied to weight the proportion of the vacancies emitted from a single pore which migrate toward pores of the different sizes. This is done by saying that that fraction of the total solid angle covering the emission to a given size is proportional to the square of its radius ($r_j^2$) divided by square of the average distance from the central pore ($\Delta x_{ij}^2$). A normalizing factor may then be found so that the total of all sizes adds to unity, or

$$\Sigma F^{N_j r_j^2}/\Delta x_{ij}^2 = \Sigma A_{ij} = 1 \qquad [8]$$

At any instant a pore will be gaining vacancies from smaller pores and losing them to larger pores. For twelve size ranges of progressively larger radius (the radii employed are integral multiples of 0.000125cm) and the exterior surface we have:

$$(i) \quad \frac{dN_1}{dt} = -4\pi r_1^2 N_1 D_h \left\{ \sum_{j=2}^{12} A_{1j} \frac{\Delta AC_{1j}}{\Delta x_{1j}} + \frac{\Delta C_{1,13}}{\Delta x_{1,13}} \right\} \qquad [9]$$

$$(ii) \quad \frac{dN_2}{dt} = 4\pi D_h \left\{ N_1 r_1^2 A_{12} \frac{\Delta C_{12}}{\Delta x_{12}} - N_2 r_2^2 \left( \sum_{j=3}^{12} A_{2j} \frac{\Delta C_{2j}}{\Delta x_{2j}} + \frac{\Delta C_{2,13}}{\Delta x_{2,13}} \right) \right\}$$

$$(xiii) \quad dN_{13} = 4\pi D_h \sum_{j=1}^{12} N_j r_j^2 \frac{\Delta C_{J,13}}{\Delta x_{J,13}}$$

The model, though admittedly crude, should show roughly the same behavior as observed in the powder compact and should give reasonable relative agreement in regard to which sizes are increasing, which decreasing, and how fast.

The calculations required to apply this set of equations to the case at hand have been carried out for each of the four times in hydrogen at each of the three temperatures. The $N_i$ were those corrected to give the measured density. However, this correction throws off the real count enough that some sizes, which are decreasing in number, appear to be increasing. For this reason it is necessary to compare our calculations with the rate of increase or decrease of pore count before density correction.

The calculated values for the rate of increase or decrease in pore sizes 1 to 12 (number per hr) and the decrease in density of the sample (cc per sec per cc) are given in tables VIII and IX for all experiments carried out in hydrogen. The experimental rate of density change is given for comparison at the bottom of each table. The discrepancies are large at low temperatures and short times, but agreement improves markedly at higher temperatures and longer times, the results at 1000°C and 1000 hr being of the same order of magnitude.

Numerical agreement in change in pore count is also poorest for the lowest temperatures and times, but the property of decrease in the number of small pores and increase in the large ones is always preserved. The point at which the rate changes from positive to negative experimentally is indicated by the positions of the lines between the columns, and it is seen that this agrees well. In table IX the measured average rate of pore count change is given for 1000°C and 100 to 1000 hr. The agreement is considerably better than one might expect in view of the approximations made earlier. Indeed, the difference for most sizes is just about the factor introduced by the density correction.

The theoretical equation, therefore, reproduces the behavior of the sample well when the pore shape has become regular, but cannot take into account the extreme irregularities of the pores in the early stages of sintering.

Several predictions may be derived from the theoretical picture proposed here.

1. In the sintering of a pure metal powder which

## Table IX. Rate of Change in Number of Pores 1000°

| | Calculated* | | | | Measured† |
|---|---|---|---|---|---|
| Time | 1 | 10 | 100 | 1000 | 100 → 1000 |
| Size‡ | | | | | |
| 1 | —1.1x10⁰§ | —4.2x10⁸ | —5.5x10⁶ | —9.9x10⁵ | —3.5x10⁴ |
| 2 | —6.1x10⁷ | —7.1x10⁰ | —2.6x10⁶ | —1.2x10⁵ | —2.4x10⁴ |
| 3 | 3.0x10⁶ | 1.0x10⁶ | —2.3x10⁵ | —3.3x10⁴ | —1.3x10⁴ |
| 4 | 1.8x10⁶ | 6.7x10⁵ | 2.0x10⁴ | —8.2x10³ | —5000 |
| 5 | 8.9x10⁵ | 3.4x10⁵ | 2.6x10⁴ | 1.9x10³ | —1200 |
| 6 | 4.9x10⁵ | 1.9x10⁵ | 1.8x10⁴ | 1.3x10³ | —220 |
| 7 | 3.0x10⁵ | 1.2x10⁵ | 1.2x10⁴ | 716 | 43‡ |
| 8 | 2.0x10⁵ | 7.4x10⁴ | 7500 | 360 | 100 |
| 9 | 1.3x10⁵ | 5.1x10⁴ | 5200 | 191 | 77 |
| 10 | 9.5x10⁴ | 3.6x10⁴ | 3700 | 128 | 61 |
| 11 | 7.1x10⁴ | 2.7x10⁴ | 2800 | 100 | 58 |
| 12 | 5.4x10⁴ | 2.0x10⁴ | 2100 | 94 | 63 |
| density (calc) | 1.3x10⁻⁸** | 7.4x10⁻⁹ | 2.5x10⁻⁹ | 5.0x10⁻¹⁰ | |
| density (meas.) | 1.0x10⁻⁵ | 9.0x10⁻⁷ | 5.0x10⁻⁸ | 3.0x10⁻⁹ | |

* Corrected for density  
‡ Uncorrected for density  
‡ See note, table VIII  

§ Pores per hr  
** cc per. sec times cc

can undergo a phase transformation, the rate of densification should show the same qualitative change at the transformation temperature as does the self diffusion coefficient of the metal.

2. A nonwetted inclusion above a minimum size should provide a condensation surface for vacancies and should be found to occupy a pore larger than itself after sintering.

3. At temperatures comparable to these studied, the largest pores will not be removed from the compact by heating alone. However, they should lose their sharp edges and should be surrounded by sound metal.

4. The distribution and amount of external surface should affect the rate of sintering, the rate being greater in samples with the greatest surface area per unit mass of powder and in those regions closest to surfaces.

5. The increased availability of vacancies may speed up the rate of dissolution of soluble bodies beyond that expected on the basis of normal diffusion measurements. Any source of fine scale porosity in a metal body should have this effect.

6. Back pressure of insoluble or difficultly soluble gases might decrease the surface energy enough to reverse the trend in density as observed for argon.

7. Compacts made under different initial conditions to produce different initial pore distributions should produce different final distributions (and therefore different properties) for the same heat treatments.

Although attempts are being made to test some of these consequences in this laboratory only the first is subject to immediate comparison with experiment. Libsch, Volterra and Wulff[15] observed a decrease in the rate of densification of iron powder compacts in the neighborhood of 900°C. This is in agreement with the sharp decrease in self diffusion rate in going from alpha to gamma iron determined by Birchenall and Mehl.[16]

## Summary

Experimental studies of the density and size distribution and shapes of pores have been carried out on copper powder compacts sintered in vacuum, hydrogen and argon for 1, 10, 100 and 1000 hr at 800°, 900° and 1000°C. It may be concluded that although the total number of pores decreases as sintering progresses, the smallest pores account for most of this decrease while the largest sizes are increasing in number, giving rise to a few pores of size larger than any existing at earlier times. Thus the average pore size increases, and progressively larger sizes are present in maximum number. Coincident with this, the pore shapes are changing from highly irregular forms to more nearly spherical. All changes proceed more rapidly as the temperature is raised. The progression of pore counts is roughly similar in hydrogen and vacuum, but samples sintered in argon first increase in density then decrease, especially at 900°C, with the eventual formation of some pores much larger than observed in any other samples.

Based upon these experimental observations a

theoretical model has been formulated, in terms of the vacancy mechanism of body diffusion, to account for the change in pore distribution and densification. It has been shown to lead to reasonable agreement with the experiments, under the most nearly ideal conditions. It is also proposed that vaporization may be an important mechanism in the tendency of pores to assume regular shapes, at least in the early stages of this process at high temperatures.

Several consequences, which may be checked experimentally, have been inferred from the theoretical model. It is found that the self diffusion coefficients of iron change at the alpha-gamma transformation temperature in the direction to be expected from the behavior of the densification rates of iron powder compacts.

## Acknowledgments

## References

[1] F. N. Rhines: Seminar on the Theory of Sintering. Trans. AIME (1946) 166, 474.

[2] A. J. Shaler: Seminar on the Kinetics of Sintering. Trans. AIME (1949) 185, 796. Jnl. of Metals, Nov. 1949. TP 2702.

[3] J. Frenkel: Viscous Flow of Crystalline Bodies Under the Action of Surface Tension. U.S.S.R. Jnl. of Phys. (1945) 9, 385.

[4] G. C. Kuczynski: Self Diffusion in Sintering of Metallic Particles. Trans. AIME (1949) 185, 169. Jnl. of Metals, Feb. 1948. TP 2528.

[5] E. Scheil: Calculation of the Number and Distribution of Sizes of Spherical Crystals in Opaque Substances. Ztsch. anorg. allg. Chem. (1931) 201, 259.

[6] H. B. Huntington and F. Seitz: Self Diffusion in Metallic Copper. Phys. Rev. (1942) 61, 315.

[7] J. S. Koehler: The Energy Stored During Work Hardening. Phys. Rev. (1941) 59, 943(A).

[8] I. Langmuir: Thoriated Tungsten Filaments. Jnl. Franklin Inst. (1934) 217, 543.

[9] Nickerson and E. Parker: The Self Surface Diffusion of Silver. Private Communication.

[10] W. A. Johnson: Self Diffusion of Silver. Trans. AIME (1941) 143, 107.

[11] P. Harteck: Measurements of the Vapor Pressure of Silver, Gold, Copper, Lead, Gallium, Tin, and Calculation of the Chemical Constants. Ztsch. Phys. Chem. (1928) 134, 1.

[12] A. L. Marshall, R. W. Dornte, F. J. Norton: The Vapor Pressure of Copper and Iron. Jnl. Am. Chem. Soc. (1937) 59, 1161.

[13] H. Udin, A. J. Shaler and J. Wulff: The Surface Tension of Solid Copper. Trans. AIME (1949) 185, 186. Jnl. of Metals, Feb. 1949. TP 2530.

[14] S. Glasstone, K. Laidler and H. Eyring: The Theory of Rate Processes. New York and London. 1941. McGraw-Hill Book Co.

[15] J. Libsch, R. Volterra and J. Wulff: The Sintering of Iron Powder. Powder Metallurgy (A Symposium) p. 384, 1942. Am. Soc. for Metals, Cleveland, Ohio.

[16] C. E. Birchenall and R. F. Mehl: Self Diffusion in Iron. Trans. AIME (1950) 188, 144. Jnl. of Metals, Jan. 1950.

# The Effects of Molybdenum and

# Commercial Ranges of Phosphorus

## Upon the Toughness of

# Manganese Steels Containing 0.40 pct Carbon

### by M. Baeyertz, W. F. Craig, Jr., and J. P. Sheehan

The loss in toughness caused by phosphorus within commercial ranges was studied in AISI-SAE 1340 steel and in molybdenum modifications of this grade. The replacement of part of the manganese by molybdenum in amounts which maintain the hardenability of the standard 1340 grade was shown to counteract to a marked degree the detrimental effects of phosphorus.

THIS paper deals with the effect of phosphorus on the toughness of 1340 steel and with the effect on toughness of replacing part of the manganese by molybdenum while retaining the same hardenability as that of 1340.

In previous work[1] a progressive decrease in toughness was observed when the phosphorus content of 5140 was raised from 0.020 to 0.036 pct; that is, from a moderate phosphorus level to one higher but yet within the AISI-SAE specification for this grade. The structural condition of the steel was tempered martensite. Toughness was evaluated by the transition temperature determined by V-notch Charpy tests. Replacement of a part of the chromium in 5140 by molybdenum provided a factor of safety against loss of toughness caused by phosphorus, especially where the steel was cooled slowly after tempering.

**Scope of the Study:** In view of the improved tolerance for phosphorus obtained by replacing a part of the chromium in 5140 with molybdenum, it seemed desirable to investigate the possibility of obtaining similar improvement in 1340 by replacing part of the manganese with molybdenum. Heats were made at different phosphorus levels, in a series that began with 1340 and ended with steels containing 0.32 to 0.35 pct Mo with 0.82 and 0.90 pct Mn. The analyses of the heats are given in table I. In order to facilitate later discussion, the 1340 heats have been placed together in the order of increasing phosphorus content, and the molybdenum modifications have been grouped according to phosphorus

*M. BAEYERTZ, Member AIME, W. F. CRAIG, JR., and J. P. SHEEHAN are Senior Metallurgist, Supervisor, Ferrous Metals Research, and Research Metallurgist, respectively, Armour Research Foundation of Illinois Inst. of Technology, Chicago, Ill.*

## Table I. Chemical Analyses

| Grade | Heat | C | Mn | P | S | Si | Mo | Mo/P |
|-------|------|-----|------|-------|-------|------|-------|------|
| 1340 | 2792 | 0.39 | 1.79 | 0.012 | 0.025 | 0.21 | 0.005 | 0.4 |
| | 2663 | 0.38 | 1.87 | 0.020 | 0.023 | 0.33 | 0.003 | 0.2 |
| | 2703 | 0.40 | 1.90 | 0.028 | 0.019 | 0.34 | 0.003 | 0.1 |
| | 2731 | 0.39 | 1.79 | 0.036 | 0.022 | 0.28 | 0.003 | 0.1 |
| Mo | 2796 | 0.38 | 0.82 | 0.010 | 0.019 | 0.22 | 0.32 | 32.0 |
| Mo-Mn | 2861 | 0.38 | 1.55 | 0.024 | 0.021 | 0.24 | 0.06 | 2.5 |
| | 2895 | 0.40 | 1.39 | 0.027 | 0.018 | 0.29 | 0.10 | 3.7 |
| | 2777 | 0.38 | 1.29 | 0.025 | 0.019 | 0.24 | 0.18 | 7.2 |
| Mo-Mn | 2872 | 0.39 | 1.43 | 0.033 | 0.024 | 0.27 | 0.12 | 3.6 |
| | 2780 | 0.39 | 1.24 | 0.035 | 0.019 | 0.26 | 0.18 | 5.1 |
| Mo | 2782 | 0.39 | 0.90 | 0.034 | 0.017 | 0.33 | 0.35 | 10.3 |

content. All of the heats were treated with aluminum, to be comparable with commercial steels made by fine grain practice.

The methods of producing and forging the steel, and of preparing, heat treating and testing the specimens were the same as those described previously in the work on 5140 and Mo-Cr steels.[1] Briefly, 500-lb laboratory induction furnace heats were made and poured in 460 lb ingots. After forging, the steel was normalized from 1550°F and tempered at 1200°F before machining the specimens. The final heat treatment was carried out on 0.016 in.-oversize Charpy blanks, and consisted of quenching in oil from 1550°F, tempering for 1 hr at 1150°F, and then quenching in water or cooling to 700°F at essentially 12, 3 or ¼°F per min. All of the specimens with controlled cooling between 1150° and 700°F were cooled in air from 700°F. Transition temperatures were determined by testing V-notch Charpy specimens over a sufficient range of temperature. Standard Jominy bars were used in evaluating hardenability.

Slow rates of cooling through the temperature range of temper embrittlement cause a loss of toughness in susceptible steels. The amount of this loss depends upon both the susceptibility of the steel to temper embrittlement and the sojourn in the embrittling temperature range that is provided by the cooling rate. The specimens that were quenched from the tempering temperature were intended to furnish a nonembrittled norm, while the other cooling rates were chosen to illustrate rates that might be encountered in commercial heat treatment.

**Hardenability of the Steels:** The Jominy hardenabilities of the various heats are recorded in table II. The specimens were standard bars, machined from normalized and tempered stock as described previously, and were quenched from 1550°F. The ASTM austenite grain sizes given in the table were determined from the Jominy bars. While the hardenabilities of the steels vary somewhat, all are within the range that might be expected from the composition limits of the standard 1340 grade.

**Impact Behavior of the Steels:** The measure of toughness used in this study is the transition temperature revealed by the relation of absorbed energy to testing temperature in the notched-bar impact tests. Fig. 1 through 11 show the impact transition curves of tempered martensites obtained from the heats under study. Each figure affords a comparison of the transitions in the same steel, as they depend upon the rate of cooling after tempering for 1 hr at 1150°F. The experimental points have been omitted from the figures to avoid confusion. The number of specimens used to determine each curve and the deviation of individual points from the curves in the figures are closely comparable with the earlier work on 5140, for which all of the experimental points were published.

A value of 40 ft-lb appears best to approximate the steepest portion of the energy curves for the 1340, Mo and Mo-Mn steels as a group. This energy value has been used arbitrarily in obtaining the transition temperatures plotted in fig. 12 and 13. Comparisons by other criteria of transition temperature as desired by the reader may be made from fig. 1 through 11.

It is desirable that comparisons of toughness be made at the same hardness level. Hardness values of the specimens used in this study are given in fig. 1 through 11, from which it will be seen that most of the values are in the range of 20/27 $R_C$. The relatively small variations in hardness were considered less objectionable than the means which would have had to be employed to avoid them—change of tempering temperature or time. For any given heat, the difference between the hardness as quenched from 1150°F and as cooled at ¼°F per min is at most 4 $R_C$ units. The difference due to the greater resistance of the molybdenum steels to softening on tempering amounts to a maximum of 7 $R_C$ units.

## Table II. Hardenabilities, Standard Jominy Test

| Grade | Heat | Pct Mn | Pct Mo | Pct P | ASTM Austenite Grain | Rockwell C Hardness at Indicated Distance From End of Specimen, in Sixteenths of Inch | | | | | | | | | | | | |
|-------|------|--------|--------|-------|----------------------|------|------|------|------|------|------|------|------|------|------|------|------|------|
| | | | | | | 2 | 4 | 6 | 8 | 10 | 12 | 14 | 16 | 20 | 24 | 30 | 40 |
| 1340 | 2792 | 1.79 | 0.005 | 0.012 | 7-9 | 54.5 | 52 | 45 | 37 | 33 | 31.5 | 31 | 31 | 30 | 29 | 27.5 | 26.5 |
| | 2663 | 1.87 | 0.003 | 0.020 | 8-9 | 55 | 54 | 51 | 46 | 41 | 37 | 34.5 | 33.5 | 32 | 31 | 30.5 | 29.5 |
| | 2703 | 1.90 | 0.003 | 0.028 | 7-9 | 55.5 | 54.5 | 53 | 50.5 | 46 | 42 | 38.5 | 35.5 | 33.5 | 32.5 | 31.5 | 30 |
| | 2731 | 1.79 | 0.003 | 0.036 | 7-9 | 56 | 55 | 53 | 50 | 46 | 41.5 | 38 | 35 | 32.5 | 31 | 30.5 | 29 |
| Mo | 2796 | 0.82 | 0.32 | 0.010 | 8-9 | 56 | 49.5 | 40.5 | 35.5 | 34 | 33 | 33 | 31.5 | 31 | 31 | 31 | 30 |
| Mo-Mn | 2861 | 1.55 | 0.06 | 0.024 | 9 | 53 | 47.5 | 37 | 34 | 32 | 30 | 29 | 29 | 28 | 28 | 27.5 | 27 |
| | 2895 | 1.39 | 0.10 | 0.027 | 8-9 | 54.5 | 50.5 | 41.5 | 34 | 33 | 32 | 31.5 | 30.5 | 30 | 29.5 | 28.5 | 27.5 |
| | 2777 | 1.29 | 0.18 | 0.025 | 8-9 | 54.5 | 52 | 43 | 36 | 24 | 33 | 32.5 | 32 | 31.5 | 31 | 30 | 29 |
| Mo-Mn | 2872 | 1.43 | 0.12 | 0.033 | 8-9 | 54.5 | 51.5 | 43 | 36 | 32.5 | 31.5 | 30.5 | 29.5 | 28.5 | 28 | 27.5 | 26.5 |
| | 2780 | 1.24 | 0.18 | 0.035 | 7-9 | 55 | 53 | 46 | 38.5 | 35.5 | 34 | 33 | 32 | 31.5 | 31 | 31 | 29 |
| Mo | 2782 | 0.90 | 0.35 | 0.034 | 7-8 | 56 | 55.5 | 53.5 | 48.5 | 42 | 39 | 37 | 35.5 | 34 | 33 | 31.5 | 30.5 |

**Fig. 1—Impact transition curves for 1340 steel.**

Specimens oil quenched from 1550°F, tempered for one hour at 1150°F and cooled at the rates indicated.
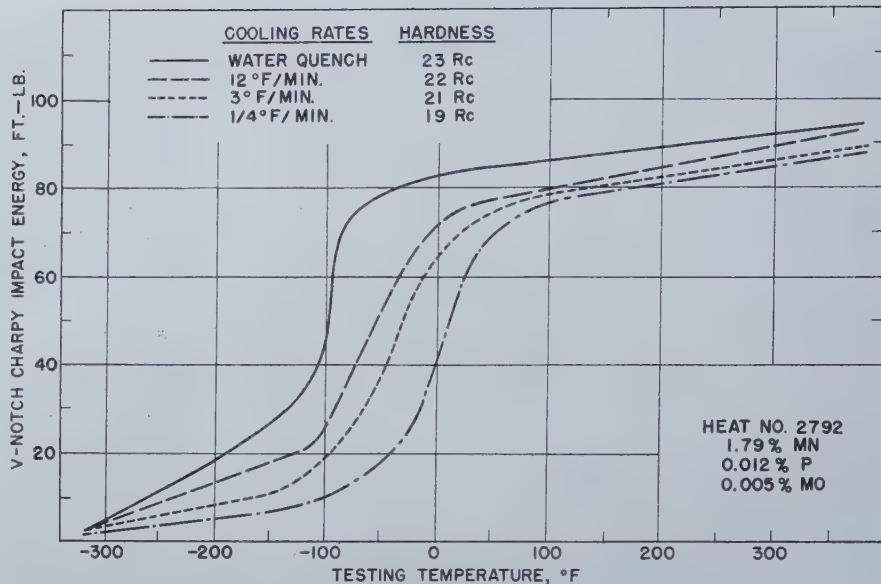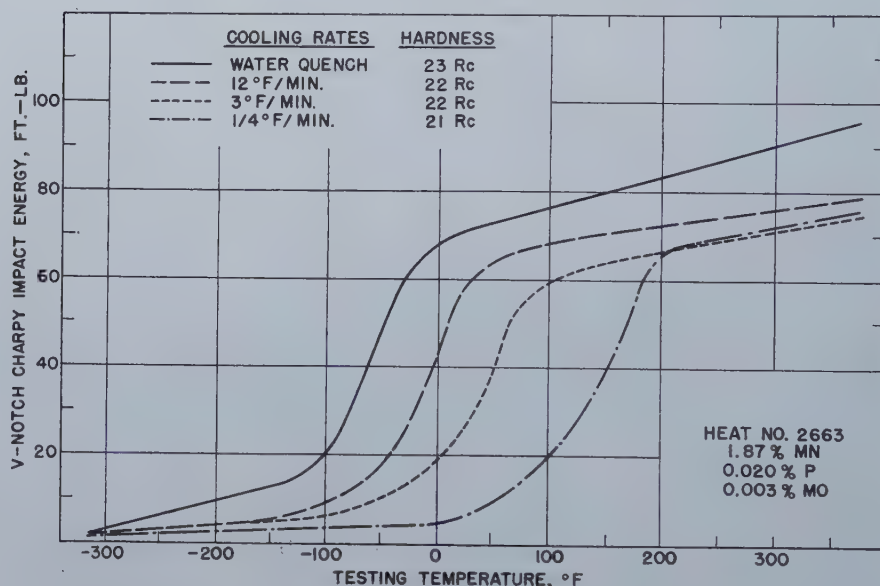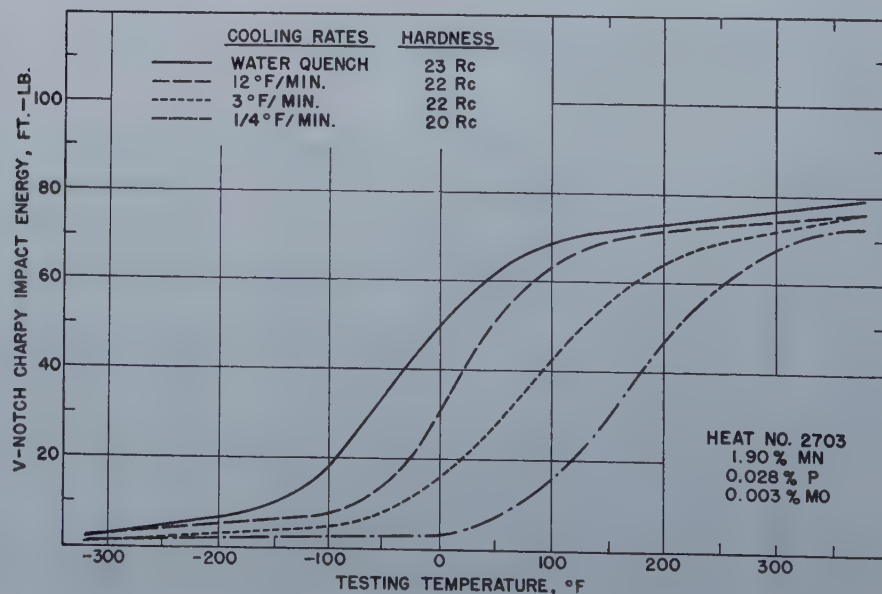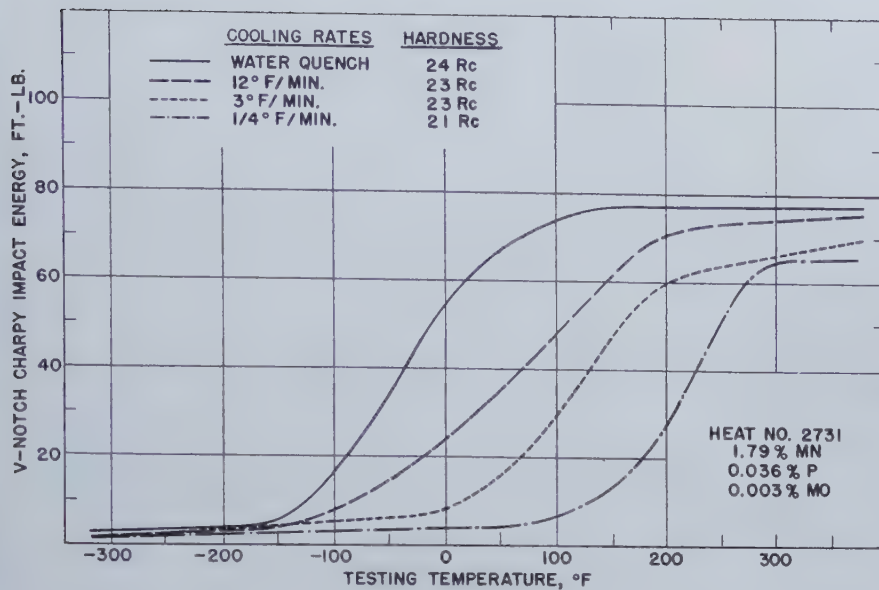
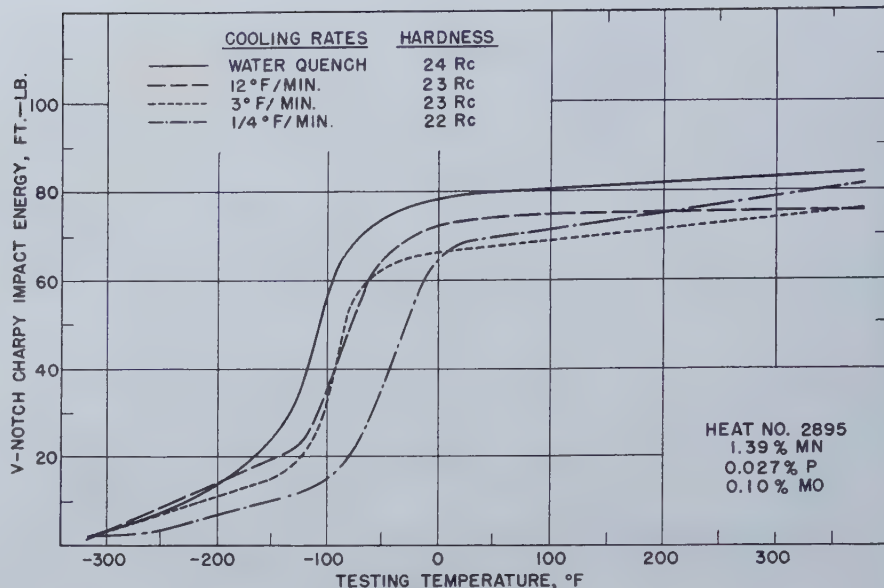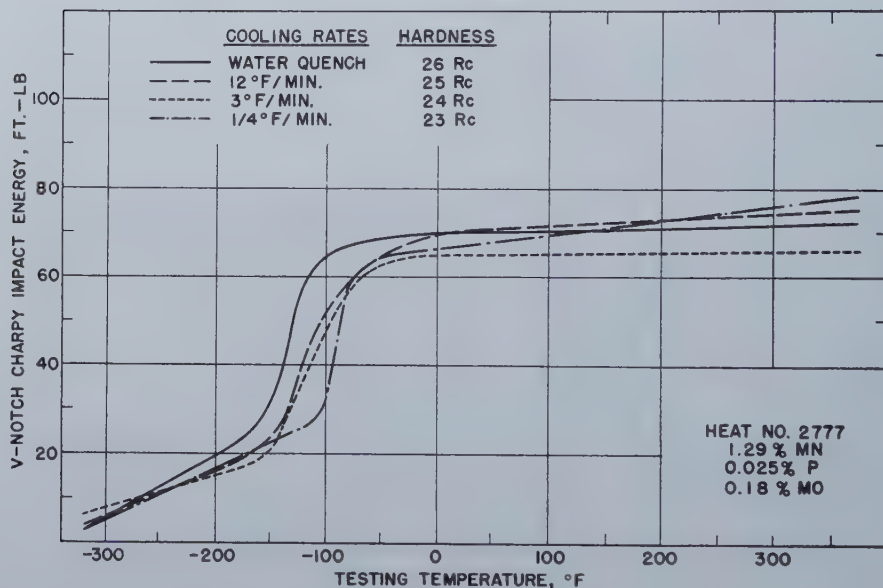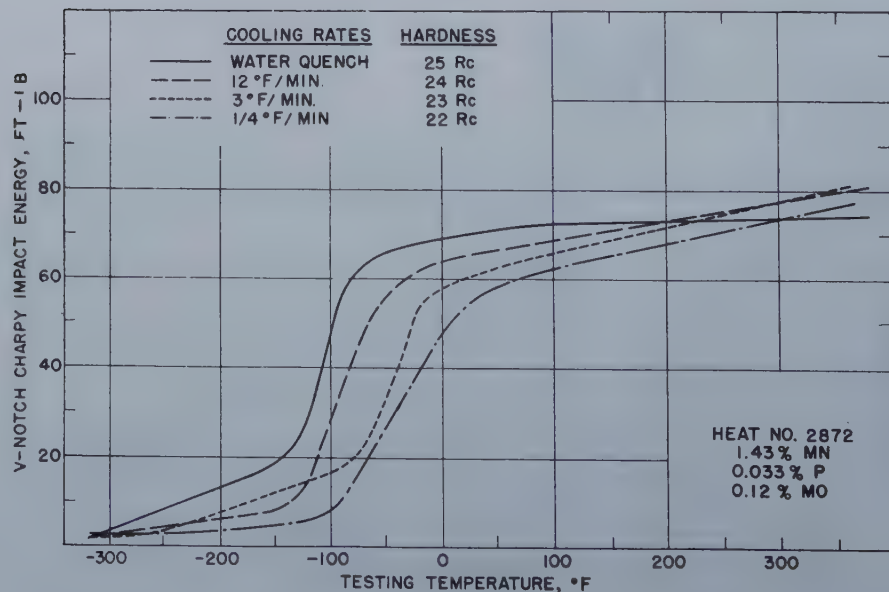| COOLING RATES | HARDNESS |
| --- | --- |
| WATER QUENCH | 23 Rc |
| 12 °F/MIN. | 22 Rc |
| 3° F/MIN. | 21 Rc |
| 1/4°F/ MIN. | 19 Rc |

HEAT NO. 2792
1.79 % MN
0.012 % P
0.005 % MO

**Fig. 2—Impact transition curves for 1340 steel.**

Specimens oil quenched from 1550°F, tempered for one hour at 1150°F and cooled at the rates indicated.

| COOLING RATES | HARDNESS |
| --- | --- |
| WATER QUENCH | 23 Rc |
| 12 °F/MIN. | 22 Rc |
| 3° F/MIN. | 22 Rc |
| 1/4°F/ MIN. | 21 Rc |

HEAT NO. 2663
1.87 % MN
0.020 % P
0.003 % MO

**Fig. 3—Impact transition curves for 1340 steel.**

Specimens oil quenched from 1550°F, tempered for one hour at 1150°F and cooled at the rates indicated.

| COOLING RATES | HARDNESS |
| --- | --- |
| WATER QUENCH | 23 Rc |
| 12 °F/MIN. | 22 Rc |
| 3° F/MIN. | 22 Rc |
| 1/4°F/ MIN. | 20 Rc |

HEAT NO. 2703
1.90 % MN
0.028 % P
0.003 % MO

Fig. 4—Impact transition curves for 1340 steel.

Specimens oil quenched from 1550°F, tempered for one hour at 1150°F and cooled at the rates indicated.
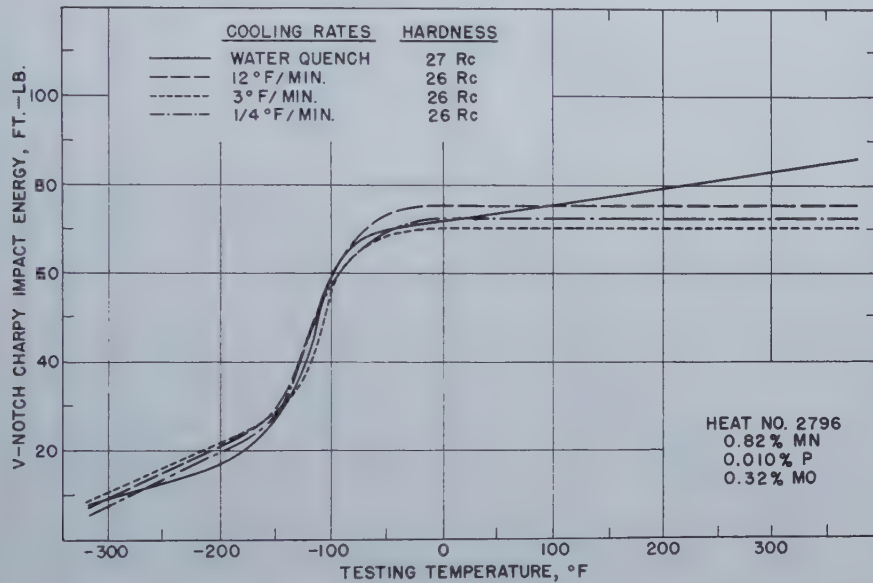


Fig. 5—Impact transition curves for molybdenum steel.

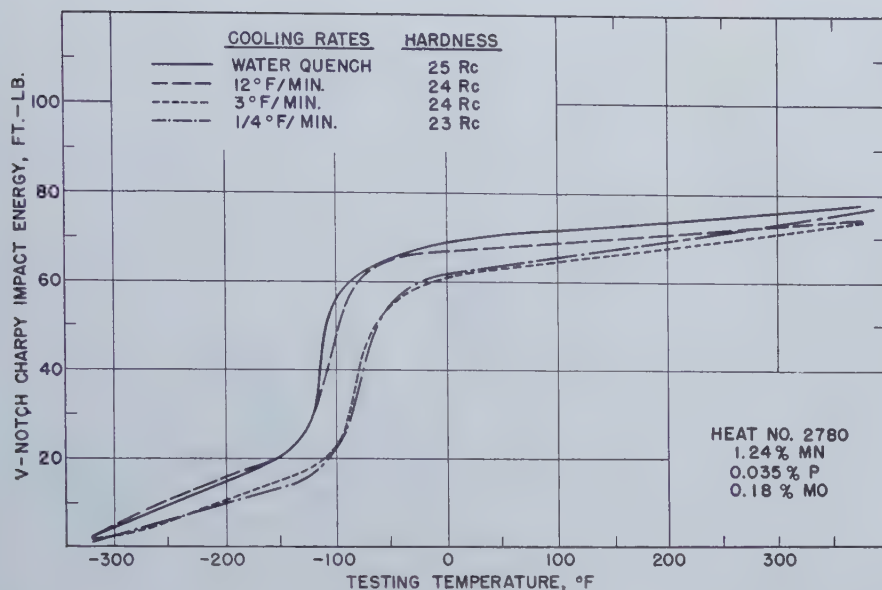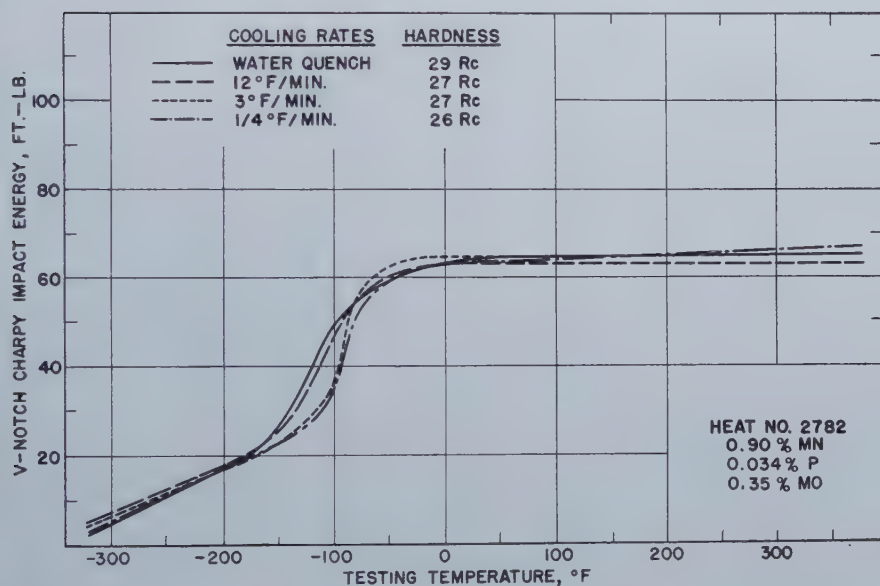Specimens oil quenched from 1550°F, tempered for one hour at 1150°F and cooled at the rates indicated.
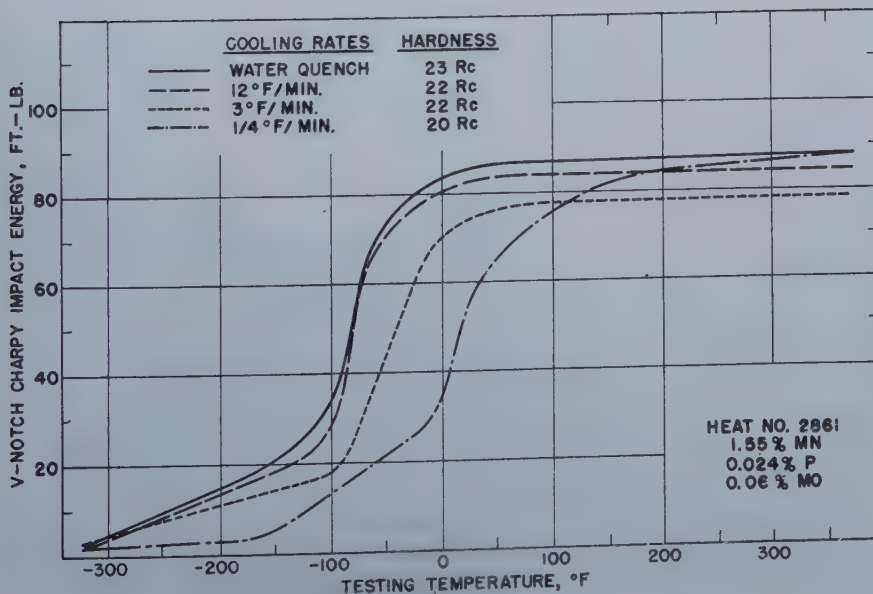


Fig. 6—Impact transition curves for molybdenum-manganese steel.

Specimens oil quenched from 1550°F, tempered for one hour at 1150°F and cooled at the rates indicated.

Fig. 7—Impact transition curves for molybdenum-manganese steel.

Specimens oil quenched from 1550°F, tempered for one hour at 1150°F and cooled at the rates indicated.

| COOLING RATES | HARDNESS |
|---|---|
| WATER QUENCH | 24 Rc |
| 12°F/MIN. | 23 Rc |
| 3°F/MIN. | 23 Rc |
| 1/4°F/MIN. | 22 Rc |

HEAT NO. 2895
1.39 % MN
0.027% P
0.10 % MO

V-NOTCH CHARPY IMPACT ENERGY, FT.-LB.
TESTING TEMPERATURE, °F

Fig. 8—Impact transition curves for molybdenum-manganese steel.

Specimens oil quenched from 1550°F, tempered for one hour at 1150°F and cooled at the rates indicated.

| COOLING RATES | HARDNESS |
|---|---|
| WATER QUENCH | 26 Rc |
| 12°F/MIN. | 25 Rc |
| 3°F/MIN. | 24 Rc |
| 1/4°F/MIN. | 23 Rc |

HEAT NO. 2777
1.29 % MN
0.025% P
0.18 % MO

V-NOTCH CHARPY IMPACT ENERGY, FT.-LB
TESTING TEMPERATURE, °F

Fig. 9—Impact transition curves for molybdenum-manganese steel.

Specimens oil quenched from 1550°F, tempered for one hour at 1150°F and cooled at the rates indicated.

| COOLING RATES | HARDNESS |
|---|---|
| WATER QUENCH | 25 Rc |
| 12°F/MIN. | 24 Rc |
| 3°F/MIN. | 23 Rc |
| 1/4°F/MIN | 22 Rc |

HEAT NO. 2872
1.43 % MN
0.033 % P
0.12 % MO

V-NOTCH CHARPY IMPACT ENERGY, FT.-IB
TESTING TEMPERATURE, °F

Fig. 10—Impact transition curves for molybdenum-manganese steel.

Specimens oil quenched from 1550°F, tempered for one hour at 1150°F and cooled at the rates indicated.



Fig. 11—Impact transition curves for molybdenum steel.

Specimens oil quenched from 1550°F, tempered for one hour at 1150°F and cooled at the rates indicated.
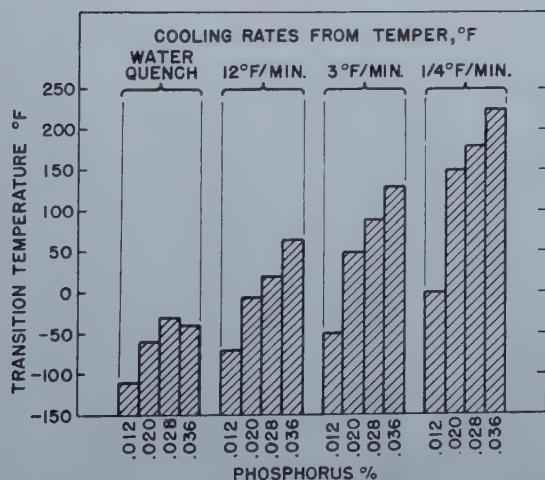


Fig. 12—Effect on transition temperature of an increase in phosphorus in 1340 steel.
Transition temperatures read from impact curves at 40 ft-lb level.

**Effect of Phosphorus in 1340 Steel:** The changes in toughness that attended an increase in phosphorus from 0.012 to 0.036 pct in 1340 steel are shown by the impact transition curves of fig. 1 through 4 and are summarized in the form of transition temperatures in fig. 12. Phosphorus caused considerable reduction in the toughness of 1340 steel, even when the specimens were quenched in water after tempering at 1150°F. Between 0.012 and 0.028 pct P the transition temperature of the water-quenched specimens rose about 80°F. However, the steel with a phosphorus content of 0.036 pct appeared inconsistent, actually showing a slightly lower transition temperature than that with 0.028 pct P.

As the cooling rate decreased, the transition temperature at each phosphorus level rose. Furthermore, the heats with 0.028 and 0.036 pct P, that had essentially the same transition temperature when quenched, developed a difference in transition temperature with slower cooling rates. When cooled at rates at 12°F per min or less, the 1340 with 0.036

**Fig. 13—Effect of replacement of part of manganese in 1340 by molybdenum.**

Transition temperatures read from impact curves at 40 ft-lb level. (Transition temperatures of 1340-0.024/0.027 pct P represent average of heats 2663 and 2703.)
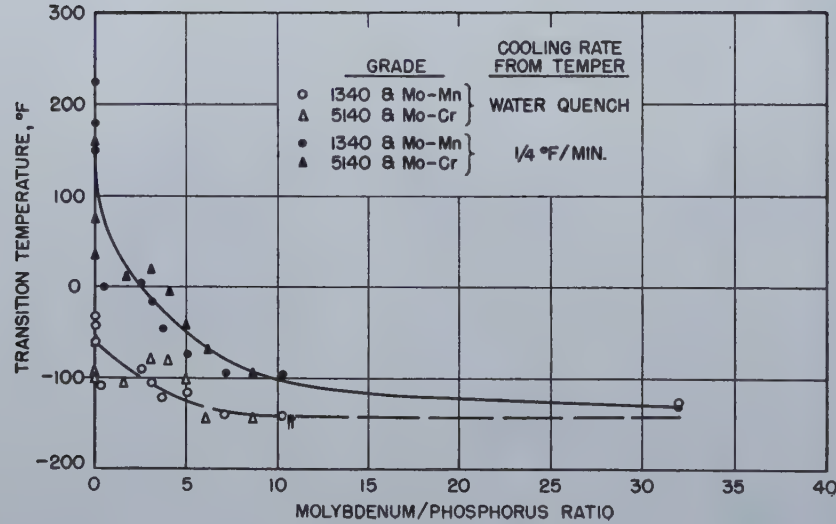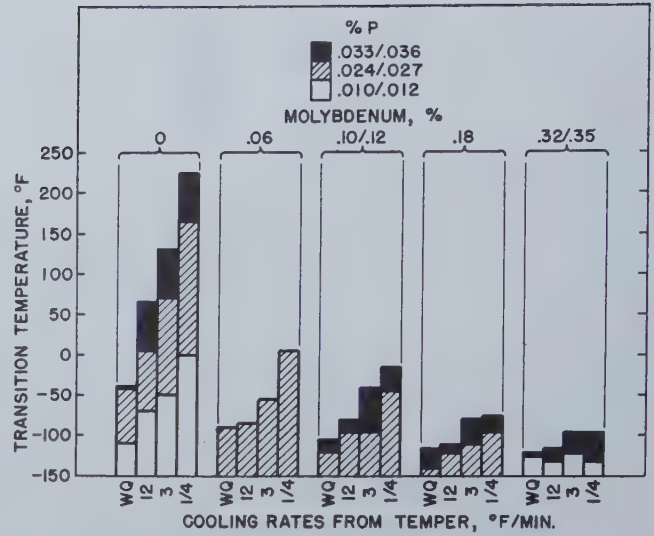


**Fig. 14—Dependence of transition temperature on Mo/P ratio and cooling rate after tempering for one hour at 1150°F.**

### Table III. Comparison of 1340, 5140, Mo-Mn and Mo-Cr Steels

| | | Transition Temperature, °F with Cooling Rate after Tempering of | | |
|---|---|---|---|---|
| Pct P | Grade | Water Quench | 3°F per min | 1/4°F per min |
| 0.020 | 1340 | — 60 | 50 | 150 |
| 0.027 | 0.10 Mo, 1.39 Mn | —120 | — 95 | — 45 |
| 0.025 | 0.18 Mo, 1.29 Mn | —140 | —110 | — 95 |
| 0.020 | 5140 | —100 | — 35 | 35 |
| 0.023 | 0.11 Mo, 0.52 Cr | —100 | — 65 | — 40 |
| 0.021 | 0.18 Mo, 0.44 Cr | —145 | —115 | — 95 |
| 0.036 | 1340 | — 40 | 130 | 225 |
| 0.033 | 0.12 Mo, 1.43 Mn | —105 | — 40 | — 15 |
| 0.035 | 0.18 Mo, 1.24 Mn | —115 | — 80 | — 75 |
| 0.036 | 5140 | — 60 | 85 | 160 |
| 0.037 | 0.11 Mo, 0.55 Cr | — 80 | — 25 | 20 |
| 0.041 | 0.16 Mo, 0.50 Cr | — 80 | — 30 | — 5 |

pct P showed a greater loss of toughness than the 1340 with 0.028 pct P. Within the scope of the data, the greatest difference in the influence of phosphorus in 1340 appears to be in the range of 0.012 to 0.020 pct P, although phosphorus contents above 0.020 pct cause an additional susceptibility to temper brittleness. Thus 1340 steel with a phosphorus content that would be considered to represent good open hearth or electric furnace practice still might show a high degree of susceptibility to embrittlement.

**Effect of Phosphorus in Mo and Mo-Mn Steels with Hardenability Similar to 1340 H Steel:** The impact transition curves of fig. 5 through 11, together with the summary of transition temperatures in fig. 13, show the extent to which replacement of a part of the manganese in 1340 by molybdenum counteracts the loss of toughness caused by phosphorus.

In a steel containing 0.010 pct P and 0.32 pct Mo, heat 2796 in fig. 5, no loss of toughness occurred even with a cooling rate as slow as ¼°F per min. The behavior of the Mo steel, fig. 5, may be compared with that of the 1340 steel containing 0.012 pct P, fig. 1. With this low phosphorus content, the 1340 steel has about the same transition temperature as the Mo steel, when the specimens were quenched in water after tempering; but, with cooling rates of 12°F per min and less the 1340 steel exhibits considerable loss of toughness. By contrast, the Mo steel retains its toughness even when cooled at a rate of ¼°F per min.

The effectiveness of the replacement of 1 pct Mn by 0.35 pct Mo in controlling loss of toughness caused by phosphorus will be evident on comparing the data from heat 2796 (0.010 pct P, 0.32 pct Mo) with that from heat 2782 (0.034 pct P, 0.35 pct Mo). Even with a cooling rate of ¼°F per min, the 0.034 pct P steel had a transition temperature of —95°F, only 35°F above that of the 0.010 pct P-Mo steel.

The progressive nature of the control of transition temperature effected by replacement of a part of the manganese in 1340 by molybdenum will be visualized readily from fig. 13. The more slowly the steel is cooled after tempering and the higher the phosphorus content, the greater must be the replacement of manganese by molybdenum to prevent an appreciable rise in transition temperature. To hold the transition temperature at —75°F or below in the 1340 steel requires the lowest phosphorus level (0.010/0.012 pct) and requires water quenching after tempering. With only 0.06 pct Mo the intermediate phosphorus level (0.024/0.027 pct) and a cooling rate after tempering of 12°F per min can be tolerated. With 0.10/0.12 pct Mo the intermediate phosphorus level and a cooling rate of 3°F per min or the highest phosphorus level (0.033/0.036 pct) and a cooling rate of 12°F per min are permitted. With 0.18 pct or more molybdenum the highest phosphorus level and slowest cooling rate (¼°F per min) do not raise the transition temperature above —75°F.

Thus it has been demonstrated that a good tolerance for phosphorus in tempered martensite can be obtained by replacing a part of the manganese in 1340 by molybdenum, without essential alteration

in the hardenability of the 1340 grade. Similar conclusions were reached earlier from a study[1] of the replacement of chromium in 5140 by molybdenum. A unique relation between molybdenum and phosphorus contents in determining the toughness of tempered steel is suggested by the dependence of transition temperature on the Mo/P ratio and the cooling rate that is shown in fig. 14. Data from all of the heats of 5140, 1340 and molybdenum modifications of both grades are included.

It may be of interest to compare 1340, 5140, and 0.16/0.18 pct Mo modifications of these grades. Table III lists pertinent transition temperatures. While the 5140 steels show somewhat less loss of toughness than the 1340 steels, when comparisons are made at the same phosphorus content and cooling rate, the maintenance of toughness in the 0.16/0.18 pct or higher Mo modifications of either grade is outstanding.

In the practical application of replacement of manganese or chromium by molybdenum, items to be considered in selecting the minimum amount of molybdenum required to guard against a detrimental loss of toughness are:

The size of section to be heat treated (cooling rate from tempering temperature).
The most critical stress state to which the part will be subjected.
The minimum expected service temperature.
The maximum phosphorus content anticipated in the steel.

While the ladle analyses of commercial alloy steels are usually well below the maximum allowed by the AISI-SAE specifications, even these moderate phosphorus contents may cause loss of toughness in some grades. This was shown to be the case in 1340. Moreover, phosphorus has a marked tendency to segregate in steel ingots. Hence, when a high degree of toughness is required, it would appear necessary to select a specification which will provide required properties in all portions of the steel actually used.

### Conclusions

1. Replacement of a part of the manganese in 1340 steel by molybdenum, in proportions required to maintain the hardenability of the grade, reduces the loss of toughness caused by phosphorus in tempered martensite.

2. The tolerance for phosphorus provided in tempered martensite by partial replacement of manganese by molybdenum depends upon the amount of the replacement and the heat treatment of the steel. Appreciable improvement resulted from as little as 0.06 pct molybdenum. With 0.18 pct Mo, toughness was virtually unaffected by the severely embrittling treatments employed in this work, even with a phosphorus content of 0.035 pct.

### Reference

[1] M. Baeyertz, W. F. Craig, Jr., and J. P. Sheehan: *Trans.* AIME (1949) **185**. *Jnl. of Metals*, Aug. 1949, TP 2654.

# The Tin-Fusion Method

## for the Determination of

## Hydrogen in Steel

by Dennis J. Carney, John Chipman, and N. J. Grant

Based on the design of vacuum fusion apparatus, an improved system has been developed solely for hydrogen analysis. A tin-iron bath permits melting and operation at 1150°C. Heating and stirring are accomplished by induction heating in a water jacketed silica tube. All grease is eliminated from the system by means of mercury valves. Routine 15 min analyses are standard. Precision of $\pm$ 0.1 parts per million for a 2 g sample is attained.

SINCE the beginning of this century it has been known that hydrogen contributes to the porosity of steel and that it is harmful to its mechanical properties. The evidence for this has been largely qualitative. Steel to which hydrogen was purposely added in sufficient amounts was shown to be either porous or brittle or both, whereas similar steel of low hydrogen content was shown to be free of porosity and to possess normal physical properties. There have been a considerable number of qualitative experiments of this type.

Also, early in this century, a few attempts were made to measure the amount of hydrogen normally dissolved in commercial steels. This was usually done by placing the sample under an inverted liquid column such as mercury and collecting the evolved gas. These attempts, while not successful in measuring actual amounts of dissolved hydrogen gas, were able to prove that this gas will diffuse out of steel at room temperature, and that the amount of hydrogen dissolved is normally very small. On the basis of such qualitative evidence, hydrogen has been and still is blamed for a great number of the troubles encountered in the steel industry.

In recent years, partial solutions for many steel-working problems have been obtained. These have led to increased interest in accurate quantitative work on hydrogen in steel, with the expectation that the results might possibly answer a few of the remaining unsolved problems. Commercially, two of the obvious questions which are in need of an answer are: (1) what are the most important sources of hydrogen, and (2) what quantity of hydrogen can be tolerated in various steels?

There are many other unanswered questions. To begin to find the answers it seemed logical to start at the beginning of steel production with the liquid metal. Further, it seemed almost imperative to solve first the problems of analysis and sampling of the metal for hydrogen. Once these problems have been solved, it would be possible to answer more of the important commercial problems mentioned above. As a consequence, it was decided to design an analytical apparatus and, upon satisfactory completion of this, to develop an accurate method of sampling liquid metal for hydrogen.

D. J. CARNEY, Student Member, is at South Works, Carnegie Illinois Steel Corp., Chicago, Ill. JOHN CHIPMAN, Member, is Professor, and N. J. GRANT, Member AIME, is Associate Professor, Mass. Inst. of Tech., Cambridge, Mass.
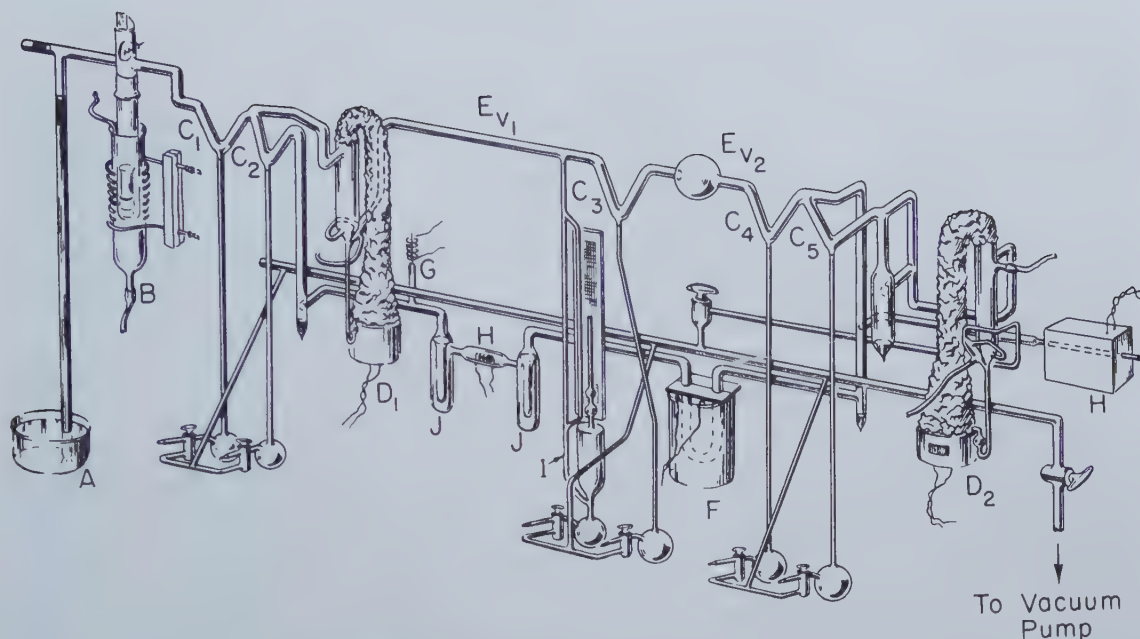
**Fig. 1—Analytical apparatus for hydrogen in steel.**

A — Mercury lift
B — Furnace
C — Mercury cut-offs
D — Mercury diffusion pumps
E — Known volumes

F — Oxidant
G — Palladium tube
H — Silver tube and platinum filament
I — McLeod gauge
J — Freeze-out traps

The intent was to develop sampling and analytical methods such that they would be rapid and simple enough to be of use on a commercial basis. For this purpose the total time of sampling and analysis had to be of the same order of magnitude as the time required for determination of carbon, manganese or sulphur, i.e., about 15 to 20 min total time. The first section of this research is devoted solely to the analytical method.

### Literature Survey

Previous to this investigation four main methods of steel analysis for hydrogen were used in the United States, Great Britain and Germany. They were: (1) the vacuum fusion method, (2) the solid state vacuum extraction method, (3) the total combustion method, and (4) the tin-fusion method. The first three methods are well described in summaries appearing in the Journal of the British Iron and Steel Institute[1] and the Transactions of the American Institute of Mining and Metallurgical Engineers[2]. In brief, the vacuum fusion method is conducted in vacuum in a graphite crucible at a temperature of 1550°-1650°C. The evolved gases are composed in general of 95 pct carbon monoxide and nitrogen and 5 pct hydrogen by volume. The gases are collected for about 30 min and circulated for another 20 min over copper oxide to convert the hydrogen to water vapor, which is absorbed or frozen out. This method had been used successfully by Derge[3, 4], who has presented a detailed discussion of it.

The method of vacuum extraction in the solid state is carried out in a silica furnace at temperatures of 400°[5], 600°[6, 7, 8], 800°[9], 1050°[10] and 1100°C[5].

At 400° and 600°C most steels are ferritic; and low-carbon steels remain in this state up to about 800°C. Since the diffusion of hydrogen is rapid and its solubility in ferrite is low, the gas is evolved rapidly and may be collected in 1 to 2 hr. At 1050° and 1100°C the steel is austenitic and the diffusion of hydrogen is slower and its solubility higher. The evolved gas is collected for periods up to 48 hr. The evolved gases in this method are about 90 pct hydrogen with the remainder carbon monoxide and nitrogen. The gases are either assumed to be 100 pct $H_2$ and measured as such, or else are analyzed by a modified Orsat apparatus. This method is being used successfully by Sims and coworkers and has been described elsewhere[10].

The total combustion method was described by G. A. Moore[11] in 1943. Moore and other workers have experienced difficulty with the accuracy and precision of this method. It is not in general use at the present time.

Perhaps the most serious objection to the vacuum fusion method is the very low percentage of hydrogen in the evolved gases, making accuracy and precision difficult. On the other hand, complete release of the hydrogen in the liquid state apparently occurs within a short time. In the vacuum extraction method from the solid state the reverse appears true. In other words, the percentage of evolved gases is high in hydrogen allowing for greater precision; however, there is a reasonable doubt that all of the hydrogen is released within the collection time.

The tin-fusion method attempts to avoid the serious objections of both of the two preceding methods. It was used for hydrogen analysis by Bennek and Klotzbach[5]. Later Bennek and others in

**Table I. Methods of Steel Analysis for Hydrogen**

| Method | Furnace Crucible | Temperature, °C | Average Compositions of Evolved Gases | Total Time of Analysis, Hours | Estimated Precision |
|---|---|---|---|---|---|
| Vacuum fusion | Graphite | 1600 | 95 pct $CO + N_2$<br>5 pct $H_2$ | 1 | 0.1 ppm |
| Vacuum extraction solid state | Silica | 1050<br>800<br>600 | 90 pct $H_2$<br>10 pct $CO + N_2$ | 48<br>1<br>1 | 0.01 ppm<br>0.1 ppm<br>0.1 ppm |
| Total combustion | Silica | 1000 | $H_2O + CO_2$ | 100? | ? |
| Tin-fusion | Silica | 1150 | See text | See text | See text |

Germany combined the solid extraction method with the tin-fusion method in one analysis. Gas was collected in the solid state for 2½ hr at 400°C and for 4 hr at 1100°C, then the sample was melted in tin and the remaining gas collected for an additional 5 hr. Elsewhere, the tin-fusion method apparently has been used only by Naughton[12] at General Electric. Naughton briefly investigated the method after using the normal vacuum fusion method. His preliminary work and a study of the published methods of analysis of steel for hydrogen indicated that tin-fusion offered promise of being rapid, accurate and precise. The various methods are summarized in table I.

## Apparatus

The apparatus is shown schematically in fig. 1 and a photograph is given in fig. 2. The apparatus was made largely from 20 mm pyrex glass tubing. A small amount of silica tubing was used for the furnace. The essential parts of the apparatus are listed in fig. 1.

A brief description of these parts and their purpose follows.

**Mercury Lift:** The mercury lift was made from 30 mm pyrex tubing. It was a mercury column of barometric height which was used for admission of samples. It allowed one to add new samples at will to an evacuated and "baked-out" system without breaking the vacuum. This was necessary since hydrogen samples can not be stored at room temperature in a furnace head under vacuum in the system.

A small plunger was placed in the "T" section at the top of the lift to keep mercury splashes within the mercury column on admission of samples.

**Furnace:** The furnace section is shown both in fig. 1 and in detail in fig. 3. The upper portion of the furnace was made of pyrex and consists of a sight glass with an optical prism for reading the bath temperature, a shutter to protect the sight glass from metal splashes, a funnel to guide the samples into the furnace crucible, and a 55/50 female ground glass joint. The lower section was composed of a 45 mm clear silica tube with a 55/50 male ground joint. The seal between the two joints was made with Apiezon W wax. The melting crucible was of opaque silica 1½ in. in diam and 4 in. long. This was set inside a short alumina crucible which was used as a heat insulator and also as a safety measure in case of cracking of the quartz melting crucible. A Vycor funnel was placed atop the melting crucible to pre-

vent splashing of metal out of the furnace when the specimen was dropped into it. The whole assembly was water-cooled by means of a pyrex jacket. The furnace was heated by means of a high frequency 7.5 kw Lepel unit.

**Mercury Cut-offs:** There were no stopcocks within the analytical portion of the apparatus. Five mercury cut-offs were used in place of stopcocks. There were two reasons for this: (1) to eliminate the possibility of hydrogen being absorbed by the stopcock grease, and (2) to obtain better control of the vacuum which is sometimes erratic when using stopcocks.

**Mercury Diffusion Pumps:** There were two three-stage mercury diffusion pumps. Pump 1 was used to evacuate the gas from the furnace, placing it in a known volume, and also to circulate the gas through the copper oxide oxidant and freeze-out traps. This pump was designed so that the outlet portion of the pump was a part of the known volume which is relatively unaffected by pumping speed or pressure of the stored gas. This pump will continue to operate at back pressures up to 20 mm of mercury. Pump 2 was used to keep all of the analytical portion of tubing which was in back of the circulating pump at a very low pressure (essentially gas free). It also isolated this section from the stopcocks used to raise and lower the mercury cut-offs, and from any back diffusion from the oil pump.

**Known Volumes:** The two known volumes indicated in fig. 1 are $V_1$, 362 ± 4 cc, and $V_2$, 650 ± 8 cc. The known volumes were calibrated by pumping prepurified nitrogen at atmospheric pressure from a small mercury-calibrated volume into the system volumes and measuring the resulting pressure with the McLeod gauge.

**Copper Oxide Oxidant:** The copper oxide furnace was simply a U tube of 20 mm pyrex tubing in a chromel-wound resistance furnace which is maintained at a temperature of 350° to 400°C. The oxidant consisted of cupric oxide made from copper gauze which was alternately oxidized and reduced with tank oxygen and hydrogen gas. This was done *in situ* by connecting the gas inlet and outlet to two small tubes joined immediately above the oxidant furnace. To assist the gas passing through the oxidant, a vacuum line was connected to the outlet nipple during the activation process.

**Palladium Tube:** The small palladium tube was used to introduce pure hydrogen into the system. It was heated by a small resistance coil while tank hydrogen was passed over it. This provided a rapid
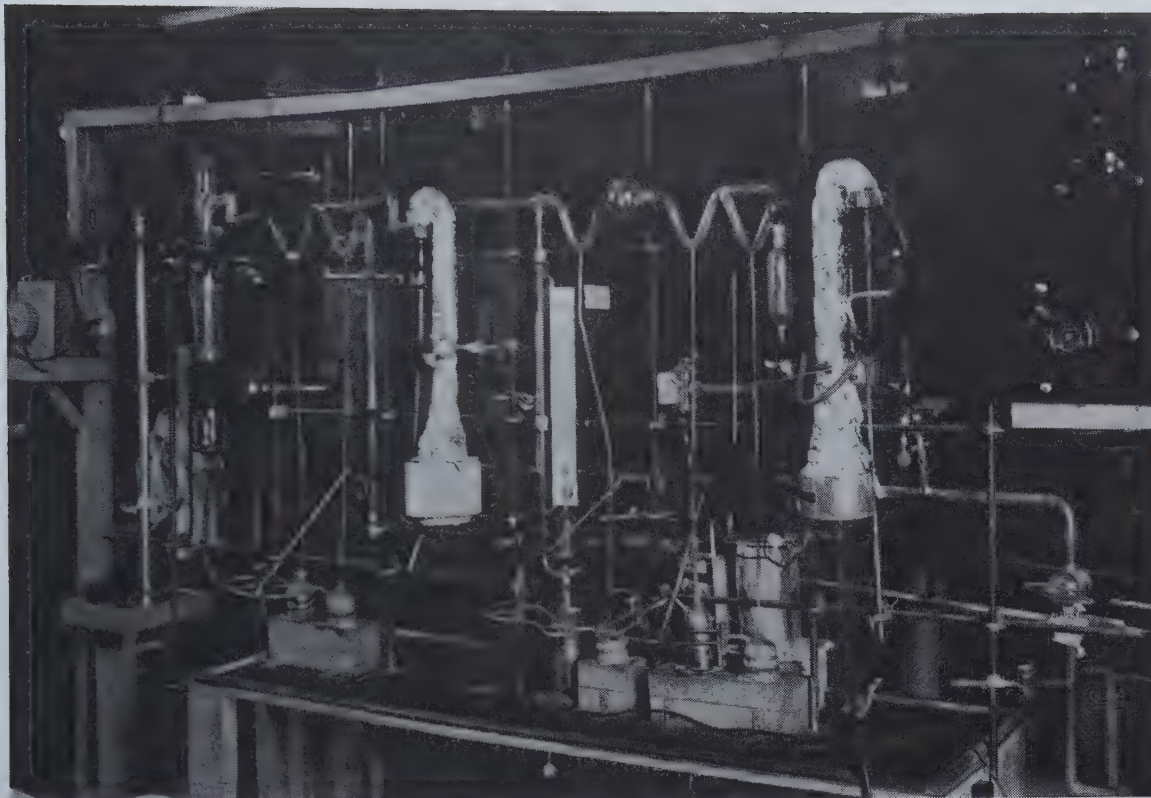
Fig. 2—Analytical apparatus for hydrogen in steel.

and convenient method of introducing pure hydrogen to be used in checking the efficiency of the analytical system.

**Silver Tube and Platinum Filament:** The silver tube and platinum filament were installed originally to take care of any hydrogen which might be evolved as methane. The silver tube when heated to 700°C allowed pure oxygen to diffuse through it from the air. This oxygen was used to combine with the methane in the presence of a heated platinum filament*.

* Only two tests were made, each indicating no methane in the evolved gases. Naughton[12] also observed that no methane is present in the gases evolved from steel. Later data on sampling which will be presented also indicate the absence of methane. Therefore, these two devices could be removed from the apparatus.

**McLeod Gauge:** A McLeod gauge was used to determine gas pressures in the known volumes. This gauge was designed to measure pressures up to 20 mm of mercury. There were three calibrated sections. The first read pressures from 20 to 0.05 mm, the second from 2 to 0.007 mm and the third from 0.2 to $10^{-6}$ mm of mercury.

**Freeze-out Traps:** The two freeze-out traps were used to keep the mercury vapor away from the platinum filament and to remove water vapor formed by the oxidant. The traps were cooled by a mixture of dry ice and acetone.

### Analytical Operation

1. The furnace crucible was initially charged with approximately 130 g of chemically pure tin pellets and 0.7 g of purified silicon metal. The furnace section was assembled, the system evacuated, and the furnace heated to 1150°C. At this tempera-ture the system was evacuated for approximately 4 hr. This is normally called "baking" or "blanking out" the apparatus.

2. After this "bake-out", the analytical section of the apparatus was checked. First, there was usually a very small build-up in pressure which appeared to come from the oxidant, freeze-out traps and mercury pump. The pressure was measured by raising the mercury in cut-offs 1 and 5 (see fig. 1) and holding for 5 min after which cut-off 4 was raised and the pressure increase, if any, was read. Second, the efficiency of the oxidant and freeze-out traps was measured. This was done by raising cut-offs 4 and 5 and allowing hydrogen to diffuse through the heated palladium tube. The amount admitted was measured by the McLeod gauge and was then circulated over the oxidant and freeze-out traps by lowering cut-off 4. The circulation was carried on until 98 to 100 pct of the admitted hydrogen had been removed. The length of time for this process determined the required circulation time, which was usually about 5 min. (Checks run at the end of the day showed little or no change in the oxidant efficiency over a period of 12 hr.)

3. The blank was measured by raising cut-offs 2 and 4 and collecting furnace gas for 10 min after which cut-off 1 was raised. The gas pressure was measured on the McLeod gauge and the gas was then circulated for the previously determined time by lowering cut-offs 2 and 4. Cut-off 4 was raised and the gas pressure again read. Any decrease in pressure measured was called the blank. The apparatus was now ready for a sample analysis.

4. The sample was washed in carbon tetrachlo-

ride, dried in a current of filtered air and weighed. With all cut-offs down, it was placed under the mercury lift and floated to the top. There it was picked up by a magnet* and pulled over to the furnace.

---

---

Any air bubbles arising out of the mercury columns when the sample was admitted were swept out while the sample was being handled by the magnet. Cut-offs 2 and 4 were then raised and the sample dropped into the furnace. As in the blank run, gas was collected for 10 min and then circulated for the required time. The decrease in pressure obtained, less any blank value, determined directly the hydrogen that was present. All cut-offs were then lowered to be ready for the next sample.

### Discussion of Procedure

**Analytical Pressure Increase:** The pressure in the analytical portion of the apparatus increased slightly with the age of the oxidant and with an increase in the amount of mercury vapor deposited in the freeze-out traps. Any oxidation of the mercury in diffusion pump I forms mercuric oxide which slowly decomposes giving another source of pressure build-up in the analytical section. Normally this pressure increase was small enough to be ignored. However, even if the pressure build-up were moderately high but constant, it would not affect the analysis since it was automatically taken care of in the blank determination.

**Oxidant Efficiency:** The oxidant efficiency obtained was very good. In approximately 80 pct of all analyses, 98 to 100 pct efficiency was obtained with a 5-min circulation period. Circulation times of over 10 min were never necessary. This may have been due partially to the fact that the evolved gases were largely hydrogen, with very little CO. Another important factor was the speed of circulation of the gases by the diffusion pump.

In a similar analytical procedure, Derge[3] observed that the freeze-out traps of acetone and dry ice at their normal temperature of —78°C would not solidify completely the water vapor formed. This was due to the fact that the equilibrium vapor pressure of dry ice at this temperature was greater than the pressure of the system. It was necessary to keep the trap temperature below —90°C, which was accomplished by bubbling air slowly through the acetone. One could easily regulate the temperature of the traps by regulating the flow of the air. This proved to be an efficient and simple method of keeping the traps at the desired temperature for long periods of time.

**Blanks:** After a 4-hr bake-out period at 1150°C, the blank was quite low as shown in table II. Most of the blank gas was pumped out within one hour and thereafter the gas was evolved more slowly. After a 2-hr bake-out in most cases it was possible to begin analyses of high hydrogen samples without a blank determination since the blank value was moderately low and was decreasing at a slow and consistent rate. The best blanks were obtained with the opaque silica crucibles. (It was possible to melt, solidify and remelt in these quartz crucibles without cracking so that the same crucible could be reused a

number of times.) Attempts to use other crucible materials such as alumina or beryllia resulted in higher blanks and in cracking of the crucibles on remelting. With quartz crucibles, a low blank was obtained more rapidly with crucibles that had previously been heated in air at a temperature of 800°C. It would be expected that a low blank could be obtained even more rapidly with clear quartz crucibles.

Since the majority of samples analyzed in this investigation weighed approximately 2 g, the blank was figured on this basis in table II. The blank was also calculated for a 10-g sample for comparison with the results of other investigations. A larger weight sample would, of course, result in even lower values. Blanks were normally determined three to four times during a day. The hydrogen values in

### Table II. Sample Blank Run

9:30 A.M. Furnace on at 1150°C, Silica Crucible,*
130g Sn, 0.7g Si

|  | Blank Values, ppm† in 10 Min. | |
|---|---|---|
|  | 2-g Sample | 10-g Sample |
| 10:30 a.m. | 1.3 | 0.36 |
| 11:30 | 0.4 | 0.08 |
| 12:00 | 0.4 | 0.08 |
| 1:30 p.m. | 0.1 | 0.02 |
| 5:30 p.m. | 0.0 | 0.00 |

* Silica crucible previously heated in air one hour at 800°C.
† See definition of ppm under "Blanks".

table II and in all subsequent figures are given as "parts per million" (ppm). These values appear as simple whole numbers which are easy to handle. The value given as ppm is converted to weight percent by moving the decimal point over four digits to the left.

**Evolved Gases:** The gases evolved from dissolved samples averaged 50 pct hydrogen by volume. The hydrogen percentage was seldom less than this and then only on low-hydrogen samples. The hydrogen was sometimes as high as 90 pct of the total gas in high-hydrogen samples. The residual gas was largely nitrogen and carbon monoxide. The small amount of silicon was added to the tin as a deoxidizer in order to keep the amount of evolved carbon monoxide low. A higher percentage of silicon could not be added since it raised the melting point of tin sharply.

There was no evidence of methane or water vapor in the evolved gas. Water vapor could be detected on a McLeod gauge of the type described by taking pressure readings on 2 of the 3 calibrated sections. If water vapor was present in the gas, it would condense in the gauge and the readings obtained on the 2 sections would not be in the perfect gas ratio. All readings were made on at least 2 of the 3 sections. In the few cases where water vapor was detected, it could usually be traced to some external cause such as adsorbed or trapped water on the surface of a poor sample and was not a part of the dissolved hydrogen.

**Time of Gas Collection:** As stated in the section on analytical procedure, the specimens were degassed for 10 min. This time was determined by collecting gas from a sample for 5 min, analyzing this portion, and then collecting gas for an additional

Glass Prism for Reading Furnace Temperature

Water Outlet

Pyrex Water Cooled Jacket

Vycor Funnel

Inner Quartz Tube

Opaque Quartz Melting Crucible

Alumina Shield
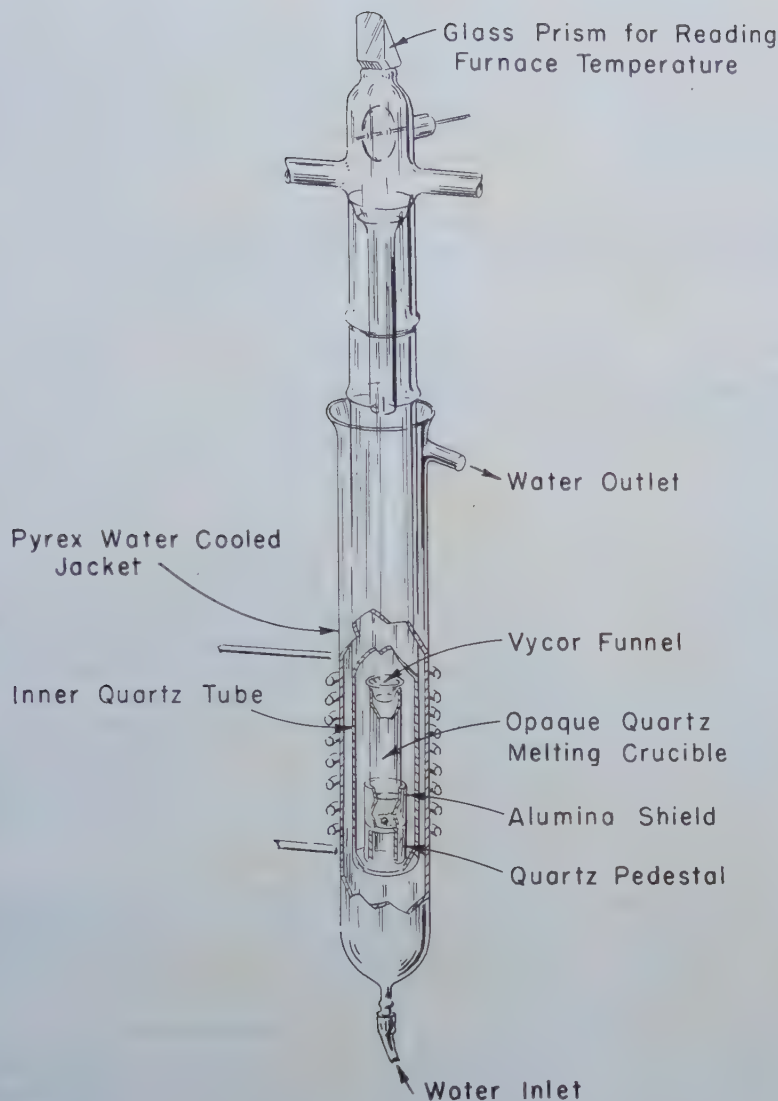
Quartz Pedestal

Water Inlet

Fig. 3—Detail of furnace.

5 min. The second 5-min collection period in all cases merely yielded the predetermined blank value.

Further evidence that a 5-min collection time was sufficient for samples which dissolved in 1 to 2 min was obtained from the liquid equilibrium samples which will be discussed later. These samples gave equally good hydrogen results when collected for 5, 10 or 15 min. This collection time was much shorter than in previous methods of analysis. It was believed due to (1) fast solution of the sample; (2) rapid pumping speed of the diffusion pumps; (3) rapid evolution of hydrogen due to constant stirring of the bath by induction heating.

**Tin Vapor:** In the past an objection to the tin-fusion method has been the vaporization of the tin metal in the vacuum. In this investigation, it did not prove to be a serious objection. The metal vapor itself was not a problem since it was easily condensed on the water-cooled furnace tube and was thereby kept out of the remainder of the system. In fact, vaporization occurred in varying degrees for all the liquid baths which were tried such as iron, copper or nickel.

A more serious objection to metal vapors in a hydrogen analysis apparatus was the possibility that

hydrogen was adsorbed by the condensate. Absorption is strongly time-dependent. The longer the time of contact between the gas and the vapor, the more chance there would be that adsorption might occur. This was illustrated experimentally by Derge[3] who bubbled known amounts of gas through liquid iron in a vacuum. He found no adsorption of the gas by the metal vapor. On the other hand, German workers did observe adsorption by tin vapor with a 12-hr gas collection. The difference in these observations was believed due primarily to the time factor. Checks were made in this investigation by heating the tin condensed on the furnace tube with a Bunsen burner after a day's run. Hydrogen was obtained from the heated condensate only when the furnace blank of hydrogen was unusually large during the entire day's run. In the normal case, when there was a small amount of blank hydrogen gas, no hydrogen was obtained from the heated condensate. Since the samples were degassed in 5 min or less at very high pumping speeds, the amount of hydrogen which would be adsorbed in this short time was insignificant. The analytical results obtained verified this viewpoint.

Various other melting baths were used experi-

mentally to obtain a lower bath temperature and less vaporization of the metal; these systems were copper-tin, copper-silicon, copper-tin-silicon, copper-aluminum, aluminum-tin, and copper-aluminum-tin. Some objections to these liquid baths were (1) formation of 2 liquid phases, (2) heavy oxide coverings, and (3) large increases in melting points after

hydrogen that was in the liquid metal was known from previous equilibrium solubility data. The problem was to sample, store and analyze samples taken from this liquid. The results of this study which will be described in another paper[14] indicate an overall accuracy of the order of a few tenths of one part per million.

## Table III. Hydrogen Results from Duplicate Steel Samples

| Treatment | Sample No. | | | |
|---|---|---|---|---|
| | 1. | 2. | 3. | 4. |
| Armco iron, pickled (HCl) | 2.4 ppm | 2.5 ppm | 2.4 ppm | 2.2 ppm |
| SAE 1020 electrolytically charged (H₂SO₄) | 1.3 | 1.5 | | |
| SAE 1020 electrolytically charged (H₂SO₄) | 3.2 | 3.1 | | |
| SAE 1020 electrolytically charged (H₂SO₄) | 4.6 | 4.3 | | |
| SAE 1020 pickled (HCl) | 4.8 | 4.6 | 4.8 | 4.5 |

addition of 6 or 7 samples. In all the metal baths used in which the samples dissolved, good hydrogen results were obtained. However, the tin bath containing 0.5 pct silicon appeared to be superior to the others in most respects.

**Accuracy and Precision:** The precision of the analytical section of the apparatus was more than adequate. The hydrogen was measured by recording pressure differences on the McLeod gauge in a known volume. The known volume normally used was measured with a precision of ± 8 cc in 650 cc. This uncertainty in volume amounts to 0.1 ppm of hydrogen for a 2-g sample of average hydrogen content. The pressure difference was usually measured on the middle section of the McLeod where the precision is 0.1 ppm for a 2-g sample. For low hydrogen samples, the difference may be read on the upper section where the precision was equivalent to 0.02 ppm.

Normally the accuracy and the precision of an analytical apparatus as a unit are determined by the use of standard samples. For hydrogen this cannot be done because there are no standards for hydrogen in steel. Further, there is no assurance that two pieces of solid steel when treated in the same manner will dissolve and retain equal amounts of hydrogen or that a single piece will dissolve hydrogen uniformly along its length.[13] As a measure of the reproducibility of the method a number of samples were either pickled or electrolytically charged in small lots and were subsequently stored and analyzed. The results of some of this work are shown in table III. While it is still difficult to distinguish by these results between the precision of the apparatus and that of the sampling and storage, the results indicate a satisfactory degree of reproducibility. The foregoing considerations and the results of analysis of approximately 600 samples within one year's time indicate precision for the analytical apparatus which is of the order of ± 0.1 ppm, and all results are therefore expressed to no less than 0.1 ppm.

The determination of the accuracy of analysis was even more difficult. In this case it was necessary to know the absolute amount of hydrogen that was in the sample before it was analyzed. Some measure of the accuracy of the analytical method used in this investigation had been obtained from the work on sampling liquid steel. In this case the amount of

## Summary

Following the basic pattern of the vacuum fusion apparatus an analytical system has been designed and built for the sole purpose of analyzing hydrogen in steel and other metals. Refinements have been incorporated which:

1. Permit fusion in an induction heated silica crucible operating at 1150°C in a fluid tin-iron bath. The furnace is water cooled to condense metal vapors and to prevent the outward diffusion of hydrogen.

2. Eliminate all grease from the system to prevent adsorption of the hydrogen.

3. Permit 15 min analysis per sample on a standard operating schedule. This is possible because of the vigorous induction stirring of the metal bath.

With this apparatus a precision of ± 0.1 ppm for a 2-g sample is attained.

## Acknowledgments

### References

[1] Fourth Report of the Oxygen Subcommittee on the Heterogeneity of Steel Ingots. *Jnl.* Iron & Steel Inst. (1943) No. II, 278.

[2] Symposium on Determination of Hydrogen in Steel. *Trans.* AIME (1945) **162**, 353.

[3] G. Derge, W. Piefer, B. Alexander: *Trans.* AIME (1945) **162**, 361.

[4] G. Derge, W. Piefer, J. H. Richards: *Trans.* AIME (1948) **176**. *Met. Tech.*, June 1948. TP 2362.

[5] H. Bennek, G. Klotzbach: *Stahl u. Eisen* (1941) **61**, 597.

[6] W. C. Newell: *Jnl.* Iron & Steel Inst. (1943) No. II, 287.

[7] W. W. Stevenson, G. E. Speight: *Jnl.* Iron & Steel Inst. (1943) No. II, 290.

[8] E. W. Colbeck, S. W. Craven: *Jnl.* Iron & Steel Inst. (1943) No. II, 298.

[9] J. G. Thompson: *Trans.* AIME (1945) **162**, 369.

[10] C. E. Sims, G. A. Moore: *Trans.* AIME (1948) **176**. *Met. Tech.*, June, 1948. TP 2368.

[11] G. A. Moore: *Trans.* AIME (1945) **162**, 404.

[12] J. Naughton: *Trans.* AIME (1945) **162**, 385.

[13] J. Seabrook: Senior Thesis, M.I.T. (1949).

[14] D. J. Carney, J. Chipman, and N. J. Grant: *Trans.* AIME (1950) **188**, 404. *Jnl. of Metals*, Feb. 1950. TP 2807.

# The Sampling and Analysis of Liquid Steel for Hydrogen

by Dennis J. Carney,

John Chipman,

and N. J. Grant

An absolute calibration has been achieved for sampling and analyzing liquid steel for hydrogen based on Sieverts' values of hydrogen solubility in iron. Further checks were made in nickel, iron-nickel, and 18-8 stainless melts. The sampling method was successfully applied to a large number of commercial steel melts in various types of furnaces. The concurrent problem of sample storage was also solved.

THE problem of sampling of liquid steel for hydrogen is more difficult than the problem of analysis. Hydrogen has a greater mobility than any other element; it is the only element that will diffuse out of steel at room temperature. In accordance with the known relation between temperature and diffusivity, the diffusion of hydrogen is extremely rapid at the temperature of liquid steel. Consequently, in the past, attempts to quench molten steel to retain the dissolved hydrogen have not been as successful as similar attempts with nitrogen or oxygen. The retention of hydrogen is especially difficult since it will continue to escape at room temperature even if the molten metal has been rapidly quenched.

D. J. CARNEY, Student Member, is Physicist, South Works, Carnegie-Illinois Steel Corporation, Chicago, Ill. JOHN CHIPMAN, Member, is Professor and N. J. GRANT, Member AIME, is Associate Professor, Mass. Inst. of Tech., Cambridge, Mass.

The hydrogen sampling methods may be classified broadly as (1) the rapid quenching techniques which attempt to preserve supersaturation and (2) those methods which attempt to collect the gases evolved as the metal freezes and cools to room temperature.

With all methods of sampling but especially with the rapid quenching methods, there is also a concurrent problem of storing the sample until analysis is undertaken. The two problems are interrelated and must be considered together when discussing liquid steel sampling techniques.

The major obstacle in liquid steel sampling has been that there was no way of evaluating properly the various sampling and storage techniques which have been developed. It has not been possible to compare the accuracy of the various methods. For evaluation of sampling methods some known standard is required; this may be found in the published work on the equilibrium solubility of hydrogen in liquid iron which has been determined in three separate investigations.[1,2,3] The data are shown in table I. Sieverts' original method of obtaining gas solubilities involved measurement of the volume of gas required to saturate the liquid metal contained in an evacuated bulb of known volume. This procedure, improved by introduction of high frequency induction heating, has yielded reproducible results which appear to be entirely dependable. Using Sieverts' method, it has been proved for iron and other metals and alloys that the hydrogen solubility is proportional to the square root of the pressure of the hydrogen gas above the liquid, so that one may work with various partial pressures of hydrogen to put different amounts of hydrogen in solution. From Sieverts' law it is possible to know accurately what amount of hydrogen is dissolved in the liquid metal at the time of sampling. The accuracy of a sampling method may be gauged by reference to this known solubility.

It was the purpose of this investigation to develop a method for sampling liquid steel and for storing the sample so that the analytical result would represent the actual hydrogen content of the metal bath. For this purpose an induction furnace was

Fig. 1—Detail of furnace.

Labels on figure (top to bottom, left to right):
Rubber Bulb
Sampling Device — Iron Pipe
Vycor Tube — Copper Mold
Shutter — Brass Tube
Window
Water Jacket — Gas Inlet
— Water Inlet
Silicone Rubber Gasket — Gas Outlet
Brick — Water Outlet
Radiation Shield
Upper Quartz Tube
Transite Box
Water Cooled Heating Element
Crucible — Chain Fall for Pouring
Insulation
Lower Quartz Tube
Brick
Silicone Rubber Gasket
Albarine Stone Base — Gas Inlet

constructed in which the bath could be held under a controlled atmosphere and from which samples could be taken by means of the "Taylor sampler"[25] without exposure of the liquid metal to air.

**Table I. Hydrogen Equilibrium Solubility Values for Liquid Iron**

| Investigator | Hydrogen Solubility at 1565°C | |
| --- | --- | --- |
| | cc per 100 g | ppm* (parts per million) |
| 1. Sieverts (1911) | 28.2 | 25.4 |
| 2. Sieverts (1938) | 26.4 | 23.7 |
| 3. Liang (1946) | 29.4 | 26.6 |
| Average Value | 28.0 | 25.1 |

* Since weight percent values for hydrogen in steel are so small as to be cumbersome the solubility is expressed in parts per million (ppm), permitting the use of simple numbers. It is noted that 1 ppm = 0.0001 wt pct.

## Literature Summary

A summary of the recent papers which have been presented concerning the sampling of liquid steel is presented below according to the country in which the work was done.

**United States:** In 1937 Hare, Peterson and Soler[4] introduced a liquid steel sampling method that was designed primarily for oxygen determinations. An evacuated steel pipe, closed at the bottom by a thin diaphragm, was inserted into a spoon of liquid metal. The liquid penetrated the diaphragm and solidified inside the pipe. The evolved gas was subsequently measured and analyzed. Variations of this method were used for hydrogen sampling by Scafe[5] and Mravec.[6]

The rapid quenching method has been used by Derge and coworkers[7, 8, 9] and by Sims, Moore, and Williams.[10, 11] Derge poured the liquid steel into a very thin wedge in a large split copper mold. The sample was stored quickly in mercury or in a sealed tube. Sims poured the liquid steel into a split copper mold with a hole 5/8 in. inside diam and approximately 1 1/4 in. long. The sample was removed rapidly and stored under mercury.

**England:** Newell[12] used a method similar to the Soler tube in which he attempted to collect gas evolved on solidification and cooling of the sample. This method has been called the "balloon tube" method. The evacuated pipette is much smaller than the Soler tube. Both the evolved gas and the solidified sample were analyzed for hydrogen.

MacKenzie[13] used a technique which collected the gas immediately after solidification of the sample. This has been called the "sealed mold" method. The liquid steel is poured into a stainless steel tube 6 in.

Fig. 2—Detail of sampler and trap door.

Rubber Bulb

$\frac{1}{8}$" Iron Pipe

Silicone Rubber Gasket

Copper Plug

Copper Mold

Vycor Glass Tube

Brass Shutter

viously described. Geller and Tak-Ho-Sun[31] used a complicated suction method of sampling steel for hydrogen. Very recently, Wentrup, Fucke and Reif[10] also described a suction method of sampling for hydrogen. The liquid steel sample was sucked into a small quartz tube. The quartz tube with the sample inside was broken off within 10 sec and stored under mercury. After 24 hr holding, the evolved gas and sample were both analyzed for hydrogen.

**Japan:** Kobayashi[20] was the first author to use the suction method with the quartz tube.

**Russia:** Chuiko has written a number of papers[21], [22], [23], [24] on hydrogen in liquid steel but only in one[24] were samples taken. The samples were poured into evacuated molds and the gas collected during solidification. After the sample had cooled, the gas which was evolved was analyzed for hydrogen. The hydrogen gas which still remained in the solid sample after cooling to room temperature was calculated on a theoretical basis developed by the author.

## Apparatus

**The Furnace:** The controlled-atmosphere induction furnace is shown in fig. 1. The essential parts of the furnace were (1) the 30-lb capacity magnesia crucible, (2) the two sections of silica tubing, 9 in. in diam, which were used to enclose the melting furnace, (3) the water-cooled brass head with a central trap door for sampling, a sight glass for reading the bath temperature, a gas inlet and a gas outlet, (4) the gas inlet at the bottom of the furnace. The furnace crucible was packed with a mixture of magnesia and alumina. Corrugated paper was placed around the inner wall of the lower silica tube before packing. This was used to prevent cracking of the silica tube when the packing expanded on heating. The paper was burned out in air by preheating the crucible with a graphite rod charge.

The two sections of silica tube were used so that the metal could be poured out of the furnace crucible at the end of an experimental heat. The top section was removed and a transite cover placed over the top of the lower silica tube. The furnace then was tilted and the metal poured.

**The Sampler:** The sampler, which was an improvement over the one described by Taylor and Chipman,[25] is shown in fig. 2. The copper mold was 1 in. od and 3½ in. long. The center was reamed out with a No. 5 tapered pin reamer and the top was threaded to fit a ⅛ in. steel pipe. These were connected by a short, small hole. To keep the metal from running up through this small hole, a copper plug was inserted into the top of the reamed hole. These items can be seen in fig. 2. The copper plug was made by cutting a ¼ in. strip of 0.01 in. copper sheet approximately 5 in. long and rolling it into a coil. The plug allowed good suction and yet kept the liquid metal from running past it. A small suction bulb was attached to the upper end of a 3 ft length of ⅛ in. iron pipe which served also as a handle. A 2 in. piece of 7 mm Vycor tubing was inserted in the lower end of the tapered hole and turned until it was tight. No cement of any kind was necessary to hold this tube in place. The Vycor tube was dipped into the bath and the metal sucked

long and 1 in. in diam. Within 15 sec after pouring, the top of the stainless steel tube is sealed off by a ground glass joint and stopcock. The evolved gas and the sample are analyzed for hydrogen. Speight and Cook[14] also used this method.

Newell,[12] Wells and Barraclough,[15] Speight and Cook,[14] and Sykes, Burton and Gregg[16] have all used the "chilled pencil test." In this sampling method, the liquid is poured into a tapered hole 6 in. long and approximately ½ in. diam in a steel or cast iron mold which is usually suspended within a water bath. The sample is removed rapidly, a section broken off and stored under mercury. Recently, Wells and Barraclough[15] and Sykes[16] and coworkers stored such samples in dry ice. This was to prevent or slow down the diffusion of hydrogen out of the sample. They reported excellent results for storage times up to 24 hr with this method. Naughton[17] stored hydrogen samples in liquid air.

**Germany:** Herasymenko and Dombrowski[18] originally developed the "sealed mold" method pre-

406—JOURNAL OF METALS, FEB. 1950, TRANSACTIONS AIME, VOL. 188

into the copper mold. Thus the copper mold was not in contact with the liquid metal. This was quite an advantage since it allowed a very rapid removal of the sample from the sampler and also kept the copper mold from being heated to a high temperature.

**The Gas:** The gases used in this investigation were hydrogen and helium, the latter being used as a diluent to vary the partial pressure of the hydrogen. For this purpose it was preferred to argon since its molecular weight is more nearly equal to that of hydrogen and errors of thermal diffusion are therefore smaller. The desired gas mixtures were
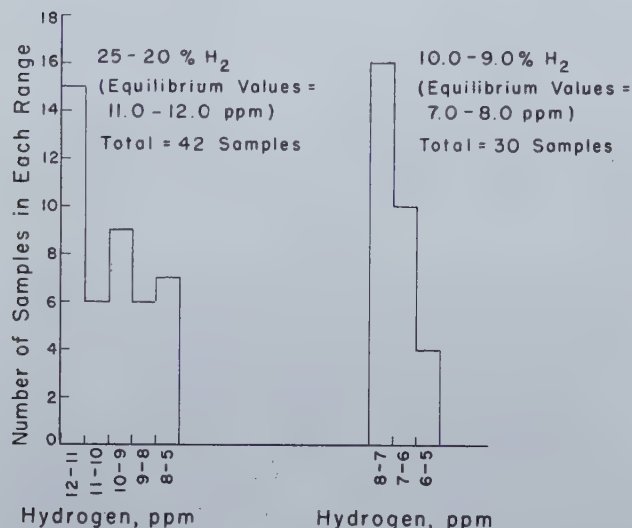


**Fig. 3—Summary of hydrogen sample values from nine iron heats.**

obtained from 4 calibrated flowmeters—two for hydrogen and two for helium since two gas inlets were used. The gases after mixing were passed through an anhydrous drying tower and into the furnace. The outlet gas was burned in air.

### Operating Procedures

**Furnace Operation:** From the experience gained in the preliminary heats, the following furnace procedure was found to be satisfactory.

The crucible was charged with approximately 15 lb of sheared Armco iron bars for the iron heats and 15 lb of alloy steel or nickel for the alloy steel and nickel heats. The upper silica tube and brass cover were placed in position and the flow of helium was started. If no gas leaks were observed, the water and power were turned on. After melt-down, 8 g of aluminum rod was dipped beneath the surface of the metal, the flow of helium was stopped and the flow of hydrogen, at approximately 5 cf per hr in the bottom inlet and 10 cf per hr in the top inlet, was started. The hydrogen flow was continued for 1 hr. This was done to saturate the liquid with hydrogen and to allow time to stabilize the bath temperature. At the end of this hour, the helium flow was again started. The rates of flow of hydrogen and helium were adjusted until the desired mixture of the two was obtained. In most runs at least two different gas mixtures were used. Metal samples for hydrogen analysis were taken from the

liquid under the higher hydrogen gas mixture, and following this, the gas was adjusted to the lower hydrogen gas mixture and samples again taken.

In spite of a reasonably tight furnace, there was still a small difference between the composition of the entering furnace gas and the exit furnace gas, the latter being usually slightly lower in hydrogen. This difference may have been due in part to small air leaks and also to reduction of the hot furnace materials by the hydrogen. In practically all the heats reported in this investigation, a 250 cc sample was taken of the exit gas and the sample analyzed for hydrogen by means of an Orsat apparatus.

The metal was deoxidized with aluminum because it was observed in preliminary heats that no matter how fast one quenched the liquid sample, a solid sample could not be obtained when the oxygen content of the bath was high. Furthermore, since the hydrogen equilibrium solubility data were obtained for low oxygen iron, a deoxidized bath was necessary. Silicon was originally used as the deoxidizing element. Large amounts of silicon were sometimes needed to deoxidize thoroughly the Armco iron and some high residual silicon contents resulted which reduced the hydrogen solubility. The silica which was formed as a deoxidation product reacted strongly with the basic magnesia crucibles. As a result of this experience, a small amount of aluminum was used as the deoxidizing element in each heat. It did not form a slag, and it was assumed that the very small amount added did not affect the hydrogen solubility.

**Temperature Measurement:** Temperatures were measured with a Leeds and Northrup optical pyrometer. Readings were taken through the pyrex sight glass in the brass head. During the hour in which the liquid was held under pure hydrogen, the melt was slowly solidified while temperature readings were taken. This measurement of the solidification temperature gave the necessary optical calibration point or constant in order to obtain the true temperature according to the approximate formula, $\frac{1}{S} - \frac{1}{T} = K$, in which $S$ is the observed temperature and $T$ the true absolute temperature. For the iron heats the temperature was then raised until it was steady at 1565°C. The estimated accuracy was ± 15°C. For the alloy steel heats the temperature measurements were not this accurate due to the uncertainty in the true solidification temperatures.

**Sampling Procedure:** Initially, the central sampling tube above the trap door was flushed with hydrogen. After this, the sampler with the cap attached was screwed into position as shown in fig. 2. The brass slide of the trap door was then pulled out and the sampler lowered into the furnace. The suction bulb was squeezed twice, and the Vycor tubing extending out of the copper mold was dipped beneath the surface of the liquid. The suction bulb was released and after a 2-sec wait the sampler was quickly pulled up into the tubing above the trap door and the brass shutter pushed back into place. The cap was loosened and the sampler taken out. The metal in the Vycor tubing protruding from the copper mold was seized with a pair of pliers and the sample pulled out of the mold. The sample was quickly quenched into water and then into a dry

ice-acetone mixture. In some cases the Vycor tube fell out of the copper mold after sampling while the sampler was being pulled out of the furnace. In these cases the sample was removed from the copper mold by tapping the mold on the floor. The total time from the aspiration of the metal into the copper mold to quenching in dry ice and acetone was usually 15 to 20 sec and never over 45 sec. After thorough quenching, the end of the sample that had been in the Vycor tube was cut off and the other end was wrapped with aluminum foil containing an identification number. The sample was quickly stored in dry ice. The surface of the samples was smooth and shiny due to rapid cooling in the hydrogen at-

the copper mold; and of the effect of water cooling the sampler. None of these indicated any marked influence on the retention of the dissolved hydrogen within the limits of the experiments. There appeared to be a very slight tendency for the thin samples to retain the very high hydrogen values a little more easily. The failure to find an appreciable benefit due to faster initial cooling in the copper sampler may be due to the sample contraction. This contraction is so fast and of such magnitude that some samples dropped out of the copper mold within 2 to 3 sec after taking the sample as the sampler was being pulled out of the furnace. Because of this contraction, an air space forms around
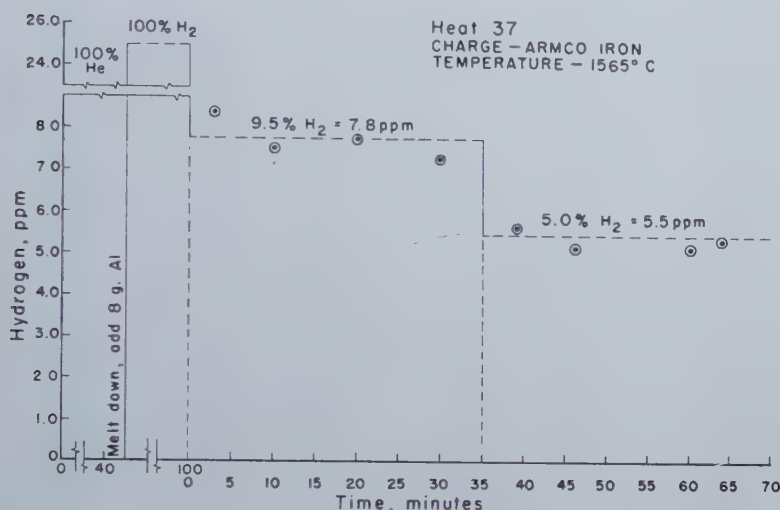


Fig. 4—Hydrogen results from Heat 37.

mosphere. Before analysis, the sample was taken out of the dry ice and a section (weighing approximately 2 g) was cut from it with an underwater cutoff wheel. This sample was dried and placed back in dry ice ready for analysis. The cutting operation required about 2 min.

### Experimental Results

**Development of Sampling and Storage Methods:** At the beginning of this investigation when the copper mold was dipped directly into the bath, the sampler was immediately removed and quenched in water. The samples taken, when using this procedure, often showed considerable water vapor on analysis. These early results, including the water vapor as hydrogen, were often twice the equilibrium value. The amount of water vapor given off was erratic but was present in most samples. Consequently, attempts were made to quench the sampler in molten tin and in mercury. Samples taken in this manner did not give off any water vapor on analysis, but the hydrogen values obtained were quite low. After this the sampler was cooled by running cold water over the surface of the copper mold. This cooled the mold to room temperature in approximately 1 min. This procedure also gave samples free of water vapor, but the hydrogen found in the analyzed samples taken in the early heats was well below the equilibrium solubility value. Studies were made of the effect of chilling the copper mold before use; of the effect of smaller size samples by using very small bores in

the sample which insulates it from the cooled copper mold. Only by using a tight copper plug at the top of the tapered hole were most of the samples kept from falling out.

The best results were obtained *not by cooling the sampler* containing the sample but by *rapidly cooling the sample itself*. A similar effect was observed by Wells and Barraclough[15] who found it necessary to remove the metal sample rapidly from a water-cooled mold and to quench it in water.

No complete study of the various storage methods was made. Comparisons were made between samples stored in dry ice and samples stored in evacuated tubes. These results indicated that dry ice storage was satisfactory for periods up to 24 hr for low alloy steels. Also, duplicates of some samples were stored for periods of 24 hr and longer. These results indicated that chilled austenitic steels and nickel could be stored for periods up to 3 days without any significant loss of hydrogen by diffusion out of the sample. The best policy with low alloy steels was to analyze the samples within a period of less than 12 hr, especially for the high hydrogen samples. Practically all the hydrogen sample analyses reported in this investigation were made after less than a 12-hr storage time.

Considerable care was necessary in handling samples. One source of trouble was contact of the sample with water and grease or oil whereby very small amounts of these could be absorbed on the surface. Water came in contact with the samples in water quenching and in using the underwater cut-

off wheel. Grease and oil came in contact with the samples from unclean tools used to handle them, from the underwater cutoff wheel when it had previously been used to cut a greasy or oily specimen, and from drying in an air blast from which the oil droplets had not been filtered out. The above sources of extraneous hydrogen were noted for the samples which had poor surface. When the sample had a poor surface, cleaning in carbon tetrachloride was not always successful.

**Sampling Liquid Iron and Liquid Nickel for Hydrogen:** 1. *Iron Heats Made Using 25 and 10 pct Hydrogen Mixtures:* Using the sampling procedure described earlier, samples were taken from the liquid iron under 100 and 50 pct hydrogen gas mixtures. These samples were completely hollow in spite of rapid cooling. However, with a 25 pct hydrogen mixture the samples were for the most part macroscopically solid. Since equilibrium is established very rapidly, as will be shown later, the liquid metal under a 25 pct hydrogen mixture contained one-half the maximum liquid solubility or 12 ppm, based on Sieverts' solubility law. Of the early samples taken from liquid iron with the 25 pct hydrogen mixture, only a few retained essentially the equilibrium amount of hydrogen. Attempts were made in 9 heats to improve the sampling technique so that all of the samples would retain all of the dissolved hydrogen. In these heats both 25 and 10 pct hydrogen mixtures were used. A summary of the results is given in fig. 3. The equilibrium value for the 25 pct mixture, depending upon the exact composition of the exit gas and upon the metal temperature, was 11.0 to 12.0 ppm, and for the 10 pct mixture it was 7.0 to 8.0 ppm. The plot gives the hydrogen values in parts per million on the ordinate and the number of samples within each range on the abscissa. These data include both the good and the poor samples from these 9 preliminary heats. The poor samples were those which were taken too slowly or which contained some porosity. Only 35 pct of the samples taken under the 25 pct hydrogen mixture retained the equilibrium amount of hydrogen but 70 pct were within 2.0 ppm of the equilibrium value. In other words, 70 pct of the samples retained 80 pct of the dissolved hydrogen. For the 10 pct hydrogen mixture, over 50 pct of the samples retained the equilibrium amount and almost 90 pct were within 1.0 ppm of this value, or 90 pct of the samples retained 85 pct of the dissolved hydrogen. Since the 25 pct mixture results in a much higher dissolved hydrogen than is normally found in commercial low alloy steels, it was decided for the subsequent melts to concentrate on the lower hydrogen mixtures. Excellent results were obtained with the lower hydrogen mixtures and are given below.

2. *Iron Heats Made Using 10 and 5 pct Hydrogen Mixtures:* Since 11.0 to 12.0 ppm is an extremely high hydrogen value for low alloy steel, 3 heats were made with the melt containing 5.0 to 8.0 ppm of dissolved hydrogen. The gas mixtures used were roughly 5 and 10 pct hydrogen. The results are summarized in table II and heat 37 is shown in fig. 4. These results indicate successful sampling since every sample retained a very high percentage of the dissolved hydrogen. An average of 94 pct of the

dissolved hydrogen was retained in the analyzed samples. From these data it appears that when molten low alloy steels contain up to 7.5 ppm of dissolved hydrogen, the sampling technique used is very accurate. In heats 38 and 39, work was also done on the rate of evolution of hydrogen from a molten bath under 100 pct helium. These results are discussed below under "Rate of Solution and Evolution of Hydrogen from Liquid Iron."

**Table II. Sampling of Remelted Armco Iron Heats at 1565°C**

| Sample | Time Minutes | Atmosphere Pct $H_2$ | Equilibrium Solubility ppm | Analysis ppm |
|---|---|---|---|---|
| | | **Heat No. 37** | | |
| | 0 | 9.5 | 7.8 | |
| 1 | 3 | 9.5 | 7.8 | 8.4 |
| 2 | 10 | 9.5 | 7.8 | 7.6 |
| 3 | 20 | 9.5 | 7.8 | 7.8 |
| 4 | 30 | 9.5 | 7.8 | 7.3 |
| | 35 | 5.0 | 5.5 | |
| 5 | 39 | 5.0 | 5.5 | 5.7 |
| 6 | 46 | 5.0 | 5.5 | 5.1 |
| 7 | 60 | 5.0 | 5.5 | 5.2 |
| 8 | 64 | 5.0 | 5.5 | 5.4 |
| | | **Heat No. 38** | | |
| | 0 | 8.4 | 7.2 | |
| 1 | 10 | 8.4 | 7.2 | 6.9 |
| 2 | 15 | 8.4 | 7.2 | 7.0 |
| 3 | 30 | 8.4 | 7.2 | 6.7 |
| 4 | 40 | 8.4 | 7.2 | 7.0 |
| | 45 | 3.6 | 4.8 | |
| 5 | 50 | 3.6 | 4.8 | 5.0 |
| 6 | 54 | 3.6 | 4.8 | 4.7 |
| 7 | 60 | 3.6 | 4.8 | 4.8 |
| 8 | 65 | 3.6 | 4.8 | 4.8 |
| | 70 – 0 | 0 | 0.0 | |
| 9 | 2 | 0 | 0.0 | 3.6 |
| 10 | 120 | 0 | 0.0 | 2.9 |
| 11 | 173 | 0 | 0.0 | 2.4 |
| 12 | 238 | 0 | 0.0 | 1.2 |
| | | **Heat No. 39** | | |
| | 0 | 9.0 | 7.5 | |
| 1 | 2 | 9.0 | 7.5 | 7.7 |
| 2 | 20 | 9.0 | 7.5 | 6.8 |
| 3 | 35 | 9.0 | 7.5 | 6.8 |
| 4 | 55 | 9.0 | 7.5 | 6.9 |
| | 65 | 5.7 | 6.0 | |
| 5 | 74 | 5.7 | 6.0 | 5.9 |
| 6 | 83 | 5.7 | 6.0 | 5.8 |
| 7 | 89 | 5.7 | 6.0 | 5.8 |
| 8 | 95 | 5.7 | 6.0 | 5.9 |
| | 100 – 0 | 0 | 0.0 | |
| 9 | 3 | 0 | 0.0 | 4.6 |
| 10 | 46 | 0 | 0.0 | 2.9 |
| 11 | 62 | 0 | 0.0 | 2.6 |
| 12 | 122 | 0 | 0.0 | 2.3 |
| 13 | 183 | 0 | 0.0 | 1.4 |
| 14 | 238 | 0 | 0.0 | 1.1 |

**Table III. Sampling of Armco Iron Heat No. 42 at 1565°C**

| Sample | Time Minutes | Atmosphere Pct $H_2$ | Equilibrium Solubility ppm | Analysis ppm |
|---|---|---|---|---|
| | 0 | 23 | 12.0 | |
| 1 | 6 | 23 | 12.0 | 11.2 |
| 2 | 12 | 23 | 12.0 | 9.4 |
| 3 | 25 | 23 | 12.0 | 10.8 |
| | 30 | 9.8 | 7.8 | |
| 4 | 36 | 9.8 | 7.8 | 7.0 |
| 5 | 44 | 9.8 | 7.8 | 7.4 |
| 6 | 55 | 9.8 | 7.8 | 7.3 |
| | 60 | 5.2 | 5.7 | |
| 7 | 66 | 5.2 | 5.7 | 5.5 |
| 8 | 71 | 5.2 | 5.7 | 5.5 |
| 9 | 75 | 5.2 | 5.7 | 5.4 |

3. *Iron Heat Made Using 25, 10 and 5 pct Hydrogen Mixtures:* A final iron heat was made using 25, 10 and 5 pct hydrogen gas mixtures. This heat is given in table III. This is a good check of the findings of the previous heats. With the 25 pct hydrogen mixture, the samples retained 80 to 85 pct of the dissolved hydrogen, while with the 10 and 5 pct mixtures, 95 pct of the hydrogen was retained in the sample.

4. *Pure Nickel Heats:* Sieverts determined the solubility of hydrogen in pure liquid nickel. At 1480°C, the solubility of hydrogen in liquid nickel under 1 atm of hydrogen is 36.0 ppm, whereas for iron it is 24.8 ppm at 1550°C. To obtain a further check on both the sampling and analytical procedure, 2 heats were made using a charge of electrolytic nickel. Because of the high hydrogen solubility, it was decided to use a 10 pct hydrogen mixture in the first heat. These results turned out so well that the second heat was made with both 25 and 10 pct hydrogen mixtures. The hydrogen values for these heats are shown in table IV. It was possible to retain very high amounts of dissolved hydrogen with liquid nickel using the described sampling method. Also it was observed while sampling nickel that one could be slower in quenching and still retain the hydrogen quite well. The data agree with Sieverts' solubility value of 36 ppm at 1480°C.

5. *Summary of Sampling Studies:* This concluded the work in which Sieverts' solubility data were available. On the basis of these solubility data, the sampling method, when used for very low alloy iron, was accurate to an average of 0.45 ppm for dissolved hydrogen contents of 7.0 to 7.5 ppm and to an average of 0.16 ppm for hydrogen contents of 6.0 ppm and below. The precision was approximately ± 0.2 ppm for all the liquid iron heats containing less than 7.5 ppm of dissolved hydrogen. For higher dissolved hydrogen contents in low alloy iron, the accuracy and precision were less than this. However, on the basis of previous work[11, 16] on sampling low alloy steel heats and the commercial sampling results given at the conclusion of this paper, it appears that the hydrogen contents of commercial low alloy steel heats are below 7.5 ppm even in the case of high hydrogen heats. For high alloy steels, especially austenitic alloys, dissolved hydrogen contents are generally much higher, but as will be shown later in the experimental alloy heats, the sampling technique is able to retain these higher dissolved hydrogen contents in high alloy steels. The above results on the pure nickel heats also serve to illustrate this point.

**Rate of Solution and Evolution of Hydrogen from Liquid Iron:** It was intended in the course of this work to study the rate of solution or evolution of hydrogen or the rate of approach to equilibrium. In the experimental procedure outlined above, it was possible to study the rate of evolution of hydrogen. As seen in table II, in going from 100 to 10 pct hydrogen and from 10 to 5 pct, the bath reached equilibrium with the lower hydrogen mixture within 5 to 6 min, and samples taken in less than this time caught the hydrogen on the way down. In all the heats made, samples taken in less than 5 min in

**Table IV. Sampling of Electrolytic Nickel Heats at 1480°C**

| | | | Heat No. 28 | |
| Sample | Time Minutes | Atmosphere Pct $H_2$ | Equilibrium Solubility ppm | Analysis ppm |
| --- | --- | --- | --- | --- |
| | 0 | 10 | 11.5 | |
| 1 | 3 | 10 | 11.5 | 12.8 |
| 2 | 7 | 10 | 11.5 | 10.3 |
| 3 | 20 | 10 | 11.5 | 11.3 |
| 4 | 35 | 10 | 11.5 | 11.2 |
| 5 | 50 | 10 | 11.5 | 11.5 |
| 6 | 55 | 10 | 11.5 | 11.2 |
| | | | Heat No. 29 | |
| | 0 | 22.1 | 16.4 | |
| 1 | 2 | 22.1 | 16.4 | 16.8 |
| 2 | 10 | 22.1 | 16.4 | 16.4 |
| 3 | 15 | 22.1 | 16.4 | 15.9 |
| 4 | 25 | 22.1 | 16.4 | 16.3 |
| | 35 | 9.5 | 11.2 | |
| 5 | 37 | 9.5 | 11.2 | 12.0 |
| 6 | 50 | 9.5 | 11.2 | 11.2 |
| 7 | 56 | 9.5 | 11.2 | 11.0 |
| 8 | 75 | 9.5 | 11.2 | 11.1 |

going from a higher to a lower hydrogen gas mixture were slightly above the equilibrium value while in no case were later samples (over 6 min) above this value. This indicates that the rate of approach to equilibrium is extremely fast under the experimental conditions used. The 5-min period required to come to equilibrium with the lower hydrogen gas mixture was the time required for the excess hydrogen gas to be swept out of the furnace atmosphere and not the time required for the melt to reach equilibrium with the contiguous gas.

Three heats were made to study the rate of solution of hydrogen or the rate of approach to equilibrium from the lower side. These heats were melted according to the described procedure, but after the metal was held under pure hydrogen for 1 hr a sample was taken. This was done to be sure that the dissolved hydrogen was extremely high as evidenced by the hollow tube samples obtained. The hydrogen was turned off and pure helium was passed over the bath. Samples were taken for the next 20 min. A 25 pct hydrogen-helium mixture was then passed over the bath and samples again taken. The results are summarized in table V. It was observed that the rate of solution was as rapid as the rate of evolution. However, in these 3 heats it appeared strange that after the initial very rapid rate of evolution of hydrogen in going from 100 pct hydrogen to 100 pct helium, the rate slowed down appreciably and all the hydrogen was not evolved after 20 min. Consequently heats 38 and 39, already discussed, were made in which the iron was held under helium for 4 hr. The results of heat 39 are shown in fig. 5. It was observed again that the hydrogen was evolved very slowly, decreasing to approximately 1.0 ppm at the end of 4 hr. In the second hour of the heat, a sample was taken from the exit gas. This sample contained no hydrogen but analyzed 0.09 pct water vapor or a partial pressure of 0.0009 atm. Thermodynamically, at equilibrium, this amount of water vapor is capable of adding approximately 2.0 ppm of hydrogen with the low oxygen content of the bath. The reaction is:

Fig. 5—Hydrogen results from Heat 39.

(Figure labels: Hydrogen, ppm on y-axis 0–7.0; Time, minutes on x-axis 0–240; "5.7% H$_2$ = 6.0 ppm"; "Heat 39 (continued) CHARGE—ARMCO IRON TEMPERATURE—1565°C"; "100% He = 0.0 ppm")
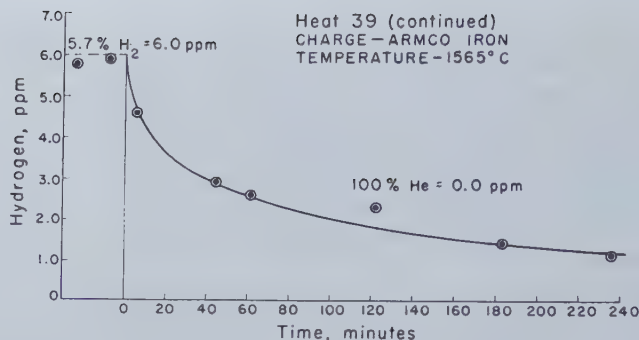
$$H_2O\ (g) = 2\underline{H} + \underline{O};\ K = \frac{(\%\ H)^2 \times \%\ O}{P_{H_2O}}$$
$$= 1.85 \times 10^{-6}\ \text{at}\ 1600°C.$$

The equilibrium constant for this reaction was obtained from the data of Chipman and Fontana[29] and Sieverts'[1] solubility data. A more complete discussion of the effect of water vapor is given in a previous paper.[30] These calculations together with the observed water vapor content indicate that water vapor could have accounted for the slow rate of evolution of hydrogen under a 100 pct helium atmosphere. The water vapor could have added hydrogen to the melt at a rate comparable to its evolution from the bath.

**Sampling Liquid Alloy Iron-Nickel Heats:** There is no hydrogen solubility data on liquid iron alloys other than iron-silicon.[3] Work had been done on some solid iron alloys such as iron-nickel,[25] iron-manganese[27] and iron-molybdenum.[28] In spite of this lack of solubility data, it was decided to make an iron-nickel alloy and an 18-8 stainless steel. This

was done mainly for the purpose of studying the precision of the sampling method with austenitic steels from which the diffusion of hydrogen is slower, thereby permitting easier retention of the dissolved hydrogen, and in which there is no phase change in the solid on cooling. One could estimate roughly from these results the solubility of hydrogen in the particular alloy made at the temperature concerned.

1. *Thirty-five Pct Nickel-Iron Heat:* The first heat was a 35 pct nickel-iron alloy which is practically the "invar" composition and is austenitic. The results are shown in table VI. A gas sample was not taken nor was the temperature accurately measured since the liquid solubility data were not available. There was a definite increase in hydrogen solubility by the addition of 35 pct nickel to iron and this agrees qualitatively with the solid equilibrium results. From these data, the liquid solubility was calculated as approximately 30.0 ppm at one atmosphere of hydrogen at 1550°C.

### Table V. Rate of Solution of Hydrogen-Armco Iron Heats

**Heat No. 33**

| Sample | Time Minutes | Atmosphere Pct H$_2$ | Solubility ppm | Analysis ppm |
|---|---|---|---|---|
| 1 | 0 | 100 | 25 | |
|   | 60 | 100 | 25 | Hollow sample |
|   | 65 | 0 | 0 | |
| 2 | 68 | 0 | 0 | 8.0 |
| 3 | 80 | 0 | 0 | 3.0 |
|   | 85 | 23 | 12.0 | |
| 4 | 89 | 23 | 12.0 | 11.3 |
| 5 | 145 | 23 | 12.0 | 10.0 |

**Heat No. 34**

| Sample | Time Minutes | Atmosphere Pct H$_2$ | Solubility ppm | Analysis ppm |
|---|---|---|---|---|
| 1 | 0 | 100 | 25 | |
|   | 60 | 100 | 25 | Hollow sample |
|   | 65 | 0 | 0 | |
| 2 | 67 | 0 | 0 | Hollow sample |
| 3 | 74 | 0 | 0 | 4.8 |
| 4 | 89 | 0 | 0 | 2.4 |
|   | 95 | 23(?) | 12.0 | |
| 5 | 100 | 23 | 12.0 | 11.5 |
| 6 | 135 | 23 | 12.0 | 10.3 |

**Heat No. 36**

| Sample | Time Minutes | Atmosphere Pct H$_2$ | Solubility ppm | Analysis ppm |
|---|---|---|---|---|
| 1 | 0 | 100 | 25 | |
|   | 60 | 100 | 25 | Hollow sample |
|   | 65 | 0 | 0 | |
| 2 | 70 | 0 | 0 | 7.6 |
| 3 | 85 | 0 | 0 | 5.6 |
| 4 | 95 | 0 | 0 | 3.3 |
|   | 100 | 25 | 12.5 | |
| 5 | 110 | 25 | 12.5 | 12.1 |

### Table VI. Sampling of Austenitic Steels
### 35 pct Nickel Heat (1500°C)

**Heat No. 24**

| Sample | Time Minutes | Atmosphere Pct H$_2$ | Hydrogen ppm |
|---|---|---|---|
| 1 | 0 | 9–10 | |
| 2 | 3 | 9–10 | 12.9 |
| 3 | 10 | 9–10 | 8.9 |
| 4 | 15 | 9–10 | 8.6 |
| 5 | 35 | 9–10 | 9.1 |
|   | 60 | 9–10 | 9.2 |

**18-8 Stainless Steel Heats (1480° C)**

**Heat No. 40**

| Sample | Time Minutes | Atmosphere Pct H$_2$ | Hydrogen ppm |
|---|---|---|---|
| 1 | 0 | 23.0 | |
| 2 | 6 | 23.0 | 12.8 |
| 3 | 12 | 23.0 | 13.3 |
|   | 25 | 23.0 | 12.1 |
| 4 | 30 | 10.5 | |
| 5 | 35 | 10.5 | 10.4 |
| 6 | 41 | 10.5 | 8.6 |
| 7 | 55 | 10.5 | 8.6 |
| 8 | 60 | 10.5 | 9.1 |
|   | 66 | 10.5 | 8.4 |

**Heat No. 41**

| Sample | Time Minutes | Atmosphere Pct H$_2$ | Hydrogen ppm |
|---|---|---|---|
| 1 | 0 | 22.0 | |
| 2 | 5 | 22.0 | 14.1 |
| 3 | 12 | 22.0 | 12.5 |
|   | 16 | 22.0 | 12.8 |
| 4 | 25 | 10.5 | |
| 5 | 31 | 10.5 | 10.1 |
| 6 | 39 | 10.5 | 9.1 |
| 7 | 45 | 10.5 | 9.0 |
| 8 | 50 | 10.5 | 8.5 |
| 9 | 59 | 10.5 | 9.1 |
|   | 63 | 10.5 | 9.1 |

2. *18-8 Stainless Steel:* Two heats of 18-8 stainless steel were melted. One-inch stainless steel rod was used as the melting charge for the first heat. The samples on the first heat were slightly magnetic so that on remelting the ingot for the second heat, 1 pct nickel was added to the charge. These samples were nonmagnetic. The heats are shown in table VI. These results were quite satisfactory and indicate that the sampling technique when used for austenitic steels was able to retain a much higher dissolved hydrogen more completely than when used for ferritic steels. From these data, the liquid solubility was calculated as being approximately 28.0 ppm for 1 atm of hydrogen at 1480°C.

### Commercial Steel Heats

At the conclusion of the above work, when it appeared that the sampling and analytical techniques were accurate, samples were taken from commercial steel heats. This work was done for the purpose of ascertaining the adaptability of the method to commercial work and not to make a thorough study of the hydrogen content of commercial steels. If the latter study were contemplated, it would require a very large amount of sampling and analysis in order to determine the average hydrogen content for the various types of steels and steelmaking practices. A total of 17 commercial heats were sampled. There were 5 acid open hearth heats, 1 basic open hearth heat, 6 basic electric heats, 3 induction furnace heats and 2 acid electric heats.

Various grades of steel were included, from plain carbon steels to 38-18 chromium-nickel-iron alloys. The furnace samples were taken from well slagged spoons which were aluminum-killed. A few samples were taken from spoons which were not killed but only if the metal had been well deoxidized previously in the furnace. Some ladle samples were taken and a few samples were taken out of risers in sand molds while castings were being poured. For this work it was possible to remove the samples from the mold and quench them faster than was possible in the experimental controlled atmosphere furnace. Also, since these samples were partially quenched in air rather than in hydrogen, they were slightly oxidized instead of being shiny as were the equilibrium samples. The results of some of these heats are summarized in table VII.

From these data a few observations were made:
1. There was a decrease in hydrogen with the carbon boil as was expected and as observed by other workers.[10]
2. There was an increase in hydrogen after furnace deoxidation in almost every heat sampled. The increase was qualitatively comparable to the relative deoxidizing power of the added elements. In other words, there was a slight increase after the manganese addition and a large increase after the silicon addition.
3. In one case of a very high alloy grade, there was a marked increase in hydrogen in the ladle after ladle deoxidation with aluminum and titanium.
4. There was an increase in hydrogen after pouring into a sand mold.
5. The average hydrogen at tap was 3.0 to 5.0 ppm for low alloy steel and 5.0 to 8.0 for very high alloy iron.

These observations were made on the basis of a

### Table VII. Summary of Hydrogen Contents of Commercial Steel Heats

| Acid Open Hearth Heats, Low Carbon Steel | | | |
| Heat No. | Sample No. | Time, Minutes, After Melt-down | Hydrogen, ppm |
| --- | --- | --- | --- |
| 1 | 1 | 45 | 2.5 |
|  | 2 | 60 | 2.4 |
|  | 3 | 75 | 2.3 |
|  |  | 96 | Si and Mn added |
|  | 4 | 105 | 3.4 |
| 2 | 1 | 60 | 4.0 |
|  | 2 | 75 | 2.7 |
|  | 3 | 90 | 2.4 |
|  | Heat poured into dry sand mold | | |
|  | 4 | Riser | 4.7 |
| 3 | 1 | 30 | 3.2 |
|  | 2 | 45 | 2.6 |
|  | 3 | 60 | 2.4 |
|  |  | 80 | Si and Mn added |
|  | 4 | 90 | 3.6 |
| 5 | 1 | 75 | 2.3 |
|  | 2 | 90 | 2.1 |
|  |  | 100 | Si and Mn added |
|  | 3 | 110 | 3.2 |

| Basic Electric Arc Heats | | | |
| Heat No. | Sample No. | Time, Minutes, After Melt-down | Hydrogen, ppm |
| --- | --- | --- | --- |
| 9 | 1 | 5 | 2.0 |
|  | 2 | 15 | 1.9 |
|  |  | 20 | Mn added |
|  | 3 | 30 | 2.3 |
|  |  | 40 | Si added |
|  | 4 | 47 | 5.5 |
| 11 | 1 | 30 | 2.8 |
|  |  | 40 | Mn added |
|  | 2 | 50 | 3.2 |
|  |  | 60 | Si added |
|  | 3 | 70 | 3.1 |

| Basic Open Hearth Heat, High Carbon | | | |
| Heat No. | Sample No. | Time, Minutes After Melt-down | Hydrogen, ppm |
| --- | --- | --- | --- |
| 12 | 1 | 90 | 4.0 |
|  |  | 105 | Si-Mn added |
|  | 2 | 115 | 4.0 |
|  |  | 125 | Mn added |
|  | 3 | 130 | 5.1 |
|  | Heat poured into ladle | | |
|  | 4 | Ladle | 5.8 |

| Acid Arc Furnace Heats 35-15 Chromium-Nickel-Iron Alloy | | | |
| --- | --- | --- | --- |
| 13 | 1 | 10 | 3.4 |
|  | Heat poured into ladle | | |
|  | 2 | Ladle | 12.1 |
|  | Ladle poured into wet sand mold | | |
|  | 3 | Mold | 13.0 |
| 14 | 1 | 10 | 8.0 |
|  | Heat poured into ladle | | |
|  | 2 | Ladle No. 1 | 6.8 |
|  | Reladled | | |
|  | 3 | Ladle No. 3 | 7.1 |

| Induction Furnace Heats 18-8 Stainless Steel | | | |
| --- | --- | --- | --- |
| 15 |  | 15 | Al added |
|  | 1 | 20 | 6.1 |
|  | Heat poured into wet sand mold | | |
|  | 2 | 30 | 6.4 |
| 16 | Heat poured into ladle | | |
|  | 1 | Ladle | 6.1 |
| 17 | Heat poured into ladle | | |
|  | 2 | Ladle | 5.2 |

relatively small number of samples. Water vapor in the slag could possibly account for the increase in hydrogen which was observed after furnace deoxidation. Calculations previously presented[30] showed the equilibrium relation between hydrogen, oxygen and water vapor in the presence of liquid steel. These calculations indicate that the lower the oxygen content of liquid steel the greater the driving force of water vapor in the direction producing hydrogen. Previous to this work, Kobayashi[20] had observed a hydrogen increase after killing liquid steel and also had submitted the hypothesis that this was due to water vapor in the slag. Chuiko[21] has supported the same viewpoint. Very recently, Wentrup[19] and coworkers reported analyses showing considerable water vapor in basic slags and a smaller amount in acid slags. They also believed that increases in hydrogen which they observed after killing the metal were due to water vapor. Much more experimental proof is necessary, however, before a definite conclusion can be made.

In general, the results obtained for low alloy steels are slightly higher than those reported by Sims and coworkers,[11] similar to some English data,[16] and lower than the data reported by other English[14] and German workers.[19] Careful review of the latter two indicated possible explanations for the high hydrogen values reported. The English workers[14] obtained considerable water vapor from their hydrogen samples during the solid extraction analyses. They attributed this to a reaction between the dissolved hydrogen and oxygen, and therefore included all the water vapor as part of the dissolved hydrogen. As observed earlier in this investigation, there is a possibility that the water vapor given off in analysis was not a part of the dissolved hydrogen in the sample.

The present work, through the necessary refinements in analytical and sampling techniques, has made it possible to reconcile the differences in results reported by other investigators. Through the use of an absolute calibration it is possible to evaluate the effects of slow sample quenching, of absorbed water vapor, and of inferior analytical methods.

It is emphasized that the proper use of the sampler requires a certain degree of manual dexterity and judicious timing on the part of the operator. The best results were obtained through frequent use.

## Acknowledgments

## Summary

A liquid steel sampling technique was developed which consisted of sucking a sample into a thick-walled copper mold, quickly pulling the sample out of the mold, and quenching it in dry ice and acetone. The total sampling time including the quench was approximately 15 sec. The samples were stored in dry ice for periods up to 12 hr. The accuracy of the method was determined by sampling metal of known hydrogen content in equilibrium with controlled hydrogen-helium mixtures. The accuracy of sampling for low alloy steel containing 12 ppm was roughly 80 pct retention of hydrogen; for metal of less than 8 ppm 95 to 100 pct of the dissolved hydrogen was recovered. For austenitic steels the sampling technique is accurate up to 12.0 ppm, and for nickel up to 16.0 ppm.

The rates of hydrogen solution and evolution were extremely fast under the experimental conditions used. Equilibrium was reached from the high and low sides within 5 min.

Seventeen commercial steel heats from various types of furnaces were sampled to prove the adaptability of the method to commercial work. The average hydrogen content at tap was 3.0 to 5.0 ppm for low alloy steels.

The method appears to be very well suited to process control of hydrogen in commercial melting furnaces and to the investigation of a variety of problems involving hydrogen in liquid steel.

## References

[1] A. Sieverts: *Ztsch. phys. Chem.* (1911) **77**, 591.
[2] A. Sieverts, G. Zapf, H. Mortiz: *Ztsch. phys. Chem.* (1938) **183**, 19.
[3] H. Liang, M. Bever, C. F. Floe: *Trans.* AIME (1946) **167**, 395. *Met. Tech.* Feb. 1946.
[4] W. Hare, L. Peterson, G. Soler: *Trans.* A.S.M. (1937) **25**, 889.
[5] R. Scafe: *Trans.* AIME (1945) **162**, 375.
[6] J. Mravec: *Trans.* AIME (1945) **162**, 398.
[7] G. Derge: *Trans.* AIME (1943) **154**, 348.
[8] G. Derge, W. Piefer, B. Alexander: *Trans.* AIME (1945) **162**, 361.
[9] G. Derge, W. Piefer, J. Richards: *Trans.* AIME (1948) **176**. *Met. Tech.* June 1948.
[10] C. Sims, G. Moore, D. Williams: *Trans.* AIME (1948) **176**. *Met. Tech.* Feb. 1948.
[11] C. Sims, G. Moore, D. Williams: *Trans.* AIME. (1948) **176**. *Met. Tech.* June 1948.
[12] W. Newell, W. Harfield: *Jnl.* Iron & Steel Inst. (1943) **11**, 407.
[13] I. Mackenzie: Contribution to Gases in Liquid Steel Study Group of the Gases and Non-metallics Subcommittee. Brit. Iron & Steel Res. Assoc. (1946).
[14] G. Speight, R. Cook: *Jnl.* Iron & Steel Inst. (1948) **160**/4, 397.
[15] J. Wells, K. Barraclough: *Jnl.* Iron & Steel Inst. (1947) **155**/1, 27.
[16] C. Sykes, H. Burton, C. Gagg: *Jnl.* Iron & Steel Inst. (1947) **156**/2, 155.
[17] J. Naughton: *Trans.* AIME (1945) **162**, 385.
[18] P. Heraysymenko, P. Dombrowsky: *Arch. f. Eisenhut.* (1940) **14**, 109.
[19] H. Wentrup, H. Fucke, O. Rief: *Stahl u. Eisen* (1949) **69**/4, 117.
[20] S. Kobayashi: *Tetsu-to-Hagane* (1937) **23**, 954.
[21] N. Chuiko: *Teoriya i Prackt. Met.* (1938) **9**, 8/7, 48.
[22] N. Chuiko: *Teoriya in Prackt. Met.* (1938) **9**/5, 31.
[23] N. Chuiko, A. Lvova: *Teoriya i Prackt. Met.* (1938) **10**/3, 30.
[24] N. Chuiko: *Stal* (1938) **8**/11, 36.
[25] C. Taylor, J. Chipman: *Trans.* AIME (1943) **154**, 228.
[26] L. Luckemeyer-Hasse, R. Schenck: *Arch. Eisenhüttenw.* (1932) **6**, 209-214.
[27] W. Baukloh, R. Müller: *Arch. Eisenhüttenw.* (1937) **11**, 509.
[28] A. Sieverts, K. Brüning: *Arch. Eisenhüttenw.* (1934) **7**, 641.
[29] J. Chipman, M. Fontana: *Trans.* A.S.M. (1936) **24**, 313.
[30] D. J. Carney, J. Chipman, N. J. Grant: AIME *Electric Furnace Steel Proceedings* (1948), p. 34.

# The Solubility of Oxygen in Liquid Iron Containing Aluminum

## by D. C. Hilty and Walter Crafts

The solubility of oxygen in iron containing aluminum has been determined at 1550°, 1600°, and 1650°C and found to be much higher than predicted from theoretical considerations, possibly due to equilibria with an iron-aluminum spinel phase rather than pure $Al_2O_3$. The presence of manganese greatly increased the deoxidizing power of aluminum.

DEOXIDATION and inclusion formation in steel have proved to be elusive phenomena that are difficult to control in spite of much effort to understand and evaluate the reactions. Study of the problem indicated that more accurate data on the solubility of oxygen in iron containing deoxidizers were essential to further progress, and an empirical determination of oxygen solubilities has been initiated at the Union Carbide and Carbon Research Laboratories, Inc. The investigation has included the effects of aluminum, silicon, manganese, and combinations of these elements at 1550°, 1600°, and 1650°C. The equipment and experimental procedure as well as the results of a study of the effects of aluminum are described below. In general, it was found that the solubility of oxygen in iron containing aluminum is much higher than predicted, possibly because of the formation of complex nonmetallic phases, and that manganese greatly increases the deoxidizing power of aluminum.

The generally accepted deoxidation curves for 1600°C are summarized in fig. 1, from "Basic Open Hearth Steelmaking"[1]. These curves are assumed to represent the solubility of oxygen in the presence of deoxidizers and should indicate the limits of miscibility gaps in the phase diagrams of the systems that control the formation and character of nonmetallic inclusions as described by Benedicks and Löfquist[2]. They were derived mainly by application of the methods of thermodynamics to the available experimental observations, and by calculations based on the thermal constants of the pure substances when experimental data were lacking. Among the more notable researches contributing to the development of knowledge of oxygen solubilities are those of Körber and Oelsen[3, 4], C. H. Herty, Jr. and associates[5, 6], Krings and Schackmann[7], Wentrup and Hieber[8], Schenck and Brüggeman[9], Vacher and Hamilton[10], and Chipman and co-authors[1, 11, 12, 13].

Practically, the deoxidation curves are of limited value in predicting oxygen content and rationalizing deoxidation practices. The reasons for this inadequacy appear to be error from inaccurate data, oversimplifying assumptions, interacting effects of combined deoxidizers, and possibly unknown extra-equilibrium and side reactions. Although inclusion formation is a very complex reaction it must be re-
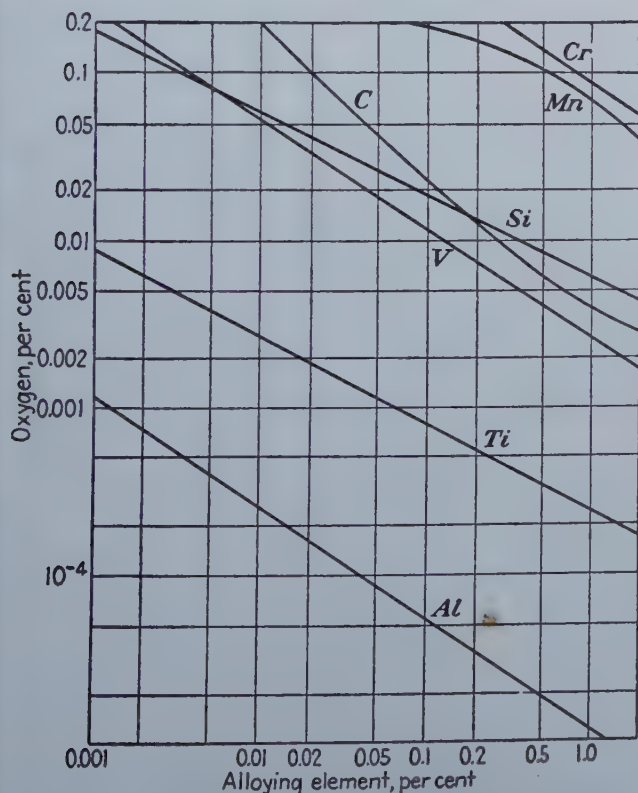


Fig. 1—Comparison of deoxidizing powers of various elements at 1600°C.

Basic Open Hearth Steelmaking.[1]

D. C. HILTY, Member AIME, is Research Metallurgist and WALTER CRAFTS, Member AIME, is Chief Metallurgist, Union Carbide and Carbon Research Laboratories, Inc., Niagara Falls, N. Y.

lated to and evaluated in terms of the deoxidation curves. For this reason it was considered that a redetermination of the deoxidation curves was essential to further solution of the deoxidation problem, and an investigation of oxygen solubilities was undertaken. The investigation of deoxidation with aluminum, alone, and to some extent in combination with silicon and manganese, is described below. A similar study of silicon and manganese is included in an accompanying paper[14].

**Experimental Furnace:** The work of Taylor and Chipman[15] on the solubility of oxygen in liquid iron and the activity of FeO in slags in contact with liquid iron suggested that a rotating crucible furnace might be particularly useful in an investigation of deoxidation equilibria. As discussed by Taylor and Chipman, the theory of such a furnace is that the forces set up by rotation of the crucible cause the surface of the molten charge to assume a concave shape. Slag rides in the liquid metal cup, so that contamination of the slag by reaction with the crucible is presumably reduced. Moreover, concentration of the slag in the cup considerably improves the possibilities for slag-sampling.

Accordingly, a rotating crucible furnace was constructed to the design shown in fig. 2. Great sturdiness and a high degree of flexibility were prime considerations in the plan of this furnace, and, as will be evident from fig. 2, the completed furnace represented a modified composite of similar furnaces described in the literature[15, 16].

The coil assembly was designed for the use of prefabricated crucibles that were centered by means of a jig that fitted on the soapstone cover of the coil. The crucibles, held in position by the jig, were packed in the coil by means of finely ground alumina, magnesia, or silica sand depending upon the type of crucible employed. The coil itself was completely encased in sillimanite cement for the dual purpose of holding the crucible packing material, which was tamped in solidly, and of protecting the coil in case a heat went through the crucible. As additional insurance against damage resulting from a breakout, the inside of the Bakelite drum upon which the slip-rings were mounted was also coated with sillimanite. The Bakelite shield mounted horizontally at the top of the drum was for the purpose of preventing metal splashings or other substances from falling on the brushes.

The rotating mechanism consisted of a 1½ hp induction motor driving a variable speed transmission coupled to the vertical shaft upon which the

coil assembly was mounted as shown in fig. 2. A continuously variable range of speed from 45 to approximately 250 rpm was obtainable, but for most of the investigation a speed of around 200 rpm was found satisfactory. By virtue of the steel shell and cover, the furnace could be operated either under vacuum or under controlled atmosphere. The water-cooled thermocouple holder mounted on the cover could be moved up and down and locked in any position. Sampling operations and the making of additions were carried out by removing the small cover plate from the sampling hole adjacent to the thermocouple holder mounting.

Provision was also made for tapping the furnace at the end of a run. Tapping was carried out by removing the metal cover and tipping the entire structure on the trunnions. As the furnace approached the horizontal, or pouring position, a portable runner was moved into position butting against the lip of the crucible. Actual melting capacity of the furnace was approximately 30 lb of iron. For most of the work in the deoxidation studies, however, it was found convenient to employ from 12 to 20 lb of metal.

**Crucibles:** For the investigation of aluminum deoxidation, high-purity alumina crucibles were em-
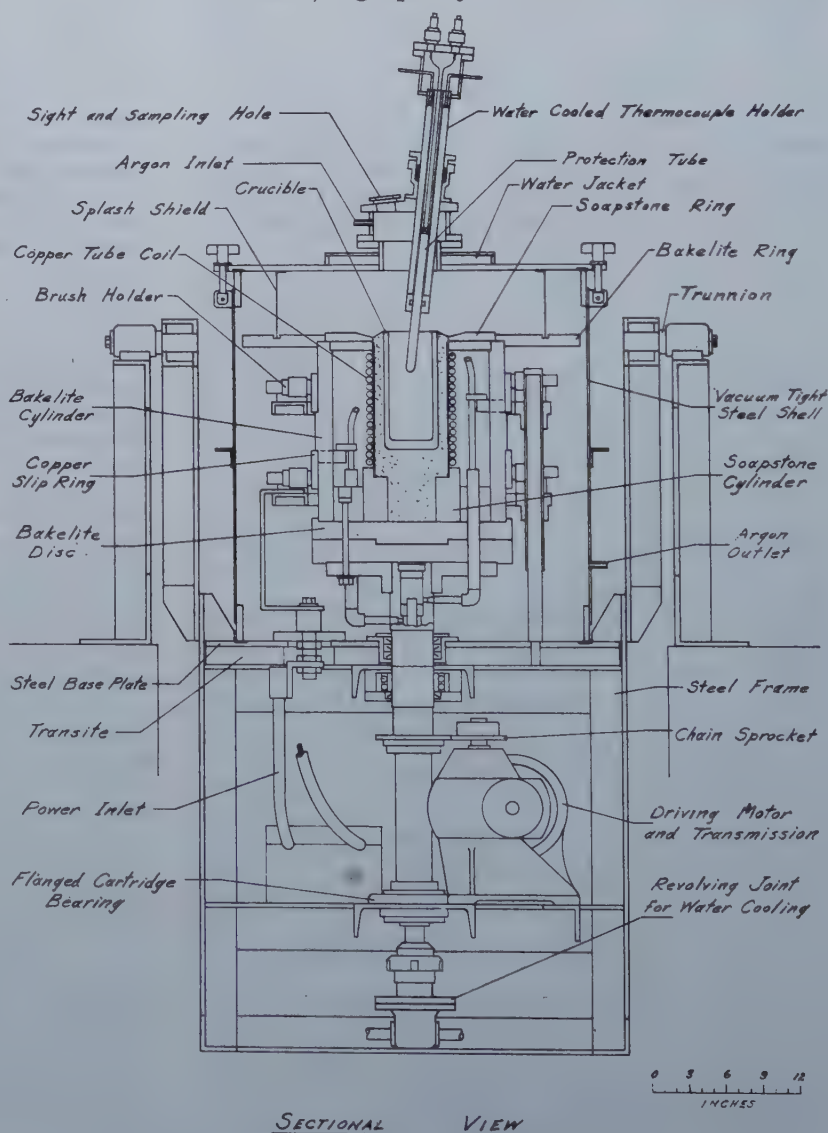


Fig. 2—Plan of
rotating furnace.

SECTIONAL VIEW

ployed. They were hand-rammed in a specially designed cast iron mold from special grade Aloxite cement containing better than 99.0 pct $Al_2O_3$ to which a small amount of water was added. After ramming, the crucibles were permitted to dry in the mold for 24 hr. They were then removed from the mold and allowed to dry for another 24 hr, after which they were fired for 8 hr at a temperature of 1200°C. The finished crucibles were reasonably dense, mechanically strong, and highly resistant to thermal spalling. It was found possible to use the same crucible for as many as five consecutive 6-hr runs. In most instances during the study of the aluminum-oxygen equilibria in molten iron, however, the crucible was changed after every 2 or 3 runs because of the buildup of crusty oxide deposits on the crucible walls and bottom as a result of what appeared to be reaction between the metal and crucible. This reaction is discussed more fully in a later section of this paper.

**Atmosphere:** All of the experimental runs were carried out in an atmosphere of argon. The furnace was initially evacuated to a pressure of 100-200 microns, and purified argon, containing 99.8-99.9 pct argon with the balance mainly nitrogen and less than 0.00015 pct other impurities, was fed directly from a cylinder through the inlet valve on the furnace cover as indicated in fig. 2. When the argon pressure inside the furnace reached atmospheric pressure, the outlet valve at the bottom of the furnace shell was opened and for the duration of the run argon was kept sweeping through the furnace chamber. Argon flow was maintained fairly constant at 3 or 4 liters per min except during sampling or the making of additions, at which times it was increased to 10 or 12 liters per min to help minimize contamination of the atmosphere resulting from the infiltration of air through the open sampling hole.

Analyses of the furnace atmosphere during operation with normal argon flow and the melt presumably at equilibrium repeatedly indicated no oxygen in the exit gas. In a test run made specifically for the purpose it was found that when the normal argon flow of 4 liters per min was maintained during sampling of the heat or during any other operation involving removal of the cover plate from the sampling hole, the oxygen content of the atmosphere immediately over the bath rose to approximately 0.1 pct; but if the argon flow was increased to 10 liters per min while the sampling hole was open, any such contamination of the atmosphere was unmeasurably small.

Contamination of the furnace atmosphere by moisture, however, proved to be a somewhat more serious problem. The source of this moisture appeared to be the furnace refractories, especially the sillimanite cement encasing the coil and coating the inside of the Bakelite drum. The argon used was practically moisture-free; moreover, moisture tests made by inserting a tube containing "Drierite," an indicating anhydrous calcium sulphate preparation which is sensitive to approximately four parts per million of moisture in air on the basis of data reported by Hammond and Withrow[17], in the gas line between the furnace and the argon cylinders gave completely negative results. On the other hand, in the early stages of the investigation, relatively large volumes of moisture were observed in the furnace.

The moisture problem was solved by carefully drying the furnace. With the furnace operating under vacuum, a charge of iron was melted, and the amount of cooling water was then reduced until it came out of the coil warm. After the heat was tapped, the furnace was immediately sealed and placed under vacuum again. When the crucible had cooled to approximately 1000°C, the cooling water was turned off, so that all refractories within the furnace chamber were heated. This procedure was repeated until a negative moisture test in the exit gas was obtained from the furnace in a regular run. By employing the above drying operation after every relining of the furnace, and by keeping the furnace sealed under argon when it was idle, contamination of the atmosphere by moisture was held to a minimum. It is considered that the actual moisture content of the atmosphere during the experimental runs was so low that it had no significant effect on the results.

**Temperature Measurement:** The temperatures chosen for determination of the oxygen solubility isotherms were 1550°, 1600°, and 1650°C. A range of ± 5°C from the specified temperature was set as the permissible limit of temperature variation for the isothermal observations. This range imposed no hardship with respect to operation of the furnace and appeared to be adequately narrow from the standpoint of any significant effect that could be detected by chemical analyses. All temperatures were measured by platinum vs. platinum + 10 pct rhodium thermocouples encased in a silica sheath mounted in a water-cooled holder as shown in fig. 2. The couples were calibrated against two standard thermocouples that were certified accurate up to at least 1575°C by the National Bureau of Standards. The calibration was also occasionally checked against the melting point of electrolytic iron (containing approximately 0.08 pct oxygen) in an alumina crucible, which was taken as 1530°C.

To make a temperature measurement, the thermocouple holder was lowered until the silica tube was plunged into the bath to a depth of approximately 2 in. Except as described below, depth of immersion of the thermocouple in the bath had no observable effect on the temperature reading provided it was greater than 1 in. The thermocouple was maintained in this position until a constant temperature indication was obtained on a direct-reading potentiometer. The time of immersion necessary for a reliable temperature measurement was on the order of 2 min. As soon as the potentiometer reading reached a constant value, the thermocouple was withdrawn from the bath and raised to the highest possible position in the furnace chamber, so that it would not interfere with sampling, and so that prolonged exposure of the thermocouple to high temperatures would be avoided.

Contamination of the thermocouples by exposure to high temperatures in the presence of silica[18] was usually observed to be a slow process resulting in gradual deterioration of the couples. It was compensated for by frequent recalibrations. Occasionally, however, especially at temperatures above 1600°C, deterioration of the couples was quite rapid, so that in the course of one run the observed temperatures might become as much as 25°C low.

Fortunately, it was discovered that an error of

Fig. 3 (above left)—FeO Inclusions in Taylor sample of oxidized electrolytic iron. X500.

Fig. 4 (below left)—FeO inclusions in sample of oxidized electrolytic iron with slightly slower quenching rate than in fig. 3. X500.

Fig. 5 (top right)—Inclusion in Taylor sample of electrolytic iron containing 0.066 pct aluminum and 0.015 pct oxygen. X2000. Fig. 6 (center right)—Inclusions in same heat as shown in fig. 5 cast in 2-in. square ingot mold; aluminum: 0.035 pct, oxygen: 0.013 pct. X500. Fig. 7 (bottom right)—Same sample as in fig. 5 after annealing for 1 hr at 1400°C. X2000.

more than 5°C in a contaminated thermocouple could be detected quite easily. With a couple contaminated sufficiently to lower its reading more than 5°C below the actual temperature, variation of temperature with depth of immersion was observed at depths considerably greater than the minimum necessary for a good couple. When a contaminated thermocouple was detected, it was immediately withdrawn from service for reconditioning and replaced with one that had been newly calibrated. By employing thermocouples of known calibration for every run and by making frequent depth of immersion tests during the progress of a run, error due to thermocouple drift because of contamination was held to a minimum. It is considered that with few exceptions the temperature observations reported in the data tables are within —5°C of the actual temperatures, so that the total deviation from the nominal temperature was from —5 to +10°C.

**Sampling of Metal:** Representative sampling of liquid metal is an important and difficult problem in investigating deoxidation phenomena. Since it has been convincingly demonstrated by Sims and Lilliqvist[19] and others[9, 20] that reaction during the cooling and solidification of molten iron tends to cause precipitation and segregation of nonmetallic phases, it is considered that the cooling rate of samples should be as fast as possible. Although practical cooling rates may not be sufficiently fast to prevent such precipitation, fast cooling should keep the inclusions small and minimize tendencies toward

their rejection. In addition, if the cooling rate is sufficiently fast to suppress the formation of large inclusions, it removes the question of whether they were present as such in the liquid metal before solidification. If inclusions of significant size are present in such a rapidly cooled specimen they may be recognized in microscopic examination, but if the specimen contains no relatively large inclusions, it may be considered to represent the liquid metal for analytical purposes.

For this investigation, the sampling device described by Taylor and Chipman[15], which has since come to be known as the "Taylor sampler," was

used. Essentially, this sampler is a heavy-wall, small-bore, copper suction-tube which gives a sample that is solidified at a very high rate. Microscopic study of samples indicated that this device would fulfill the requirements discussed above.

The effect of the Taylor sampler on the precipitation of inclusions is illustrated by fig. 3 to 7. Fig. 3 illustrates FeO inclusions in a sample taken at approximately 1650°C from an electrolytic iron melt saturated with oxygen. Fig. 4 shows similar inclusions in a large drop of metal that clung suspended to the tip of the sampler as the latter was withdrawn from the melt, so that the rate of cooling of this metal, although still quite rapid, was not so fast as that of the sample proper. The suppression of inclusion growth resulting from the rapid quench is evident.

Similar behavior is indicated by fig. 5 which illustrates a sample taken at a temperature of approximately 1650°C from a melt of electroyltic iron to which aluminum had been added. Even at a magnification of 2000 diam, no oxide inclusions were visible in spite of the fact that chemical analyses of the sample indicated the presence of 0.066 pct aluminum and 0.015 pct oxygen. When this same heat was cast in a 2-in. square cast iron ingot mold, so that the freezing rate was relatively slow in comparison to the Taylor sample, the composition changed to 0.035 pct aluminum and 0.013 pct oxygen, and inclusions typical of aluminum-killed steel formed as shown in fig. 6. The sample illustrated in fig. 5 was annealed for 1 hr at 1400°C in an atmosphere of argon with a resultant formation of the inclusions shown in fig. 7. It is apparent that the rate of cooling of the Taylor sample effectively retards the precipitation and growth of inclusions.

Not all of the samples taken during the study of the aluminum-oxygen equilibria were so free from visible inclusions as the one illustrated by fig. 5. Some of them occasionally contained minute inclusions more or less similar to those shown in fig. 7. Such observations, however, were considered not to be evidence of sample contamination but to be an indication of the extreme quenching rate necessary for the suppression of inclusion precipitation, a rate that could not always be achieved, even with the drastic quench of the Taylor sampler.

Before being submitted to chemical analysis, all samples were carefully examined for defects that might cause erroneous analytical results, and if the defects could not be removed, the samples were discarded. The most troublesome defect was a type of skin lamination or cold shut that was particularly prevalent in samples taken at the lower temperatures from heats containing substantial amounts of aluminum or silicon. Manganese appeared to alleviate the condition. Slag contamination of the samples was encountered unless the slag volume was kept fairly small. Generally, these defects were fairly obvious, but in some instances they could be detected only by a macroetching treatment that was given all samples.

**Sampling of Slag:** The low slag volumes that were found necessary for the successful conduct of the experimental runs made slag sampling difficult. Moreover, sampling was not improved by the fact that many of the slags, particularly those of the aluminum study reported in this paper, were solid

under the conditions of the runs and were present as dry, frangible films on the surface of the metal. The sampling method that proved most effective was as follows: A clean, cold steel rod ¼ to ⅜ in. in diam was lowered into the furnace through the sampling hole until it just touched the surface of the heat. A small amount of slag, with or without some metal, would usually freeze to the tip of the rod. The rod was immediately raised until the tip was at the level of the argon inlet orifice, and the sample was cooled in the incoming stream of argon. When cool, the samples were pulverized in a steel mortar and then passed through a 100-mesh screen to remove metal that had also frozen to the rod. Many of the slag samples were too small for reliable chemical analysis. Most of them, however, were suitable for X ray diffraction examination for identification of the phases present.

**Analytical Methods:** As has been pointed out by Chipman[1, 11], a major obstacle attending studies of deoxidation with aluminum has been the lack of a reliable analytical method for determining low concentrations of aluminum in iron. The recent development of sensitive colorimetric methods for aluminum, however, has now materially lessened this handicap.

The aluminum results reported herein were obtained by a spectrophotometric method using aluminon as the indicator after removing iron and other interfering elements by means of cupferron. This method, which is applicable to aluminum contents as low as a fraction of a part per million, was developed by J. B. Culbertson and R. M. Fowler of the Union Carbide and Carbon Research Laboratories, Inc. The precision of the method may be inferred from a test that was made on carbonyl iron with the following results:

| Size of Sample | Aluminum—Pct |
|---|---|
| 5.0 g | $0.0012_2$ |
| 50.0 g | $0.0010_4$ |
| 100.0 g | $0.0012_8$ |
| Reagent blank | $0.00006_5$ |

Aluminum analyses were made on chips machined from the complete cross-section of the Taylor sample. Total aluminum was determined, since it was considered that all of the aluminum present in a sample had been in solution in the liquid metal at the time the sample was taken.

Analyses for oxygen were made by the conventional vacuum fusion technique which appeared to give results reproducible within ± 0.001 pct oxygen. In preparation for vacuum fusion analysis, the samples were macroetched in 50 pct HCl to eliminate all traces of scale or rust and to reveal any defects not already detected. Following pickling, they were washed with water, acetone, and ether and were then stored in a dessicator to await analysis.

Slag samples were analyzed by the customary procedures and were X rayed by the powder diffraction method using chromium radiation. In the study of aluminum, very few slag samples were of sufficient size or were sufficiently free from contamination with finely divided particles of metal to warrant chemical analysis. All samples were X rayed, however, with iron lines in the diffraction patterns being disregarded.

**Experimental Procedure:** The basic furnace charge consisted of approximately 15 lb of electrolytic iron. To facilitate charging and melting in the rotating furnace, it was found convenient to premelt the electrolytic iron and forge a slug fitting the rotating crucible. Composition of the electroyltic iron slugs as charged was as follows:

| Element | Pct |
|---|---|
| Carbon | 0.002 |
| Manganese | 0.0006 |
| Phosphorus | 0.0012 |
| Sulphur | 0.010 |
| Silicon | <0.001 |
| Aluminum (soluble) | 0.0002 |
| Aluminum (insoluble) | 0.0005 |
| Copper | Trace |
| Nickel | Trace |

For certain runs, it was desired to start out with a charge containing a high concentration of aluminum. This aluminum was, therefore, incorporated in the electrolytic iron during the premelting operation.

When the charge in the rotating furnace had been melted, the temperature of the bath was adjusted to within ± 5°C of the desired level and held constant for sufficient time to attain equilibrium. After an addition of deoxidizer or ferric oxide, the heat was permitted to come to the new equilibrium before a sample was taken. The time interval varied from 15 min to several hours but usually was about 30 min. This cycle of addition and sampling operations was repeated throughout the duration of a run which lasted from 4 to 7 hr. In some cases, several successive samples were taken over a period of time with no additions in order to make sure that equilibrium was actually being attained. Additions were made in the form of high-purity aluminum welding rod, distilled manganese, refined silicon metal, and C.P. ferric oxide.

**Aluminum and Oxygen in Liquid Iron:** The initial work in the rotating furnace was a study of the aluminum-oxygen equilibria in liquid iron. The experimental results are listed in table I.* From these

---
* For tables I, II, III, and IV (5 pages) order Document 2737 from American Documentation Institute, 1719 N Street, N.W., Washington 6, D.C., remitting $0.50 for microfilm (images 1 in. high on standard 35 mm motion picure film) or $0.50 for photocopies (6x8 in.) readable without optical aid.
---

data, isothermal oxygen solubility curves were plotted as illustrated in fig. 8. It is evident that the data could be represented almost equally well by curves of somewhat different slopes from those shown. The curves, as drawn, appear to suggest that the metal was in equilibrium with pure solid $Al_2O_3$. Such an inference, however, is not supported by the evidence and is not intended to be implied.

The point of origin at approximately 0.002 pct aluminum and 0.08 pct oxygen of the 1600°C curve in fig. 8 is considered to be reasonably well established. It is the end point that was reached either by melting oxidized electrolytic iron in the alumina crucible or by adding iron oxide to a melt initially containing aluminum. The data are insufficient for locating this point at the other temperatures.

The phases in contact with the liquid metal were studied qualitatively. A fairly large sample of the solid phase at low aluminum concentrations in the bath was obtained during a run in which a charge

containing aluminum was oxidized down to the end point. The X ray diffraction pattern of this sample corresponded to that of iron-aluminum spinel. Chemical analysis gave the following results:

| Element | Pct |
|---|---|
| Aluminum | 44.68 |
| Iron | 21.70 |
| Oxygen | 33.98 |
| Total | 100.36 |

which are calculated to correspond to a composition of 69.9 pct $FeO.Al_2O_3$ and 30.4 pct $Fe_3O_4$. The melting point was determined to be 1700°C ± 20°C. It is inferred, therefore, that at least through a limited range of aluminum concentration above the invariant point the metal may be in equilibrium with an iron oxide-rich iron-aluminum spinel. During another run in which the end point was being approached merely by melting a charge of oxidized electrolytic iron, a sample of the liquid slag phase was obtained. The sample was inadequate for chemical analysis, but X ray diffraction indicated it to be a mixture of FeO and $FeO.Al_2O_3$. At aluminum contents in the metal on the order of 0.10 pct and over, X ray diffraction examination of the nonmetallic phases indicated mixtures of $FeO.Al_2O_3$ and $Al_2O_3$.

In view of the above observations, it seems probable that the true solubility curves may be more complex than indicated. The curves of fig. 8, however, are considered to represent the order of magnitude of the oxygen solubilities observed in this investigation. The results can be expressed approximately by the equation:

$$Log\ K = Log\ \%\ \underline{Al}^2 \cdot \%\ \underline{O}^3 = -\frac{58,600}{T} + 22.75 \quad [1]$$

in which $T$ is the absolute temperature. This equation represents a so-called "deoxidation constant" through the range of temperatures and compositions studied and is not considered to have any other significance.

Apparently, the only previous laboratory study of the deoxidation of iron with aluminum reported in
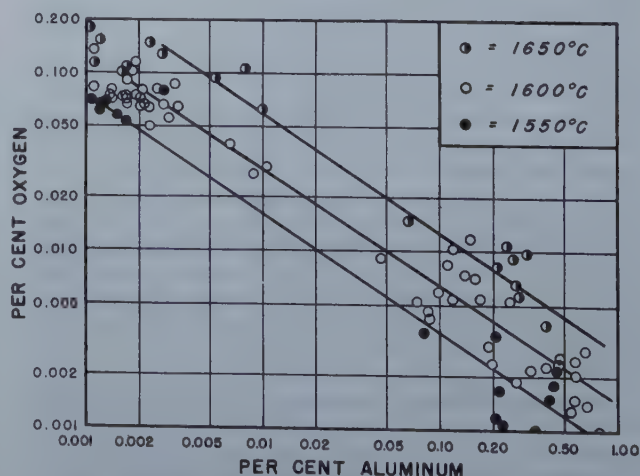


Fig. 8—Solubility of oxygen in liquid iron containing aluminum.
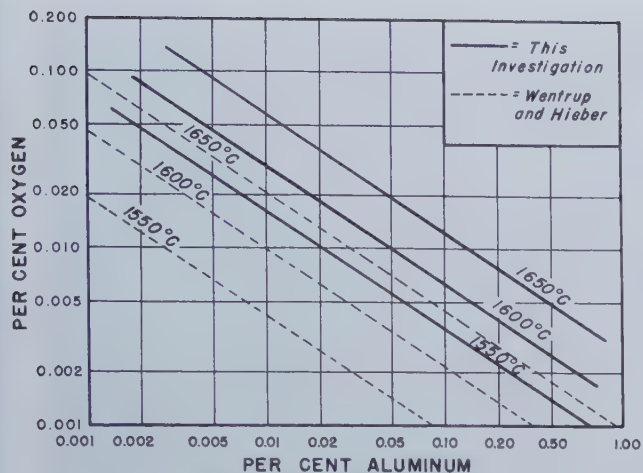
Fig. 9—Comparison of experimental aluminum deoxidation curves.

was varied. Only the 1600°C temperature range was covered by the experimental results, which are given in tables II, III, and IV.* By plotting the aluminum

---

and oxygen contents of the metal for the silicon and manganese ranges indicated, the average oxygen solubility curves shown in fig. 10, 11, and 12 were obtained. In these figures the 1600°C curve already determined for aluminum, alone, is indicated for reference.

In fig. 10, illustrating the effect of 0.25 pct silicon on deoxidation with aluminum, no curve has been drawn because none seems warranted on the basis of the data. The points at high aluminum contents appear to be within the range that would be expected for aluminum, alone. The points at low aluminum contents, at the left of the diagram, although considerably below the aluminum curve, are at the oxygen level that was found[14] to be the limit of oxygen solubility for this amount of silicon in

the literature is that of Wentrup and Hieber[5], who attempted to evaluate a deoxidation constant experimentally. These authors concluded that their results over the temperature range of 1600-1720°C could be expressed by the equation:

$$\text{Log K} = \text{Log } \% \underline{Al}^2 \times \% \underline{O}^3 = -\frac{71,200}{T} + 27.98. \quad [2]$$

In fig. 9, the present results are compared with those of Wentrup and Hieber calculated by means of Eq 2. It will be evident that, although they differ somewhat, they are of the same order of magnitude. Wentrup and Hieber measured temperature with a Bioptex color pyrometer which they assumed gave a direct reading of the true temperature of the liquid metal, and they quenched their samples by pouring a portion of their heats into a small mold. Presumably, much of the actual difference can be attributed to the different methods of temperature measurement employed in the two investigations and to a more rapid quench of the samples in the present study.

**Aluminum, Silicon, Manganese, and Oxygen in Liquid Iron:** The solubility of oxygen in liquid iron containing aluminum in the presence of silicon and manganese was also investigated to a limited extent. Rotating furnace runs were made in which the manganese and silicon contents of the bath were held relatively constant, and the aluminum content



Fig. 11—Effect of 0.46 pct manganese on the solubility of oxygen in liquid iron containing aluminum.
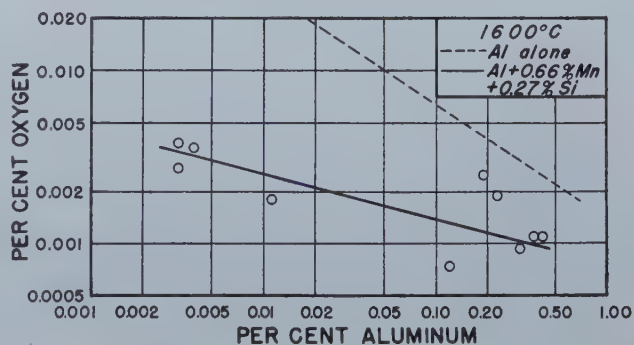


Fig. 12—Effect of 0.66 pct manganese and 0.27 pct silicon on the solubility of oxygen in liquid iron containing aluminum.

the absence of aluminum. It is inferred, therefore, that the influence of silicon on deoxidation with aluminum is relatively minor.

On the other hand, the curve of fig. 11, showing the effect of approximately 0.46 pct manganese on the aluminum-oxygen relation in molten iron, indicates that manganese substantially lowers the solubility of oxygen below the limit observed for aluminum alone. Similarly, the curve of fig. 12, for aluminum in the presence of 0.66 pct manganese and 0.27 pct silicon shows a lowering of the oxygen solubility beyond that indicated by fig. 11. In view of the results illustrated by fig. 10, however, it is



Fig. 10—Effect of 0.25 pct silicon on the solubility of oxygen in liquid iron containing aluminum.

Fig. 13 (top left)—
Reaction product
extending from walls
and bottom of crucible
into metal bath.

Fig. 14 (top right)—
Effect of manganese
on condition shown
in fig. 13.

Fig. 15 (bottom left)—
Effect of silicon on
condition shown
in fig. 13.

Fig. 16 (bottom right)—
Effect of manganese
and silicon on
condition shown
in fig. 13.
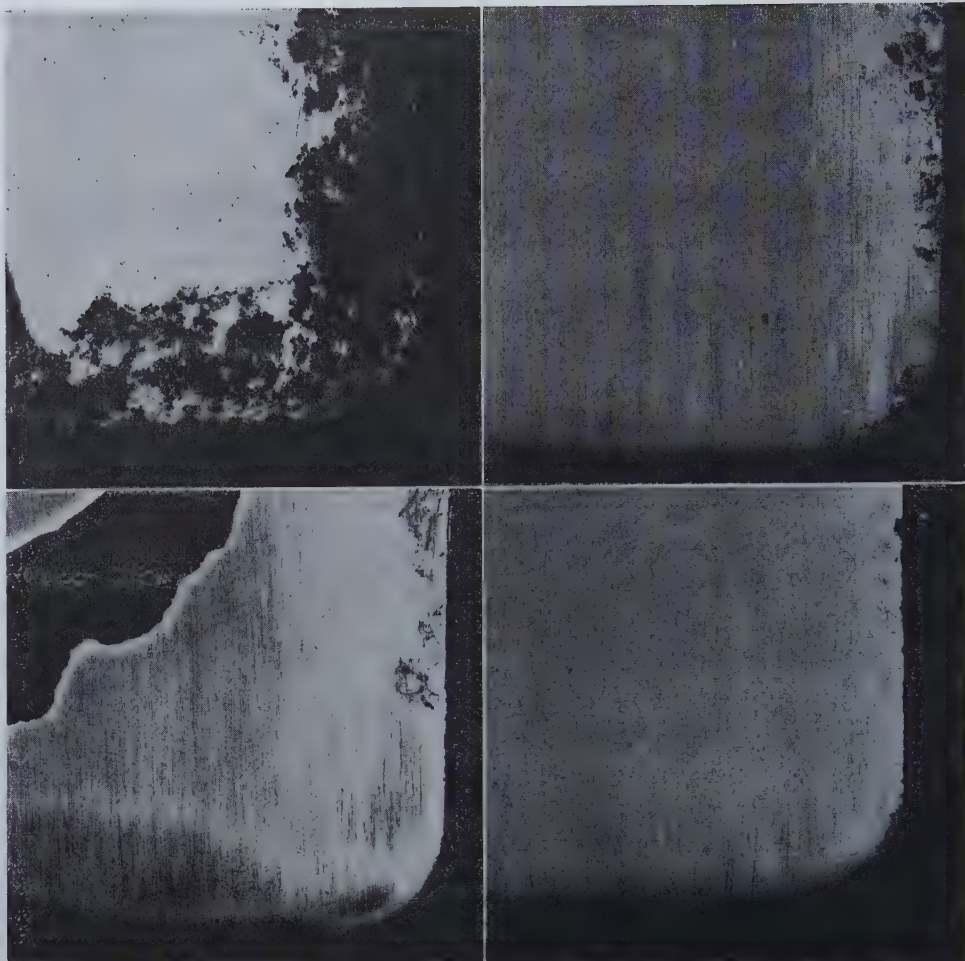
considered that the additional reduction in oxygen solubility apparent in fig. 12 is due to the increased manganese concentration rather than to any appreciable influence of the silicon.

**Crucible Reaction:** During the experimental runs, unusual difficulty in attaining equilibrium was experienced because of what appeared to be extensive reaction between the liquid metal and the alumina crucible. Although it was worse at the lower aluminum concentrations (below approximately 0.10 pct), the reaction persisted throughout the range of aluminum contents studied.

It seemed to be characteristic of the reaction that if equilibrium were being approached by adding aluminum to a high-oxygen, low-aluminum bath, small additions of aluminum were not retained by the bath for any length of time until the aluminum content of the metal exceeded 0.10 pct. On the other hand, when the bath contained a relatively high aluminum concentration initially, excessive additions of ferric oxide were required to effect an incremental lowering of the aluminum content. In the latter case, the addition of ferric oxide was frequently observed to be followed immediately by an initial drop in the aluminum content of the metal followed by a slow increase until the new equilibrium was reached.

The reaction was accompanied by what appeared to be a growth of oxidic reaction products extending into the melt from the walls and bottom of the cru-

cible. This condition is illustrated by fig. 13 which is a photograph of a bottom corner of the vertical cross section of a heat that was permitted to solidify in the crucible under slow rotation. When manganese and/or silicon were present in the bath, however, the deposition of nonmetallics on the crucible walls and bottom appeared to be greatly reduced as shown by fig. 14, 15, and 16. Fig. 14 is a photograph similar to fig. 13 of a heat that contained 0.40 pct manganese; fig. 15 illustrates a heat that had a silicon content of 0.25 pct; and fig. 16 shows a heat that contained 0.58 pct manganese and 0.27 pct silicon.

These reaction products extending out into the bath seriously interfered with the sampling of the metal. If the sampler were plunged too close to the walls or the bottom of the crucible, some of the reaction products would be broken off and drawn into the sampler with the liquid metal. Such contamination of the samples was readily detected by the microscopic examination to which all samples of this investigation were submitted before analysis. A micrograph of a polished section from a sample containing these reaction products is shown in fig. 17. The strong resemblance to the typical oxide clusters usually observed in aluminum-killed steel is notable. The inclusions in the sample illustrated by fig. 17 were extracted electrolytically with the result shown in fig. 18. Their appearance is strongly suggestive of a dendritic character. The residue illustrated in fig. 18 was identified by X ray diffrac-

Fig. 17—Reaction products trapped in Taylor sample. X500.



Fig. 18—Inclusions extracted from sample shown in fig. 17. X500.
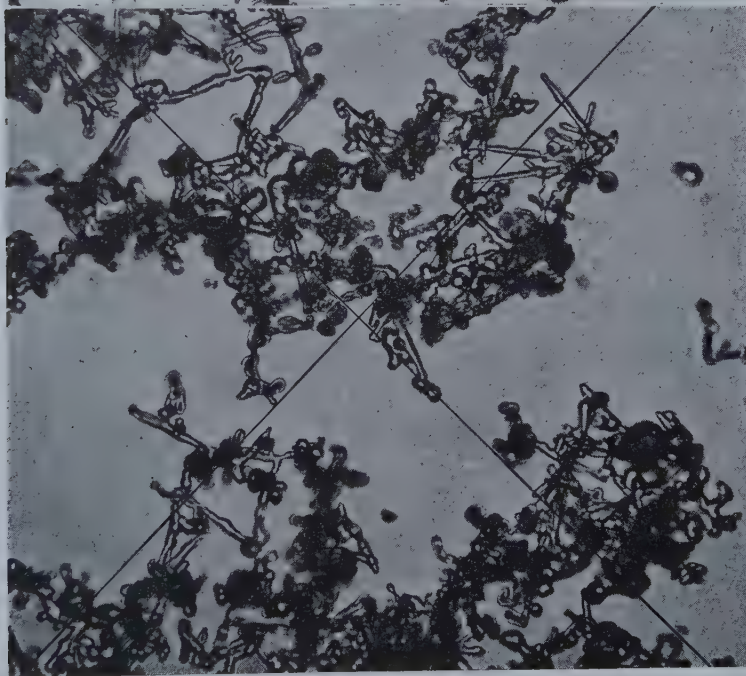
tion as a mixture of iron-aluminum spinel (FeO. Al$_2$O$_3$ phase) and some Al$_2$O$_3$.

A possible explanation of this reaction is suggested by the work of White[21]. From a careful study of the reduction curves of Schenck, Franz, and Willeke[22] and with consideration for the dissociation pressure relationships that must obtain, White deduced the schematic phase distribution shown in fig. 19 for the system Fe-Al-O.

The implications of this diagram regarding reactions that may occur within a relatively small composition range at low aluminum concentrations in the metallic phase are significant. In this connection, it is worthy of note that the composition and constitution of the nonmetallic phase observed in the present investigation to be in equilibrium with liquid

metal phase at low aluminum concentrations, as described in a preceding section, appear to correspond approximately to White's point A in fig. 19. The observations of spinel phase or mixtures of spinel and alumina at somewhat higher aluminum contents in the bath also appear to agree with the phase distribution suggested by White. This phase distribution may be modified by the presence of manganese and/or silicon.

This crucible reaction strongly suggests that pure, solid Al$_2$O$_3$ cannot coexist with liquid iron of the composition studied. On the basis of the above discussion, it is inferred that the solubility of oxygen in liquid iron containing aluminum within the range of steelmaking concentrations is limited by the

**Fig. 19—Phase distribution in system Fe-Al-O.**

After White.[21]
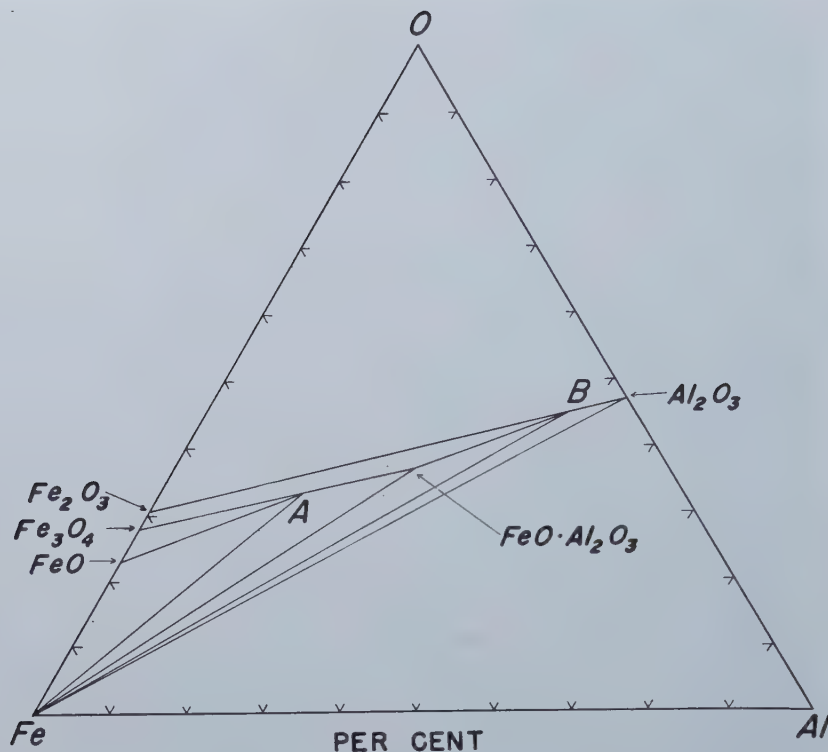
formation of a phase or phases richer in iron oxide than $Al_2O_3$.

**Comparison with Theoretical Aluminum Deoxidation Curve:** The curve generally employed for describing the deoxidizing power of aluminum is the aluminum curve of fig. 1. This curve was derived by Chipman[1, 11] from a thermodynamic calculation of the equilibrium constant of the reaction:

$$Al_2O_3 \text{ solid} = 2\underline{Al} + 3\underline{O}$$

in which aluminum and oxygen dissolved in liquid iron were assumed to be in equilibrium with pure, solid $Al_2O_3$. In fig. 20, the present oxygen solubility results for a temperature of 1600°C are compared with this theoretical curve. It is apparent that the present results indicate an oxygen solubility approximately 100-fold greater than that predicted by the calculation.

One explanation of this apparent discrepancy has been given by Chipman in a recent publication[23] in which he pointed out that the thermodynamic calculations give the *activity* and not the *concentration* of oxygen dissolved in the liquid metal, and that in systems such as this the activity coefficient of oxygen in the metal phase may be considerably less than unity. An alternative explanation is suggested by the observations of the present investigation, which indicate that liquid iron of the compositions considered here may not actually attain equilibrium with pure $Al_2O_3$ as necessarily assumed for the calculations. Instead, the equilibria may be with phases of presumably higher oxygen activity than pure, solid $Al_2O_3$.

## Summary

In order to study deoxidation reactions in molten iron, a rotating crucible induction furnace was constructed, and an experimental technique involving close temperature control and drastically quenched samples was developed, so that the isothermal solubility of oxygen in liquid iron containing one or more deoxidizers could be investigated.

By means of this equipment and technique, deoxidation curves for aluminum at 1550°, 1600°, and 1650°C were obtained which, although oversimplified, are believed to be representative the order of magnitude of oxygen solubility in liquid iron containing small quantities of aluminum.

The results are at wide variance with the theoretical curve of Chipman[1], either because the theoretical curve predicts the activity rather than the concentration of oxygen in the liquid metal, or because the metal phase is not actually in equilibrium with pure, solid $Al_2O_3$ as was assumed for the calculations. Throughout the range of aluminum concentrations investigated, the experimental melts could not be brought into equilibrium with the pure $Al_2O_3$ crucible but appeared to react rather extensively with the crucible. It is inferred that in deoxidation of iron with aluminum, the nonmetallic phases involved are not pure, solid $Al_2O_3$ but are phases of compositions intermediate between $Al_2O_3$ and iron oxide.

Observations on melts containing manganese in addition to aluminum indicated that manganese greatly increases the deoxidizing power of aluminum at concentrations within the usual steelmaking range. On the other hand, silicon appeared to have no significant effect on the deoxidizing power of aluminum.
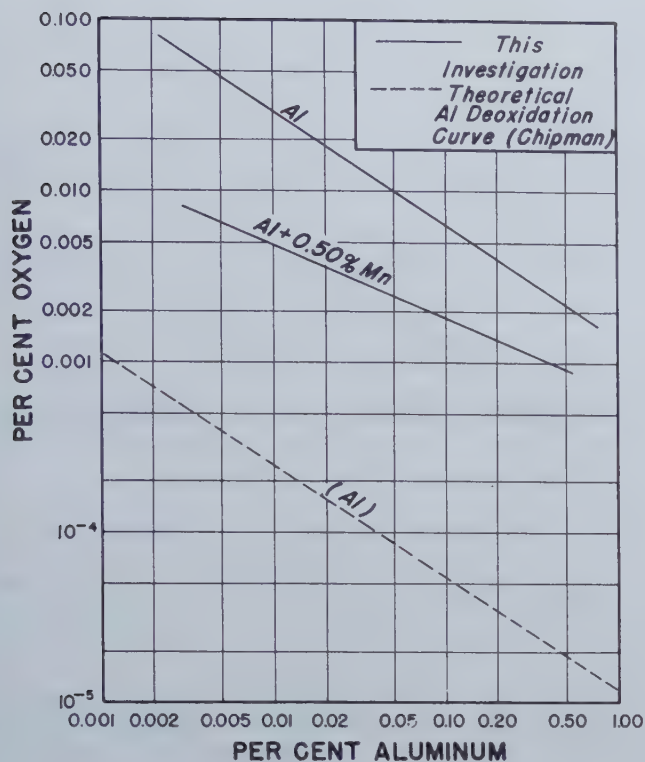
Fig. 20—Comparison with theoretical aluminum
deoxidation curve.

Massachusetts Institute of Technology, who was consulted throughout the course of the investigation and generously contributed valuable suggestions and criticisms.

Acknowledgment is also due to A. B. Kinzel, President, Union Carbide and Carbon Research Laboratories, Inc. for his constructive and steadfast encouragement, and to L. V. Spangberg for the design and construction of the rotating furnace, R. M. Fowler, Chief Chemist, H. L. Hamner, and J. B. Culbertson for chemical analysis, W. D. Forgeng for X ray and metallographic examination, and particularly to J. J. Darby and J. J. Mikula for their wholehearted assistance in conducting the investigation.

Recognition should also be accorded to Electro Metallurgical Division, Union Carbide and Carbon Corporation, for sponsoring a long-continued program on deoxidation and for permission to publish the results.

### References

[1] "Basic Open Hearth Steelmaking." Physical Chemistry of Steelmaking Committee, AIME, New York, N. Y., 1944.

[2] C. Benedicks and H. Löfquist: Nonmetallic Inclusions in Iron and Steel. John Wiley and Sons, Inc., New York, N. Y., 1931.

[3] F. Körber and W. Oelsen: Über die Beziehungen zwischen manganhaltigem Eisen und Schlacken, die fast nur aus Manganoxydul und Eisenoxydul besteben. Mitt. K.-W. Inst. f.d. Eisenforsch., Dusseldorf, (1932) 14, 181-204.

[4] F. Körber and W. Oelsen: Die Grundlagen der Desoxydation mit Mangan und Silizium. Mitt. K.-W. Inst. f.d. Eisenforsch., Dusseldorf, (1933) 15, 271-309.

[5] C. H. Herty, Jr. and G. R. Fitterer: The Physical Chemistry of Steelmaking: Deoxidation with Silicon and the Formation of Ferrous Silicate Inclusions in Steel. U. S. Bur. of Mines, Carnegie Inst. of Tech., and Min. and Met. Advisory Boards Coop. Bull. 36, Pittsburgh, Pa. 1928.

[6] C. H. Herty, Jr., G. R. Fitterer, and J. M. Byrns: The Physical Chemistry of Steelmaking: Deoxidation of Steel with Aluminum. Ibid., Bull. 46.

[7] W. Krings and H. Schackman: Über Gleichgewichte zwischen Metallen und Schlacken im Schmelzflusse, I. Ztsch. anorg. allg. Chem. (1931) 202, 99-112.

[8] H. Wentrup and G. Hieber: Umsetzungen zwischen Aluminum und Sauerstoff in Eisenschmelzen. Archiv. f. d. Eisenhuttenw. (1939) 13, 15-20.

[9] H. Schenck and E. O. Brüggeman: Untersuchungen über die Chemie des sauren Siemens-Martin-Verfahrens. Archiv. f. d. Eisenhuttenw. (1935-1936) 9, 543-553.

[10] H. C. Vacher and E. H. Hamilton: The Carbon-oxygen Equilibrium in Liquid Iron. Trans. AIME (1931) 95, 124-140.

[11] J. Chipman: Deoxidation of Steel. Trans. A.S.M. (1934) 22, 385-433.

[12] S. Marshall and J. Chipman: The Carbon-oxygen Equilibrium in Liquid Iron. Trans. A.S.M. (1942) 30, 695-746.

[13] J. Chipman and N. J. Grant: The Induction Furnace as a High-Temperature Calorimeter and the Heat of Solution of Silicon in Liquid Iron. Trans. A.S.M. (1943) 31, 365-379.

[14] D. C. Hilty and Walter Crafts: The Solubility of Oxygen in Liquid Iron Containing Silicon and Manganese. Trans. AIME (1950) 188, 425. Jnl. of Metals, Feb. 1950.

[15] C. R. Taylor and J. Chipman: Equilibria of Liquid Iron and Simple Basic and Acid Slags in a Rotating Induction Furnace. Trans. AIME (1943) 154, 228-245.

[16] E. P. Barrett, W. F. Holbrook, and C. E. Wood: Induction Furnaces for Rotating Liquid Crucibles. Trans. AIME (1939) 135, 73-84.

[17] W. A. Hammond and J. R. Withrow: Soluble Anhydrite as a Dessicating Agent. Ind. and Eng. Chem. (1935) 25, 653-659.

[18] British Iron and Steel Research Association: Symp. on the Contamination of Platinum Thermocouples. Jnl. Iron and Steel Inst., London, (1947) 155, 213-231.

[19] C. E. Sims and G. A. Lillieqvist: Inclusions — Their Effect, Solubility, and Control in Cast Steel. Trans. AIME (1932) 100, 154-195.

[20] W. Crafts, J. J. Egan, and W. D. Forgeng: Formation of Inclusions in Steel Castings. Trans. AIME, (1940) 140, 233-262.

[21] J. White: The Physical Chemistry of Open-hearth Slags. Jnl. Iron and Steel Inst. London, (1943) 148, II, 579-688.

[22] R. Schenck, H. Franz, and H. Willeke: Gleichgewichtsuntersuchungen über die Reduktions — Oxydations — und Kohlungsvorgange beim Eisen, IX., Ztsch. f. anorg u. allge. Chemie (1929) 184, 1-38.

[23] J. Chipman: Another Look at the Problem of Steel Deoxidation. Metal Progress, (1949) 56, No. 2, 211-221.

# Solubility of Oxygen in Liquid Iron

## Containing Silicon and Manganese

### by D. C. Hilty and Walter Crafts

Determination of the solubility of oxygen in iron containing silicon, or manganese, or both, has confirmed the earlier work on silicon, shown that manganese is more effective than expected, and has demonstrated that the combination of silicon and manganese is a much stronger deoxidizer than might have been inferred from their individual effects.

SILICON and manganese are of primary importance in the deoxidation of steel, and a study has been made at the Union Carbide and Carbon Research Laboratories, Inc. of the solubility of oxygen in iron in the presence of silicon and manganese, singly and in combination, as a basis for more effective control of inclusion formation.

The investigation was carried out with the same equipment and experimental procedure that were used in the determination of the oxygen solubility of iron containing aluminum[1]. The heats were melted in a rotating crucible furnace under an argon atmosphere. Bath temperatures were controlled by platinum/platinum + 10 pct rhodium thermocouples to attain equilibrium at 1550°, 1600°, and 1650°C, so that oxygen solubility isotherms were determined directly without requiring calculation from a temperature coefficient. A detailed description of the furnace and procedure is given in the paper on aluminum deoxidation[1].

Oxygen solubility in the presence of more than 0.10 pct silicon was found to approximate earlier determinations closely, but some deviation was observed at lower silicon contents. Manganese appeared to be more effective than had been anticipated. The combination of silicon and manganese lowered the solubility for oxygen markedly as compared with either silicon or manganese alone. Although the solubility for oxygen in the presence of both silicon and manganese represents only a part of the information needed to control inclusion formation, it suggests a partial explanation of the benefits of this combination that have been observed in practice.

**Manganese and Oxygen in Liquid Iron:** The study of oxygen in iron in the presence of manganese was carried out in magnesia crucibles of the type furnished commercially for laboratory induction furnaces. Alumina crucibles were unsatisfactory, because the work on the aluminum-oxygen equilibria in iron[1] had shown that merely melting iron in an alumina crucible limited the solubility of oxygen to a level considerably below that anticipated for moderate concentrations of manganese. Silica crucibles appeared unsuitable because of the dangers of excessive fluxing by the melt. Moreover, as will be shown later, melting iron in a silica crucible also limits the oxygen content below that in equilibrium with
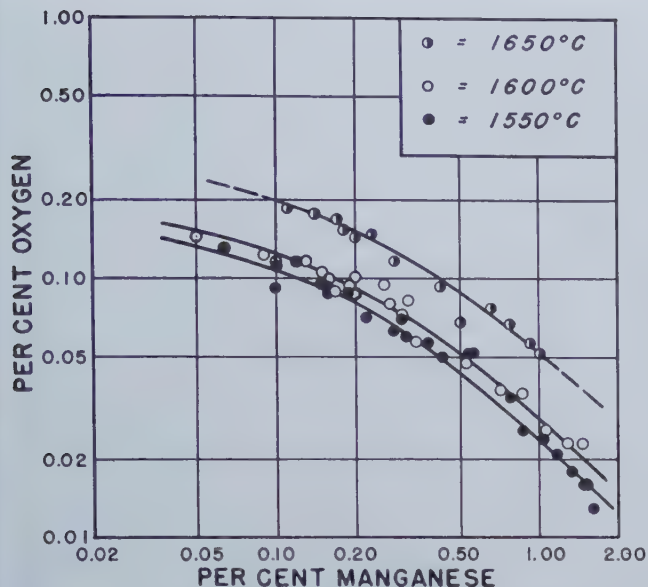
**Fig. 1—Solubility of oxygen in iron containing manganese.**
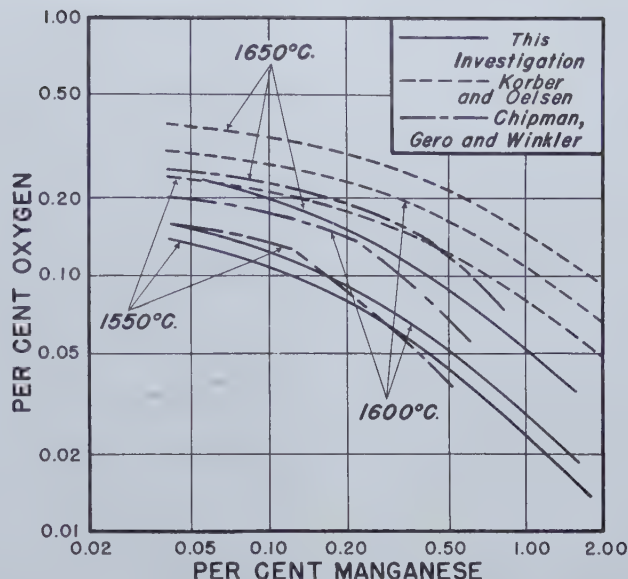


**Fig. 2—Comparison of present manganese results with those of other investigators.**

manganese, alone. It is presumed, on the other hand, that at steelmaking temperatures the influence of magnesia on the solubility of oxygen in the metallic phase of the iron-manganese-oxygen system is quite small.

Determinations of manganese contents of the bath were made by the conventional analytical method for manganese in steel. Analyses for oxygen in the metal were by vacuum fusion. The results obtained from samples taken during the experimental runs are listed in table I.* A plot of these data gave

* For Tables I through VI order Document 2736 from American Documentation Institute, 1719 N Street, N. W., Washington, D. C., remitting $0.50 for microfilm (images 1 in. high on standard 35 mm motion picture film) or $2.20 for photocopies (6x8 in.) readable without optical aid.

the isothermal oxygen solubility curves shown in fig. 1.

Most previous investigations[2,3,4,5] of equilibrium in the iron-manganese-oxygen system, among which the work of Körber and Oelsen[2] is outstanding, have been devoted to an evaluation of the equilibrium constant for the reaction of manganese dissolved in the liquid metal with iron oxide in the liquid slag as expressed by the equations:

$$(FeO) + \underline{Mn} = (MnO) + Fe \qquad [1]†$$

$$K_{Mn} = \frac{\% \ (MnO)}{\% \ (FeO) \cdot \% \ \underline{Mn}} \qquad [2]$$

† Conventionally, underlining of the symbols in a steelmaking reaction indicates that those substances are dissolved in the liquid iron, while parentheses indicate solution in the slag.

Körber and Oelsen represented their results over a wide temperature range by the equation:

$$Log \ K_{Mn} = \frac{6234}{T} - 3.03 \qquad [3]$$

where $T$ is the absolute temperature.

Recently, Chipman, Gero, and Winkler[6] have recalculated the free energy of Eq 1 from lately published thermodynamic data for the individual substances involved. By combining this result with a number of observations on experimental melts

under liquid FeO-MnO slags they have obtained the equation:

$$Log \ K_{Mn} = \frac{6440}{T} - 2.95 \qquad [4]$$

In the present investigation an attempt was made to secure a check on the value of $K_{Mn}$ without success. The manganese slags were of such a nature that they would not remain well down in the rotating cup of metal but crept up the walls of the cup toward the rim where they could not be sampled. When an effort was made to keep some slag on the surface of the cup by increasing the slag volume, it was found that the slag volume necessary was so large that it became chilled on the top surface and could not be considered representative of the true equilibrium slag; in addition, the large slag volumes caused extensive fluxing of the thermocouple protection tube during temperature measurements, so that the samples obtained were excessively contaminated with silica. Consequently, all of the results from these runs with high slag volume were discarded, and the attempt to determine the equilibrium constant, $K_{Mn}$, was abandoned.

Both Körber and Oelsen[2] and Chipman, Gero, and Winkler[6] made direct observations of the solubility of oxygen in the metal. From their data Körber and Oelsen concluded that the oxygen content of the metal in this system is dependent solely on the iron oxide content of the slag according to the Nernst partition principle. They determined the partition coefficient:

$$L_o = \frac{\% \ \underline{O}}{\% \ (FeO)} \qquad [5]$$

over a range of temperatures, and by combining the result with Eq 3 they calculated deoxidation curves for manganese. Similarly, Chipman, Gero, and Winkler employed the partition coefficient, $L_o$, derived from the work of Taylor and Chipman[7] on the solubility of oxygen in pure iron, to calculate manganese deoxidation curves from Eq 4 representing their experimental results. At the higher manganese

**Fig. 3—Silicon-oxygen equilibrium in liquid iron at 1550°C.**
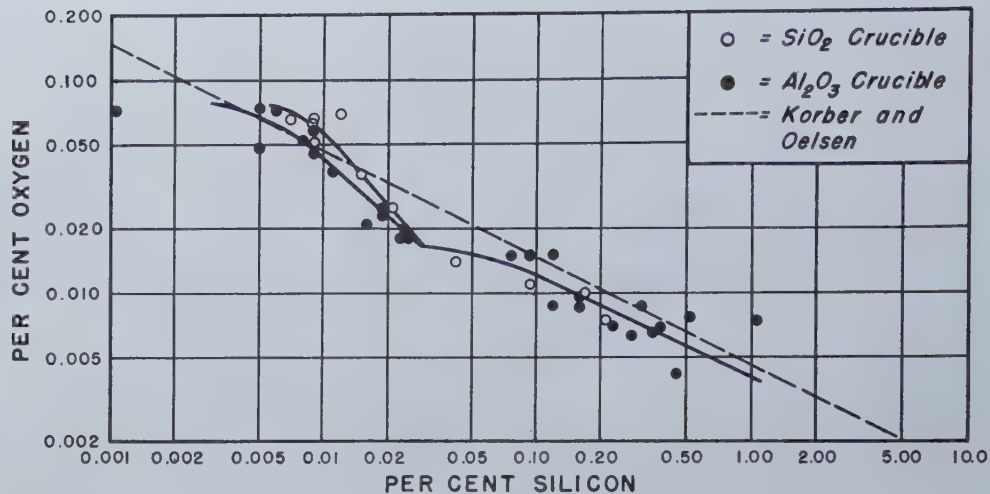


**Fig. 4—Silicon-oxygen equilibrium in liquid iron at 1600°C.**
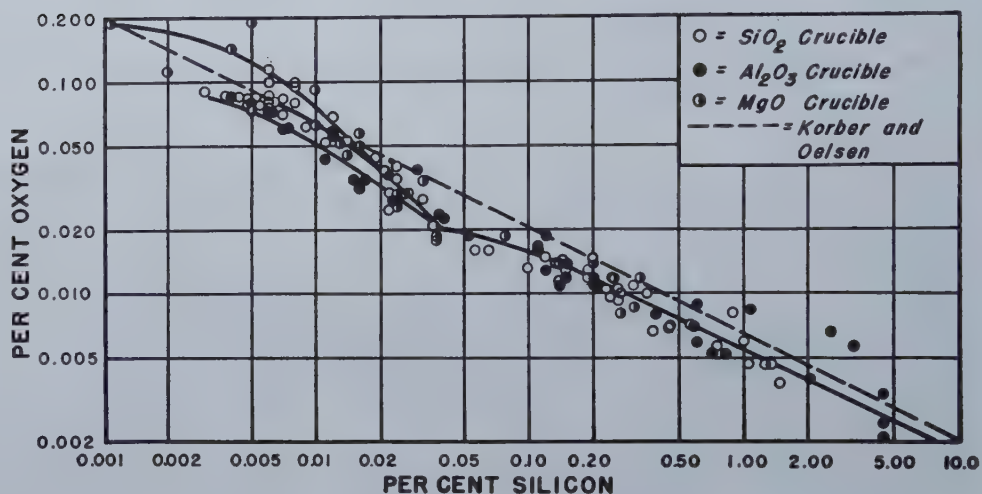


**Fig. 5—Silicon-oxygen equilibrium in liquid iron at 1650°C.**
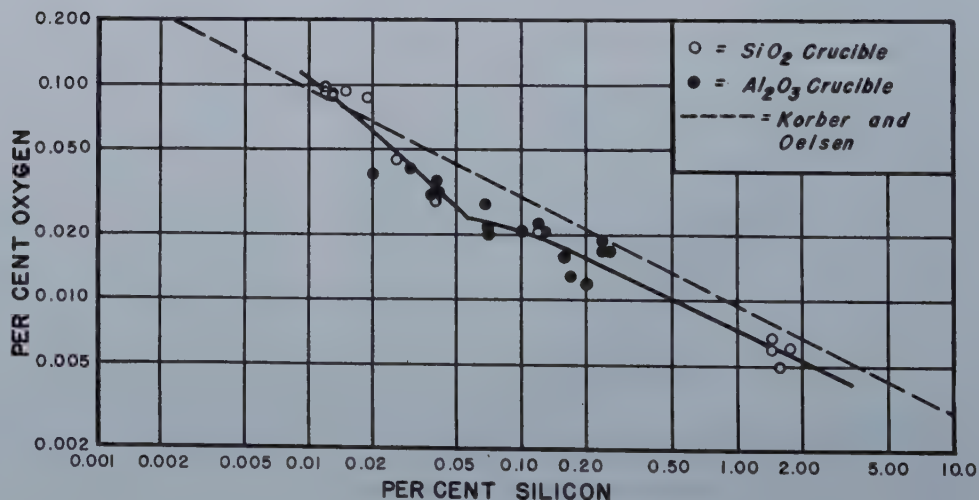
concentrations the calculation was modified to include the assumption of a solid slag phase.

In fig. 2 the results of the present study are compared with those of Körber and Oelsen and Chipman, Gero and Winkler. It will be evident from fig. 2 that the oxygen solubilities determined in this investigation are of a totally different order of magnitude from those predicted by Körber and Oelsen. In view of the work of Taylor and Chipman[7] and of Sloman[8], however, the values of the partition coefficient, $L_o$, derived by Körber and Oelsen and applied by them in calculating the solubility isotherms, ap-
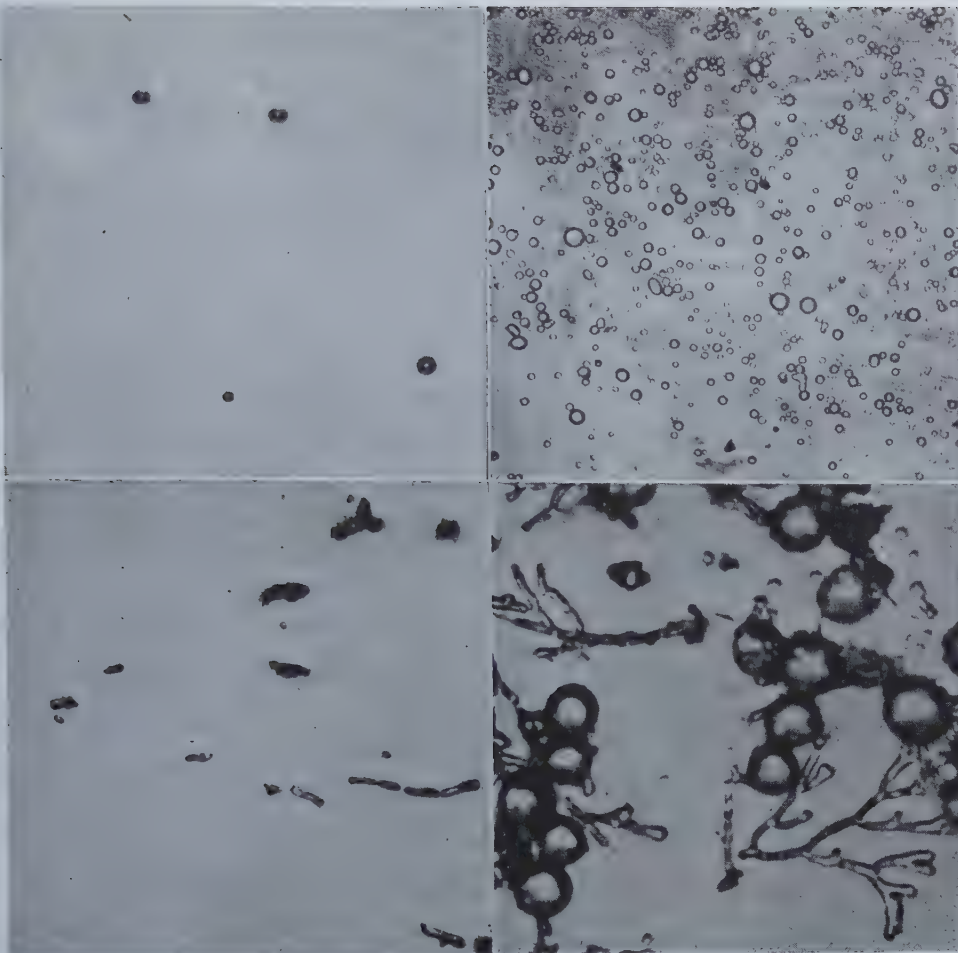
Fig. 6 (upper left)—Type of inclusions present in metallographic specimens of heats containing 1.75 pct, 0.17 pct, and 0.14 pct silicon.

Fig. 7 (upper right)—Appearance of silica globules extracted from heats represented by fig. 6.

Fig. 8 (lower left)—Inclusions in metallographic specimen from near the center of a heat containing 0.14 pct silicon.

Fig. 9 (lower right)—Inclusions extracted from specimen shown in fig. 8.

pear to have been 40 to 50 pct too high. Moreover, it is probable that the temperatures reported by Körber and Oelsen were somewhat lower than the true temperatures, because the vapors of manganese and manganese oxides over their melts admittedly interfered with their optical pyrometer readings.

At the higher manganese concentrations the increased rate of slope of the curves is probably indicative of the solid slag phase. The manganese content at which the slag changes from liquid to solid increases with temperature. Presumably, therefore, these curves should show inflections corresponding to the points of isothermal invariant equilibrium. Apparently, however, the magnitude of the inflections is so small that it was beyond the sensitivity of the present study. Visual observations of the character of the slag during the various runs suggested that the transition might come at around 0.10 pct manganese in the bath at 1550°C, approximately 0.20 pct manganese at 1600°C, and in the vicinity of 0.60 pct manganese at 1650°C. These observations are in good agreement with what would be estimated from consideration of Eq 4 and the FeO-MnO diagram of Hay, Howat, and White[9].

The position of the 1600°C curve in relation to the curves for 1550° and 1650°C, as illustrated by fig. 1, is believed to reflect the disproportionately higher solubility of oxygen in pure iron at higher temperatures implied by the data as compared with the curve of Taylor and Chipman[7] and the similarity

of FeO and MnO which have been shown[9, 10] to be completely miscible in all proportions in both the liquid and solid states.

On the basis of these solubility curves, it is apparent that the deoxidizing power of manganese is considerably greater than has heretofore been assumed.

**Silicon and Oxygen in Liquid Iron:** Since it was expected (c.f. *Basic Open Hearth Steelmaking[11]*) that the type of refractory in which the experimental melts were made might have a profound influence on the solubility of oxygen in liquid iron in the presence of silicon, the iron-silicon-oxygen equilibria were studied in magnesia, silica, and alumina crucibles. The magnesia crucibles were similar to those employed for the investigation of manganese; the silica crucibles, also obtained commercially, were pure, vitreous silica; while the alumina crucibles were made up for the purpose[1]. A few alumina crucibles made commercially from alumina bonded with approximately 12 pct silica were also employed.

Silicon contents of most of the metal samples in the very low silicon range were determined by a modification of the highly-sensitive silico-molybdate colorimetric method of Clausen and Roussopoulas[12] adapted for this investigation by R. C. Shubert and R. M. Fowler of these Laboratories. In the higher silicon ranges (above approximately 0.20 pct) analyses were by the conventional gravimetric method. Oxygen contents were determined by

vacuum fusion. Slag samples of sufficient size were analyzed by the customary procedures. All slags, however, were examined by X ray diffraction for identification of the phases present.

Of the several attempts to evaluate a silicon deoxidation constant experimentally, including the studies of Herty and Fitterer[13], Körber and Oelsen[14], Zapffe and Sims[15], Schenck and Brüggeman[16], Derge[17], and others, the investigation of Körber and Oelsen[14] has received the greatest attention. For the effect of temperature on the equilibrium constant of the reaction:

$$SiO_{2\,solid} + 2\,\underline{Fe} = 2\,(FeO) + \underline{Si} \qquad [6]$$

Körber and Oelsen expressed their results by the equation:

$$Log\,K_{Si} = Log\,\%\,\underline{Si} \cdot (\%\,FeO)^2 = -\frac{19,057}{T} + 11.101 \qquad [7]$$

which Chipman[11] has converted to:

$$Log\,K_{Si} = Log\,\%\,\underline{Si}\,(\%\,\underline{O})^2 = -\frac{26,050}{T} + 9.51 \quad [8]$$

for the reaction of silicon with oxygen dissolved in the metal. The points of three-phase equilibrium at constant temperature, i.e., liquid metal in contact with liquid iron silicate slag and solid silica, representing the maximum oxygen and minimum silicon contents to which Eq 8 is applicable were reported by Körber and Oelson to be 0.084 pct oxygen and 0.002 pct silicon at 1550°C, 0.105 pct oxygen, and 0.003 pct silicon at 1600°C, and 0.13 pct oxygen and 0.006 pct silicon at 1650°C. Körber and Oelsen, however, made no truly isothermal study of oxygen solubility over a range of silicon contents.

The experimental results obtained during the current investigation are given in tables II, III, and IV segregated according to type of crucible employed for the rotating furnace runs. From these data oxygen solubility curves were plotted for 1550°, 1600°, and 1650°C as illustrated by fig. 3, 4, and 5 in which the silicon deoxidation curves of Körber and Oelsen calculated by Eq 8 are also indicated for comparison.

At first glance, it may appear that there is small justification for drawing the curves in the manner shown. Actually, each of the groups of data could be represented by single straight lines on these logarithmic plots. Upon closer examination, however, it was found that the best single straight lines that could be drawn through the points not only showed less agreement with the data but were inconsistent with each other at the different temperatures. On the other hand, the remarkable degree of consistency with which the apparent break in the curves shows up at different temperatures, in different crucibles, and, as will be shown below, in the presence of manganese, cannot be ignored. Consequently, and in view of other considerations discussed below, the solubility curves of fig. 3, 4, and 5 have been drawn as two intersecting curves which fit the data quite well in comparison with the straight lines predicted by Körber and Oelsen.

Above 0.10 pct silicon the slope of the curve is actually 2.13, but the results are fitted approximately by the equation:

$$Log\,K = Log\,\%\,\underline{Si} \cdot \%\,O^2 = -\frac{18,050}{T} + 5.10 \qquad [9]$$

It should be noted that this equation does not refer



Fig. 10 — FeO inclusions in heat containing 0.015 pct silicon.

to an equilibrium constant but is considered to be a representation of an empirical silicon deoxidation constant for liquid metal in equilibrium with silica.

Another unexpected result evident from fig. 3, 4, and 5 is the apparent lack of any significant effect of the crucible on the solubility of oxygen in liquid iron containing silicon except at very low silicon contents where a slight influence is indicated. By means of thermodynamics it has been predicted[11] that the deoxidizing power of silicon should be considerably increased for iron melted in magnesia or alumina refractories, because the activity of SiO_2 is reduced by the formation of stable magnesium or aluminum silicates. It is apparent, however, that in the present experiments such a tendency was not observed. The small deviations of the magnesia and alumina crucible curves at very low silicon contents are in line with the observed effects of alumina and magnesia crucibles on the solubility of oxygen in liquid iron in the absence of additions of a deoxidizer[1,7]. It is notable that the analytical and X ray results of slag samples listed in tables III and IV suggest that at silicon contents over approximately 0.05 pct the slags from heats melted in alumina crucibles were saturated with silica, while those from a run made in magnesia were saturated with forsterite or enstatite.

The exact significance of the apparent discontinuities in the solubility isotherms could not be determined directly and can only be inferred. The problem was investigated experimentally at some length, and a number of miscellaneous observations were made which, considered in toto, appear to suggest a reasonable explanation.

The invariant points indicated by the breaks in the curves ought to correspond to points of three-phase equilibrium involving liquid metal, liquid slag, and solid silica. However, repeated tests in which plain electrolytic iron (containing oxygen) was melted in a silica crucible, or in which an excess of oxygen was added to a melt containing silicon gave a result at 1600°C of approximately 0.006 pct silicon and 0.085 pct oxygen in the metal in fair agreement with the results of Körber and Oelsen[14] for liquid iron under a silica saturated slag. Moreover, for the runs made in a silica crucible, both the
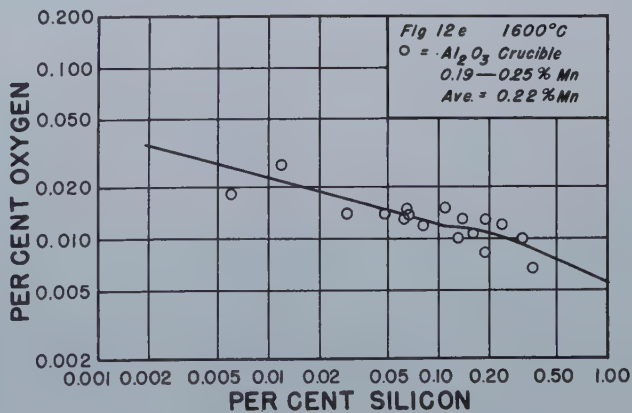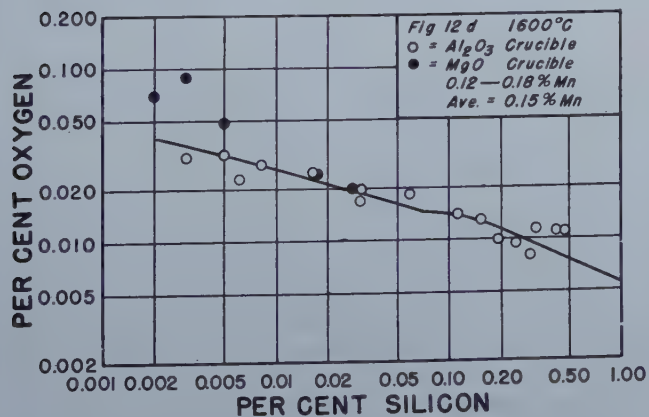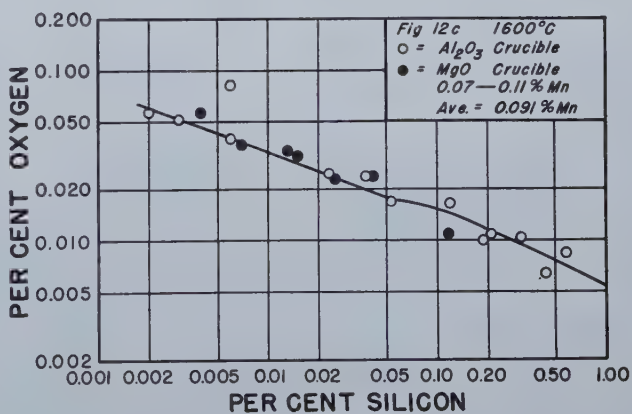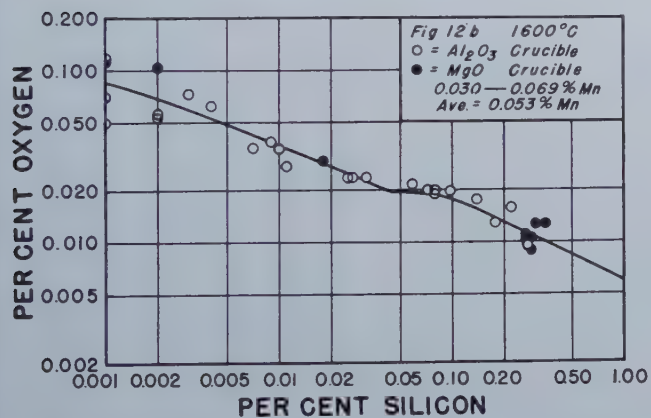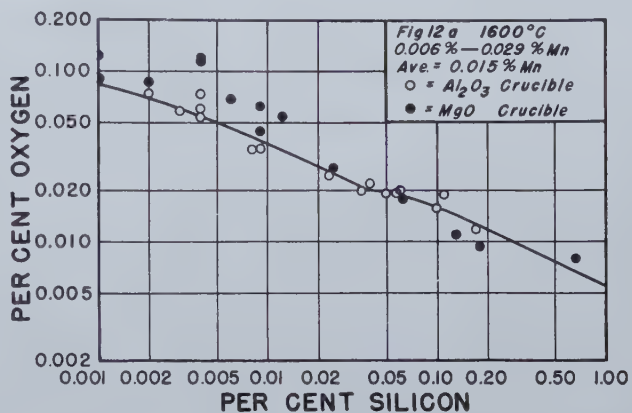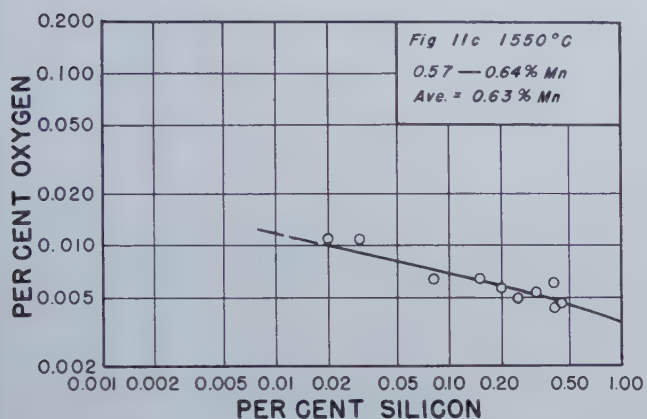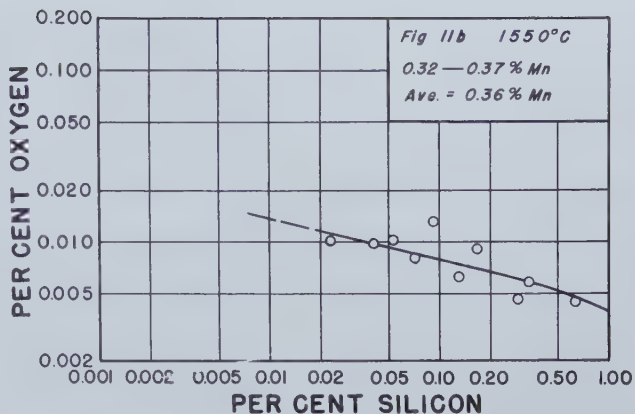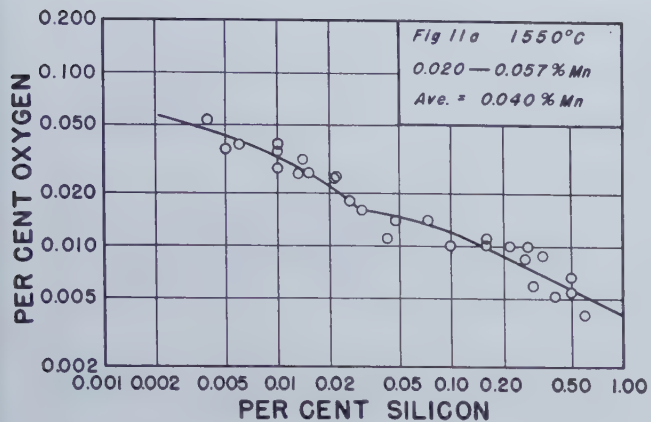
Fig. 11—Effect of manganese on the solubility of oxygen in liquid iron containing silicon at 1550°C.

Fig. 12—Effect of manganese on the solubility of oxygen in liquid iron containing silicon at 1600°C.
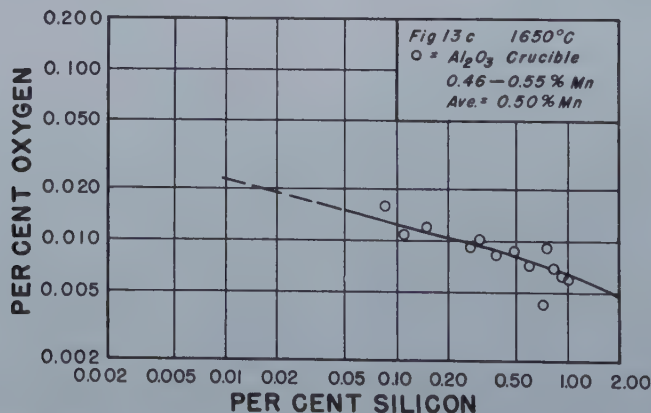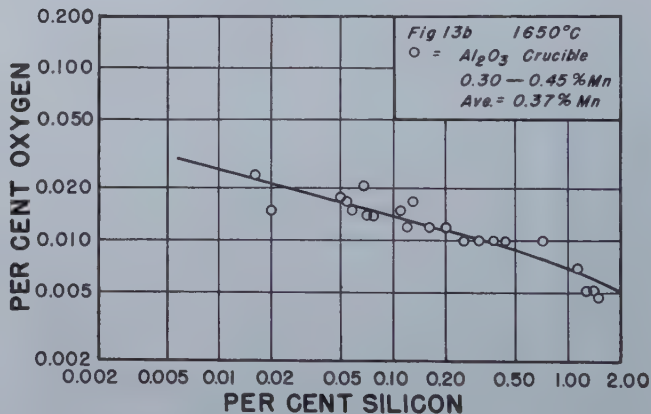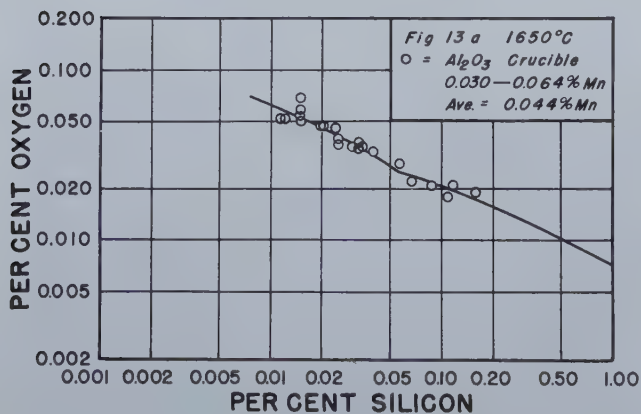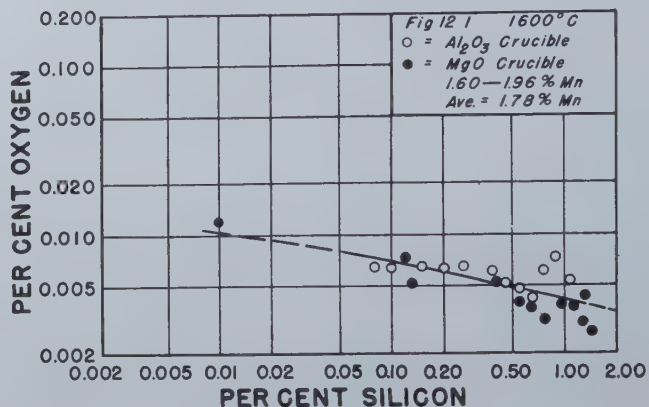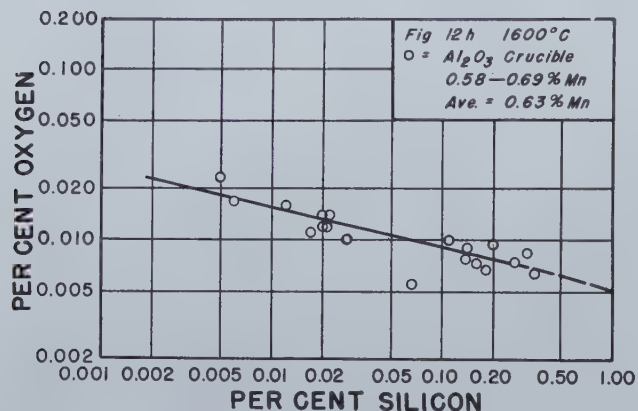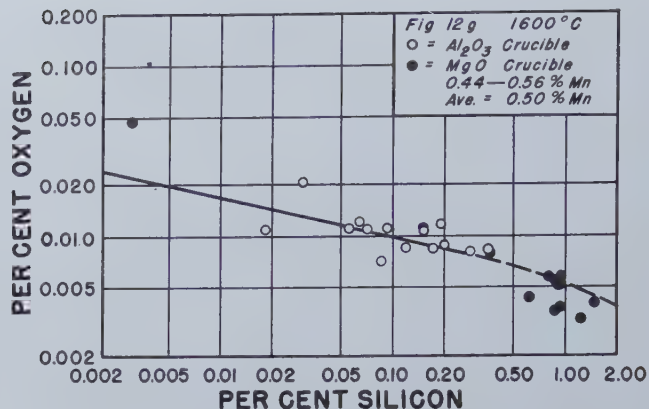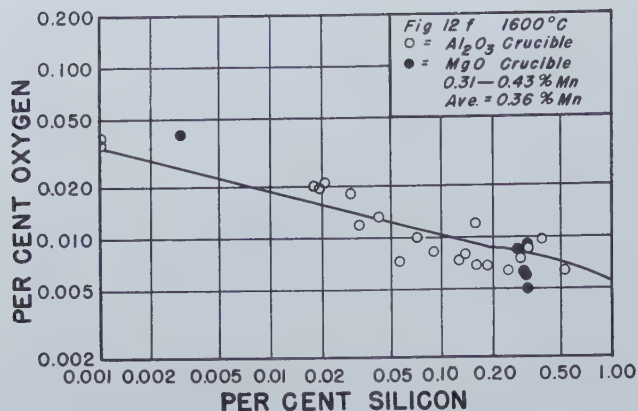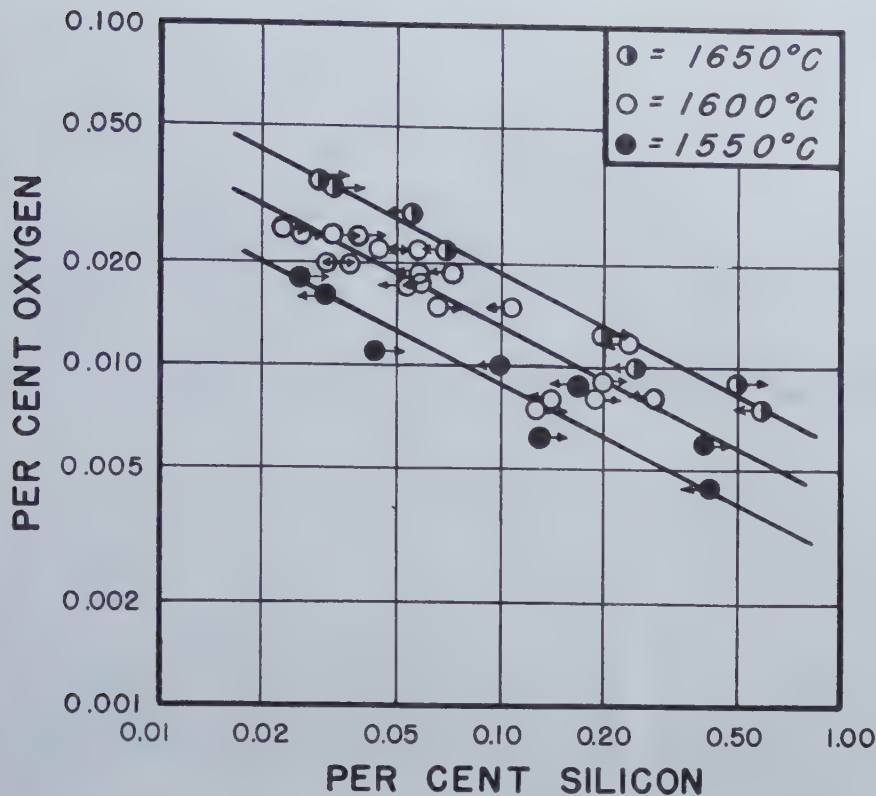
Fig. 12 (continued)—Effect of manganese on the solubility of oxygen in liquid iron containing silicon at 1600°C.

Fig. 13—Effect of manganese on the solubility of oxygen in liquid iron containing silicon at 1650°C.

**Fig. 14—Lines of two-fold saturation of the metal for any manganese content.**

Arrows pointing to right indicate observations just before appearance of film; arrows pointing left indicate observations immediately after appearance of film (see text).
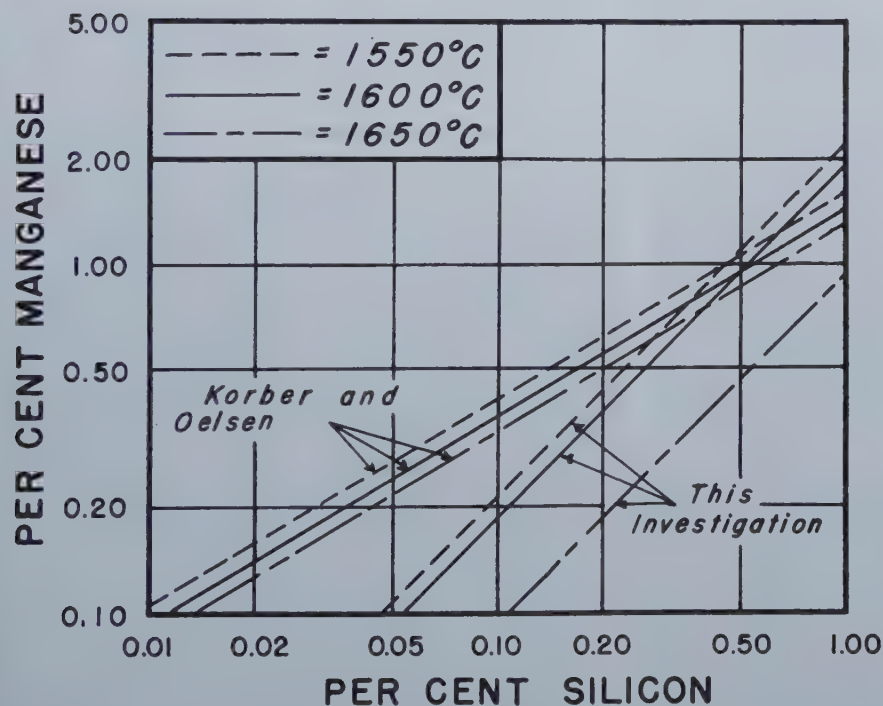


**Fig. 15—Manganese and silicon contents of liquid iron in equilibrium with silica-saturated slags.**

chemical analyses and the X ray results of slag samples indicated the presence of excess silica in the slag at all silicon concentrations in the metal above this end-point. This was not true for runs made in alumina and magnesia crucibles (see tables II, III, and IV).

On the other hand, during the conduct of the experimental runs in all crucibles it was observed that the indicated breaks in the oxygen solubility curves seemed to coincide with a visible change in the appearance of the slag. At silicon contents below the breaks, the slag appeared completely liquid and

formed a small puddle at the bottom of the rotating metal cup. At silicon contents above the breaks in the curves, the slag changed quite sharply to a thin, tough film that was either solid or of very high viscosity, and that completely enveloped the surface of the metal like a skin. When this scum was removed, as by sampling, a new film formed promptly. Samples of this film invariably included a considerable amount of metal, so that chemical analyses of slags at the higher silicon contents could not be considered reliable.
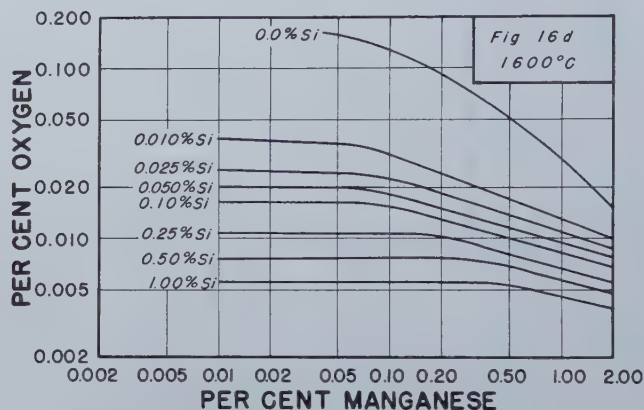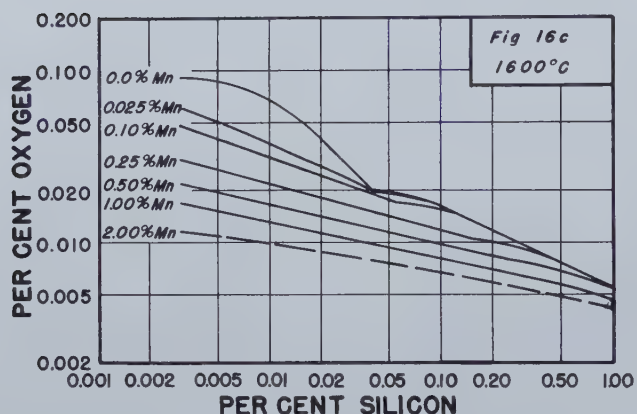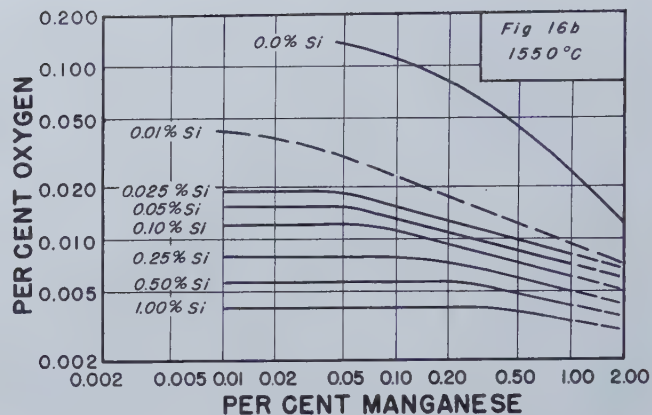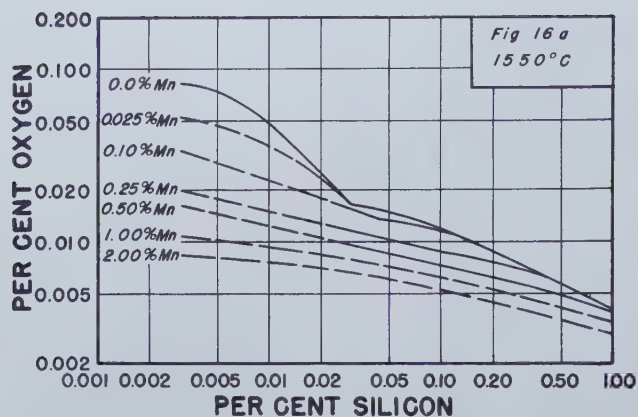
It was also observed during the making of the
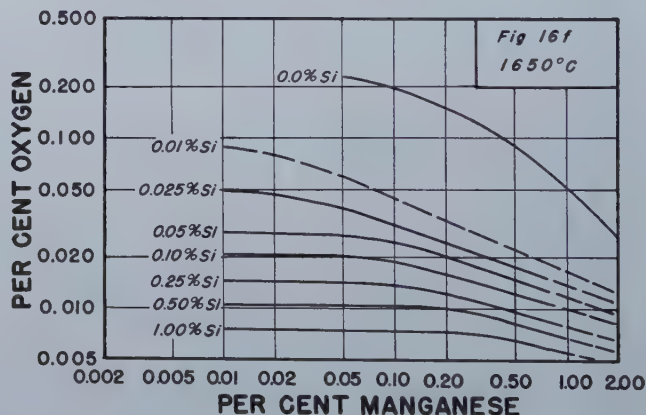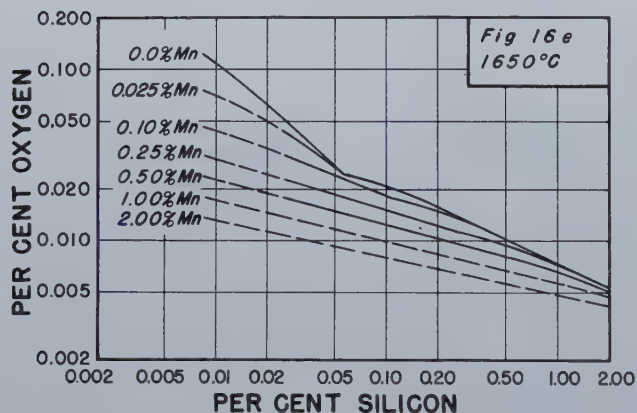
Fig. 16—Solubility of oxygen in liquid iron containing manganese and silicon.

runs that maintenance of equilibrium at silicon contents in the range between the breaks in the curves and the end-point in a silica crucible was practically impossible under the conditions of this study. Left to themselves, melts in this range slowly lost silicon and absorbed oxygen until the end-point was reached. At silicon contents above the breaks, however, equilibrium could readily be maintained over a long period of time.

As explained by Benedicks and Löfquist[18] deoxidation-type inclusions in steel are directly related to the nonmetallic phases in equilibrium with the liquid metal at the time freezing begins. Accordingly, at the conclusion of several of the runs

in silica crucibles, the melts were permitted to freeze in the furnace under the argon atmosphere, and the inclusions in the solidified metal were studied.

The inclusions in a polished section of a heat containing 1.75 pct silicon are shown in fig. 6. These inclusions were extracted electrolytically with the result illustrated by fig. 7. By means of refractive index measurements and X ray diffraction they were identified as globules of so-called "cristobalite glass." Observations similar to these were made on heats containing 0.17 and 0.14 pct silicon respectively.

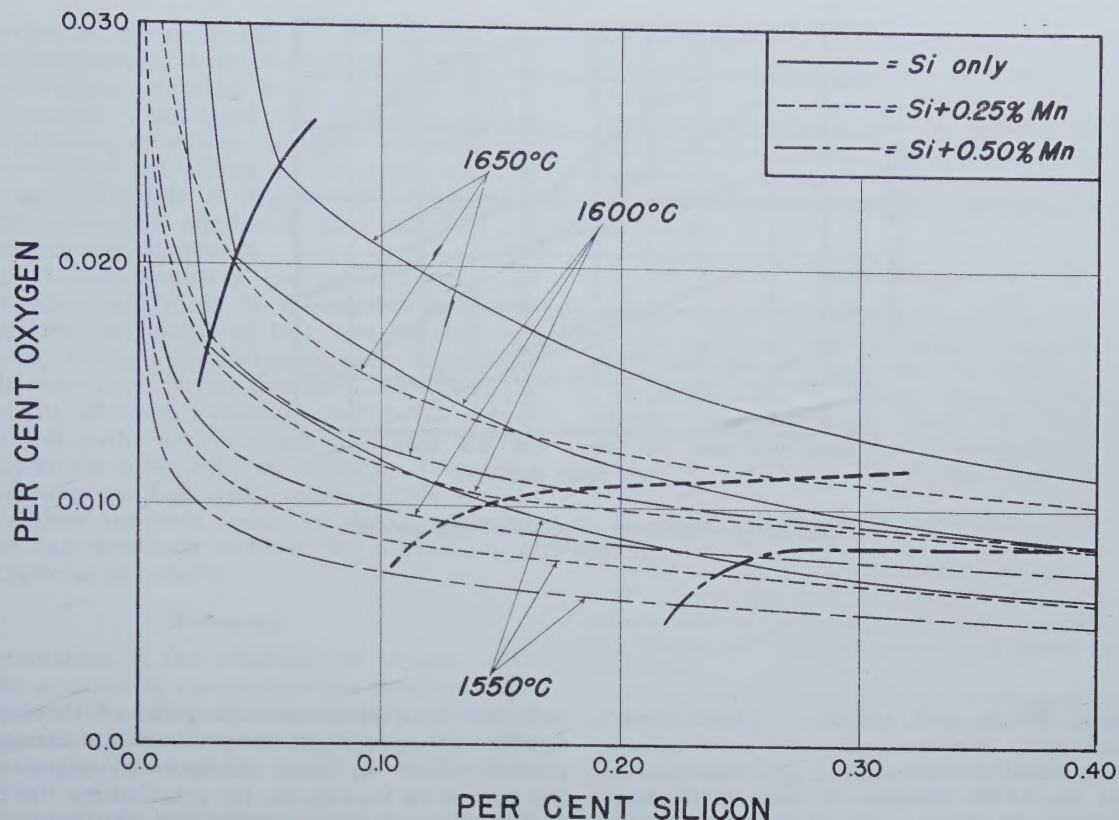In addition, a few unusual inclusions of the type

Fig. 17—Effect of manganese on deoxidation with silicon.

shown in fig. 8 were observed in a specimen cut from near the center of the 0.14 pct silicon heat. The inclusions extracted from this specimen are illustrated in fig. 9. The spherical inclusions were the same as the silica globules described above, but the small, branched particles resembling "wishbones" were identified as crystals of cristobalite. It is reasoned that the latter inclusions may be part of a metal — silica eutectic formed by the last liquid to solidify.

The inclusions in a heat containing 0.015 pct silicon are shown in fig. 10. These were extracted electrolytically and identified by X ray diffraction as FeO. This same heat also contained a completely enclosed pocket or pipe cavity in which some of the precipitating nonmetallic phase had collected during solidification of the metal. By X rays this slag was observed to consist mainly of FeO with a trace of fayalite (2 FeO.SiO$_2$). Chemical analysis gave a result of 87.0 pct FeO and 12.2 pct SiO$_2$. These results of inclusion studies strongly suggest that metal containing silicon in excess of the concentrations at the breaks in the oxygen solubility curves is saturated with silica, but that metal having silicon contents below the breaks in the curves is not.

On the basis of the foregoing observations, it is inferred that the discontinuities in the isothermal oxygen solubility curves of fig. 3, 4, and 5 do actually represent the invariant points of two-fold saturation at which the liquid metal is saturated

with slag phase and solid silica phase. At higher silicon concentrations, the metal appears to be in true equilibrium with solid silica, but at lower silicon contents the equilibrium is with a slag phase of variable composition — and, as suggested by heavy fuming at low silicon concentrations, possibly relatively high vapor pressure — whose identity in runs made in a silica crucible was obscured because of reaction with the crucible.

It is notable that both Herty and Fitterer[13] and Zapffe and Sims[15], in their attempts to evaluate the silicon deoxidation constant for metal in equilibrium with pure silica, also observed deviations from the theoretical oxygen solubility curve at approximately the same silicon contents reported here. Herty and Fitterer attributed this to fluxing of SiO$_2$ inclusions by FeO so that the inclusions were not retained in the metal. Zapffe and Sims considered it might be due to the formation of SiO.

It is considered, therefore, that the curves of fig. 3, 4, and 5 represent solubility isotherms for oxygen in liquid iron containing silicon, and that the inflections in the curves are the points of invariant, three-phase equilibrium. Consequently, at silicon contents above these points the metal is in equilibrium with solid silica phase, and at lower silicon concentrations, the metal is in equilibrium with a liquid slag phase of widely variable composition. For practical purposes, at silicon concentrations over 0.10 pct the product of the silicon content of the metal and the square of the oxygen content may be regarded as constant.
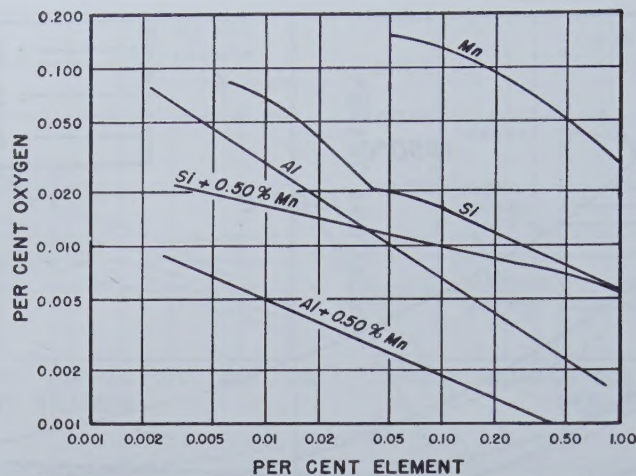
**Fig. 18—Comparison of deoxidizing powers
at 1600°C.**

**Manganese, Silicon, and Oxygen in Liquid Iron:**
Up to the present time no study of the solubility
of oxygen in liquid iron containing both manganese
and silicon but in the absence of silica saturation
has been reported. Körber and Oelsen[14] investi-
gated deoxidation with manganese and silicon in a
silica crucible with varying temperature and de-
rived the equilibrium constant equation:

$$\text{Log } K_{MnSi} = \text{Log } \frac{\% \text{ Si } (\% \text{ MnO})^2}{\% \underline{\text{Mn}}^2} = \frac{-3177}{T} + 4.757 \quad [10]$$

for the reaction:

$$SiO_{2 \text{ solid}} + 2 \underline{\text{Mn}} = 2 (MnO) + \underline{\text{Si}} \quad [11]$$
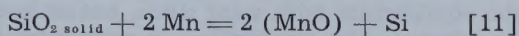
The field of deoxidation so important to steelmak-
ing in other than acid furnaces, however, does not
appear to have been covered experimentally. In
the present investigation, therefore, most of the
experimental runs for the study of the manganese-
silicon-oxygen equilibria in liquid iron were car-
ried out in alumina crucibles, with a few runs be-
ing made in magnesia. No changes in experimental
procedure were involved. The experimental results
are tabulated in tables V and VI.

By plotting the oxygen and silicon contents of
the metal for various limited ranges of manganese
concentrations, oxygen solubility isotherms were
obtained as illustrated by fig. 11, 12, and 13. It is
evident from these curves that, as in the case of
silicon, alone, the effect of type of crucible is not
great. There is a tendency for the oxygen solubili-
ties at very low silicon contents to be somewhat
higher in magnesia crucibles than in alumina, but
this is compatible with the observations reported
above. For the sake of consistency, the curves have
been drawn principally with respect to the alumina
crucible data. In presenting these data, aluminum
concentration in the metal is considered so low as
to be essentially without effect.

It will also be evident that the discontinuities
corresponding to the beginning of silica saturation
are quite apparent in those curves where there are

sufficient data to locate this point of three-phase
equilibrium at constant temperature and manganese
concentration. In those manganese ranges where
the data were inadequate for establishing the break
in the curve, it was located with the help of the
curves of fig. 14.

During the conduct of some of the experimental
runs, reasonably accurate observations of the first
appearance or of the disappearance of the persis-
tent film considered to indicate saturation of the
metal with silica phase, as described in the preced-
ing section, were recorded in the heat logs. By
plotting the silicon and oxygen contents of samples
taken from the melts of various manganese con-
tents immediately before and immediately after
these observations, the curves of fig. 14 were ob-
tained. The intersection of an oxygen solubility
curve from fig. 11, 12, or 13 at any manganese con-
tent with the appropriate temperature curve from
fig. 14 corresponds to the invariant point at con-
stant temperature and manganese content and is
the break in the oxygen solubility curve.

The manganese and silicon contents of the metal
at these invariant points correspond to those cal-
culated by Körber and Oelsen[14] by means of Eq 10
for metal in equilibrium with silica-saturated slags.
The present results are quite different from those
of Körber and Oelsen, as shown in fig. 15. The tem-
perature coefficient indicated in fig. 15 conforms
to that observed for the effect of temperature on
the manganese-oxygen equilibria shown in fig. 1.

From the experimental curves of fig. 1, 3, 4, 5,
11, 12, and 13, complete families of curves showing
the effect of manganese on the silicon-oxygen equi-
libria and the effect of silicon on the manganese-
oxygen equilibria were constructed as illustrated
in fig. 16. The dashed portions of these curves are
based on what appears to be a reasonable extrapo-
lation of the experimental data.

To illustrate the effect of manganese on deoxida-
tion with silicon within the composition and tem-
perature ranges of particular interest in normal
steelmaking processes, the results of this study have

been plotted as shown in fig. 17. The pronounced effect of manganese in increasing the deoxidizing power of silicon, especially in the range of silicon contents usually considered for furnace deoxidation or blocking practices, is quite evident. For example, at 0.10 pct silicon in the bath, 0.25 pct manganese is indicated to improve the deoxidizing power of silicon by almost 30 pct, and 0.50 pct manganese nearly doubles it.

In fig. 17, the boundary curves delineating the fields of silica saturation of the molten metal, as suggested by the results of this investigation, are also shown for the indicated manganese concentrations. It may be inferred that compositions lying to the right of these boundary curves, or whose solidification paths intersect the boundary curves, will precipitate solid $SiO_2$ on cooling. The effect of manganese in displacing these curves toward higher silicon contents, and thereby presumably reducing the tendency toward the formation of $SiO_2$ inclusions, is notable.

## Summary

Determination of the solubility of oxygen in liquid iron containing manganese has indicated that manganese is 50 to 70 pct more effective in limiting the oxygen solubility than has previously been considered on the basis of the work of Körber and Oelsen[2].

The solubility of oxygen in liquid iron containing silicon has been observed to agree fairly well with that reported by Körber and Oelsen[14]. It is indicated, however, that below a silicon content of approximately 0.05 pct the metal is no longer saturated with silica, and the oxygen solubility ceases to conform to the conventional deoxidation constant equation.

Silicon and manganese in combination have been found to be very substantially more effective than either element individually. Within the usual range of steelmaking compositions, silicon in the presence of 0.50 pct manganese has been observed to be practically equivalent to aluminum without manganese in limiting the oxygen content of steel. Manganese also appears to displace the region of silica saturation of the metal toward higher silicon and lower oxygen contents.

From the results of this investigation and those presented in the aluminum paper[1], fig. 18 has been prepared showing a comparison of the deoxidizing abilities of manganese, silicon, aluminum, and combinations of these elements at 1600°C.

## References

[1] D. C. Hilty and Walter Crafts: The Solubility of Oxygen in Liquid Iron Containing Aluminum. *Trans.* AIME **188**, 414. *Jnl. of Metals,* Feb. 1950.

[2] F. Körber and W. Oelsen: Über die Beziehungen zwischen manganhaltigem Eisen und Schlacken, die fast nur aus Manganoxydul und Eisenoxydul bestehen. *Mitt. K-W. Inst. f. Eisenforschung,* Düsseldorf (1932) **14**, 181-204.

[3] C. H. Herty, Jr.: Chemical Equilibrium of Manganese, Carbon and Phosphorus in the Basic Open Hearth Process. *Trans.* AIME (1926) **73**, 1107-1131.

[4] P. Oberhoffer and H. Schenck: Theoretische und experimentelle Untersuchungen über die Desoxydation des Eisens mit Mangan. *Stahl und Eisen* (1927) **47**, 1526-1536.

[5] H. Schenck: Introduction to the Physical Chemistry of Steelmaking. (translation) British Iron and Steel Research Association, London, 1945; cf. Einführung in die physikalische Chemie der Eisenhüttenprozesse, Julius Springer, Berlin, 1932 and 1934.

[6] J. Chipman, J. B. Gero, and T. B. Winkler: The Manganese Equilibrium under Simple Oxide Slags. *Trans.* AIME **188**, 341. *Jnl. of Metals,* Feb. 1950.

[7] C. R. Taylor and J. Chipman: Equilibria of Liquid Iron and Simple Basic and Acid Slags in a Rotating Induction Furnace. *Trans.* AIME (1943) **154**, 228-245.

[8] H. A. Sloman: Third Report of the Oxygen Subcommittee of the Committee on the Heterogeneity of Steel Ingots. *Jnl.* Iron and Steel Inst., London (1941) **143**, 311.

[9] Phase Diagrams for Ceramists. *Jnl. Am. Cer. Soc.:* Part II, Nov. 1947.

[10] A. H. Jay and K. W. Andrews: Note on Oxide Systems Pertaining to Steel-Making Furnace Slags. *Jnl.* Iron and Steel Inst. London (1945) **152**, 15-18.

[11] Basic Open Hearth Steelmaking. AIME, New York, 1944, Chap. 16.

[12] D. F. Clausen and H. D. Roussopoulas: The Molybdenum Blue Reaction for the Determination of Silicon in Steel. *Anachem News* (1946) **6**, 41-44.

[13] C. H. Herty, Jr. and G. R. Fitterer: The Physical Chemistry of Steelmaking: Deoxidation with Silicon and the Formation of Ferrous Silicate Inclusions in Steel. U. S. Bur. Mines, Carnegie Inst. of Tech., and Min. and Met. Advisory Boards Coop. Bul. 36, Pittsburgh, Pa. 1928.

[14] F. Körber and W. Oelsen: Die Grundlagen der Desoxydation mit Mangan und Silizium. *Mitt. K.W. Inst. f.d. Eisenforsch.* Düsseldorf (1933) **15**, 271-309.

[15] C. A. Zapffe and C. E. Sims: Silicon-oxygen Equilibria in Liquid Iron. *Trans.* AIME (1943) **154**, 192-220.

[16] H. Schenck and E. O. Bruggemann: Untersuchungen über die Chemie des sauren Siemens-Martin-Verfahrens. *Archiv. f.d. Eisenhüttenw.* (1935-1936) **9**, 543-553.

[17] G. Derge: The Distribution of Oxygen Between Molten Iron and Iron Oxide-Silica Slags. Amer. Iron and Steel Inst., 1949, (Preprint).

[18] C. Benedicks and H. Löfquist: Nonmetallic Inclusions in Iron and Steel. John Wiley and Sons, Inc., N. Y., 1931.